Doctoral Thesis

Design for Amphiphilic Nanoparticles and Development of Radical Ion Reactions

両親媒性ナノ粒子の設計とラジカルイオン反応の開発

Tokyo University of Agriculture & Technology

Graduate School of Bio-Applications and Systems Engineering

Naoya Maeta

Table of Contents

Chapter 1
General Introduction

1.1. Properties of Nanoparticles and Applications.

Nanoparticles (NPs) are very small particles less than 100 nm and have unique physicochemical properties that depend on the size, thus their applications in a wide range of fields such as pharmaceuticals, cosmetics, functional materials have been investigated.[1] For example, polymer-nanocomposite is a material that is given the functionality of nanoparticles by homogeneous dispersion of the nanoparticles in the polymer.[2]

However, there are several problems in the application of nanoparticles. One of them is “high cohesiveness”. This is due to the high surface energy of nanoparticles compared with bulk material. In order to take advantage of the nanoparticle functionalities, it is essential to develop the new methods and technologies to solve these problems, and it will lead to the expansion of the use of nanoparticles.

In this chapter, research examples about nanoparticle dispersion in solvents and research applications about catalytic reactions using nanoparticles would be reviewed.

1.2. Ligand Design for Dispersion Control of Nanoparticles in Solvents

Over the past decade, nanotechnology has grown significantly and now accounts for a significant portion of current research in both academic and industrial fields. Nanoparticles are positioned as one of the most important platforms of technically useful materials due to their inherent magnetic, electrical and optical physicochemical properties.[3] Extensive and intensive efforts to produce nanoparticles of well-defined size and morphology have led to the development of classes of various functional materials and devices.[3] To achieve such applications, development of in-solution processing technique is required to stable and homogeneous colloidal dispersion in solvent. Although various organic ligands have been devised, and surface modifiers have been used to improve the dispersibility of nanoparticles in organic solvents,[5] the relationship between the structure and the function of nanoparticle-ligand complexes remains elusive and is often controversial.[6] Previous colloidal dispersion models are often insufficient to predict the functionalities of nanoparticles in solution and have been described very recently both experimentally and theoretically.[7] In addition, even small differences in nanoparticles, additives, and ligands can have significant effects on solution properties, so their selection must be careful.

In generally, ligand design is intended for dispersion in high or low polarity solvents, thus the types of solvent that can disperse the nanoparticle-ligand complex are limited (Fig. 1-1, 1-2).[8][9] For example, hydrophobic alkyl ligands such as octadecyl and oleyl group are used to achieve dispersion in low-polarity solvents as shown in Fig. 1-2. Hydrophobic nanoparticles are dispersible in hydrophobic solvents, but aggregate in hydrophilic solvents. Therefore, appropriate ligands have been required to disperse nanoparticles in each solvent. Since ligands have been selected empirically so far, trial and error have been required to find the suitable ligand.

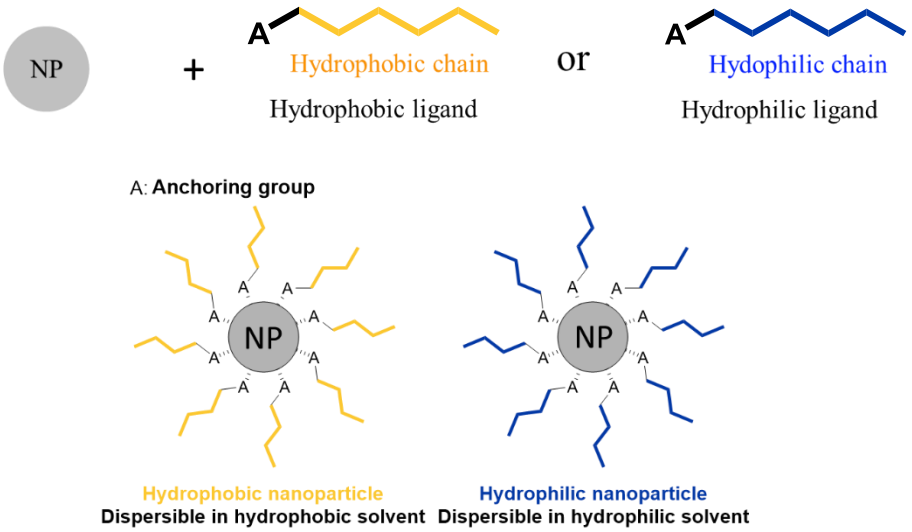

Fig. 1-1 Surface Modification for Nanoparticle by Hydrophobic or Hydrophilic Ligand.

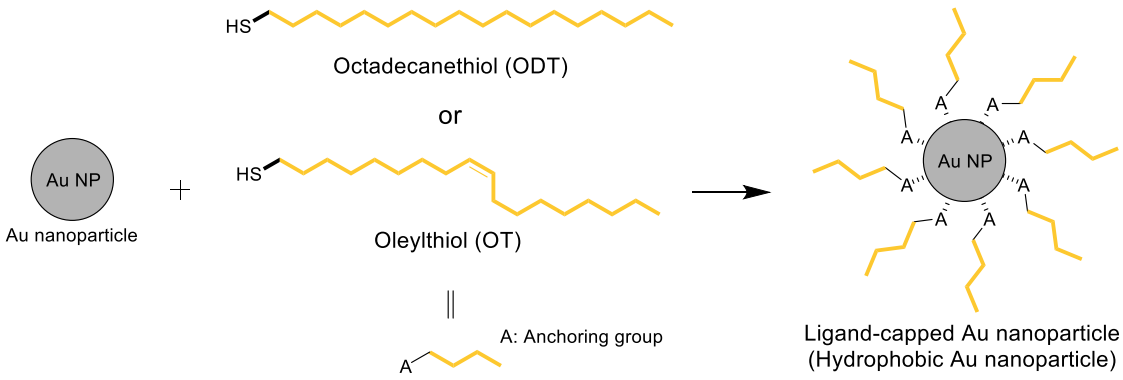

Fig. 1-2 Fabrication of ODT-Capped Au Nanoparticle

In order to overcome these current situations, a guideline for designing ligands based on experimental data is required. On the other hand, only a few studies have focused on the ligand structure and the dispersibility of nanoparticles, and their relationships are still controversial. In recent years, Peng *et al.* reported a work evaluating the dispersibility of nanoparticles from the viewpoint of solubility in solvents, and found that the crystallinity between ligands greatly contributes to the solubility of nanoparticles (Fig. 1-3).[7] This result supports the fact that many studies have empirically used bulky ligands such as oleyl groups.[8][9] In other words, small differences in the molecular structure of the ligand affect the

dispersibility and functionality of the nanoparticle in solvent, thus the design of the ligand is very important to expand the applicability of the nanoparticle.

Fig. 1-3 Difference of Dispersion State by Changing Molecular Structure of Ligands.

When converting hydrophobic nanoparticles to hydrophilic nanoparticles, the ligand exchange method is effective. Ligand exchange is a method of replacing the ligand on the particle surface by adding a large amount of different ligand (Fig. 1-4).[9] However, ligand exchange is required complicated processing and it is difficult to evaluate the produced nanoparticles. Hence, it is required for the development of simple surface modification methods that enables thorough evaluation of nanoparticles.

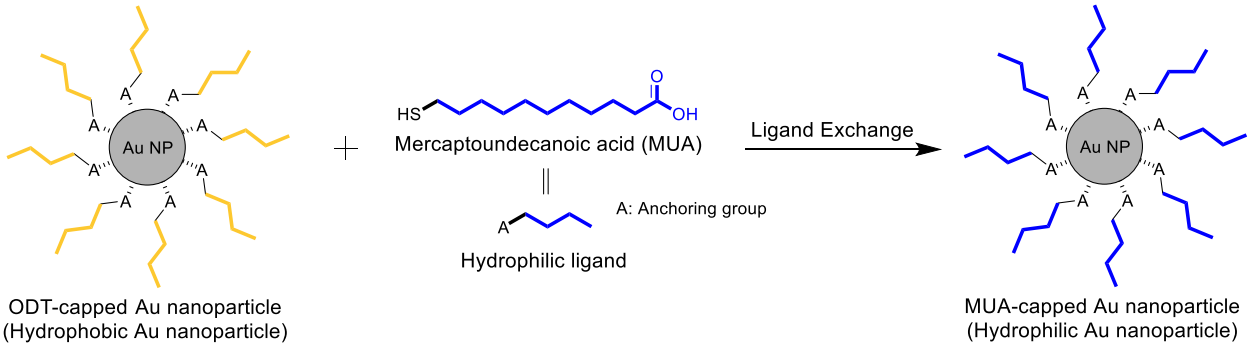

Fig. 1-4 Ligand Exchange from Hydrophobic Ligand to Hydrophilic Ligand.

In recent years, biological application research using nanoparticles as a carrier for drug delivery has been rapidly developed. In particular, Au nanoparticles have been used in many studies because of their high bioadaptability and membrane permeability.[10] The design and evaluation of amphiphilic ligands is important for biological applications of Au nanoparticles. A research investigating the dispersion mechanism of ligand-coated Au nanoparticles using ^{1}H-NMR is shown in Fig. 1-5 and Fig. 1-6.[11]

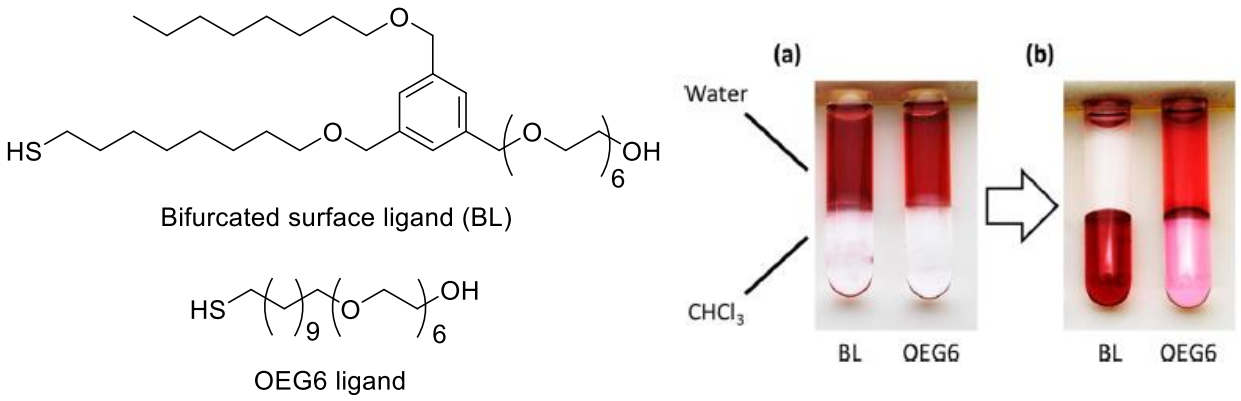

Fig. 1-5 BL or OEG6 Ligand Structure and Dispersibility of Ligand-Coated Au Nanoparticle. (Phase transfer of Au nanoparticles (10 nm in diameter) from water to $CHCl_3$ (a) before mixing and (b) after mixing.)

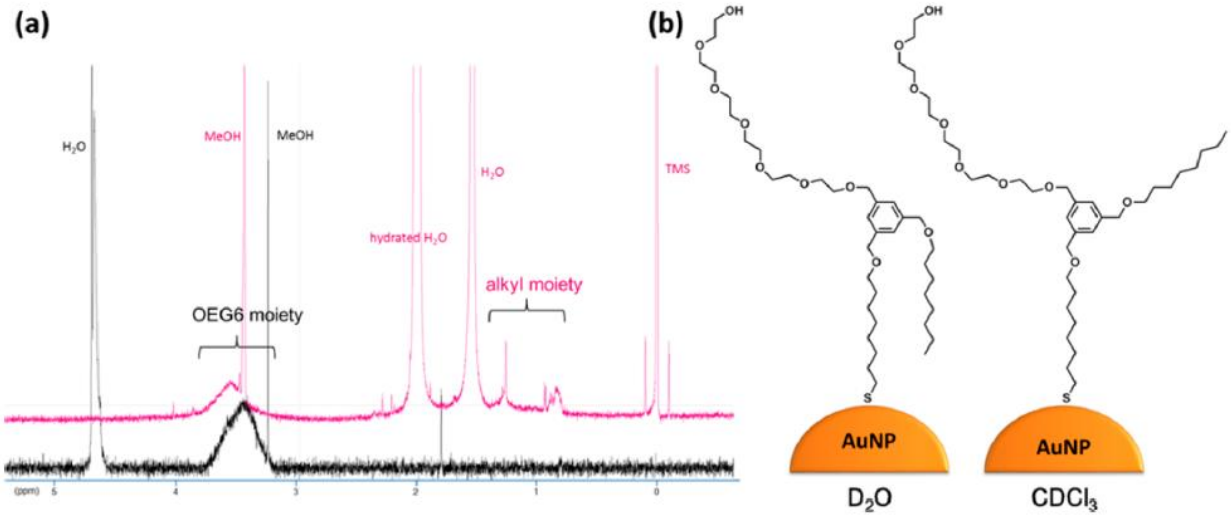

Fig. 1-6 ^{1}H-NMR Measurement of BL-Coated Au Nanoparticles for Estimation of Dispersion Mechanism. ((a) ^{1}H-NMR measurement in D_2O (black) and $CDCl_3$ (red) and (b) estimation of dispersion mechanism in each solvent.)

Fig.1-5 shows the phase transfer from water to chloroform of BL or OEG ligand-coated Au nanoparticles. Each Au nanoparticle was dispersed in water (Fig. 1-5 (a)), and the two-phase solvent was vigorously mixed. Although BL-coated Au nanoparticles were transferred from water to chloroform, OEG6 ligand-coated Au nanoparticles were hardly transferred (Fig. 1-5 (b)). From these results, it was suggested that the alkyl arm of the BL greatly contributed to the phase transfer to chloroform.

Fig. 1-6 shows the estimation of the dispersion mechanism of BL-coated Au nanoparticles by ^{1}H-NMR measurement. In general, NMR can analyze free molecules in solution, but it is difficult to analyze molecules near the particle surface due to restricted molecule mobility. In $CDCl_3$, peaks of both the alkyl moiety and the OEG6 moiety were confirmed (red). However, in D_2O, the peak of the OEG6 moiety was only confirmed (black). From these results, the dispersion mechanism was estimated in Fig. 1-6 (b). From fig. 1-6(b), the alkyl chain was folded in D_2O, and the motion was significantly restricted. Therefore, it was suggested that observation by ^{1}H-NMR became difficult. On the other hand, since both OEG6 chain and alkyl chain could move freely in chloroform, it was suggested that both chains could be observed by ^{1}H-NMR. From these results, it was possible to estimate indirectly the behavior of the ligand on the particle surface in different solvents, although the elucidation of the dispersion mechanisms is still controversial.

The ligand design for incorporating amphiphilic Au nanoparticles into cells is shown in Fig. 1-7.[12]

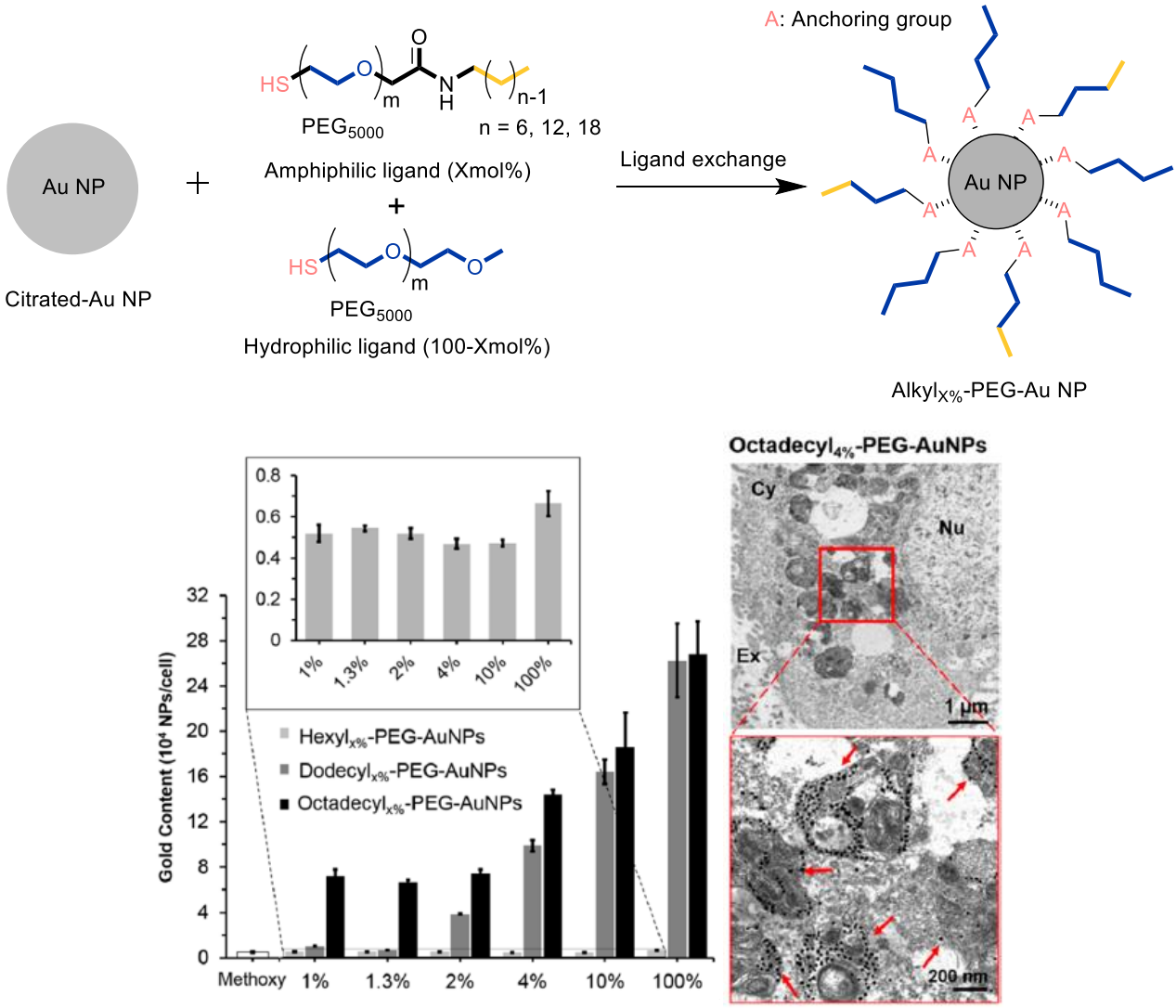

Fig. 1-7 Alkyl-PEG Coated Amphiphilic Au Nanoparticle and Cellular Uptake of Amphiphilic Au Nanoparticle Varying Alkyl Chain and Alkyl Amount.

Figure 1-7 shows an example of biomedical application using amphiphilic nanoparticles. The purpose of this research is to design the ligand to incorporate highly biocompatible Au nanoparticles into cells. Au nanoparticles are known as carriers for delivering drugs into cells. In this research, Lok *et al.* worked on the preparation of Au nanoparticles modified with amphiphilic ligands having both PEG and alkyl chains and evaluated the effects of alkyl chain length and amount on the uptake of Au nanoparticles into cells. From the experimental results, as the length of the terminal alkyl chain increased, the incorporation of Au nanoparticles into the cell proceeded efficiently. This is because the affinity between the amphiphilic ligand (Octadecyl$_{4\%}$-PEG-Au NPs) with long alkyl chain and the hydrophobic cell membrane is increased, and the cell membrane permeability is increased. As in this example, the development of amphiphilic ligands for various nanoparticles would be very important research subject in biological, catalytic and material applications.

1.3. Catalytic Applications of Semiconductor Nanoparticle Photocatalyst

One of the nanoparticle applications is the use as a catalyst. In recent years, inorganic oxide nanoparticles, metal nanoparticles and quantum dots have been used for organic synthesis by light irradiation and nanoparticle activation. Compared to transition metal photocatalysts and organic molecular photocatalysts, nanoparticle photocatalysts have the advantages of being inexpensive, low toxicity and stable in air.[13] The schematic diagram of nanoparticle photocatalysis is shown below (Fig. 1-8). [14]

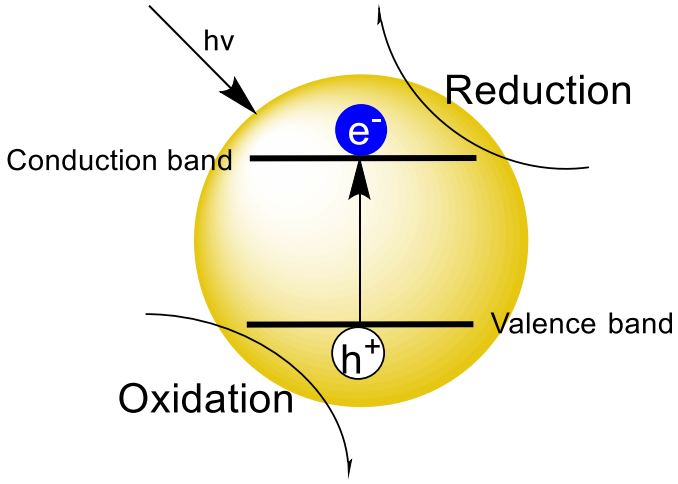

Fig. 1-8 Schematic Diagram of Nanoparticle Photocatalysis.

Nanoparticle photocatalysis refers to the redox reaction by holes (h^+) and excited electrons (e^-) that are generated by light irradiation. For many years, “degradative reactions” that decompose harmful organic molecules in water has been the mainstream of research on the redox action of nanoparticles.[15] However, in recent years, “synthetic reactions” using nanoparticle photocatalysis in organic solvents for the construction of complex organic molecules have also been rapidly developed with the reaction development using transition metal and organic molecule photocatalysts. This development has been led to the expansion of the use of nanoparticle photocatalysts.

As an example, decarboxylative cycloaddition reaction by TiO_2 photocatalysis is shown below (Scheme 1-1).[16]

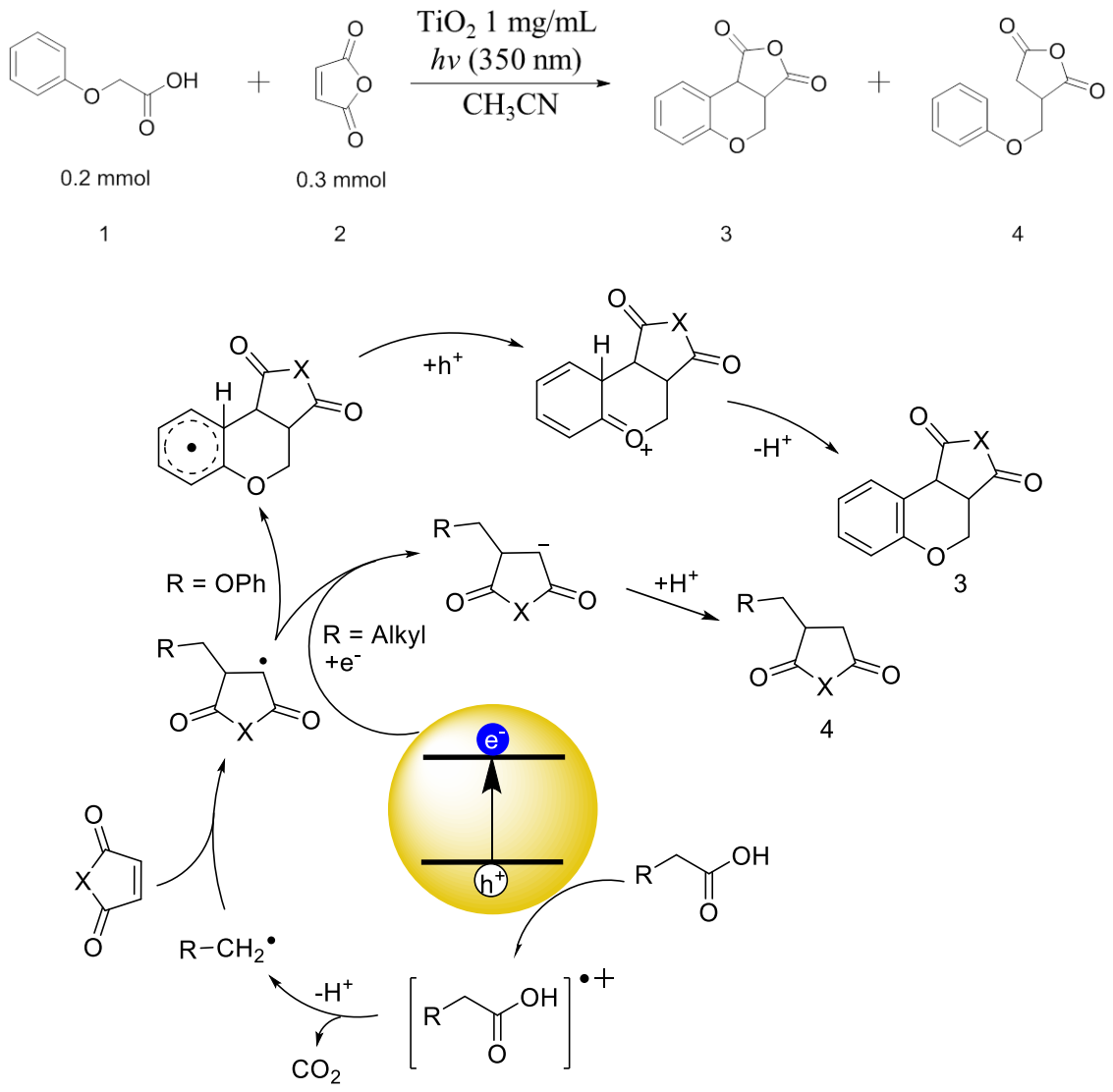

Scheme 1-1 Decarboxylative Cycloaddition Reaction by TiO_2 Photocatalysis.

This reaction is the decarboxylative cycloaddition reaction between Phenoxyacetic acid (1) and Maleic acid anhydride (2) under argon atmosphere. Product 3 is obtained by utilizing hole oxidation of TiO_2. On the other hand, the product 4 is obtained by utilizing both hole oxidation and excited electron reduction of TiO_2. In this reaction, it was also found that when the TiO_2 concentration was increased from 1 mg/mL to 5 mg/mL, the ratio of product 3 : product 4 changed from 1.0 : 1.3 to 1.0 : 0.3. From this result, it was confirmed that the reaction using only hole oxidation proceeded preferentially by increasing the amount of TiO_2. Therefore, it was suggested that the excited electrons were consumed by the solvent or could not be used efficiently by diffusing in the particles.

Examples of such decarboxylative cycloaddition reactions using TiO_2 photocatalysts have also been reported using amino acids such as proline, and nanoparticle photocatalysts are expected to be applicable to a wide range of synthetic reactions. [13][17] In synthetic reaction using photocatalysts, radicals are generated in many cases, and highly reactive radical intermediate is cross-coupled with substrate to give a product. Although radical reactions have many variations, there are also problems that side reactions are likely to occur due to the high reactivity of radical intermediates. Therefore, it is necessary not only to develop the photocatalyst but also to devise how to stabilize unstable radicals and incorporate them into the reaction. In addition, it is essential to understand the intermolecular and intramolecular electron transfer to know the reaction mechanism.

As an example, a C-C bond formation reaction using hydrophobic ligand-coated CdSe quantum dots photocatalyst is shown (Fig. 1-9). [18]

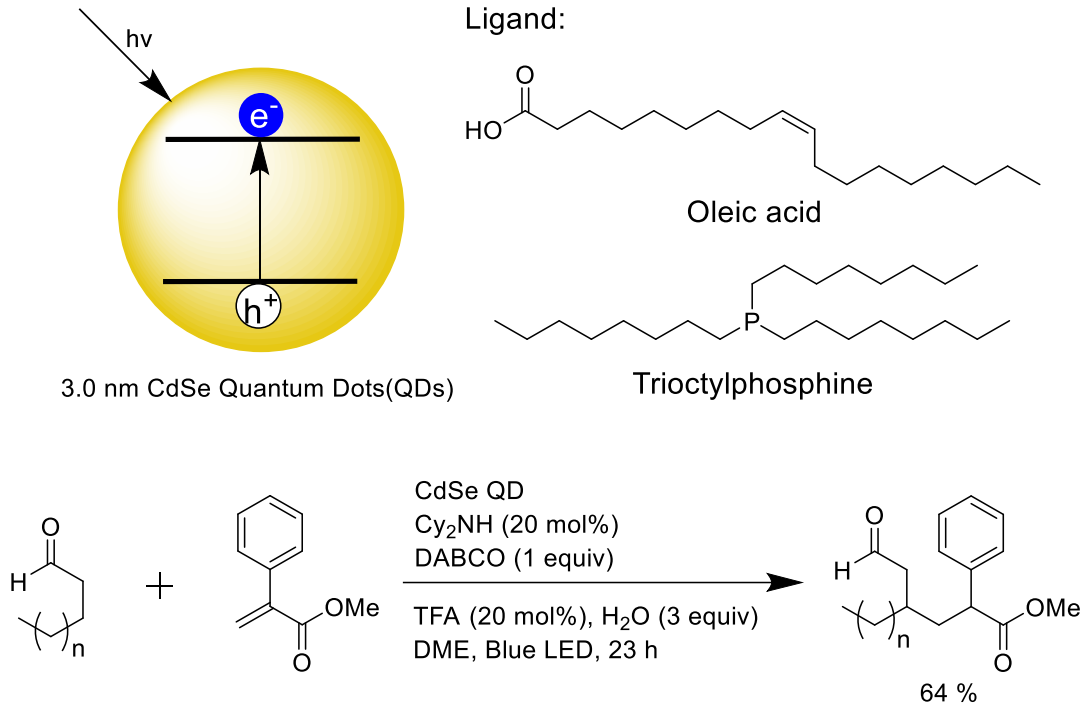

Fig. 1-9 Photocatalytic C-C Coupling Using CdSe Quantum Dots (QDs).

In this research, CdSe QDs with hydrophobic ligands are used as photocatalysts to achieve five types of C-C bond forming reactions including β-alkylation of aldehydes. This research is one of the few examples using ligand-coated nanoparticles for photocatalytic reactions. This reaction was completed with only 0.0008 mol% catalyst amount and the yield is like those of existing transition metal photocatalysts such as Ru and Ir complex. This is due to the synergistic effect of holes and excited electrons existing everywhere on the nanoparticle surface. This work would be a breakthrough for nanoparticle photocatalysis using ligand-coated nanoparticles.

However, there are some challenges in this work. One is that the window of oxidation potential (+0.75 V) and reduction potential (-1.59 V) of CdSe QDs is narrow. For this reason, substrates that can be

oxidized and reduced is limited for reactions. Another is low quantum yield. Especially, in β-alkylation reaction of aldehyde, the quantum yield is low about 0.31%. This means that only one of the 323 photoexcited electrons can be used. Furthermore, since hydrophobic ligands are used, the solvent system and additives are limited to use for reaction.

In order to solve these problems, the use of nanoparticles with high oxidation potential such as TiO_2, ZrO_2 and ZnO and high reduction potential such as ZnS and ZnSe are necessary to construct synthetic reaction systems. On the other hand, it is important to develop nanoparticle materials that extend the lifetime of generated hole-electron pairs. In addition, the development of the methods such as modification of organic molecules to the nanoparticle surface is also important to prevent recombination of holes (h^+) and excited electrons (e^-).[19] Therefore, in order to establish the synthetic reaction systems using nanoparticle photocatalyst, basic research on both “construction of reaction system” and “interface design of nanoparticle” would be required.

1.4. Reactions Induced by Radical (Ion) Species

The development of organic synthesis is significantly important in the manufacture of pharmaceuticals, fine chemicals and functional materials. In particular, “molecular targeted drugs” and “antibody drugs” that act specifically on target proteins and genes are attracting attention in the field of drug synthesis.[20] Along with this, the required molecular structure has become more complex. On the other hand, reduction of waste in each manufacturing process is desired in the industry field. For efficiently obtaining the desired product, the development of an environmentally friendly and sustainable method is required.[21]

Most reactions in synthetic organic chemistry is “electron-matched reactions” involving electron pair transfer between electron-poor and electron-rich molecules. On the other hand, electronically mismatched reactions between electron-rich and electron-poor molecules are known to not proceed with classical synthesis methods (Scheme 1-2). Since a bond is formed between an electron rich molecule and an electron poor molecule in electron-matched reactions, either molecule must be electron rich or electron poor. Hence, the substrates that can be used for the reaction have been limited (Scheme 1-3). As a result, the synthesis of precursor is required to obtain the target compound. From the viewpoint of the atom economy and step economy, the development of innovative synthesis methods is required.[22] Atom economy and step economy are concepts that minimize the waste of atoms and steps. These concepts are important in terms of environmental harmony and efficient production.

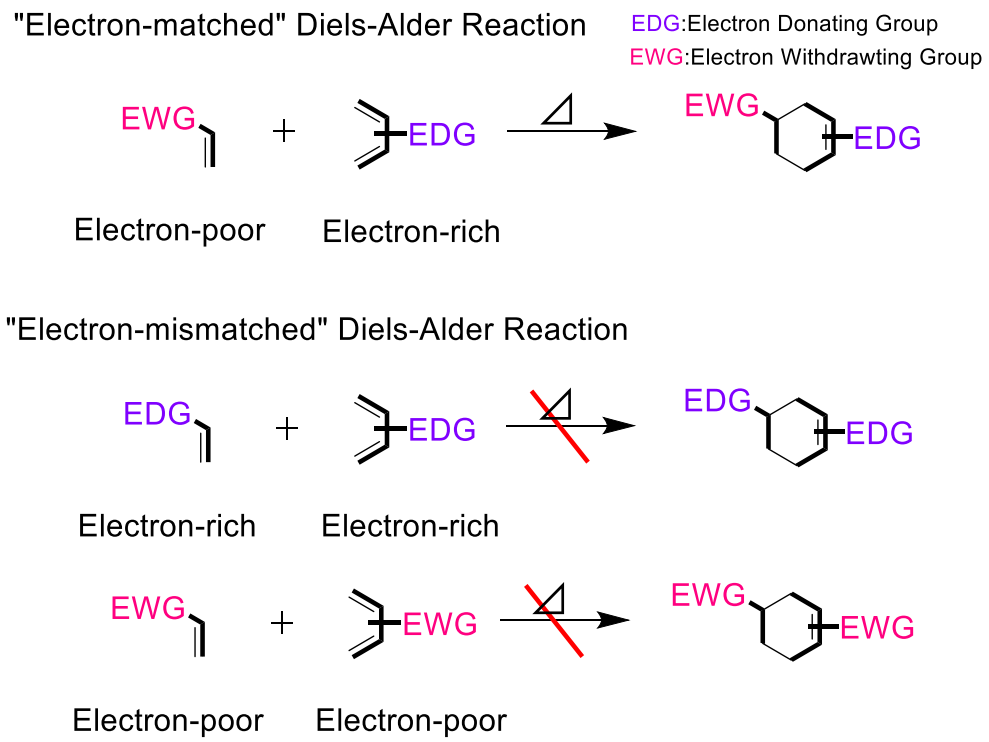

Scheme 1-2 Electron-matched and Electron-mismatched Diels-Alder Reaction.

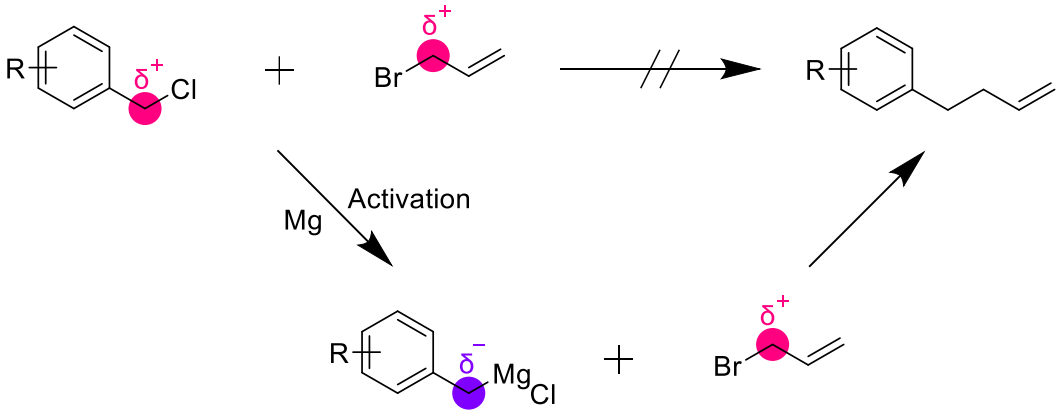

Scheme 1-3 Carbon Activation in Grignard Reaction (Ion Reaction).

In recent years, environmentally friendly methods using light and electricity are attracting attention and are rapidly developing.[23][24] Reaction development using “photocatalyst” has been energetically worked in the field of synthetic organic chemistry, and new molecular conversions utilizing unique reactivity has attracted attention. Photocatalytic reaction refers to "radical (ion) reaction" with single electron transfer (SET) which utilizes the unique reactivity of radical or radical ion species (Scheme 1-4, 1-5). [24][25] In particular, the reaction by “electron-rich molecules” or “electron-poor molecules” which is impossible in classical reactions proceeds in case of radical ion reactions.

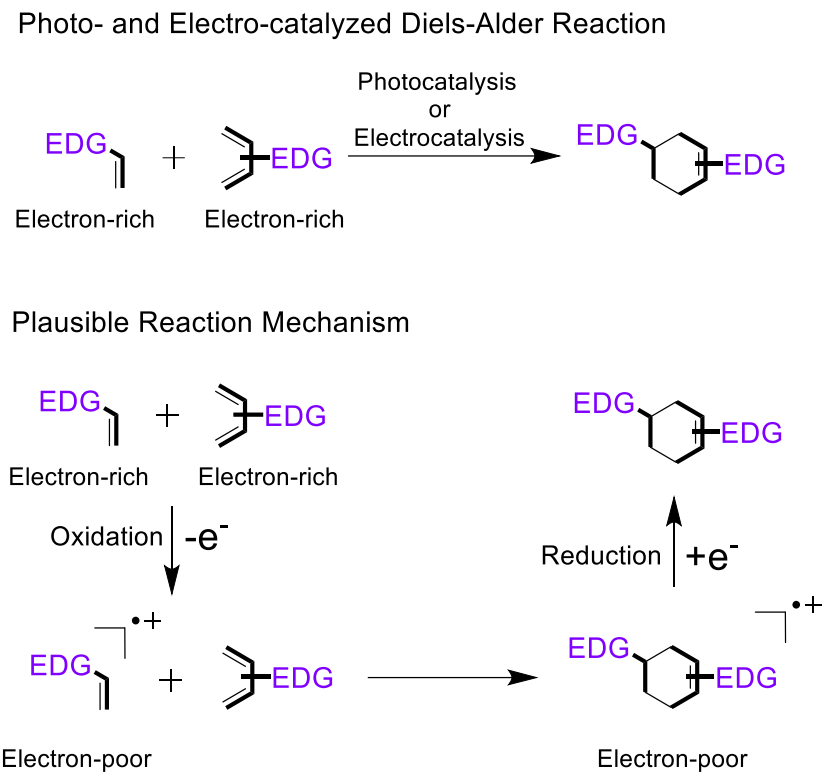

Scheme 1-4 SET-induced Diels-Alder Reaction and Plausible Reaction Mechanism.

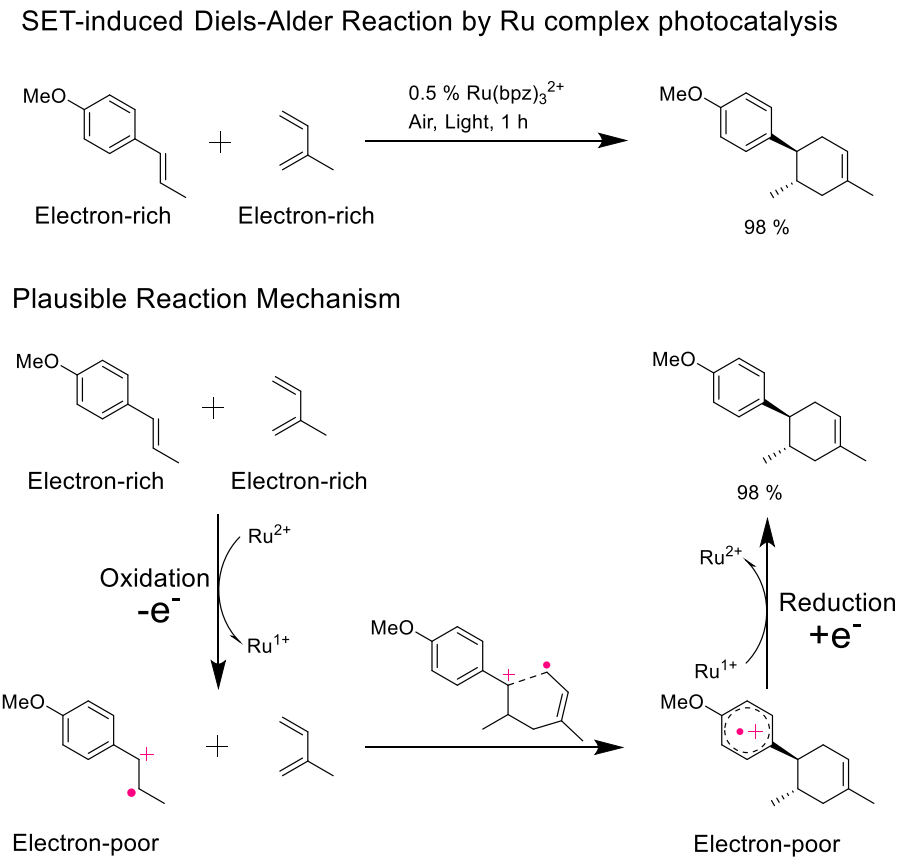

Scheme 1-5 Reaction Mechanism in Diels-Alder Reaction by Ru Complex Photocatalysis.

As shown in Scheme 1-4 and Scheme 1-5, since SET type reaction proceeds only by “exchange of an electron”, SET reaction is said an elegant reaction from the viewpoint of the atom economy.[26] If reaction active species such as radicals and radical ions could be used as expected, sophisticated reactions would be designed. Moreover, more complex molecules would be efficiently synthesized in a short process.

As described above, in ligand design for stable and homogeneous dispersion of nanoparticles in solvents, surface modification using a hydrophobic ligand or a hydrophilic ligand has been the mainstream. Therefore, it was necessary to select an appropriate ligand for solvent type. In addition, since various nanoparticles and organic solvents are used in the application of catalysts and materials, preparation of nanoparticles that can be dispersed in various organic solvents is desired. Accordingly, development of amphiphilic ligands applicable to nanoparticles having different surface structures is desired. On the other hand, as for the relationship between the ligand structure and the dispersibility of the nanoparticles in solvent, examples using a hydrophobic ligand have been reported, but using an amphiphilic ligand have not been reported. By evaluating the relationship between the structure of the amphiphilic ligand and the dispersibility of the nanoparticles, it is expected that a clue toward the preparation of the amphiphilic particles could be obtained.

In the application of nanoparticles to photocatalysts, their use in synthesis reactions is limited, although they have unique functions superior to existing photocatalysts. Promotion of reaction development using nanoparticle photocatalysts is expected to contribute to the acquisition of new reactivity and the development of environmentally friendly synthetic methods. Accordingly, the reactivity of radicals and radical ions have not been elucidated, and it is also important to analyze the reaction mechanism using these reactive species.

1.5. The Purpose of This Work

Based on the challenges described in Chapter 1, by designing and synthesizing amphiphilic ligands that can maintain the stable and homogeneous nanoparticle dispersion in complex reaction systems, structure-function relationship between nanoparticles and amphiphilic ligands should be evaluated. In addition, by constructing the radical ion reaction system using nanoparticle photocatalyst and applying the experimental and computational chemistry approach, it is possible to construct a carbon skeleton that is difficult to synthesize with classical methods, and it is possible to analyze the reaction mechanism in detail.

Hence, the purpose of this work is “evaluation of relationship between nanoparticle dispersibility and amphiphilic ligand structure for preparation of amphiphilic nanoparticles” and “development of radical ion reaction using nanoparticle photocatalyst” for establishment of radical ion reaction system by nanoparticle photocatalysis.

In chapter 2, relationship between ligand structure and dispersibility was evaluated for preparation of amphiphilic TiO_2 nanoparticles dispersible in various solvents. In chapter 3, relationship between ligand structure and dispersibility was evaluated for preparation of amphiphilic Ag nanoparticles dispersible in various solvents. The reason for selecting TiO_2 and Ag nanoparticles is to exhibit unique properties such as high photocatalytic activity and surface plasmon resonance by light irradiation. In addition, TiO_2 nanoparticles (metal oxide) and Ag nanoparticles (metal) have different surface structures, which is important information for evaluating the versatility of amphiphilic ligands. Therefore, TiO_2 and Ag nanoparticles were selected as representatives of nanoparticles.

In chapter 4, electron-mismatched [2 + 2] cycloaddition reaction was developed for the construction of radical ion reaction system by TiO_2 photocatalysis. In chapter 5, electron transfer of [2 + 2] cycloaddition reaction was analyzed by applying the experimental and computational chemical approach.

1.6. References

[1] (a) Jung, S. K.; Hwang, I.; Chang, D.; Park, K. Y.; Kim, S. J.; Seong, W. M.; Eum, D.; Park, J.; Kim, B.; Kim, J.; Heo, J. H.; Kang, K. Nanoscale Phenomena in Lithium-Ion Batteries. *Chem. Rev.*, ASAP article. (b) Qiu, J.; Camargo, P. H. C.; Jeong, U.; Xia, Y. Synthesis, Transformation, and Utilization of Monodispersed Colloidal Spheres. *Chem. Rev.* **2019**, *52*, 3475-3487. (c) Yu, J. R.; Yao, W. Y.; Wang, Y.; Fei, X.; Qi, P.; Lin, S.; Kaplan, D. L.; Buehler, M. J.; Ling, S. Biological Material Interfaces as Inspiration for Mechanical and Optical Material Designs. *Chem. Rev.* **2019**, *119*, 12279-12336. (d) Peynshaert, K; Manshian, B. B.; Joris, F.; Braeckmans, K.; Smedt, S. C. D.; Demeester, J.; Soenen, S. J. Exploiting Intrinsic Nanoparticle Toxicity: The Pros and Cons of Nanoparticle-Induced Autophagy in Biomedical Research. *Chem. Rev.* **2014**, *114*, 7581-7609.

[2] (a) Shifrina, Z. B.; Matveeva, V. G.; Bronstein, L. M. Role of Polymer Structures in Catalysis by Transition Metal and Metal Oxide Nanoparticle Composites. *Chem. Rev.*, ASAP article.

[3] (a) Ulbrich, K..; Holà, K.; Šubr, V.; Bakandritsos, A.; Tucek, J.; Zboril, R. Targeted Drug Delivery with Polymers and Magnetic Nanoparticles: Covalent and Noncovalent Approaches, Release Control, and Clinical Studies. *Chem. Rev.* **2016**, *116*, 5338–5431. (b) Gawande, M. B.; Goswami, A.; Felpin, F-X; Asefa, T.; Huang, X.; Silva, R.; Zou, X.; Zboril, R.; Varma, R. S. Cu and Cu-Based Nanoparticles: Synthesis and Applications in Catalysis. *Chem. Rev.* **2016**, *116*, 3722–3811. (c) Kamaly, K.; Yameen, B.; Wu, J.; Farokhzad, O. C. Degradable Controlled-Release Polymers and Polymeric Nanoparticles: Mechanisms of Controlling Drug Release. *Chem. Rev.* **2016**, *116*, 2602–2663. (d) Feliu, N.; Docter, D.; Heine, M.; Pino, P.;Ashraf, S.; Kolosnjaj-Tabi, J.; Macchiarini, P.; Nielsen, P.; Alloyeau, D.; Gazeau, F.; Stauber, R. H.; Parak, W. J. In vivo Degeneration and The Fate of Inorganic Nanoparticles. *Chem. Soc. Rev.* **2016**, *45*, 2440–2457. (e) Edel, J. B.; Kornyshev, A. A.; Kucernaka, A. R.; Urbakh, M. Fundamentals and Applications of Self-Assembled Plasmonic Nanoparticles at Interfaces. *Chem. Soc. Rev.* **2016**, *45*, 1581–1596. (f) Karimi, M.; Ghasemi, A.; Zangabad, P. S.; Rahighi, R.; Basri, S. M. M.; Mirshekari, H.; Amiri, M.; Pishabad, Z. S.; Aslani, A.; Bozorgomid, M.; Ghosh, D.; Beyzavi, A.; Vaseghi, A.; Aref, A. R.; Haghani, L.; Bahramia, S.; Hamblin, M. R. Smart Micro/Nanoparticles in Stimulus-Responsive Drug/Gene Delivery Systems. *Chem. Soc. Rev.* **2016**, *45*, 1457–1501.

[4] (a) Khosousi, A. Z.; Dhirani, Al-A.; Charge Transport in Nanoparticle Assemblies. *Chem. Rev.* **2008**, *108*, 4072–4124. (b) Burda, C.; Chen, X.; Narayanan, R.; El-Sayed, M. A. Chemistry and Properties of Nanocrystals of Different Shapes. *Chem. Rev.* **2005**, *105*, 1025–1102.

[5] (a) Sekiguchi, S.; Niikura, K.; Matsuo, Y.; Ijiro, K. Hydrophilic Gold Nanoparticles Adaptable for Hydrophobic Solvents. *Langmuir* **2012**, *28*, 5503–5507. (b) Qi, L.; Sehgal, A.; Castaing, J-C.; Chapel, J-P.; Fresnais, J.; Berret, J-F.; Cousin, F. Redispersible Hybrid Nanopowders: Cerium Oxide Nanoparticle Complexes with Phosphonated-PEG Oligomers. *ACS Nano* **2008**, *2*, 879–888. (c) Studart, A. R.; Amstad, E.; Gauckler, L. J. Colloidal Stabilization of Nanoparticles in Concentrated Suspensions *Langmuir* **2007**, *23*, 1081–1090. (d) Traina, C. A.; Schwartz, J. Surface Modification of Y_2O_3 Nanoparticles. *Langmuir* **2007**, *23*, 9158–9161.

[6] (a) Bauer, C. A.; Stellacci, F.; Perry, J. W. Relationship Between Structure and Solubility of

Thiol-Protected Silver Nanoparticles and Assemblies. *Top. Catal.* **2008**, *47*, 32−41. (b) Yin, Y.; Alivisatos. A. P. Colloidal nanocrystal synthesis and the organic–inorganic interface. *Nature* **2005**, *437*, 664−670. (c) Jackson, A. M.; Myerson. J. W.; Stellacci, F. Spontaneous assembly of subnanometre-ordered domains in the ligand shell of monolayer-protected nanoparticles. *Nat. Mater.* **2004**, *3*, 330−336.

[7] (a) Yang, Y.; Qin, H.; Peng, X. Intramolecular Entropy and Size-Dependent Solution Properties of Nanocrystal–Ligands Complexes. *Nano Lett.* **2016**, *16*, 2127–2132. (b) Yang, Y.; Qin, H.; Jiang, M.; Lin, L.; Fu, T.; Dai, X.; Zhang, Z.; Niu, Y.; Cao, H.; Jin, Y.; Zhao, F.; Peng, X. Entropic Ligands for Nanocrystals: From Unexpected Solution Properties to Outstanding Processability. *Nano Lett.* **2016**, *16*, 2133–2138.

[8] Fratoddi, I. Hydrophobic and Hydrophilic Au and Ag nanoparticles. Breakthroughs and Perspectives. *Nanomaterials* **2017**, *8*, 11.

[9] (a) Vo, D. Q.; Shin, E. W.; Kim, J-S.; Kim, S. Low-Temperature Preparation of Highly Conductive Thin Films from Acrylic Acid-Stabilized Silver Nanoparticles Prepared through Ligand Exchange. *Langmuir* **2016**, *26*, 17435-17443. (b) Portilla, L.; Halik, M. Smoothly Tunable Surface Properties of Aluminum Oxide Core–Shell Nanoparticles By A Mixed-Ligand Approach. *ACS Appl. Mater. Interfaces* **2014**, *6*, 5977-5982. (c) Kim, S-G.; Hagura, N.; Iskandar, F.; Okuyama, K. Characterization of Silica-Coated Ag Nanoparticles Synthesized Using A Water-Soluble Nanoparticle Micelle. *Adv. Powder. Technol.* **2009**, *20*, 94-100.

[10] (a) Zhao, N.; Yan, L.; Zhao, X.; Chen, X.; Li, A.; Zheng, D.; Zhou, X.; Dai, X.; Xu, F. J. Versatile Types of Organic/Inorganic Nanohybrids: From Strategic Design to Biomedical Applications. *Chem. Rev.* **2019**, *119*, 1666-1762. (b) Chen, G.; Roy, I.; Yang, C.; Prasad, P. N. Nanochemistry and Nanomedicine for Nanoparticle-based Diagnostics and Therapy. *Chem. Rev.* **2016**, *116*, 2826-2885.

[11] Niikura, K.; Kobayashi, K.; Takeuchi, C.; Fujitani, N.; Takahara, S.; Ninomiya, T.; Hagiwara, K.; Mitomo, H.; Ito, Y.; Osada, Y.; Ijiro, K. Amphiphilic Gold Nanoparticles Displaying Flexible Bifurcated Ligands as a Carrier for siRNA Delivery into the Cell Cytosol. *ACS Appl. Mater. Interfaces* **2014**, *6*, 22146-22154.

[12] Ho, L. W. C.; Yung, W-Y.; Sy, K. H. S.; Li, H. Y.; Choi, C. K. K.: Leung, K. C-F.; Lee, T. W. Y.; Choi, C. H. J. Effect of Alkylation on the Cellular Uptake of Polyethylene Glycol-Coated Gold Nanoparticles. *ACS Nano* **2017**, *11*, 6085-6101.

[13] (a) Ravelli, D.; Protti, S.; Fagnoni, M. Carbon−Carbon Bond Forming Reactions via Photogenerated Intermediates. *Chem. Rev.* **2016**, *116*, 9850–9913. (b) Manley, D. W.; Walton, J. C. Preparative Semiconductor Photoredox Catalysis: An Emerging Theme in Organic Synthesis. *Beilstein J. Org. Chem.* **2015**, *11*, 1570–1582. (c) Kisch, H. Semiconductor Photocatalysis—Mechanistic and Synthetic Aspects. *Angew. Chem., Int. Ed.* **2013**, *52*, 812–847. (d) Scaiano, J. C.; Stamplecoskie, K. Can Surface Plasmon Fields Provide a New Way to Photosensitize Organic Photoreactions? From Designer Nanoparticles to Custom Applications. *J. Phys. Chem. Lett.* **2013**, *4*, 1177–1187. (e) Scaiano, J. C.; Stamplecoskie, K. Can Surface Plasmon Fields Provide a New Way to Photosensitize Organic Photoreactions? From Designer Nanoparticles to Custom Applications. *J. Phys. Chem. Lett.* **2013**, *4*, 1177–1187. (f) Fagnoni, M.; Dondi,

D.; Ravelli, D.; Albini, A. Photocatalysis for the Formation of the C−C Bond. *Chem. Rev.* **2007**, *107*, 2725–2756.

[14] Kisch, H. Semiconductor Photocatalysis for Chemoselective Radical Coupling Reactions. Acc. *Chem. Res.* **2017**, *50*, 1002–1010.

[15] (a) Anwer, H.; Mahmood, A.; Kim, J. L. K-H.; Park, J-W.; Yip, A. C. K. Photocatalysts for Degradation of Dyes in Industrial Effluents: Opportunities and Challenges. *Nano Res.* **2019**, *5*, 955-972. (b) Nosaka Y.; Nosaka, A. Y. Generation and Detection of Reactive Oxygen Species in Photocatalysis. *Chem. Rev.* **2017**, *117*, 11302–11336. (c) Ajmal, A.; Majeed, I.; Malik, R. N.; Idrissc, H.; Nadeem, M. A. Principle and Mechanisms of Photocatalytic Dye Degradation on TiO_2 Based Photocatalysts: A Comparative Overview. *RSC Adv.* **2014**, *4*, 37003-37026.

[16] Manley, D. W.; McBurney, R. T.; Miller, P.; Howe, R. F.; Rhydderch, S.; Walton, J. C. Unconventional Titania Photocatalysis: Direct Deployment of Carboxylic Acids in Alkylations and Annulations. *J. Am. Chem. Soc.* **2012**, *134*, 13580−13583.

[17] Noble, A.; Macmillan, D. W. C. Photoredox α-Vinylation of α-Amino Acids and N-Aryl Amines. *J. Am. Chem. Soc.* **2014**, *136*, 5257−5260.

[18] Caputo, J. A.; Frenette, L.C.; Zhao, N.; Sowers, K. L.; Krauss, T. D.; Weix, D. J. General and Efficient C–C Bond Forming Photoredox Catalysis with Semiconductor Quantum Dots. *J. Am. Chem. Soc.***2017**, *139*, 4250-4253.

[19] (a) Weiss, E. A. Designing the Surfaces of Semiconductor Quantum Dots for Colloidal Photocatalysis. *ACS Energy Lett.* **2017**, *2*, 1005–1013. (b) Harris, R. D.; Homan, S. B.; Kodaimati, M.; He, C.; Nepomnyashchii, A. B.; Swenson, N. K.; Lian, S.; Calzada, R.; Weiss, E. A. Electronic Processes within Quantum Dot-Molecule Complexes. *Chem. Rev.* **2016**, *116*, 12865–12919.

[20] (a) Srinivasarao, M.; Low, P. S. Ligand-Targeted Drug Delivery. *Chem. Rev.* **2017**, *117*, 12133-12164. (b) Wong, P. T.; Choi, S. K. Mechanisms of Drug Release in Nanotherapeutic Delivery Systems. *Chem. Rev.* **2015**, *115*, 3388-3432. (c) Wang, R. E.; Liu, T.; Wang, Y.; Cao, Y.; Du, J.; Luo, X.; Deshmukh, V.; Kim, C. H.; Lawson, B. R.; Tremblay, M. S.; Young, T. S.; Kazane, S. A.; Wang, F.; Schultz, P. G. An Immunosuppressive Antibody–Drug Conjugate. *J. Am. Chem. Soc.* **2015**, *137*, 3229-3232.

[21] (a) Sheldon, R. A.; Woodley, O. J. M. Role of Biocatalysis in Sustainable Chemistry. *Chem. Rev.* **2018**, *118*, 801-838. (b) Clarke, C. J.; Tu, W. C.; Levers, O.; Bröhl, A.; Hallett, J. P. Green and Sustainable Solvents in Chemical Processes. *Chem. Rev.* **2018**, *118*, 747-800.

[22] (a) Burns, N. Z.; Baran, P. S.; Hoffmann, R. W. Redox Economy in Organic Synthesis. *Angew. Chem., Int. Ed.* **2009**, *48*, 2854-2867. (b) Trost B.M. The atom economy- a search for synthetic efficiency. *Science* **1991,** *254***,** 1471-1477.

[23] Yan, M.; Kawamata, Y.; Baran, P. S. Synthetic Organic Electrochemical Methods Since 2000: On the Verge of a Renaissance. *Chem. Rev.* **2017**, *117*, 13230-13319.

[24] (a) Kärkäs, M. D.; Porco Jr., J. A.; Stephenson, C. R. J. Photochemical Approaches to Complex Chemotypes: Applications in Natural Product Synthesis *Chem. Rev.* **2016**, *116*, 9683–9747. (b) Skubi, K. L.; Blumand, T. R.; Yoon, T. P. Dual Catalysis Strategies in Photochemical Synthesis. *Chem. Rev.* **2016**, *116*,

10035–10074. (c) Hopkinson, M. N.; Tlahuext-Aca, A.; Glorius, F. Merging Visible Light Photoredox and Gold Catalysis. *Acc. Chem. Res.* **2016**, *49*, 2261–2272. (d) Fabry, D. C.; Magnus Rueping, M. Merging Visible Light Photoredox Catalysis with Metal Catalyzed C–H Activations: On the Role of Oxygen and Superoxide Ions as Oxidants. *Acc. Chem. Res.* **2016**, *49*, 1969–1979. (e) Ghosh, I.; Marzo, L.; Das, A.; Shaikh, R.; König, B. Visible Light Mediated Photoredox Catalytic Arylation Reactions. *Acc. Chem. Res.* **2016**, *49*, 1566–1577. (f) Tellis, J. C.; Kelly, C. B.; Primer, D. N.; Jouffroy, M.; Patel, N. R.; Molander, G. A. Single-Electron Transmetalation via Photoredox/Nickel Dual Catalysis: Unlocking a New Paradigm for sp3–sp2 Cross-Coupling. *Acc. Chem. Res.* **2016**, *49*, 1429–1439. (g) Prier, C. K.; Rankic, D. A.; MacMillan, D. W. C. Visible Light Photoredox Catalysis with Transition Metal Complexes: Applications in Organic Synthesis. *Chem. Rev.***2013**, *113*, 5322-5363.

[25] (a) Shin, J. H.; Seong, E. Y.; Mun, H. J.; Jang, Y. J.; Kang, E. J. Electronically Mismatched Cycloaddition Reactions via First-Row Transition Metal, Iron(III)−Polypyridyl Complex. *Org. Lett.* **2018**, *20*, 5872−5876. (b) Zhao, Y.; Antonietti, M. Visible-Light-Irradiated Graphitic Carbon Nitride Photocatalyzed Diels-Alder Reactions with Dioxygen as Sustainable Mediator for Photoinduced Electrons. *Angew. Chem., Int. Ed.* **2017**, *56*, 9336−9340. (c) Lin, S.; Ischay, M. A.; Fry, C. G.; Yoon, T. P. Radical Cation Diels−Alder Cycloadditions by Visible Light Photocatalysis. *J. Am. Chem. Soc.* **2011**, *133*, 19350−19353.

[26] Studer, A.; Curran, D. P. The electron is a catalyst. *Nat. Chem.* **2014**, *6*, 765−773.

Chapter 2
Preparation of TiO_2 Nanoparticles with Flexible Dispersibility in Various Solvents

2.1. Introduction

"Surface modification of the nanoparticle with ligand" is one of the methods for homogeneous dispersion of nanoparticles in organic solvents. In the industry, cheaply available natural products and surfactants are often used as ligands. However, since natural products and surfactants are often mixtures, the dispersion/aggregation behavior is difficult to discuss strictly from chemical perspective. In addition, although polymeric and/or oligomeric ligands have been generally used for surface modification of nanoparticles, their motions were very complicated and difficult to evaluated. Since solvent systems used in material processing and catalytic reaction are complex, it is desired to design the flexible ligands and produce nanoparticles with flexible dispersibility.

In our previous works, the surface modification of TiO_2 and Ag nanoparticles by the amphiphilic ligand for stable colloidal dispersion in various solvents has been developed (Fig. 2-1).[28][29] However, it is difficult to investigate the relationship between the ligand structure and the nanoparticle functionality in case of using the ligand of unclear molecular structure. To better understand the relationship between ligand structure and nanoparticle functionality, it is necessary to discuss using high purity and low molecular weight ligand.

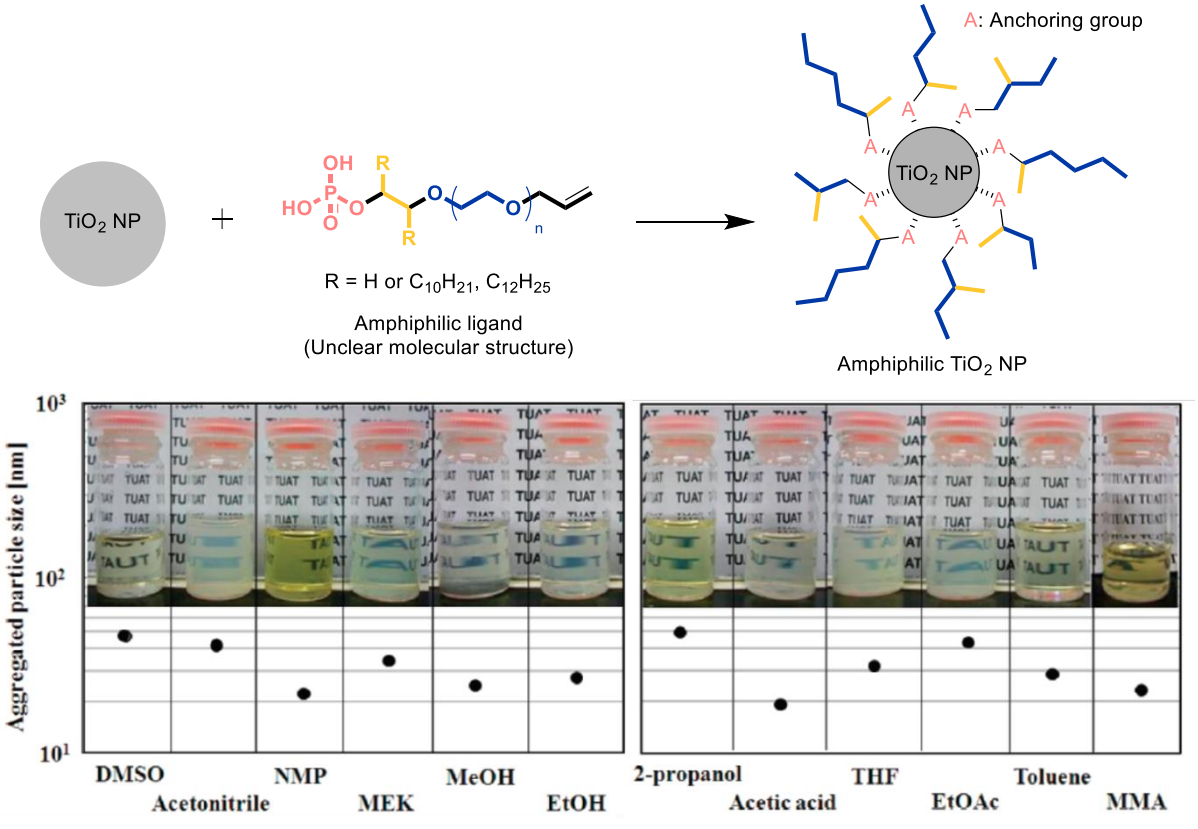

Fig. 2-1 Surface Modification by Amphiphilic Ligand with Unclear Molecular Structure.

The purpose of this work is to investigate the relationship between ligand structure and nanoparticle dispersibility toward the preparation of nanoparticles with flexible dispersibility in various solvents. As a ligand structure, linear organic ligand having both hydrophobic alkyl chain and hydrophilic ethylene glycol chain was designed and synthesized. Phosphonic acid was used as the binding group for TiO_2 nanoparticle (Fig. 2-2). Investigation of the relationship between the structure of the amphiphilic ligand and the nanoparticle dispersibility was not reported so far, suggesting that it would provide much insight into the design of low-molecular amphiphilic ligands.

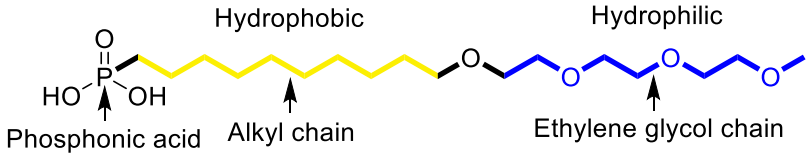

Fig. 2-2 Example of Structure of Amphiphilic Ligand.

2.2. Experimental Procedure

General Remarks

All reagents and solvents were purchased from commercial sources and used without further purification. Reactions were monitored by thin-layer chromatography (TLC) carried out on silica gel plates, with detection by UV absorption (254 nm) and by heating the plates after dipping them in a solution of 12 M molybdo(VI) phosphoric acid n-hydrate in 95% ethanol. Silica gel (particle size 40−50 μm) was used for column chromatography. ^{1}H NMR spectra were collected on a 500 MHz NMR spectrometer using the deuterated solvent as an internal deuterium reference. Chemical shift data are given in δ units calibrated with residual protic solvent. The multiplicity of a signal is indicated as follows: s, singlet; d, doublet; t, triplet; q, quartet; quint, quintet; m, multiplet. ^{13}C NMR spectra were collected at 125 MHz with proton decoupling using the deuterated solvent as an internal carbon reference. Chemical shift data are given in δ units calibrated with residual solvent. High-resolution mass spectra (HRMS) were collected on electrospray ionization (ESI)- or direct analysis in real time (DART)-time-of-flight (TOF) spectrometers.

Williamson Reactions

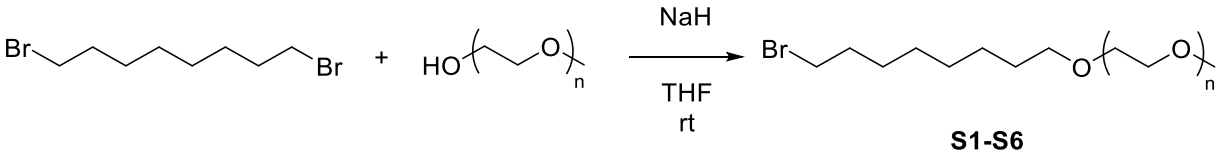

To a solution of the respective oligoethylene glycol monomethyl ether (15.0 mmol) in THF (40 mL) stirring at r.t., NaH (60% dispersion in paraffin liquid, 900 mg, 22.5 mmol) was added. The resulting reaction mixture was stirred at r.t. for 10 min and the respective dibromoalkane (22.5 mmol) was added. The resulting reaction mixture was stirred at r.t. for additional overnight, diluted with MeOH (40 mL), and concentrated *in vacuo*. Silica gel column chromatography (hexane/EtOAc = 4/1-1/1) gave the corresponding product **S1**–**S6** in 22–54% yield as a pale yellow oil.

Michaelis-Arbuzov Reactions

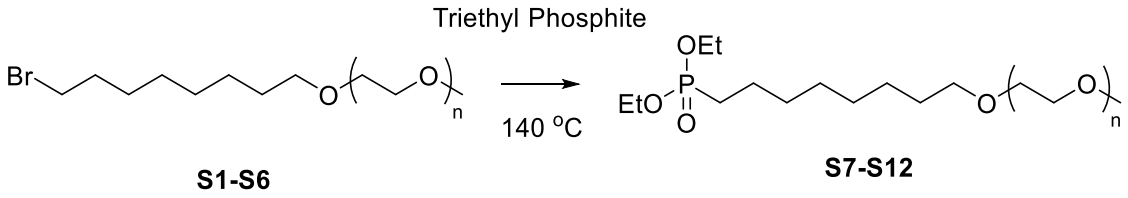

The respective substrate **S1**–**S6** (5.0 mmol) was added into triethyl phosphite (1.73 mL, 10.0 mmol). The resulting reaction mixture was stirred at 140 °C for 24 h and concentrated *in vacuo*. Silica gel column chromatography (EtOAc/MeOH = 20/1) gave the corresponding product **S7**–**S12** in 74–97% yield as a colorless oil.

Hydrolysis Reactions

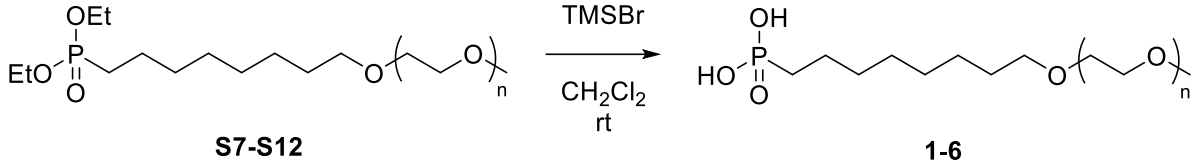

S7-S12 **1-6**

To a solution of the respective substrate **S7**– **S12** (3.0 mmol) in CH_2Cl_2 (30 mL) stirring at r.t., TMSBr (30.0 mmol) was added. The resulting reaction mixture was stirred at r.t. for 24 h, diluted with water (60 mL), and organic layer was separated. Aqueous layer was saturated with NaCl and extracted with CH_2Cl_2 (30 mL x 3). The combined organic layer was dried over Na_2SO_4, filtered, and concentrated *in vacuo*. Silica gel column chromatography (EtOAc/MeOH = 1/1) gave the corresponding amphiphilic small molecule ligands **1-6** in 42–65% yield as a white solid.

Preparation and Analysis of the TiO_2 Nanoparticle-Ligands Complexes

To a solution of the respective ligand **1-6** (85.9–132 mg, 0.32 mmol, 5.4 μmol/m^2) in water (9.0 g) stirring at r.t., aqueous 4.0 nm TiO_2 nanoparticles (20wt%, 1.0 g, 295 m^2/g) was added. The resulting reaction mixture was stirred at r.t. for 3 h and centrifuged at 30000 G for 5 min. The recovered precipitate was washed with water and concentrated *in vacuo* to give the corresponding nanoparticle-ligands complexes as a white powder. The saturated adsorption amount was measured by CHN organic elemental analyzer (JM-10 Micro coder, J Science Lab. Co. Ltd.). Particle size of TiO_2 nanoparticle-ligands complex was measured by transmission electron microscope (TEM).

Investigation on the Solubility and Dispersibility of the TiO_2 Nanoparticle-Ligands Complexes

To various organic solvents (1.94 g), the respective TiO_2 nanoparticle-ligands complex (3wt%, 60 mg) was added and sonicated for 30 min. Dispersibility of the ligand-modified TiO_2 nanoparticle was measured by dynamic light scattering (DLS, Malvern HPP5001) and small angle X-ray scattering (SAX).

2.3. Results and Discussion

2.3.1. Designed and Synthesized Amphiphilic Ligand Structure

In this work, the amphiphilic ligand shown in Fig. 2-3 was designed and synthesized, and the relationship between the ligand structure and nanoparticle dispersibility was investigated.

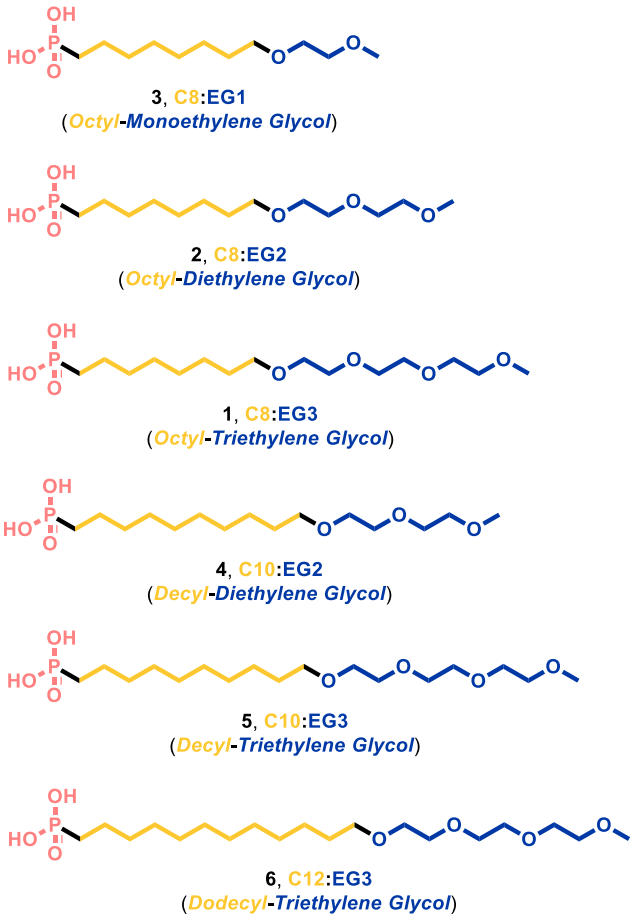

Fig. 2-3 Designed and Synthesized Amphiphilic Ligand for TiO_2 Nanoparticle in This Work

2.3.2. General Surface Modification Procedure

First, ligand modification was carried out using ligand 1 (C8EG3) in aqueous dispersion of TiO_2 nanoparticles (Figs. 2-4 and 2-5).

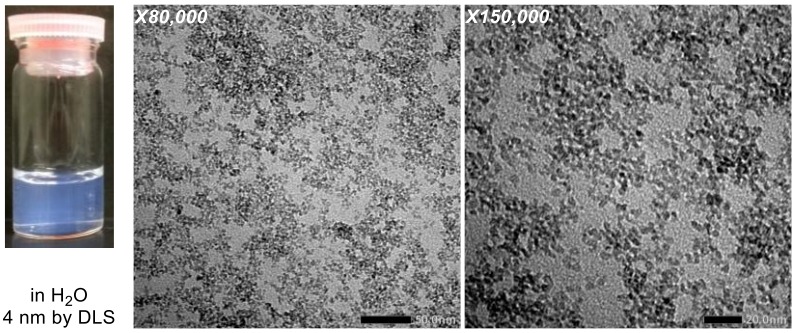

Fig. 2-4 Photograph and TEM Images of the Aqueous Dispersion TiO_2 Nanoparticles.

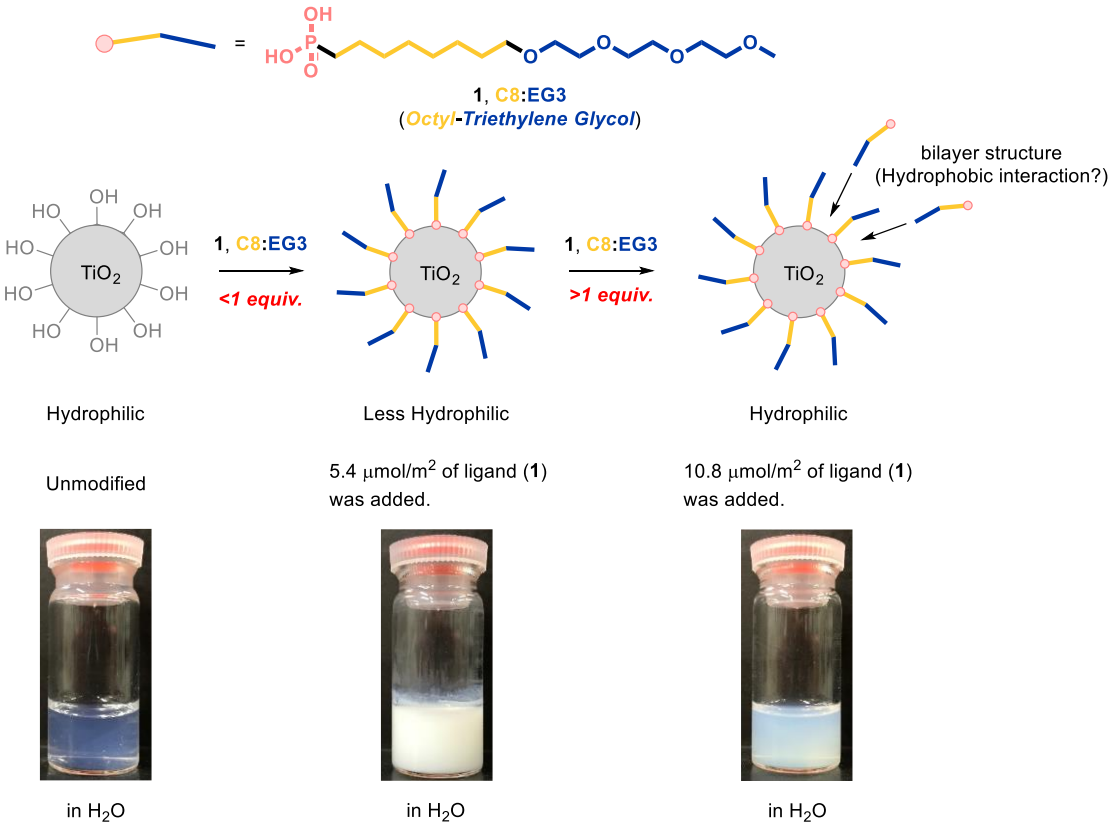

Fig. 2-5 Schematic Illustration and Photographs of Anchoring Behavior.

When ligand 1 was added little by little into the aqueous TiO_2 dispersion (primary particle size 4.0 nm) shown in Fig. 2-4, the transparent solution gradually became cloudy as shown in Fig. 2-5. Furthermore, when additional ligands were added, the state of solution changed to a translucent solution again. From these results, the OH groups on the particle surface are filled by adding a ligand and binding the ligand to the particle surface, and then the solution becomes cloudy by reducing the affinity to water. (single layer).

In addition, it was considered that the affinity to water was regained again, because the ligands were formed in bilayer as additional ligand was added. Ligand-coated TiO_2 nanoparticles were collected by centrifuging and washing. The saturated adsorption amounts were 4.3 μmol / m^2.

2.3.3. Evaluation of the Dispersibility of Ligand-modified TiO_2 Nanoparticles

The collected particles were dispersed in methanol (high-polarity solvent) and toluene (low-polarity solvent). In methanol, the DLS diameter (10 nm) was the almost same as the primary particle diameter (4.0 nm), indicating good dispersibility. However, the particle aggregated in toluene (Fig. 2-6).

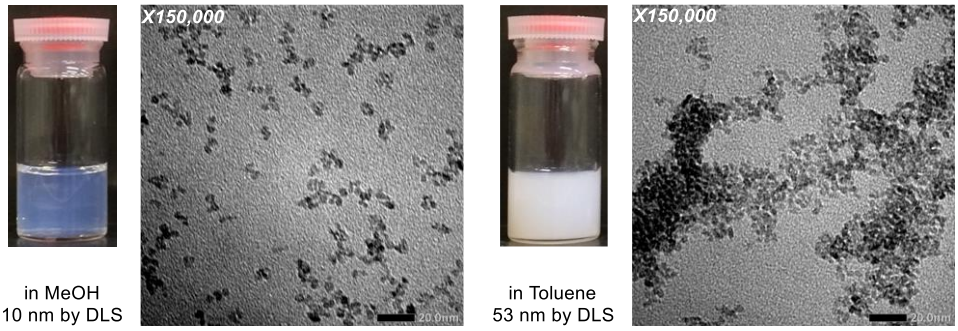

Fig. 2-6 Photographs and TEM Images of Solutions of the Nanoparticle-Ligand 1 Complexes at 3.0wt% in Methanol (Left) and Toluene (Right).

From this result, it was considered that the hydrophobicity of the ligand is simply insufficient, thus flexible dispersibility can be obtained by modifying the more hydrophobic ligand. Therefore, ligands 2 (C8EG2) and ligand 3 (C8EG1) with short hydrophilic ethylene glycol chains were modified on the surface by the same method to increase the hydrophobicity (Fig. 2-7). Both saturated adsorption amounts were 4.6 μmol / m^2.

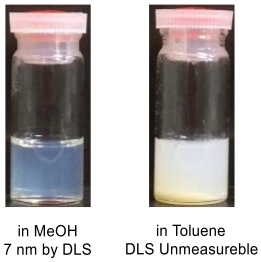

Fig. 2-7 Photographs of Solutions of the Nanoparticle-Ligand 3 Complexes at 3.0wt% in Methanol (Left) and Toluene (Right).

As shown in Fig. 2-7, TiO_2 nanoparticles modified with ligand 3 aggregated in toluene despite increasing hydrophobicity. However, good dispersibility was exhibited in methanol. Similar results were obtained with ligand 2. From these results, it was suggested that the C8 amphiphilic ligands of this system

could not obtain enough hydrophobicity for dispersion in hydrophobic solvents.

Next, ligand 4 (C10EG2) having higher hydrophobicity than ligand 2 (C8EG2) was modified to TiO_2 nanoparticles. As a result, although the hydrophobicity of the ligand was increased, the same result was obtained as when the ligand 2 (C8EG2) was used (Fig. 2-8).

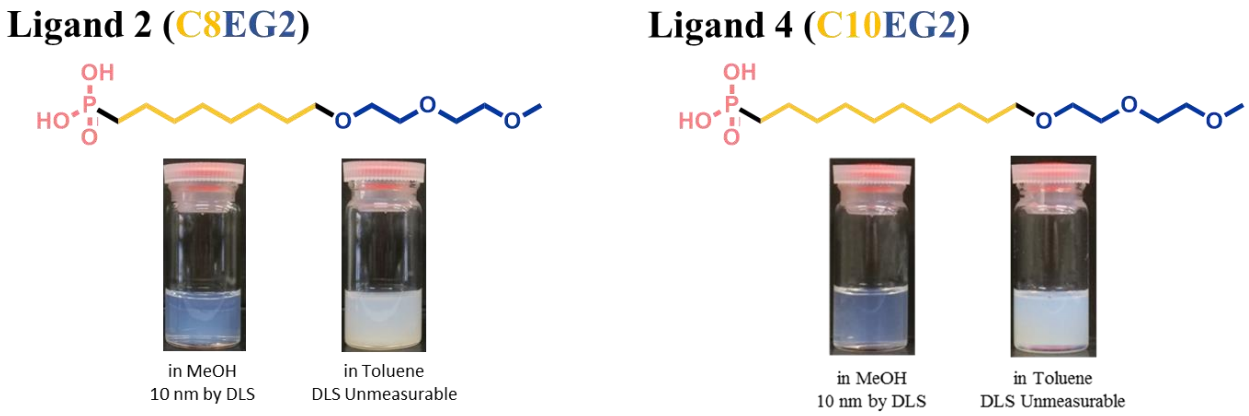

Fig. 2-8 Dispersibility in Solvent of Ligand 2- and Ligand 4-modified TiO_2 Nanoparticles.

On the other hand, ligand 5 (C10EG3) having higher hydrophilicity than ligand 4 (C10EG2) was modified to TiO_2 nanoparticles. The saturated adsorption amounts were 4.6 μmol / m^2 (ligand 5). As a result, although the hydrophilicity of the ligand was increased, ligand 5-modified TiO_2 nanoparticle was dispersed not only in methanol but also in toluene (Fig. 2-9).

Fig. 2-9 Dispersibility in Solvent of Ligand 5-modified TiO_2 Nanoparticles.

Despite extending the hydrophilic chain, dispersibility of TiO_2 nanoparticles in toluene was improved. Further experiments were investigated to explain this paradox.

TiO_2 nanoparticles modified with hydrophobic or hydrophilic ligands were synthesized and their dispersibility was evaluated (Fig. 2-10).

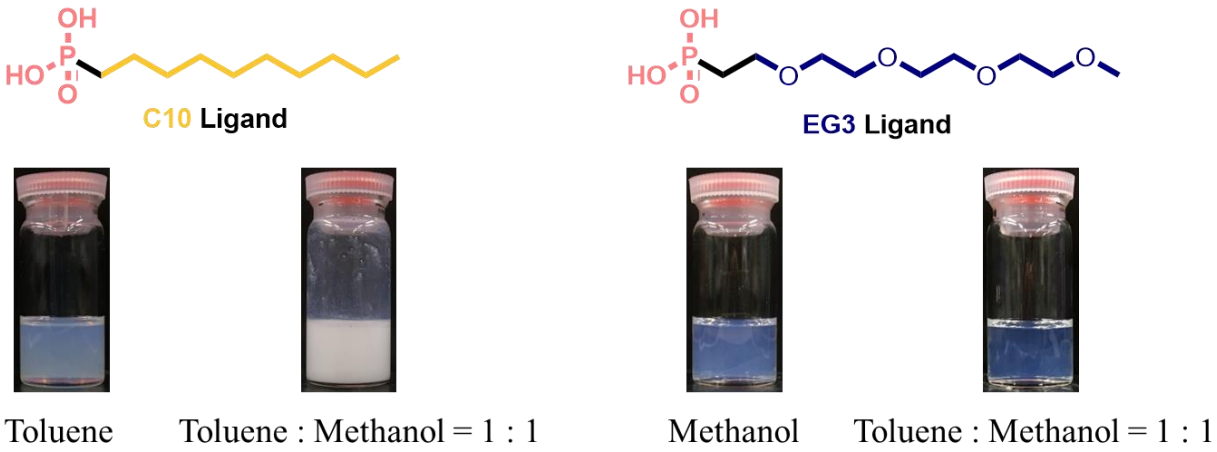

Fig. 2-10 C10- and EG3-modified TiO_2 Nanoparticles in Toluene+Methanol Solution.

The TiO_2 nanoparticles modified with the C10 ligand showed good dispersibility in toluene, but aggregated in the toluene-methanol mixed solution (Toluene : Methanol = 1 : 1). On the other hand, the TiO_2 nanoparticles modified with EG3 ligand showed good dispersibility not only in methanol but also in the toluene-methanol mixed solution (Toluene : Methanol = 1 : 1). These results suggested that, although the ethylene glycol chain is a hydrophilic group, it is a dispersing group that gives a certain degree of flexible dispersibility.

Next, the ligand 6 with long hydrophobic chain were modified by the same method, and the dispersibility was evaluated (Fig. 2-11). The saturated adsorption amounts were 5.0 μmol / m^2 (ligand 6).

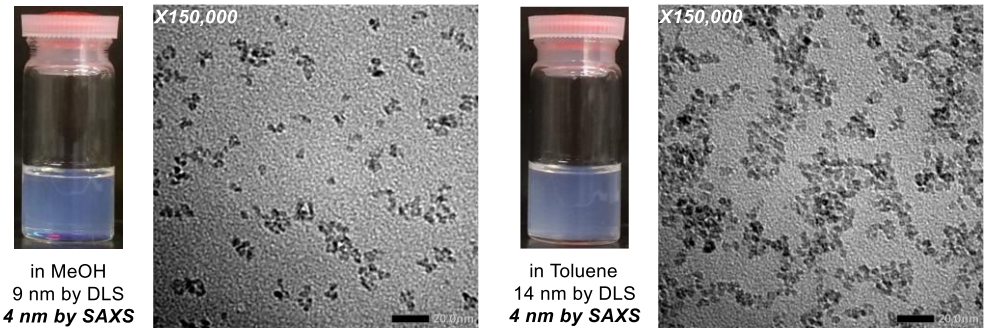

Fig. 2-11 Photographs and TEM Images of Solutions of the Nanoparticle-Ligand 6 Complexes at 3.0wt% in Methanol (Left) and Toluene (Right).

TiO_2 nanoparticles modified with ligand 6 show good dispersibility in both methanol and toluene (Fig. 2-11). Similar results were obtained with ligand 5.

These results indicated that slight differences in hydrophobicity and hydrophilicity significantly affect the dispersibility of nanoparticles. On the other hand, it was suggested that the dispersibility of the nanoparticles was not simply determined by the hydrophilicity or hydrophobicity of the ligand. Furthermore, since a larger change was observed in the dispersibility when the ethylene glycol chain was extended than when the alkyl chain was extended, it was suggested that the arrangement of the alkyl chain and the ethylene chain is also greatly effected on the dispersibility. In other words, the combination of ligand length, chain arrangement, and hydrophilic / hydrophobic balance would determine the dispersibility of nanoparticles. To confirm these hypotheses, evaluation using ligands such as C12EG2 and C8EG4 would be effective. In addition, although it is complicated and huge computational cost, molecular dynamics calculation might be one of the effective methods.

Finally, ligand 6-coated TiO_2 nanoparticles were dispersed in various solvents, and those dispersibility was evaluated (Fig. 2-12).

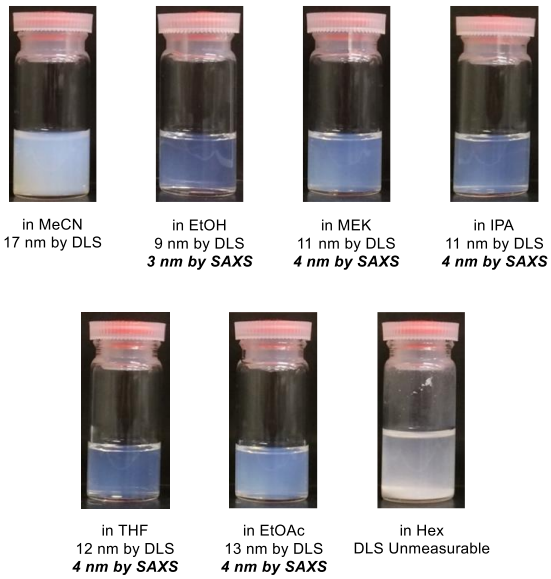

Fig. 2-12　Photographs of Solutions of Nanoparticle-Ligand 6 Complexes at 3.0wt% in Various Organic Solvents.

Ligand 6 coated TiO_2 nanoparticles show good dispersibility in various organic solvents (Fig. 2-12). On the other hand, the reason for aggregation in acetonitrile (MeCN) and hexane (Hex) was thought to be simply because the hydrophilicity and hydrophobicity of the solvent were too high.

2.4. Summary

In this chapter, the ligand structure for the preparation of TiO_2 nanoparticles with flexible dispersibility in various solvents was investigated.

The dispersibility of TiO_2 nanoparticles modified with ligands having different lengths of ethylene glycol chain and alkyl chain based on ligand 3 (C8EG3) was investigated. TiO_2 nanoparticles modified with ligand 3 were dispersed in methanol, but aggregated in toluene. Despite modification of the ligand to increase hydrophobicity, ligand 2 (C8EG2) and ligand 1 (C8EG1) with short ethylene glycol chain modified TiO_2 nanoparticles aggregated in toluene, but dispersed in methanol. On the other hand, from the comparison results of ligands, it was suggested that the dispersibility of the nanoparticles is not simply determined by the hydrophilicity and hydrophobicity of the ligand, but by the ligand length, chain arrangement, and the balance between hydrophilicity and hydrophobicity. In addition, it was confirmed that ligand 6-modified TiO_2 nanoparticles dispersed in various organic solvents.

TiO_2 nanoparticles with flexible dispersibility in various solvents were prepared by optimizing the ligand structure. Using ligands with slightly different structures, the relationship between the dispersibility of nanoparticles and the ligand structure was investigated, and important knowledge on the design of small molecule ligands for nanoparticles was obtained.

2.5. References

[27] Iijima, M.; Kobayakawa, M.; Yamazaki, M.; Ohta, Y.; Kamiya, H. Anionic Surfactant with Hidrophobic and Hydrophilic Chains for Nanoparticle Dispersion and Shape Memory Polymer Nanocomposites. *J. Am. Chem. Soc.* **2009**, *131*, 16342-16343.

[28] Iijima, M.; Kamiya, H. Layer-by-Layer Surface Modification of Functional Nanoparticles for Dispersion in Organic Solvents. *Langmuir* **2010**, *26*, 17943-17948.

Chapter 3
Preparation of Ag Nanoparticles with Flexible Dispersibility in Various Solvents

3.1. Introduction

In surface modification of nanoparticles, the combination of particle type and binding group of ligands is very important, because it determines the binding strength between particle surface and ligand. Therefore, combinations of particle types and binding groups are still significant research subject (Fig. 3-1).[29]

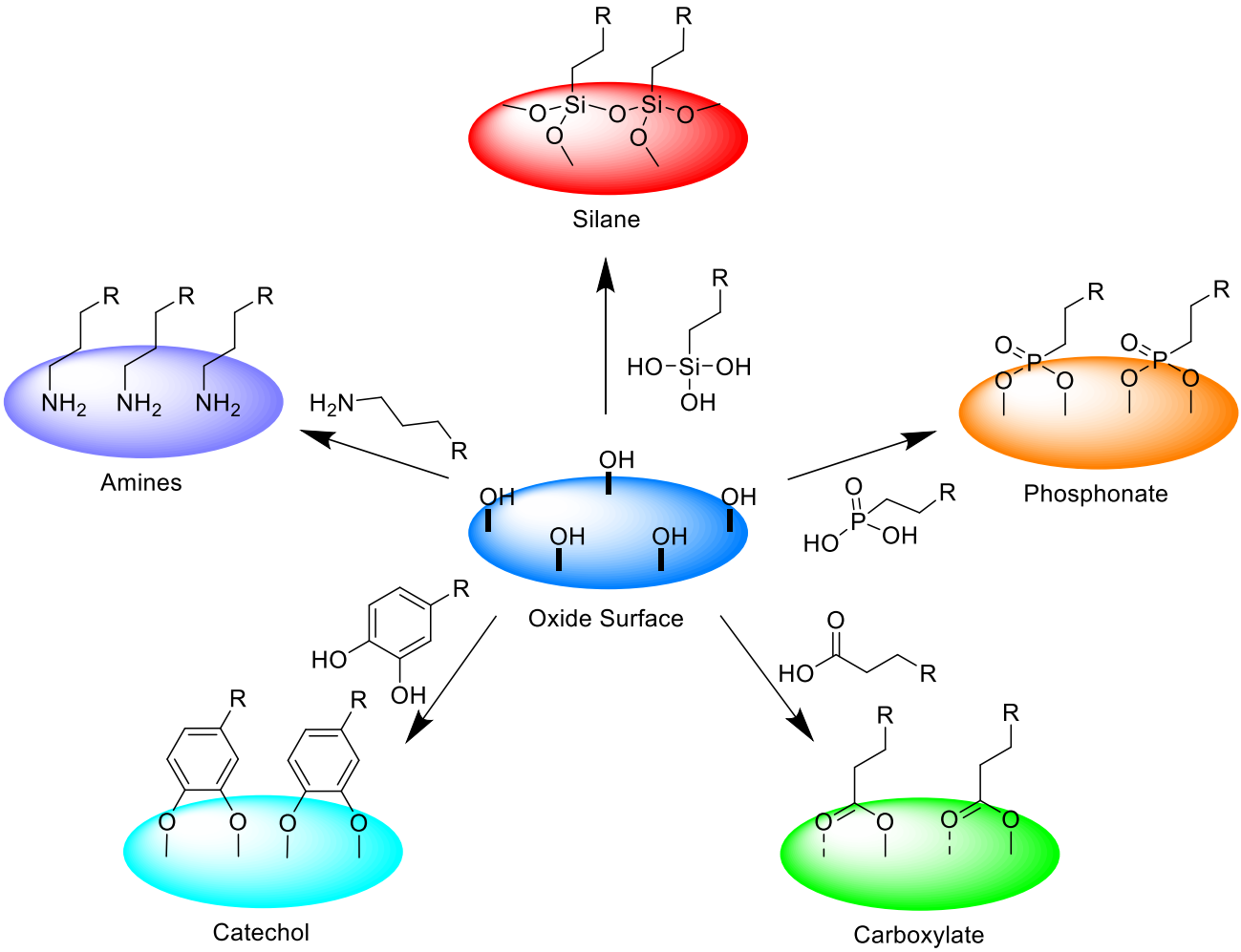

Fig. 3-1 Bonding of Various Binding Groups to Inorganic Oxide Surface

In recent years, NMR measurement for understanding the behavior of organic molecules at particle interfaces has been developed widely and intensively.[30] This method is a powerful tool for knowing the strength of the binding group bonded to the particle surface. As shown in Fig. 3-1, there are various combinations of inorganic oxides and binding groups. Depending on the bonding group of the ligand, the bonding mode and the bonding strength are also different. Similarly, there are various combinations of metal nanoparticles and binding groups, which are also still important research subjects. However, the influence of the combination of particle surface structure and binding group on the nanoparticle dispersibility has not been enough understood.

The purpose of this work is to evaluate the influence of the difference between particle type and amphiphilic ligand structure on the dispersibility of Ag nanoparticles by modifying amine ligands with the same structure as used in Chapter 2. As a ligand structure, linear organic ligand having both hydrophobic alkyl chain and hydrophilic ethylene glycol chain was designed and synthesized. Amine was used as the bonding group for Ag nanoparticle (Fig. 3-2). There are no papers discussing the effect of the relationship between the particle type and the amphiphilic ligand structure on the dispersibility of nanoparticles, thus this work provides important knowledge in ligand design according to particle type.

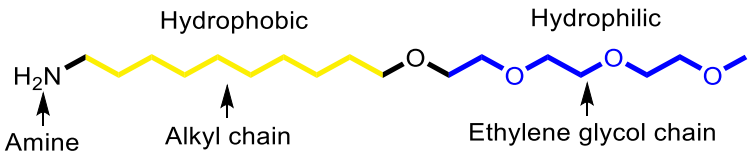

Fig. 3-2 Example of Structure of Amphiphilic Ligand.

3.2. Experimental Procedure

General Remarks

All reagents and solvents were purchased from commercial sources and used without further purification. Reactions were monitored by thin-layer chromatography (TLC) carried out on silica gel plates, with detection by UV absorption (254 nm) and by heating the plates after dipping them in a solution of 12 M molybdo(VI) phosphoric acid n-hydrate in 95% ethanol. Silica gel (particle size 40−50 μm) was used for column chromatography. ^{1}H NMR spectra were collected on a 500 MHz NMR spectrometer using the deuterated solvent as an internal deuterium reference. Chemical shift data are given in δ units calibrated with residual protic solvent. The multiplicity of a signal is indicated as follows: s, singlet; d, doublet; t, triplet; q, quartet; quint, quintet; m, multiplet. ^{13}C NMR spectra were collected at 125 MHz with proton decoupling using the deuterated solvent as an internal carbon reference. Chemical shift data are given in δ units calibrated with residual solvent. High-resolution mass spectra (HRMS) were collected on electrospray ionization (ESI)- or direct analysis in real time (DART)-time-of-flight (TOF) spectrometers.

General Procedure for Williamson Reactions.

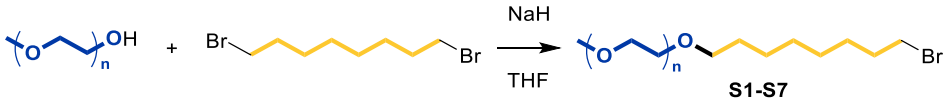

To a solution of the respective oligoethylene glycol monomethyl ether (15.0 mmol) in THF (40 mL) stirring at rt, NaH (60% dispersion in paraffin liquid, 900 mg, 22.5 mmol) was added. The resulting reaction mixture was stirred at rt for 10 min and the respective dibromoalkane (22.5 mmol) was added. The resulting reaction mixture was stirred at rt overnight, diluted with MeOH (40 mL), and concentrated *in vacuo*. Silica gel column chromatography (Hex/EtOAc = 4/1–1/1) gave the corresponding products **S1**–**S7** in 22–54% yields as pale yellow oils.

General Procedure for Gabriel Reactions.

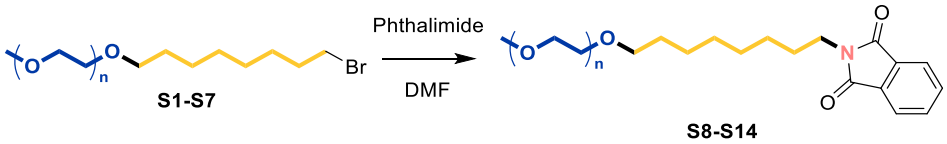

To a solution of the respective substrate **S1**–**S7** (10.0 mmol) in DMF (50 mL) stirring at 80 ºC, phthalimide potassium salt (3.70 g, 20.0 mmol) was added. The resulting reaction mixture was stirred at 80 ºC for 3 h, diluted with water (250 mL), and extracted with EtOAc (50 mL x 3). The combined organic layer was dried over Na_2SO_4, filtered, and concentrated *in vacuo*. Silica gel column chromatography (Hex/EtOAc = 3/1–1/1) gave the corresponding products **S8**–**S14** in 74–97% yields as colorless oils or white amorphous solids.

General Procedure for Deprotection Reactions.

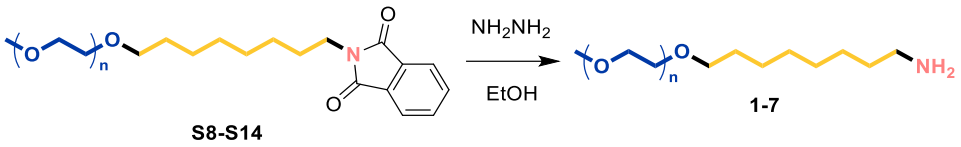

To a solution of the respective substrate **S8**– **S14** (5.0 mmol) in EtOH (50 mL) stirring at 60 ºC, TMSBr (50.0 mmol) was added. The resulting reaction mixture was stirred at 60 ºC for 4 h, filtered, and concentrated *in vacuo*. Silica gel column chromatography (MeOH including 1% TEA) gave the corresponding amphiphilic amines **1-7** in 81–92% yields as pale yellow oils or white amorphous solids.

Preparation and Analysis of the Ag Nanoparticle

To a solution of the respective amine (0.60 mmol) in THF (5 mL) stirring at rt, silver nitrate (34.0 mg, 0.20 mmol) was added (*Note: silver nitrate is not fully soluble in THF*). The resulting reaction mixture was sonicated for 5 min and ascorbic acid (52.8 mg, 0.30 mmol) was added. The resulting reaction mixture was stirred at r.t. for 2 h, then filtered, and concentrated *in vacuo* to give the corresponding amine-capped Ag nanoparticles (about 10 nm). Particle size of Ag nanoparticle-ligands complex was measured by TEM analysis.

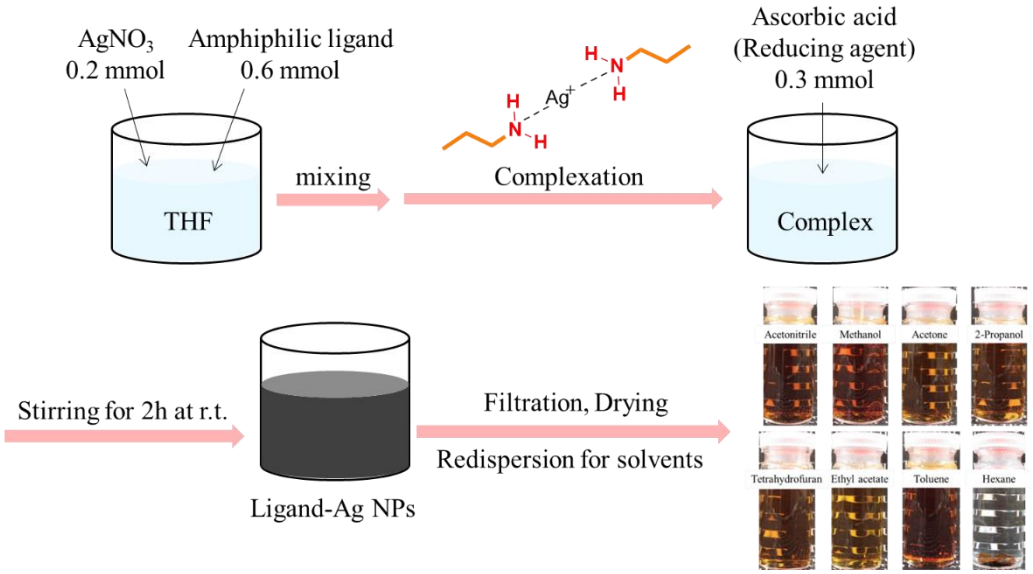

Investigation on the Solubility and Dispersibility of the Ag Nanoparticle-Ligands Complexes

To various organic solvents (5 mL), the respective Ag nanoparticle-ligands complex (2 mg) was added and sonicated for 30 min. Dispersibility of the ligand-modified Ag nanoparticle was measured by DLS.

3.3. Results and Discussion

3.3.1. Designed and Synthesized Amphiphilic Ligand Structure

In the case of Ag nanoparticles, the ligands shown in Fig. 3-3 were designed and synthesized as well as Chapter 2. Ligand-coated Ag nanoparticles were prepared and dispersibility was evaluated.

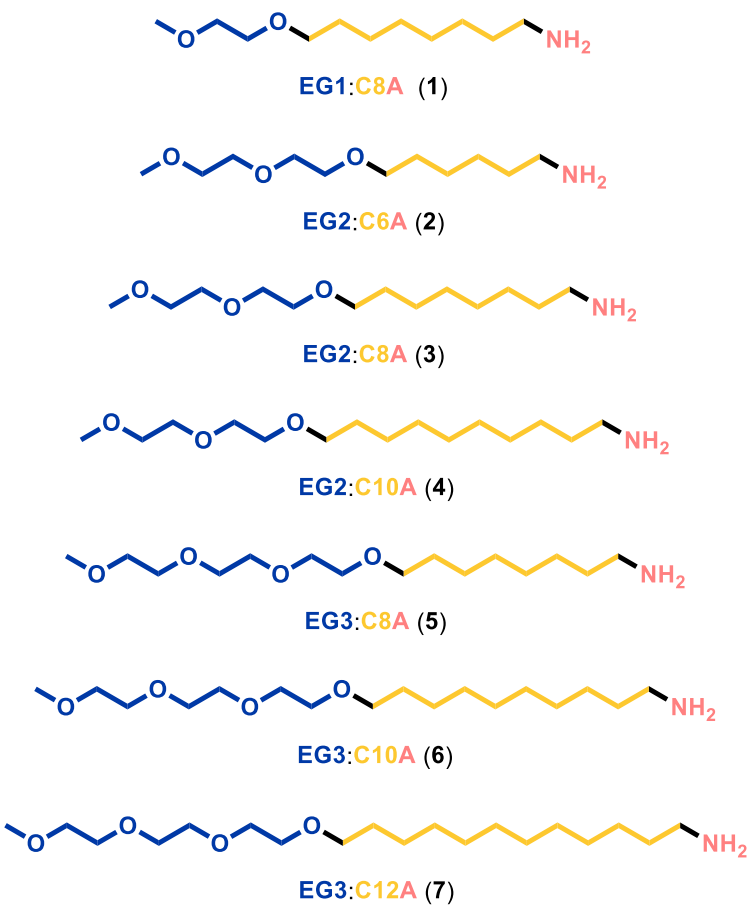

Fig. 3-3 Designed and Synthesized Amphiphilic Ligand for Ag Nanoparticle in This Work

3.3.2. Evaluation of the Dispersibility of Ligand-modified Ag Nanoparticles

First, Ag nanoparticles coated by ligands 1, 2 and 3 were prepared and evaluated the dispersibility in methanol and toluene (Figs. 3-4 and 3-5). The preparation method of ligand-coated Ag nanoparticles is shown in Supporting Information.

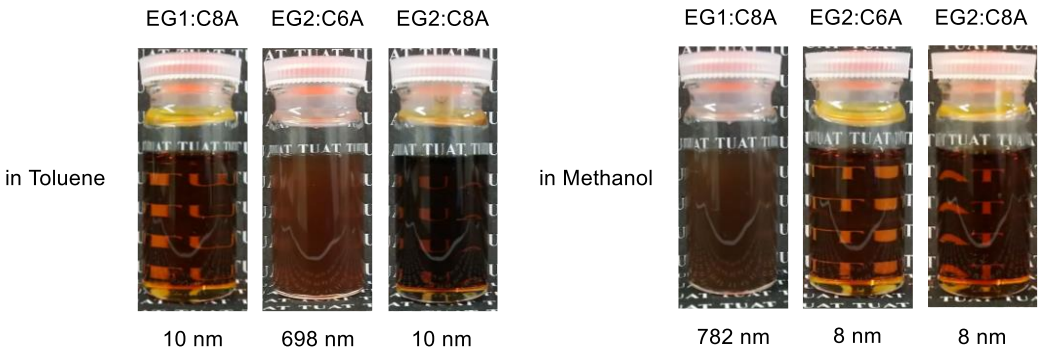

Fig. 3-4 Pictures and DLS Diameters of Amine-Coated Ag Nanoparticles.

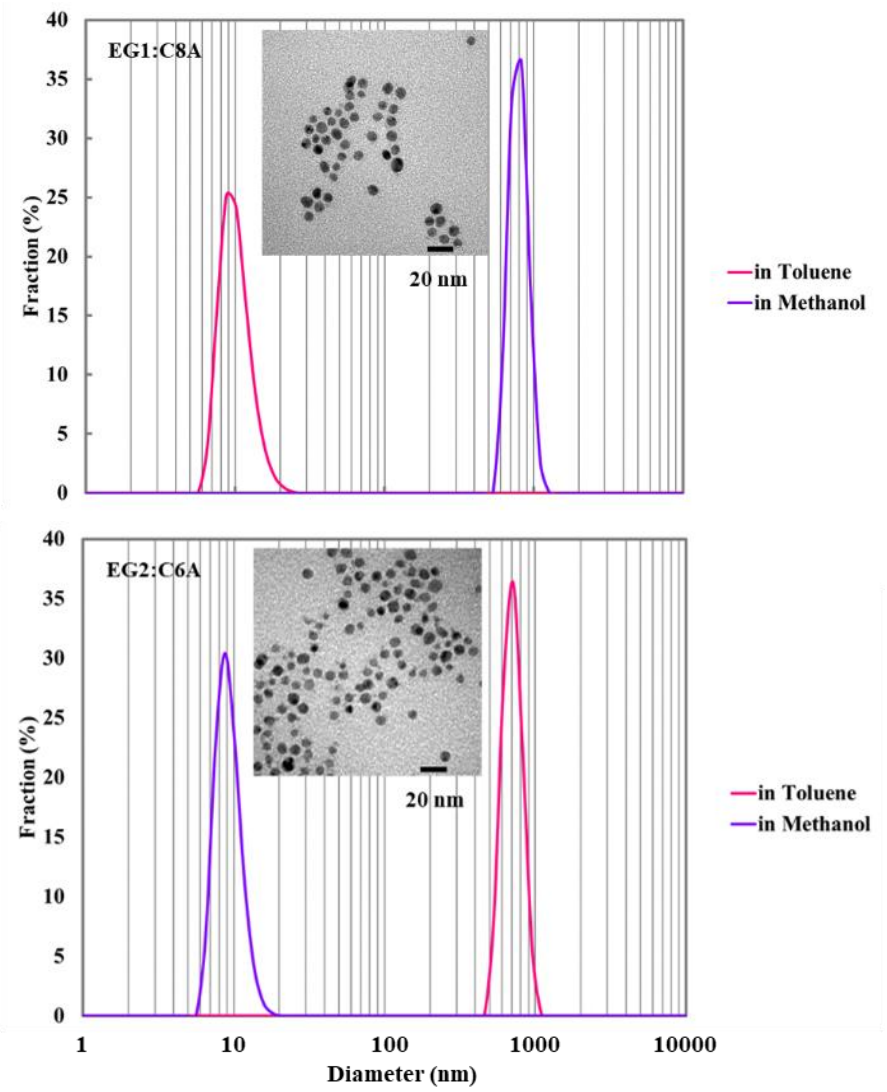

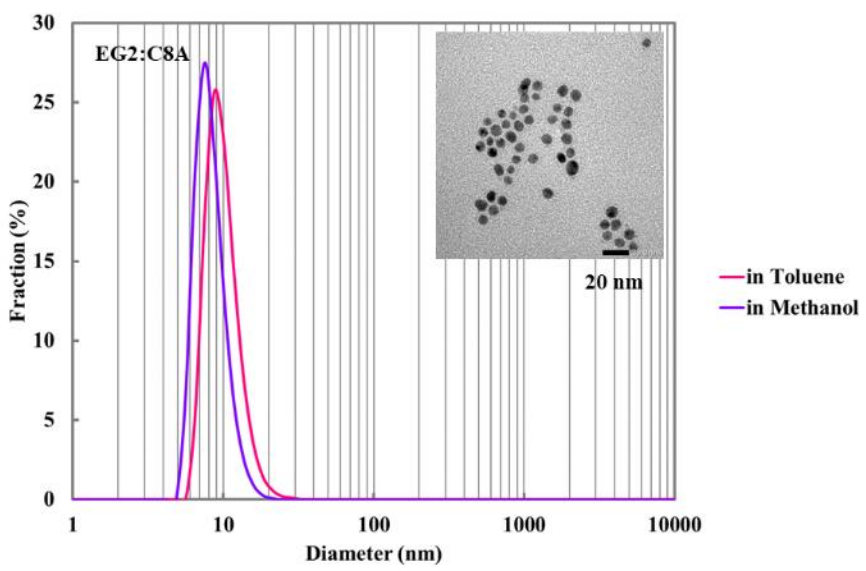

Fig. 3-5　Size Distribution of Ligand-coated Ag Nanoparticles in each Solvent (DLS) and TEM Images of Amine-Coated Ag nanoparticles.

From Fig. 3-4 and Fig. 3-5, the ligand 1 (C8EG1) -coated Ag nanoparticles were dispersed in toluene, but aggregated in methanol. Ligand 2 (C6EG2) -coated Ag nanoparticles were dispersed in methanol, but aggregated in toluene. On the other hand, ligand 3 (C8EG2) coated Ag nanoparticles showed good dispersibility in both methanol and toluene. However, the nanoparticles formed aggregates in just a few days. From these results, it was shown that the hydrophobic / hydrophilic balance and ligand length are important for dispersion in both methanol and toluene, even for Ag nanoparticles.

Moreover, when C8EG1 and C8EG2 ligands with the same molecular structure were modified on TiO_2 nanoparticles and Ag nanoparticles, the results showed that the dispersibility of nanoparticles was significantly different (Fig. 3-6). This is due to the difference in the "surface structure" between TiO_2 nanoparticles with hydrophilic OH groups on the particle surface and Ag nanoparticles without hydrophilic OH groups. In addition, it was suggested that the difference in the "binding group" between the phosphonic acid and the primary amine bound to the particle surface would need to consider.

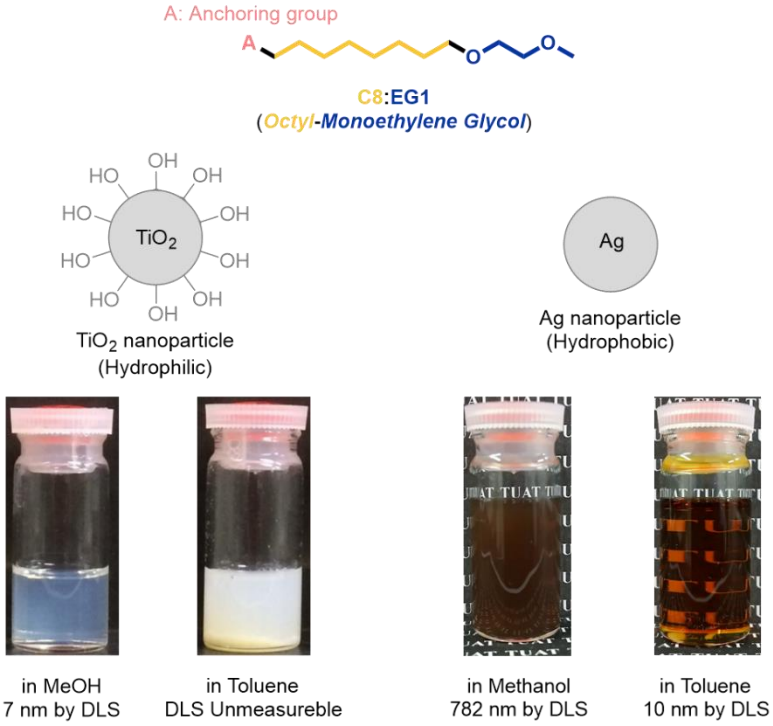

Fig. 3-6 Effect of Differences in Particle Surface Structure on Dispersibility of Nanoparticles.

Moreover, it was suggested that steric hindrance was necessary to maintain the dispersibility of the nanoparticles for a long period of time. Therefore, Ag nanoparticles coated by ligands 4, 5, 6 and 7 with longer alkyl chain and ethylene glycol chain that can be expected to have steric hindrance were prepared. Dispersibility was evaluated by dispersing these Ag nanoparticles in methanol and toluene (Fig. 3-7).

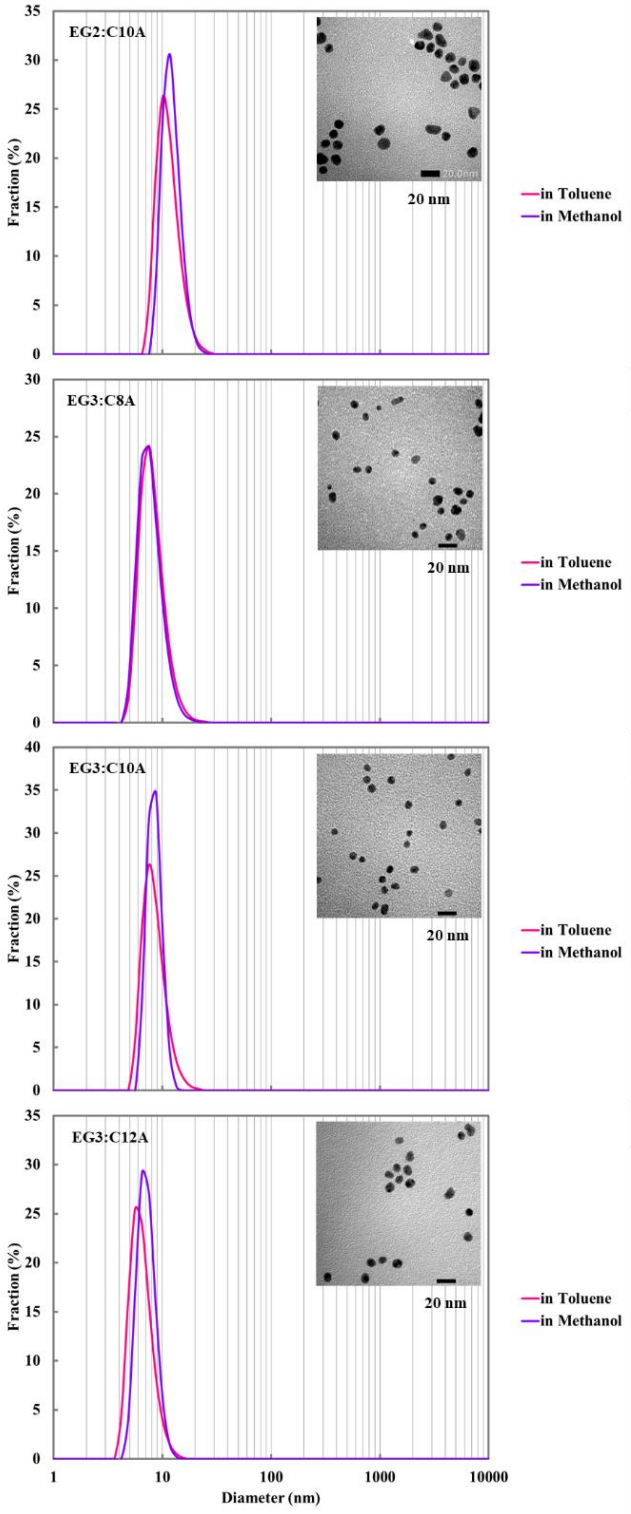

Fig. 3-7　Size Distribution of Ligand-coated Ag Nanoparticles in each Solvent (DLS) and TEM Images of Amine-Coated Ag Nanoparticles.

Fig. 3-7 shows that Ag nanoparticles coated by ligands 4, 5, 6 and 7 show good dispersibility in both methanol and toluene. On the other hand, it was found that only Ag nanoparticles coated by ligand 7 (C12EG3) maintain dispersibility for more than one month. It was also found that the ligand 7-coated Ag nanoparticles can be dispersed in various organic solvents and maintain dispersibility for more than one month (Fig. 3-8 and 3-9). This was suggested to be due to the effect of preventing reaggregation by long ligand chains after dispersing in the solvent.

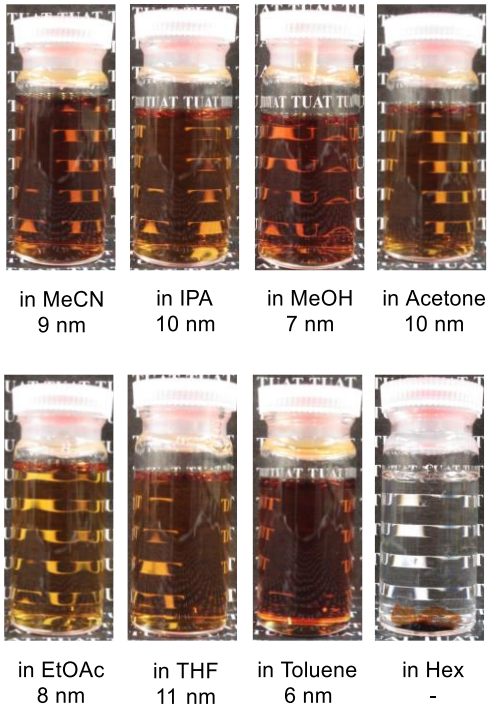

Fig. 3-8 Pictures and DLS Diameters of Ligand 7 Coated Ag Nanoparticles in Various Organic Solvents.

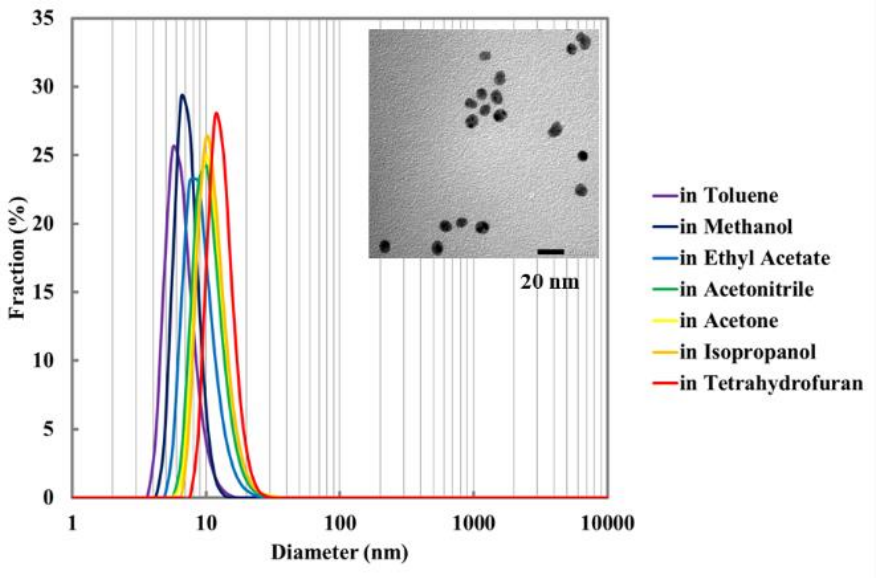

Fig. 3-9 DLS Profiles and TEM Images of Ligand 7 Coated Ag Nanoparticles in Various Solvents.

From these results, it was suggested that the hydrophobic/hydrophilic balance and ligand length are important to homogeneous dispersion of the Ag nanoparticles in various organic solvents. Moreover, it was suggested that steric hindrance by long chain ligand is efficient to maintain the dispersibility of Ag nanoparticles in a solvent for a long period of time.

3.4. Summary

In this chapter, the effect of particle type and bonding group on the dispersibility of Ag nanoparticles modified by amine ligands with the same structure as used in Chapter 2 was investigated.

In the case of Ag nanoparticles, it was found that the balance between the hydrophobicity and hydrophilicity of the ligand is important for dispersibility in organic solvents as well as TiO_2 nanoparticles. In addition, the slight difference in the ligand structure also significantly affected the dispersibility of Ag nanoparticles. On the other hand, when C8EG1 and C8EG2 ligands were modified on TiO_2 nanoparticles and Ag nanoparticles, the dispersibility of each nanoparticle was significantly different. This is due to the difference in the "surface structure" between TiO_2 nanoparticles with hydrophilic OH groups on the particle surface and Ag nanoparticles without hydrophilic OH groups. In addition, it was suggested that the difference in the "bonding group" between the phosphonic acid and the primary amine bound to the particle surface would affect the dispersibility of the nanoparticles.

From the above, the dispersibility of the nanoparticles was significantly different by depending on the particle type, the ligand structure and their combinations. In particular, when using small ligands, "sensitive molecular design" would be required. The results of Chapter 2 and 3 support the possibility of maintaining the dispersibility of nanoparticles even in complex solvent systems, and would become a guideline for interface design and nanoparticle catalyst utilization.

3.5. References

[29] Pujari, S. P.; Scheres, L.; Marcelis, A. T. M.; Zuilhof, H. Covalent Surface Modification of Oxide Surfaces. *Angew. Chem., Int. Ed.* **2014**, *53*, 6322–6356.

[30] (a) Wu, M.; Vartanian, A. M.; Chong, G.; Pandiakumar, A. K.; Hamers, R. J.; Hernandez, R.; Murphy, C. J. Solution NMR Analysis of Ligand Environment in Quaternary Ammonium-Terminated Self-Assembled Monolayers on Gold Nanoparticles: The Effect of Surface Curvature and Ligand Structure. *J. Am. Chem. Soc.* **2019**, *141*, 4316-4327. (b) Smith, A. M.; Marbella, L. E.; Johnston, K. A.; Hartmann, M. J.; Crawford, S. E.; Kozycz, L. M.; Seferos, D. S.; Millstone, J. E. Quantitative Analysis of Thiolated Ligand Exchange on Gold Nanoparticles Monitored by ^{1}H NMR Spectroscopy. *Anal. Chem.* **2015**, *87*, 2771−2778. (c) Fritzinger, B.; Capek, R. K.; Lambert, K.; Martins, J. C.; Hens, Z. Utilizing self-exchange to address the binding of carboxylic acid ligands to CdSe quantum dots. *J. Am. Chem. Soc.* **2010**, *132*, 10195–10201.

Chapter 4
Radical Cation Induced [2 + 2] Cycloaddition Reaction Using TiO_2 Photocatalyst

4.1. Introduction

Development of heterogeneous reactions such as photocatalytic reactions and electrocatalytic reactions is attracting attention as an environmentally friendly chemical process. In particular, the research using the TiO_2 photocatalysis has rapidly developed since Honda-Fujishima effect published at Nature in 1972 was reported. [31] Looking at application examples focused on synthetic reactions, most reactions have been molecular transformations utilizing "radicals".[32] On the other hand, molecular transformation utilizing "radical ions" has been almost no examples. An example of cycloaddition reaction utilizing radical ion species is shown below (Scheme 4-1).[33]

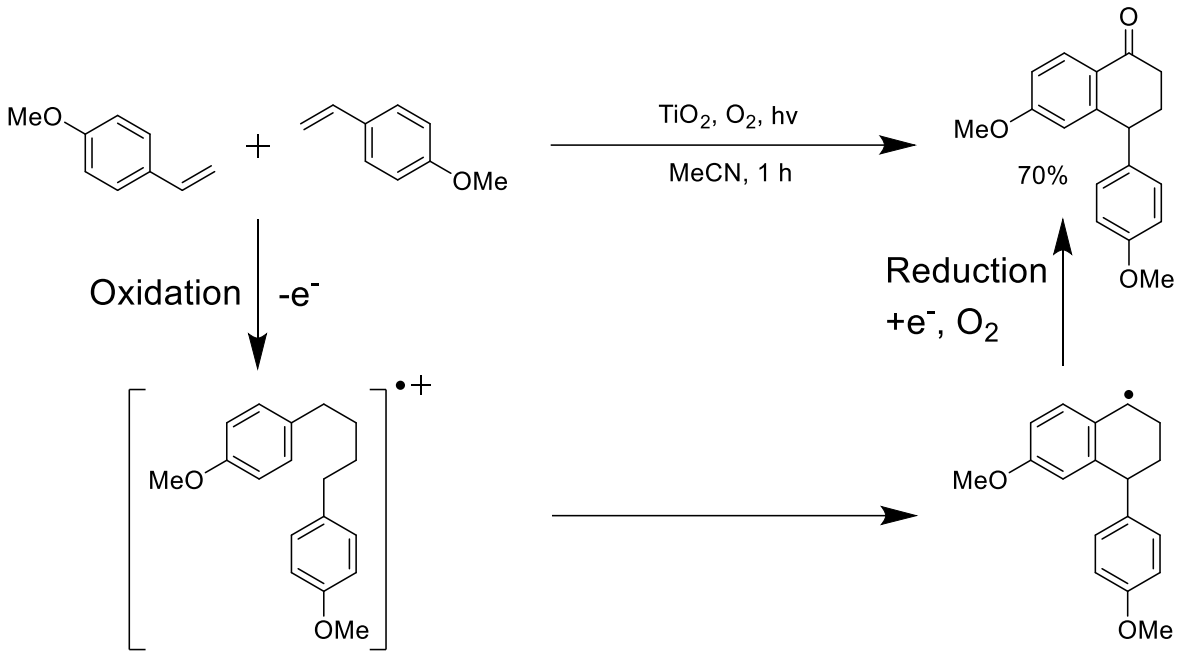

Scheme 4-1 Prausible Reaction Mechanism of Homo-Cyclization Reaction by TiO_2 Photocatalysis.

This reaction is a homo-cyclization reaction between styrenes, which forms C-C bond via a radical cation intermediate after single electron oxidation of styrene. This research result is one of the few examples of radical ion reaction systems constructed using TiO_2 photocatalysis. By establishing a radical ion reaction system using nanoparticle photocatalyst, it is expected that a new reaction field could be constructed, and the new molecular design could be realized.

The solvent system used in organic electrolysis can be used as a reference in constructing radical ion reaction system in heterogeneous system. Chiba *et al*. have reported various reaction developments using nitromethane/lithium perchlorate as a solvent system for organic electrolysis. [34] In addition, it has been found that the effect of the salt is important for using radical ions stably in the reaction, indicating that the supporting salt in organic electrolysis is not an electrolyte simply. [35] Furthermore, it has been shown that the counter anion is significantly related to the stability of the radical cation in reaction system.[36]

We have been working on the establishment of radical cation reaction system using TiO_2 photocatalyst and nitromethane/lithium perchlorate so far. An example is shown below (Scheme 4-2). [37]

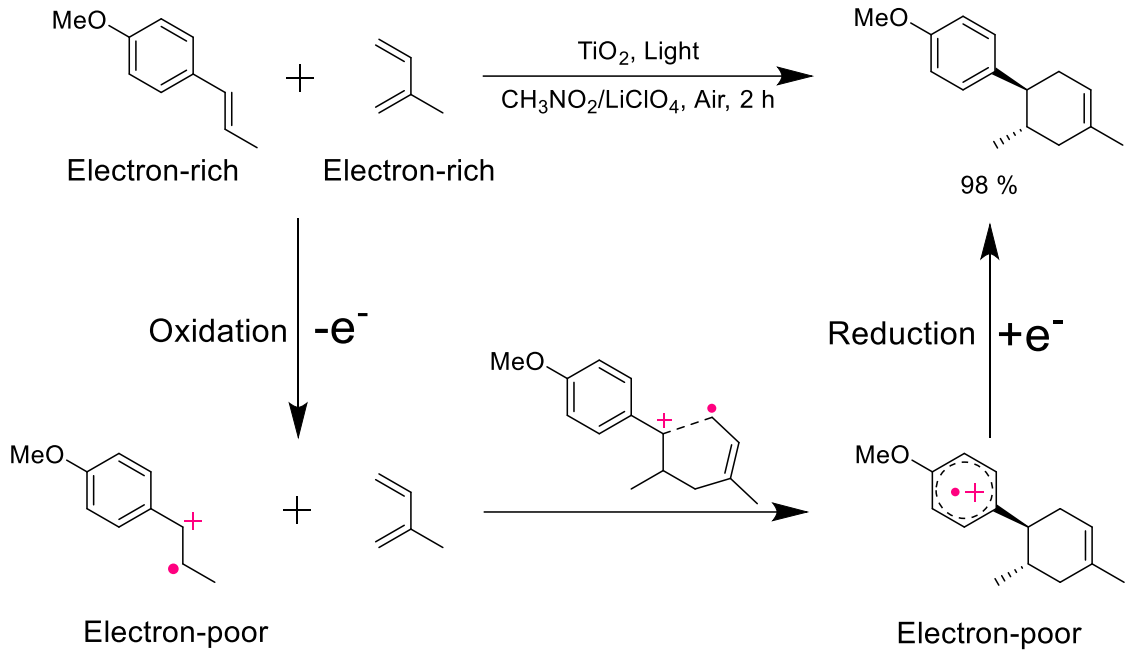

Scheme 4-2 Diels-Alder Reaction by TiO_2 Photocatalysis.

The Diels-Alder reaction shown in Scheme 4-2 is a reaction carried out using various catalysts, but Scheme 4-2 is the first example carried out using TiO_2 photocatalyst. In this work, molecular transformations that are difficult with transition metal catalysts and organic molecular catalysts have been achieved, and the synergistic effect of holes and excited electrons has been proven. Moreover, it was shown that the nitromethane/lithium perchlorate system used in organic electrolysis was effective in the radical cation reaction system using TiO_2 photocatalyst.

The purpose of this work is to establish the radical cation reaction system using TiO_2 photocatalyst and to construct the cyclic compound that cannot be synthesized in one step by the classical method. In addition, the intermolecular and intramolecular electron transfer process was analyzed by an experimental and computational chemistry approach. A deep understanding of electron transfer will provide a new perspective on synthetic organic chemistry.

In this work, four-membered ring forming reactions using nanoparticle photocatalysts were carried out. (Scheme 4-3).

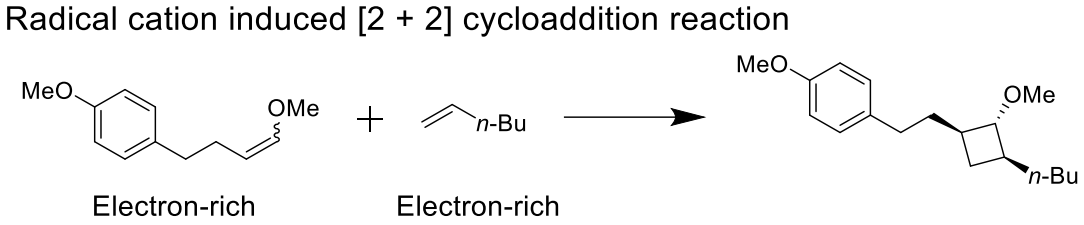

Scheme 4-3 Radical Cation Induced Reactions by TiO_2 Photocatalysis.

4.2. Experimental Procedure

General Remarks

All reagents and solvents were purchased from commercial sources and used without further purification. Reactions were monitored by thin-layer chromatography (TLC) carried out on silica gel plates, with detection by UV absorption (254 nm) and by heating the plates after dipping them in a solution of 12 M molybdo(VI) phosphoric acid n-hydrate in 95% ethanol. Silica gel (particle size 40−50 μm) was used for column chromatography. ^{1}H NMR spectra were collected on a 500 MHz NMR spectrometer using the deuterated solvent as an internal deuterium reference. Chemical shift data are given in δ units calibrated with residual protic solvent. The multiplicity of a signal is indicated as follows: s, singlet; d, doublet; t, triplet; q, quartet; quint, quintet; m, multiplet. ^{13}C NMR spectra were collected at 125 MHz with proton decoupling using the deuterated solvent as an internal carbon reference. Chemical shift data are given in δ units calibrated with residual solvent. High-resolution mass spectra (HRMS) were collected on electrospray ionization (ESI)-or direct analysis in real time (DART)-time-of-flight (TOF) spectrometers. Structure optimizations of all stationary points and frequency analyses were carried out at the B3LYP level of density functional theory (DFT) with the 6-311++G(2d,2p) basis set in nitromethane (PCM model). No imaginary frequency was observed for all compounds. Calculations of the radical cations (**1**$^{\bullet+}$, **3**$^{\bullet+}$, **30**$^{\bullet+}$, **31**$^{\bullet+}$, **32**$^{\bullet+}$, **33**$^{\bullet+}$) were carried out with a methyl group instead of the *n*-butyl group for simplification.

Synthesis and Characterization Data

General Procedure for the Synthesis of Enol Ethers (from Substituted Phenylpropionic Acids)

The enol ethers were synthesized from the respective substituted phenylpropionic acids (if available) in 3 steps, including Weinreb amide synthesis, lithium aluminum hydride reduction, and Wittig reaction. To a solution of the respective substituted phenylpropionic acid (30.0 mmol) and *N*,*O*-dimethylhydroxylamine hydrochloride (4.39 g, 45.0 mmol) in dichloromethane (80 mL) stirred at room temperature were added *N*,*N*'-diisopropylcarbodiimide (6.97 mL, 45.0 mmol), 4-dimethylaminopyridine (36.7 mg, 0.30 mmol), and *N*,*N*-diisopropylethylamine (10.3 mL, 60.0 mmol). The resulting reaction mixture was stirred at room

temperature overnight, diluted with water, and extracted with dichloromethane. The combined organic layers were dried over sodium sulfate, filtered, and concentrated in vacuo. Silica gel column chromatography (hexane/ethyl acetate = 1/1) gave the respective Weinreb amides in 61−67% yield. To a solution of the respective Weinreb amide (18.0 mmol) in tetrahydrofuran (80 mL) stirred at 0 °C was added lithium aluminum hydride (751 mg, 19.8 mmol). The resulting reaction mixture was stirred at 0 °C until the starting material was consumed (checked by thin layer chromatography), diluted with water, and extracted with ethyl acetate. The combined organic layers were dried over sodium sulfate, filtered, concentrated in vacuo, and used without further purification. To a solution of (methoxymethyl)triphenylphosphonium chloride (12.3 g, 36.0 mmol) in tetrahydrofuran (80 mL) stirred at 0 °C was added potassium *tert*-butoxide (3.03 g, 27.0 mmol). After the color turned red, the crude aldehyde was added, stirred at 0 °C until the starting material was consumed (checked by thin layer chromatography), diluted with water, and extracted with ethyl acetate. The combined organic layers were dried over sodium sulfate, filtered, and concentrated in vacuo. Silica gel column chromatography (hexane/ethyl acetate = 20/1) gave the desired enol ethers in 28−31% yield over 2 steps.

General Procedure for the Synthesis of Enol Ethers (from the Respective Substituted Benzaldehydes)

The enol ethers were synthesized from the respective substituted benzaldehydes (if the corresponding substituted phenylpropionic acids were not available) in 5 steps including Wittig reaction and acid hydrolysis. To a solution of (methoxymethyl)triphenylphosphonium chloride (34.3 g, 100.0 mmol) in tetrahydrofuran (160 mL) stirred at 0 °C was added potassium *tert*-butoxide (8.42 g, 75.0 mmol). After the color turned red, the respective substituted benzaldehyde (50.0 mmol) was added, and the reaction was stirred at 0 °C until the starting material was consumed (checked by thin layer chromatography), diluted with water, and extracted with ethyl acetate. The combined organic layers were dried over sodium sulfate, filtered, and concentrated in vacuo. Silica gel column chromatography (hexane/ethyl acetate = 20/1) gave the respective enol ethers in 87−93% yield. To a solution of the respective enol ether (45.0 mmol) in acetone (100 mL) stirred at room temperature was added a catalytic amount of concentrated sulfuric acid. The resulting reaction mixture was stirred at room temperature until the starting material was consumed (checked by thin layer chromatography), diluted with water, and extracted with ethyl acetate. The combined organic layers were dried over sodium sulfate, filtered, and concentrated in vacuo. Silica gel column chromatography (hexane/ethyl acetate = 5/1) gave the respective substituted benzaldehydes in 35−40% yield. The repetitive Wittig reactions and acid hydrolysis gave the desired enol ethers in 25−30% yield over 3 steps.

General Procedure for the [2 + 2] Cycloadditions

To a solution of $LiClO_4$ (1.0 M) in CH_3NO_2 and TiO_2 nanoparticle powder (P25, 20 nm, 50 m^2/g) stirred at room temperature were added the respective enol ethers and alkenes. The resulting reaction mixture was stirred at room temperature in front of a 15 W UV lamp (365 nm) until the starting material was consumed (checked by thin layer chromatography), diluted with water, and extracted with ethyl acetate. The combined organic layers were dried over sodium sulfate, filtered, and concentrated in vacuo. Yields were determined by

^{1}H NMR analysis using benzaldehyde as an internal standard. Silica gel column chromatography (hexane/ethyl acetate = 50/1) gave the desired cycloadduct.

Theoretical Calculations

Structure optimizations of all stationary points and frequency analyses were carried out at the B3LYP level of density functional theory (DFT) with the 6-311++G(2d,2p) basis set in nitromethane (PCM model). No imaginary frequency was observed for all compounds.

4.3. Results and Discussion

4.3.1. General Reaction Condition

First, the scheme and photograph of the [2 + 2] cycloaddition reaction are shown in Fig. 4-1.

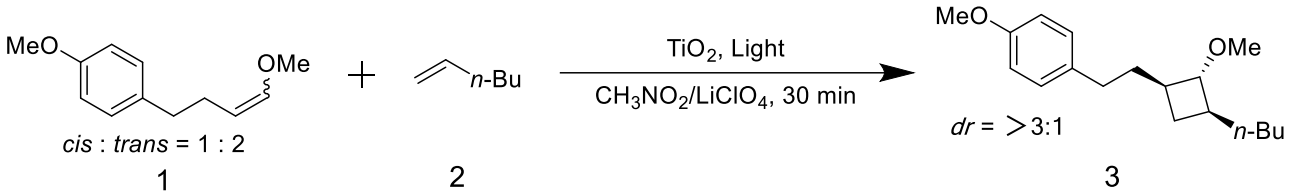

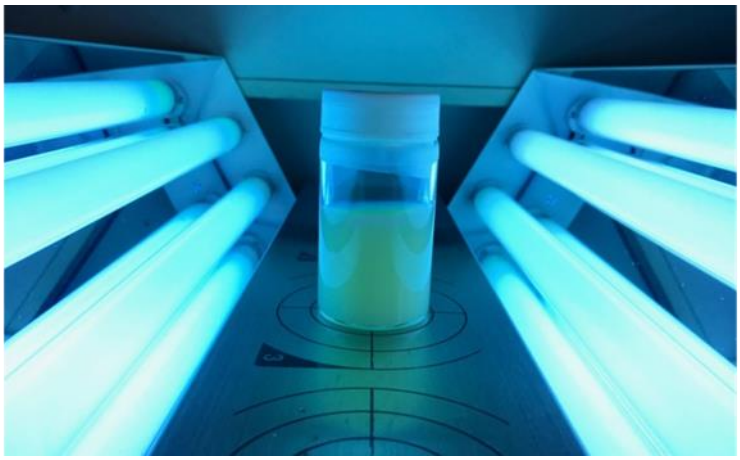

Fig. 4-1 Condition and Photograph of Photocatalytic Reaction.

This reaction is [2 + 2] cycloaddition reaction between electron-rich enol ether and olefin. TiO_2 nanoparticles were used for the photocatalyst, and nitromethane / lithium perchlorate system was used for the solvent system.

4.3.2. Optimization of Reaction Conditions

The optimization of reaction conditions were shown below (Table 4-1).

Table 4-1 Optimization of the Conditions for the [2 + 2] Cycloaddition.

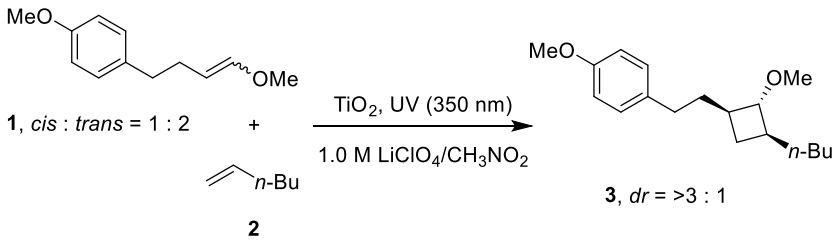

entry	conditions[a]	yield (%)[b]
1	-	68 (0)
2	5 min	68 (0)
3	3 min	67 (0)
4	1 min	29 (1)
5	no TiO_2, no light	0 (99)
6	no light	0 (0)
7	no TiO_2	trace (63)
8	air	68 (0)
9	H_2O (1 eq)	67 (0)
10	air, H_2O (1 eq)	67 (0)

[a]Unless otherwise stated, reactions were carried out on a 0.20 mmol scale of the enol ether (**1**) with 20 eq of 1-hexene (**2**) and 100 mg of TiO_2 in 4 mL of CH_3NO_2 using a 15 W UV lamp at rt for 30 min under Ar atmosphere. [b]Yields were determined by ^1H NMR analysis using benzaldehyde as an internal standard and recovered starting material was reported in parenthesis.

In this reaction, it was found that the starting material was consumed in 3 min to give the desired product 3 (entry 1-3). When the reaction was stopped at 1 min, the yield of the desired product was drastically reduced, but the starting material was almost consumed (entry 4). It was suggested that the rate-determining step of this reaction was not the hole oxidation of substrate 1 by TiO_2 photocatalysis but the nucleophilic attack of olefin for radical cations. In addition, the desired product was not obtained under no TiO_2 and no light conditions, and the starting material was recovered (entry 5). In the absence of light, the desired product was not obtained, and the starting materials was consumed, indicating that

aldehyde was produced (entry 6). This was due to acid hydrolysis by solvent system. When light was irradiated without TiO_2, the desired product was hardly obtained (entry 7). Furthermore, since the reaction proceeded even in the presence of a small amount of water in air atmosphere, it was suggested that the reactivity between the radical cation and the olefin is better than the reactivity between the radical cation and the reactive oxygen species (ROS) generated during the reaction (entry 8-10).

The experimental results on the substrate concentration and catalyst amount were shown below (Table 4-2).

Table 4-2 Competition Experiments between the [2 + 2] Cycloaddition and Dimerization.

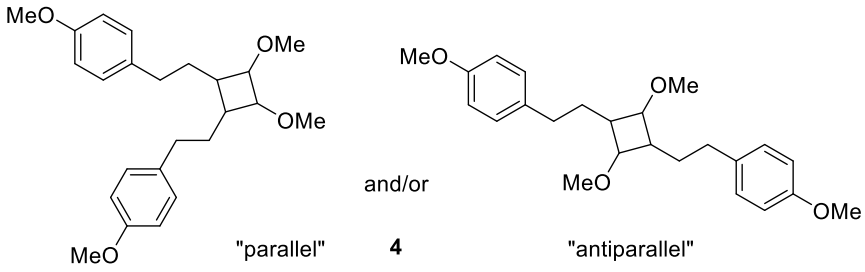

entry	amount of **1** + **2** (mmol)[a]	yield (%)[b,c] of **3** + **4**
1	0.20 (40 μmol/m^2) + 4.0 (1.0 M, 20 eq)	68 (0) + 7
2	0.20 (40 μmol/m^2) + 8.0 (2.0 M, 40 eq)	71 (0) + 8
3	0.10 (20 μmol/m^2) + 4.0 (1.0 M, 40 eq)	71 (0) + 7
4	0.05 (10 μmol/m^2) + 4.0 (1.0 M, 80 eq)	82 (0) + 5
5	0.02 (4 μmol/m^2) + 4.0 (1.0 M, 200 eq)	87 (0) + 3
6	0.20 (40 μmol/m^2) + 4.0 (0.1 M, 20 eq)[d]	74 (0) + 9
7	0.20 (4 μmol/m^2) + 4.0 (0.1 M, 20 eq)[d, e]	75 (0) + 5
8	0.20 (4 μmol/m^2) + 8.0 (0.2 M, 40 eq)[d, e]	86 (0) + 4

[a]Reactions were carried out with 100 mg of TiO_2 in 4 mL of CH_3NO_2 using a 15 W UV lamp at rt for 30 min under Ar atmosphere. TiO_2 surface area was estimated to be 50 m^2/g by BET measurement.
[b]Yields were determined by ^{1}H NMR analysis using benzaldehyde as an internal standard.
[c]Recovered starting material was reported in parenthesis.
[d]40 mL of CH_3NO_2 was used.
[e]1000 mg of TiO_2 was used.

It was found that even if the olefin concentration was increased, the yield of the desired product 3 was about 70% in both cases (entry 1 and 2). This is due to the olefin has reached saturated concentration in nitromethane. Moreover, it was confirmed that the yield of the desired product 3 increased from 68% to 87% as the concentration of the starting material 1 decreased from 0.20 mmol to 0.02 mmol (entry 1, 3, 4 and 5). Furthermore, when the amount of TiO_2 was increased to 10 times that of entry 1 and 2, it was confirmed that the yield increased (entry 7-8). From these results, it was considered that the yield of the desired product 3 is simply due to the processing ability based on the surface area of TiO_2, regardless of the concentration of olefin 2.

4.3.3. Plausible Reaction Mechanism in [2 + 2] Cycloaddition Reaction

The reaction mechanism of this reaction was shown below (Fig. 4-2).

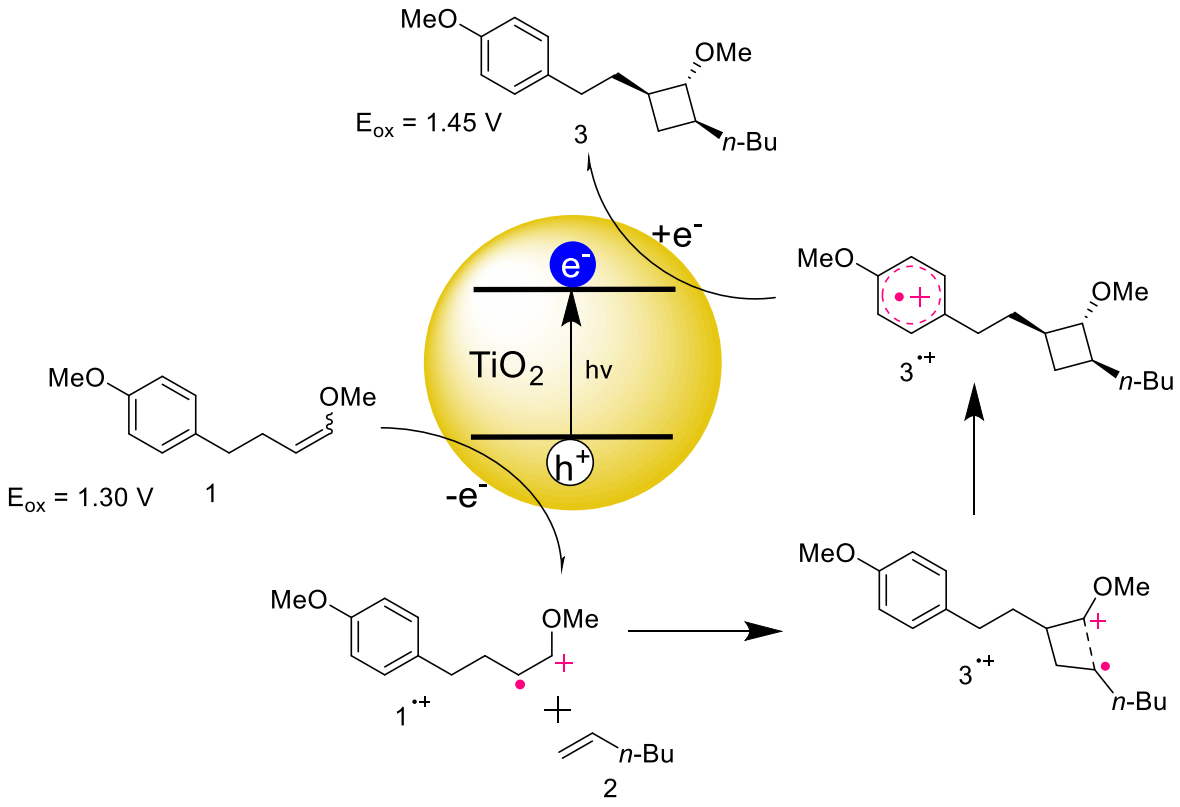

Fig. 4-2 Plausible Reaction Mechanism of Radical Cation Induced [2 + 2] Cycloaddition Reaction

This reaction starts by generating radical cations by hole oxidation of enol ether. The generated radical cation reacts with the olefin to form a C-C bond. Thereafter, a four-membered ring is formed by intramolecular reduction from the aromatic ring, leading to long-lived radical cation. Finally, the excitation electron is received and the desired product 3 is obtained through single electron reduction. In other words, this reaction is a “redox neutral” reaction that begins with single electron oxidation and ends with single electron reduction.

4.3.4. Scope & Limitation of [2 + 2] Cycloaddition Reactions

The experimental results of functional group resistance of olefins are shown below (Table 4-3).

Table 4-3 Hexene Variation for the [2 + 2] Cycloaddition.

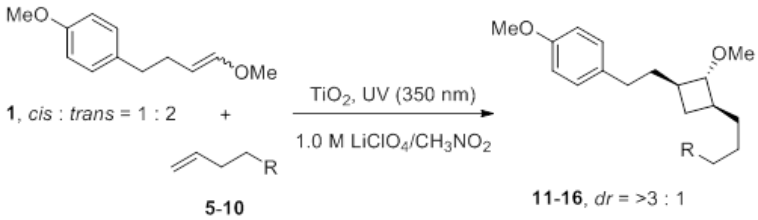

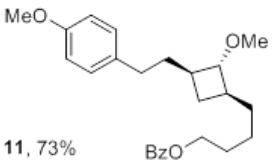

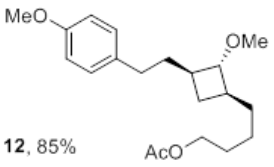

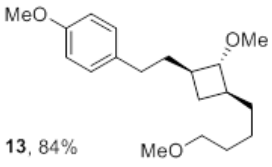

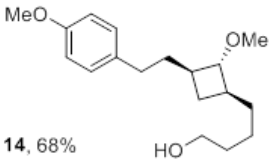

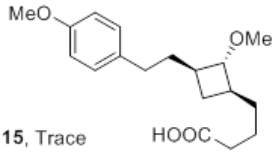

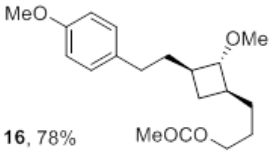

[a]Reactions were carried out on a 0.20 mmol scale of the enol ether (**1**) with 40 eq of the hexene (**5-10**) and 1000 mg of TiO_2 in 40 mL of CH_3NO_2 using a 15 W UV lamp at rt for 30 min under Ar atmosphere.
[b]Yields were determined by ^1H NMR analysis using benzaldehyde as an internal standard.

The desired products 11, 12, 13, 14 and 16 were obtained in the yield of 73% -85%, so it was showed that benzoyl, acetyl, ether, alcohol and ester groups could be used in this reaction. On the other hand, in the case of olefin 9, the desired product 15 was hardly obtained. From the result of analyzing the structure of the product by NMR, aldehyde was obtained by acid hydrolysis of the enol ether, because the functional group of the olefin 9 is the acidic carboxy group. The mechanism of aldehyde formation by acid hydrolysis is shown below (Scheme 4-4).

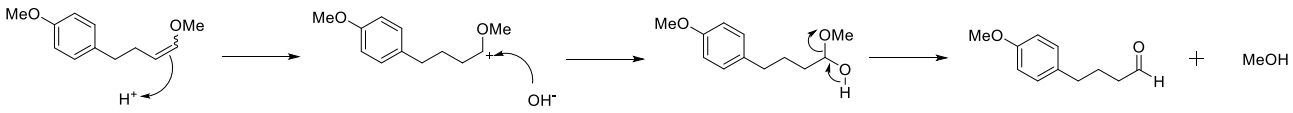

Scheme 4-4 Aldehyde Generation Mechanism by Acid Hydrolysis.

As shown in Scheme 4-4, the olefin having acidic functional group such as carboxy group or sulfo group might not be applicable to this reaction unless the equivalent is reduced. In addition, olefins having basic functional groups such as amino groups caused an acid/base reaction with acidic atmosphere of nitromethane/lithium perchlorate solvent system.

The experimental results of various substitution of alkenes were shown below (Table 4-4).

Table 4-4 Alkene Variation for the [2 + 2] Cycloaddition.

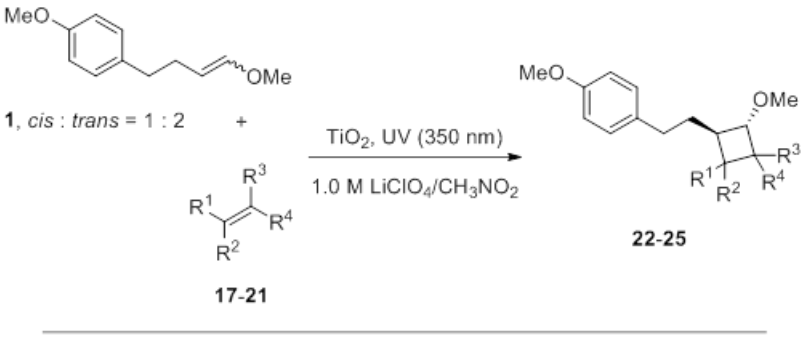

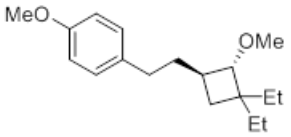

22, 88%
dr = >10 : 1

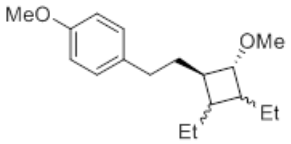

23, <50% from *cis*-3-hexene (**20**)[c]
23, <40% from *trans*-3-hexene (**21**)[c]

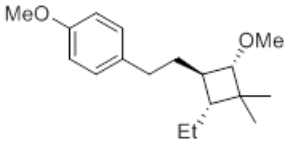

24, 76%[d]
dr = >3 : 1

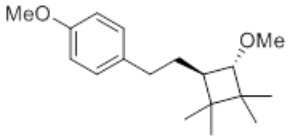

25, 48%[d]
dr = >10 : 1

[a]Reactions were carried out on a 0.20 mmol scale of the enol ether (**1**) with 40 eq of the alkene (**17-21**) and 1000 mg of TiO_2 in 40 mL of CH_3NO_2 using a 15 W UV lamp at rt for 30 min under Ar atmosphere.
[b]Yields were determined by ^1H NMR analysis using benzaldehyde as an internal standard.
[c]Inseparable diastereomixtures were obtained.
[d]Reaction was carried out for 2 h.

It was found that the yield was different significantly with various olefin substitution patterns (Table 3-4). This result was considered from the viewpoint of reaction mechanism. The difference of the reactivity between enol ether and alkene when olefin 17 and olefin 21 were used is shown (Scheme 4-5).

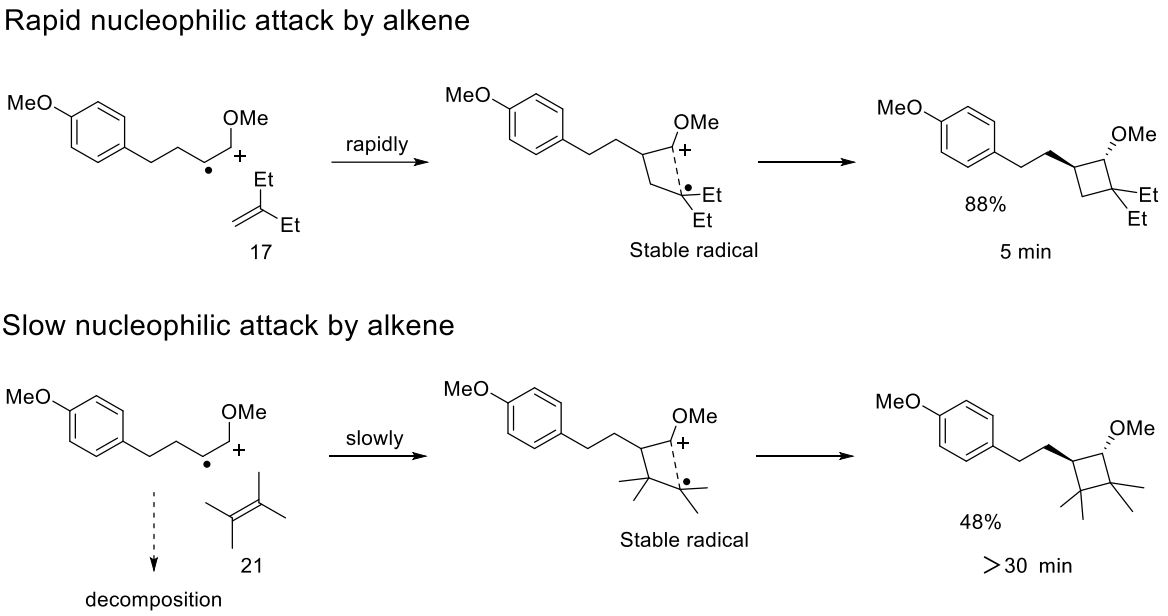

Scheme 4-5 The Difference of Nucleophilic Attack by Alkene.

Four-membered ring forming reaction is significantly influenced by two factors.

The first is the reactivity between enol ether radical cations and olefins. As shown in Scheme 4-4 above, a olefin that is sterically open on one side of the double bond is prone to nucleophilic attack on the radical cation intermediate, so it forms a bond quickly. On the other hand, as shown in Scheme 4-4 lower, both sides of the double bond are all buried, and the nucleophilic attack on the radical cation intermediate is difficult. Therefore, the enol ether was decomposed, and the reaction time was prolonged. It was suggested that the olefin structure determines the reactivity.

The second is the radical stability after one bond is formed. In general, the radical stability is higher in the order of tertiary radicals, secondary radicals and primary radicals, so both intermediates form stable radicals. Therefore, it was suggested that both reactions proceed smoothly after forming one bond.

In other words, the reactivity in this reaction is determined mainly by two factors: one is the reaction rate between enol ether and olefin, and another is the radical stability generated during the reaction. In addition, since the electron transfer in the molecule is very fast, the rate-limiting step is a bond forming process of enol ether and olefin.

The results of investigating the effect of aromatic ring substituents on the reaction were shown below (Table 4-5).

Table 4-5 Substitution Variation of Aromatic Ring for the [2 + 2] Cycloaddition.

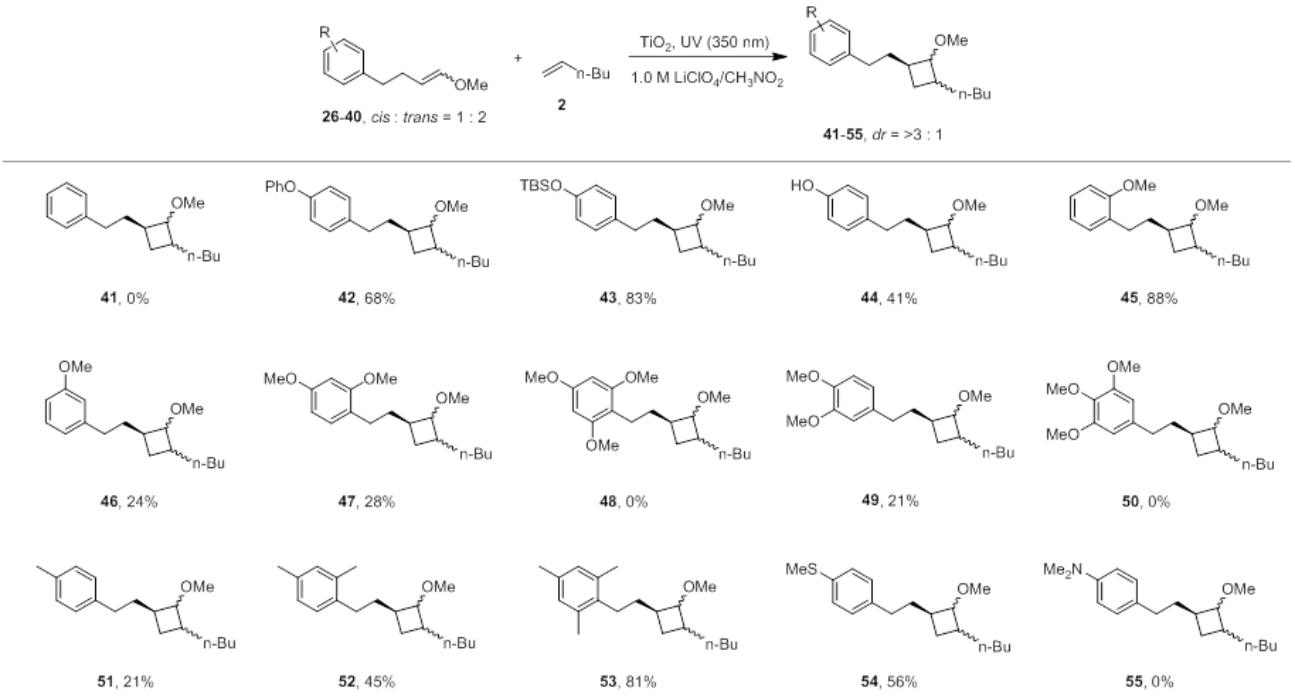

[a]Reactions were carried out on a 0.02 mmol scale of the enol ether (**26-40**) with 200 eq of the alkene (**2**) and 100 mg of TiO_2 in 4 mL of CH_3NO_2 using a 15 W UV lamp at rt for 30 min under Ar atmosphere.
[b]Yields were determined by ^1H NMR analysis using benzaldehyde as an internal standard.
[c]Inseparable diastereomixtures were obtained.
[d]Reaction was carried out for 2 h.

The reactions using substrate 1 and substrate 26 were compared. In the reaction of the substrate 1 having the MeO group which is an electron donating group on the aromatic ring and the olefin 2, the yield of the desired product 3 was 87%. On the other hand, in the reaction of the substrate 26 having no substituent on the aromatic ring and the olefin 2, the yield of the desired product 41 was 0%. However, the reaction of substrate 26 and olefin 2 was found to give the metathesis product as the main product. The plausible metathesis generation mechanism is shown (Scheme 4-6).

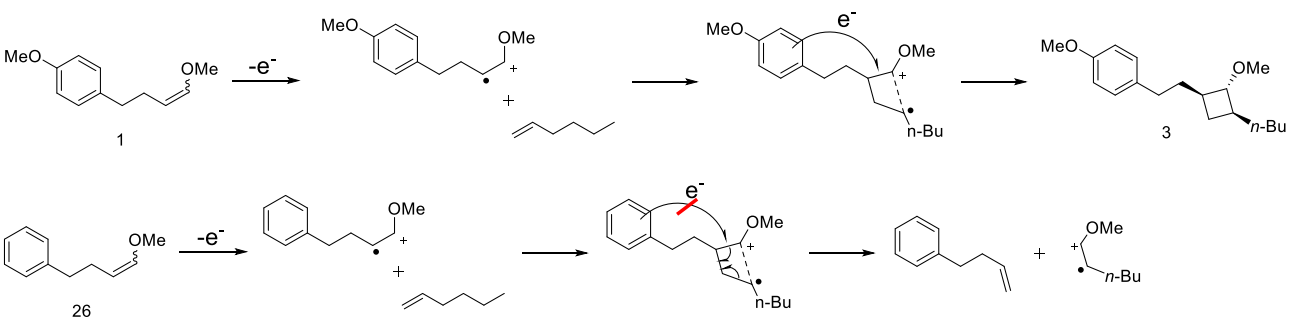

Scheme 4-6 Plausible Metathesis Generation Mechanism.

From Scheme 4-6, when the aromatic ring has the MeO electron donating group, intramolecular single electron reduction from the aromatic ring proceeded to form four-membered ring. On the other hand, when the aromatic ring does not have a substituent, intramolecular single electron reduction from the aromatic ring did not proceed and could not lead to the formation of a four-membered ring. Therefore, the bond is broken to give metathesis product. In order to form a four-membered ring, it is necessary to have the electron-donating substituent on the aromatic ring.

4.3.5. DFT Calculation of Radical Cation Intermediate

Furthermore, the analysis by computational chemistry of the electron transfer process in this reaction was carried out using density functional theory calculations (DFT calculations) (Scheme 4-7). Note that in the actual calculation, the CH_3 group was used instead of the *n*-Butyl group in order to simplify the calculation. The calculation level is B3LYP / 6-311 ++G (2d, 2p).

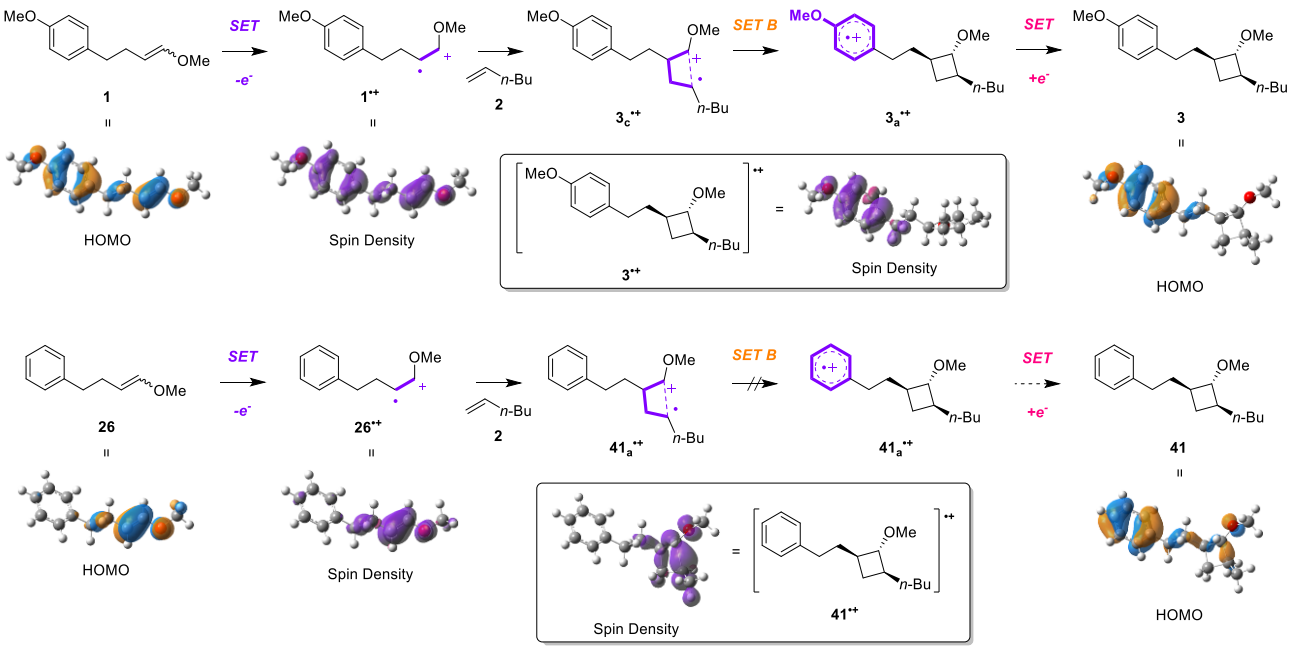

Scheme 4-7 Spin Densities and HOMOs of Plausible Reaction Mechanism for the [2 + 2] Cycloaddition.

From Scheme 4-7, the spin densities after single electron oxidation of substrate 1 and substrate 26 are both distributed on enol ether, so it was confirmed that a reactive site exists on enol ether. The critical difference is the spin density of the radical cation intermediate after formation of the bond with olefin 2. The structure of radical cation 3 in Scheme 4-6 above shows that the four-membered ring is completely closed, and the spin density is localized on the aromatic ring. On the other hand, the structure of the radical cation 41 in Scheme 4-6 below shows that the bond of the four-membered ring is not closed, and the spin density is localized on the four-membered ring. The bond length in the radical cation is shown

below (Fig. 4-3).

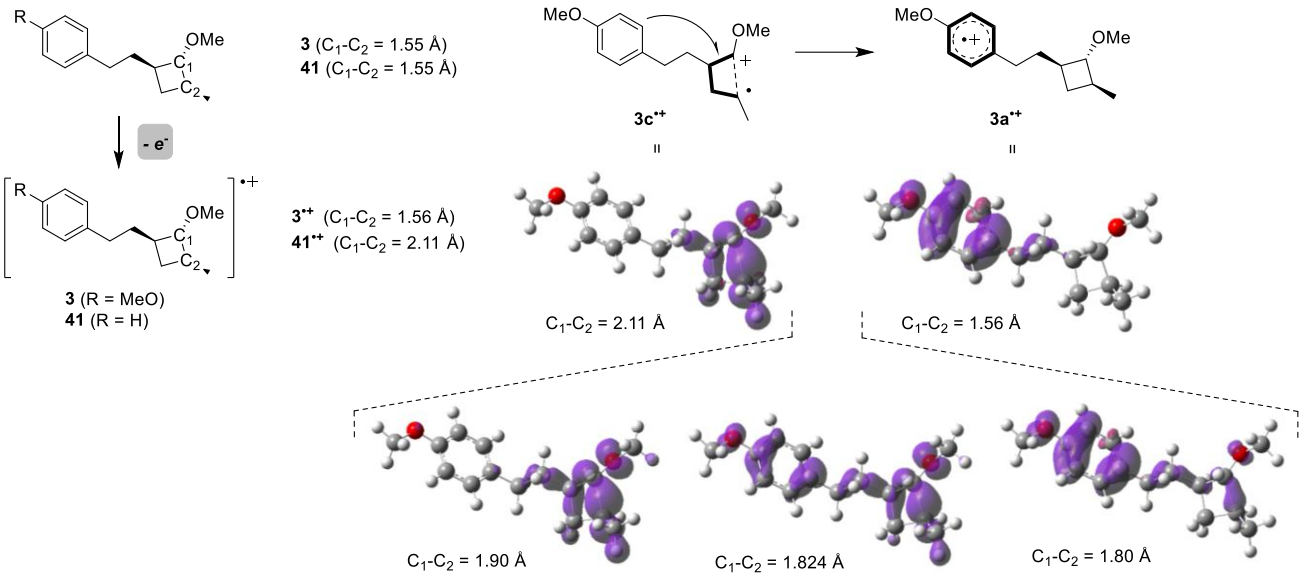

Fig. 4-3 C_1-C_2 Bond Length and Spin Density shift of Radical Cation Intermediate (C_1-C_2 bond length: from 2.11 Å to 1.56 Å).

From Fig. 4-3, the length of the C_1-C_2 bond in the four-membered ring product is 1.55 Å (four-membered ring product 3) and 1.55 Å (four-membered ring product 41), respectively. On the other hand, in the state of radical cation, the length of C_1-C_2 bond is 1.56 Å (radical cation $3^{\cdot +}$) and 2.11 Å (radical cation $41^{\cdot +}$), respectively. Since the length of general C-C bond is 1.54 Å, it was confirmed that the bond of radical cation $41^{\cdot +}$ having no MeO group is not closed. In addition, when the length of the C_1-C_2 bond of the radical cation $3^{\cdot +}$ with a MeO group was set to 2.11 Å and the structure was optimized, it was found that spin density was localized in the four-membered ring. The intramolecular single electron transfer from the methoxyphenyl group to the four-membered ring could be showed as spin density shift by DFT calculations. Furthermore, when the calculation was carried out while gradually shortening the C_1-C_2 bond length of the radical cation $3^{\cdot +}$ from 2.11 Å to 1.56 Å, it was found that the spin density shift occurred between 1.90 Å and 1.80 Å. It was also found that spin density was delocalized at about 1.824 Å. Given that the length of the C_1-C_2 bond in the final four-membered ring product 3 is 1.56 Å, intramolecular single electron transfer would be completed earlier than the four-membered ring was completely formed.

From these calculation results, when the aromatic ring has a MeO group, intramolecular single electron transfer (SET) proceeds from the aromatic ring to the four-membered ring. It was suggested that the spin density was distributed on the aromatic ring, and then the radical cation was stabilized. On the other hand, when the aromatic ring has no substituent, intramolecular electron transfer from the aromatic ring to the four-membered ring did not proceed, suggesting that the four-membered ring was not formed. From the above, the results of DFT calculations corresponded well to the experimental results, and were powerful

tool for understanding the electron transfer process during the reaction that could not be seen with the eyes.

4.3.6. CV Measurement and DFT Calculation of Enol Ether

The effect of the substitution position of the MeO group on the formation of four-membered ring is discussed below. Cyclic voltammetry (CV) measurement results, HOMO and spin density distributions of *o*-MeO, *m*-MeO and *p*-MeO enol ether were shown in Fig. 4-4.

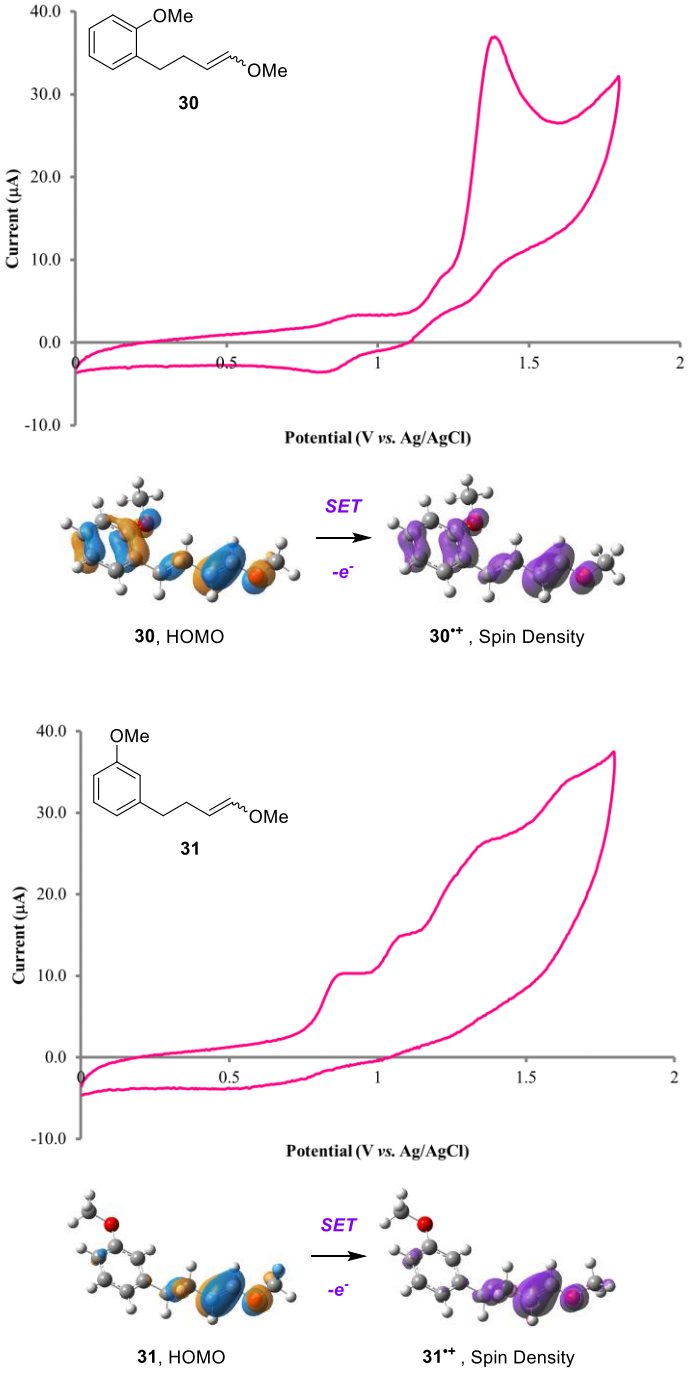

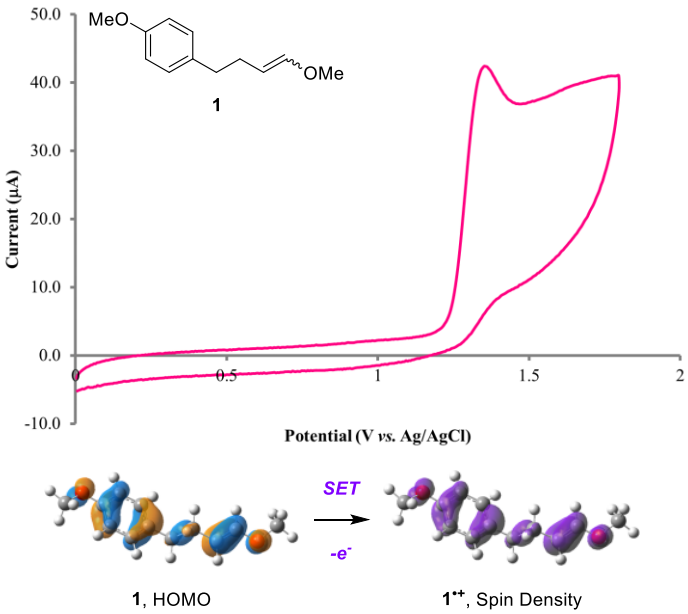

Fig. 4-4　CV Measurements and DFT Calculations of Enol Ethers.

From Table 4-5, the yields of the target products 3, 45 and 46 were 87%, 88% and 24% respectively. It was found that the yield of the desired product was significantly decreased when the *meta*-substituted substrate was used. This result was considered from the results of CV and DFT calculations.

From Fig. 4-4, the oxidation potentials of *ortho*- and *para*-substituted enol ethers are 1.39 V and 1.36 V respectively, and the CV waveforms were similar. In both cases, the distribution of HOMO and spin density obtained from the results of DFT calculations also corresponded well. On the other hand, *meta*-substituted enol ethers were different from *ortho*- and *para*-substitutions, and some oxidation waves could be confirmed. The lowest oxidation peak was 0.87 V. In addition, the distribution of HOMO and spin density obtained from the results of DFT calculations corresponded well with the substrate 26 having no substituent in the aromatic ring.

From these results, it was considered that the substitution position of the aromatic ring substituent was significantly related to the stabilization of the radical cation, and it was suggested that the orientation might be involved.

The effect of aromatic ring substituents on four-membered ring formation was discussed below. Fig. 4-5 shows the distribution of HOMO, spin density and results of CV measurement of substrates 32 and 33 with increased number of MeO group substitution.

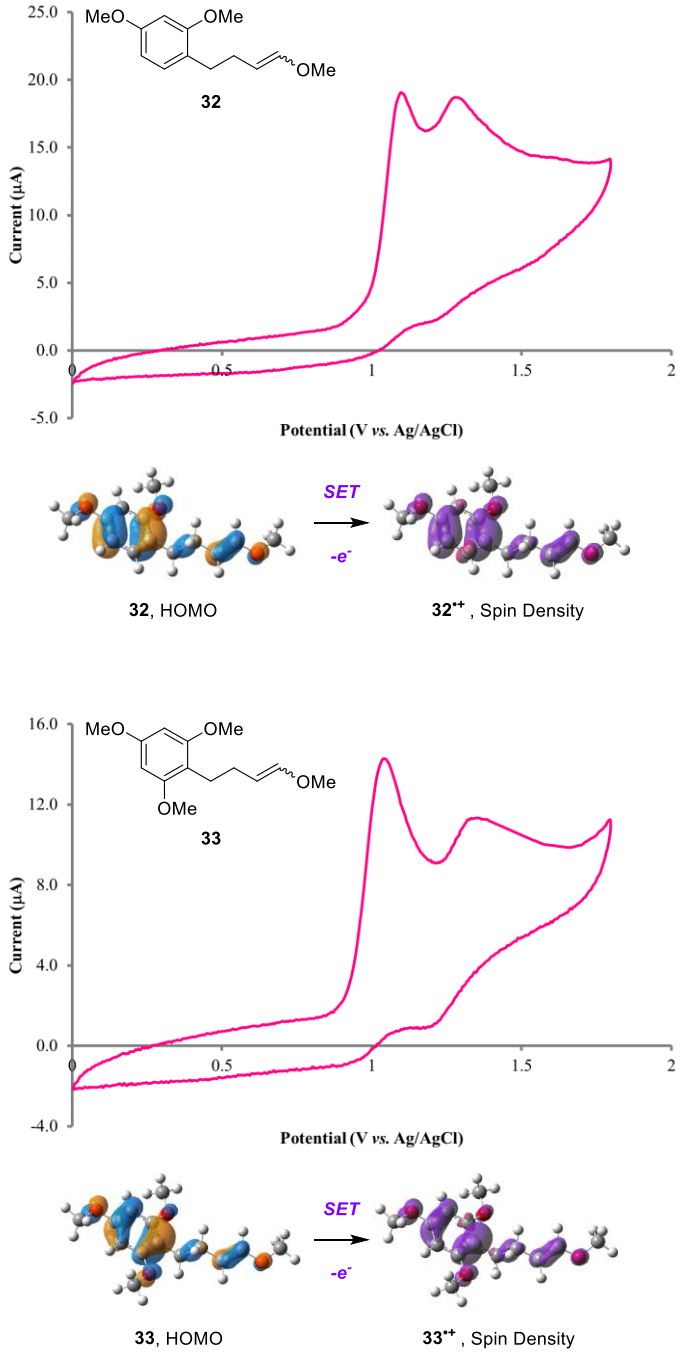

Fig. 4-5 CV Measurements and DFT Calculations of 2,4-Dimethoxy and 2,4,6-Trimethoxy Enol Ethers.

From Table 4-5, the yields of the target products 47 and 48 were 28% and 0% respectively, and it was found that the yield of the desired product significantly decreased as the number of MeO group substitutions increased. This result was considered from the results of CV and DFT calculations.

The oxidation potential of substrates 32 and 33 in Fig. 4-5 was about 1.0 V. On the other hand, the spin density was slightly different from substrate 1, and the distribution was localized in the aromatic ring moiety rather than the enol ether moiety. A conceptual diagram of the reaction was shown below (Scheme 4-8).

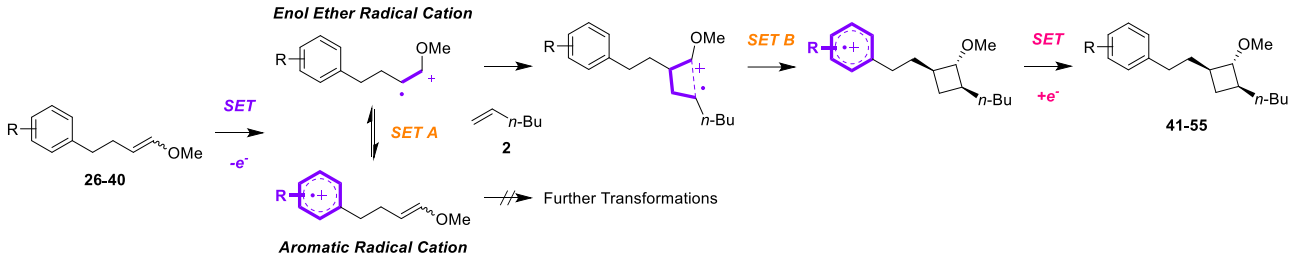

Scheme 4-8 Plausible Reaction Mechanism for the [2 + 2] Cycloaddition.

As shown in Fig. 4-5 and Scheme 4-8, the electron density of the aromatic ring was increased as the number of the electron-donating MeO groups increased. As a result, the ability to stabilize the radical cations by the aromatic ring was enhanced. Therefore, it is difficult to leave the reactivity in the enol ether moiety. From these results, it is considered that the analysis of the electron transfer process using DFT calculations provides a clue to know whether the reaction proceeds without synthesizing the substrate.

4.3.7. Competition between Four-membered Ring Products and Metathesis Products

The reaction results when Me group is used as an electron donating substituent were shown in Scheme 4-9.

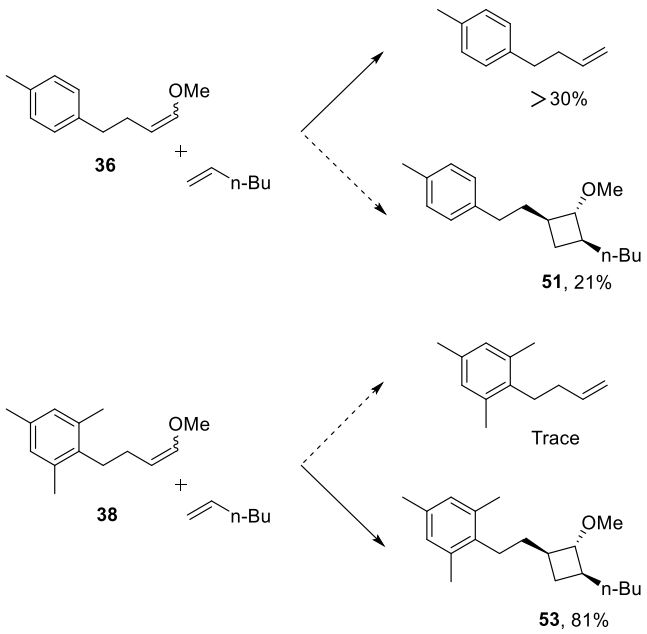

Scheme 4-9 Relationship between the Number of Methyl Groups and the Synthetic Outcome.

As shown in Scheme 4-9, when the substrate 36 having monomethyl group was used in the reaction, the yield of the desired product 51 was 21%, and the yield of the metathesis product was more than 30%. On the other hand, when the substrate 38 having trimethyl group was used in the reaction, the yield of the desired product 53 was 81%, and almost no metathesis product was obtained.

It is considered that the substrate 36 having monomethyl group has low electron density of the aromatic ring, and the intramolecular electron transfer to the four-membered ring was not smoothly occurred. On the other hand, since the substrate 38 having trimethyl group has the almost same desired yield as that of the substrate 1 having monomethoxy group, the substrate 38 has the electron density distribution very similar to that of the substrate 1. From these results, it was suggested that the balance of the electron density of the enol ether and the aromatic ring is important to obtain four membered ring products with good yield.

4.3.8. Relationship between Oxidation-Reduction Potential of Enol Ether and Product Yield

The relationship between oxidation potential and desired product yield is shown below (Fig. 4-6).

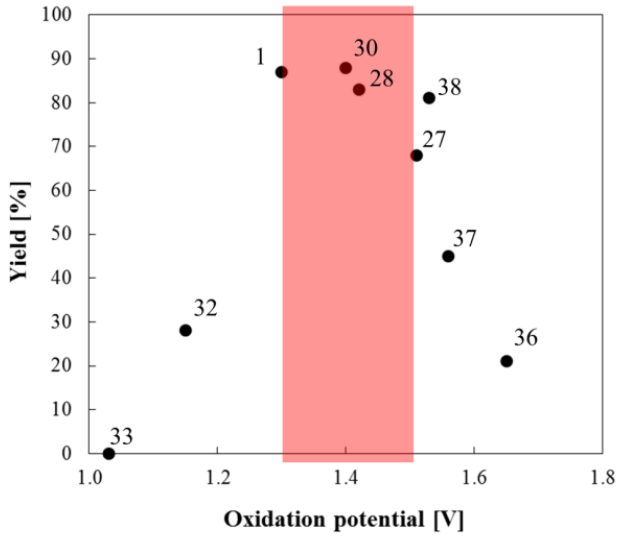

Fig. 4-6 Relationship between Oxidation Potential of Substrate and Product Yield.

From Fig. 4-6, it was found that when the oxidation potential of the substrate was between about 1.3-1.5 V, the yield of the desired product was more than 80%. In other words, if the oxidation potential could be tuned between 1.3-1.5 V, the reaction would proceed smoothly. By measuring the oxidation potential before carrying out the reaction, it would be possible to predict how much the reaction would proceed. Analysis of the electron transfer process combined with experimental results, CV measurement and DFT calculations would help to design new reactions.

4.4. Summary

In this chapter, the establishment of radical cation reaction system using TiO_2 photocatalyst and the analysis of the inter/intramolecular electron transfer processes were worked on.

By using TiO_2 photocatalyst and nitromethane / lithium perchlorate system, the reaction between electron-rich enol ether and olefin was promoted. In addition, four-membered ring skeleton that could not be synthesized in one step by the classical synthesis method was constructed by using TiO_2 photocatalysis. It is considered that TiO_2 photocatalyst would become the powerful oxidation and reduction option to build C-C bond in radical cation reaction system. In particular, when a substrate having an electron donating group was used in the reaction, a four-membered ring was formed. However, when a substrate having no substituent was used, a four-membered ring was not formed. This is because the intramolecular electron transfer from the aromatic ring to the four-membered ring was not occurred smoothly. In addition, since the position and number of substituents have a great influence on the formation of a four-membered ring, it was found that the substituent of the aromatic ring is significantly important for obtaining the desired product.

Regarding the electron transfer process of the reaction, analysis by CV measurements and DFT calculations in addition to experimental results have made it possible to understand more reasonably. A deep understanding of electron transfer could be expected to lead to the development of new molecular designs and new reactions.

4.5. References

[31] Fujishima, A.; Honda, K. Electrochemical Photolysis of Water at a Semiconductor Electrode. *Nature* **1972**, *238*, 37–38.

[32] (a) Hodgson, G. K.; Scaiano, J. C. Heterogeneous Dual Photoredox-Lewis Acid Catalysis Using a Single Bifunctional Nanomaterial. *ACS Catal.* **2018**, *8*, 2914−2922. (b) Pitre, S. P.; Scaiano, J. C.; Yoon, T. P. Photocatalytic Indole Diels–Alder Cycloadditions Mediated by Heterogeneous Platinum-Modified Titanium Dioxide. *ACS Catal.* **2017**, *7*, 6440–6444. (c) Pitre, S. P.; Yoon, T. P.; Scaiano, J. C. Titanium Dioxide Visible Light Photocatalysis: Surface Association Enables Photocatalysis with Visible Light Irradiation. *Chem. Commun.* **2017**, *53*, 4335–4338. (d) Zoller, J.; Fabry, D. C.; Rueping, M. Unexpected Dual Role of Titanium Dioxide in the Visible Light Heterogeneous Catalyzed C−H Arylation of Heteroarenes. *ACS Catal.* **2015**, *5*, 3900–3904. (e) Vila, C.; Rueping, M. Visible-light mediated heterogeneous C–H functionalization: oxidative multi-component reactions using a recyclable titanium dioxide (TiO_2) catalyst. *Green Chem.* **2013**, *15*, 2056−2059. (f) Manley, D. W.; McBurney, R. T.; Miller, P.; Walton, J. C. Titania-Promoted Carboxylic Acid Alkylations of Alkenes and Cascade Addition−Cyclizations. *J. Org. Chem.* **2014**, *79*, 1386−1398.

[33] Liu, Y.; Zhang, M.; Tung, C.-H.; Wang, Y. TiO_2 Photocatalytic Cyclization Reactions for the Syntheses of Aryltetralones. *ACS Catal.* **2016**, *6*, 8389–8394.

[34] (a) Okada, Y.; Yamaguchi, Y.; Chiba, K. Substitution Pattern-Selective Olefin Cross-Couplings.

ChemElectroChem **2019**, *6*, 4165−4168. (b) Okada, Y.; Yamaguchi, Y.; Ozaki, A.; Chiba, K. Aromatic "Redox Tag"-Assisted Diels−Alder Reactions by Electrocatalysis. *Chem. Sci.* **2016**, *7*, 6387−6393. (c) Yamaguchi, Y.; Okada, Y.; Chiba, K. Understanding the Reactivity of Enol Ether Radical Cations: Investigation of Anodic Four-Membered Carbon Ring Formation. *J. Org. Chem*. **2013**, *78*, 2626−2638. (d) Okada, Y.; Nishimoto, A.; Akaba, R.; Chiba, K. Electron-Transfer-Induced Intermolecular [2 + 2] Cycloaddition Reactions Based on the Aromatic "Redox Tag" Strategy. *J. Org. Chem.* **2011**, *76*, 3470−3476. (e) Okada, Y.; Akaba, R.; Chiba, K. Electrocatalytic Formal [2 + 2] Cycloaddition Reactions between Anodically Activated Aliphatic Enol Ethers and Unactivated Olefins Possessing an Alkoxyphenyl Group. *Org. Lett.* **2009**, *11*, 1033−1035.

[35] Imada, Y.; Yamaguchi, Y.; Shida, N.; Okada, Y.; Chiba, K. Entropic Electrolytes for Anodic Cycloadditions of Unactivated Alkene Nucleophiles. *Chem. Commun.* **2017**, *53*, 3960−3963.

[36] (a) Shida, N.; Imada, Y.; Nagahara, S.; Okada, Y.; Chiba, K. Interplay of Arene Radical Cations with Anions and Fluorinated Alcohols in Hole Catalysis. *Comm. Chem.* **2019**, *2*, Article number: 24, (b) Farney, E. P.; Chapman, S. J.; Swords, W. B.; Torelli, M. D.; Hamers, R. J.; Yoon, T. P. Discovery and Elucidation of Counteranion Dependence in Photoredox Catalysis. *J. Am. Chem. Soc.* **2019**, *141*, 6385-6391.

[37] Nakayama, K.; Maeta, N.; Horiguchi, G.; Kamiya, H.; Okada, Y. Radical Cation Diels−Alder Reactions by TiO_2 Photocatalysis. *Org. Lett.* **2019**, *21*, 2246−2250.

Chapter 5
Probing Intramolecular Electron Transfer in [2 + 2] Cycloaddition Reaction

5.1. Introduction

In the radical reaction, Complex electron exchanges cause chain reactions that break down or build molecules. Therefore, it is difficult to understand bond breaking and bond formation mechanisms in radical reactions compared to ion reactions. Single electron transfer between molecules is due to a simple redox process and is not difficult to understand. On the other hand, intramolecular single electron transfer is very important and complicated for understanding the reaction mechanism. In particular, understanding where and how the electrons have transferred in a molecule is an important clue in designing the reaction. However, the understanding the reaction mechanism with single electron transfer has relied on empirical rules and has not been well understood so far.

In recent years, not only the electron transfer in a molecule but also between particle and molecule has been worked experimentally. [38] This result would significantly assist the construction of the electron transfer reaction systems using nanoparticles, and might be a guide for designing the interface of nanoparticles (Fig. 5-1).

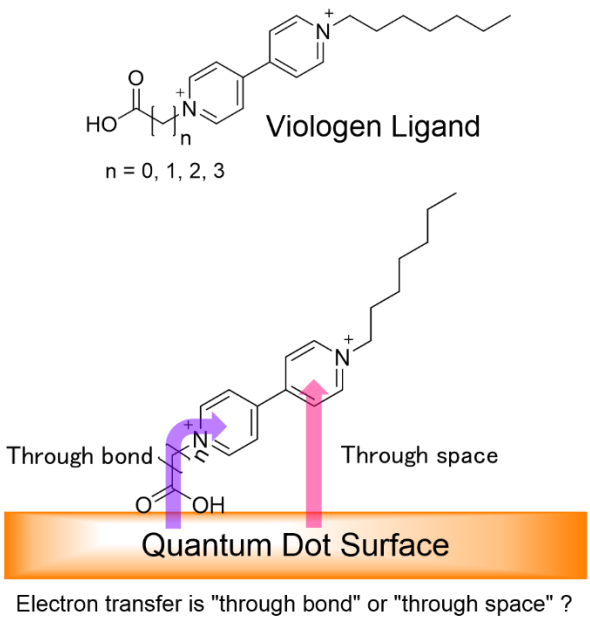

Fig. 5-1 Electron Transfer between Quantum Dot and Molecule.

The purpose of this work is to rationally understand intramolecular electron transfer by experimental results and DFT calculations using [2 + 2] cycloaddition reaction as a model. By detailed electron transfer analysis, it is possible to know how intramolecular electron transfer is determined. The results of this work could be expected to lead to a deeper and rational understanding of the reaction mechanism in single electron transfer reactions and to assist in the design of new molecules.

5.2. Experimental Procedure

General Remarks

All reagents and solvents were purchased from commercial sources and used without further purification. Reactions were monitored by thin-layer chromatography (TLC) carried out on silica gel plates, with detection by UV absorption (254 nm) and by heating the plates after dipping them in a solution of 12 M molybdo(VI) phosphoric acid n-hydrate in 95% ethanol. Silica gel (particle size 40−50 μm) was used for column chromatography. ^{1}H NMR spectra were collected on a 500 MHz NMR spectrometer using the deuterated solvent as an internal deuterium reference. Chemical shift data are given in δ units calibrated with residual protic solvent. The multiplicity of a signal is indicated as follows: s, singlet; d, doublet; t, triplet; q, quartet; quint, quintet; m, multiplet. ^{13}C NMR spectra were collected at 125 MHz with proton decoupling using the deuterated solvent as an internal carbon reference. Chemical shift data are given in δ units calibrated with residual solvent. High-resolution mass spectra (HRMS) were collected on electrospray ionization (ESI)-or direct analysis in real time (DART)-time-of-flight (TOF) spectrometers. Structure optimizations of all stationary points and frequency analyses were carried out at the B3LYP level of density functional theory (DFT) with the 6-311G++(2d,2p) basis set in nitromethane (PCM model). No imaginary frequency was observed for all compounds. Calculations of the radical cations (**3**$^{\bullet+}$, **10**$^{\bullet+}$, **12**$^{\bullet+}$, **15**$^{\bullet+}$, **16**$^{\bullet+}$, **18**$^{\bullet+}$) were carried out with a methyl group instead of the *n*-butyl group for simplification.

Synthesis and Characterization Data

General Procedure for the Synthesis of Enol Ethers (6-9)

The enol ethers were synthesized from the respective carboxylic acids or aldehydes according to chapter 4.

General Procedure for the TiO_2 Photocatalytic Reactions

To a solution of $LiClO_4$ (1.0 M) in CH_3NO_2 (4 mL) stirred at room temperature were added the respective enol ethers (0.20 mmol) and 1-hexene (503 μL, 4.0 mmol). The resulting reaction mixture was stirred at room temperature in front of a 15 W UV lamp (365 nm) until the starting material was consumed (checked by TLC), diluted with water, and extracted with EtOAc. The combined organic layers were dried over Na_2SO_4, filtered, and concentrated in vacuo. Yields reported in the manuscript were determined by ^{1}H NMR analysis. Unless otherwise stated, silica gel column chromatography was carried out on 0.40 mmol scale (2 batches of the reactions) using Hex/EtOAc = 50/1 as an eluent.

Theoretical Calculations

Structure optimizations of all stationary points and frequency analyses were carried out at the B3LYP level of density functional theory (DFT) with the 6-311++G(2d,2p) basis set in nitromethane (PCM model). No imaginary frequency was observed for all compounds.

5.3. Results and Discussion

5.3.1. Effect of Linker Length on Product Structure and DFT Calculation of Four-membered Products

In this work, the electron transfer process was analyzed in more detail using the [2 + 2] cycloaddition reaction between enol ether and olefin as a model. The electron transfer process of four-membered ring forming reaction and metathesis reaction is shown below (Scheme 5-1).

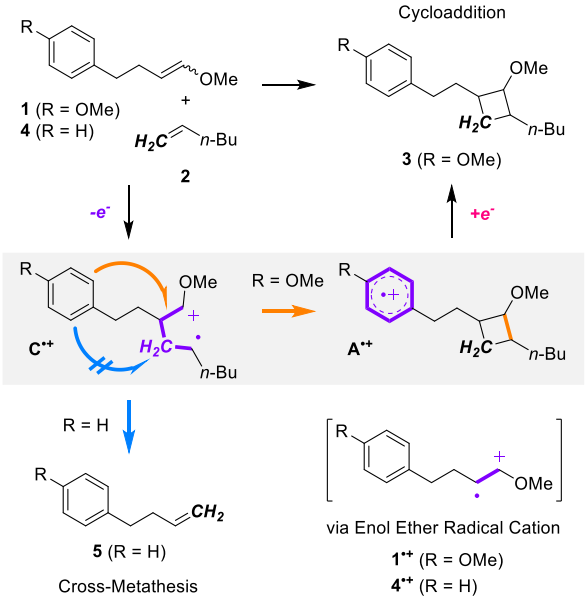

Scheme 5-1 Electron Transfer Process in Cycloaddition *vs* Cross Metathesis.

As described in Chapter 4, when the enol ether has an appropriate electron donating group (R = MeO), the four-membered ring forming reaction proceeded. Moreover, when enol ether has no substituent (R = H), the metathesis reaction proceeded. Which reaction proceeds is mainly related to the rate of intramolecular electron transfer and the thermodynamic stability of the radical cation intermediate. Therefore, the effect of linker length on the product was investigated. The molecular structure of substrate and the product yield after reaction are shown in Fig. 5-2 and Table 5-1.

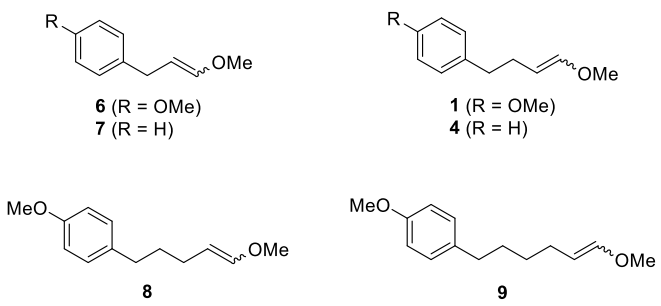

Fig. 5-2 Designed and Synthesized Substrates with Different Linker Length.

Table 5-1　Reaction Using Substrates with Different Linker Length.

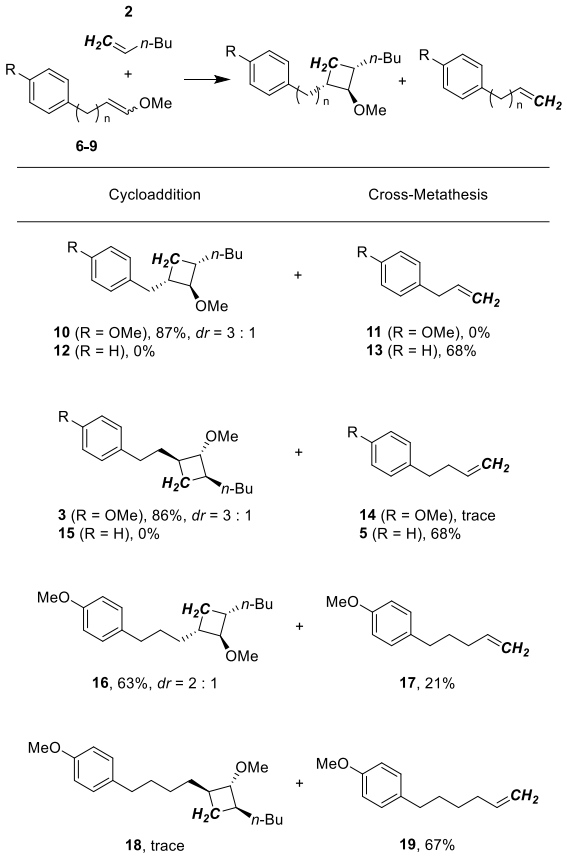

[a]Reactions were carried out on a 0.20 mmol scale of the enol ethers (**6-9**) with 20 equiv of 1-hexene (**2**) and 100 mg TiO_2 in 4 mL of 1.0 M $LiClO_4/CH_3NO_2$ using a 15 W UV lamp (365 nm) at rt for 30 min under air.

First, as shown in Fig. 5-2 and Table 5-1, when substrate 6 having a MeO group and short linker length (n = 1) was used, four-membered ring forming reaction proceeded in the yield of 87%. On the other hand, when the substrate 7 having no MeO group and short linker length (n = 1) was used, the metathesis reaction proceeded in the yield of 68%. These results showed that the same results as the linker length (n = 2) described in chapter 4. Therefore, the electron transfer from aromatic ring to four-membered ring was not occurred smoothly by shortening the linker length (substrates 7 and 12). The DFT calculations for the reaction products $10^{\bullet+}$ and $12^{\bullet+}$ with short linker length were shown below (Fig. 5-3).

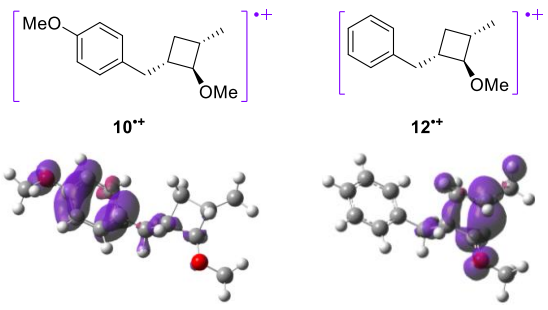

Fig. 5-3　DFT Calculation of Shorter Linker Four-membered Products.

From Fig. 5-3, the spin density of the radical cation 10 $^{\bullet+}$ was localized on the aromatic ring. On the other hand, the spin density of the radical cation 12$^{\bullet+}$ was localized on the four-membered ring and the bond was not closed. This DFT calculations corresponded well with the results of Scheme 4-6 in Chapter 4. It was suggested that the reaction using a substrate with short linker length was dominated by thermodynamic stability rather than the rate of intramolecular electron transfer.

Next, substrates 8 and 9 having longer linker length were used in the reaction. When using the substrate 8 (n = 3), the yield of the four-membered ring product 16 was 63% and the metathesis product 17 was 21%. It was found that both a four-membered ring product and a metathesis product were obtained. Furthermore, when using the substrate 9 (n = 4), the metathesis product 19 was 67% and the 4-membered ring product 18 was hardly obtained. It was found that the electron transfer in the molecule was not smoothly occurred as the linker length became longer, and the metathesis reaction was prioritized over the four-membered ring forming reaction. DFT calculations of radical cation 16 $^{\bullet+}$ and 18 $^{\bullet+}$ with long linker were shown below in Fig. 5-4.

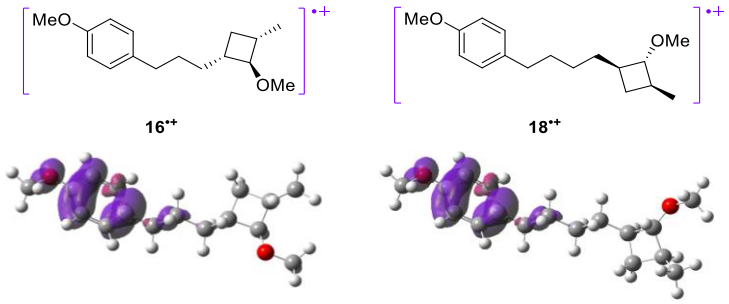

Fig. 5-4 DFT Calculation of Longer Linker Four-membered Products.

Fig. 5-4 shows that the spin densities of the four-membered ring products 16 $^{\bullet+}$ and 18 $^{\bullet+}$ are both localized on the aromatic ring. From above, the localization of spin density on the aromatic ring showed that the single electron transfer from the aromatic ring to the four-membered ring proceeded, and the four-membered ring was formed. However, the experimental results showed that the electron transfer from the aromatic ring to four-membered ring did not proceed, and the results of DFT calculations did not correspond to the experimental results.

The results of DFT calculations just show quantum stability and do not consider the rate of electron transfer. On the other hand, the experimental results take into consideration both the quantum stability and the rate of electron transfer. In other words, the experimental results seem to support the fact that the bond breaking proceeded preferentially over the four-membered ring formation due to kinetic control.

5.3.2. Analysis of Intramolecular Electron Transfer by Using Rigid and Flexible Linker Substrate

Herein, a question was raised about how intramolecular electron transfer proceeds in this reaction. Therefore, a new molecular design was attempted to investigate whether the electron transfer was through bond or through space (Fig. 5-5).

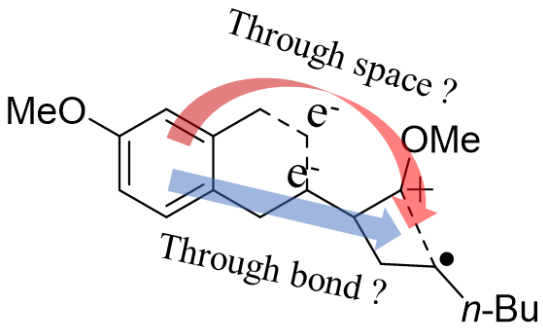

Fig. 5-5 Electron Transfer Processes from Aromatic Ring to Cyclobutyl Radical Cation.

To obtain further insight into the intramolecular SET mechanism, enol ethers (20-23) were synthesized (Fig. 5-6).

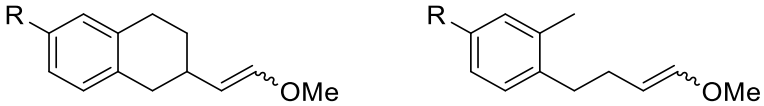

20 (R = OMe)
22 (R = H)

21 (R = OMe)
23 (R = H)

Fig. 5-6 Enol Ether with Rigid or Flexible Linker.

Enol ethers (20, 22) have a rigid linker, and the aromatic ring and enol ether moiety are inaccessible to each other. As controls, the enol ether (21, 23) were synthesized to have a flexible linker with an aromatic ring of the same electron density as the enol ether (20, 22). The reaction of enol ether (20-23) and 1-hexene (2) were summarized (Scheme 5-2).

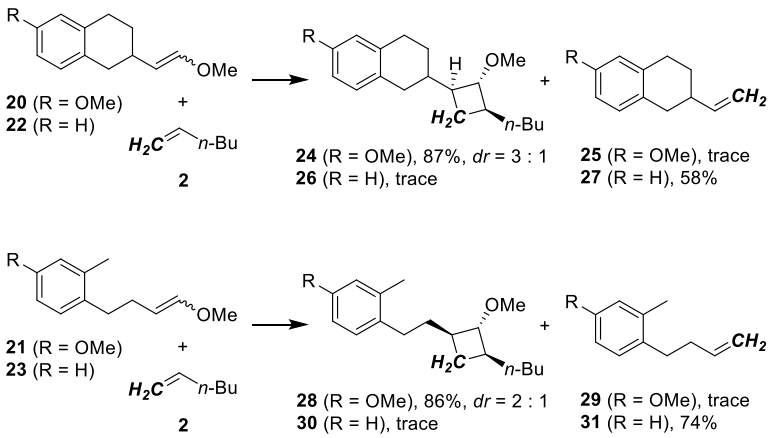

Scheme 5-2　Reactions of Enol Ether with Rigid or Flexible Linker *vs* Olefin.

Enol ethers with methoxyphenyl rings (20, 21) selectively gave cycloadducts (24, 28), but almost no metathesis products (25, 29) were obtained. On the other hand, when enol ether (22, 23) having no methoxy group was used instead, cross-metathesis took place selectively and almost no cycloaddition occurred. These results showed that intramolecular SET from the methoxyphenyl ring to the cyclobutyl radical cation is indeed important for ring closure. In addition, it was suggested that the flexibility of the linker connecting the electron donor (methoxyphenyl ring) and the electron acceptor (cyclobutyl radical cation) has almost no impact on the effectiveness of intramolecular SET. Taken together, it could be said that intramolecular SET can occur not only through space but also through bonding.

A correct and deep understanding of electron transfer is very important for the use of radicals and radical ions. These results would be useful for designing new molecules and constructing reaction systems.

5.4. Summary

In this chapter, rational and deep understanding of intramolecular electron transfer by experimental results and DFT calculations using [2 + 2] cycloaddition reaction as a model was worked on.

By the approach that combined experimental results and DFT calculations, the electron transfer in the [2 + 2] cycloaddition reaction was analyzed in more detail using the synthetic outcome as a probe. In addition, Whether the synthetic outcome was due to the rate of electron transfer and/or thermodynamic stability was investigated. In the reaction using short linker substrate, the experimental results and the DFT calculation corresponded well, suggesting that the reaction depends on thermodynamic stability. On the other hand, in the reaction using substrate with long linker, the experimental results and the DFT calculation results did not correspond, suggesting that the reaction depends on the rate of electron transfer rather than thermodynamic stability.

A deep understanding of electron transfer could be expected to lead to the development of new molecular designs and new reaction systems. In addition, the establishment of the radical ion reaction systems using nanoparticle photocatalyst would opened up a new path for organic reactions.

5.5. References

[38] Knowles, K. E.; Peterson, M. D.; McPhail, M. R.; Weiss, E. A. Exciton Dissociation within Quantum Dot-Organic Complexes: Mechanisms, Use as a Probe of Interfacial Structure, and Application. *J. Phys. Chem. C* **2013**, *117*, 10229-10243.

Chapter 6
Conclusion

6. Conclusion

In this research, “design of nanoparticle interface” and “development of radical ion reaction using nanoparticles” for the establishment of radical ion reaction system using nanoparticle catalyst were worked on.

In chapter 2, some small amphiphilic ligands were designed and synthesized for the preparation of TiO_2 nanoparticles with flexible dispersibility in various solvents, and the relationship between nanoparticle dispersibility and ligand structure was investigated. From experimental results, it was found that the nanoparticle dispersion in the solvent could not be determined simply by the hydrophobicity and hydrophilicity of the ligand. Moreover, it was found that the length of the hydrophobic/hydrophilic chain and the balance between the hydrophobicity and the hydrophilicity were important for the dispersion of nanoparticle-ligand complex. In addition, it was found that slight differences in ligand structure greatly affect the dispersibility of nanoparticles. Therefore, “sensitive molecular design” would be required for preparation of nanoparticles with flexible dispersibility in various solvents.

In chapter 3, the influence of the difference between particle type and bonding group on the dispersibility of Ag nanoparticles by modifying amine ligands with the same structure as used in chapter 2 was investigated. From experimental results, it was found that the balance between the hydrophobicity and hydrophilicity of the ligand is important for dispersibility in organic solvents as well as TiO_2 nanoparticles. In addition, the slight difference in the ligand structure also greatly affected the dispersibility of Ag nanoparticles. On the other hand, when C8EG1 and C8EG2 ligands with the same molecular structure were modified on TiO_2 nanoparticles and Ag nanoparticles, the dispersibility of the nanoparticles was significantly different. This is due to the difference in the “surface structure” between TiO_2 nanoparticles with hydrophilic OH groups on the particle surface and Ag nanoparticles without hydrophilic OH groups. In addition, it was suggested that the difference in the “binding group” between the phosphonic acid and the primary amine bound to the particle surface would affect the dispersibility of the nanoparticle.

In chapter 4, the establishment of radical cation reaction system using TiO_2 photocatalyst was worked on. In addition, the intermolecular and intramolecular electron transfer processes were analyzed by experimental and computational chemistry approach. From experimental results, the reaction of electron-rich enol ether and olefin was promoted by using TiO_2 photocatalyst and nitromethane / lithium perchlorate system. Therefore, it was suggested that TiO_2 photocatalyst would become the powerful oxidation and reduction option to build C-C bond in radical cation reaction systems. A four-membered ring was formed when the substrate having electron donating group was used in the reaction. On the other hand, a four-membered ring was not formed when the substrate having no substituent was used. It was suggested by DFT calculations that the intramolecular electron transfer from the aromatic ring to the

four-membered ring is important for four-membered ring formation. Regarding the electron transfer process of the reaction, analysis by CV measurements and DFT calculations in addition to experimental results have made it possible to understand more reasonably.

In chapter 5, rational and deep understanding of intramolecular electron transfer by experimental results and DFT calculations using [2 + 2] cycloaddition reaction as a model was worked on. By the approach that combined experimental results and DFT calculations, the electron transfer in the [2 + 2] cycloaddition reaction was analyzed in more detail using the synthetic outcome as a probe. In addition, Whether the synthetic outcome was due to the rate of electron transfer and/or thermodynamic stability was investigated. From experimental results, the experimental results and the DFT calculation corresponded well when using short linker substrate, suggesting that the reaction depends on thermodynamic stability. On the other hand, the experimental results and the DFT calculation results did not correspond when using long linker substrate, suggesting that the reaction depends on the rate of electron transfer rather than thermodynamic stability.

The results of this research strongly promote the establishment of reaction systems using nanoparticle photocatalysts. It could be expected to contribute to the achievement of new molecular transformations using nanoparticle interfaces as a new reaction field and the construction of environmentally friendly and sustainable chemical processes. The preparation of nanoparticles with flexible dispersibility in various solvents would be significantly related not only to the use of catalysts, but also to applications as nanocomposites and drug delivery. In addition, the construction of radical ion reaction systems using nanoparticles and the analysis of electron transfer processes would provide the new insights in the field of organic synthesis.

Chapter 7
Acknowlegdement

7. Acknowledgement

Many people thank you for proceeding with this research. First, Prof. Kamiya advised me on setting research themes and making presentations that would be easy for anyone to listen to. Next, Assistant Prof. Okada taught me the fun of chemistry. I am very grateful that I have been given various opportunities to think about my growth as a researcher. I feel like a moment from the launch of the theme of organic synthesis to the present, because there have been too many events in the laboratory for five years. It was a very fulfilling day. In addition, Prof. Ogino, Prof. Quan, Prof. Tominaga, Associate Prof. Nakata, and Associate Prof. Akai taught me how to develop a logical story in compiling a doctoral thesis. Finally, my family and lab members were mentally supported in various situations. Thank you very much.

Chapter 8
Publications

8. Publications

(1) Okada, Y.; Ishikawa, K.; Maeta, N.; Kamiya, H. Understanding the Colloidal Stability of Nanoparticle-Ligand Complexes: Design, Synthesis, and Structure-Function Relationship Studies of Amphiphilic Small-Molecule Ligands. *Chem. Eur. J.* **2018**, *24*, 1853-1858. (Chapter 2)

(2) Maeta, N.; Kamiya, H.; Okada, Y. Direct Monitoring of Molecular Events at the Surface: One-Step Access to Flexibly Stable Colloidal Ag Nanoparticles. *Langmuir* **2018**, *34*, 5495-5504. (Chapter 3)

(3) Okada, Y.; Maeta, N.; Nakayama, K.; Kamiya, H. TiO_2 Photocatalysis in Aromatic "Redox Tag"-Guided Intermolecular Formal [2+2] Cycloadditions. *J. Org. Chem.* **2018**, *83*, 4948-4962. (Chapter 4)

(4) Maeta, N.; Kamiya, H.; Okada, Y. Probing Intramolecular Electron Transfer in Redox Tag Processes. *Org. Lett.* **2019**, 21, 8519-8522. (Chapter 5)

Chapter 9
Supporting Information

9. Supporting Information

9.1. NMR and Mass Information in Chapter 2

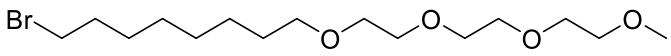

S1

^{1}H-NMR (500 MHz, $CDCl_3$) δ 3.66 (8H, m), 3.58 (2H, m), 3.55 (2H, m), 3.45 (2H, t, *J* = 6.8 Hz), 3.41 (2H, t, *J* = 7.0 Hz), 3.38 (3H, s), 1.85 (2H, quin, *J* = 7.2 Hz), 1.58 (2H, m), 1.42 (2H, quin, *J* = 6.8 Hz), 1.32 (6H, m); ^{13}C-NMR (125 MHz, $CDCl_3$) δ 71.9, 71.4, 70.6, 70.6, 70.6, 70.5, 70.0, 59.0, 34.0, 32.8, 29.6, 29.2, 28.7, 28.1, 26.0; HRMS $[M + Na]^+$ calculated for $C_{15}H_{31}O_4BrNa$ 377.1303, found 377.1289.

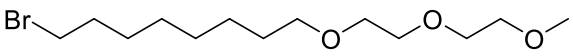

S2

^{1}H-NMR (500 MHz, $CDCl_3$) δ 3.65 (4H, m), 3.60 (2H, m), 3.56 (2H, m), 3.45 (2H, t, *J* = 6.7 Hz), 3.41 (2H, t, *J* = 6.9 Hz), 3.39 (3H, s), 1.85 (2H, quin, *J* = 7.3 Hz), 1.57 (2H, m), 1.42 (2H, quin, *J* = 6.8 Hz), 1.32 (6H, m); ^{13}C-NMR (125 MHz, $CDCl_3$) δ 72.0, 71.4, 70.7, 70.5, 70.1, 59.1, 34.0, 32.8, 29.6, 29.3, 28.7, 28.1, 26.0; HRMS $[M + Na]^+$ calculated for $C_{13}H_{27}O_3BrNa$ 333.1041, found 333.1069.

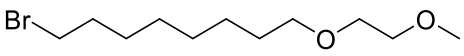

S3

^{1}H-NMR (500 MHz, $CDCl_3$) δ 3.58 (2H, m), 3.54 (2H, m), 3.46 (2H, t, *J* = 6.6 Hz), 3.41 (2H, t, *J* = 6.9 Hz), 3.39 (3H, s), 1.85 (2H, quin, *J* = 7.2 Hz), 1.60 (2H, m), 1.42 (2H, quin, *J* = 7.0 Hz), 1.32 (6H, m); ^{13}C-NMR (125 MHz, $CDCl_3$) δ 71.9, 71.4, 69.9, 59.0, 33.8, 32.7, 29.5, 29.2, 28.6, 28.0, 25.9; HRMS $[M + Na]^+$ calculated for $C_{11}H_{23}O_2BrNa$ 289.0779, found 289.0870.

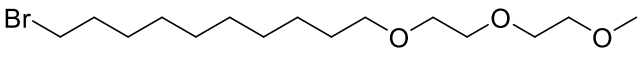

S4

^{1}H NMR (500 MHz, $CDCl_3$) δ 3.65 (4H, m), 3.60 (2H, m), 3.56 (2H, m), 3.45 (2H, t, *J* = 6.7 Hz), 3.41 (2H, t, *J* = 7.0 Hz), 3.38 (3H, s), 1.85 (2H, quint, *J* = 7.5 Hz), 1.58 (2H, m), 1.42 (2H, m), 1.29 (10H, m); ^{13}C NMR δ 72.0, 71.5, 70.7, 70.5, 70.0, 59.0, 34.0, 32.8, 29.6, 29.5, 29.4, 29.4, 28.8 ,28.2, 26.1; HRMS $[M + Na]^+$ calculated for $C_{15}H_{31}O_3BrNa$ 361.1354, found 361.1371.

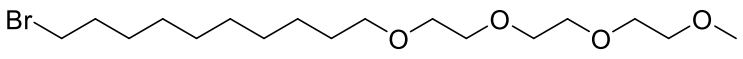

S5

^{1}H-NMR (500 MHz, $CDCl_3$) δ 3.66 (8H, m), 3.58 (2H, m), 3.55 (2H, m), 3.45 (2H, t, *J* = 6.9 Hz), 3.41 (2H, t, *J* = 6.9 Hz), 3.38 (3H, s), 1.85 (2H, quin, *J* = 7.3 Hz), 1.57 (2H, quin, *J* = 7.3 Hz), 1.42 (2H, quin, *J* = 7.4 Hz), 1.29 (10H, m); ^{13}C-NMR (125 MHz, $CDCl_3$) δ 71.8, 71.4, 70.5, 70.5, 70.4, 70.0, 58.9, 33.9, 32.7, 29.5, 29.4, 29.3, 29.3, 28.7, 28.1, 26.0; HRMS $[M + Na]^+$ calculated for $C_{17}H_{35}O_4BrNa$ 405.1616, found 405.1609.

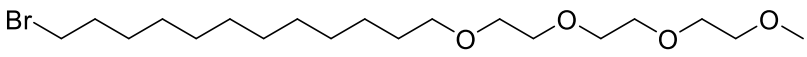

S6

^{1}H-NMR (500 MHz, $CDCl_3$) δ 3.65 (8H, m), 3.58 (2H, m), 3.56 (2H, m), 3.45 (2H, t, *J* = 6.7 Hz), 3.41 (2H, t, *J* = 6.9 Hz), 3.38 (3H, s), 1.85 (2H, quin, *J* = 7.1 Hz), 1.58 (2H, quin, *J* = 6.9 Hz), 1.42 (2H, quin, *J* = 7.1 Hz), 1.27 (14H, m); ^{13}C-NMR (125 MHz, $CDCl_3$) δ 71.8, 71.3, 70.5, 70.5, 70.5, 70.4, 69.9, 58.9, 33.8, 32.8, 29.5, 29.4, 29.4, 29.4, 29.4, 29.3, 28.7, 28.0, 26.0; HRMS $[M + Na]^+$ calculated for $C_{19}H_{39}O_4BrNa$ 433.1929, found 433.1932.

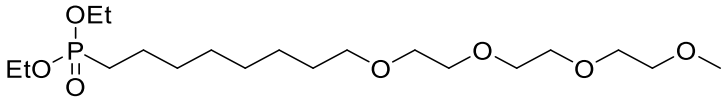

S7

^{1}H-NMR (500 MHz, $CDCl_3$) δ 4.08 (4H, m), 3.65 (8H, m), 3.57 (4H, m), 3.44 (2H, t, *J* = 6.9 Hz), 3.38 (3H, s), 1.72 (2H, m), 1.57 (2H, m), 1.32 (14H, m); ^{13}C-NMR (125 MHz, $CDCl_3$) δ 71.9, 71.4, 70.6, 70.4, 70.0, 61.5, 61.4, 59.0, 30.6, 30.4, 29.5, 29.2, 29.0, 26.2, 26.0, 25.0, 22.3, 16.5, 16.4; HRMS $[M + Na]^+$ calculated for $C_{19}H_{41}O_7PNa$ 435.2488, found 435.2487.

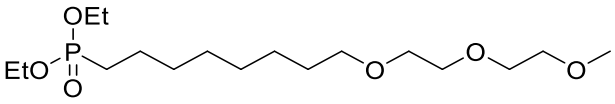

S8

^{1}H-NMR (500 MHz, $CDCl_3$) δ 4.09 (4H, m), 3.65 (4H, m), 3.60 (2H, m), 3.56 (2H, m), 3.45 (2H, t, *J* = 6.9 Hz), 3.39 (3H, s), 1.72 (2H, m), 1.58 (4H, m), 1.32 (14H, m); ^{13}C-NMR (125 MHz, $CDCl_3$) δ 72.1, 71.6, 70.8, 70.7, 70.2, 61.6, 61.5, 59.2, 30.8, 30.7, 29.7, 29.4, 29.2, 26.4, 26.2, 25.3, 22.5, 16.7, 16.6; HRMS $[M + Na]^+$ calculated for $C_{17}H_{37}O_6PNa$ 391.2225, found 391.2239.

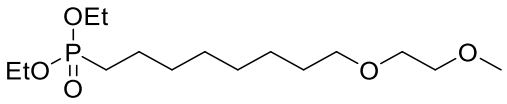

S9

^{1}H-NMR (500 MHz, $CDCl_3$) δ 4.09 (4H, m), 3.57 (2H, m), 3.54 (2H, m), 3.45 (2H, t, *J* = 6.9 Hz), 3.39 (3H, s), 1.71 (2H, m), 1.59 (4H, m), 1.32 (14H, m); ^{13}C-NMR (125 MHz, $CDCl_3$) δ 72.1, 71.7, 70.1, 61.6, 61.5, 59.2, 30.8, 30.6, 29.7, 29.3, 29.2, 26.4, 26.2, 25.2, 22.5, 16.7, 16.6; HRMS $[M + Na]^+$ calculated for $C_{15}H_{33}O_5PNa$ 347.1963, found 347.1974.

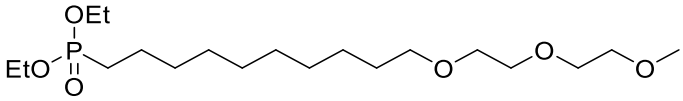

S10

^{1}H-NMR (500 MHz, $CDCl_3$) δ 4.13-4.03 (4H, m), 3.67-3.63 (4H, m), 3.61-3.58 (4H, m), 3.57-3.54 (2H, m), 3.45 (2H, t, *J* = 6.9 Hz), 3.38 (3H, s), 1.78-1.65 (4H, m), 1.63-1.54 (4H, m), 1.40-1.22 (18H, m); ^{13}C-NMR (125 MHz, $CDCl_3$) δ 72.0,71.6, 70.8, 70.6, 70.1, 61.5, 61,4, 59.1, 30.8, 30.6, 29.7, 29.6, 29.5, 29.4, 29.2, 26.3, 26.2, 25.2, 22.5, 16.6; HRMS $[M + Na]^+$ calculated for $C_{19}H_{41}O_6PNa$ 419.2538, found 419.2530.

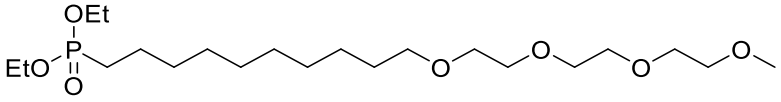

S11

^{1}H-NMR (500 MHz, $CDCl_3$) δ 4.09 (4H, m), 3.66 (8H, m), 3.57 (4H, m), 3.45 (2H, t, *J* = 6.9 Hz), 3.39 (3H, s), 1.73 (2H, m), 1.58 (4H, m), 1.31 (18H, m); ^{13}C-NMR (125 MHz, $CDCl_3$) δ 72.0,71.6, 70.7, 70.6, 70.6, 70.1, 61.5, 61,4, 59.1, 30.7, 30.6, 29.7, 29.5, 29.5, 29.4, 29.1, 26.3, 26.1, 25.2, 22.5, 16.6,16.5; HRMS $[M + Na]^+$ calculated for $C_{21}H_{45}O_7PNa$ 463.2801, found 463.2774.

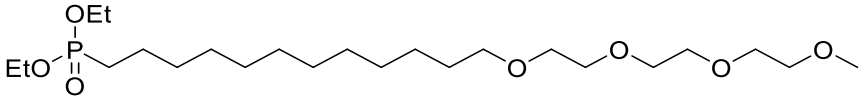

S12

^{1}H-NMR (500 MHz, $CDCl_3$) δ 4.09 (4H, m), 3.65 (8H, m), 3.57 (4H, m), 3.45 (2H, t, *J* = 6.9 Hz), 3.39 (3H, s), 1.72 (2H, m), 1.58 (4H, m), 1.31 (22H, m); ^{13}C-NMR (125 MHz, $CDCl_3$) δ 71.9, 71.5, 70.6, 70.5,70.0, 61.4, 61.3, 59.0, 30.7, 30.5, 29.6, 29.6, 29.5, 29.4, 29.1, 26.2, 26.1, 25.1, 22.4, 16.5, 16.5; HRMS $[M + Na]^+$ calculated for $C_{23}H_{49}O_7PNa$ 491.3114, found 491.3114.

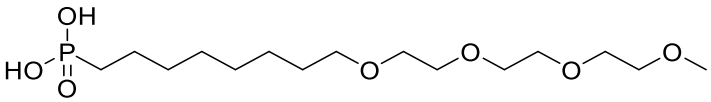

1

^{1}H-NMR (500 MHz, $CDCl_3$) δ 3.66 (8H, m), 3.57 (4H, m), 3.45 (2H, t, *J* = 6.6 Hz), 3.39 (3H, s), 1.73 (2H, m), 1.57 (4H, m), 1.37 (2H, m), 1.30 (6H, m); ^{13}C-NMR (125 MHz, $CDCl_3$) v 72.0, 71.6, 70.7, 70.7, 70.6, 70.5, 70.1, 59.1, 30.6, 30.5, 29.6, 29.2, 29.1, 26.1, 22.4; HRMS $[M + Na]^+$ calculated for $C_{15}H_{33}O_7PNa$ 379.1862, found 379.1847.

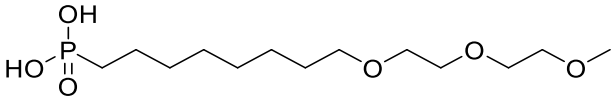

2

^{1}H-NMR (500 MHz, $CDCl_3$) δ 3.65 (4H, m), 3.60 (2H, m), 3.56 (2H, m), 3.45 (2H, t, *J* = 6.8 Hz), 3.39 (3H, s), 1.73 (2H, m), 1.57 (4H, m), 1.31 (8H, m); ^{13}C-NMR (125 MHz, $CDCl_3$) δ 72.1, 71.6, 70.8, 70.6, 70.2, 59.2, 30.6, 30.5, 29.7, 29.3, 29.1, 26.1, 22.3; HRMS $[M + Na]^+$ calculated for $C_{13}H_{29}O_6PNa$ 335.1599, found 335.1621.

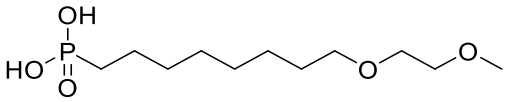

3

^{1}H-NMR (500 MHz, $CDCl_3$) δ 3.58 (2H, m), 3.55 (2H, m), 3.46 (2H, t, *J* = 6.9 Hz), 3.39 (3H, s), 1.73 (2H, m), 1.59 (4H, m), 1.32 (8H, m); ^{13}C-NMR (125 MHz, $CDCl_3$) δ 72.1, 71.7, 70.1, 59.2, 30.6, 30.5, 29.7, 29.3, 29.1, 26.1, 22.2; HRMS $[M + Na]^+$ calculated for $C_{11}H_{25}O_5PNa$ 291.1337, found 291.1349.

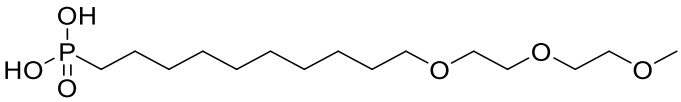

4

^{1}H-NMR (500 MHz, $CDCl_3$) δ 3.68-3.63 (4H, m), 3.62-3.58 (2H, m), 3.58-3.55 (2H, m), 3.45 (2H, t, *J* = 6.9 Hz), 3.39 (3H, s), 1.80-1.68 (2H, m), 1.68-1.53 (4H, m), 1.42-1.20 (12H, m); ^{13}C-NMR (125 MHz, $CDCl_3$) δ 72.0, 71.6, 70.7, 70.6, 70.1, 59.1, 30.6, 30.4, 29.6, 29.5, 29.5, 29.3, 29.1, 26.1, 22.1; HRMS $[M + Na]^+$ calculated for $C_{15}H_{33}O_6PNa$ 363.1912, found 363.1898.

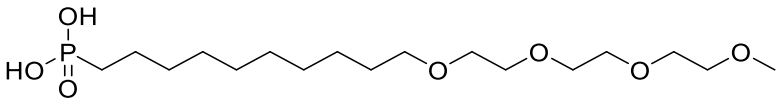

5

^{1}H-NMR (500 MHz, $CDCl_3$) δ 3.65 (8H, m), 3.57 (4H, m), 3.45 (2H, t, *J* = 6.4 Hz), 3.39 (3H, s), 1.73 (2H, m), 1.57 (4H, m), 1.31 (12H, m); ^{13}C-NMR (125 MHz, $CDCl_3$) δ 72.1, 71.7, 70.8, 70.7, 70.6, 70.2, 59.2, 30.7, 30.5, 29.7, 29.6, 29.6, 29.4, 29.2, 26.2, 25.1, 22.2; HRMS $[M + Na]^+$ calculated for $C_{17}H_{37}O_7PNa$ 407.2175, found 407.2151.

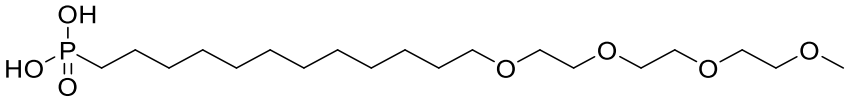

6

^{1}H-NMR (500 MHz, $CDCl_3$) δ 3.66 (8H, m), 3.57 (4H, m), 3.45 (2H, t, *J* = 6.9 Hz), 3.39 (3H, s), 1.73 (2H, m), 1.57 (4H, m), 1.30 (16H, m); ^{13}C-NMR (125 MHz, $CDCl_3$) δ 72.1, 71.7, 70.8, 70.7, 70.6, 70.2, 59.2, 30.7, 30.5, 29.8, 29.7, 29.7, 29.6, 29.5, 29.2, 26.2, 22.2; HRMS $[M + Na]^+$ calculated for $C_{19}H_{41}O_7PNa$ 435.2488, found 435.2491.

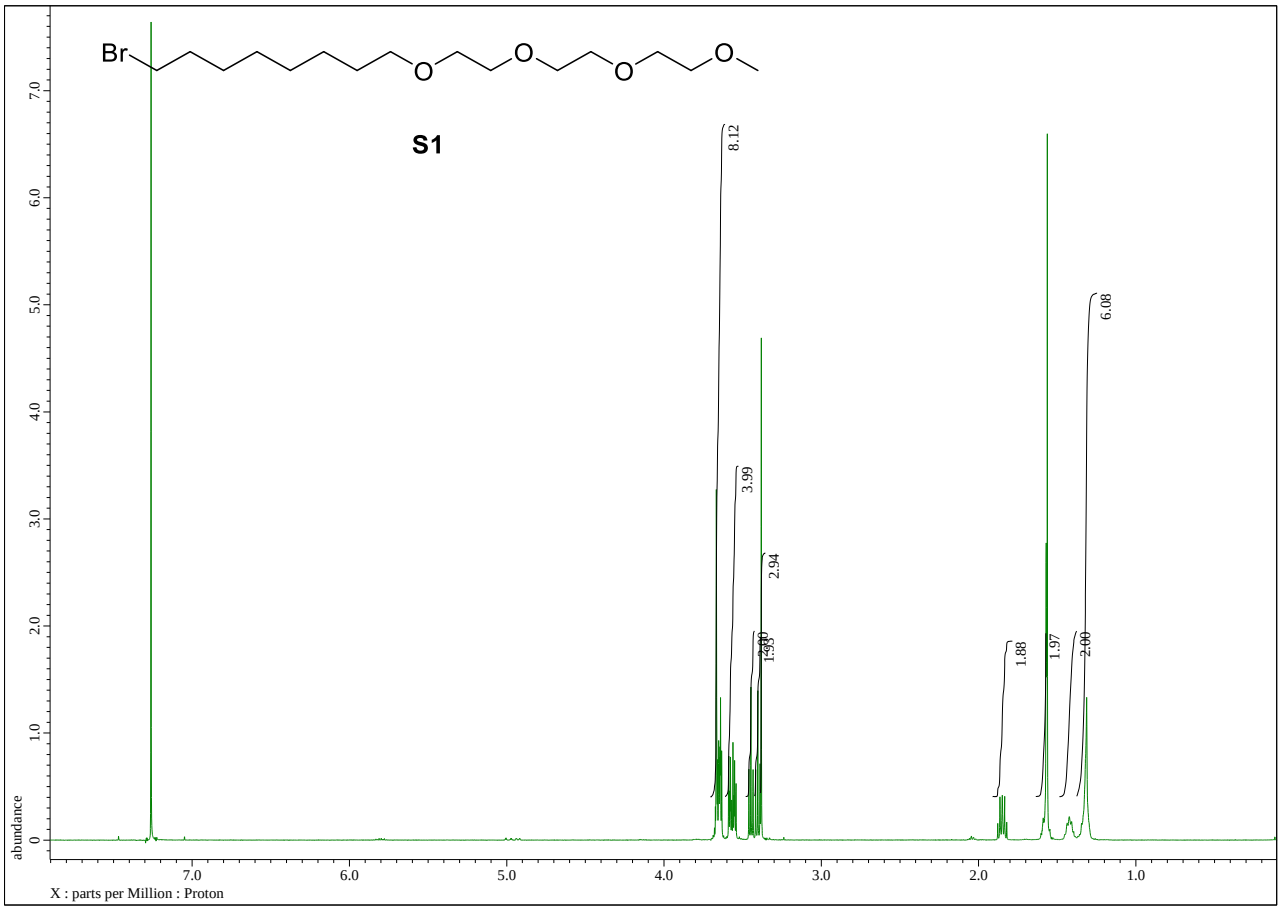
Br
O
O
O
O
S1
8.12
3.99
2.94
1.88
1.97
2.00
6.08
abundance
X : parts per Million : Proton

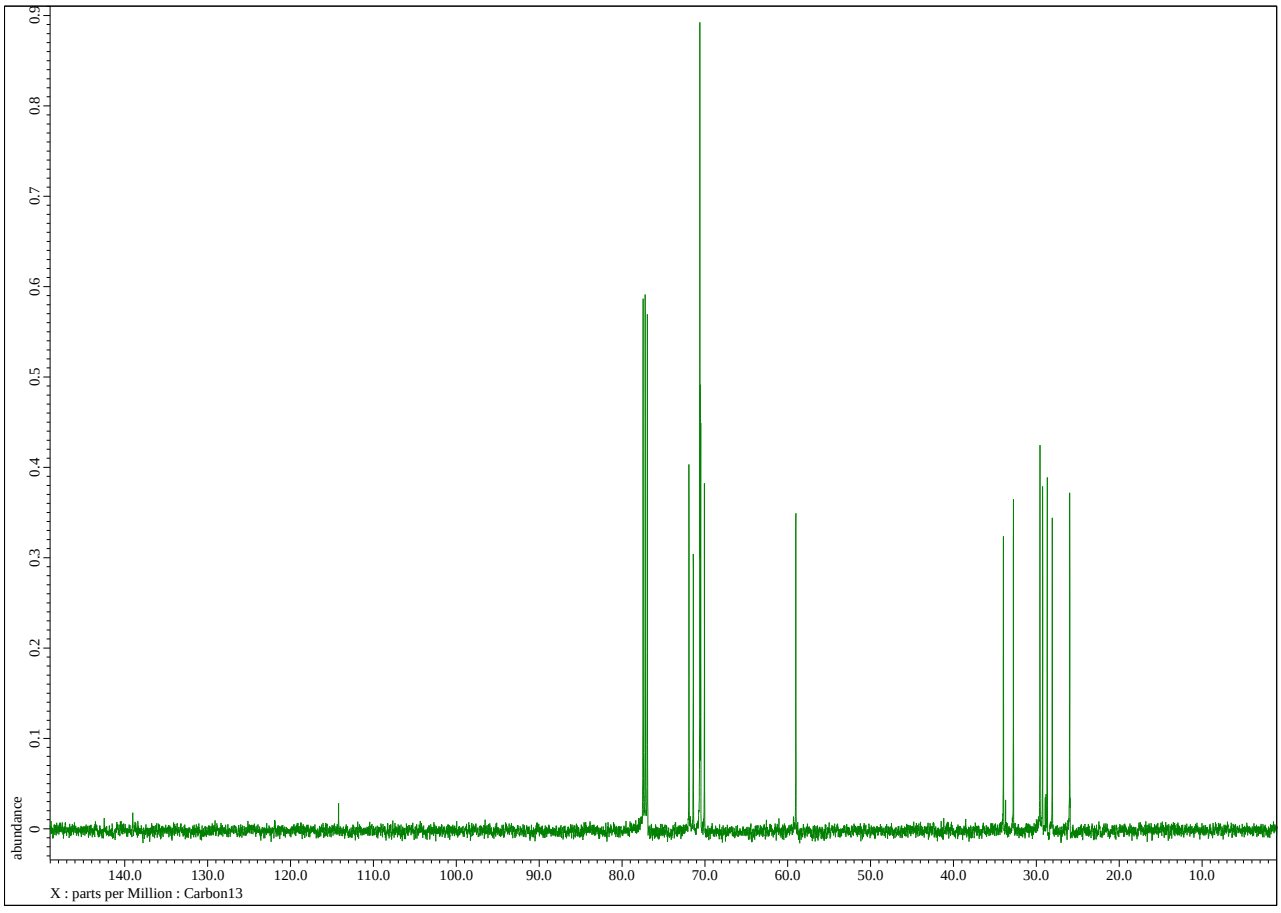
abundance
X : parts per Million : Carbon13

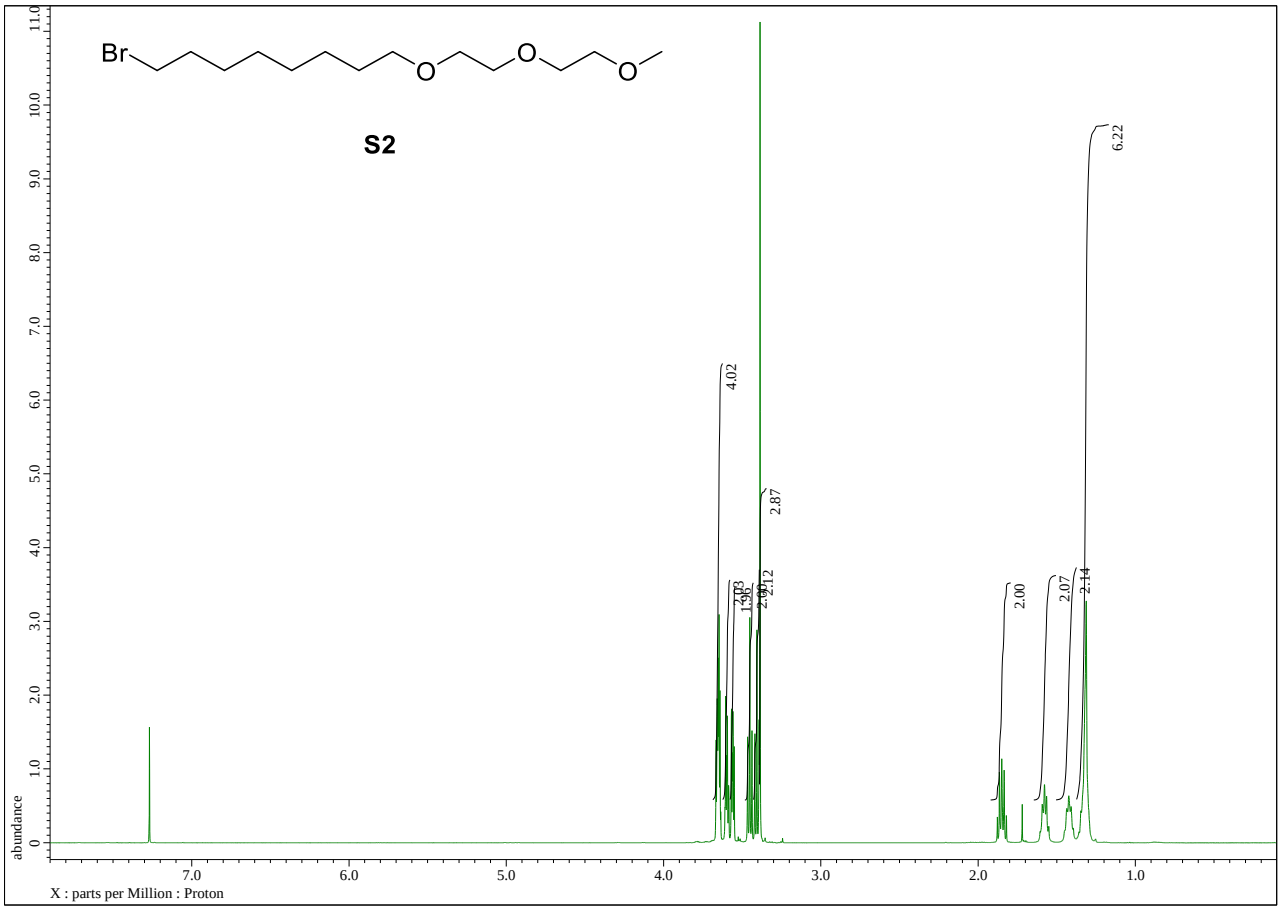
Br
O
O
O
S2
4.02
2.87
2.00
2.07
2.14
6.22
abundance
X : parts per Million : Proton

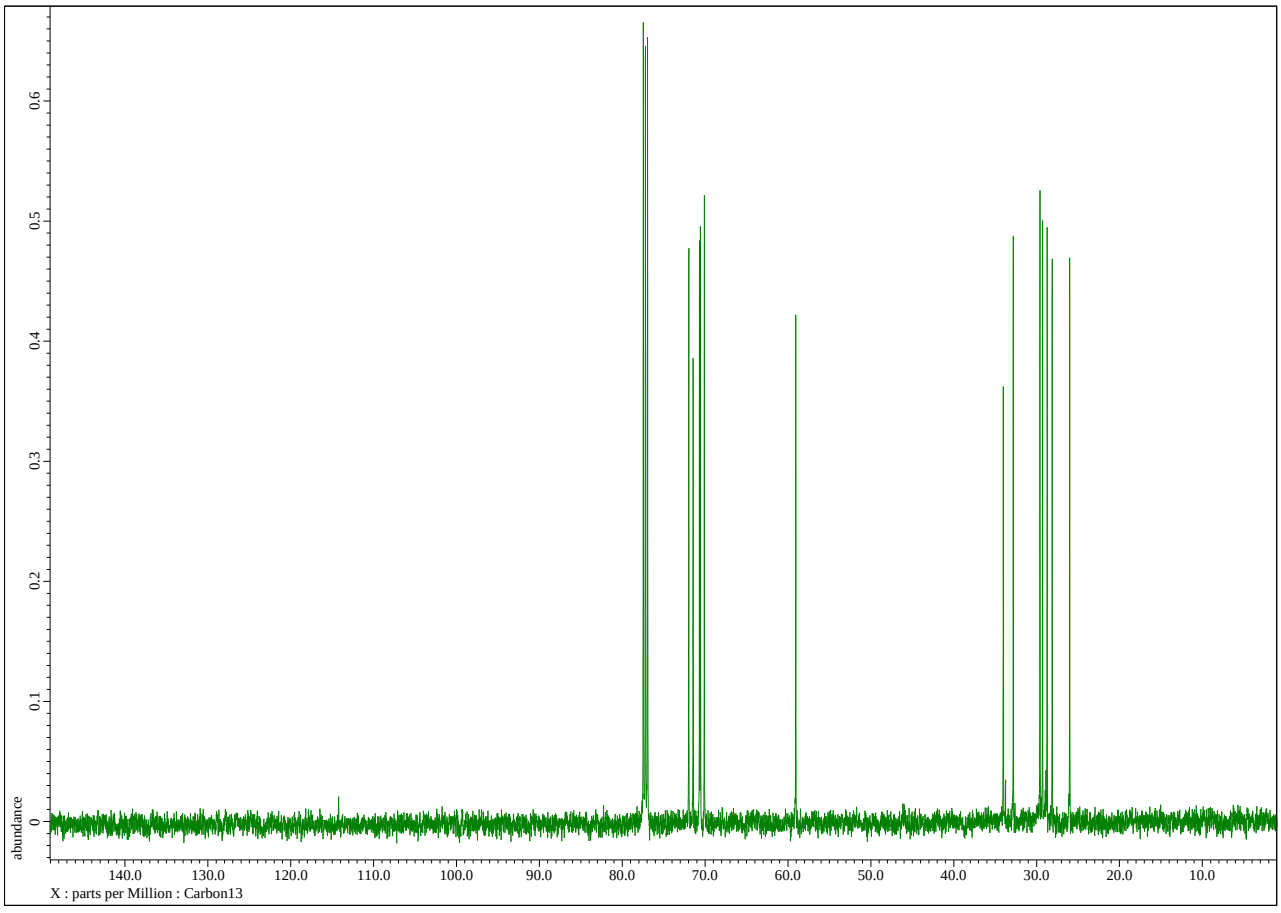
abundance
X : parts per Million : Carbon13

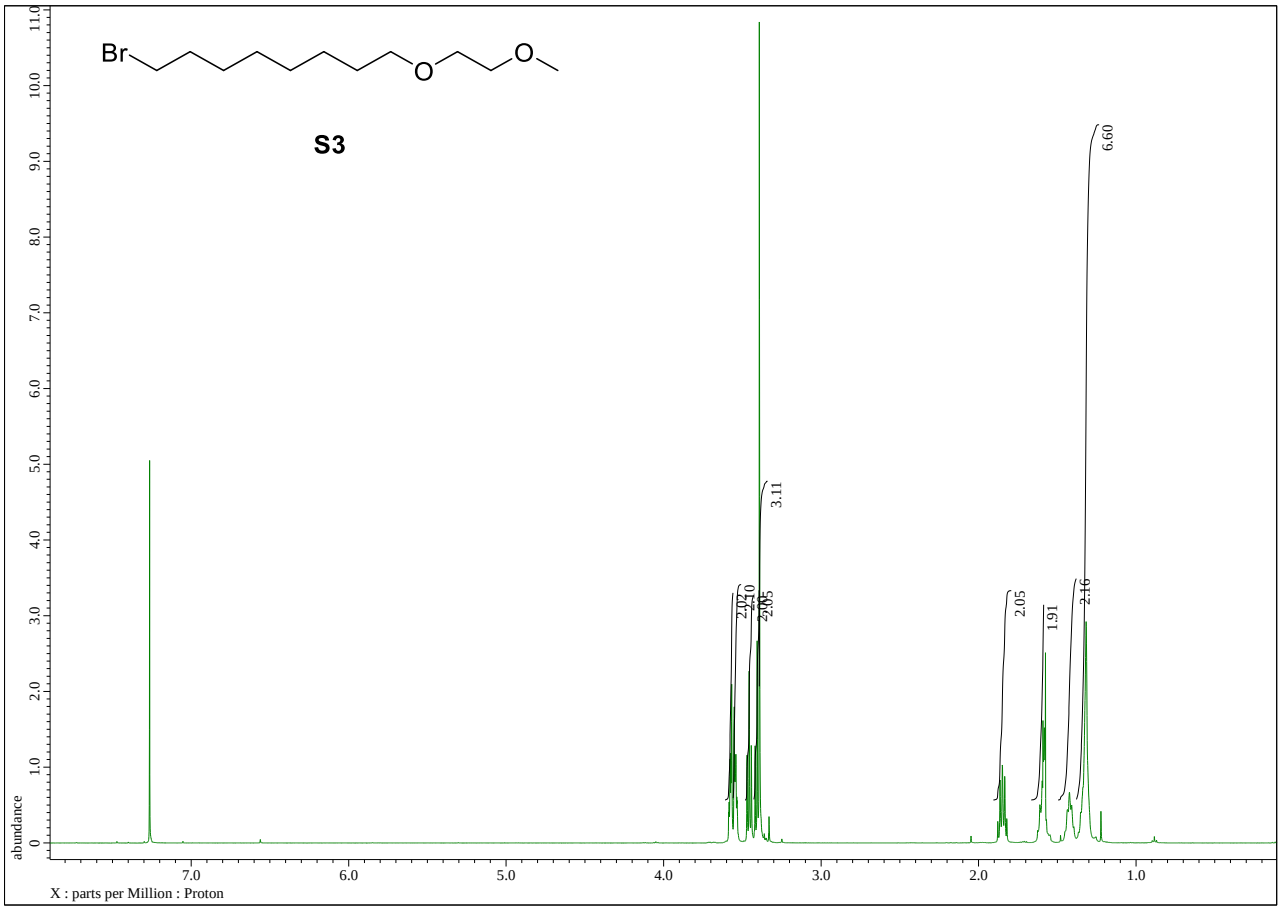
Br
O
O
S3
6.60
3.11
2.07
2.10
2.05
2.05
1.91
2.16
abundance
X : parts per Million : Proton

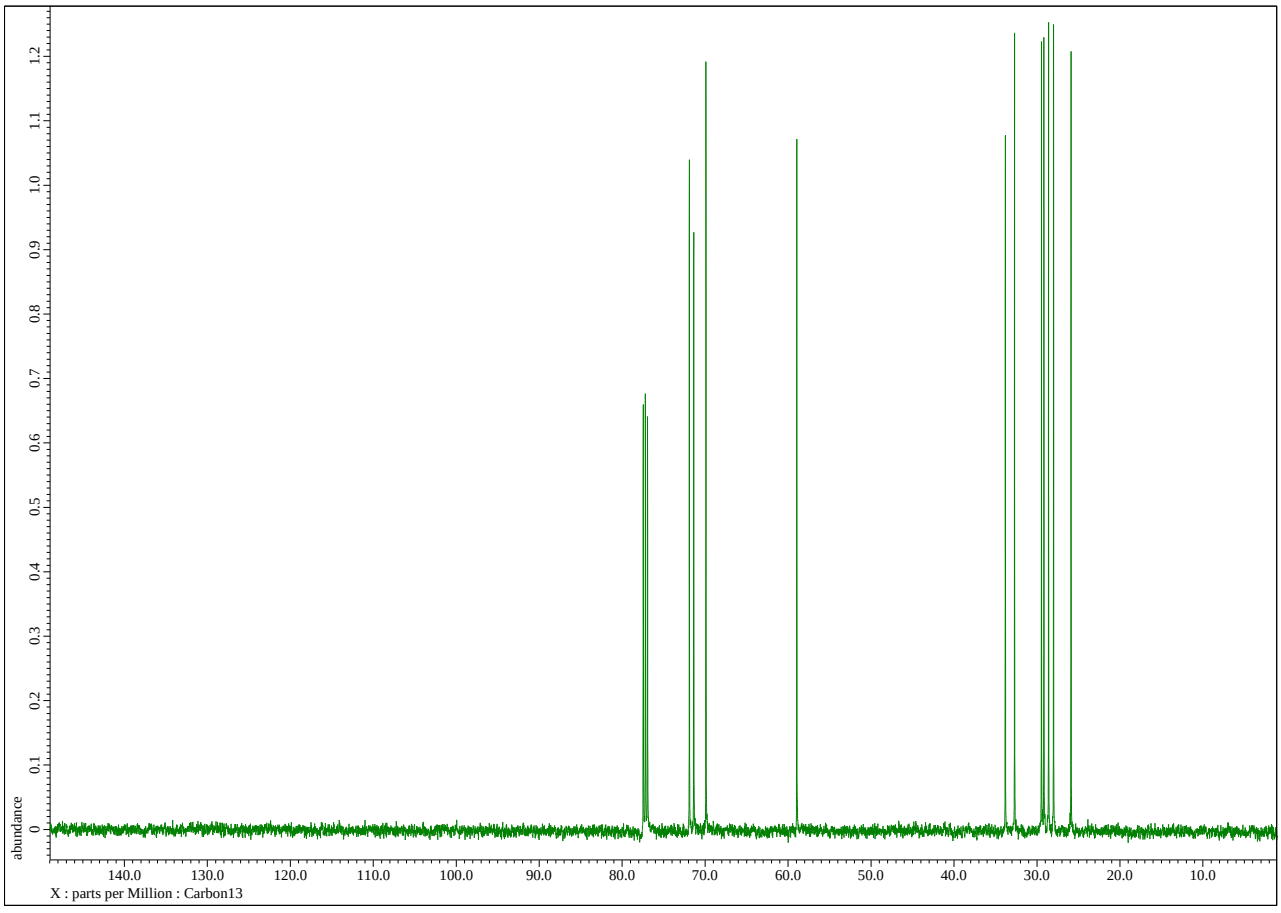
abundance
X : parts per Million : Carbon13

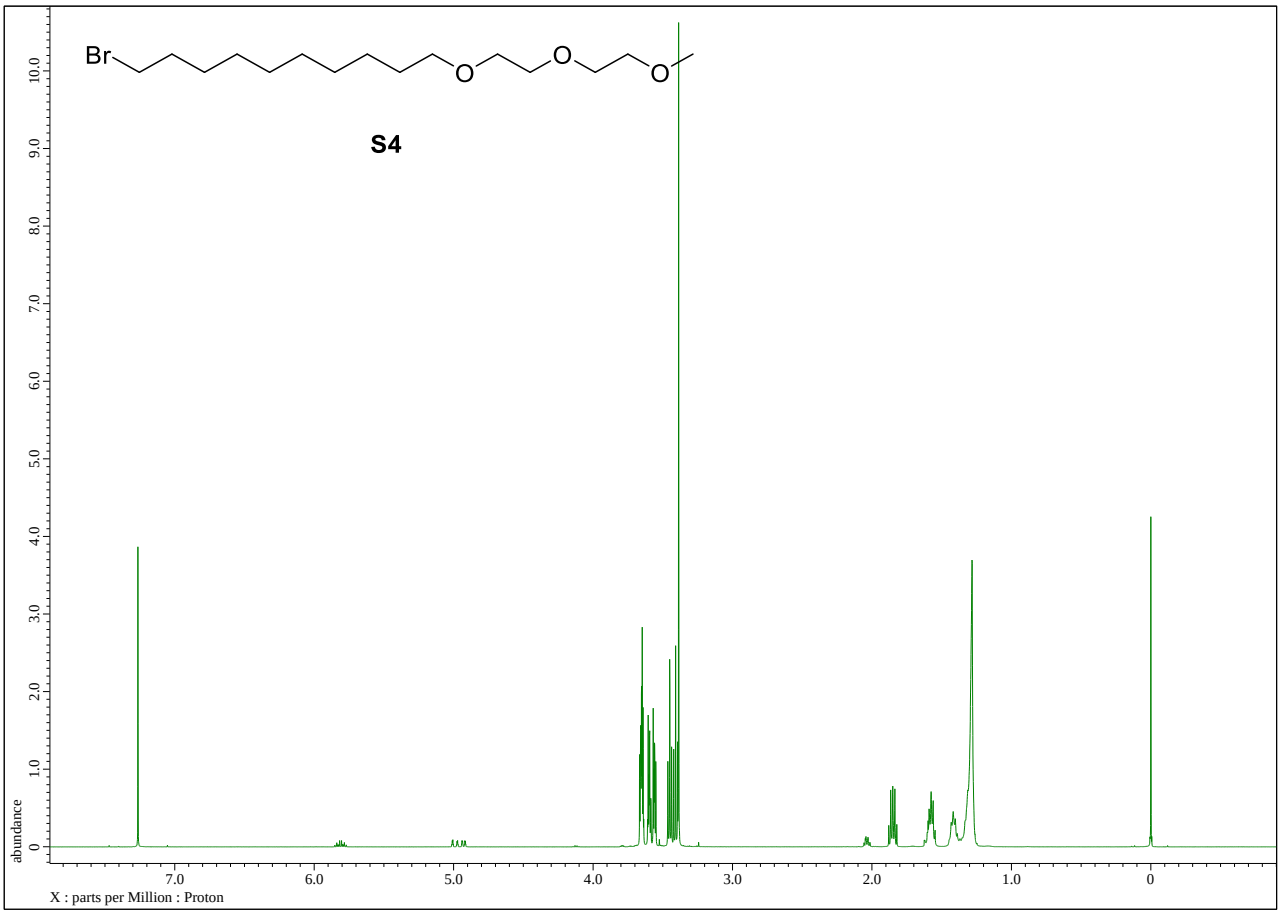
Br
O
O
O
S4
abundance
X : parts per Million : Proton

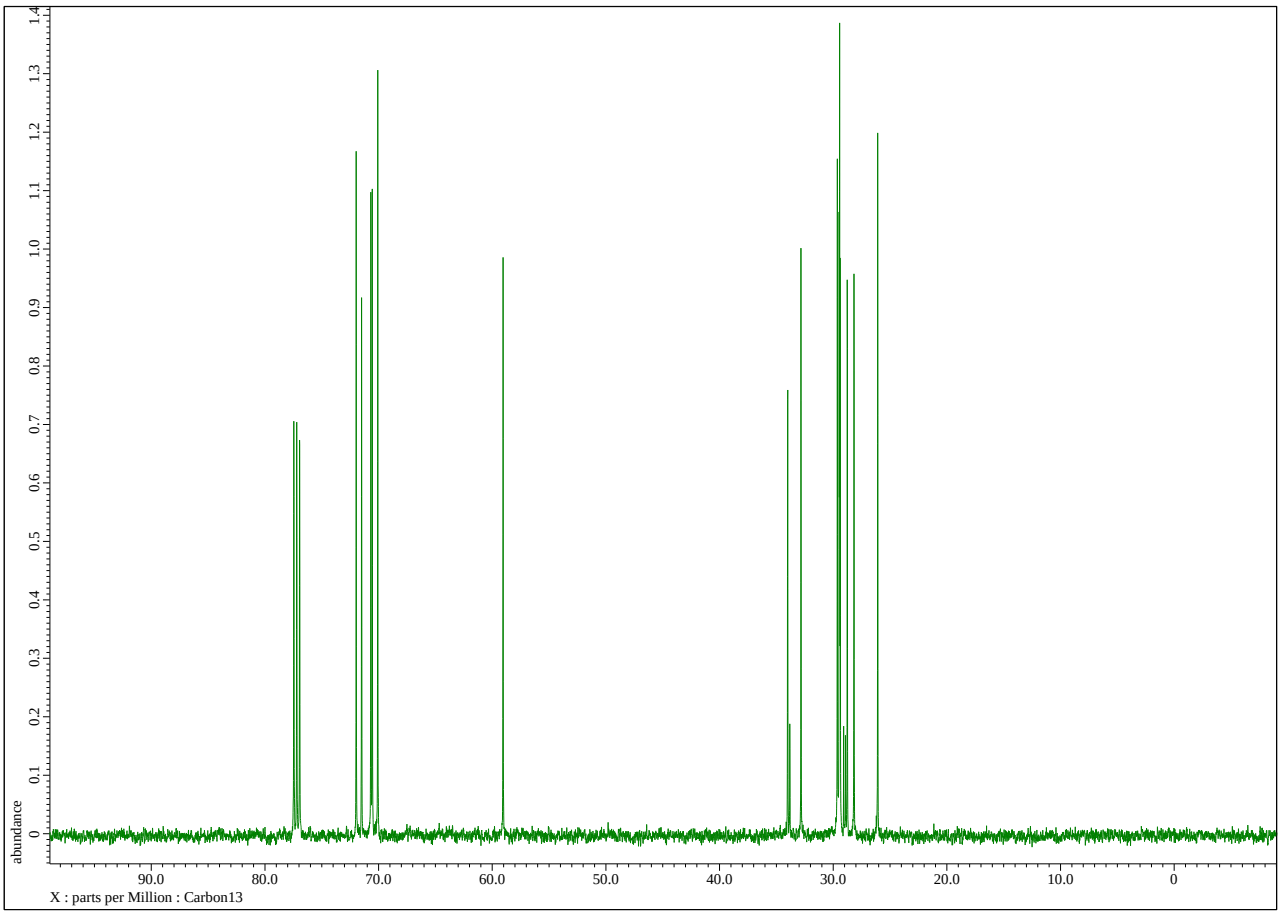
abundance
X : parts per Million : Carbon13

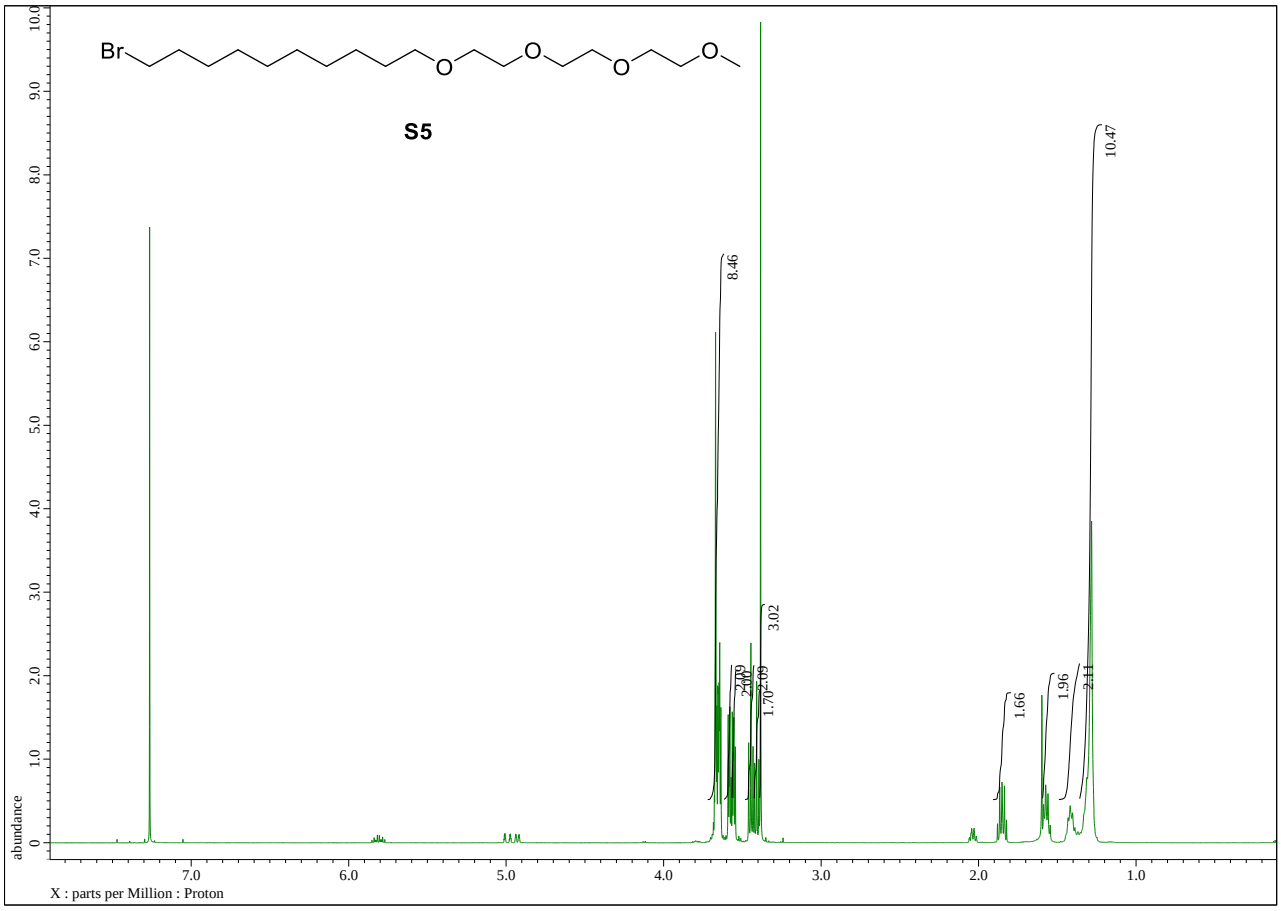
Br
O
O
O
O
S5
10.47
8.46
3.02
2.09
2.09
2.00
1.70
1.66
1.96
2.11
abundance
X : parts per Million : Proton

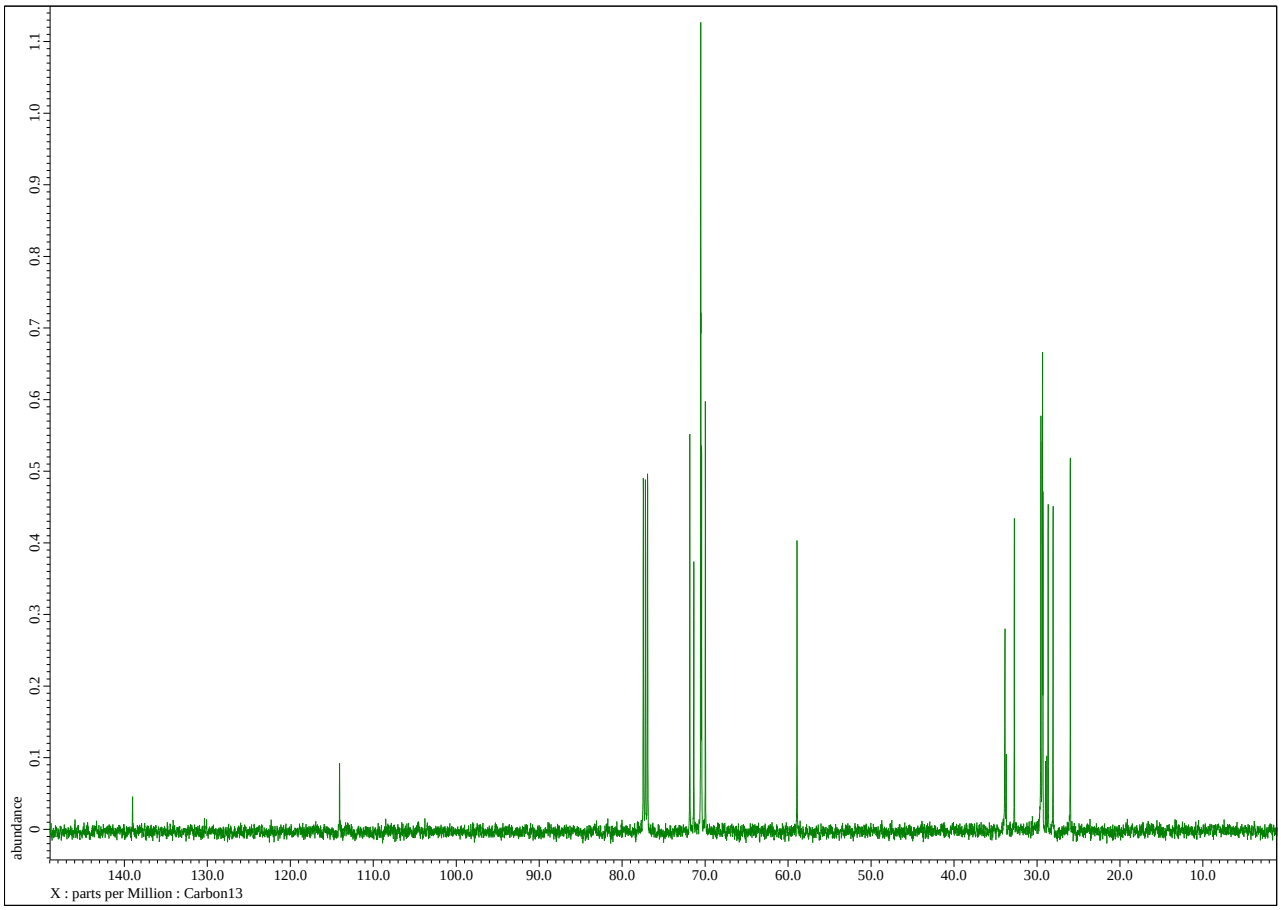
abundance
X : parts per Million : Carbon13

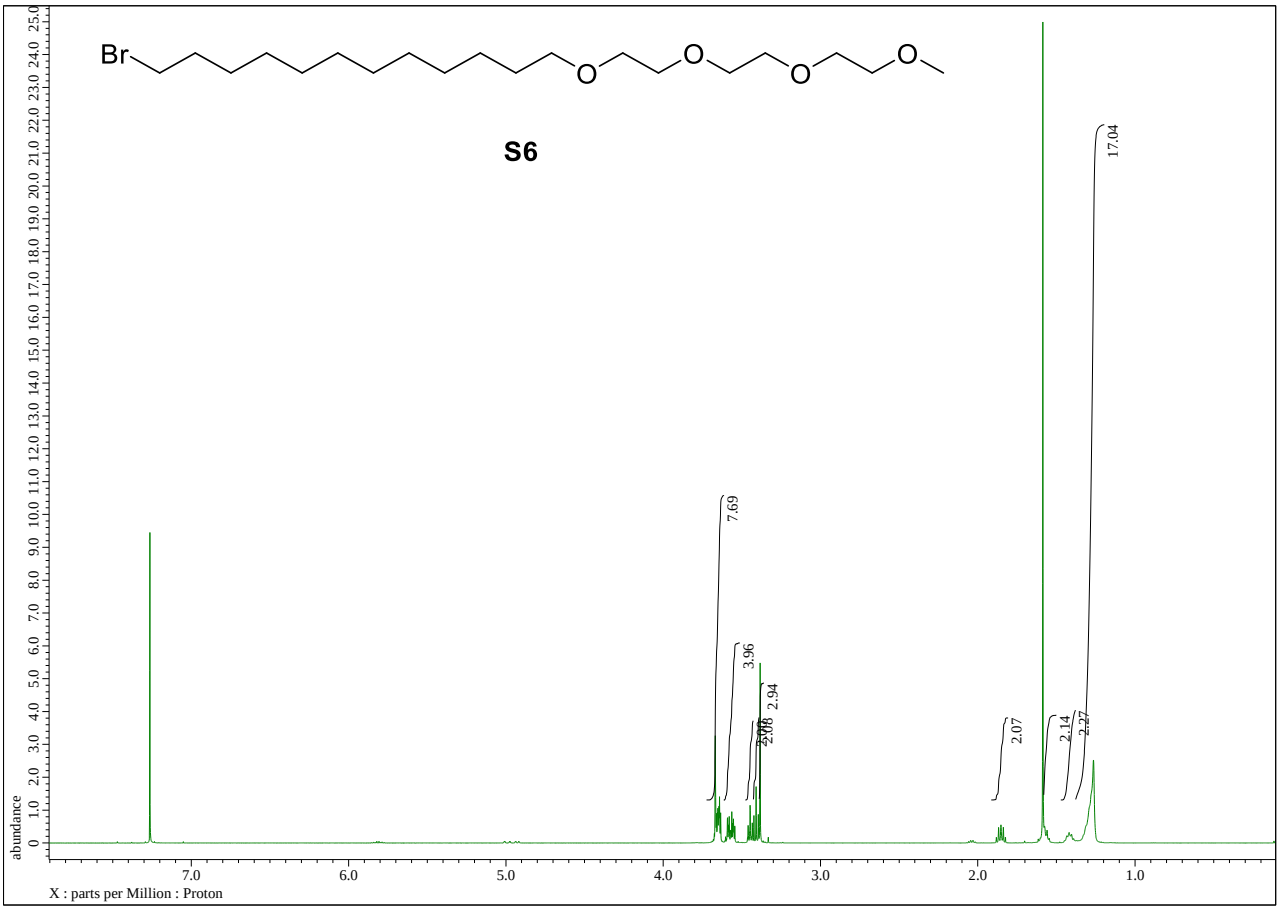
Br
O
O
O
O
S6
7.69
3.96
2.94
2.07
2.14
2.27
17.04
abundance
X : parts per Million : Proton

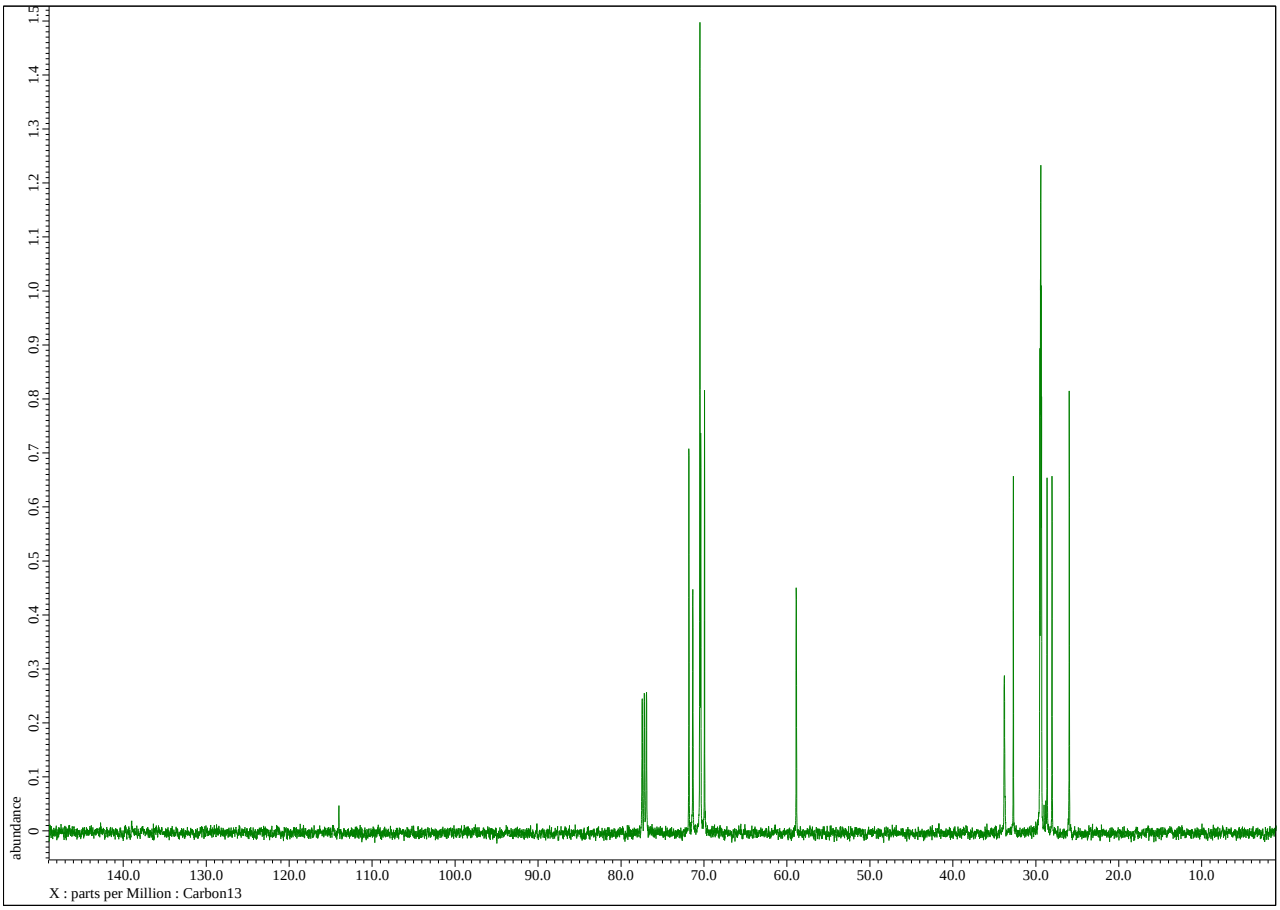
abundance
X : parts per Million : Carbon13

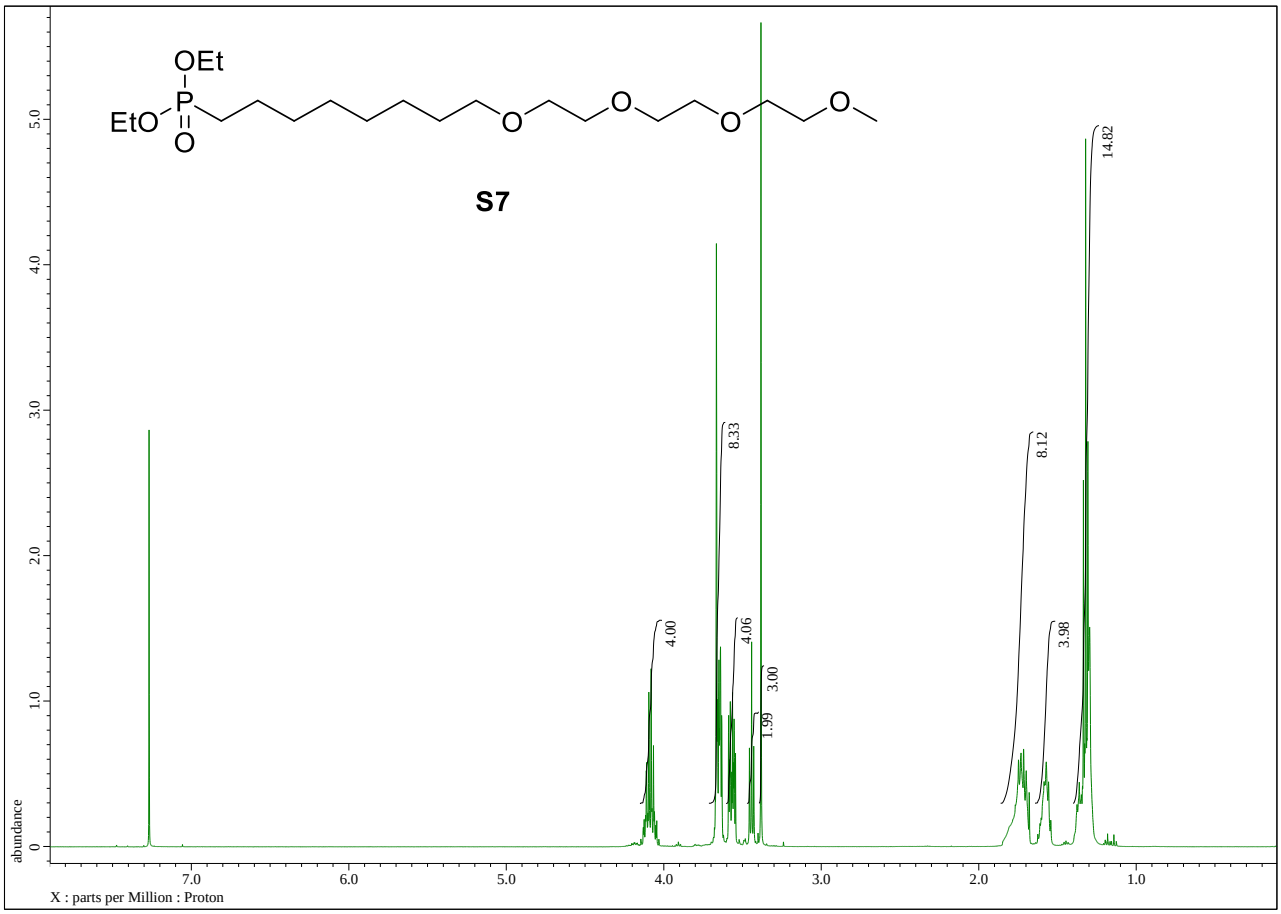
OEt
EtO
P
O
O
O
O
O
S7
14.82
8.33
8.12
4.00
4.06
3.98
3.00
1.99
abundance
X : parts per Million : Proton

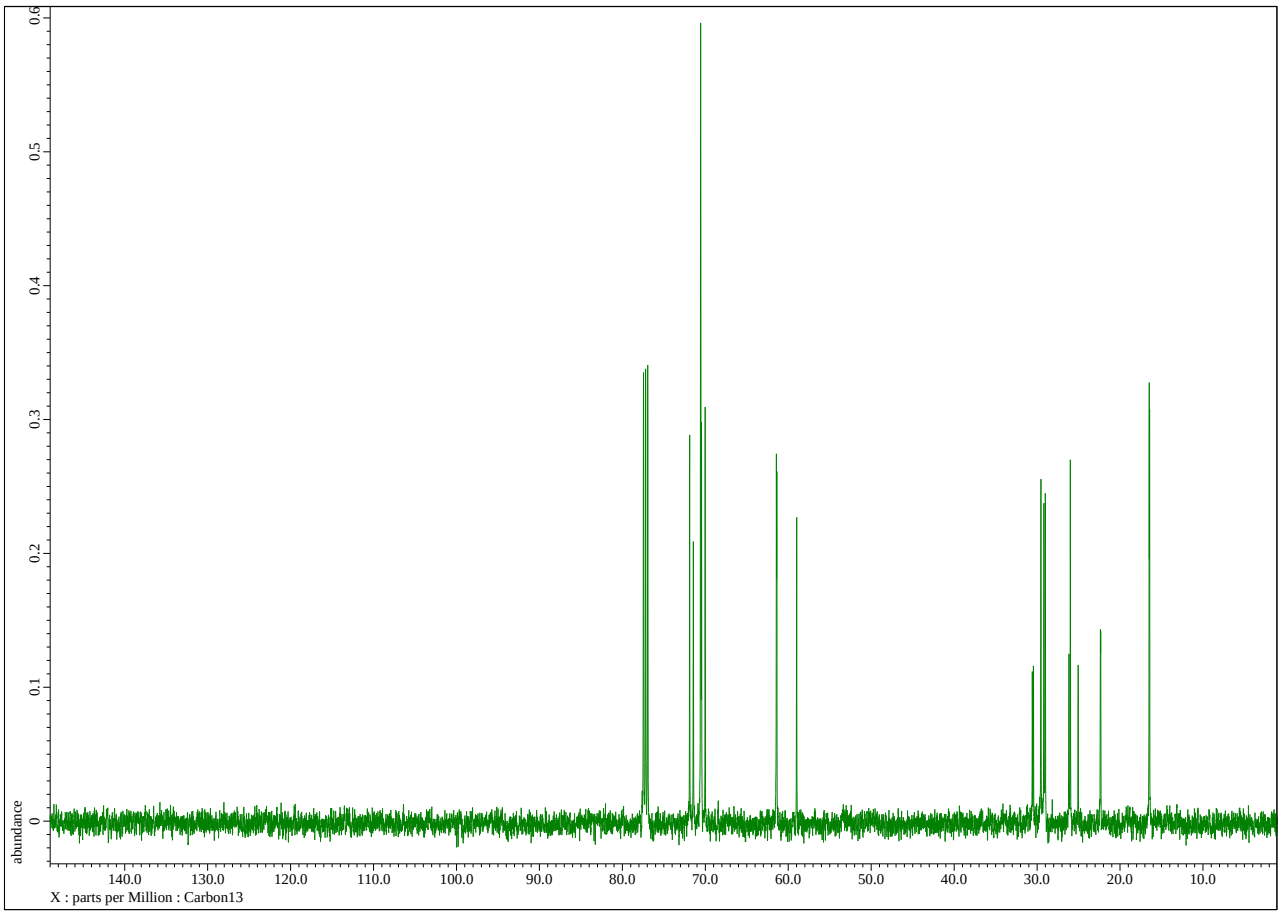
abundance
X : parts per Million : Carbon13

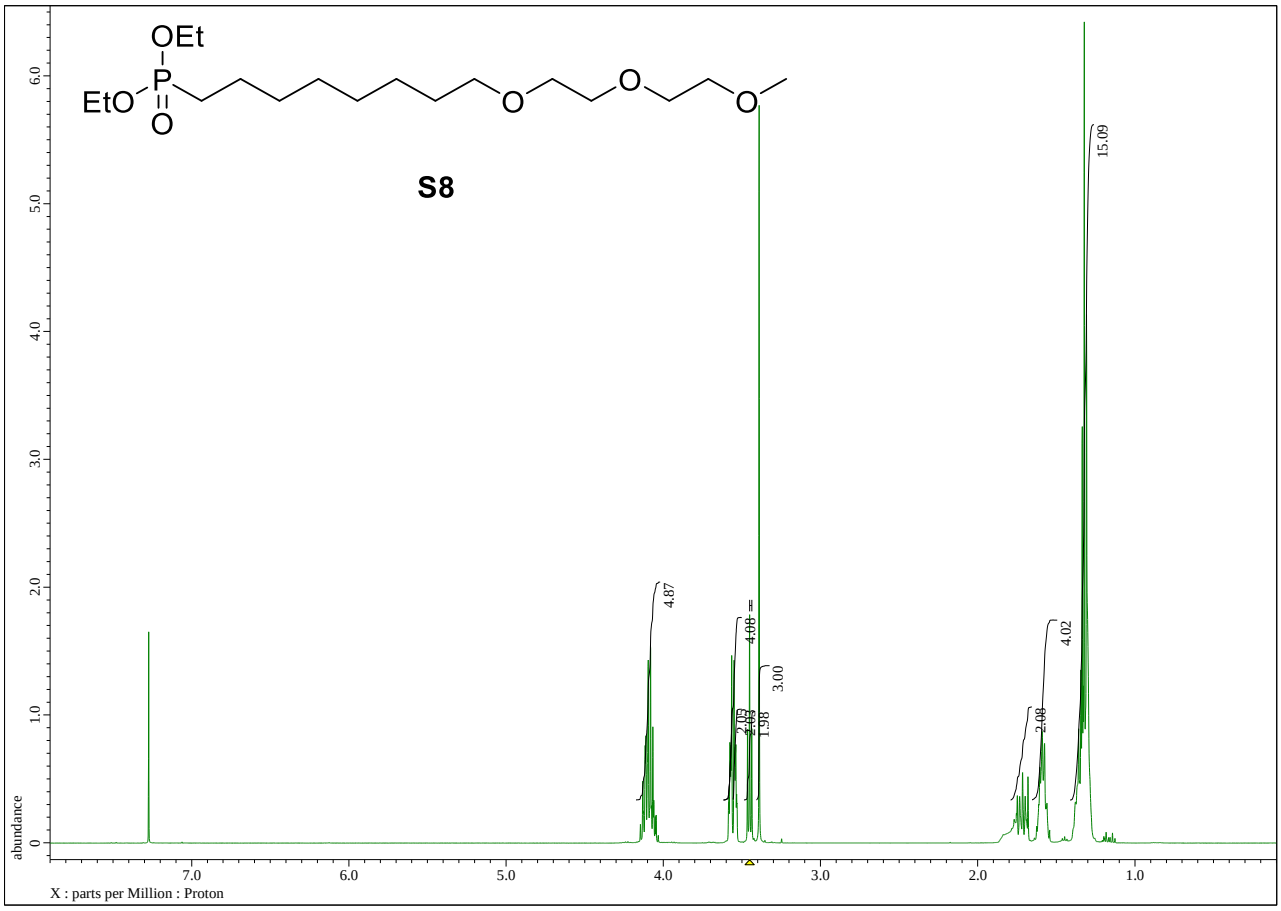
OEt
EtO
P
O
O
O
O
S8
4.87
4.06
4.03
3.00
2.09
2.03
1.98
4.02
2.08
15.09
abundance
X : parts per Million : Proton

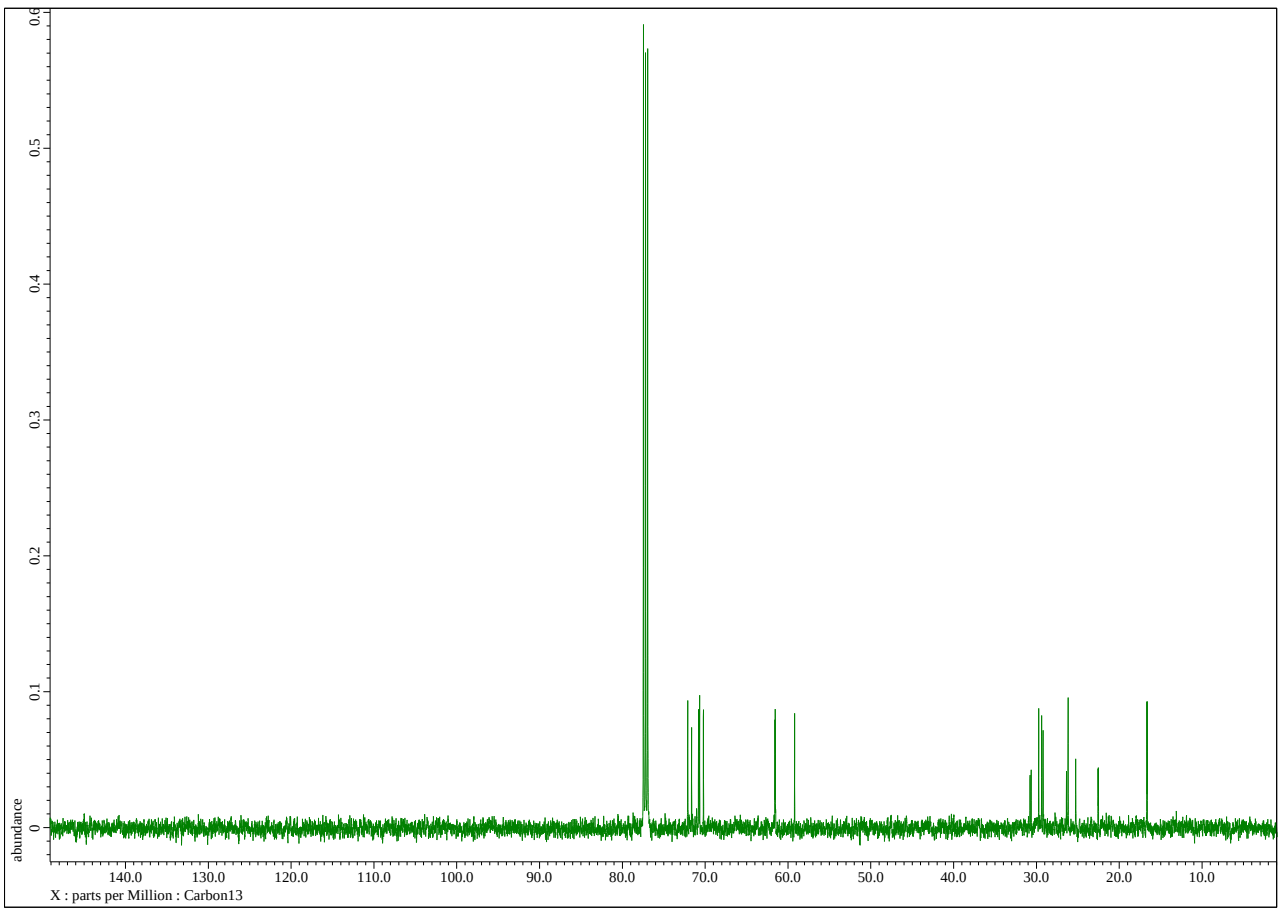
abundance
X : parts per Million : Carbon13

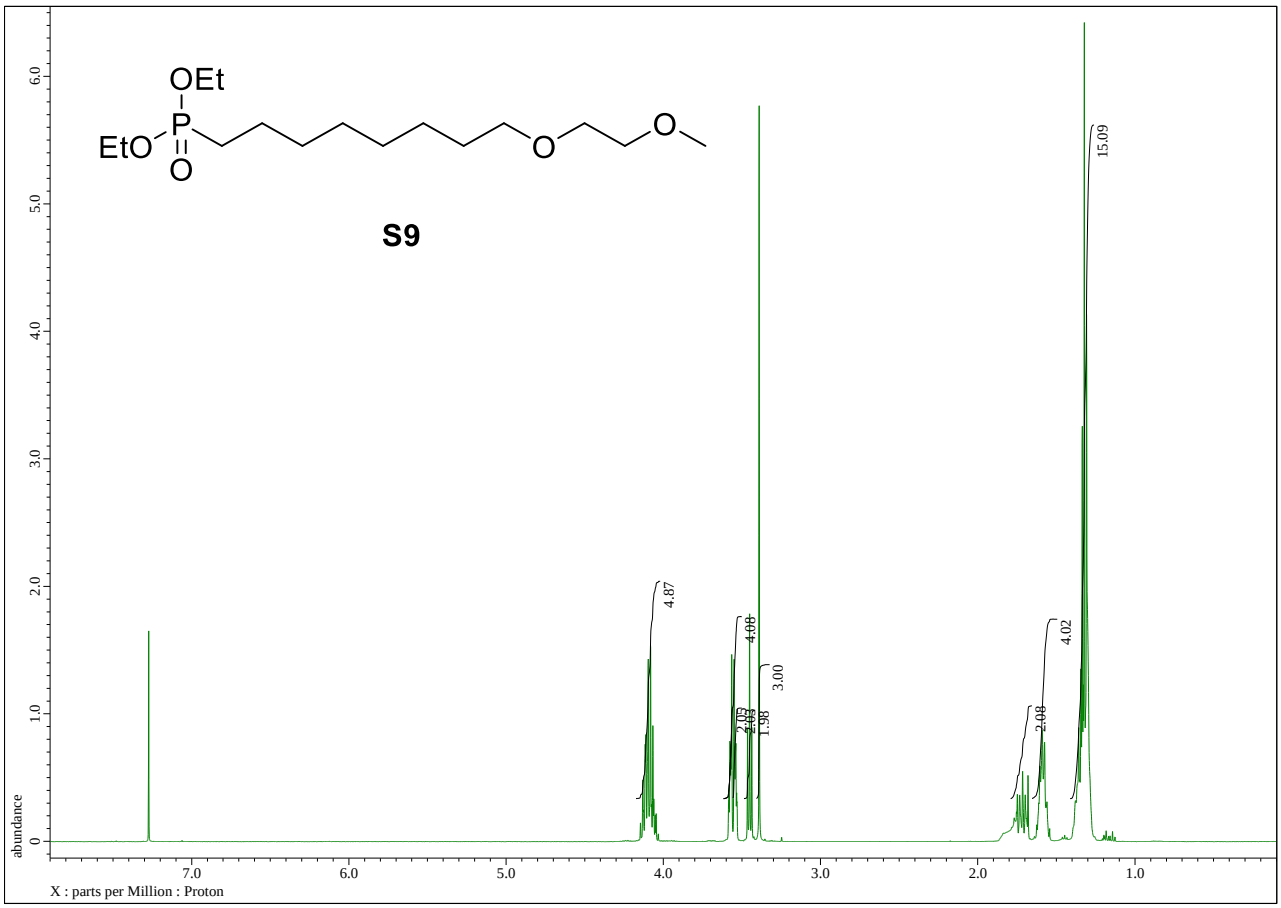
OEt
EtO
P
O
O
O
S9
4.87
4.08
3.00
2.09
2.03
1.98
4.02
2.08
15.09
abundance
X : parts per Million : Proton

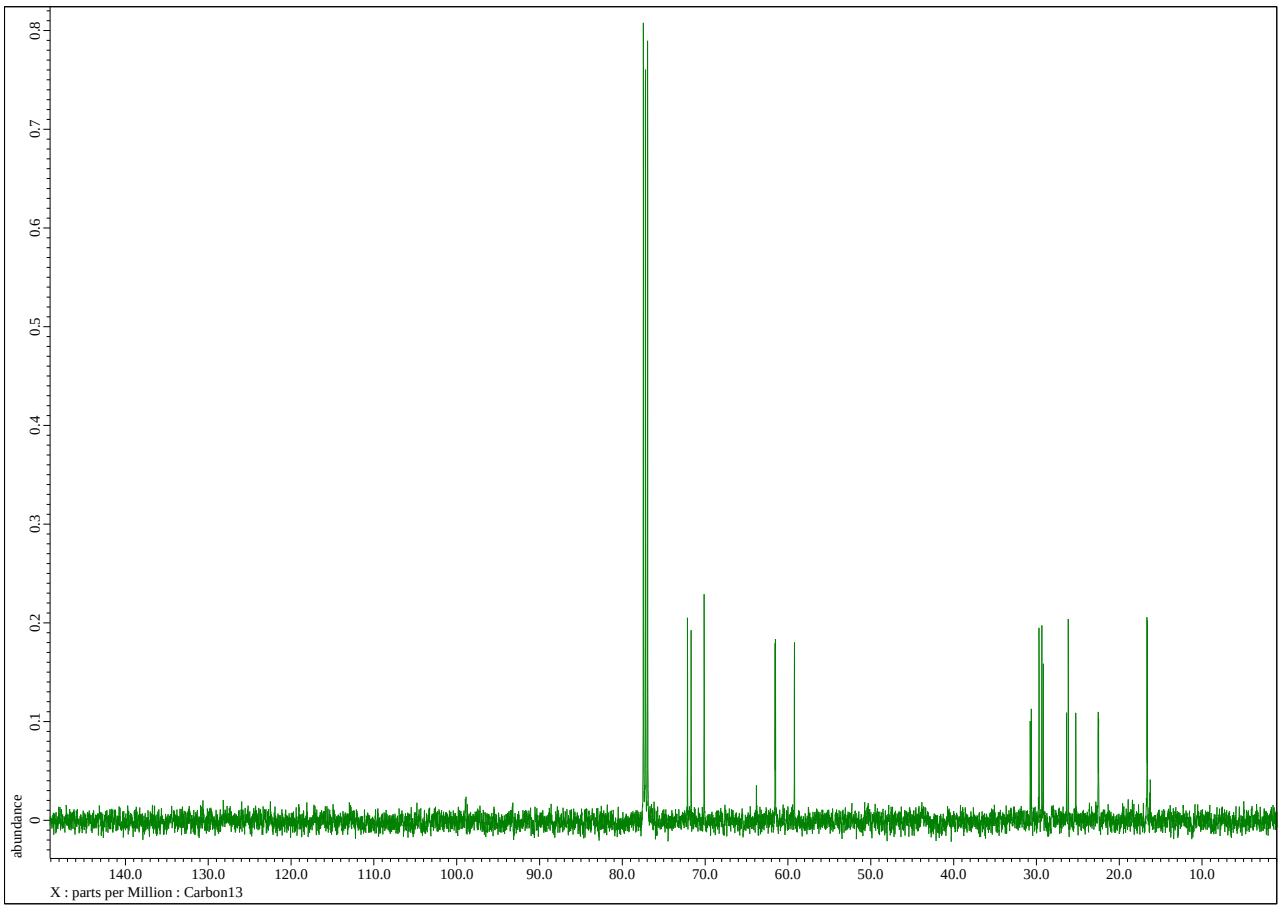
abundance
X : parts per Million : Carbon13

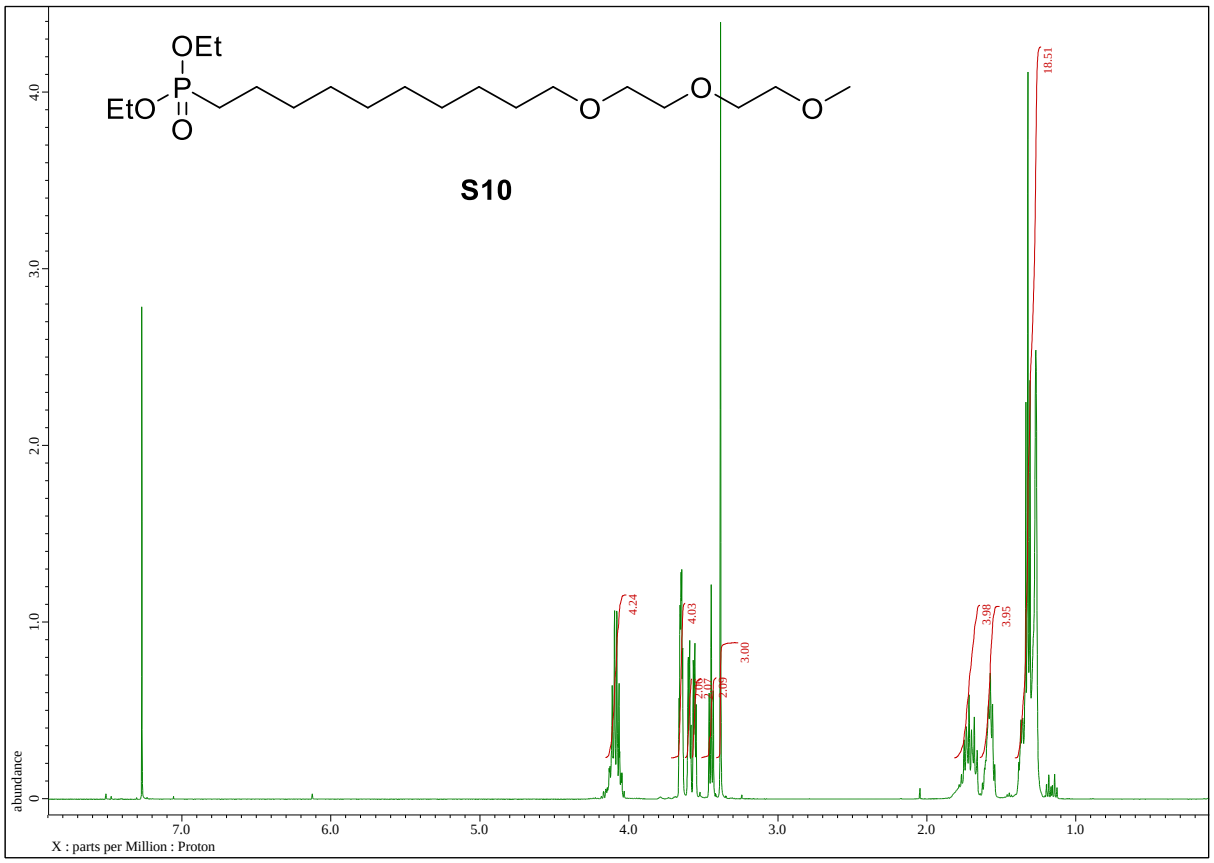
OEt
EtO
P
O
O
O
O
S10
4.24
4.03
4.00
3.98
3.95
3.00
2.03
18.51
abundance
X : parts per Million : Proton

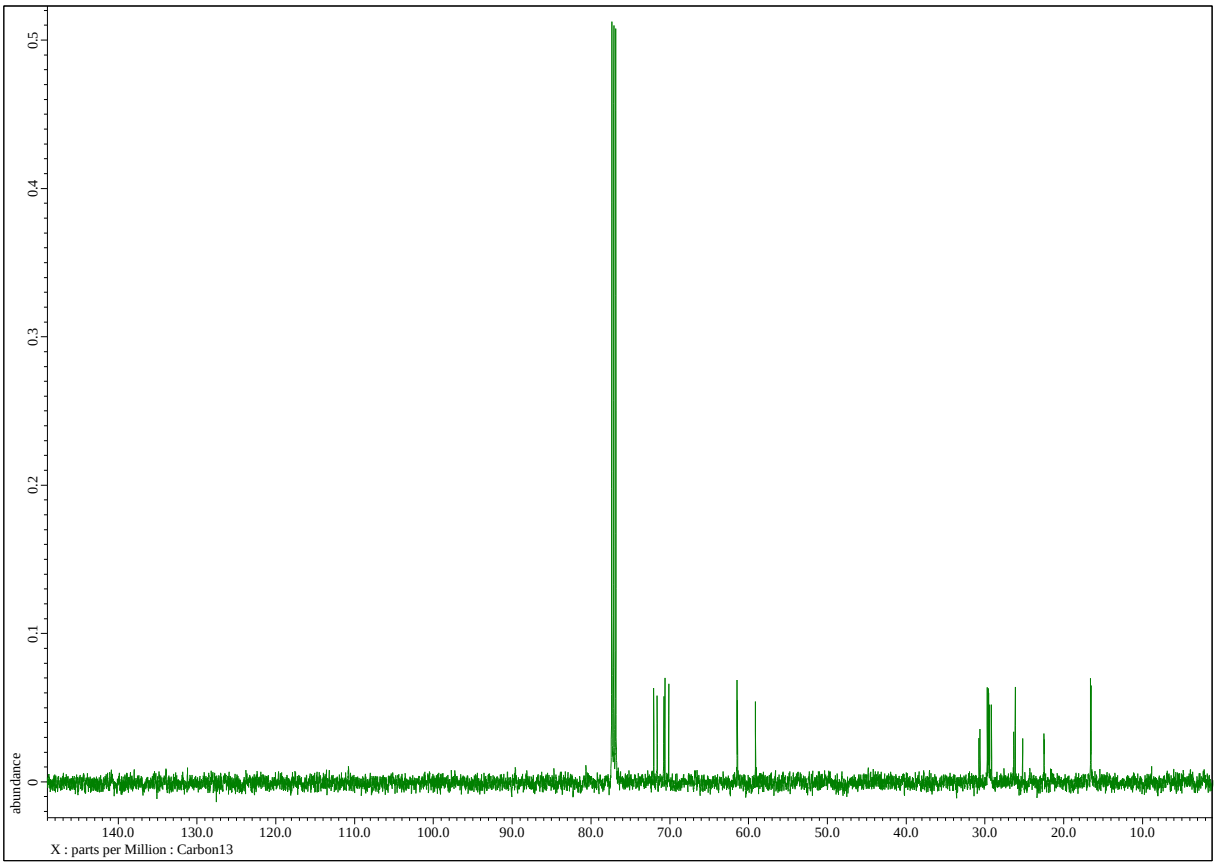
abundance
X : parts per Million : Carbon13

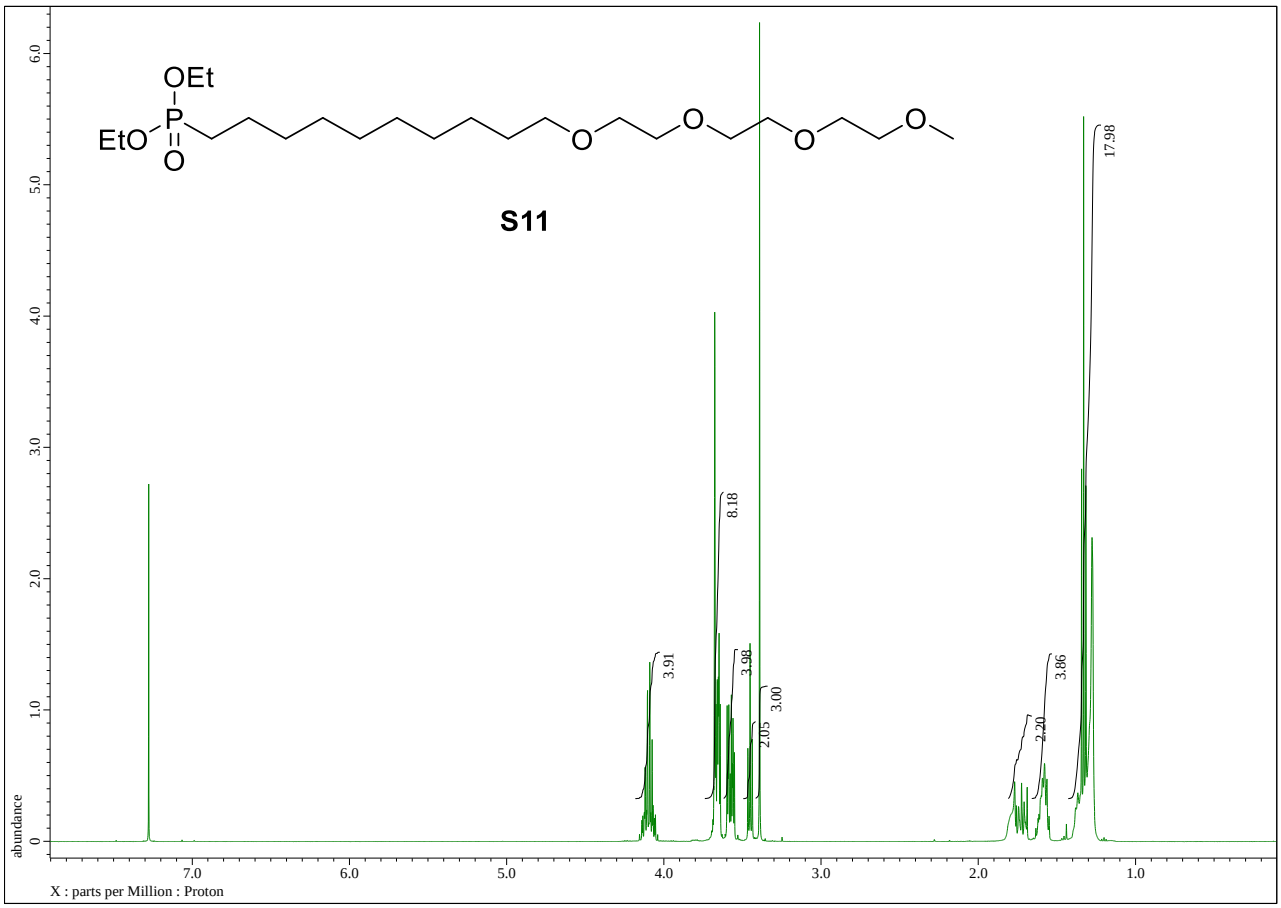
OEt
EtO
P
O
O
O
O
O
S11
17.98
8.18
3.91
3.98
3.00
2.05
3.86
2.20
abundance
X : parts per Million : Proton

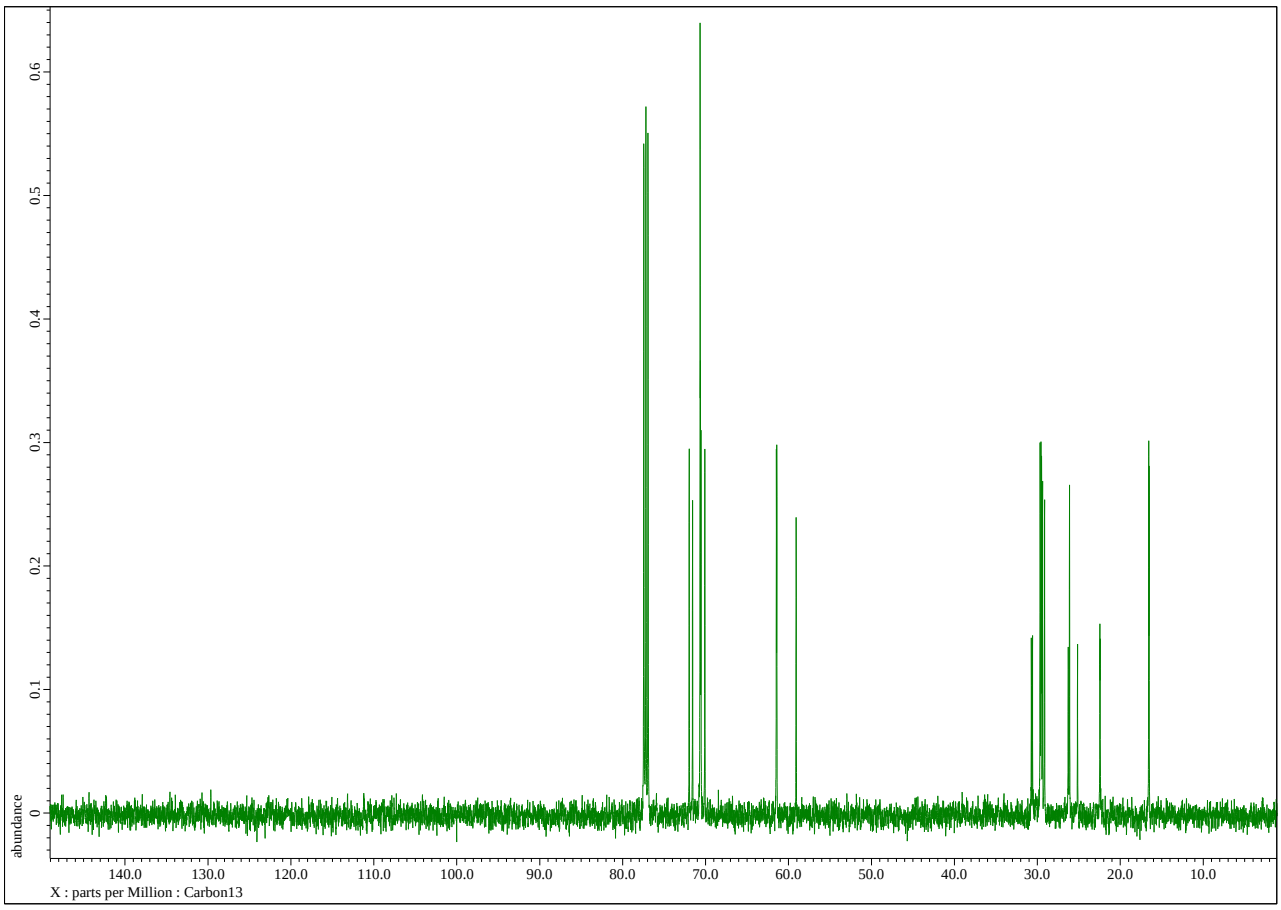
abundance
X : parts per Million : Carbon13

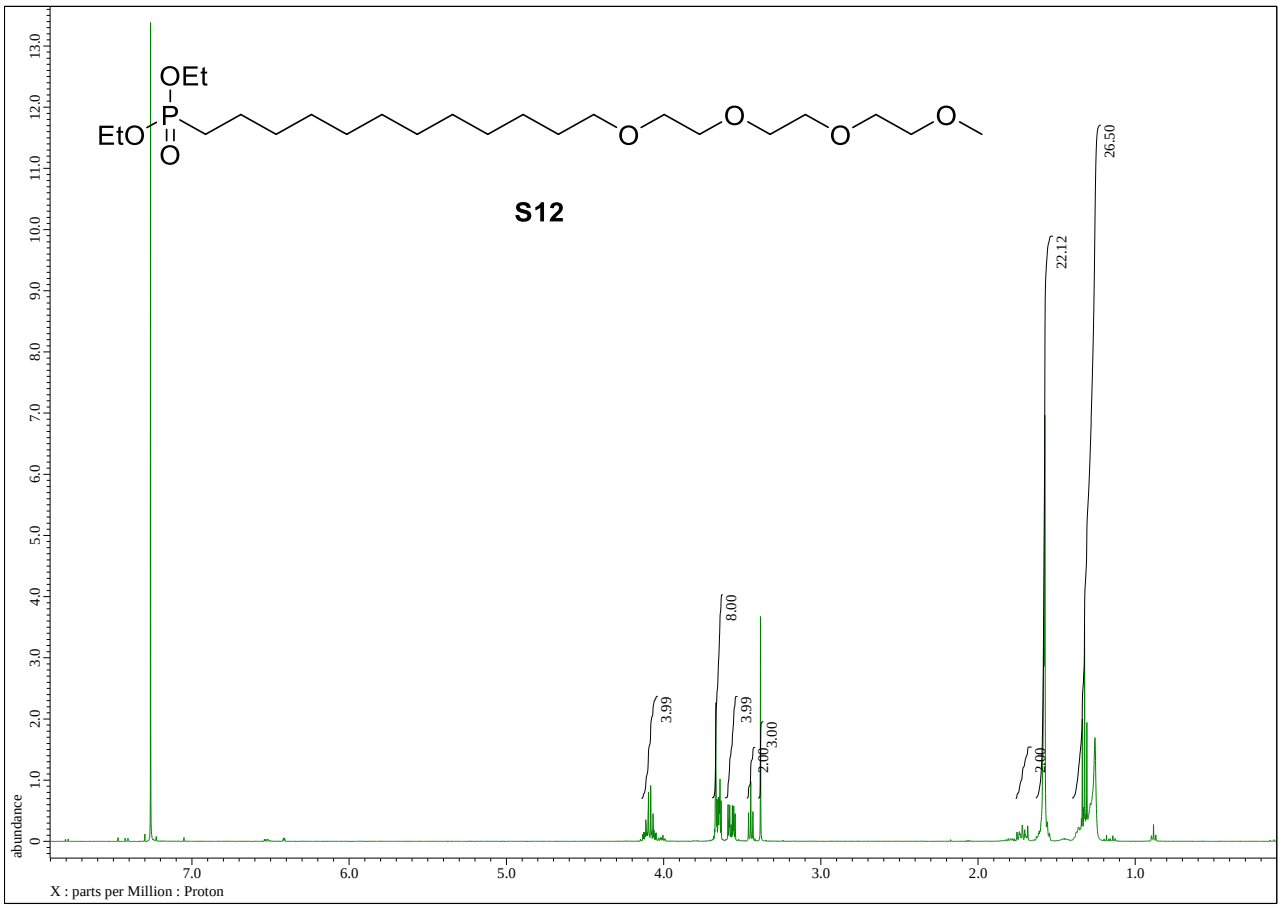
OEt
EtO
P
O
O
O
O
O
S12
26.50
22.12
8.00
3.99
3.99
3.00
2.00
2.00
abundance
X : parts per Million : Proton

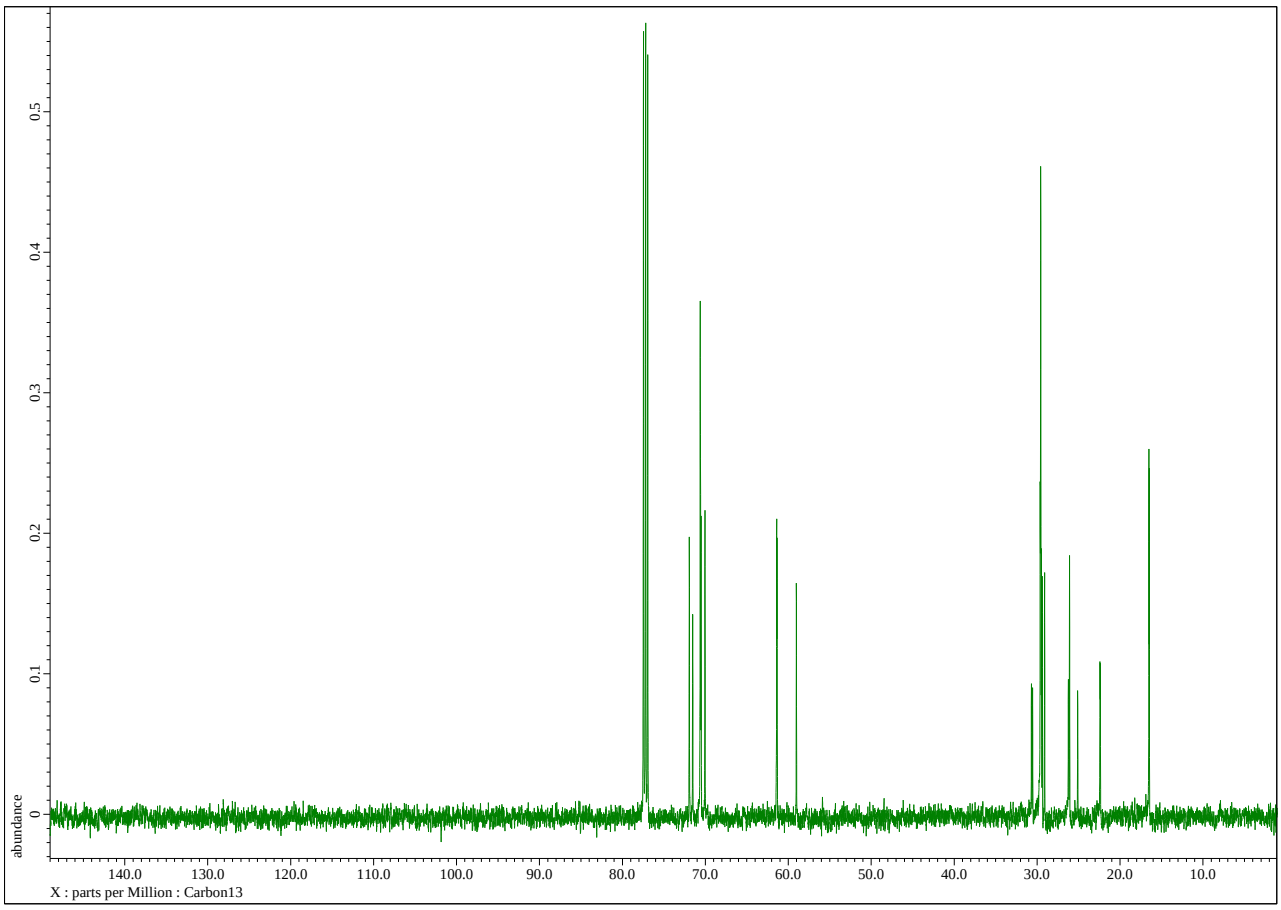
abundance
X : parts per Million : Carbon13

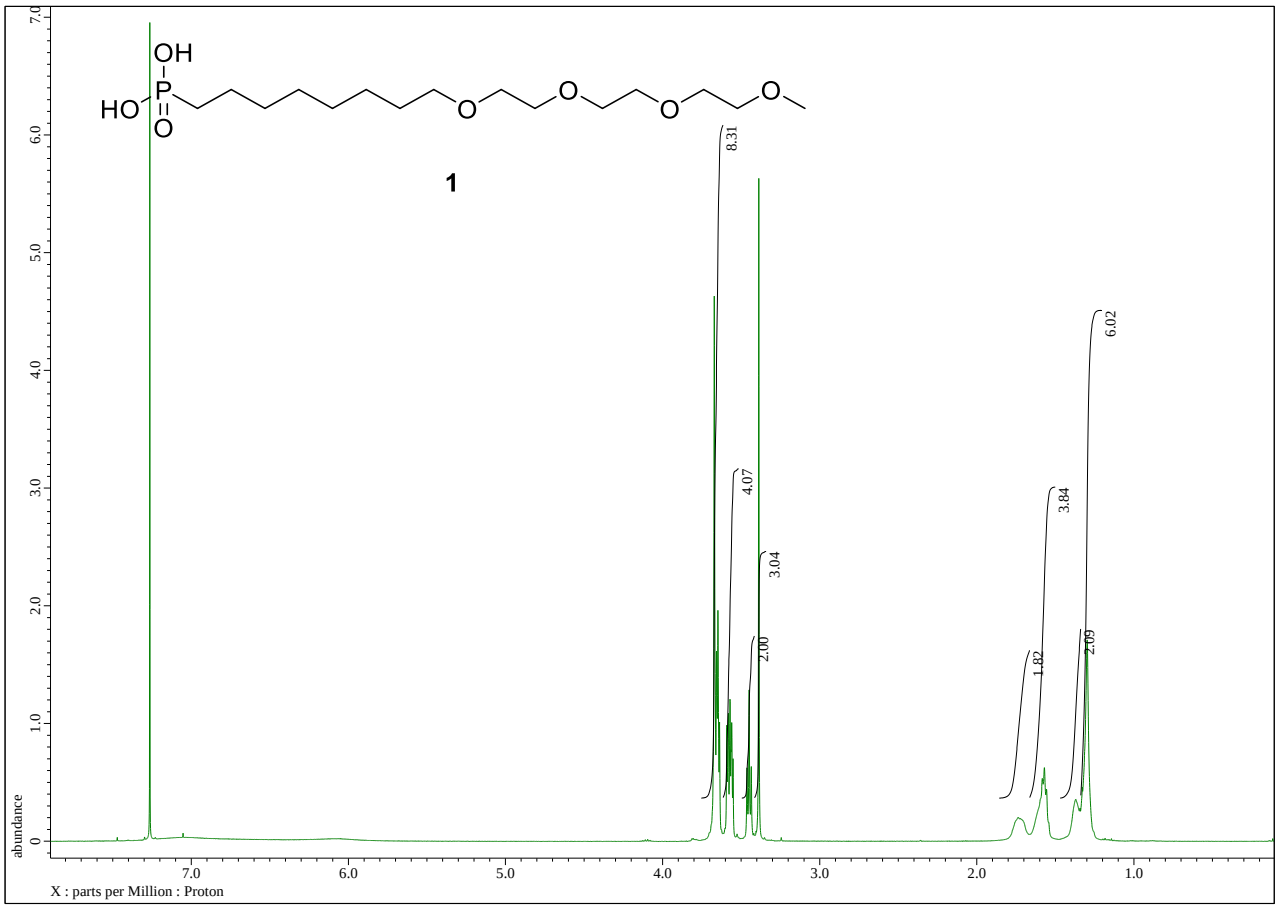
OH
HO
P
O
O
O
O
O
1
8.31
4.07
3.04
2.00
1.82
3.84
2.09
6.02
abundance
X : parts per Million : Proton

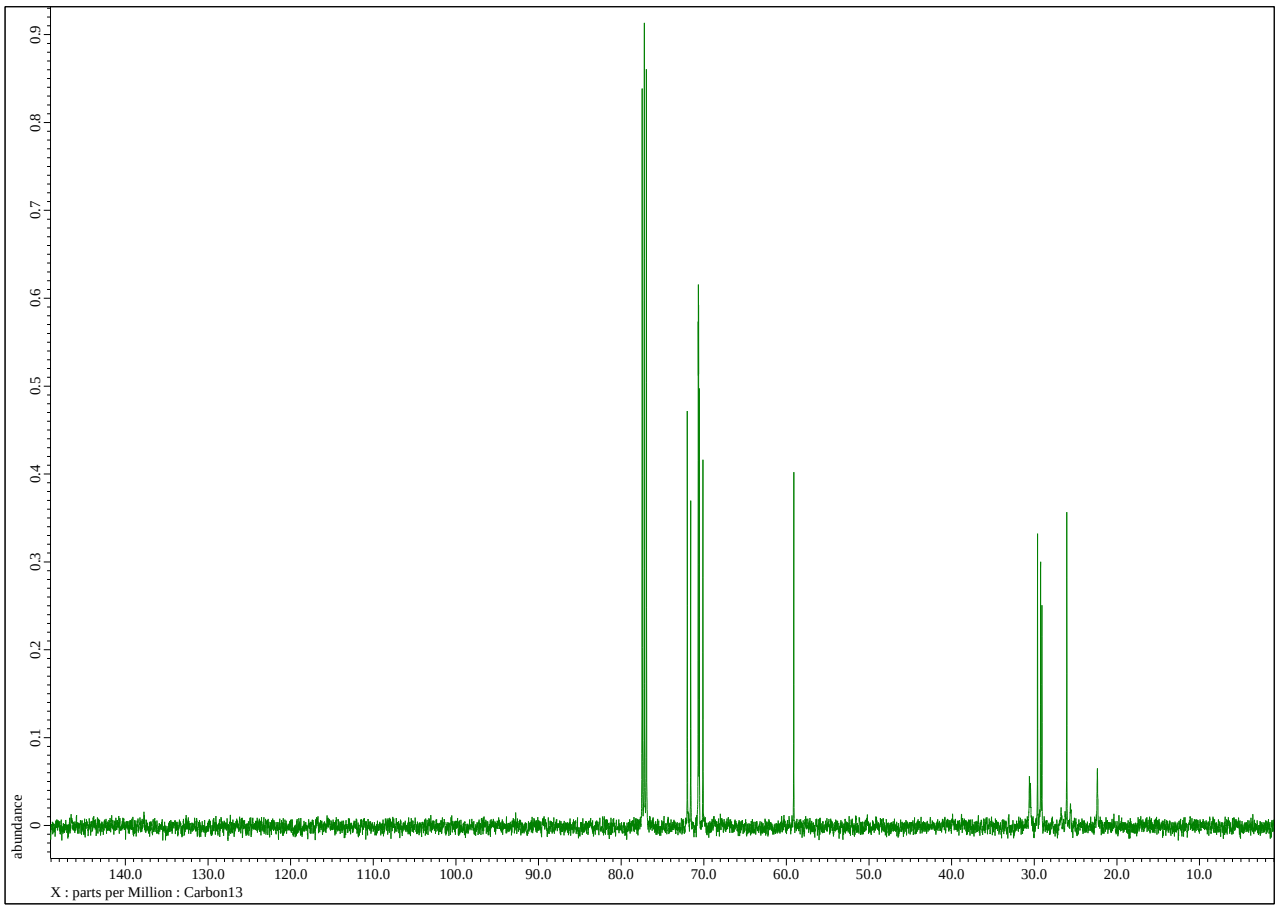
abundance
X : parts per Million : Carbon13

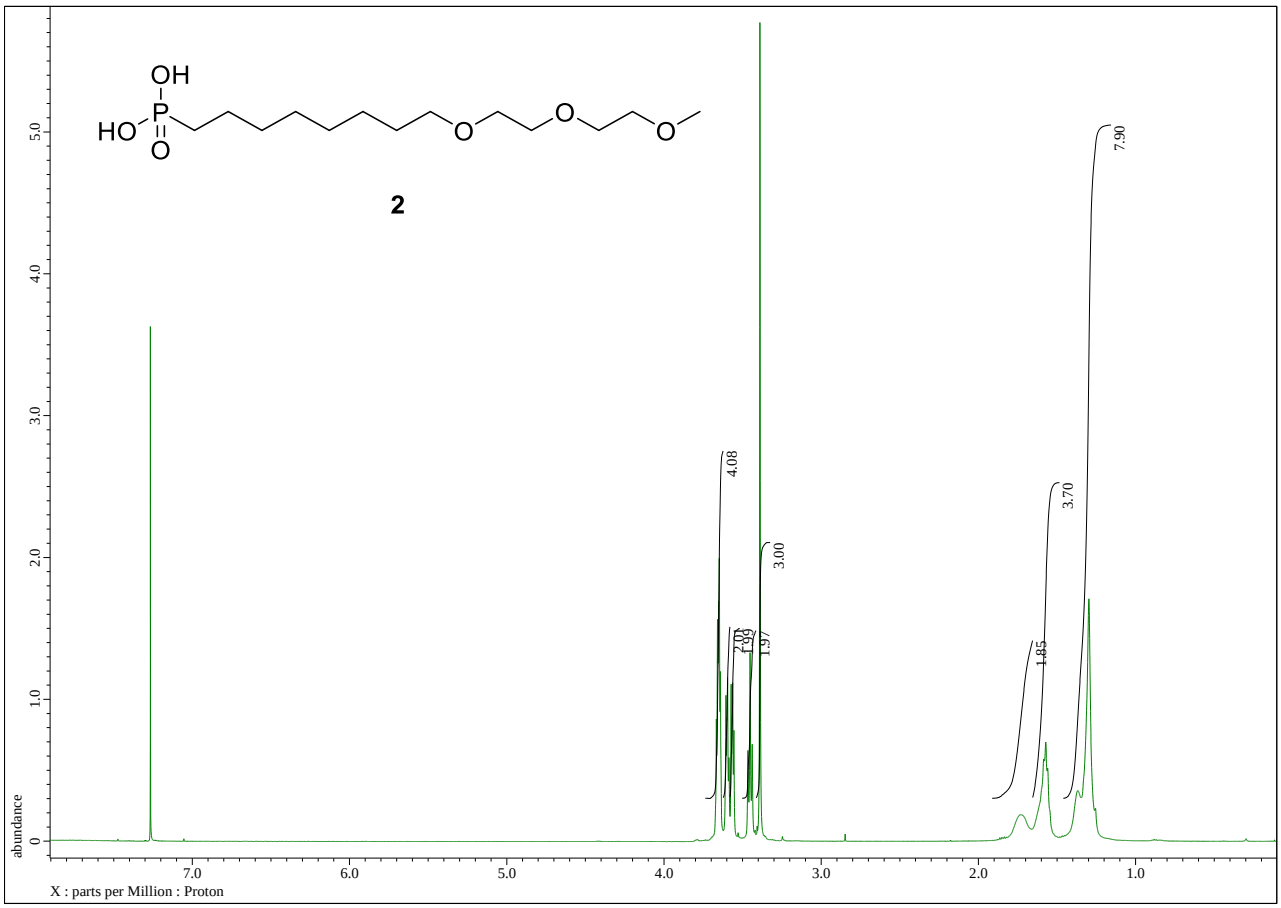
OH
HO
P
O
O
O
O
2
4.08
3.00
2.00
1.92
1.97
1.85
3.70
7.90
abundance
X : parts per Million : Proton

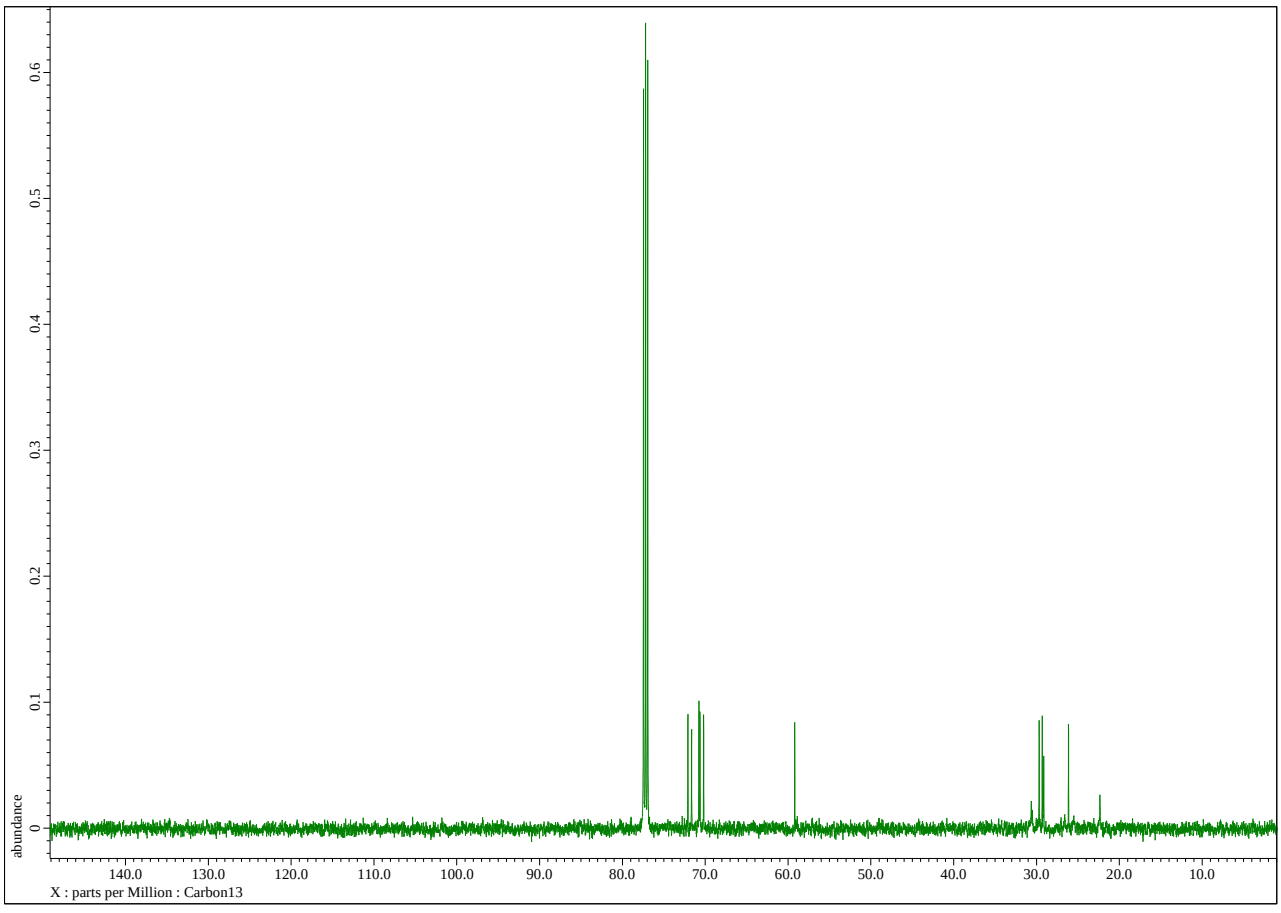
abundance
X : parts per Million : Carbon13

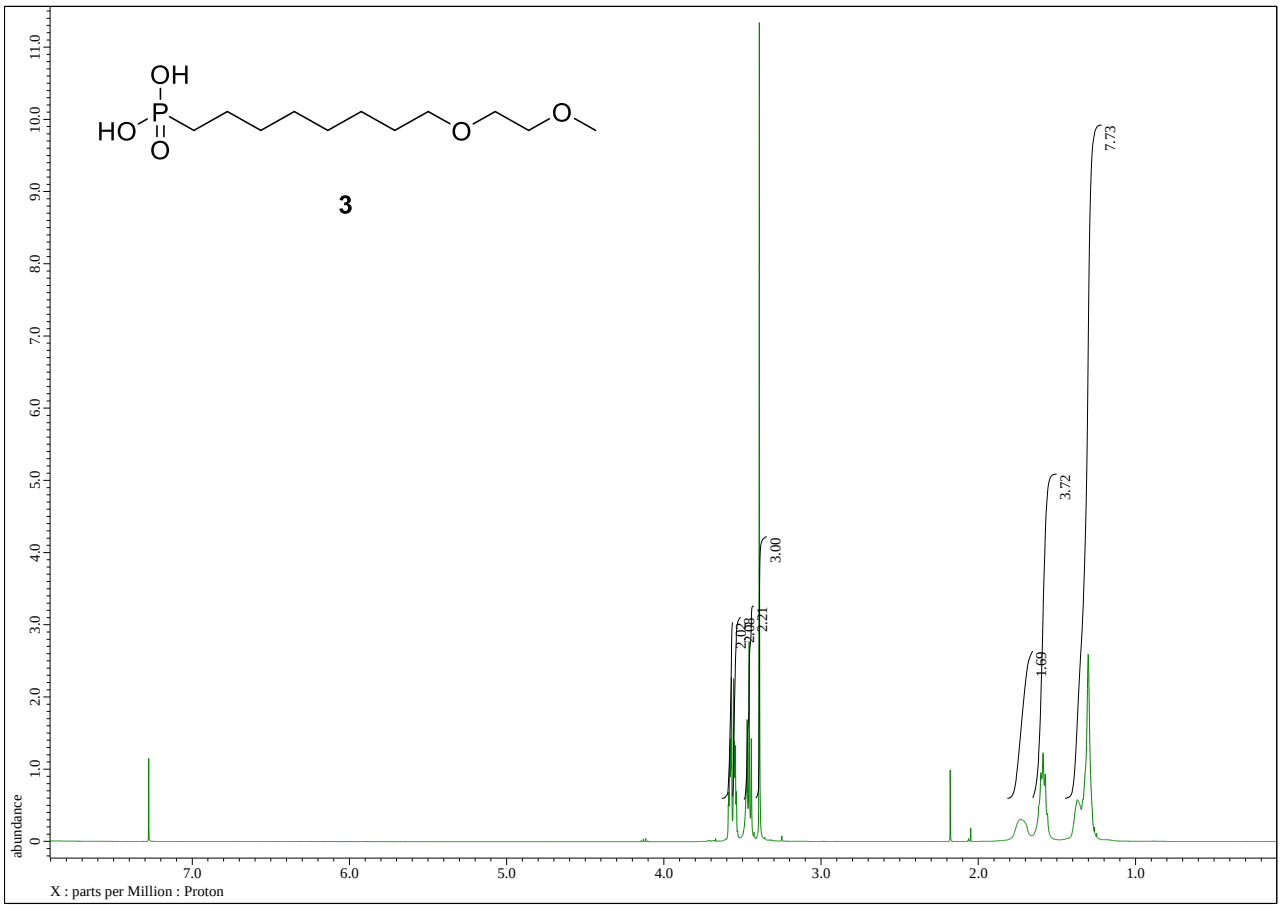
OH
HO
P
O
O
O
3
7.73
3.72
3.00
2.21
2.08
2.07
1.69
abundance
X : parts per Million : Proton

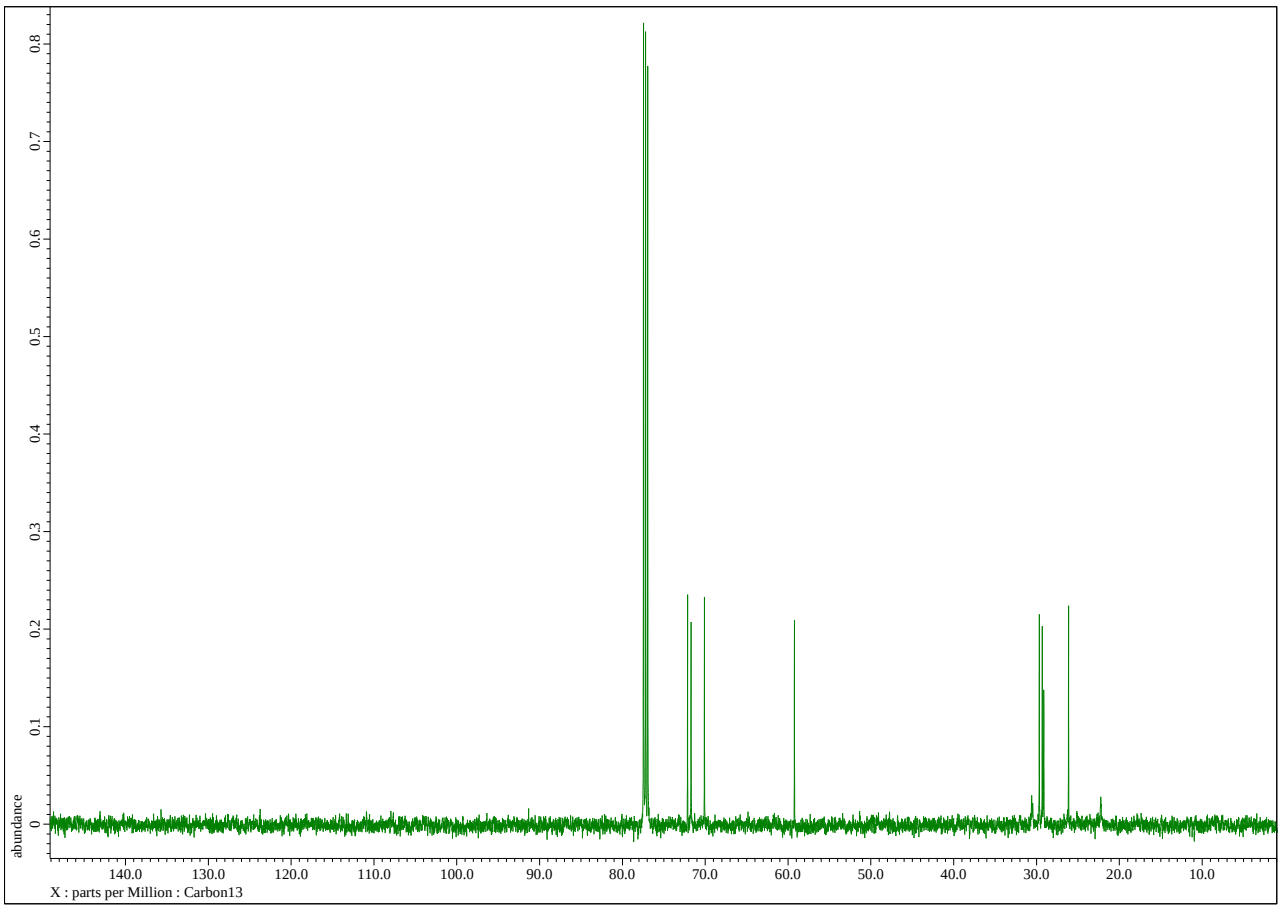
abundance
X : parts per Million : Carbon13

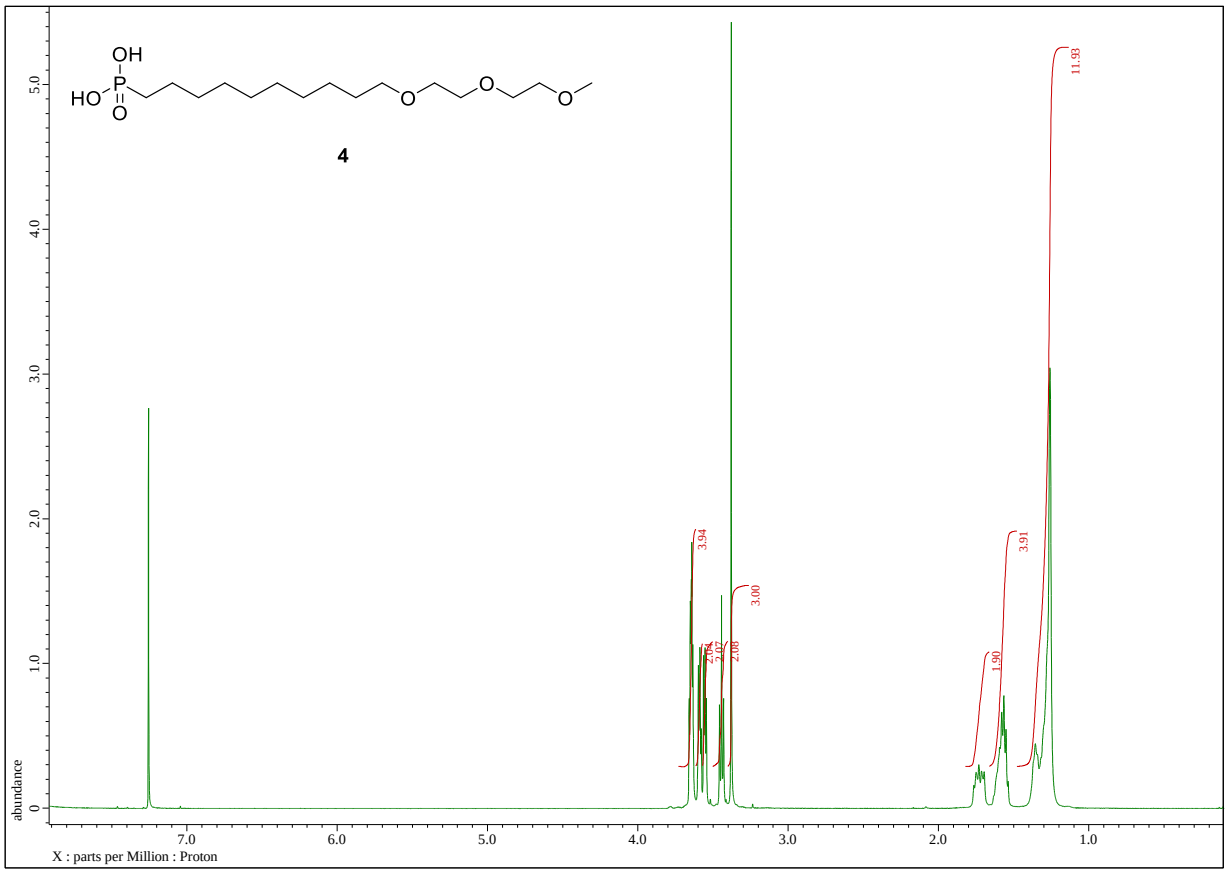
OH
HO
P
O
O
O
O
4
11.93
3.94
3.91
3.00
2.08
1.90
abundance
X : parts per Million : Proton

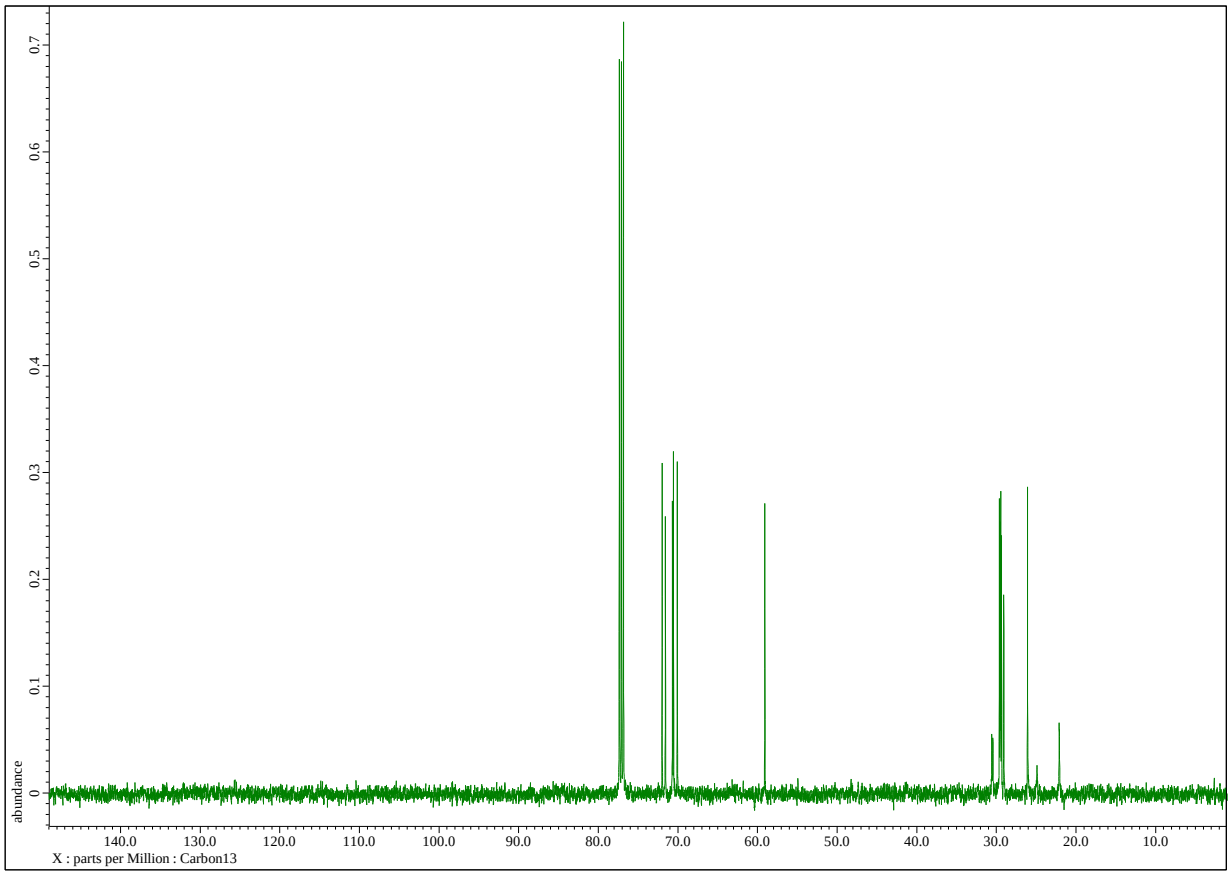
abundance
X : parts per Million : Carbon13

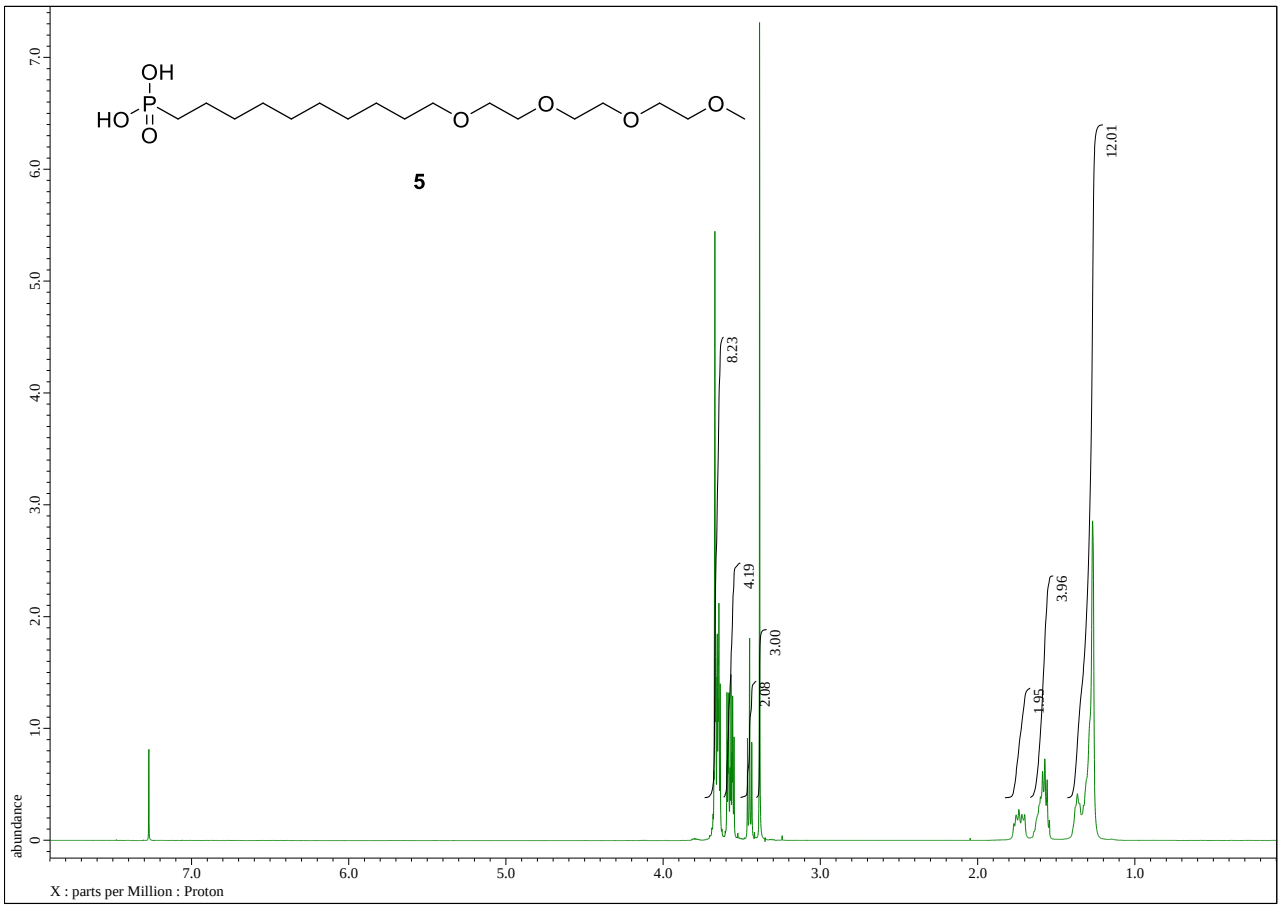
OH
HO
P
O
O
O
O
O
5
12.01
8.23
4.19
3.96
3.00
2.08
1.95
abundance
X : parts per Million : Proton

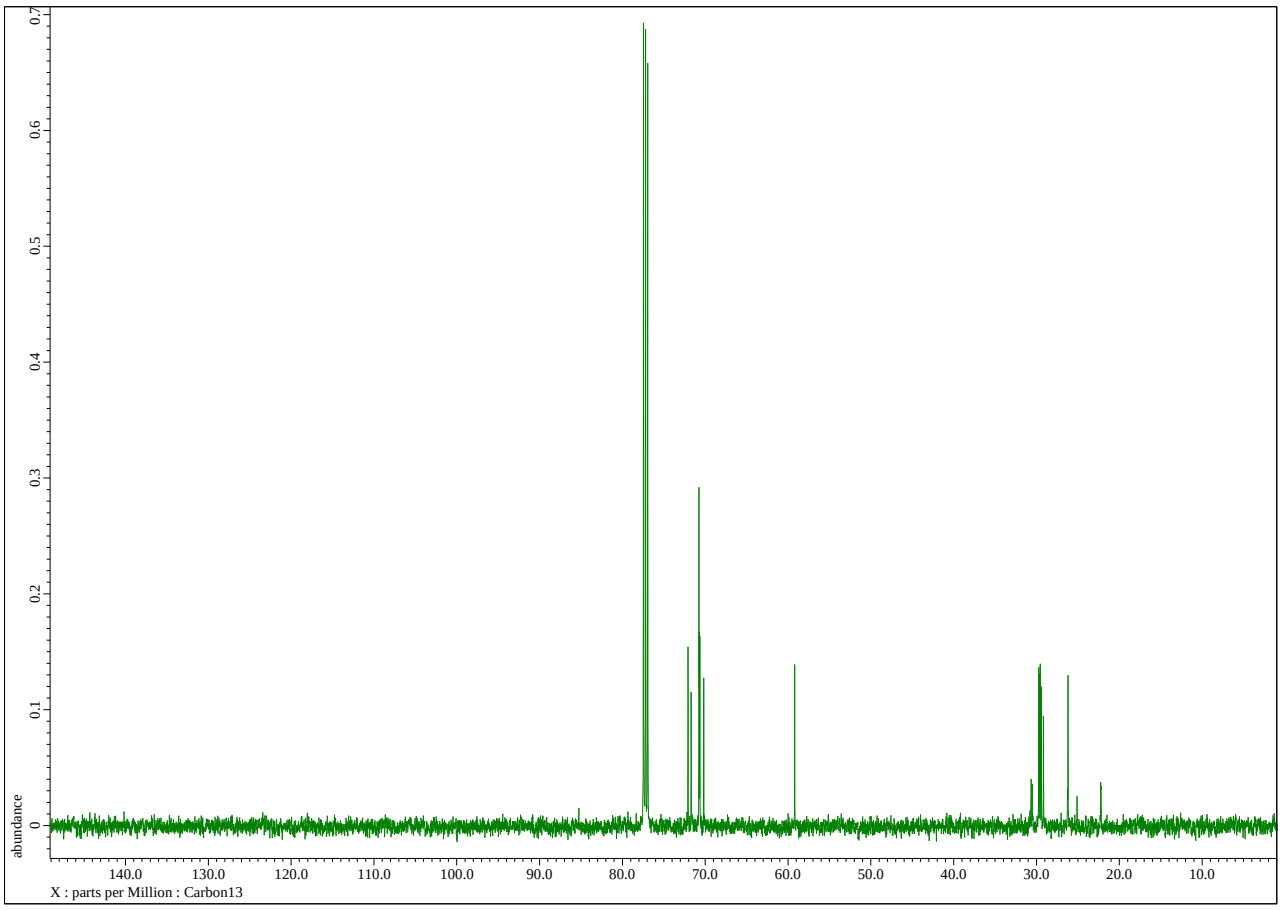
abundance
X : parts per Million : Carbon13

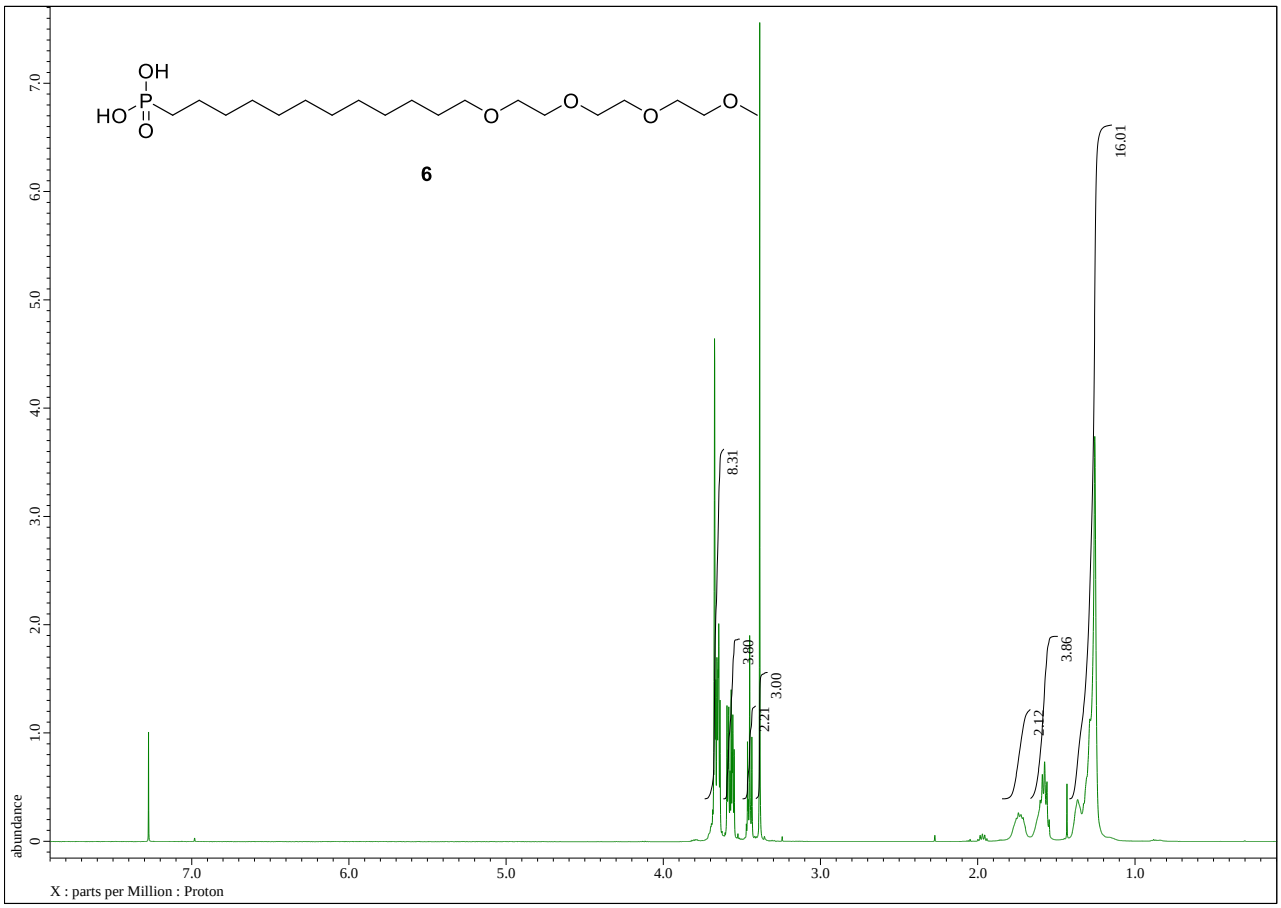
OH
HO
P
O
O
O
O
O
6
16.01
8.31
3.00
2.21
2.12
3.86
abundance
X : parts per Million : Proton

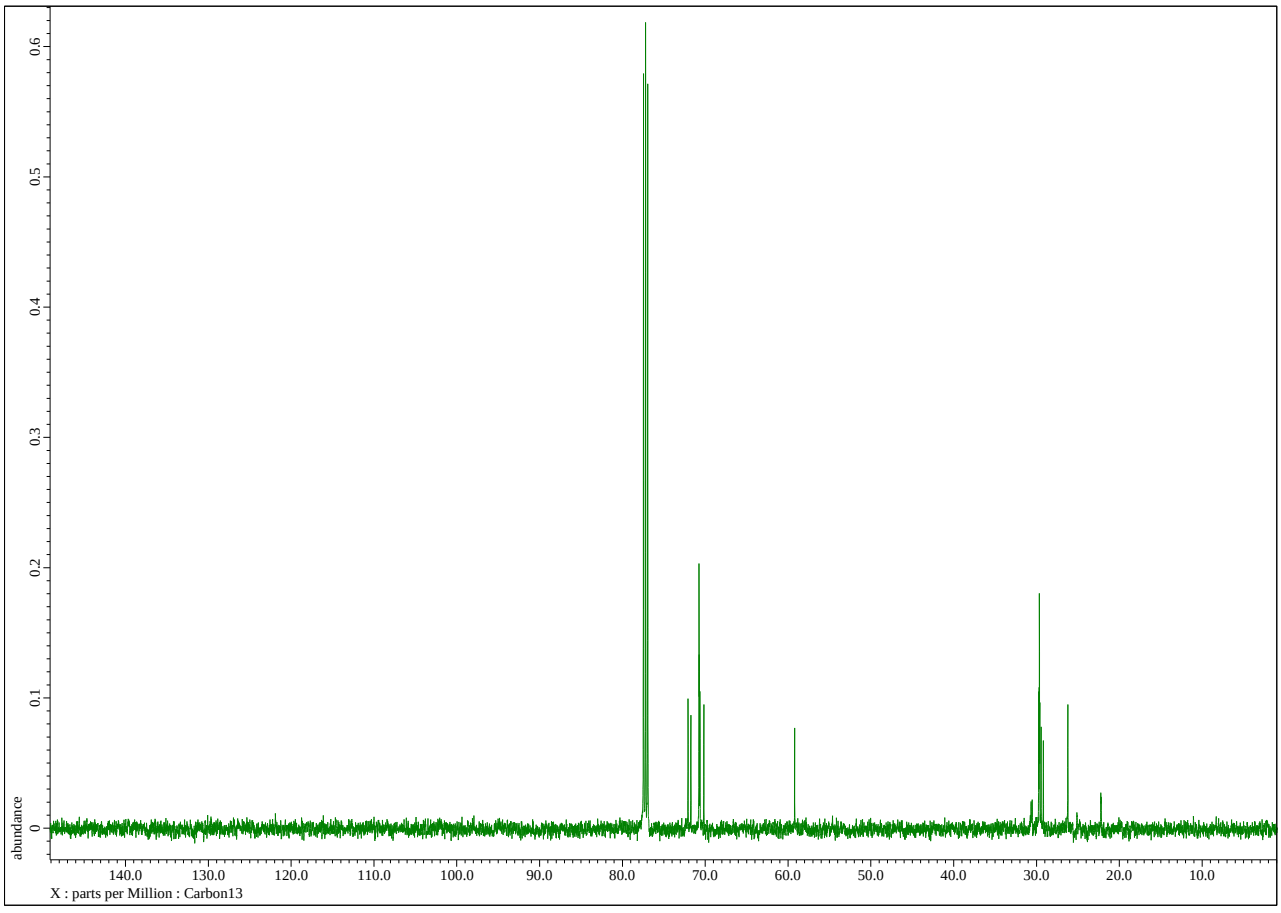
abundance
X : parts per Million : Carbon13

8.2. NMR and Mass Information in Chapter 3

S1

1-Bromo-8-(2-methoxyethoxy)octane ***(S1)***. ^{1}H NMR (500 MHz, $CDCl_3$) δ 3.58 (2H, m), 3.54 (2H, m), 3.46 (2H, t, J = 6.6 Hz), 3.41 (2H, t, J = 6.9 Hz), 3.39 (3H, s), 1.85 (2H, quint, J = 7.2 Hz), 1.60 (2H, m), 1.42 (2H, quint, J = 7.0 Hz), 1.32 (6H, m); ^{13}C NMR (125 MHz, $CDCl_3$) δ 71.9, 71.4, 69.9, 59.0, 33.8, 32.7, 29.5, 29.2, 28.6, 28.0, 25.9; HRMS $[M + Na]^+$ calculated for $C_{11}H_{23}O_2BrNa$ 289.0779, found 289.0870.

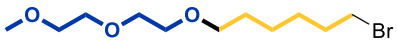

S2

1-Bromo-6-(2-(2-methoxyethoxy)ethoxy)hexane ***(S2)***. ^{1}H NMR (500 MHz, $CDCl_3$) δ 3.65 (4H, m), 3.60 (2H, m), 3.56 (2H, m), 3.46 (2H, t, J = 6.6 Hz), 3.41 (2H, t, J = 6.8 Hz), 3.39 (3H, s), 1.86 (2H, quint, J = 7.6 Hz), 1.60 (2H, m), 1.45 (2H, m), 1.37 (2H, m); ^{13}C NMR (125 MHz, $CDCl_3$) δ 71.9, 71.1, 70.6, 70.5, 70.0, 59.0, 33.8, 32.7, 29.4, 27.9, 25.3; HRMS $[M + Na]^+$ calculated for $C_{11}H_{23}O_3BrNa$ 305.0728, found 305.0707.

S3

1-Bromo-8-(2-(2-methoxyethoxy)ethoxy)octane ***(S3)***. ^{1}H NMR (500 MHz, $CDCl_3$) δ 3.65 (4H, m), 3.60 (2H, m), 3.56 (2H, m), 3.45 (2H, t, J = 6.7 Hz), 3.41 (2H, t, J = 6.9 Hz), 3.39 (3H, s), 1.85 (2H, quint, J = 7.3 Hz), 1.57 (2H, m), 1.42 (2H, quint, J = 6.8 Hz), 1.32 (6H, m); ^{13}C NMR (125 MHz, $CDCl_3$) δ 72.0, 71.4, 70.7, 70.5, 70.1, 59.1, 34.0, 32.8, 29.6, 29.3, 28.7, 28.1, 26.0; HRMS $[M + Na]^+$ calculated for $C_{13}H_{27}O_3BrNa$ 333.1041, found 333.1069.

S4

1-Bromo-10-(2-(2-methoxyethoxy)ethoxy)decane ***(S4)***. ^{1}H NMR (500 MHz, $CDCl_3$) δ 3.65 (4H, m), 3.60 (2H, m), 3.56 (2H, m), 3.45 (2H, t, J = 6.7 Hz), 3.41 (2H, t, J = 7.0 Hz), 3.38 (3H, s), 1.85 (2H, quint, J = 7.5 Hz), 1.58 (2H, m), 1.42 (2H, m), 1.29 (10H, m); ^{13}C NMR δ 72.0, 71.5, 70.7, 70.5, 70.0, 59.0, 34.0, 32.8, 29.6, 29.5, 29.4, 29.4, 28.8 ,28.2, 26.1; HRMS $[M + Na]^+$ calculated for $C_{15}H_{31}O_3BrNa$ 361.1354, found 361.1371.

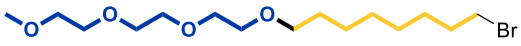

S5

19-Bromo-2,5,8,11-tetraoxanonadecane ***(S5)***. ^{1}H NMR (500 MHz, $CDCl_3$) δ 3.66 (8H, m), 3.58 (2H, m), 3.55 (2H, m), 3.45 (2H, t, J = 6.8 Hz), 3.41 (2H, t, J = 7.0 Hz), 3.38 (3H, s), 1.85 (2H, quint, J = 7.2 Hz), 1.58 (2H, m), 1.42 (2H, quint, J = 6.8 Hz), 1.32 (6H, m); ^{13}C NMR (125 MHz, $CDCl_3$) δ 71.9, 71.4, 70.6, 70.6, 70.6, 70.5, 70.0, 59.0, 34.0, 32.8, 29.6, 29.2, 28.7, 28.1, 26.0; HRMS $[M + Na]^+$ calculated for $C_{15}H_{31}O_4BrNa$ 377.1303, found 377.1289.

S6

*21-Bromo-2,5,8,11-tetraoxahenicosane (**S6**)*. ^{1}H NMR (500 MHz, $CDCl_3$) δ 3.66 (8H, m), 3.58 (2H, m), 3.55 (2H, m), 3.45 (2H, t, J = 6.9 Hz), 3.41 (2H, t, J = 6.9 Hz), 3.38 (3H, s), 1.85 (2H, quint, J = 7.3 Hz), 1.57 (2H, quint, J = 7.3 Hz), 1.42 (2H, quint, J = 7.4 Hz), 1.29 (10H, m); ^{13}C NMR (125 MHz, $CDCl_3$) δ 71.8, 71.4, 70.5, 70.5, 70.4, 70.0, 58.9, 33.9, 32.7, 29.5, 29.4, 29.3, 29.3, 28.7, 28.1, 26.0; HRMS $[M + Na]^+$ calculated for $C_{17}H_{35}O_4BrNa$ 405.1616, found 405.1609.

S7

*23-Bromo-2,5,8,11-tetraoxatricosane (**S7**)*. ^{1}H NMR (500 MHz, $CDCl_3$) δ 3.65 (8H, m), 3.58 (2H, m), 3.56 (2H, m), 3.45 (2H, t, J = 6.7 Hz), 3.41 (2H, t, J = 6.9 Hz), 3.38 (3H, s), 1.85 (2H, quint, J = 7.1 Hz), 1.58 (2H, quint, J = 6.9 Hz), 1.42 (2H, quint, J = 7.1 Hz), 1.27 (14H, m); ^{13}C NMR (125 MHz, $CDCl_3$) δ 71.8, 71.3, 70.5, 70.5, 70.5, 70.4, 69.9, 58.9, 33.8, 32.8, 29.5, 29.4, 29.4, 29.4, 29.4, 29.3, 28.7, 28.0, 26.0; HRMS $[M + Na]^+$ calculated for $C_{19}H_{39}O_4BrNa$ 433.1929, found 433.1932.

S8

*2-(8-(2-Methoxyethoxy)octyl)isoindoline-1,3-dione (**S8**)*. ^{1}H NMR (500 MHz, $CDCl_3$) δ 7.84 (2H, m), 7.71 (2H, dd, J = 5.4, 3.1 Hz), 3.67 (2H, t, J = 7.3 Hz), 3.57 (2H, m), 3.54 (2H, m), 3.44 (2H, t, J = 6.8 Hz), 3.39 (3H, s), 1.66 (2H, m), 1.58 (2H, m), 1.32 (8H, m); ^{13}C NMR (125 MHz, $CDCl_3$) δ 168.5, 133.9, 132.2, 123.2, 72.1, 71.6, 70.0, 59.1, 38.1, 29.6, 29.4, 29.2, 28.7, 26.9, 26.1; HRMS $[M + Na]^+$ calculated for $C_{19}H_{27}NO_4Na$ 356.1838, found 356.1820.

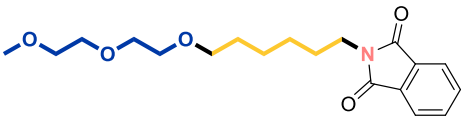

S9

*2-(6-(2-(2-Methoxyethoxy)ethoxy)hexyl)isoindoline-1,3-dione (**S9**)*. ^{1}H NMR (500 MHz, $CDCl_3$) δ 7.84 (2H, m), 7.71 (2H, dd, J = 5.4, 3.1 Hz), 3.68 (2H, t, J = 7.4 Hz), 3.64 (4H, m), 3.57 (4H, m), 3.44 (2H, t, J = 6.7 Hz), 3.38 (3H, s), 1.68 (2H, m), 1.58 (2H, m), 1.37 (4H, m); ^{13}C NMR (125 MHz, $CDCl_3$) δ 168.5, 133.9, 132.2, 123.2, 72.0, 71.3, 70.7, 70.6, 70.1, 59.1, 38.0, 29.5, 28.6, 26.8, 25.8; HRMS $[M + Na]^+$ calculated for $C_{19}H_{27}NO_5Na$ 372.1787, found 372.1758.

S10

2-(8-(2-(2-Methoxyethoxy)ethoxy)octyl)isoindoline-1,3-dione (***S10***). ^{1}H NMR (500 MHz, $CDCl_3$) δ 7.84 (2H, m), 7.71 (2H, dd, *J* = 5.3, 3.0 Hz), 3.67 (2H, t, *J* = 7.3 Hz), 3.65 (4H, m), 3.59 (2H, m), 3.56 (2H, m), 3.44 (2H, t, *J* = 6.8 Hz), 3.38 (3H, s), 1.66 (2H, m), 1.56 (2H, m), 1.31 (8H, m); ^{13}C NMR (125 MHz, $CDCl_3$) δ 168.5, 133.9, 132.2, 123.2, 72.0, 71.5, 70.7, 70.6, 70.1, 59.1, 38.1, 29.7, 29.4, 29.2, 28.7, 26.9, 26.1; HRMS $[M + Na]^+$ calculated for $C_{21}H_{31}NO_5Na$ 400.2100, found 400.2106.

S11

2-(10-(2-(2-Methoxyethoxy)ethoxy)decyl)isoindoline-1,3-dione (***S11***). ^{1}H NMR (500 MHz, $CDCl_3$) δ 7.84 (2H, dd, *J* = 5.0, 3.0 Hz), 7.71 (2H, dd, *J* = 5.5, 2.5 Hz), 3.66 (6H, m), 3.59 (2H, m), 3.56 (2H, m), 3.44 (2H, t, *J* = 7.0 Hz), 3.38 (3H, s), 1.66 (2H, m), 1.56 (2H, m), 1.28 (12H, m); ^{13}C NMR (125 MHz, $CDCl_3$) δ 168.4, 133.8, 132.2, 123.1, 72.0, 71.5, 70.7, 70.5, 70.1, 59.0, 38.0, 29.6, 29.5, 29.4, 29.2, 28.6, 26.7, 26.1; HRMS $[M + Na]^+$ calculated for $C_{23}H_{35}NO_5Na$ 428.2413, found 428.2420.

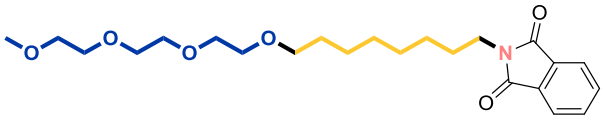

S12

2-(2,5,8,11-Tetraoxanonadecan-19-yl)isoindoline-1,3-dione (***S12***). ^{1}H NMR (500 MHz, $CDCl_3$) δ 7.84 (2H, m), 7.71 (2H, dd, *J* = 5.4, 3.1 Hz), 3.65 (10H, m), 3.56 (4H, m), 3.43 (2H, t, *J* = 6.7 Hz), 3.38 (3H, s), 1.67 (2H, m), 1.56 (2H, m), 1.31 (8H, m); ^{13}C NMR (125 MHz, $CDCl_3$) δ 168.4, 133.8, 132.1,123.1, 71.9, 71.4, 70.6, 70.5, 70.0, 59.0, 38.0, 29.6, 29.3, 29.1, 28.5, 26.8, 26.0; HRMS $[M + Na]^+$ calculated for $C_{23}H_{35}NO_6Na$ 444.2362, found 444.2350.

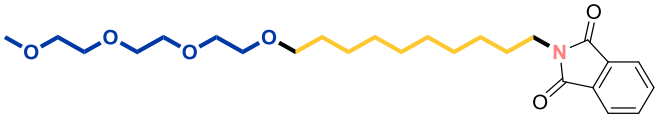

S13

2-(2,5,8,11-Tetraoxahenicosan-21-yl)isoindoline-1,3-dione (***S13***). ^{1}H NMR (500 MHz, $CDCl_3$) δ 7.84 (2H, m), 7.71 (2H, m), 3.66 (10H, m), 3.57 (4H, m), 3.44 (2H, t, *J* = 6.9 Hz), 3.38 (3H, s), 1.67 (2H, m), 1.56 (2H, m), 1.29 (12H, m); ^{13}C NMR (125 MHz, $CDCl_3$) δ 168.5, 133.9, 132.2, 123.2, 72.0, 71.5, 70.7, 70.5, 70.1, 59.1, 38.1, 29.7, 29.5, 29.4, 29.2, 28.6, 26.9, 26.1; HRMS $[M + Na]^+$ calculated for $C_{25}H_{39}NO_6Na$ 472.2675, found

472.2670.

S14

*2-(2,5,8,11-Tetraoxatricosan-23-yl)isoindoline-1,3-dione (**S14**)*. ^{1}H NMR (500 MHz, $CDCl_3$) δ 7.84 (2H, m), 7.71 (2H, dd, *J* = 5.5, 3.1 Hz), 3.66 (10H, m), 3.56 (4H, m), 3.44 (2H, t, *J* = 7.0 Hz), 3.38 (3H, s), 1.67 (2H, m), 1.58 (2H, m), 1.28 (16H, m); ^{13}C NMR (125 MHz, $CDCl_3$) δ 168.4, 133.8, 132.1, 123.1, 71.9, 71.5, 70.6, 70.6, 70.5, 70.0, 59.0, 38.0, 29.6, 29.5, 29.5, 29.2, 28.6, 26.8, 26.1; HRMS $[M + Na]^+$ calculated for $C_{27}H_{43}NO_6Na$ 500.2988, found 500.2983.

1

*8-(2-Methoxyethoxy)octan-1-amine (EG1:C8A, **1**)*. ^{1}H NMR (500 MHz, $CDCl_3$) δ 3.57 (2H, m), 3.54 (2H, m), 3.45 (2H, t, *J* = 6.9 Hz), 3.39 (3H, s), 2.67 (2H, t, *J* = 7.0 Hz), 1.59 (2H, quint, *J* = 6.8 Hz), 1.44 (2H, m), 1.31 (8H, m); ^{13}C NMR (125 MHz, $CDCl_3$) δ 72.1, 71.6, 70.0, 59.1, 42.1, 33.4, 29.6, 29.5, 29.4, 26.9, 26.1; HRMS $[M + Na]^+$ calculated for $C_{11}H_{25}NO_2Na$ 226.1783, found 226.1757.

2

*6-(2-(2-Methoxyethoxy)ethoxy)hexan-1-amine (EG2:C6A, **2**)*. ^{1}H NMR (500 MHz, $CDCl_3$) δ 3.65 (4H, m), 3.60 (2H, m), 3.56 (2H, m), 3.46 (2H, t, *J* = 7.0 Hz), 3.39 (3H, s), 2.68 (2H, t, *J* = 7.0 Hz), 1.60 (2H, m), 1.44 (2H, m), 1.34 (4H, m); ^{13}C NMR (125 MHz, $CDCl_3$) δ 71.9, 71.3, 70.6, 70.5, 70.0, 59.0, 41.9, 33.3, 29.6, 26.7, 25.9; HRMS $[M + Na]^+$ calculated for $C_{11}H_{25}NO_3Na$ 242.1732, found 242.1735.

3

*8-(2-(2-Methoxyethoxy)ethoxy)octan-1-amine (EG2:C8A, **3**)*. ^{1}H NMR (500 MHz, $CDCl_3$) δ 3.65 (4H, m), 3.60 (2H, m), 3.56 (2H, m), 3.45 (2H, t, *J* = 6.9 Hz), 3.39 (3H, s), 2.67 (2H, t, *J* = 6.9 Hz), 1.58 (2H, quint, *J* = 6.6 Hz), 1.43 (2H, m), 1.30 (8H, m); ^{13}C NMR (125 MHz, $CDCl_3$) δ 71.9, 71.4, 70.6, 70.5, 70.0, 59.0, 42.1, 33.6, 29.6, 29.4, 26.8, 26.0; HRMS $[M + Na]^+$ calculated for $C_{13}H_{29}NO_3Na$ 270.2045, found 270.2057.

4

*10-(2-(2-Methoxyethoxy)ethoxy)decan-1-amine (EG2:C10A, **4**)*. ^{1}H NMR (500 MHz, $CDCl_3$) δ 3.65 (4H, m), 3.60 (2H, m), 3.56 (2H, m), 3.45(2H, t, *J* = 7.0 Hz), 3.39 (3H, s), 2.68 (2H, t, *J* = 7.0 Hz), 1.58 (2H, m), 1.42 (4H, m), 1.29 (12H, m); ^{13}C NMR (125 MHz, $CDCl_3$) δ 72.0, 71.6, 70.7, 70.6, 70.1, 59.1, 42.2, 33.7, 29.7,

29.6, 29.6, 29.5, 27.0, 26.2; HRMS $[M + Na]^+$ calculated for $C_{15}H_{33}NO_3Na$ 298.2358, found 298.2329.

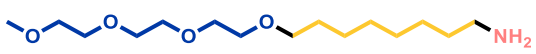

5

2,5,8,11-Tetraoxanonadecan-19-amine (EG3:C8A, ***5****)*.[12] ^1H NMR (500 MHz, $CDCl_3$) δ 3.66 (8H, m), 3.58 (2H, m), 3.55 (2H, m), 3.45 (2H, t, J = 6.8 Hz), 3.38 (3H, s), 2.67 (2H, t, J = 7.1 Hz), 1.57 (2H, quint, J = 6.8 Hz), 1.43 (2H, m), 1.32 (8H, m); ^{13}C NMR (125 MHz, $CDCl_3$) δ 71.5, 70.9, 70.2, 70.1, 69.6, 58.5, 41.6, 33.1, 29.2, 29.0, 26.4, 25.6; HRMS $[M + Na]^+$ calculated for $C_{15}H_{33}NO_4Na$ 314.2307, found 314.2328.

6

2,5,8,11-Tetraoxahenicosan-21-amine (EG3:C10A, ***6****)*. ^1H NMR (500 MHz, $CDCl_3$) δ 3.65 (8H, m), 3.57 (4H, m), 3.45(2H, t, J = 7.0 Hz), 3.38 (3H, s), 2.67 (2H, t, J = 7.0 Hz), 1.57 (2H, m), 1.43 (2H, m), 1.28 (12H, m); ^{13}C NMR (125 MHz, $CDCl_3$) δ 71.9, 71.5, 70.6, 70.6, 70.5, 70.0, 59.0, 42.2, 33.8, 29.6, 29.5, 29.5, 29.4, 26.9, 26.0; HRMS $[M + Na]^+$ calculated for $C_{17}H_{37}NO_4Na$ 342.2620, found 342.2628.

7

2,5,8,11-Tetraoxatricosan-23-amine (EG3:C12A, ***7****)*. ^1H NMR (500 MHz, $CDCl_3$) δ 3.65 (8H, m), 3.58 (2H, m), 3.55 (2H, m), 3.45 (2H, t, J = 6.8 Hz), 3.38 (3H, s), 2.68 (2H, t, J = 7.0 Hz), 1.57 (2H, quint, J = 7.2 Hz), 1.44 (2H, m), 1.28 (16H, m); ^{13}C NMR (125 MHz, $CDCl_3$) δ 72.0, 71.6, 70.7, 70.7, 70.6, 70.1, 59.1, 41.7, 32.8, 29.7, 29.6, 29.5, 27.0, 26.2; HRMS $[M + Na]^+$ calculated for $C_{19}H_{41}NO_4Na$ 370.2933, found 370.2958.

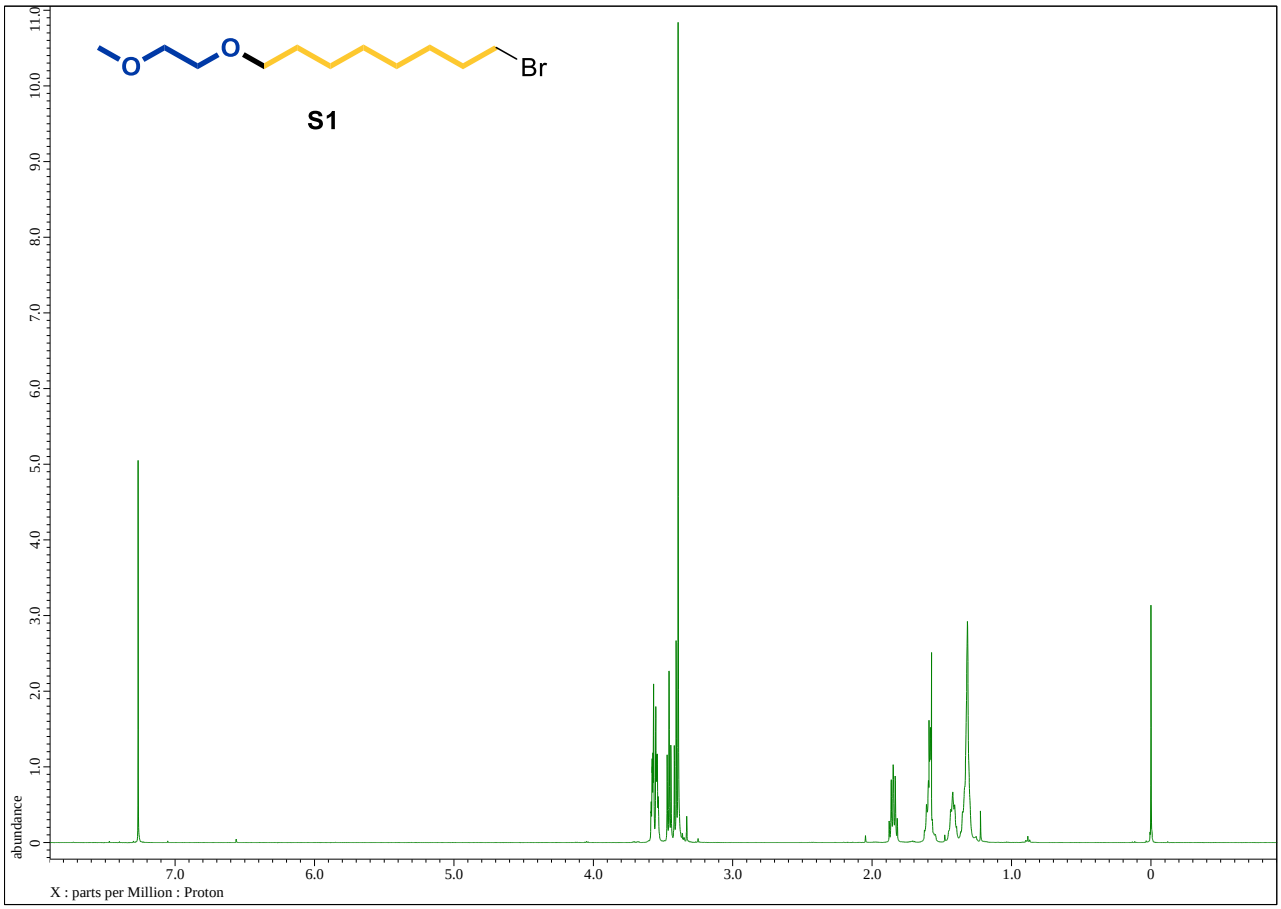
O
O
Br
S1
abundance
X : parts per Million : Proton

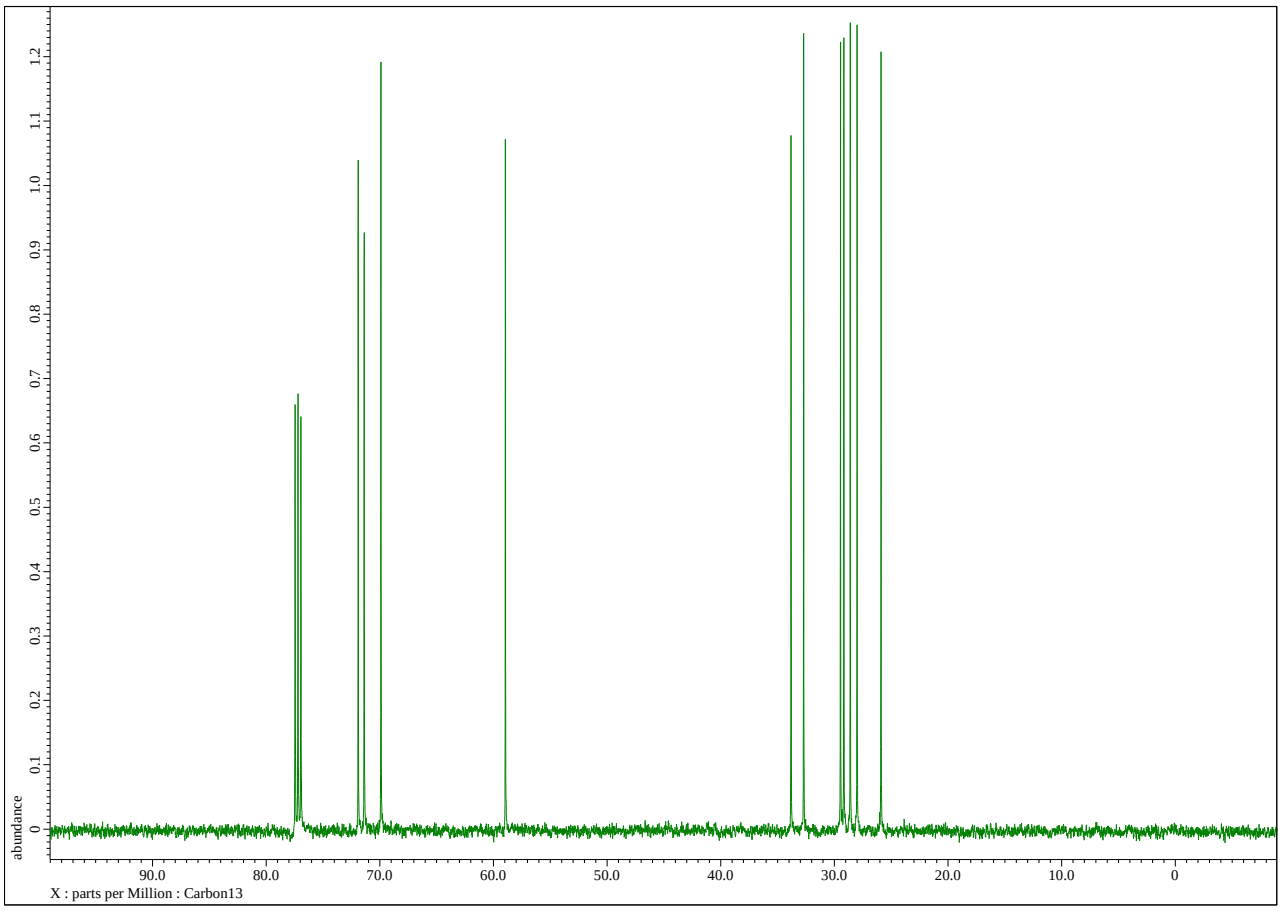
abundance
X : parts per Million : Carbon13

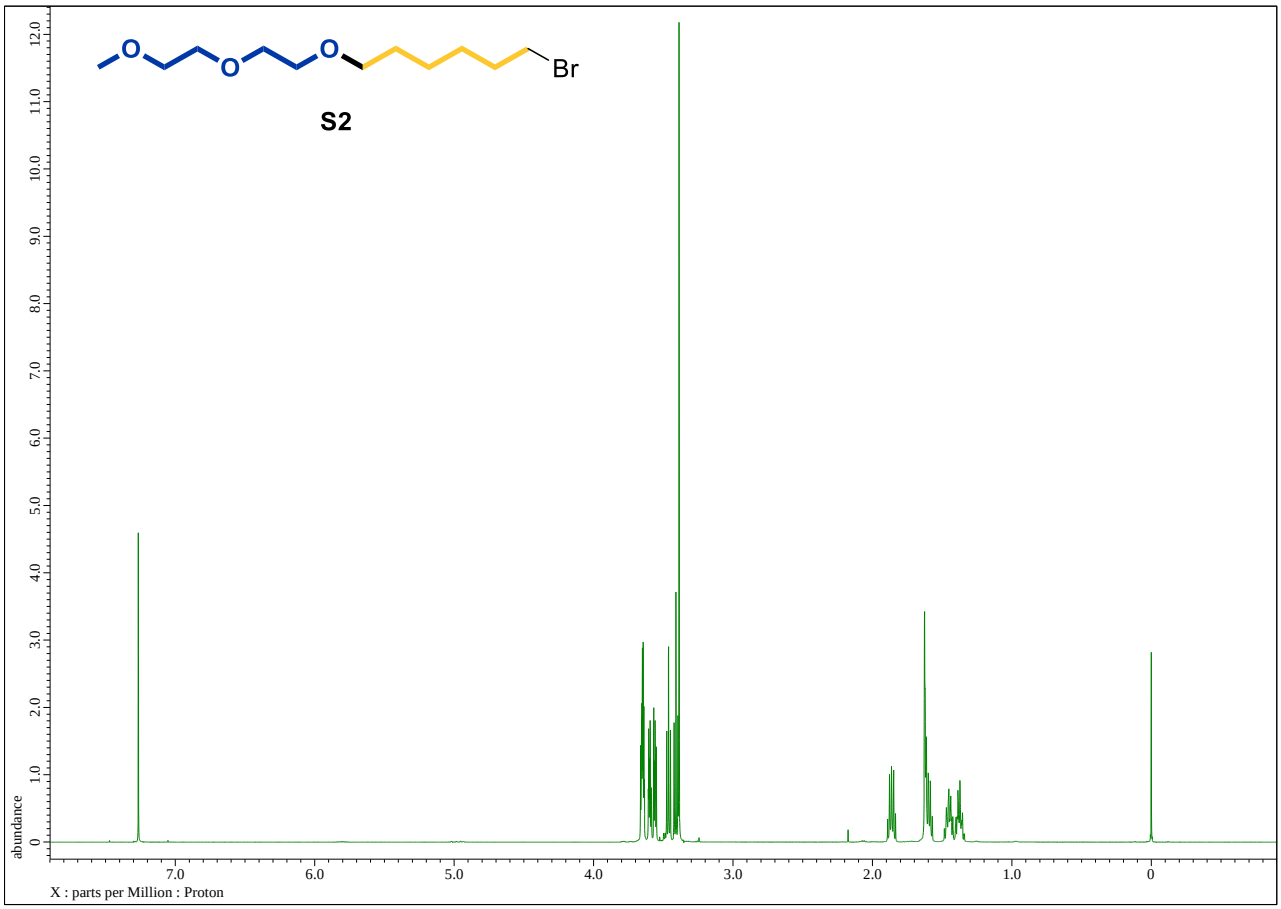
S2
Br
abundance
X : parts per Million : Proton

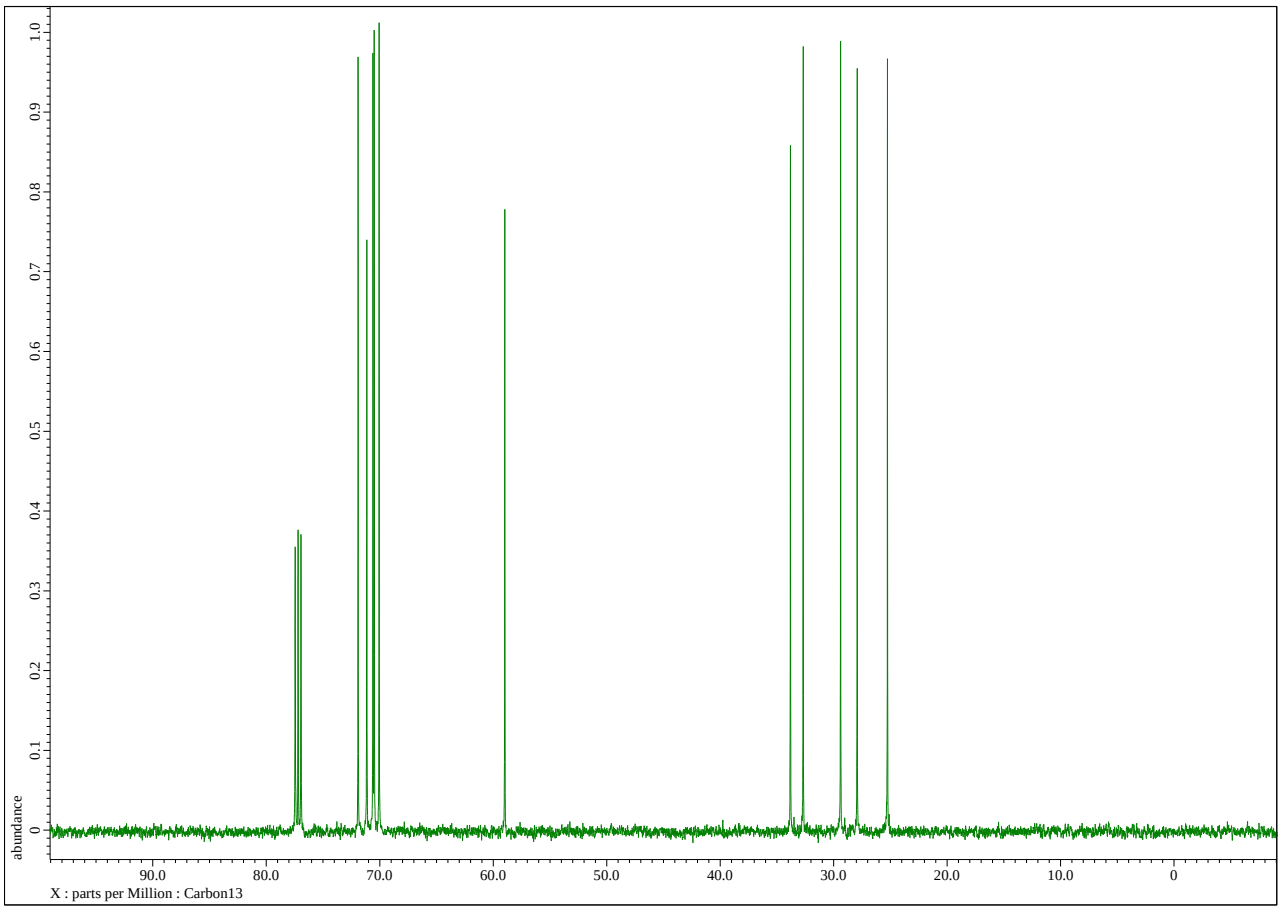
abundance
X : parts per Million : Carbon13

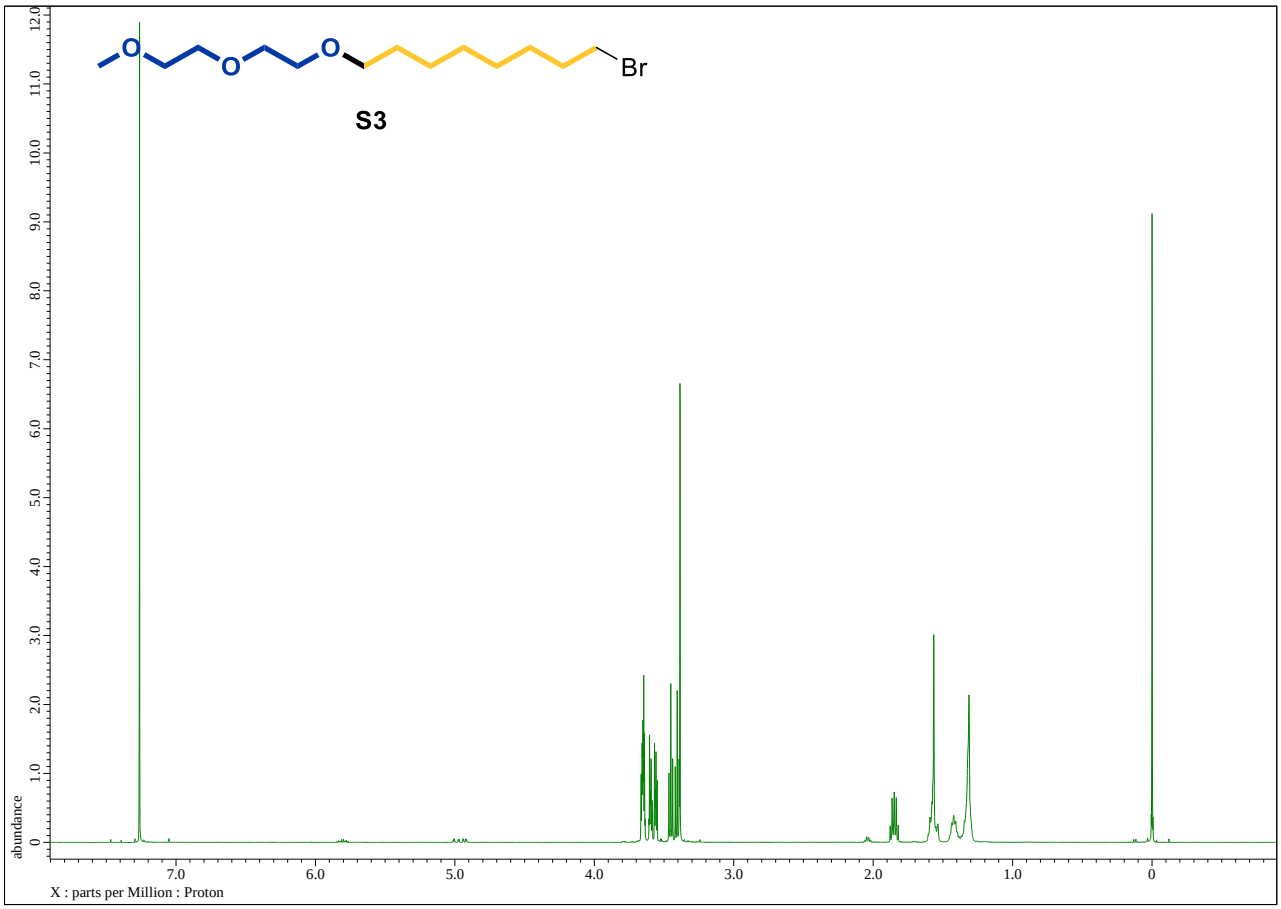
O
O
O
Br
S3
abundance
12.0
11.0
10.0
9.0
8.0
7.0
6.0
5.0
4.0
3.0
2.0
1.0
0
7.0
6.0
5.0
4.0
3.0
2.0
1.0
0
X : parts per Million : Proton

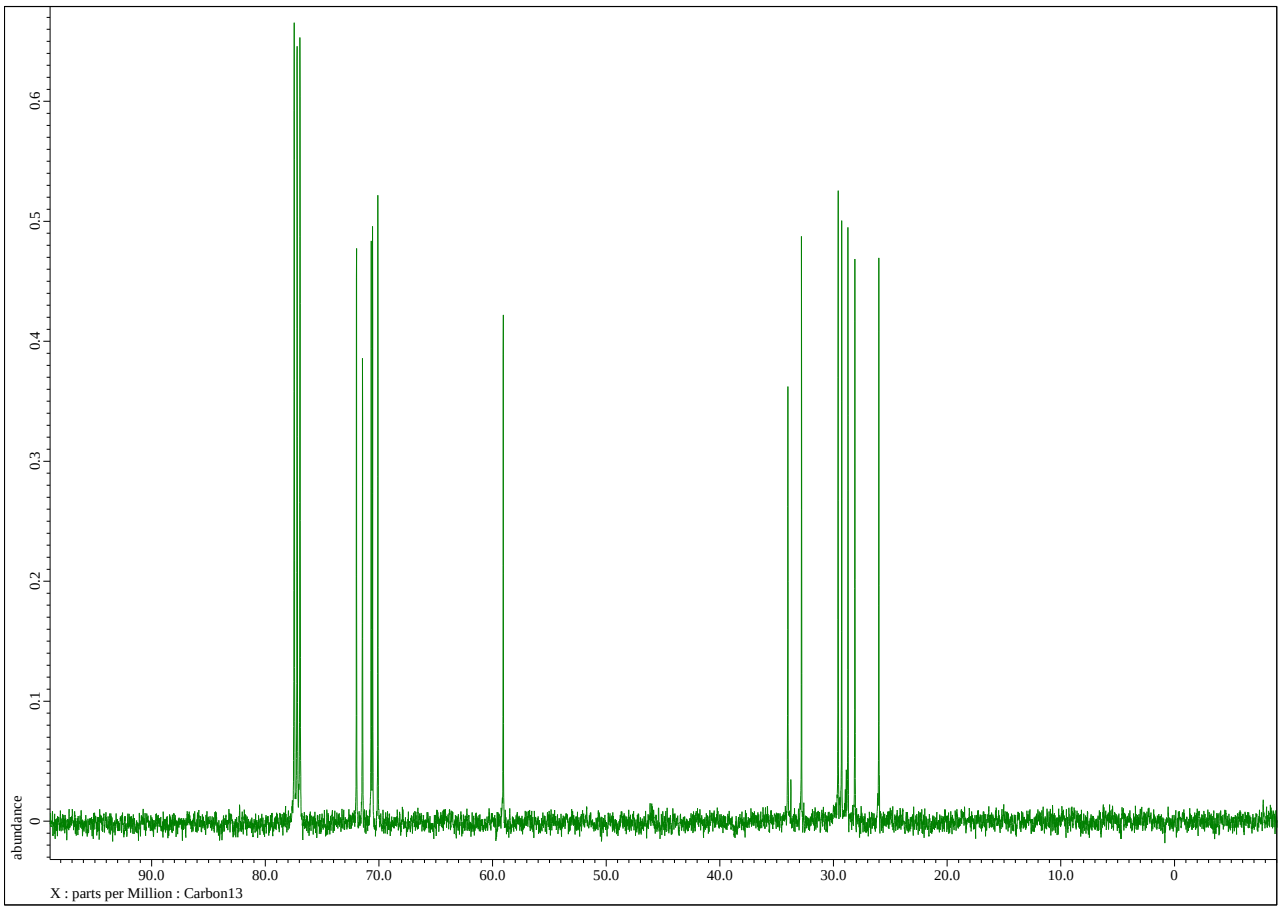
abundance
0.6
0.5
0.4
0.3
0.2
0.1
0
90.0
80.0
70.0
60.0
50.0
40.0
30.0
20.0
10.0
0
X : parts per Million : Carbon13

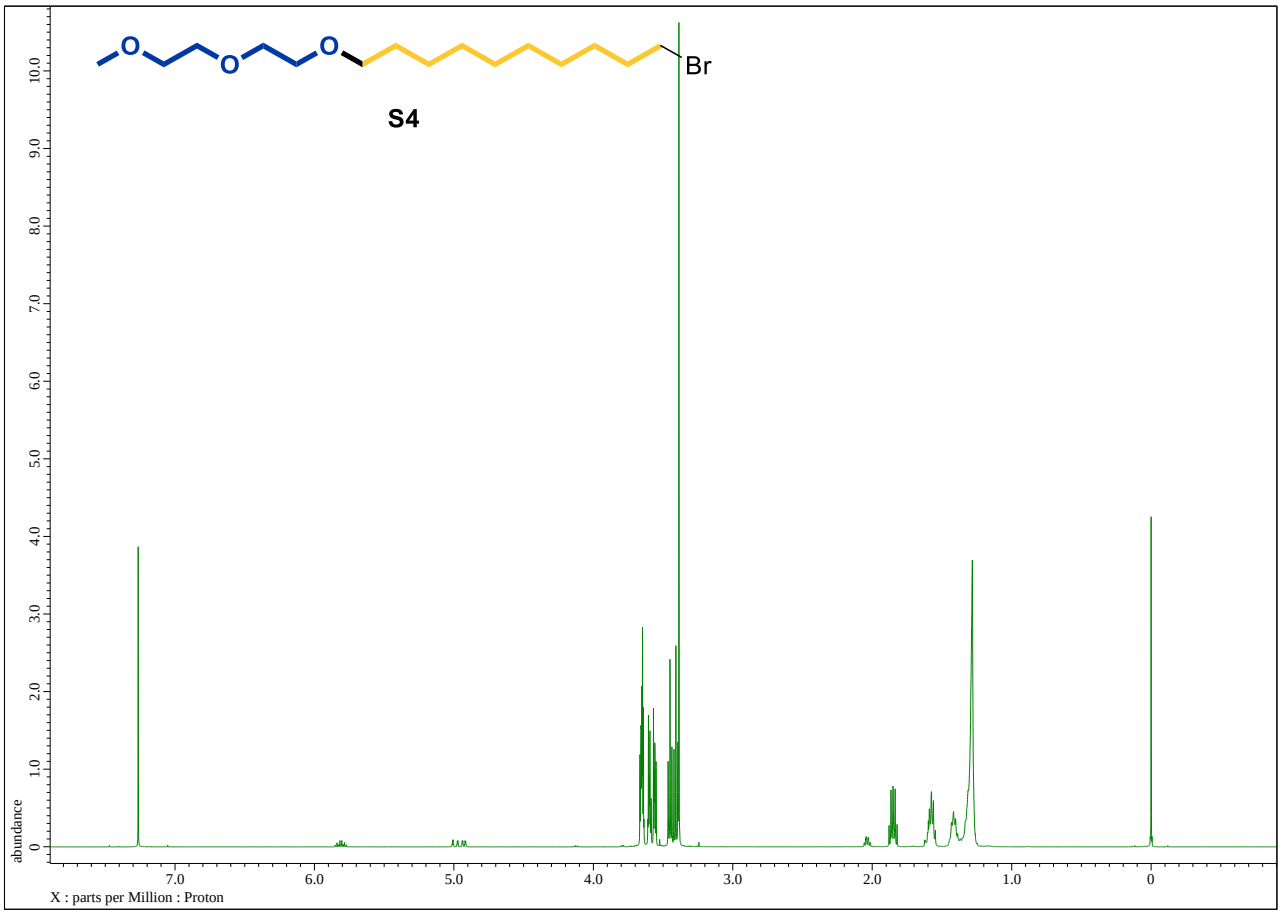
O
O
O
Br
S4
abundance
X : parts per Million : Proton

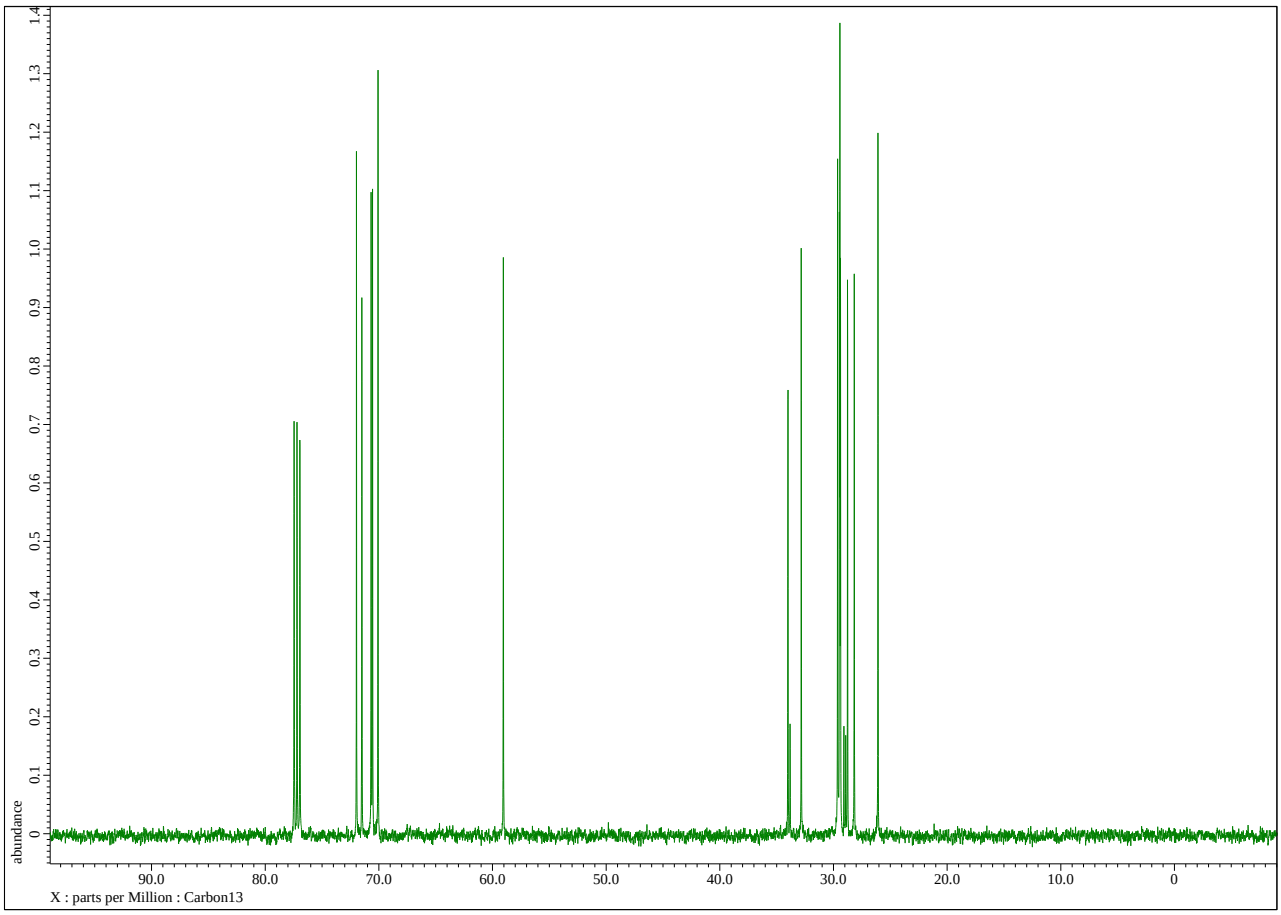
abundance
X : parts per Million : Carbon13

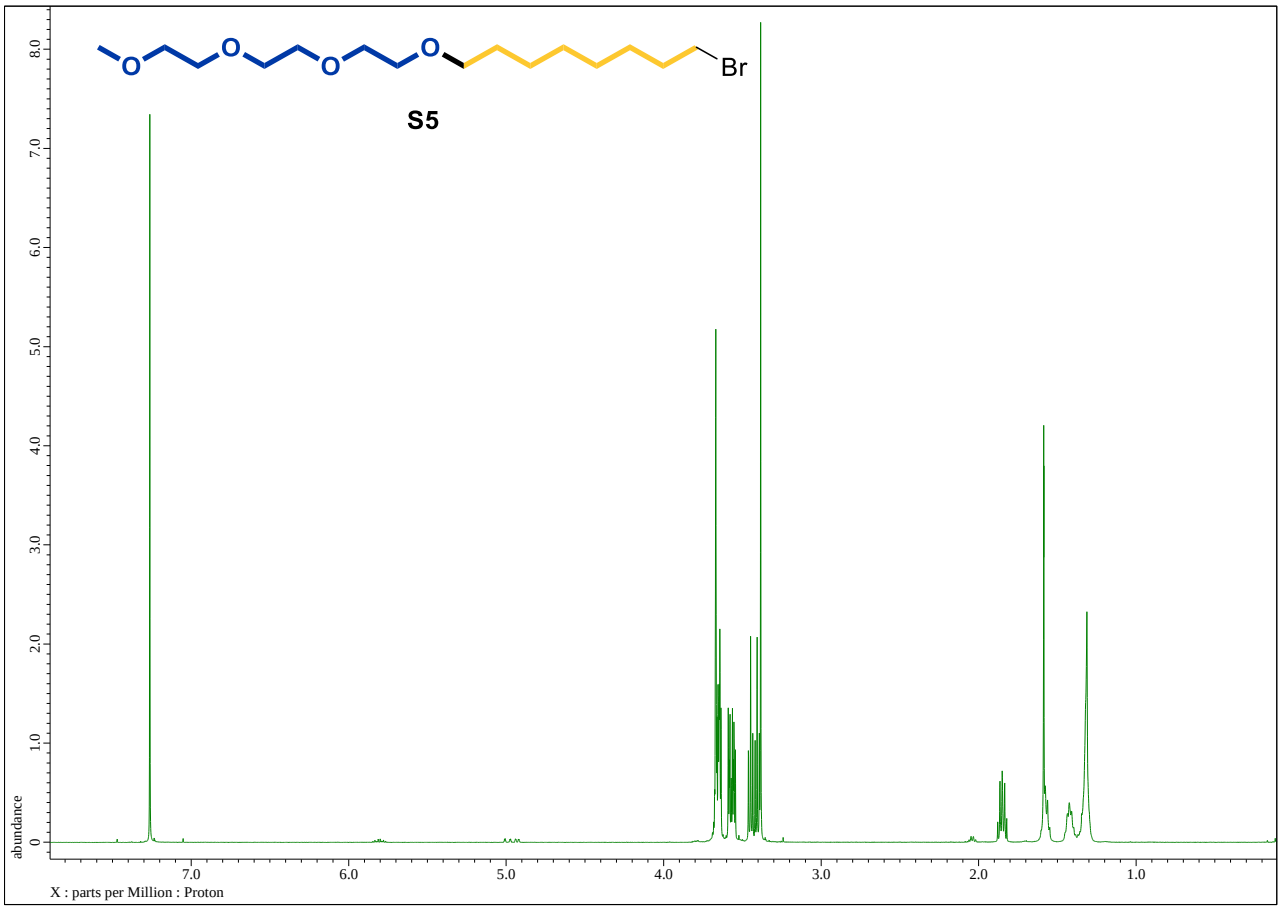
Br
S5
abundance
X : parts per Million : Proton

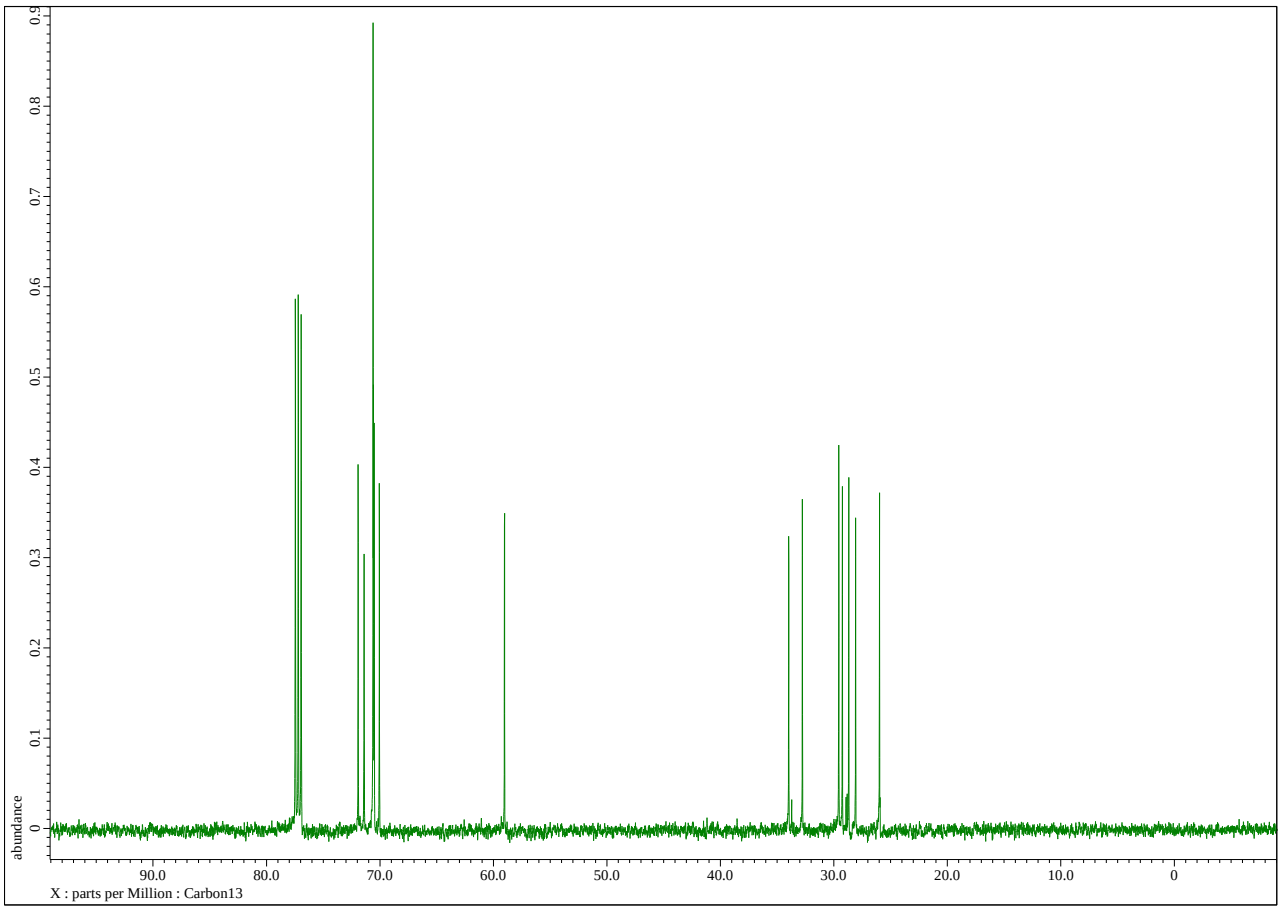
abundance
X : parts per Million : Carbon13

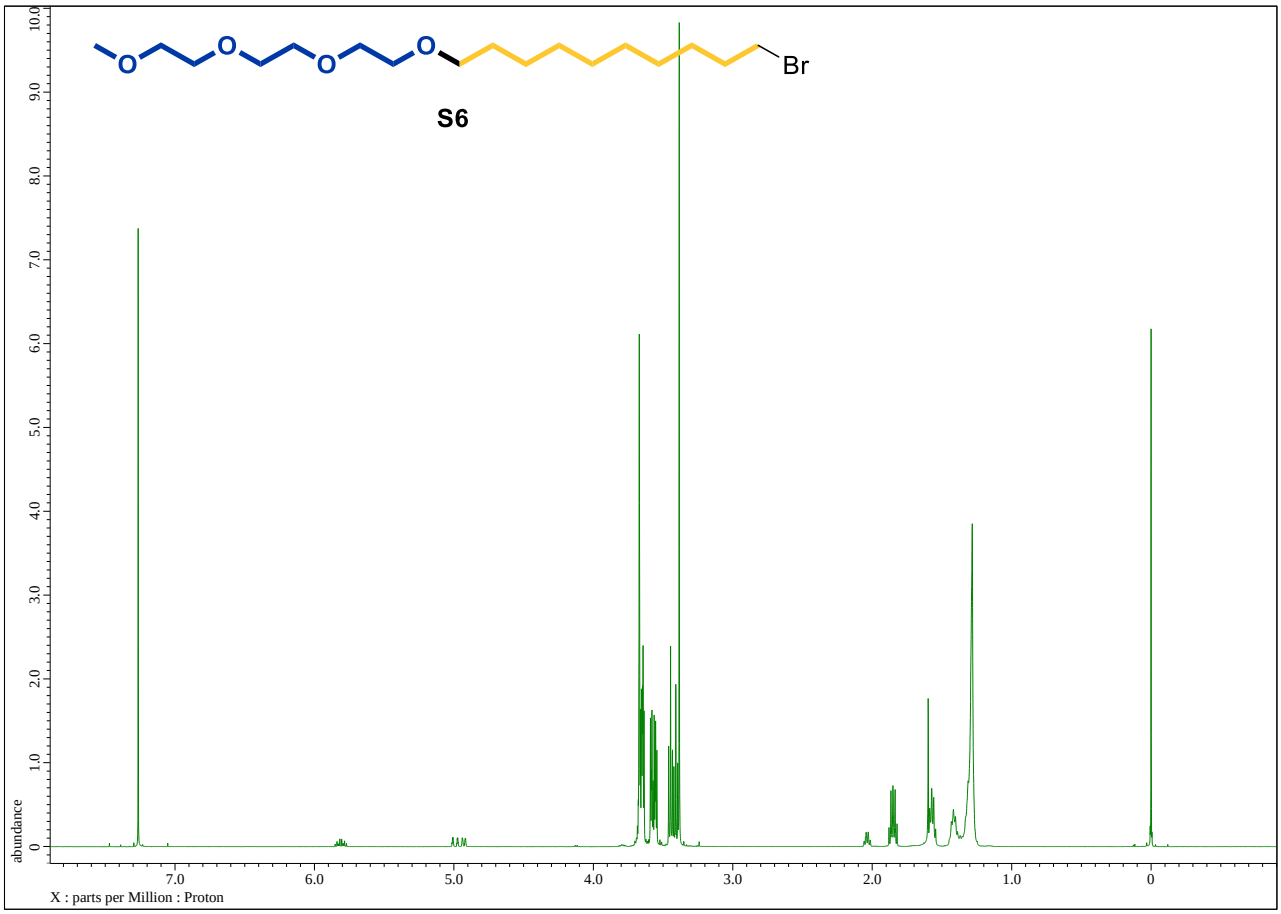
O
O
O
O
Br
S6
abundance
X : parts per Million : Proton

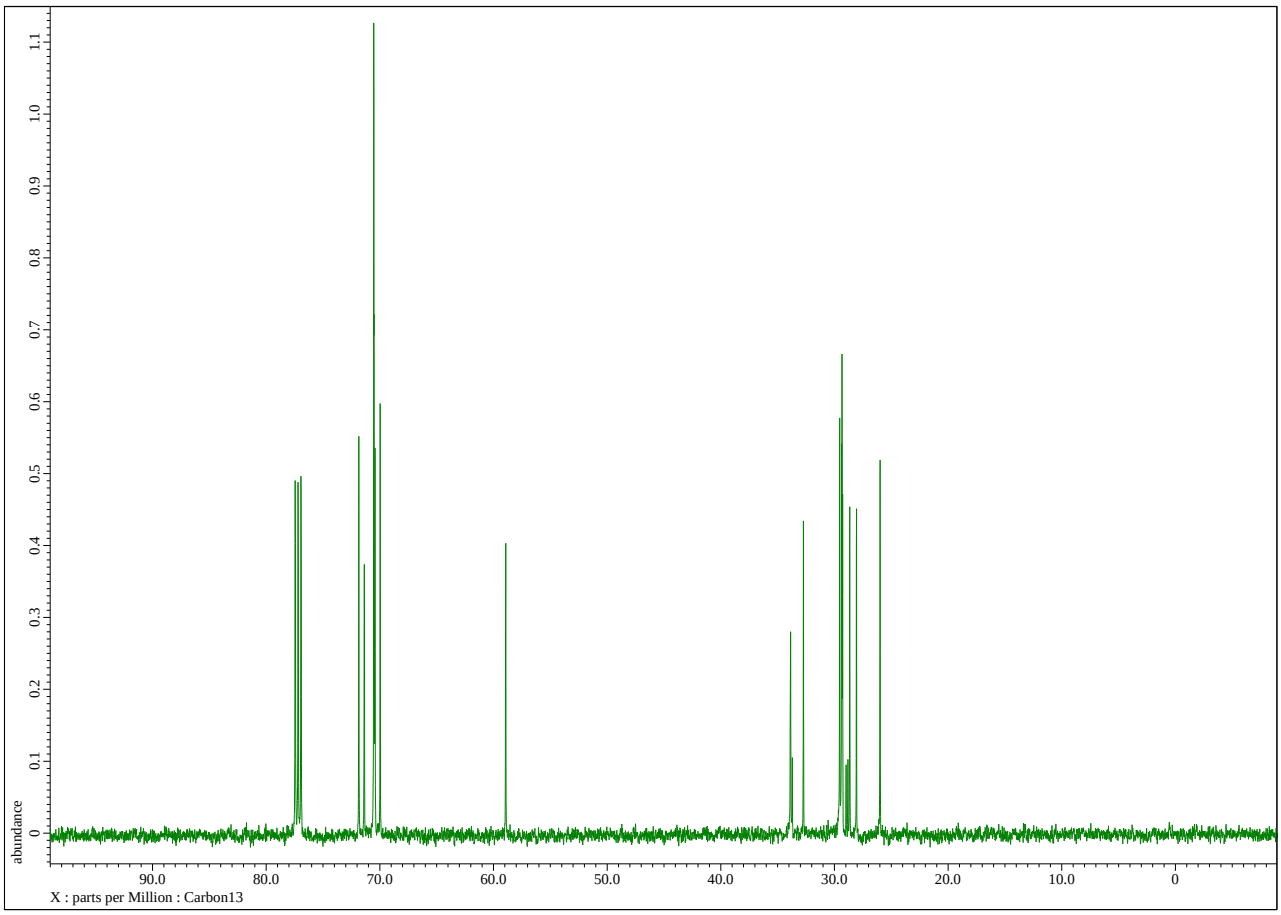
abundance
X : parts per Million : Carbon13

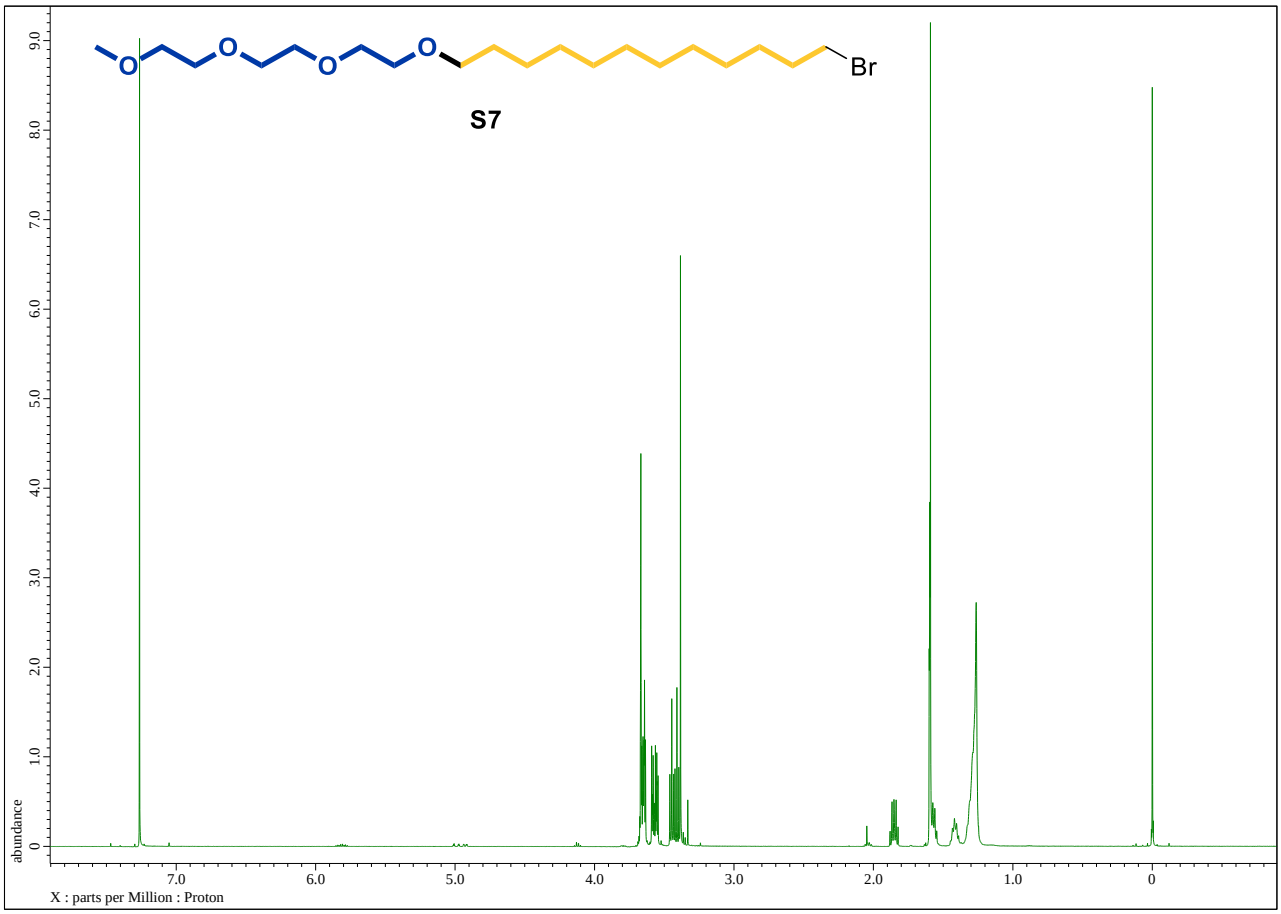
O
O
O
O
Br
S7
abundance
X : parts per Million : Proton

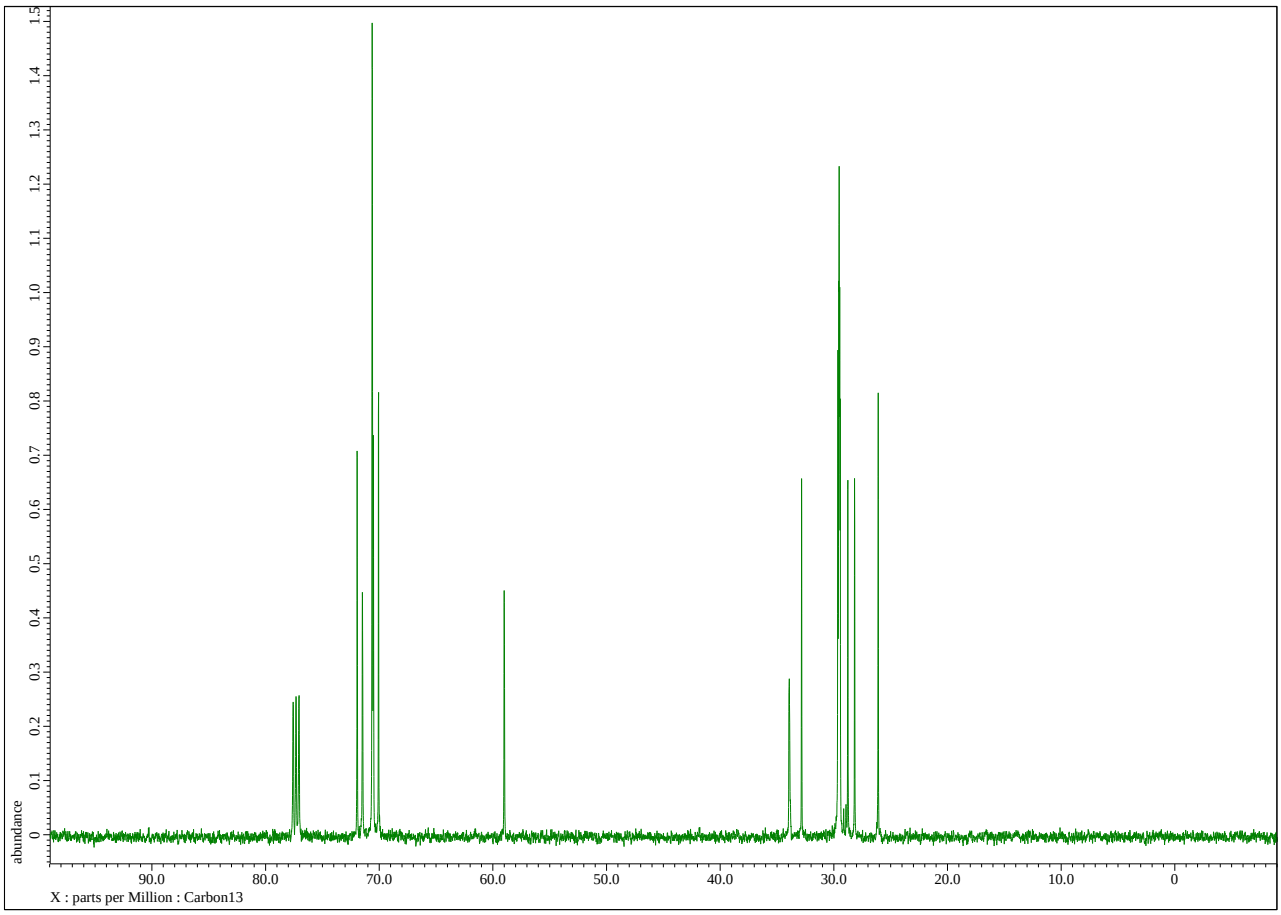
abundance
X : parts per Million : Carbon13

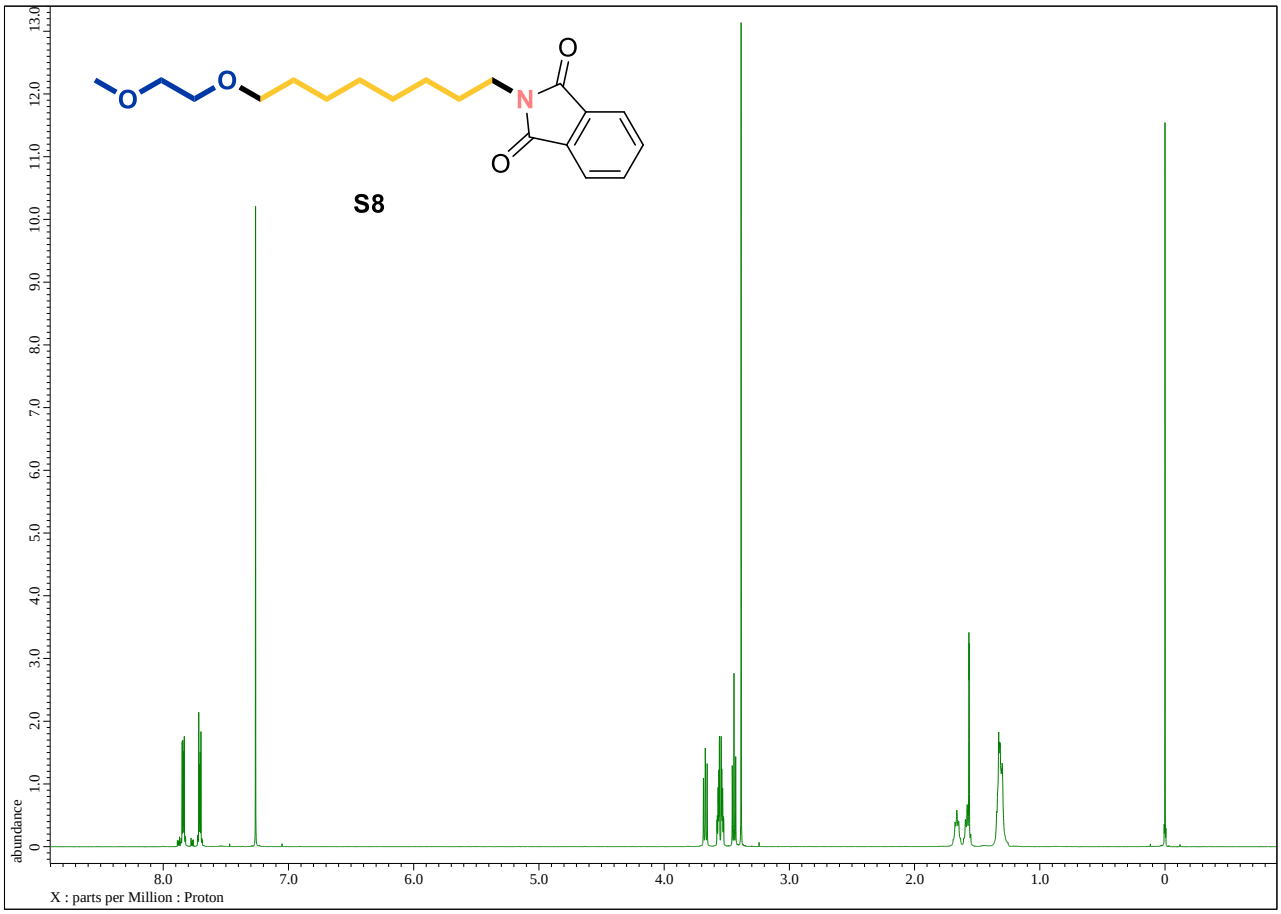
S8
abundance
X : parts per Million : Proton

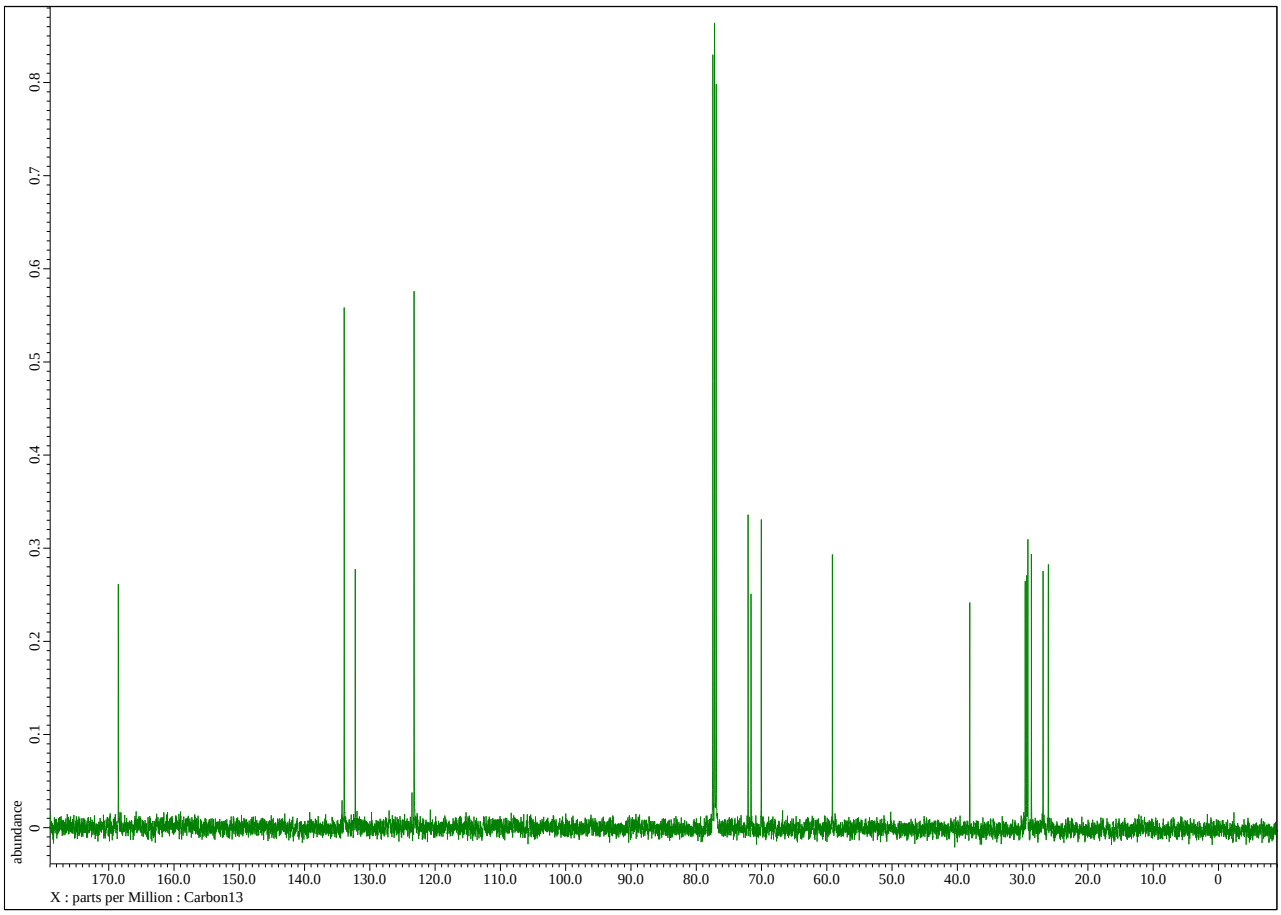
abundance
X : parts per Million : Carbon13

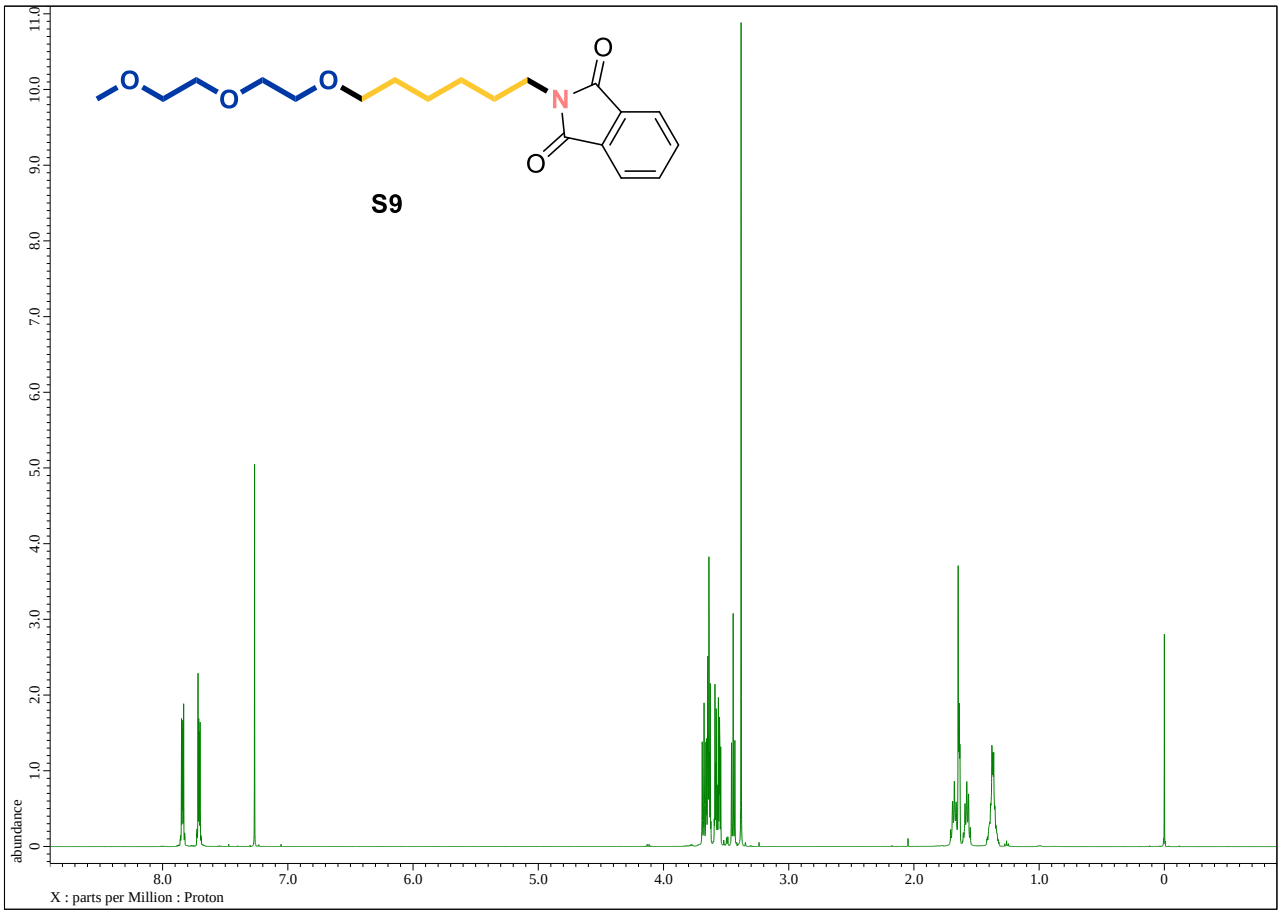
S9
abundance
X : parts per Million : Proton

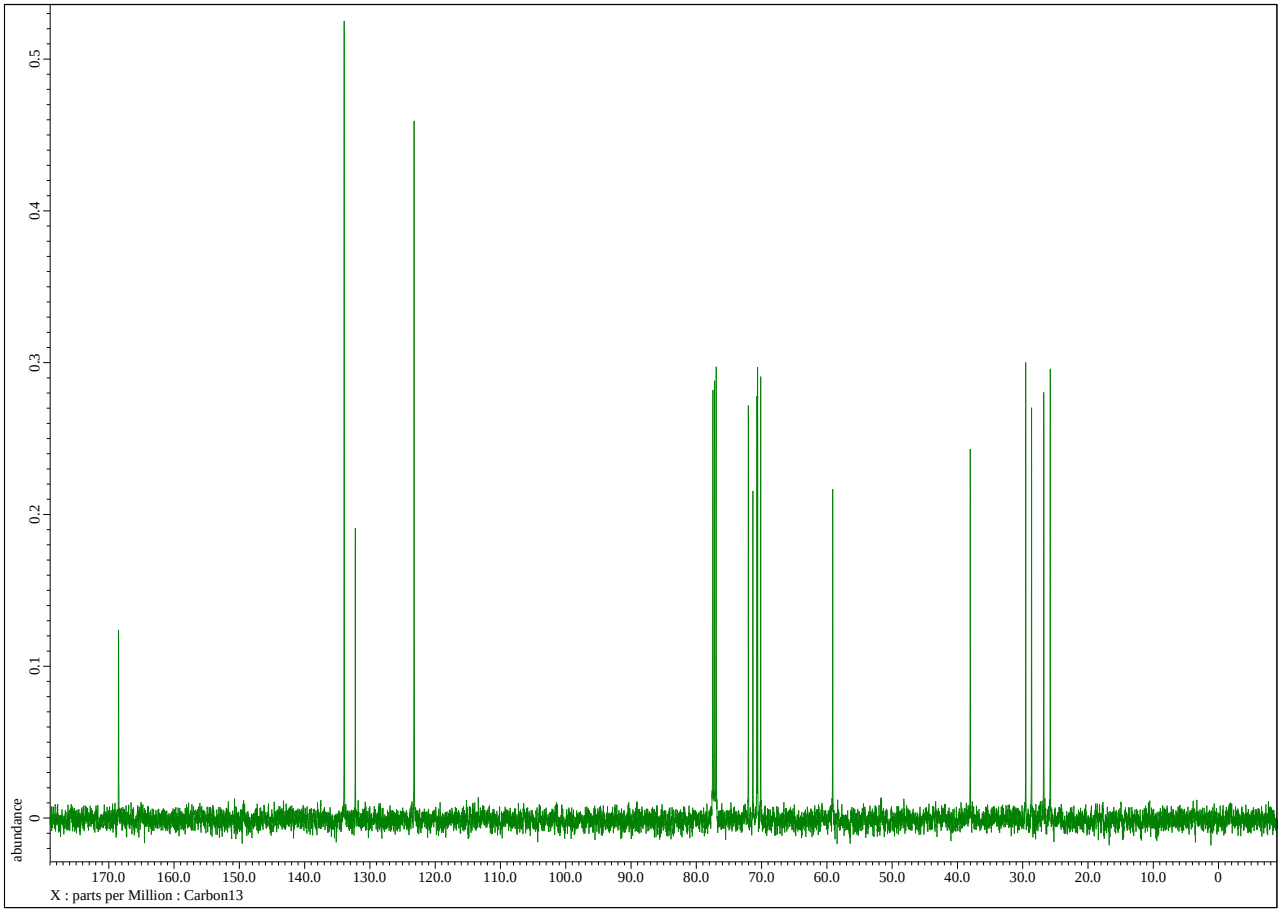
abundance
X : parts per Million : Carbon13

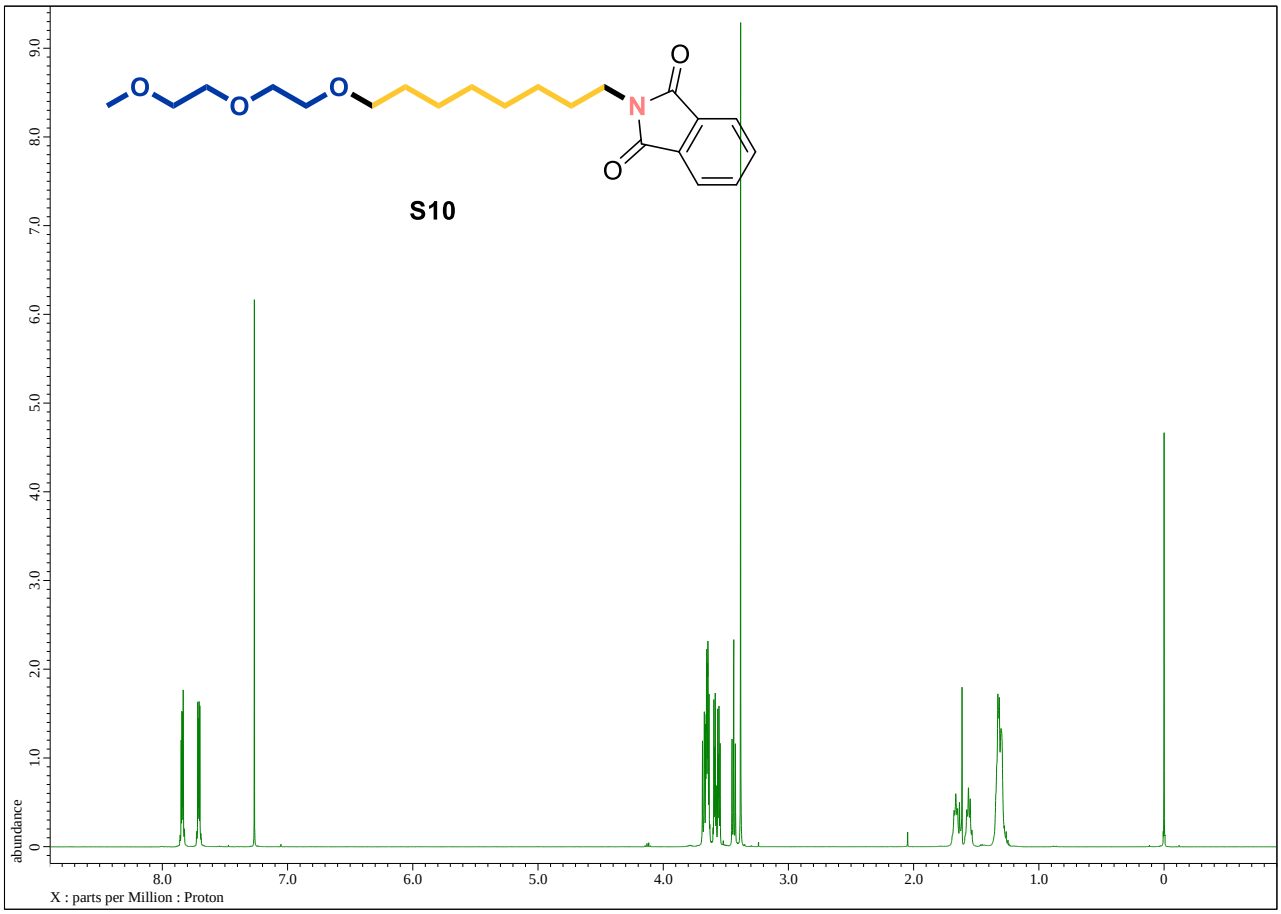
S10
abundance
X : parts per Million : Proton

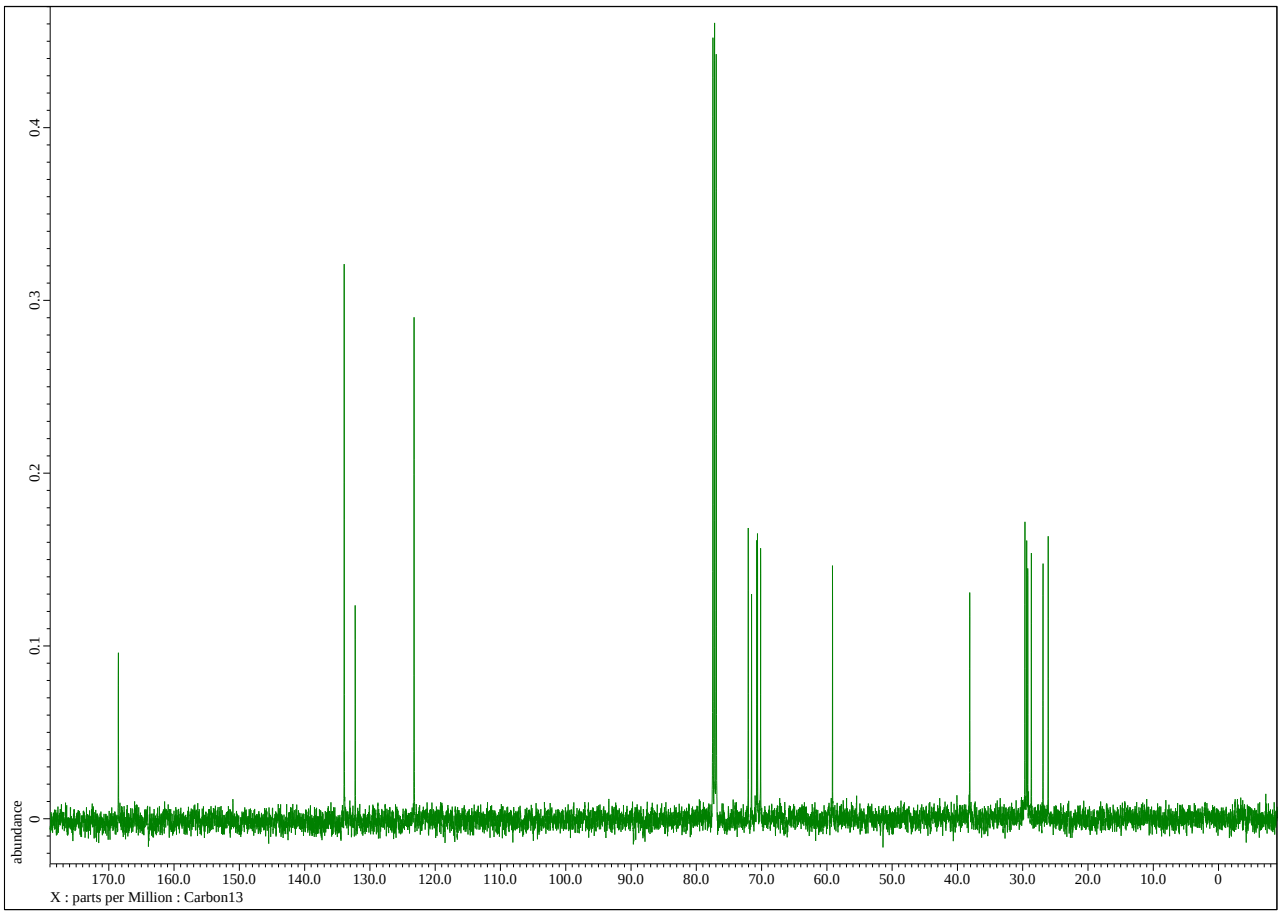
abundance
X : parts per Million : Carbon13

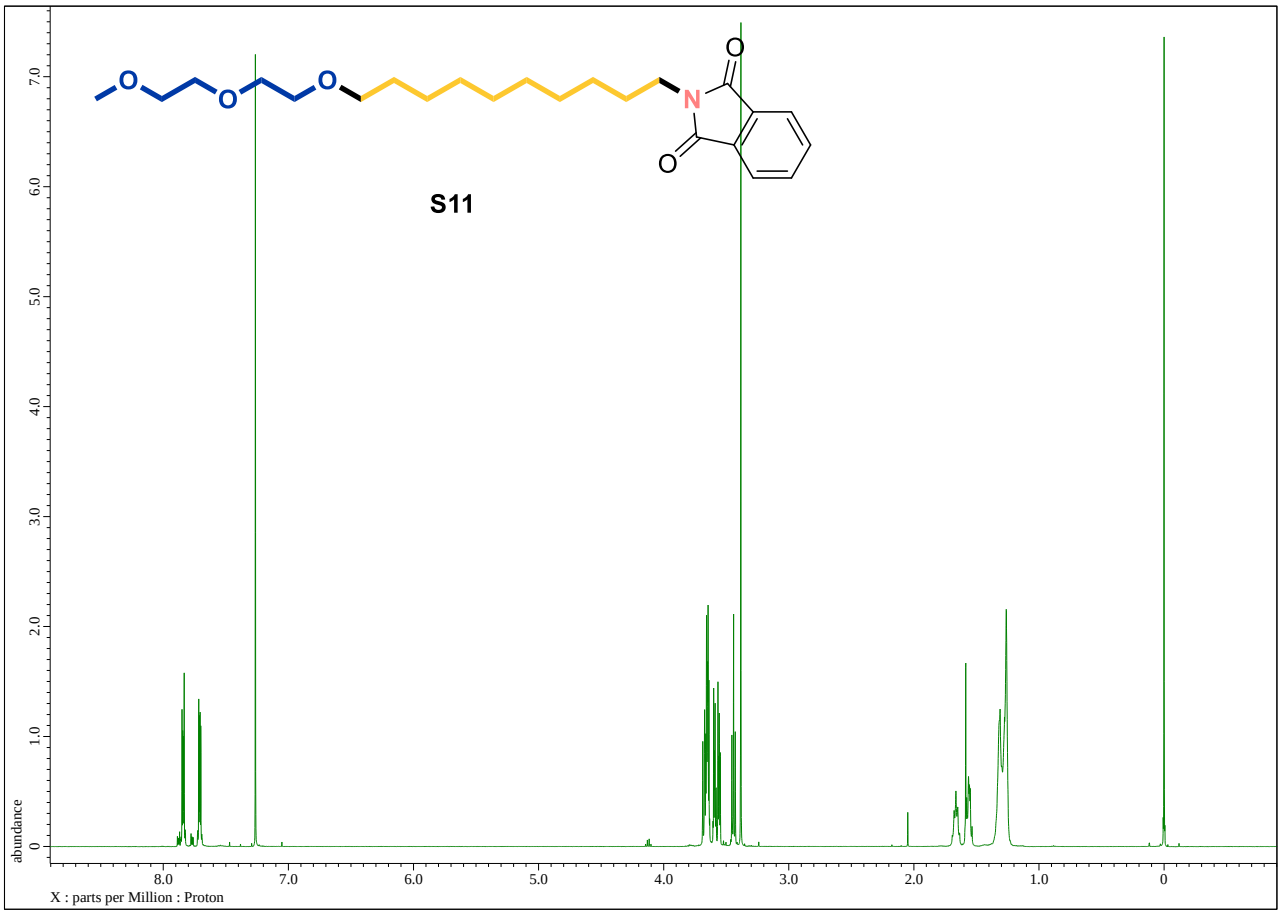
S11
abundance
X : parts per Million : Proton

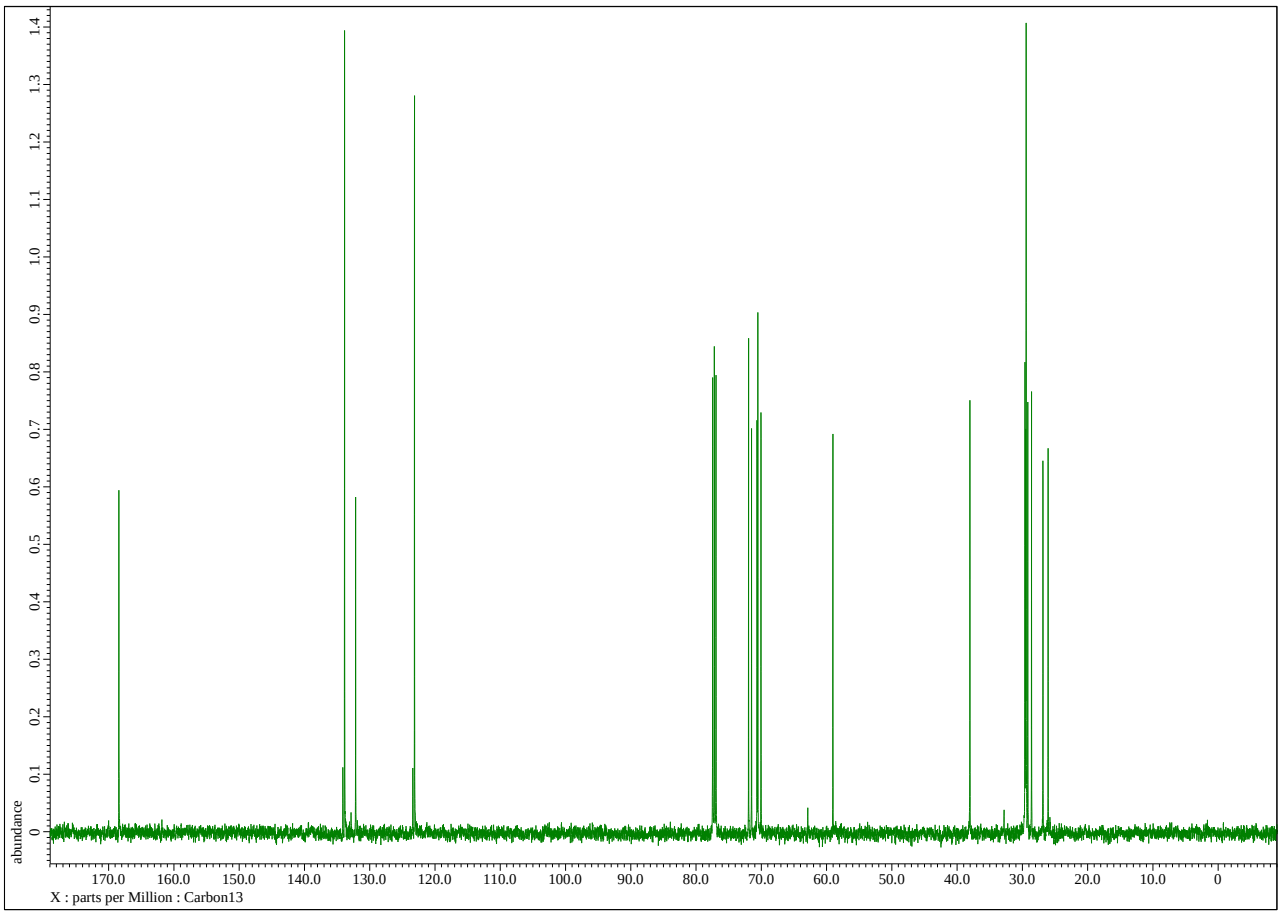
abundance
X : parts per Million : Carbon13

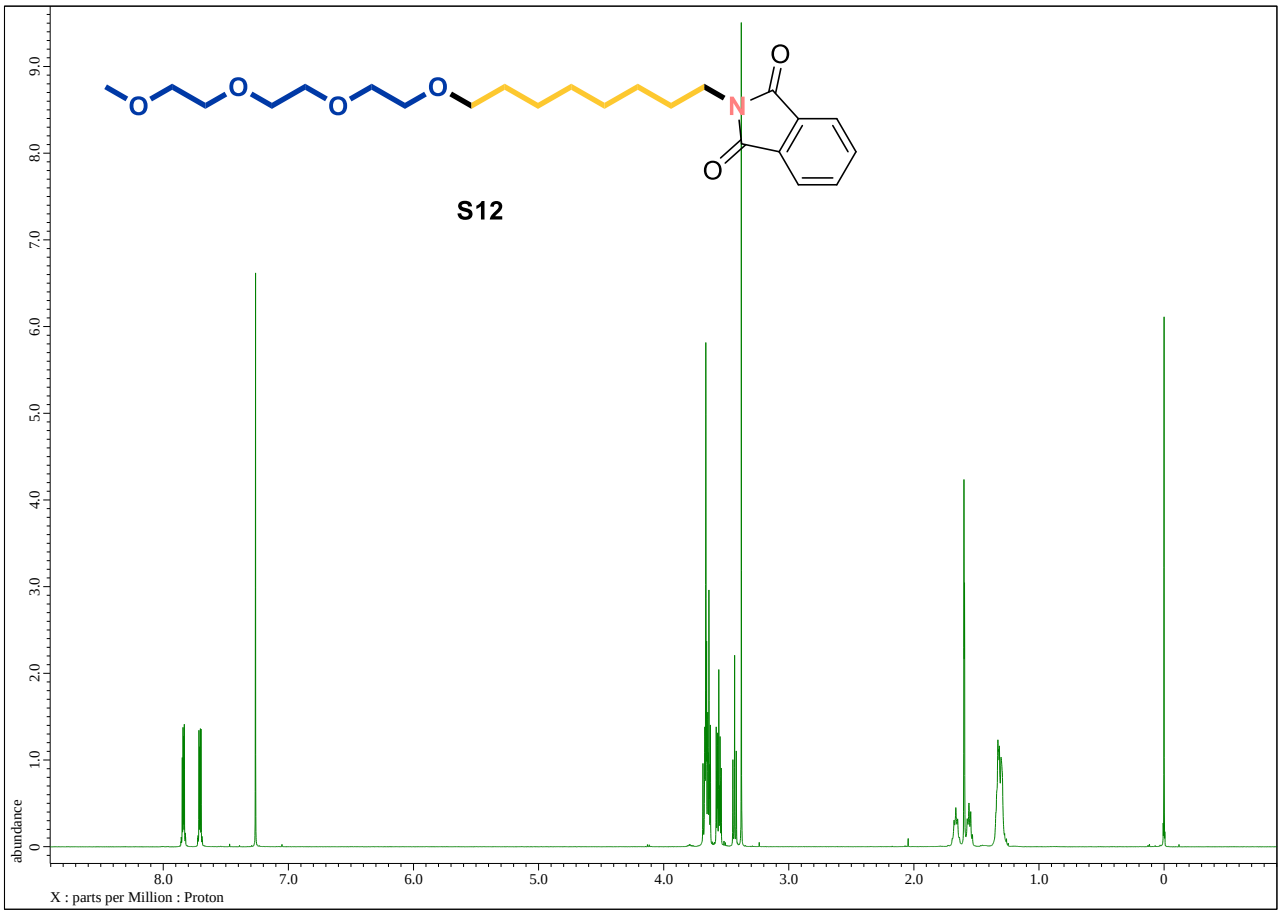
S12
abundance
X : parts per Million : Proton

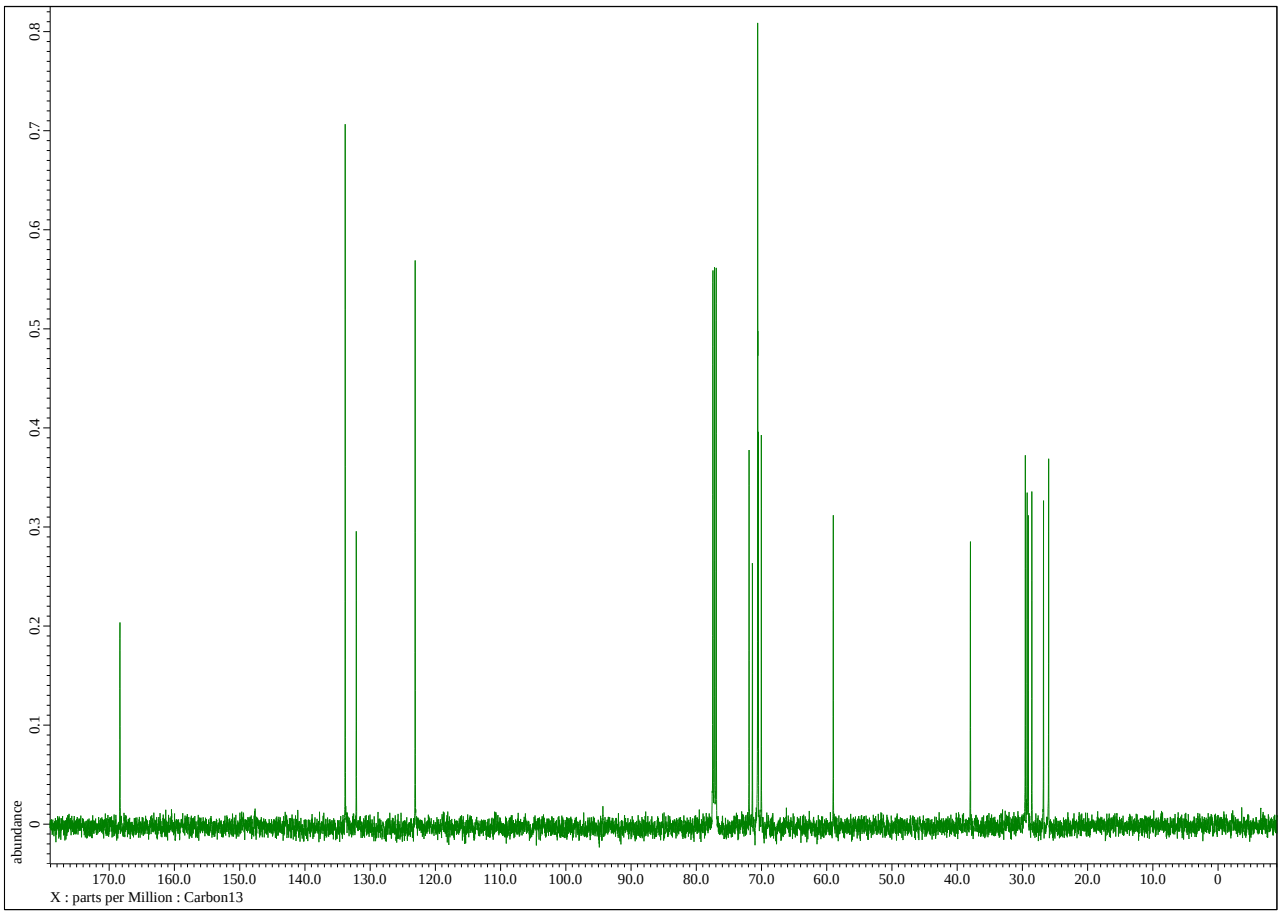
abundance
X : parts per Million : Carbon13

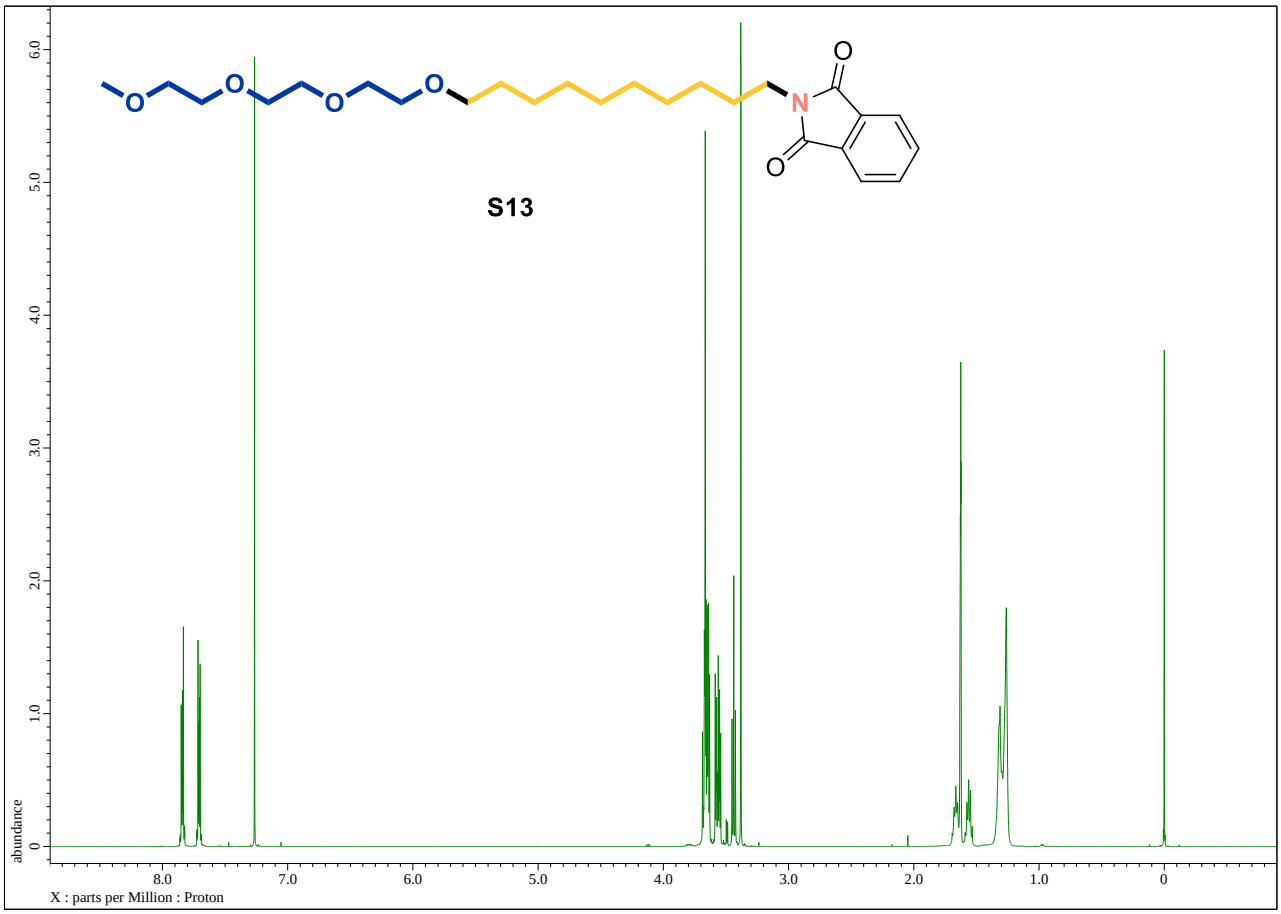
S13
O
O
O
O
N
O
abundance
6.0
5.0
4.0
3.0
2.0
1.0
0
8.0
7.0
6.0
5.0
4.0
3.0
2.0
1.0
0
X : parts per Million : Proton

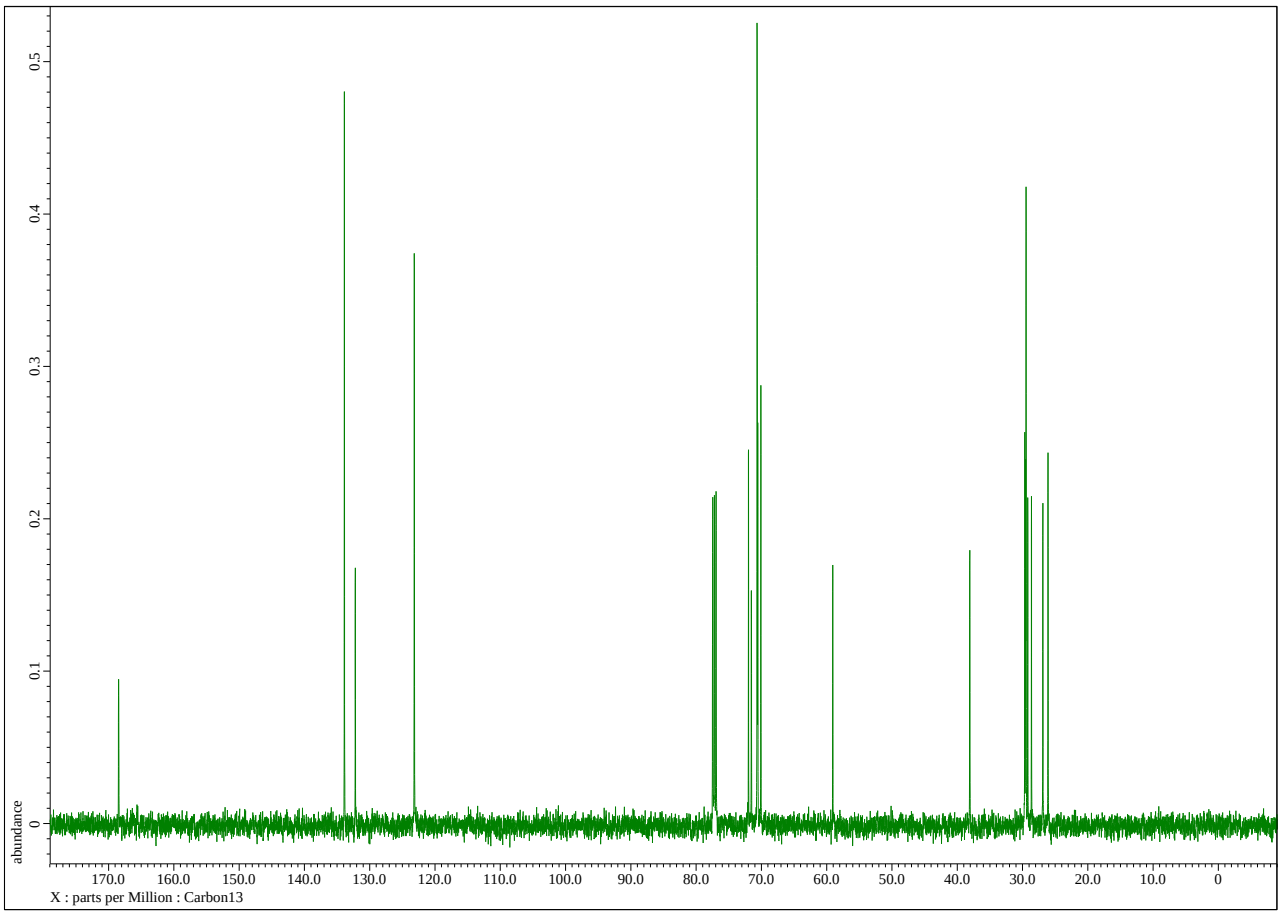
abundance
0.5
0.4
0.3
0.2
0.1
0
170.0
160.0
150.0
140.0
130.0
120.0
110.0
100.0
90.0
80.0
70.0
60.0
50.0
40.0
30.0
20.0
10.0
0
X : parts per Million : Carbon13

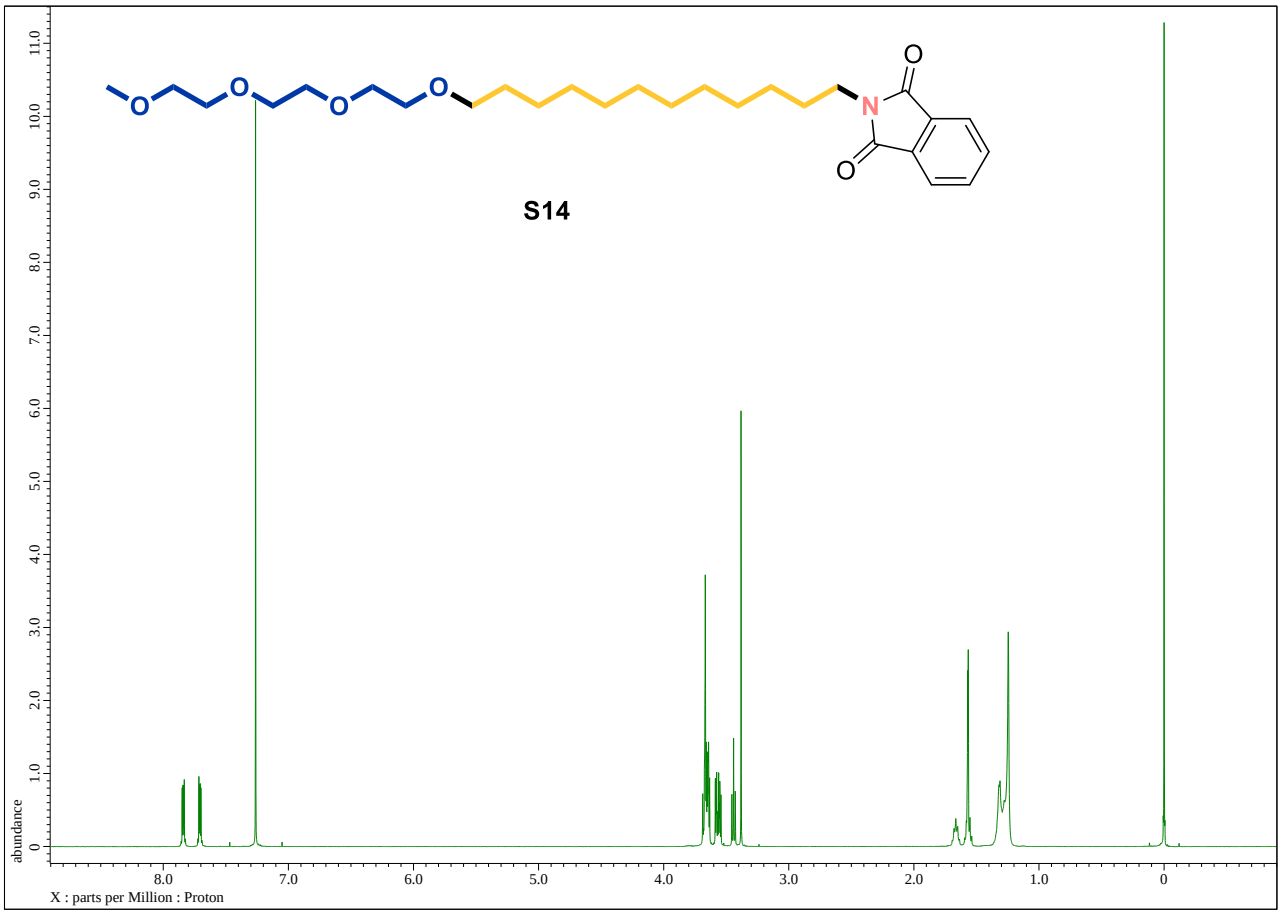
S14
abundance
X : parts per Million : Proton

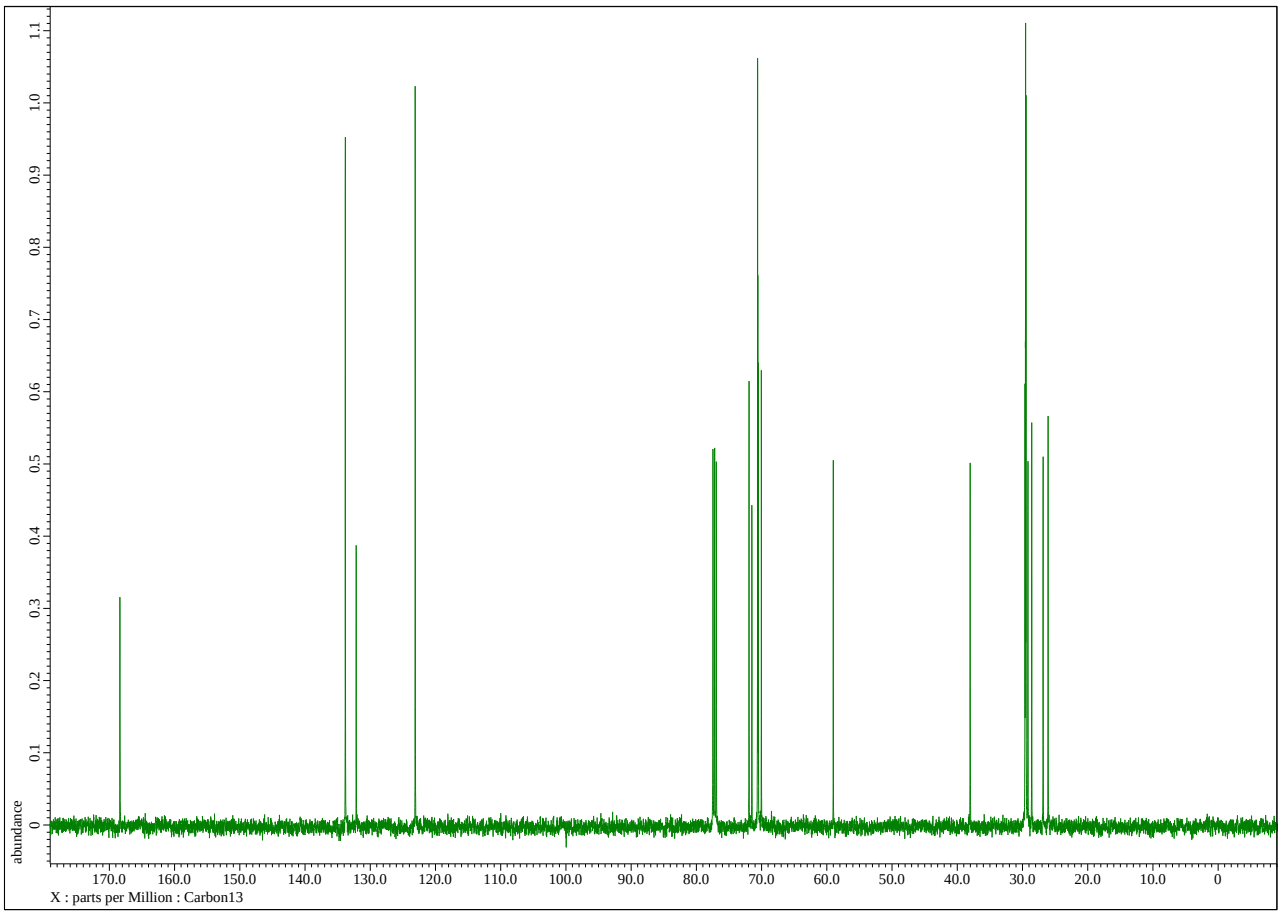
abundance
X : parts per Million : Carbon13

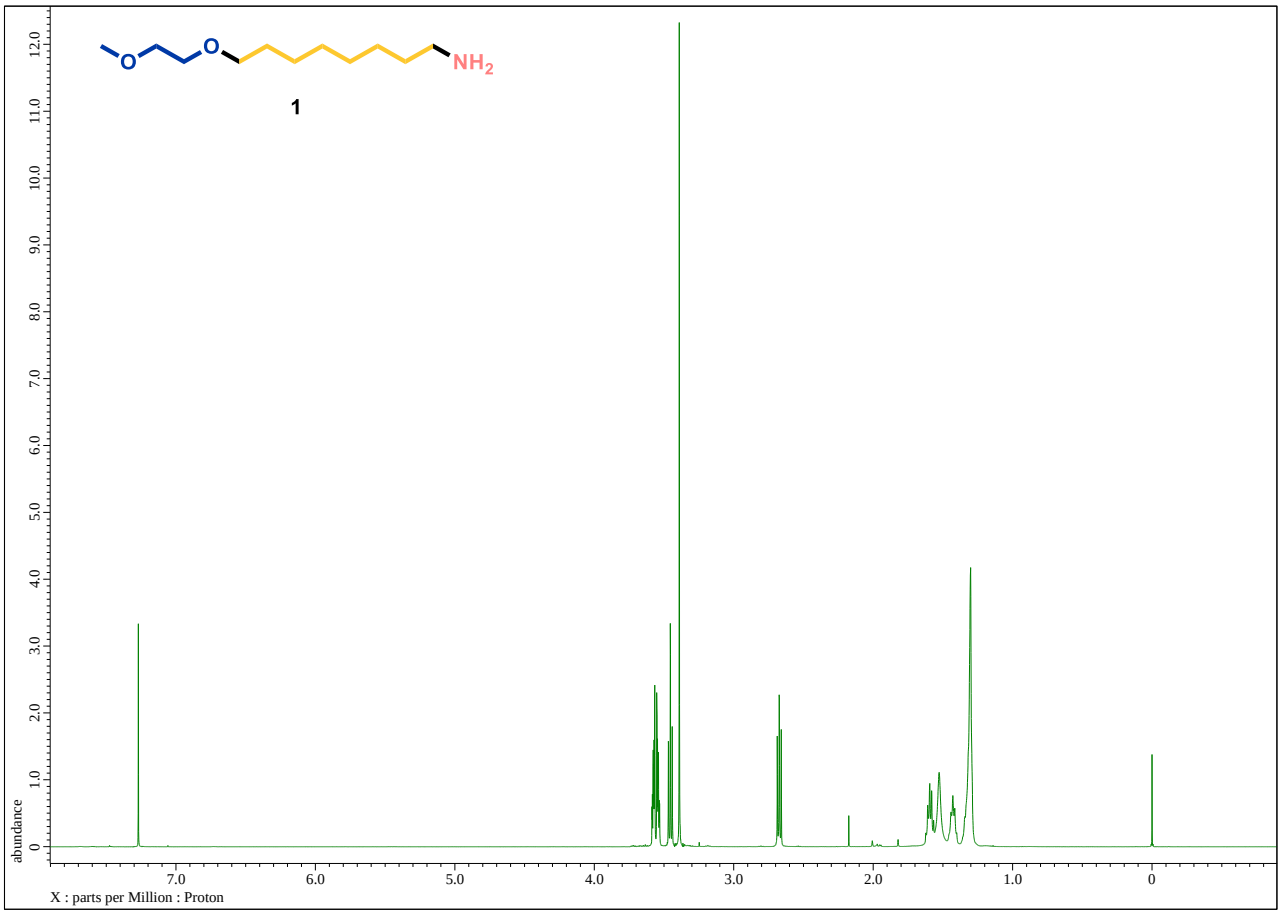
O
O
NH2
1
abundance
X : parts per Million : Proton

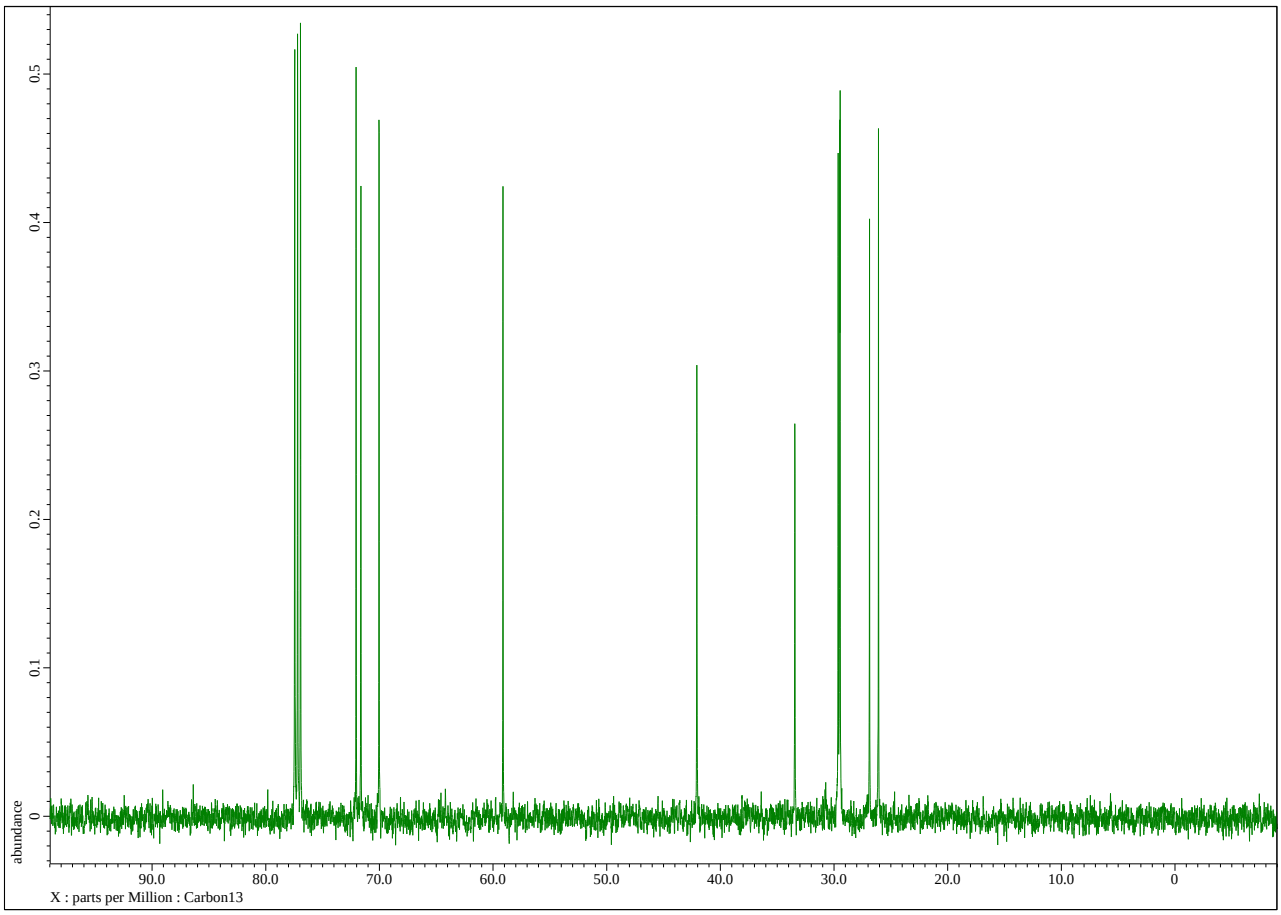
abundance
X : parts per Million : Carbon13

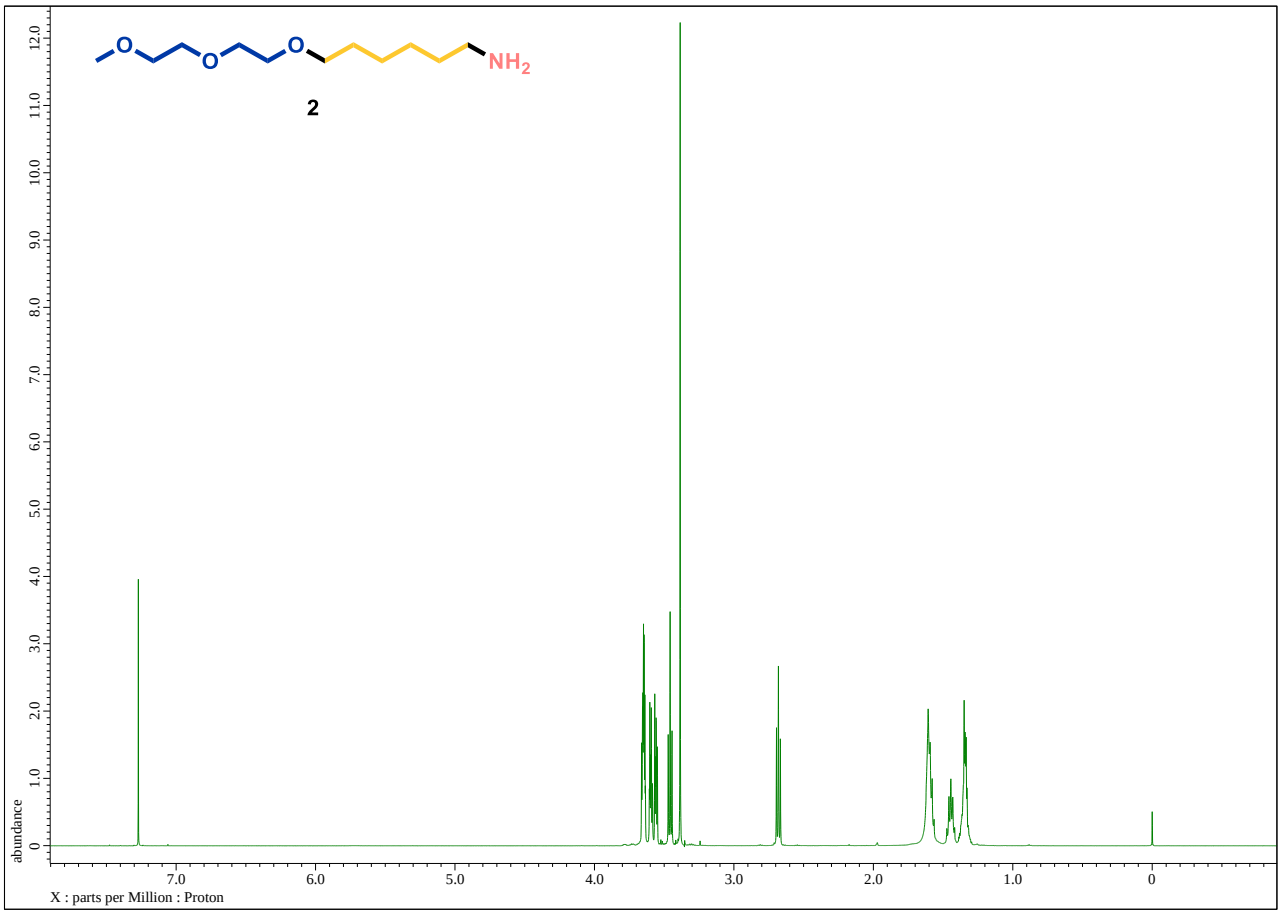
O
O
O
NH2
2
abundance
X : parts per Million : Proton

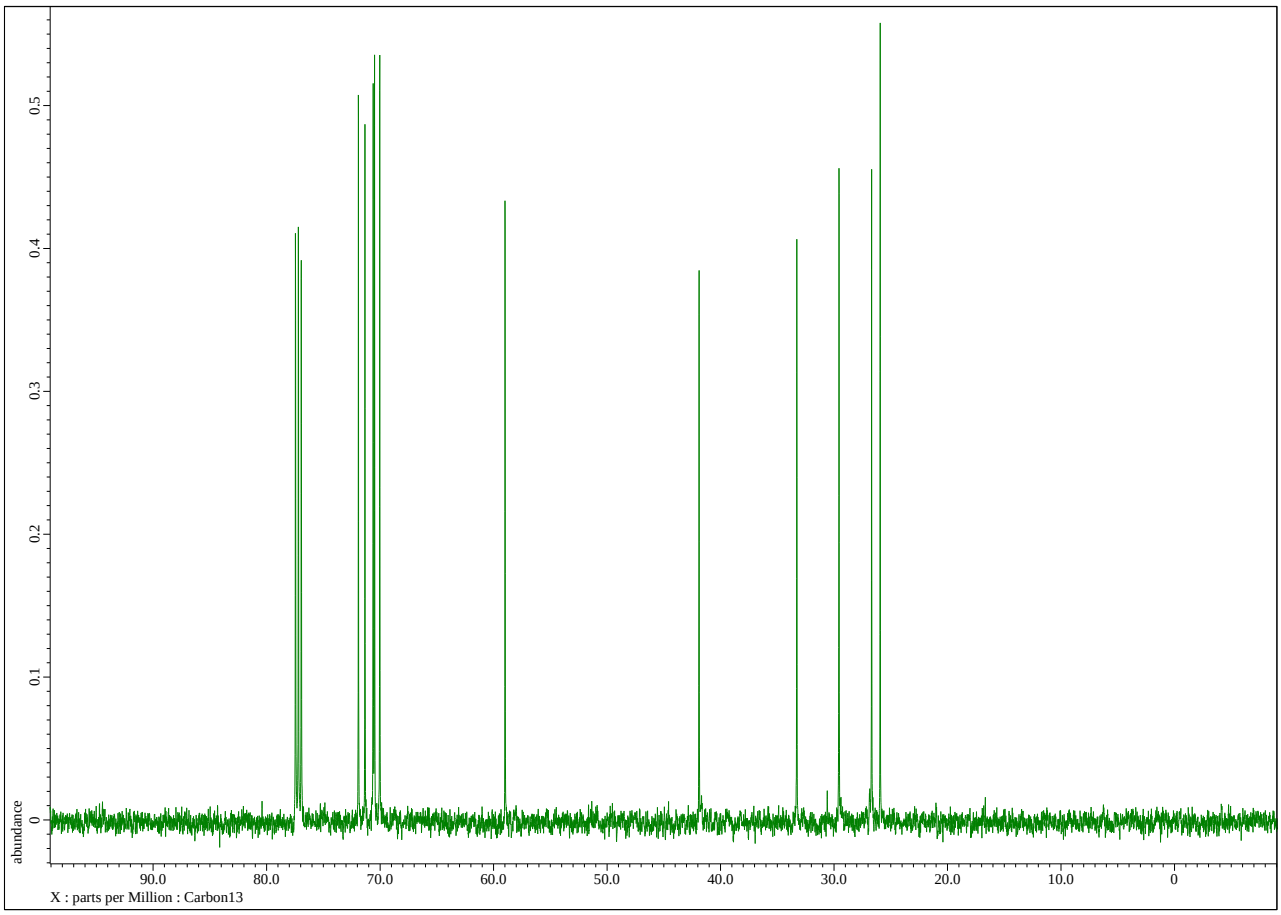
abundance
X : parts per Million : Carbon13

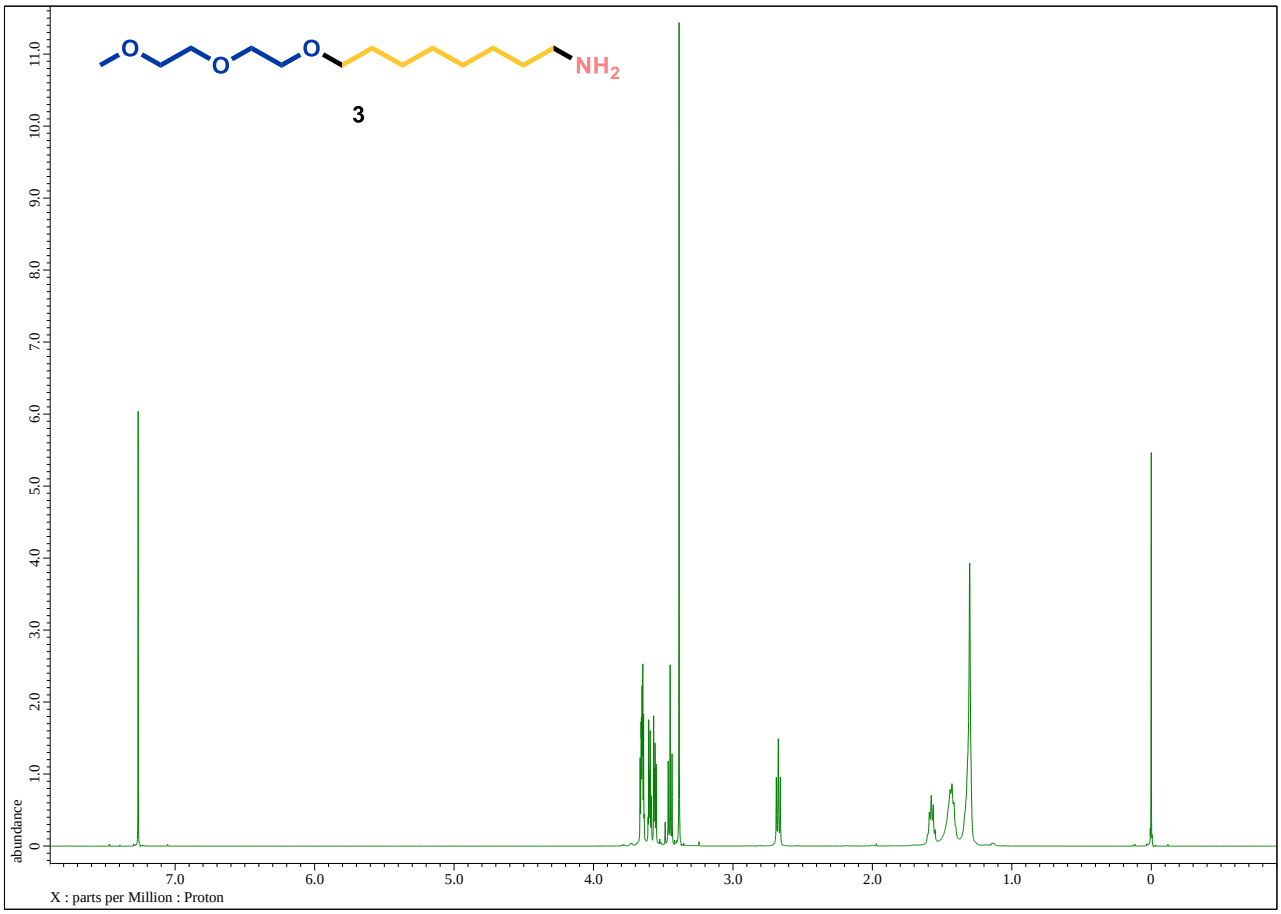
O
O
O
NH2
3
abundance
X : parts per Million : Proton

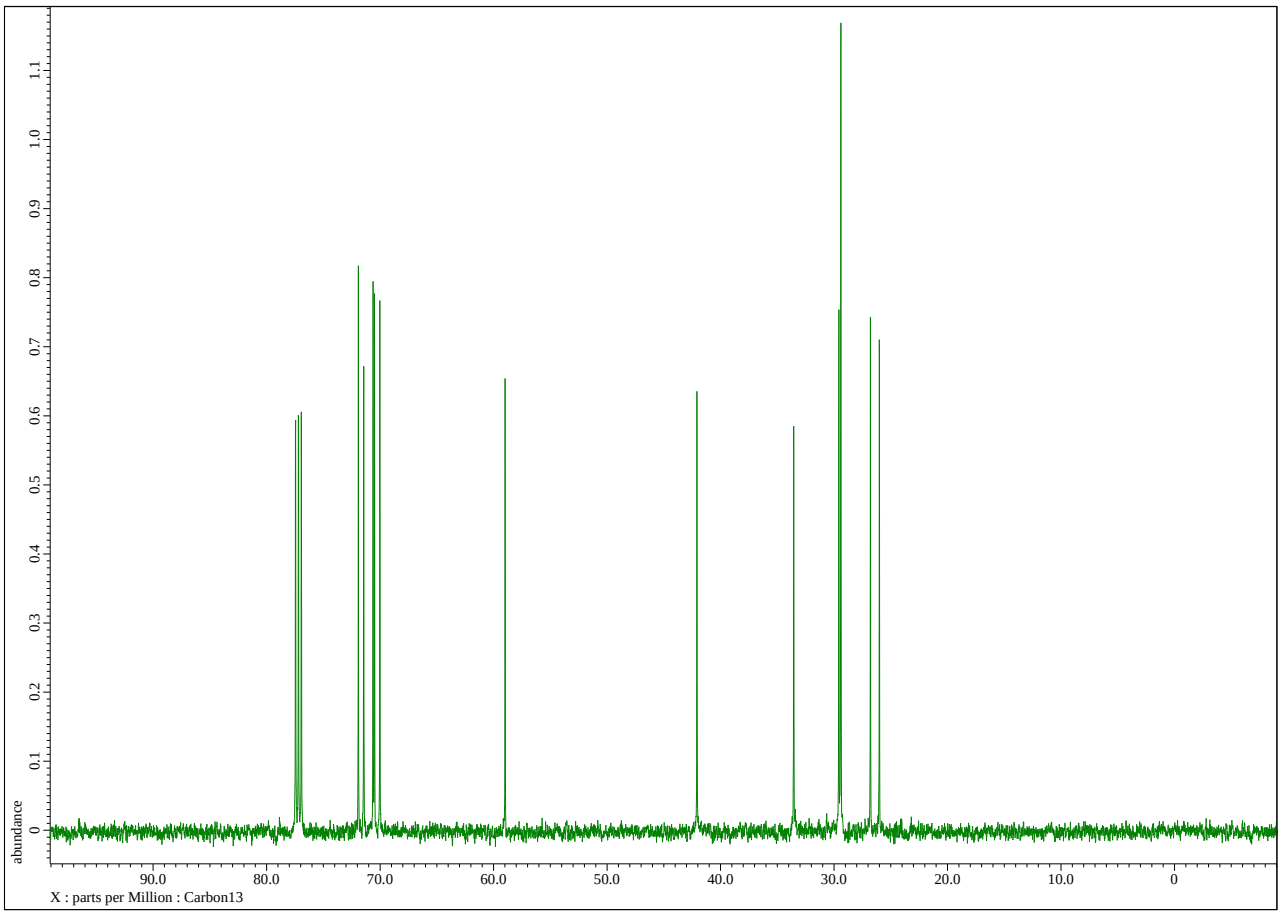
abundance
X : parts per Million : Carbon13

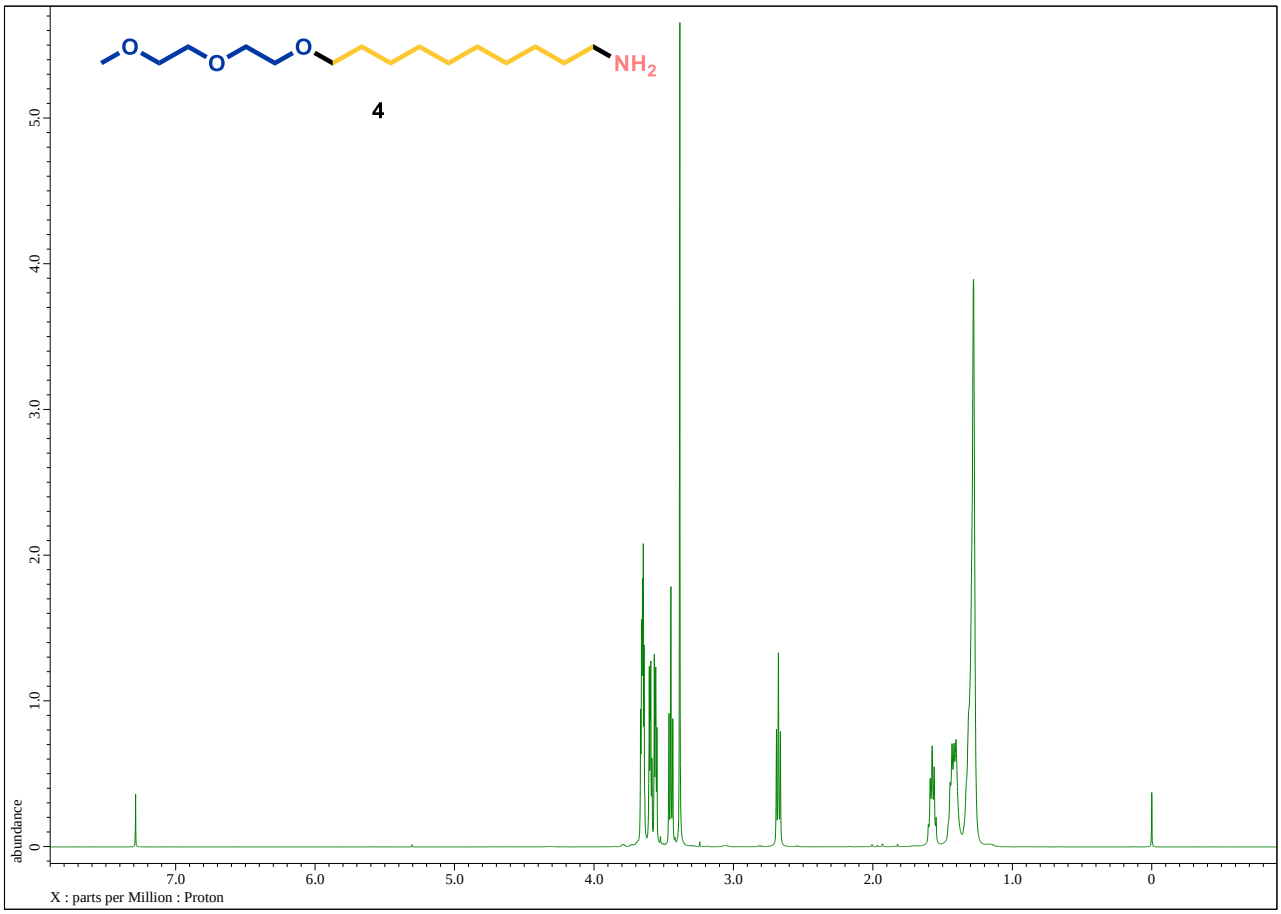
O
O
O
NH2
4
abundance
0
1.0
2.0
3.0
4.0
5.0
7.0
6.0
5.0
4.0
3.0
2.0
1.0
0
X : parts per Million : Proton

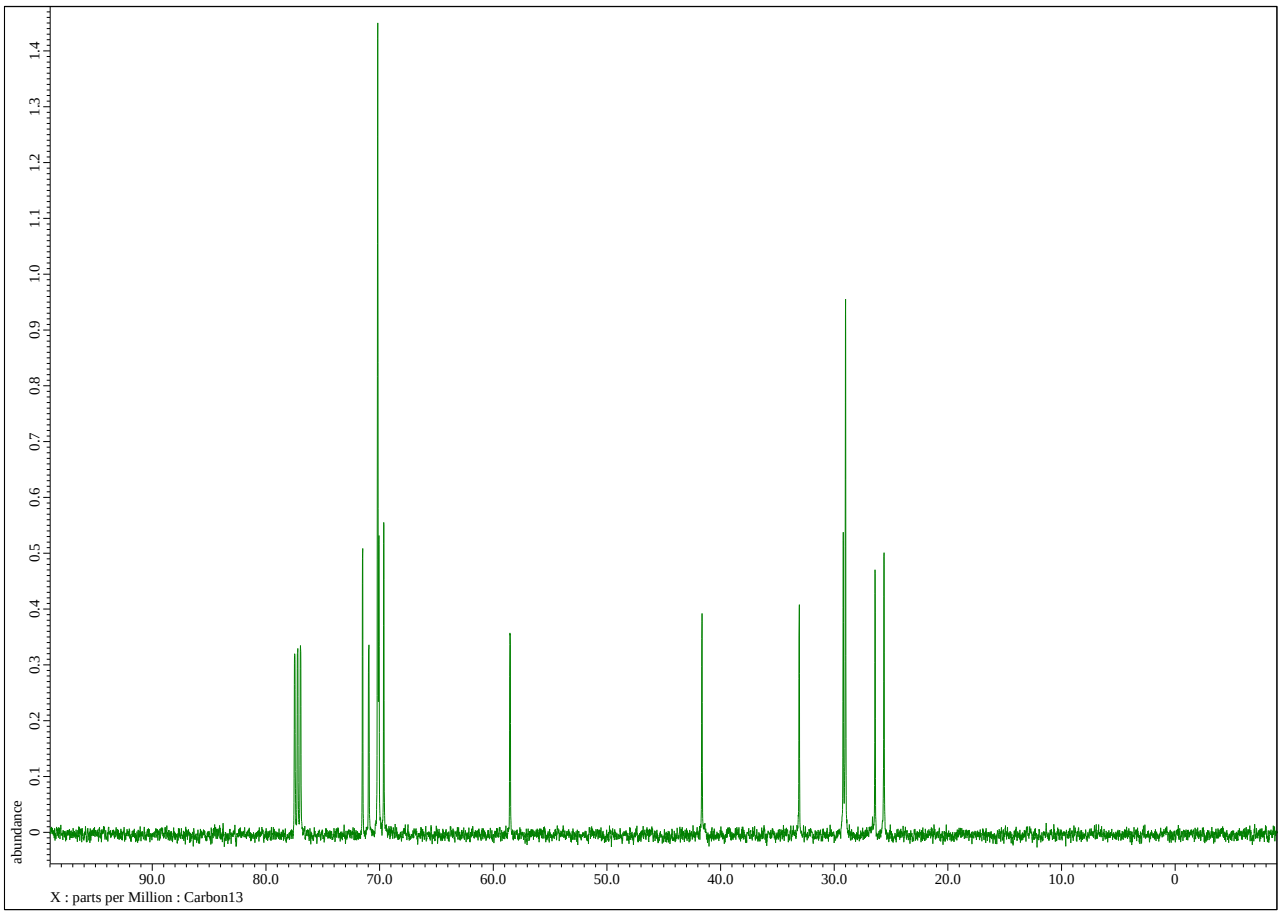
abundance
0
0.1
0.2
0.3
0.4
0.5
0.6
0.7
0.8
0.9
1.0
1.1
1.2
1.3
1.4
90.0
80.0
70.0
60.0
50.0
40.0
30.0
20.0
10.0
0
X : parts per Million : Carbon13

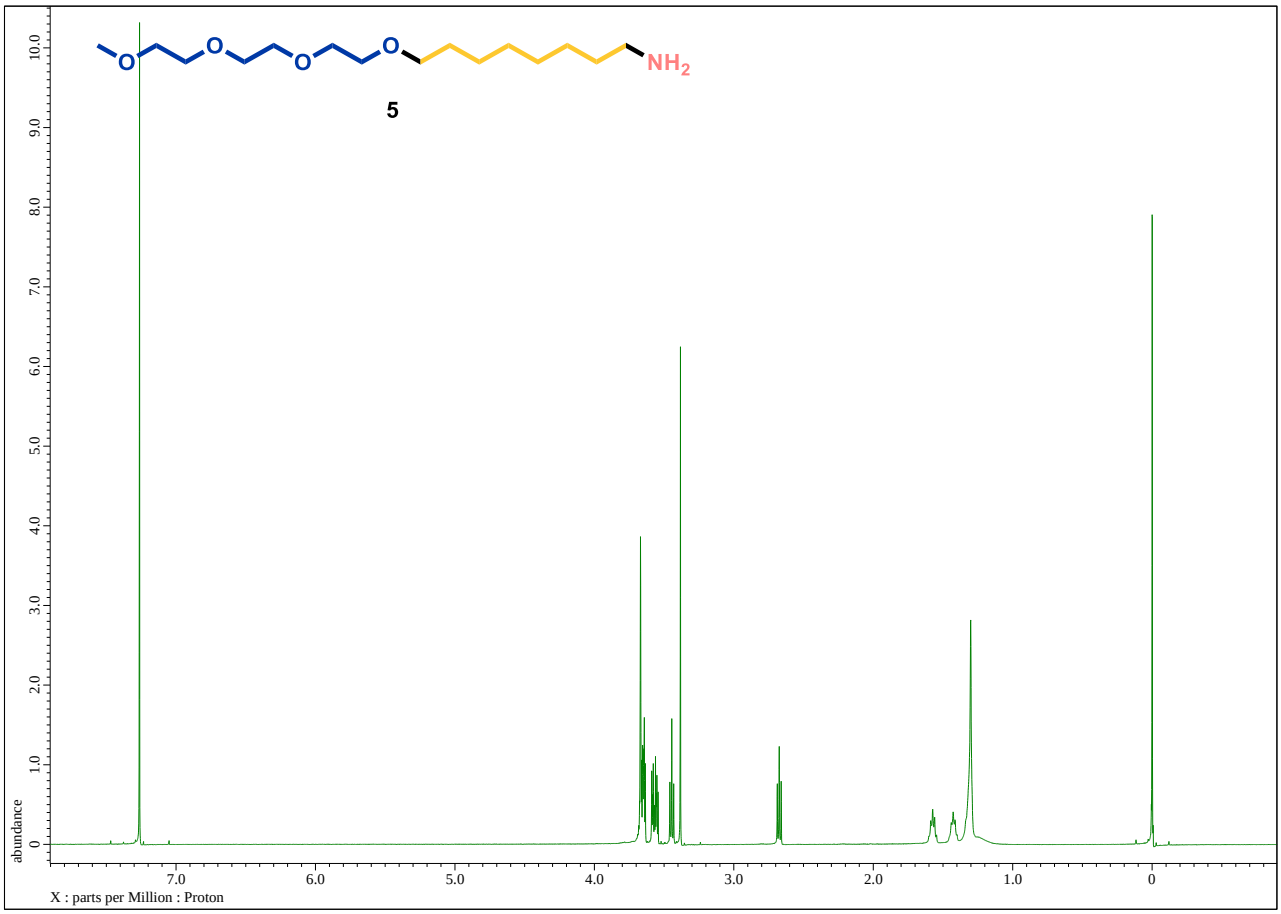
O
O
O
O
NH2
5
abundance
X : parts per Million : Proton

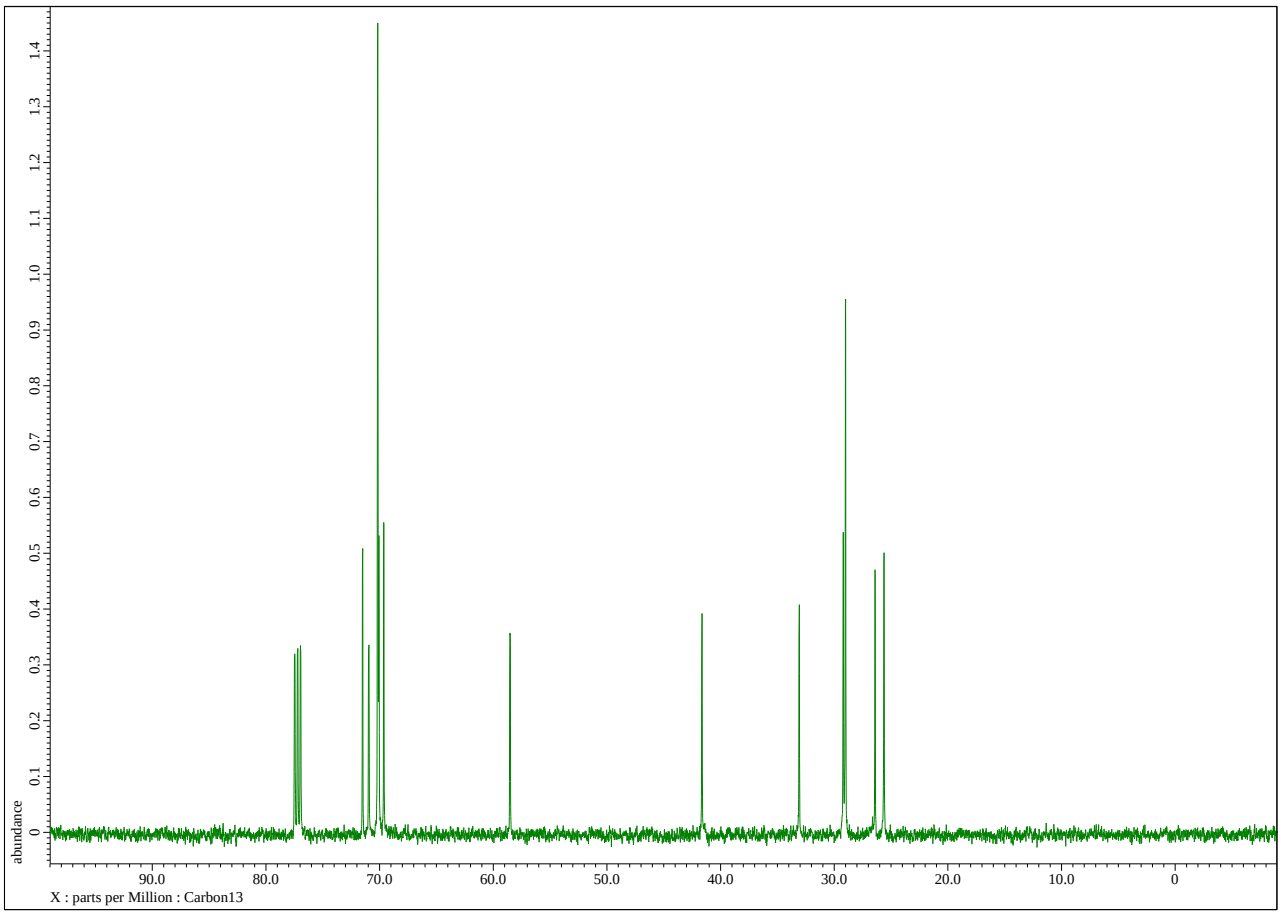
abundance
X : parts per Million : Carbon13

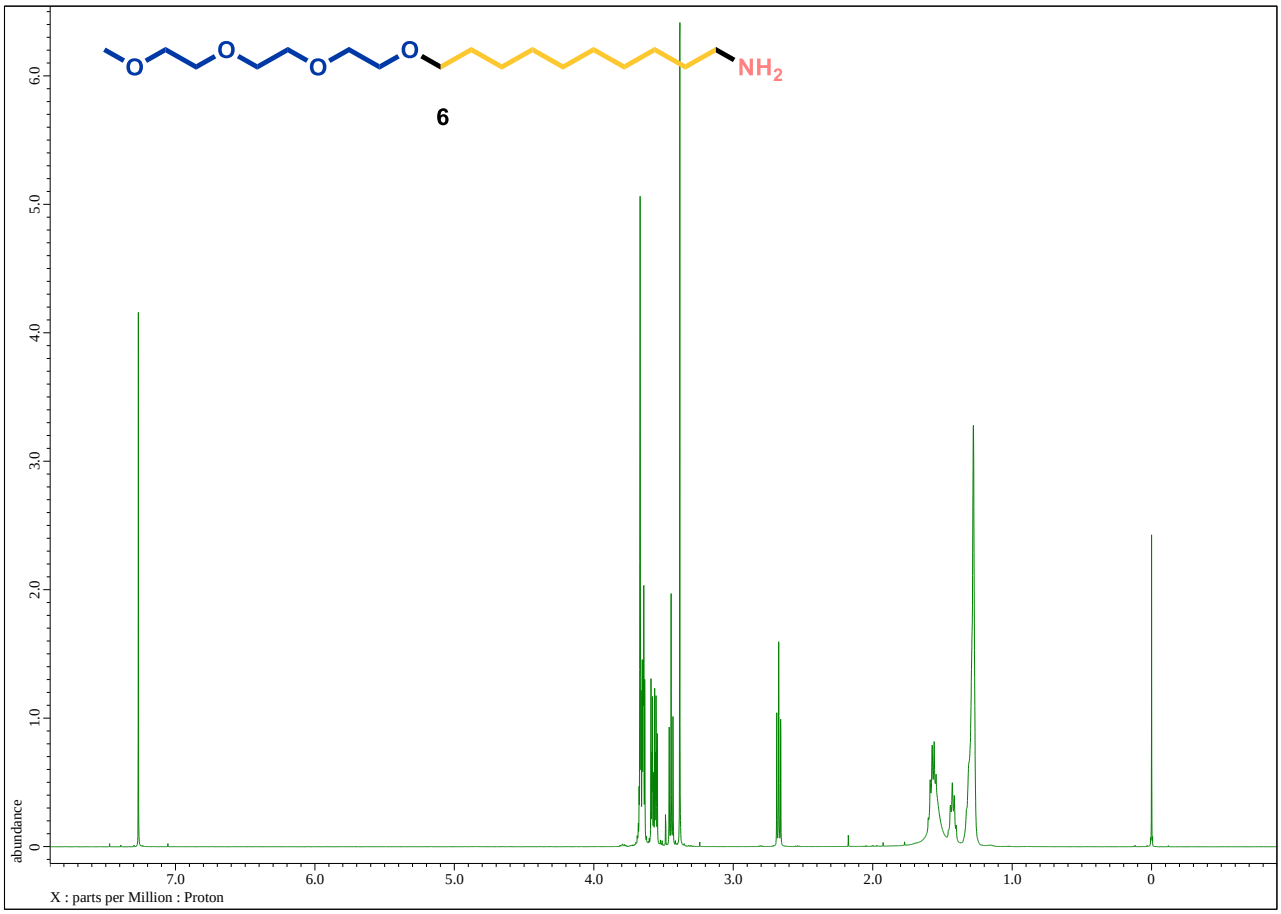
O
O
O
O
NH2
6
abundance
X : parts per Million : Proton

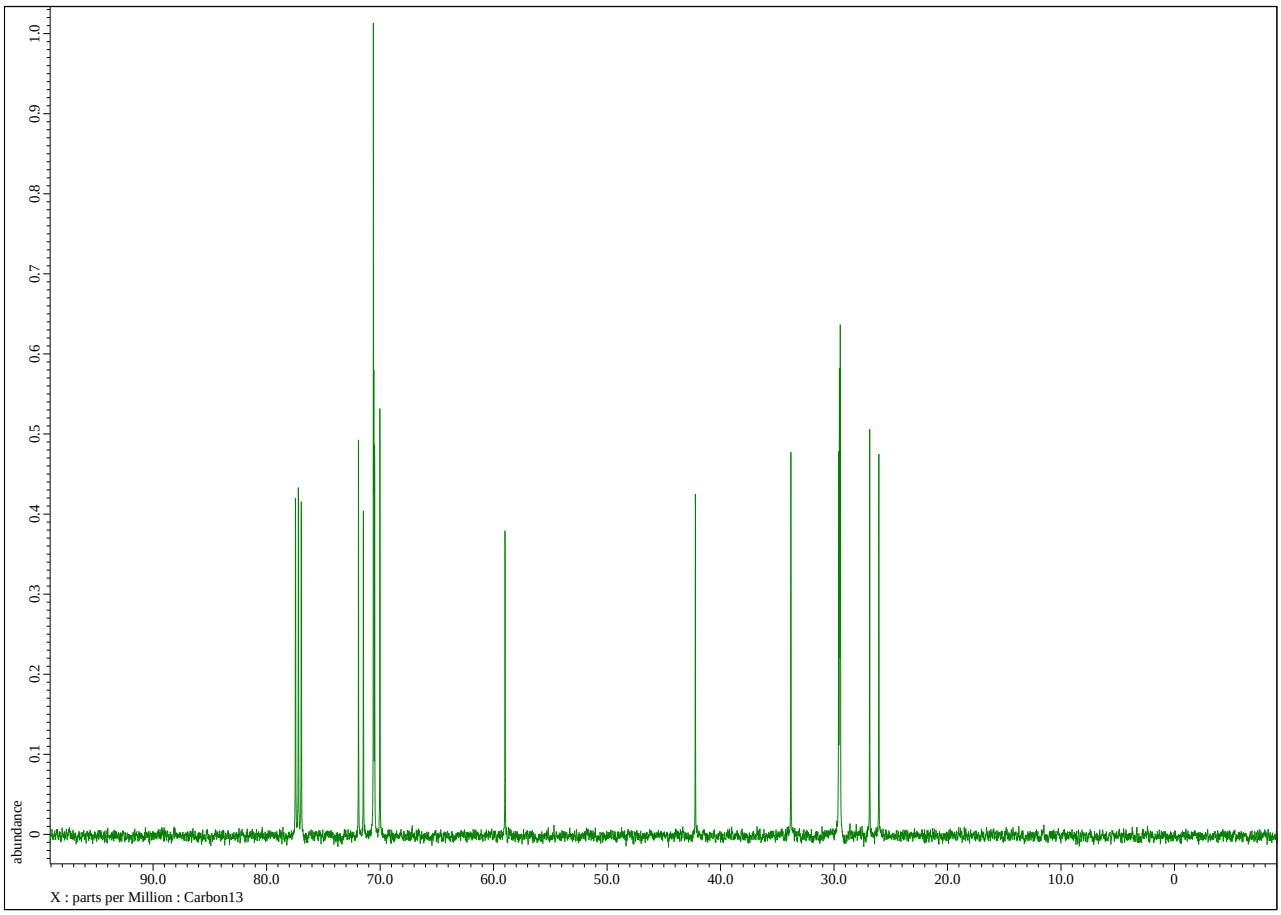
abundance
X : parts per Million : Carbon13

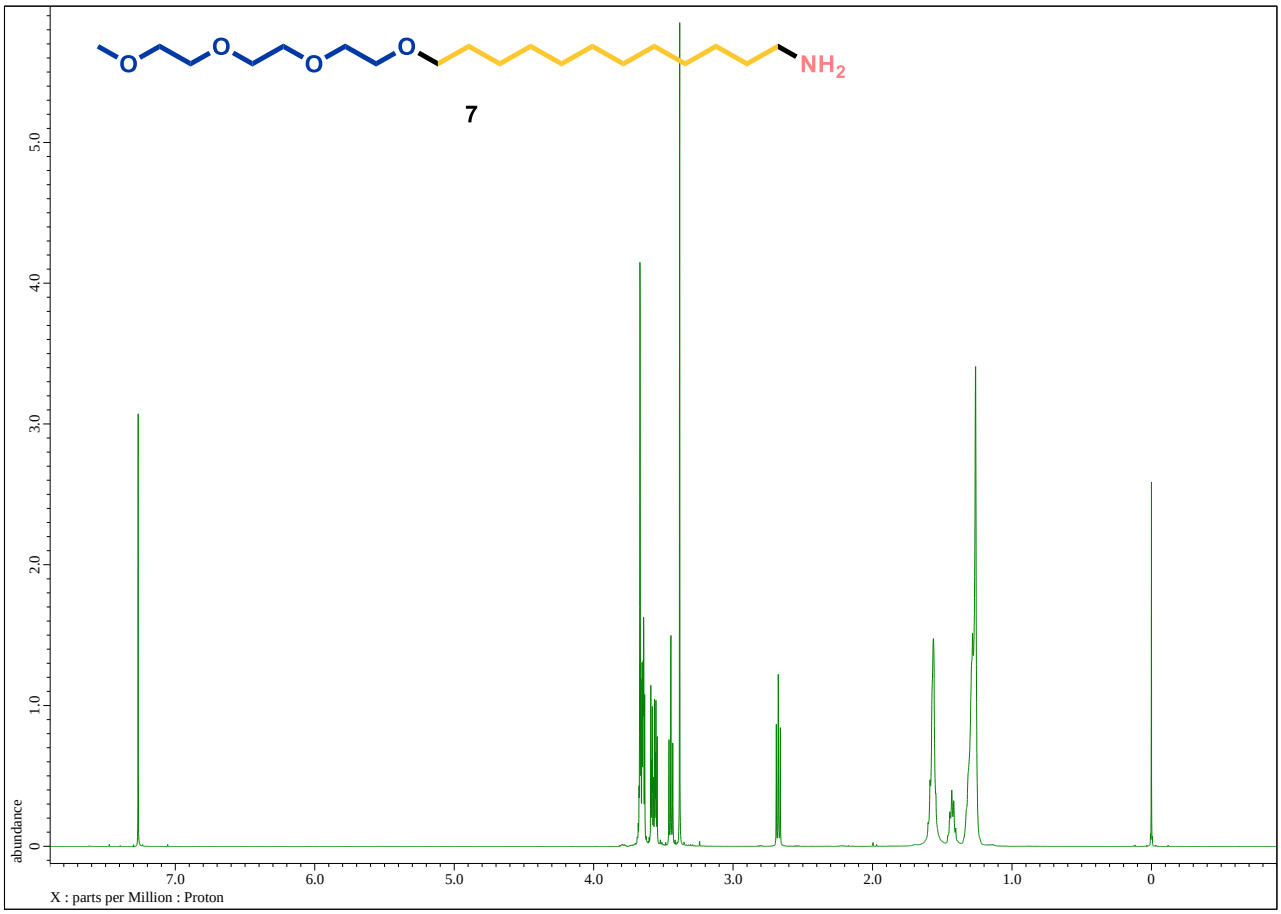
7
NH2
abundance
X : parts per Million : Proton

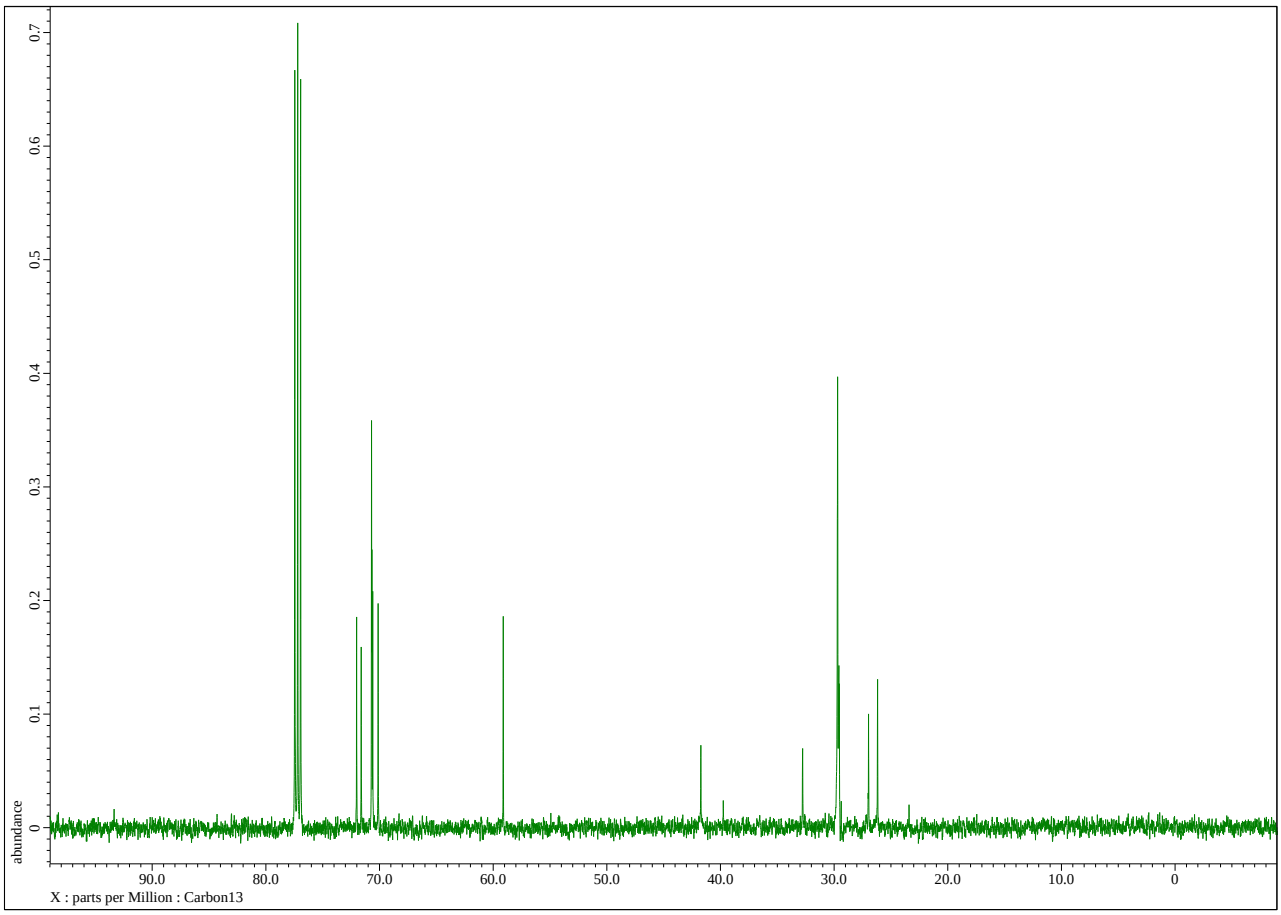
abundance
X : parts per Million : Carbon13

8.3. NMR and DFT Information in Chapter 4

*1-Methoxy-4-(4-methoxybut-3-en-1-yl)benzene (**1**, cis : trans = 1 : 2)*

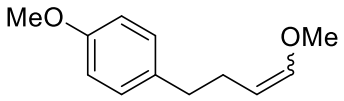

1, *cis* : *trans* = 1 : 2

cis: ^{1}H NMR ($CDCl_3$, 500 MHz) δ 7.12 (2H, d, *J* = 8.6 Hz), 6.82 (2H, d, *J* = 8.6 Hz), 5.87 (1H, dt, *J* = 6.3, 1.7 Hz), 4.36 (1H, dt, *J* = 7.3, 6.3 Hz), 3.78 (3H, s), 3.56 (3H, s), 2.60 (2H, t, *J* = 7.3 Hz), 2.35 (2H, dq, *J* = 7.3, 1.7 Hz); ^{13}C NMR (125 MHz, $CDCl_3$) δ 157.8, 146.5, 134.4, 129.4, 113.7, 106.1, 59.6, 55.3, 35.1, 25.9.
trans: ^{1}H NMR ($CDCl_3$, 500 MHz) δ 7.09 (2H, d, *J* = 8.6 Hz), 6.83 (2H, d, *J* = 8.6 Hz), 6.29 (1H, dt, *J* = 12.6, 1.2 Hz), 4.74 (1H, dt, *J* = 12.6, 7.3 Hz), 3.79 (3H, s), 3.49 (3H, s), 2.59 (2H, t, *J* = 7.3 Hz), 2.20 (2H, dq, *J* = 7.3, 1.2 Hz); ^{13}C NMR (125 MHz, $CDCl_3$) δ 157.8, 147.5, 134.2, 129.5, 113.8, 102.3, 55.9, 55.3, 36.6, 30.1. ; HRMS $[M + H]^+$ calculated for $C_{12}H_{17}O_2$ 193.1229, found 193.1250.

*1-(2-((1R,2R,3S)-3-butyl-2-methoxycyclobutyl)ethyl)-4-methoxybenzene (**3**, all trans)*

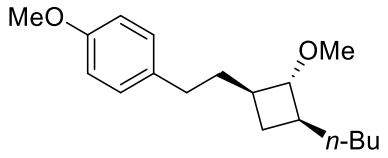

3, *all trans*

^{1}H NMR ($CDCl_3$, 500 MHz) δ 7.08 (2H, d, *J* = 8.6 Hz), 6.81 (2H, d, *J* = 8.6 Hz), 3.78 (3H, s), 3.30 (3H, s), 3.11 (1H, t, *J* = 6.8 Hz), 2.59-2.43 (2H, m), 2.07-1.82 (4H, m), 1.65-1.53 (2H, m), 1.36-1.17 (5H, m), 0.88 (3H, t, *J* = 7.1 Hz), 0.72 (1H, q, *J* = 9.1 Hz); ^{13}C NMR (125 MHz, $CDCl_3$) δ 157.8, 134.8, 129.4, 113.9, 86.6, 56.6, 55.4, 40.7, 40.2, 37.6, 35.1, 33.0, 29.8, 25.6, 22.9, 14.3. ; HRMS $[M + H]^+$ calculated for $C_{18}H_{29}O_2$ 277.2168, found 277.2177.

*hex-5-en-1-yl benzoate (**5**)*

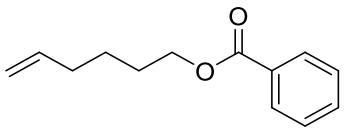

5

^{1}H NMR ($CDCl_3$, 500 MHz) δ 8.04 (2H, d, *J* = 8.5 Hz), 7.55 (1H, t, *J* = 7.0 Hz), 7.44 (2H, t, *J* = 8.0 Hz), 5.82 (1H, ddt, *J* = 17.2, 10.3, 6.9 Hz), 5.03 (1H, dq, *J* = 17.2, 1.7 Hz), 4.97 (1H, dd, *J* = 10.3, 1.7 Hz), 4.33 (2H, t, *J* = 6.5 Hz), 2.13 (2H, dt, *J* = 7.5, 6.9 Hz), 1.79 (2H, quin, *J* = 7.5 Hz), 1.55 (2H, quin, *J* = 7.0 Hz); ^{13}C NMR (125 MHz, $CDCl_3$) δ 166.7, 138.4, 132.9, 130.5, 129.6, 128.4, 115.0, 65.0, 33.4, 28.3, 25.4. ; HRMS $[M + H]^+$ calculated for $C_{13}H_{17}O_2$ 205.1229, found 205.1205.

6-methoxyhex-1-ene (7)

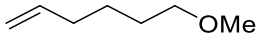

7

^{1}H NMR ($CDCl_3$, 500 MHz) δ 5.81 (1H, ddt, *J* = 17.2, 10.3, 6.3 Hz), 5.01 (1H, dq, *J* = 17.2, 1.7 Hz), 4.95 (1H, d, *J* = 10.3 Hz), 3.38 (2H, t, *J* = 6.3 Hz), 3.33 (3H, s), 2.07 (2H, dt, *J* = 7.5, 6.9 Hz), 1.59 (2H, quin, *J* = 7.5 Hz), 1.45 (2H, quin, *J* = 7.5 Hz) ; ^{13}C NMR (125 MHz, $CDCl_3$) δ 138.8, 114.6, 72.8, 58.6, 33.7, 29.2, 25.6. ; HRMS [M + H]+ calculated for C7H15O 115.1124, found 115.1100.

*4-((1S,2R,3R)-2-methoxy-3-(4-methoxyphenethyl)cyclobutyl)butyl benzoate (**11**, all trans)*

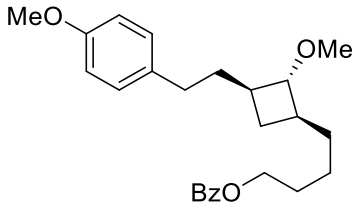

11, *all trans*

^{1}H NMR ($CDCl_3$, 500 MHz) δ 8.04 (2H, dd, *J* = 8.6, 1.2 Hz), 7.55 (1H, tt, *J* = 6.6, 1.7 Hz), 7.44 (2H, t, *J* = 8.0 Hz), 7.08 (2H, d, *J* = 8.6 Hz), 6.81 (2H, d, *J* = 8.6 Hz), 4.31 (2H, t, *J* = 6.9 Hz), 3.78 (3H, s), 3.29 (3H, s), 3.12 (1H, t, *J* = 6.9 Hz), 2.57-2.45 (2H, m), 2.08-1.94 (3H, m), 1.92-1.85 (1H, m), 1.79-1.72 (2H, m), 1.69-1.58 (2H, m), 1.46-1.37 (3H, m), 0.74 (1H, q, *J* = 9.7 Hz) ; ^{13}C NMR (125 MHz, $CDCl_3$) δ 166.8, 157.8, 134.7, 133.0, 130.6, 129.7, 129.3, 128.5, 113.9, 86.5, 65.7, 56.7, 55.4, 40.6, 40.3, 37.6, 35.0, 32.9, 28.9, 25.5, 24.0. ; HRMS $[M + H]^+$ calculated for $C_{25}H_{33}O_4$ 397.2380, found 397.2392.

*4-((1S,2R,3R)-2-methoxy-3-(4-methoxyphenethyl)cyclobutyl)butyl acetate (**12**, all trans)*

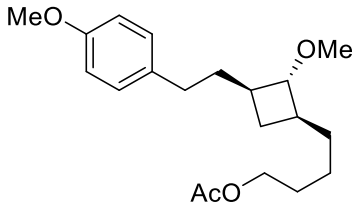

12, *all trans*

^{1}H NMR ($CDCl_3$, 500 MHz) δ 7.08 (2H, d, *J* = 8.6 Hz), 6.82 (2H, d, *J* = 8.6 Hz), 4.05 (2H, t, *J* = 6.9 Hz), 3.78 (3H, s), 3.29 (3H, s), 3.11 (1H, t, *J* = 6.9 Hz), 2.57-2.45 (2H, m), 2.05 (3H, s), 2.04-1.84 (3H, m), 1.65-1.57 (5H, m), 1.40-1.25 (3H, m), 0.72 (1H, q, *J* = 9.7 Hz) ; ^{13}C NMR (125 MHz, $CDCl_3$) δ 171.4, 157.8, 134.6, 129.3, 113.9, 86.5, 64.7, 56.6, 55.4, 40.5, 40.3, 37.6, 34.9, 32.9, 28.8, 25.5, 23.9, 21.2. ; HRMS $[M + H]^+$ calculated for $C_{20}H_{31}O_4$ 335.2223, found 335.2225.

*1-methoxy-4-(2-((1R,2R,3S)-2-methoxy-3-(4-methoxybutyl)cyclobutyl)ethyl)benzene (**13**, all trans)*

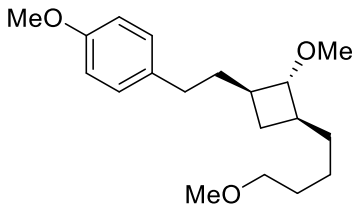

13, *all trans*

^{1}H NMR ($CDCl_3$, 500 MHz) δ 7.08 (2H, d, *J* = 8.6 Hz), 6.82 (2H, d, *J* = 8.6 Hz), 3.78 (3H, s), 3.36 (2H, t, *J* = 6.9 Hz), 3.32 (3H, s), 3.29 (3H, s), 3.11 (1H, t, *J* = 6.9 Hz), 2.56-2.45 (2H, m), 2.27-1.92 (2H, m), 1.91-1.83 (1H, m), 1.64-1.51 (5H, m), 1.38-1.25 (3H, m), 0.72 (1H, q, *J* = 9.7 Hz) ; ^{13}C NMR (125 MHz, $CDCl_3$) δ 157.8, 134.7, 129.4, 113.8, 86.5, 73.0, 58.7, 56.6, 55.4, 40.7, 40.2, 37.6, 35.3, 32.9, 29.9, 25.5, 24.2. ; HRMS $[M + H]^+$ calculated for $C_{19}H_{31}O_3$ 307.2274, found 307.2281.

*4-((1S,2R,3R)-2-methoxy-3-(4-methoxyphenethyl)cyclobutyl)butan-1-ol (**14**, all trans)*

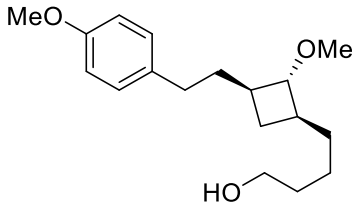

14, *all trans*

^{1}H NMR ($CDCl_3$, 500 MHz) δ 7.08 (2H, d, *J* = 8.6 Hz), 6.82 (2H, d, *J* = 8.6 Hz), 3.79 (3H, s), 3.64 (2H, t, *J* = 6.3 Hz), 3.30 (3H, s), 3.12 (1H, t, *J* = 6.9 Hz), 2.57-2.45 (2H, m), 2.07-1.93 (2H, m), 1.92-1.84 (1H, m), 1.64-1.51 (4H, m), 1.41-1.26 (4H, m), 0.73 (1H, q, *J* = 9.2 Hz) ; ^{13}C NMR (125 MHz, $CDCl_3$) δ 157.8, 134.7, 129.4, 113.9, 86.5, 63.1, 56.6, 55.4, 40.6, 40.2, 37.6, 35.1, 32.9, 32.9, 25.6, 23.7. ; HRMS $[M + H]^+$ calculated for $C_{18}H_{29}O_3$ 293.2117, found 293.2114.

*methyl 4-((1S,2R,3R)-2-methoxy-3-(4-methoxyphenethyl)cyclobutyl)butanoate (**16**, all trans)*

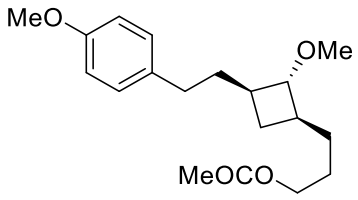

16, *all trans*

^{1}H NMR ($CDCl_3$, 500 MHz) δ 7.08 (2H, d, *J* = 8.6 Hz), 6.81 (2H, d, *J* = 8.6 Hz), 3.78 (3H, s), 3.66 (3H, s), 3.29 (3H, s), 3.11 (1H, t, *J* = 6.9 Hz), 2.54-2.44 (2H, m), 2.30 (2H, t, J = 5.7 Hz), 2.07-1.92 (3H, m), 1.91-1.84 (1H, m), 1.63-1.55 (4H, m), 1.40-1.33 (1H, m), 0.73 (1H, q, *J* = 9.7 Hz) ; ^{13}C NMR (125 MHz, $CDCl_3$) δ 174.3, 157.8, 134.6, 129.3, 113.8, 86.3, 56.6, 55.4, 51.6, 40.3, 40.2, 37.5, 34.7, 34.1, 32.8, 25.4, 22.9. ; HRMS $[M + H]^+$ calculated for $C_{19}H_{29}O_4$ 321.2144, found 321.2165.

*1-(2-((1R,2S)-3,3-diethyl-2-methoxycyclobutyl)ethyl)-4-methoxybenzene (**22**, all trans)*

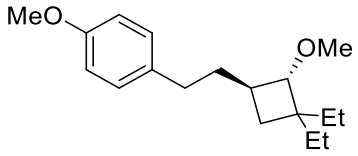

22, *all trans*

^{1}H NMR ($CDCl_3$, 500 MHz) δ 7.09 (2H, d, *J* = 8.6 Hz), 6.82 (2H, d, *J* = 8.6 Hz), 3.78 (3H, s), 3.29 (3H, s), 3.15 (1H, d, *J* = 7.5 Hz), 2.57-2.44 (2H, m), 2.15-2.06 (1H, m), 1.91-1.83 (1H, m), 1.71 (1H, t, *J* = 10.3 Hz), 1.64-1.52 (3H, m), 1.50-1.41 (2H, m), 1.40-1.32 (1H, m), 0.82 (3H, t, *J* = 7.5 Hz), 0.81 (3H, t, *J* = 7.5 Hz); ^{13}C NMR (125 MHz, $CDCl_3$) δ 157.8, 134.9, 129.4, 113.9, 88.1, 58.1, 55.4, 45.1, 38.4, 38.1, 33.0, 31.4, 30.3, 23.3, 8.8, 8.1. ; HRMS $[M + H]^+$ calculated for $C_{18}H_{29}O_2$ 277.2168, found 277.2181.

*1-(2-((1R,2S,3S,4R)-2,3-diethyl-4-methoxycyclobutyl)ethyl)-4-methoxybenzene (**23**, all trans)*

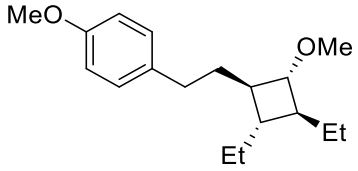

23, *all trans*

^{1}H NMR ($CDCl_3$, 500 MHz) δ 7.10 (2H, d, *J* = 8.6 Hz), 6.82 (2H, d, *J* = 8.6 Hz), 3.79 (3H, s), 3.30 (3H, s), 3.04 (1H, t, *J* = 6.9 Hz), 2.57 (2H, t, *J* = 8.0 Hz), 1.78-1.71 (2H, m), 1.71-1.65 (1H, m), 1.62-1.55 (1H, m), 1.54-1.46 (4H, m), 1.09-1.02 (1H, quin, *J* = 7.5 Hz), 0.91 (3H, t, *J* = 7.5 Hz), 0.87 (3H, t, *J* = 7.5 Hz); ^{13}C NMR (125 MHz, $CDCl_3$) δ 157.8, 135.0, 129.3, 113.9, 84.0, 56.5, 55.4, 48.1, 46.0, 40.7, 37.6, 33.2, 29.1, 27.8, 12.1. ; HRMS $[M + H]^+$ calculated for $C_{18}H_{29}O_2$ 277.2168, found 277.2168.

*1-(2-((1R,2R,4S)-2-ethyl-4-methoxy-3,3-dimethylcyclobutyl)ethyl)-4-methoxybenzene (**24**, all trans)*

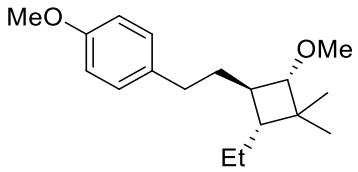

24, *all trans*

^{1}H NMR ($CDCl_3$, 500 MHz) δ 7.10 (2H, d, *J* = 8.6 Hz), 6.82 (2H, d, *J* = 8.6 Hz), 3.78 (3H, s), 3.31 (3H, s), 2.98 (1H, d, *J* = 7.5 Hz), 2.58-2.49 (2H, m), 1.79-1.67 (3H, m), 1.37 (2H, dq, *J* = 8.0, 7.5 Hz), 1.16 (3H, s), 1.03 (1H, m), 0.95 (3H, s), 0.85 (3H, t, *J* = 7.5 Hz); ^{13}C NMR (125 MHz, $CDCl_3$) δ 157.7, 135.0, 129.3, 113.8, 87.3, 57.8, 55.3, 45.6, 44.9, 40.8, 37.4, 33.2, 30.8, 23.2, 15.8, 13.3. ; HRMS $[M + H]^+$ calculated for $C_{18}H_{29}O_2$ 277.2168, found 277.2186.

*1-methoxy-4-(2-((1R,4S)-4-methoxy-2,2,3,3-tetramethylcyclobutyl)ethyl)benzene (**25**, all trans)*

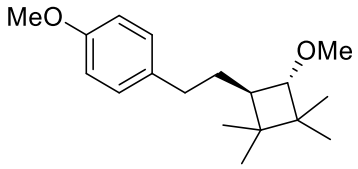

25, *all trans*

^{1}H NMR ($CDCl_3$, 500 MHz) δ 7.10 (2H, d, *J* = 8.6 Hz), 6.82 (2H, d, *J* = 8.6 Hz), 3.78 (3H, s), 3.30 (3H, s), 3.13 (1H, d, *J* = 8.6 Hz), 2.51 (2H, t, *J* = 8.0 Hz), 1.90 (1H, dt, *J* = 8.0, 7.5 Hz), 1.70-1.63 (2H, m), 1.00 (3H, s), 0.99 (3H, s), 0.91 (6H, s); ^{13}C NMR (125 MHz, $CDCl_3$) δ 157.8, 135.2, 129.3, 113.8, 86.7, 58.2, 55.4, 48.6, 42.6, 34.8, 33.9, 31.5, 24.6, 23.8, 20.8, 18.7. ; HRMS $[M + H]^+$ calculated for $C_{18}H_{29}O_2$ 277.2168, found 277.2139.

*(4-methoxybut-3-en-1-yl)benzene (**26**, cis : trans = 1 : 1)*

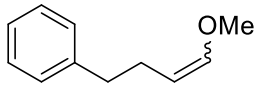

26, *cis* : *trans* = 1 : 1

cis: ^{1}H NMR ($CDCl_3$, 500 MHz) δ 7.28 (2H, m), 7.18 (2H, d, *J* = 7.5 Hz), 7.17 (1H, tt, *J* = 8.0, 1.2 Hz), 5.87 (1H, dt, *J* = 6.3, 1.7 Hz), 4.37 (1H, dt, *J* = 6.9, 6.9 Hz), 3.55 (3H, s), 2.66 (2H, t, *J* = 7.5 Hz), 2.39 (2H, dq, *J* = 7.3, 1.2 Hz); ^{13}C NMR (125 MHz, $CDCl_3$) δ 146.6, 142.4, 128.6, 128.3, 125.8, 106.1, 59.6, 36.1, 25.7.
trans: ^{1}H NMR ($CDCl_3$, 500 MHz) δ 7.28 (2H, m), 7.20 (2H, d, *J* = 7.5 Hz), 7.17 (1H, dt, *J* = 8.0, 1.2 Hz), 6.30 (1H, dt, *J* = 12.6, 1.2 Hz), 4.76 (1H, dt, *J* = 12.6, 7.5 Hz), 3.49 (3H, s), 2.65 (2H, t, *J* = 8.0 Hz), 2.24 (2H, dq, *J* = 7.5, 1.2 Hz); ^{13}C NMR (125 MHz, $CDCl_3$) δ 147.6, 142.1, 128.6, 128.4, 125.9, 102.3, 56.0, 37.6, 30.0. ; HRMS $[M + H]^+$ calculated for $C_{11}H_{15}O$ 163.1124, found 163.1095.

*1-(4-methoxybut-3-en-1-yl)-4-phenoxybenzene (**27**, cis : trans = 1 : 2)*

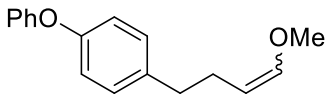

27, *cis : trans* = 1 : 2

cis: ^{1}H NMR ($CDCl_3$, 500 MHz) δ 7.31 (2H, dt, *J* = 8.0, 1.2 Hz), 7.17 (2H, d, *J* = 8.6 Hz), 7.07 (1H, dt, *J* = 7.5, 1.2 Hz), 6.98 (2H, d, *J* = 8.0 Hz), 6.93 (2H, d, *J* = 8.6 Hz), 5.89 (1H, dt, *J* = 6.3, 1.2 Hz), 4.37 (1H, dt, *J* = 6.9, 6.3 Hz), 3.56 (3H, s), 2.64 (2H, t, *J* = 7.5 Hz), 2.38 (2H, dq, *J* = 7.5, 1.2 Hz); ^{13}C NMR (125 MHz, $CDCl_3$) δ 157.9, 155.1, 146.7, 137.5, 129.8, 129.8, 123.0, 119.1, 118.5, 106.0, 59.6, 35.3, 25.8.
trans: ^{1}H NMR ($CDCl_3$, 500 MHz) δ 7.32 (2H, dt, *J* = 8.0, 1.2 Hz), 7.13 (2H, d, *J* = 8.6 Hz), 7.08 (1H, dt, *J* = 7.5, 1.2 Hz), 6.99 (2H, dd, *J* = 8.6, 1.2 Hz), 6.93 (2H, d, *J* = 8.0 Hz), 6.30 (1H, dt, *J* = 12.6, 1.2 Hz), 4.75 (1H, dt, *J* = 12.6, 7.5 Hz), 3.50 (3H, s), 2.63 (2H, t, *J* = 8.0 Hz), 2.23 (2H, dq, *J* = 7.5, 1.2 Hz); ^{13}C NMR (125 MHz, $CDCl_3$) δ 157.8, 155.2, 147.7, 137.1, 129.8, 123.1, 119.1, 118.6, 102.3, 56.1, 36.8, 30.1. ; HRMS $[M + H]^+$

calculated for $C_{17}H_{19}O_2$ 255.1386, found 255.1368.

*tert-butyl(4-(4-methoxybut-3-en-1-yl)phenoxy)dimethylsilane (**28**, cis : trans = 1 : 1)*

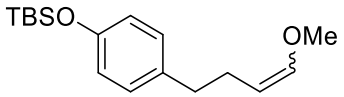

28, *cis : trans* = 1 *:* 1

cis: ^{1}H NMR ($CDCl_3$, 500 MHz) δ 7.04 (2H, d, *J* = 8.6 Hz), 6.74 (2H, d, *J* = 8.6 Hz), 5.86 (1H, dt, *J* = 5.7, 1.7 Hz), 4.35 (1H, dt, *J* = 7.5, 6.3 Hz), 3.55 (3H, s), 2.58 (2H, t, *J* = 7.5 Hz), 2.34 (2H, dq, *J* = 7.5, 1.2 Hz), 0.97 (9H, s), 0.17 (6H,s); ^{13}C NMR (125 MHz, $CDCl_3$) δ 153.6, 146.4, 135.1, 129.4, 119.8, 106.2, 59,6, 35.3, 30.1, 25.8, 18.3, -4.3.

trans: ^{1}H NMR ($CDCl_3$, 500 MHz) δ 7.01 (2H, d, *J* = 8.0 Hz), 6.75 (2H, d, *J* = 8.6 Hz), 6.28 (1H, dt, *J* = 12.6, 1.2 Hz), 4.73 (1H, dt, *J* = 12.6, 7.5 Hz), 3.48 (3H, s), 2.57 (2H, t, *J* = 8.0 Hz), 2.19 (2H, dq, *J* = 7.5, 1.2 Hz), 0.97 (9H,s), 0.18 (6H, s); ^{13}C NMR (125 MHz, $CDCl_3$) δ 153.7, 147.5, 134.8, 129.4, 119.9, 102.4, 55.9, 36.7, 30.1, 25.9, 25.8, -4.3. ; HRMS $[M + H]^+$ calculated for $C_{17}H_{29}O_2Si$ 293.1938, found 293.1945.

*4-(4-methoxybut-3-en-1-yl)phenol (**29**, cis : trans = 1 : 1)*

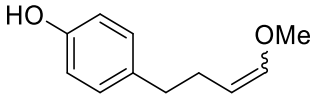

29, *cis* : *trans* = 1 : 1

cis: ^{1}H NMR ($CDCl_3$, 500 MHz) δ 7.04 (2H, d, *J* = 8.0 Hz), 6.73 (2H, d, *J* = 8.0 Hz), 5.87 (1H, dt, *J* = 6.3, 1.7 Hz), 4.37 (1H, dt, *J* = 7.5, 6.3 Hz), 3.55 (3H, s), 2.57 (2H, t, *J* = 6.9 Hz), 2.34 (2H, dq, *J* = 7.5, 1.2 Hz); ^{13}C NMR (125 MHz, $CDCl_3$) δ 153.7, 146.3, 134.4, 129.6, 115.2, 106.5, 59.6, 35.1, 25.9.

trans: ^{1}H NMR ($CDCl_3$, 500 MHz) δ 7.02 (2H, d, *J* = 8.6 Hz), 6.74 (2H, d, *J* = 8.6 Hz), 6.28 (1H, dt, *J* = 12.6, 1.2 Hz), 4.77 (1H, dt, *J* = 12.6, 7.5 Hz), 3.49 (3H, s), 2.56 (2H, t, *J* = 8.0 Hz), 2.18 (2H, dq, *J* = 8.0, 1.3 Hz); ^{13}C NMR (125 MHz, $CDCl_3$) δ 153.8, 147.2, 134.1, 129.7, 115.3, 102.9, 56.1, 36.5, 30.1. ; HRMS $[M + H]^+$ calculated for $C_{11}H_{15}O_2$ 179.1073, found 179.1063.

*1-methoxy-2-(4-methoxybut-3-en-1-yl)benzene (**30**, cis : trans = 1 : 2)*

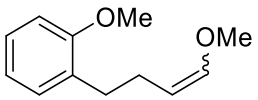

30, *cis* : *trans* = 1 : 2

cis: ^{1}H NMR ($CDCl_3$, 500 MHz) δ 7.17 (1H, dt, *J* = 8.0, 1.7 Hz), 7.15 (1H, d, *J* = 6.9 Hz), 6.87 (1H, dt, *J* = 6.9, 1.2 Hz), 6.83 (1H, d, *J* = 8.0 Hz), 5.86 (1H, dt, *J* = 6.3, 1.2 Hz), 4.38 (1H, dt, *J* = 7.5, 6.3 Hz), 3.82 (3H, s), 3.55 (3H, s), 2.66 (2H, t, *J* = 6.9 Hz), 2.37 (2H, dq, *J* = 7.5, 1.2 Hz); ^{13}C NMR (125 MHz, $CDCl_3$) δ 157.7, 146.3, 130.7, 129.9, 127.0, 120.3, 110.3, 106.7, 59.5, 55.3, 30.3, 24.0.

trans: ^{1}H NMR ($CDCl_3$, 500 MHz) δ 7.17 (1H, dt, *J* = 8.0, 1.7 Hz), 7.12 (1H, dd, *J* = 6.9, 1.2 Hz), 6.87 (1H, dt, *J* = 6.9, 1.2 Hz), 6.84 (1H, d, *J* = 8.0 Hz), 6.30 (1H, d, *J* = 12.6 Hz), 4.78 (1H, dt, *J* = 12.6, 7.5 Hz), 3.82 (3H, s), 3.49 (3H, s), 2.65 (2H, t, *J* = 8.0 Hz), 2.20 (2H, dq, *J* = 7.5, 1.2 Hz); ^{13}C NMR (125 MHz, $CDCl_3$) δ 147.3, 130.5, 129.9, 127.1, 120.4, 110.3, 102.9, 55.9, 55.3, 31.9, 28.2. ; HRMS $[M + H]^+$ calculated for $C_{12}H_{17}O_2$ 193.1229, found 193.1204.

*1-methoxy-3-(4-methoxybut-3-en-1-yl)benzene (**31**, cis : trans = 1 : 1)*

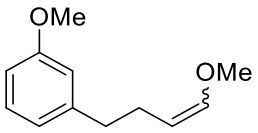

31, *cis* : *trans* = 1 : 1

cis: ^{1}H NMR ($CDCl_3$, 500 MHz) δ 7.20 (1H, t, *J* = 7.5 Hz), 6.80 (1H, d, *J* = 7.5 Hz), 6.75-6.71 (2H, m), 5.87 (1H, dt, *J* = 6.3, 1.2 Hz), 4.36 (1H, dt, *J* = 7.5, 6.3 Hz), 3.79 (3H, s), 3.56 (3H, s), 2.64 (2H, t, *J* = 6.9 Hz), 2.39 (2H, dq, *J* = 7.5, 1.2 Hz); ^{13}C NMR (125 MHz, $CDCl_3$) δ 159.7, 146.6, 144.1, 129.3, 121.1, 114.3, 111.2, 106.1, 59.8, 56.1, 36.1, 25.6.

trans: ^{1}H NMR ($CDCl_3$, 500 MHz) δ 7.18 (1H, t, *J* = 7.5 Hz), 6.77 (1H, d, *J* = 7.5 Hz), 6.75-6.71 (2H, m), 6.31 (1H, dt, *J* = 12.6, 1.2 Hz), 4.75 (1H, dt, *J* = 12.6, 7.5 Hz), 3.80 (3H, s), 3.49 (3H, s), 2.63 (2H, t, *J* = 6.3 Hz), 2.24 (2H, dq, *J* = 7.5, 1.2 Hz); ^{13}C NMR (125 MHz, $CDCl_3$) δ 159.8, 147.7, 143.8, 129.4, 121.1, 114.4, 111.2, 102.4, 59.8, 55.3, 37.6, 29.8. ; HRMS $[M + H]^+$ calculated for $C_{12}H_{17}O_2$ 193.1229, found 193.1210.

*2,4-dimethoxy-1-(4-methoxybut-3-en-1-yl)benzene (**32**, cis : trans = 1 : 2)*

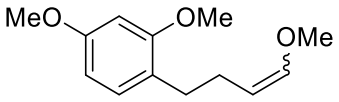

32, *cis* : *trans* = 1 : 2

cis: ^{1}H NMR ($CDCl_3$, 500 MHz) δ 7.05 (1H, d, *J* = 8.0 Hz), 6.43 (1H, d, *J* = 2.9 Hz), 6.41 (1H, dd, *J* = 8.0, 2.3 Hz), 5.86 (1H, dt, *J* = 6.3, 1.2 Hz), 4.37 (1H, dt, *J* = 7.5, 6.3 Hz), 3.79 (3H, s), 3.79 (3H, s), 3.56 (3H, s), 2.59 (2H, t, *J* = 7.5 Hz), 2.33 (2H, dq, *J* = 7.5, 1.7 Hz); ^{13}C NMR (125 MHz, $CDCl_3$) δ 159.1, 158.4, 146.2, 129.9, 123.0, 106.7, 103.7, 98.4, 59.4, 55.2, 55.2, 29.6, 24.1.

trans: ^{1}H NMR ($CDCl_3$, 500 MHz) δ 7.01 (1H, d, *J* = 8.0 Hz), 6.44 (1H, d, *J* = 2.3 Hz), 6.41 (1H, dd, *J* = 8.0, 2.3 Hz), 6.29 (1H, dt, *J* = 12.6, 1.4 Hz), 4.77 (1H, dt, *J* = 12.6, 7.5 Hz), 3.79 (3H, s), 3.79 (3H, s), 3.49 (3H, s), 2.58 (2H, t, *J* = 8.0 Hz), 2.16 (2H, dq, *J* = 7.5, 1.2 Hz); ^{13}C NMR (125 MHz, $CDCl_3$) δ 159.2, 158.3, 147.2, 130.1, 122.7, 103.7, 102.8, 98.4, 55.7, 55.2, 55.1, 31.2, 28.4. ; HRMS $[M + H]^+$ calculated for $C_{13}H_{19}O_3$ 223.1335, found 223.1357.

*1,3,5-trimethoxy-2-(4-methoxybut-3-en-1-yl)benzene (**33**, cis : trans = 1 : 2)*

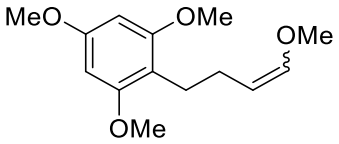

33, *cis* : *trans* = 1 : 2

cis: ^{1}H NMR ($CDCl_3$, 500 MHz) δ 6.12 (2H, s), 5.83 (1H, dt, *J* = 6.3, 1.7 Hz), 4.40 (1H, dt, *J* = 7.5, 6.3 Hz), 3.80 (3H, s), 3.79 (6H, s), 3.54 (3H, s), 2.61 (2H, t, *J* = 7.5 Hz), 2.23 (2H, dq, *J* = 7.5, 1.7 Hz); ^{13}C NMR (125 MHz, $CDCl_3$) δ 159.3, 159.0, 145.8, 111.5, 107.5, 90.6, 59.5, 55.8, 55.3, 23.9, 22.8.

trans: ^{1}H NMR ($CDCl_3$, 500 MHz) δ 6.28 (1H, d, *J* = 12.6 Hz), 6.12 (2H, s), 4.80 (1H, dt, *J* = 12.6, 7.5 Hz), 3.80 (3H, s), 3.79 (6H, s), 3.49 (3H, s), 2.59 (2H, t, *J* = 8.0 Hz), 2.05 (2H, dq, *J* = 7.5, 1.2 Hz); ^{13}C NMR (125 MHz, $CDCl_3$) δ 159.3, 158.9, 146.9, 111.1, 103.5, 90.5, 59.5, 55.6, 55.3, 27.8, 24.1. ; HRMS $[M + H]^+$ calculated for $C_{14}H_{21}O_4$ 253.1441, found 253.1468.

*1,2-dimethoxy-4-(4-methoxybut-3-en-1-yl)benzene (**34**, cis : trans = 1 : 2)*

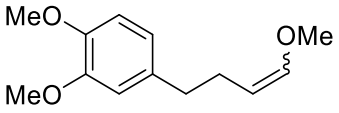

34, *cis* : *trans* = 1 : 2

cis: ^{1}H NMR ($CDCl_3$, 500 MHz) δ 6.80 (1H, d, *J* = 3.7 Hz), 6.76-6.72 (1H, m), 6.72-6.70 (1H, m), 5.88 (1H, dt, *J* = 5.7, 1.2 Hz), 4.37 (1H, dt, *J* = 7.5, 6.3 Hz), 3.88 (3H, s), 3.85 (3H, s), 3.57 (3H, s), 2.61 (2H, t, *J* = 7.5 Hz), 2.37 (2H, dq, *J* = 7.5, 1.7 Hz); ^{13}C NMR (125 MHz, $CDCl_3$) δ 148.5, 146.9, 146.3, 134.9, 120.2, 111.7, 111.0, 105.9, 55.8, 55.8, 55.6, 35.4, 25.6.

trans: ^{1}H NMR ($CDCl_3$, 500 MHz) δ 6.78 (1H, s), 6.76-6.72 (1H, m), 6.72-6.70 (1H, m), 6.31 (1H, dt, *J* = 12.6, 1.2 Hz), 4.75 (1H, dt, *J* = 12.6, 6.9 Hz), 3.88 (3H, s), 3.86 (3H, s), 3.49 (3H, s), 2.60 (2H, t, *J* = 7.5 Hz), 2.22 (2H, dq, *J* = 7.5, 1.2 Hz); ^{13}C NMR (125 MHz, $CDCl_3$) δ 148.6, 147.3, 147.0, 134.6, 120.3, 111.8, 111.1, 102.2, 55.8, 55.8, 55.6, 36.9, 29.9. ; HRMS $[M + H]^+$ calculated for $C_{13}H_{19}O_3$ 223.1335, found 223.1319.

*1,2,3-trimethoxy-5-(4-methoxybut-3-en-1-yl)benzene (**35**, cis : trans = 1 : 1)*

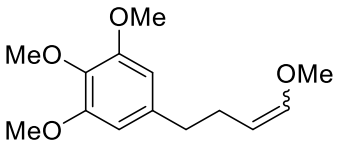

35, *cis* : *trans* = 1 : 1

cis: ^{1}H NMR ($CDCl_3$, 500 MHz) δ 6.43 (1H, s), 6.40 (1H, s), 5.90 (1H, dt, *J* = 6.3, 1.7 Hz), 4.37 (1H, dt, *J* = 7.5, 6.3 Hz), 3.85 (6H, s), 3.82 (3H, s), 3.58 (3H, s), 2.61 (2H, t, *J* = 8.6 Hz), 2.39 (2H, dq, *J* = 7.5, 1.7 Hz); ^{13}C NMR (125 MHz, $CDCl_3$) δ 152.9, 147.5, 137.8, 135.9, 105.3, 102.1, 59.5, 56.0, 55.9, 37.8, 25.5.

trans: ^{1}H NMR ($CDCl_3$, 500 MHz) δ 6.43 (1H, s), 6.40 (1H, s), 6.33 (1H, dt, *J* = 12.6, 1.1 Hz), 4.76 (1H, dt, *J* = 12.6, 7.5 Hz), 3.85 (6H, s), 3.83 (3H, s), 3.50 (3H, s), 2.60 (2H, t, *J* = 8.0 Hz), 2.24 (2H, dq, *J* = 7.5, 1.2

Hz); ^{13}C NMR (125 MHz, $CDCl_3$) δ 153.0, 146.5, 138.1, 136.0, 105.8, 105.2, 60.8, 56.0, 55.9, 36.3, 29.9. ; HRMS $[M + H]^+$ calculated for $C_{14}H_{21}O_4$ 253.1441, found 253.1456.

*1-(4-methoxybut-3-en-1-yl)-4-methylbenzene (**36**, cis : trans = 1 : 1)*

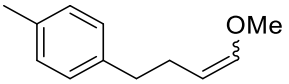

36, *cis* : *trans* = 1 : 1

cis: ^{1}H NMR ($CDCl_3$, 500 MHz) δ 7.11-7.05 (4H, m), 5.87 (1H, dt, *J* = 6.3, 1.2 Hz), 4.36 (1H, dt, *J* = 6.9, 6.3 Hz), 3.56 (3H, s), 2.62 (2H, t, *J* = 7.5 Hz), 2.37 (2H, dq, *J* = 7.5, 1.2 Hz), 2.31 (3H, s); ^{13}C NMR (125 MHz, $CDCl_3$) δ 146.5, 139.3, 135.2, 129.0, 128.5, 106.2, 59.6, 35.6, 30.1, 21.2.
trans: ^{1}H NMR ($CDCl_3$, 500 MHz) δ 7.11-7.05 (4H, m), 6.30 (1H, dt, *J* = 12.6, 1.2 Hz), 4.75 (1H, dt, *J* = 12.6, 7.5 Hz), 3.49 (3H, s), 2.61 (2H, t, *J* = 8.0 Hz), 2.32 (3H, s), 2.21 (2H, dq, *J* = 7.5, 1.2 Hz); ^{13}C NMR (125 MHz, $CDCl_3$) δ 147.5, 139.0, 135.3, 129.1, 128.5, 102.5, 56.0, 37.1, 25.8, 21.2. ; HRMS $[M + H]^+$ calculated for $C_{12}H_{17}O$ 177.1280, found 177.1266.

*1-(4-methoxybut-3-en-1-yl)-2,4-dimethylbenzene (**37**, cis : trans = 1 : 2)*

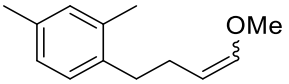

37, *cis* : *trans* = 1 : 2

cis: ^{1}H NMR ($CDCl_3$, 500 MHz) δ 7.05 (1H, d, J = 8.0 Hz), 6.97-6.92 (2H, m), 5.89 (1H, dt, *J* = 6.3, 1.5 Hz), 4.40 (1H, dt, *J* = 7.5, 6.3 Hz), 3.57 (3H, s), 2.60 (2H, t, *J* = 7.5 Hz), 2.32 (2H, q, *J* = 7.5 Hz), 2.28 (3H, s), 2.28 (3H, s); ^{13}C NMR (125 MHz, $CDCl_3$) δ 146.6, 137.5, 136.0, 135.3, 131.0, 128.8, 126.6, 106.3, 59.6, 33.0, 24.6, 21.0, 19.4.
trans: ^{1}H NMR ($CDCl_3$, 500 MHz) δ 7.02 (1H, d, J = 7.5 Hz), 6.97-6.92 (2H, m), 6.33 (1H, d, *J* = 12.6 Hz), 4.79 (1H, dt, *J* = 12.6, 7.5 Hz), 3.50 (3H, s), 2.60 (2H, t, *J* = 7.5 Hz), 2.28 (3H, s), 2.27 (3H, s), 2.17 (2H, q, *J* = 7.5 Hz); ^{13}C NMR (125 MHz, $CDCl_3$) δ 147.5, 137.2, 135.8, 135.4, 131.1, 129.0, 126.7, 102.7, 56.0, 34.5, 28.9, 21.0, 19.4. ; HRMS $[M + H]^+$ calculated for $C_{13}H_{19}O$ 191.1437, found 191.1448.

*2-(4-methoxybut-3-en-1-yl)-1,3,5-trimethylbenzene (**38**, cis : trans = 1 : 2)*

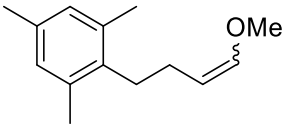

38, *cis* : *trans* = 1 : 2

cis: ^{1}H NMR ($CDCl_3$, 500 MHz) δ 6.82 (2H, s), 5.91 (1H, dt, *J* = 6.3, 1.2 Hz), 4.45 (1H, dt, *J* = 7.5, 6.3 Hz), 3.58 (3H, s), 2.62 (2H, t, *J* = 8.6 Hz), 2.31 (6H, s), 2.24 (3H, s), 2.20 (2H, dq, *J* = 6.9, 1.2 Hz); ^{13}C NMR (125 MHz, $CDCl_3$) δ 146.7, 136.2, 135.8, 134.9, 128.9, 106.5, 59.6, 29.8, 23.8, 20.0, 19.8.

trans: ^{1}H NMR ($CDCl_3$, 500 MHz) δ 6.83 (2H, s), 6.36 (1H, dt, *J* = 12.6, 1.2 Hz), 4.82 (1H, dt, *J* = 12.6, 7.5 Hz), 3.52 (3H, s), 2.62 (2H, t, *J* = 8.0 Hz), 2.29 (6H, s), 2.24 (3H, s), 2.07 (2H, dq, *J* = 6.9, 1.2 Hz); ^{13}C NMR (125 MHz, $CDCl_3$) δ 147.4, 136.3, 136.1, 135.1, 129.1, 102.8, 56.0, 31.1, 27.7, 21.0, 20.0. ; HRMS $[M + H]^+$ calculated for $C_{14}H_{21}O$ 205.1593, found 205.1564.

*(4-(4-methoxybut-3-en-1-yl)phenyl)(methyl)sulfane (**39**, cis : trans = 1 : 2)*

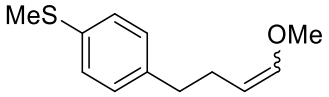

39, *cis* : *trans* = 1 : 2

cis: ^{1}H NMR ($CDCl_3$, 500 MHz) δ 7.19 (2H, d, *J* = 8.6 Hz), 7.13 (2H, d, *J* = 8.6 Hz), 5.87 (1H, dt, *J* = 6.0, 1.2 Hz), 4.34 (1H, dt, *J* = 7.5, 6.3 Hz), 3.56 (3H, s), 2.62 (2H, t, *J* = 6.9 Hz), 2.46 (3H, s), 2.36 (2H, dq, *J* = 7.5, 1.2 Hz); ^{13}C NMR (125 MHz, $CDCl_3$) δ 146.6, 139.6, 135.1, 129.1, 127.2, 105.8, 59.6, 35.5, 25.6, 16.5.
trans: ^{1}H NMR ($CDCl_3$, 500 MHz) δ 7.20 (2H, d, *J* = 8.0 Hz), 7.10 (2H, d, *J* = 8.6 Hz), 6.29 (1H, dt, *J* = 12.6, 1.2 Hz), 4.73 (1H, dt, *J* = 12.6, 6.9 Hz), 3.49 (3H, s), 2.61 (2H, t, *J* = 8.0 Hz), 2.47 (3H, s), 2.21 (2H, dq, *J* = 7.5, 1.2 Hz); ^{13}C NMR (125 MHz, $CDCl_3$) δ 147.7, 139.2, 135.3, 129.2, 127.2, 102.1, 56.0, 37.0, 29.8, 16.4. ; HRMS $[M + H]^+$ calculated for $C_{12}H_{17}OS$ 209.1001, found 209.0080.

*4-(4-methoxybut-3-en-1-yl)-N,N-dimethylaniline (**40**, cis : trans = 1 : 2)*

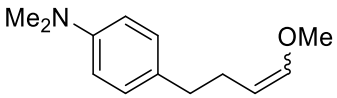

40, *cis* : *trans* = 1 : 2

cis: ^{1}H NMR ($CDCl_3$, 500 MHz) δ 7.09 (2H, d, *J* = 8.6 Hz), 6.70 (2H, d, *J* = 8.6 Hz), 5.87 (1H, dt, *J* = 5.7, 1.2 Hz), 4.37 (1H, dt, *J* = 7.5, 6.3 Hz), 3.56 (3H, s), 2.90 (6H, s), 2.57 (2H, t, *J* = 6.9 Hz), 2.35 (2H, dq, *J* = 7.5, 1.7 Hz); ^{13}C NMR (125 MHz, $CDCl_3$) δ 149.1, 146.3, 130.7, 129.1, 113.1, 106.5, 59.6, 41.1, 35.1, 26.0.
trans: ^{1}H NMR ($CDCl_3$, 500 MHz) δ 7.06 (2H, d, *J* = 8.6 Hz), 6.70 (2H, d, *J* = 8.6 Hz), 6.31 (1H, dt, *J* = 12.6, 1.3 Hz), 4.77 (1H, dt, *J* = 12.6, 7.5 Hz), 3.49 (3H, s), 2.91 (6H, s), 2.55 (2H, t, *J* = 6.9 Hz), 2.19 (2H, dq, *J* = 7.5, 1.2 Hz); ^{13}C NMR (125 MHz, $CDCl_3$) δ 149.2, 147.4, 130.4, 129.2, 113.1, 102.7, 56.0, 41.0, 36.5, 30.3. ; HRMS $[M + H]^+$ calculated for $C_{13}H_{20}NO$ 206.1546, found 206.1573.

*1-(2-((1R,2R,3S)-3-butyl-2-methoxycyclobutyl)ethyl)-4-phenoxybenzene (**42**, all trans)*

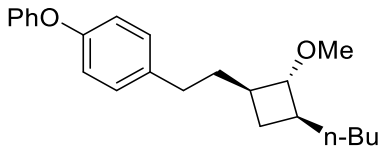

42, *all trans*

^{1}H NMR ($CDCl_3$, 500 MHz) δ 7.32 (1H, d, *J* = 8.6 Hz), 7.31 (1H, d, *J* = 8.6 Hz), 7.13 (2H, d, *J* = 8.0 Hz),

7.07 (1H, tt, *J* = 7.5, 1.2 Hz), 6.98 (2H, d, *J* = 8.0 Hz), 6.92 (2H, d, *J* = 8.6 Hz), 3.31 (3H, s), 3.11 (1H, t, *J* = 6.9 Hz), 2.61-2.50 (2H, m), 2.07-1.87 (4H, m), 1.67-1.55 (2H, m), 1.36-1.19 (5H, m), 0.89 (3H, t, *J* = 7.5 Hz), 0.73 (1H, q, *J* = 9.2 Hz) ; ^{13}C NMR (125 MHz, $CDCl_3$) δ 157.9, 155.1, 137.7, 129.8, 129.7, 123.0, 119.2, 118.6, 86.6, 56.6, 40.7, 40.2, 37.4, 35.2, 33.1, 29.8, 25.6, 22.9, 14.3. ; HRMS $[M + H]^+$ calculated for $C_{23}H_{31}O_2$ 339.2325, found 339.2295.

*tert-butyl(4-(2-((1R,2R,3S)-3-butyl-2-methoxycyclobutyl)ethyl)phenoxy)dimethylsilane (**43**, all trans)*

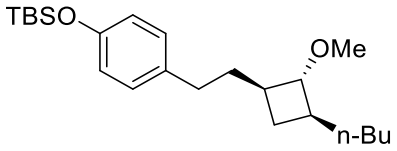

43, *all trans*

^{1}H NMR ($CDCl_3$, 500 MHz) δ 7.01 (2H, d, *J* = 8.6 Hz), 6.73 (2H, d, *J* = 8.6 Hz), 3.30 (3H, s), 3.10 (1H, t, *J* = 6.9 Hz), 2.56-2.44 (2H, m), 2.05-1.83 (4H, m), 1.63-1.53 (2H, m), 1.34-1.18 (5H, m), 0.97 (9H, s), 0.88 (3H, t, *J* = 6.9 Hz), 0.70 (1H, q, *J* = 9.7 Hz), 0.18 (6H, s); ^{13}C NMR (125 MHz, $CDCl_3$) δ 153.7, 135.4, 129.3, 119.9, 86.6, 56.6, 40.7, 40.3, 37.5, 35.1, 33.1, 29.8, 25.9, 25.6, 22.9, 18.4, 14.3, -4.3. ; HRMS $[M + H]^+$ calculated for $C_{23}H_{41}O_2Si$ 377.2877, found 377.2869.

*4-(2-((1R,2R,3S)-3-butyl-2-methoxycyclobutyl)ethyl)phenol (**44**, all trans)*

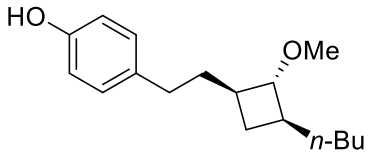

44, *all trans*

^{1}H NMR ($CDCl_3$, 500 MHz) δ 7.02 (2H, d, *J* = 8.3 Hz), 6.73 (2H, d, *J* = 8.3 Hz), 3.31 (3H, s), 3.12 (1H, t, *J* = 6.9 Hz), 2.56-2.43 (2H, m), 2.06-1.92 (3H, m), 1.92-1.83 (1H, m), 1.62-1.53 (2H, m), 1.35-1.18 (5H, m), 0.88 (3H, t, *J* = 6.9 Hz), 0.71 (1H, q, *J* = 9.2 Hz); ^{13}C NMR (125 MHz, $CDCl_3$) δ 153.8, 134.7, 129.5, 86.6, 6.6, 40.7, 40.1, 37.5, 35.1, 32.9, 29.8, 2.6, 22.9, 14.3. ; HRMS $[M + H]^+$ calculated for $C_{17}H_{27}O_2$ 263.2012, found 263.2030.

*1-(2-((1R,2R,3S)-3-butyl-2-methoxycyclobutyl)ethyl)-2-methoxybenzene (**45**, all trans)*

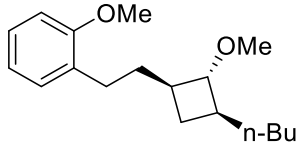

45, *all trans*

^{1}H NMR ($CDCl_3$, 500 MHz) δ 7.15 (1H, dt, *J* = 7.5, 1.7 Hz), 7.11 (1H, dd, *J* = 7.5, 1.7 Hz), 6.86 (1H, t, *J* = 7.5 Hz), 6.82 (1H, d, J = 8.0 Hz), 3.81 (3H, s), 3.30 (3H, s), 3.11 (1H, t, *J* = 6.9 Hz), 2.62-2.51 (2H, m),

2.08-1.84 (4H, m), 1.63-1.53 (2H, m), 1.36-1.19 (5H, m), 0.88 (3H, t, *J* = 6.9 Hz), 0.73 (1H, q, *J* = 9.7 Hz); ^{13}C NMR (125 MHz, $CDCl_3$) δ 157.6, 131.1, 129.9, 127.0, 120.5, 110.4, 86.7, 56.6, 55.4, 40.7, 40.6, 35.6, 35.1, 29.8, 28.2, 25.6, 22.9, 14.2. ; HRMS $[M + H]^+$ calculated for $C_{18}H_{29}O_2$ 277.2168, found 277.2177.

*1-(2-((1R,2R,3S)-3-butyl-2-methoxycyclobutyl)ethyl)-3-methoxybenzene (**46**, all trans)*

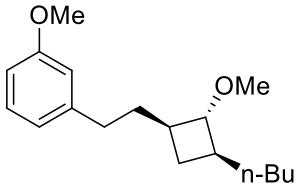

46, *all trans*

^{1}H NMR ($CDCl_3$, 500 MHz) δ 7.19 (1H, dd, *J* = 8.6, 7.5 Hz), 6.77 (1H, d, *J* = 8.0 Hz), 6.74-6.71 (2H, m), 3.80 (3H, s), 3.30 (3H, s), 3.11 (1H, t, *J* = 6.9 Hz), 2.61-2.48 (2H, m), 2.08-1.87 (4H, m), 1.66-1.54 (2H, m), 1.36-1.17 (5H, m), 0.88 (3H, t, *J* = 6.9 Hz), 0.73 (1H, q, *J* = 9.7 Hz); ^{13}C NMR (125 MHz, $CDCl_3$) δ 159.7, 144.3, 129.4, 120.9, 114.3, 111.1, 86.5, 56.6, 55.3, 40.7, 40.2, 37.3, 35.2, 33.9, 29.8, 25.6, 22.9, 14.3. ; HRMS $[M + H]^+$ calculated for $C_{18}H_{29}O_2$ 277.2168, found 277.2145.

*1-(2-((1R,2R,3S)-3-butyl-2-methoxycyclobutyl)ethyl)-2,4-dimethoxybenzene (**47**, all trans)*

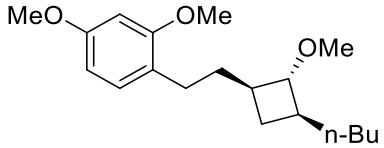

47, *all trans*

^{1}H NMR ($CDCl_3$, 500 MHz) δ 7.01 (1H, d, *J* = 8.0 Hz), 6.43 (1H, d, *J* = 2.9 Hz), 6.40 (1H, dd, *J* = 7.5, 2.9 Hz), 3.79 (6H, s), 3.31 (3H, s), 3.10 (1H, t, *J* = 6.9 Hz), 2.55-2.43 (2H, m), 2.07-1.90 (3H, m), 1.88-1.80 (1H, m), 1.60-1.51 (2H, m), 1.36-1.19 (5H, m), 0.88 (3H, t, *J* = 6.8 Hz), 0.72 (1H, q, *J* = 9.7 Hz); ^{13}C NMR (125 MHz, $CDCl_3$) δ 169.1, 158.4, 130.0, 123.4, 103.8, 98.6, 86.7, 56.6, 55.5, 55.4, 40.7, 40.6, 35.9, 35.1, 29.8, 27.5, 25.6, 22.9, 14.3. ; HRMS $[M + H]^+$ calculated for $C_{19}H_{31}O_3$ 307.2274, found 307.2284.

*1-(2-((1R,2R,3S)-3-butyl-2-methoxycyclobutyl)ethyl)-4-methylbenzene (**51**, all trans)*

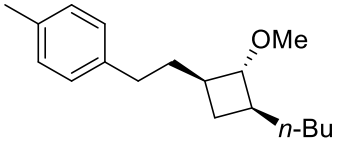

51, *all trans*

^{1}H NMR ($CDCl_3$, 500 MHz) δ 7.11-7.04 (4H, m), 3.30 (3H, s), 3.11 (1H, t, *J* = 6.8 Hz), 2.58-2.47 (2H, m), 2.31 (3H, s), 2.07-1.85 (4H, m), 1.65-1.52 (2H, m), 1.36-1.20 (5H, m), 0.88 (3H, t, *J* = 7.5 Hz), 0.72 (1H, q, *J*

= 9.7 Hz); ^{13}C NMR (125 MHz, $CDCl_3$) δ 139.6, 135.2, 129.1, 128.3, 86.6, 56.6, 40.7, 40.3, 37.5, 35.1, 33.4, 29.8, 25.6, 22.9, 21.2, 14.3. ; HRMS $[M + H]^+$ calculated for $C_{18}H_{29}O$ 261.2219, found 261.2244.

*1-(2-((1R,2R,3S)-3-butyl-2-methoxycyclobutyl)ethyl)-2,4-dimethylbenzene (**52**, all trans)*

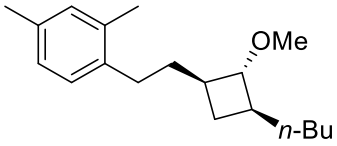

52, *all trans*

^{1}H NMR ($CDCl_3$, 500 MHz) δ 7.01 (1H, d, *J* = 7.5 Hz), 6.96-6.91 (2H, m), 3.31 (3H, s), 3.11 (1H, t, *J* = 7.5 Hz), 2.54-2.45 (2H, m), 2.28 (3H, s), 2.26 (3H, s), 2.10-1.92 (3H, m), 1.87-1.79 (1H, m), 1.61-1.50 (2H, m), 1.37-1.19 (5H, m), 0.88 (3H, t, *J* = 7.5 Hz), 0.74 (1H, q, *J* = 9.7 Hz); ^{13}C NMR (125 MHz, $CDCl_3$) δ 137.7, 135.7, 135.3, 131.1, 128.8, 126.7, 86.6, 56.7, 40.7, 40.6, 36.3, 35.2, 30.8, 29.8, 25.7, 22.9, 21.0, 19.3, 14.2. ; HRMS $[M + H]^+$ calculated for $C_{19}H_{31}O$ 275.2376, found 275.2387.

*2-(2-((1R,2R,3S)-3-butyl-2-methoxycyclobutyl)ethyl)-1,3,5-trimethylbenzene (**53**, all trans)*

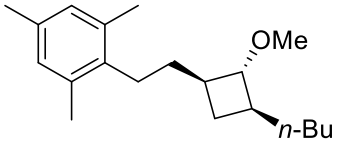

53, *all trans*

^{1}H NMR ($CDCl_3$, 500 MHz) δ 6.82 (2H, s), 3.32 (3H, s), 3.11 (1H, t, *J* = 6.9 Hz), 2.52 (2H, t, J = 8.6 Hz), 2.27 (6H, s), 2.23 (3H, s), 2.15-1.93 (3H, m), 1.75-1.67 (1H, m), 1.63-1.55 (1H, m), 1.49-1.18 (6H, m), 0.89 (3H, t, *J* = 6.9 Hz), 0.77 (1H, q, *J* = 9.7 Hz); ^{13}C NMR (125 MHz, $CDCl_3$) δ 136.3, 135.9, 135.0, 129.0, 86.6, 56.7, 41.2, 40.8, 35.2, 34.9, 29.8, 27.3, 25.6, 22.9, 20.9, 19.8, 14.3. ; HRMS $[M + H]^+$ calculated for $C_{20}H_{33}O$ 289.2532, found 289.2533.

*(4-(2-((1R,2R,3S)-3-butyl-2-methoxycyclobutyl)ethyl)phenyl)(methyl)sulfane (**54**, all trans)*

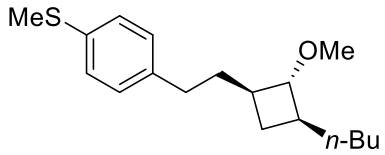

54, *all trans*

^{1}H NMR ($CDCl_3$, 500 MHz) δ 7.18 (2H, d, *J* = 8.0 Hz), 7.09 (2H, d, *J* = 8.0 Hz), 3.29 (3H, s), 3.10 (1H, t, *J* = 6.9 Hz), 2.58-2.47 (2H, m), 2.46 (3H, s), 2.05-1.83 (4H, m), 1.65-1.53 (2H, m), 1.35-1.19 (5H, m), 0.88 (3H, t, *J* = 6.9 Hz), 0.71 (1H, q, *J* = 9.7 Hz); ^{13}C NMR (125 MHz, $CDCl_3$) δ 139.9, 135.2, 129.1, 127.4, 86.6, 56.6, 40.8, 40.2, 37.3, 35.1, 33.3, 29.8, 25.6, 22.9, 16.6, 14.2. ; HRMS $[M + H]^+$ calculated for $C_{18}H_{29}OS$ 293.1940, found 293.1957.

Cartesian Coordinates of the Optimized Structure for the Ground State of *para*-Methoxy Enol Ether (**1**) Calculated at the B3LYP/6-311++G(2d,2p) Level in Nitromethane (PCM model). Total Energy: -617.51959388 hartree/particle.

Symbol	X	Y	Z
C	0.6945193	-0.1865819	0.5784544
C	1.5920136	-1.2068187	0.2713730
C	1.1838731	1.1256850	0.5737626
C	2.9289645	-0.9484401	-0.0340302
C	2.5080743	1.4047084	0.2735309
C	3.3920950	0.3664972	-0.0350879
H	3.5880857	-1.7718596	-0.2609409
H	2.8758698	2.4215927	0.2780517
C	-1.6540454	-0.4125365	-0.3923932
H	-1.2440349	-1.1028298	-1.1358729
H	-1.5896240	0.5869858	-0.8276287
C	-0.7591500	-0.4772165	0.8676714
H	-0.8522974	-1.4694174	1.3140981
H	-1.1404934	0.2349513	1.6019780
C	-3.0876989	-0.7583005	-0.1145279
H	-3.3049982	-1.7572805	0.2496050
C	-4.0945407	0.0972959	-0.2709881
H	-3.9417201	1.1097266	-0.6320949
C	-6.3641272	0.7307993	-0.3836004
H	-6.3868009	0.8232207	-1.4709178
H	-7.3244584	0.3663246	-0.0315391
H	-6.1611737	1.7065781	0.0615910
O	-5.3875697	-0.2298370	0.0267763
H	1.2507869	-2.2346146	0.2717957
H	0.5171693	1.9444192	0.8142925
C	5.6204524	-0.2873873	-0.6314143
H	6.5615016	0.2214081	-0.8156951
H	5.7408834	-0.9838944	0.1999128
H	5.3225304	-0.8356173	-1.5266329
O	4.6783440	0.7365971	-0.3150893

Cartesian Coordinates of the Optimized Structure for the Ground State of the Radical Cation of *para*-Methoxy Enol Ether (**1**$^{\cdot+}$) Calculated at the B3LYP/6-311++G(2d,2p) Level in Nitromethane (PCM model). Total Energy: -617.30788871 hartree/particle.

Symbol	X	Y	Z
C	0.6538627	-0.1968342	0.5912473
C	1.5703513	-1.2244735	0.2910688
C	1.1125378	1.1377968	0.5522598
C	2.8890068	-0.9541862	-0.0041983
C	2.4211313	1.4295055	0.2590973
C	3.3288801	0.3847400	-0.0253481
H	3.5703239	-1.7633836	-0.2116189
H	2.7831519	2.4469935	0.2424576
C	-1.6243350	-0.6063184	-0.4607039
H	-1.1993017	-1.4320438	-1.0290493
H	-1.4895146	0.3147657	-1.0233807
C	-0.7628342	-0.5038694	0.8958693
H	-0.8643112	-1.4567481	1.4109731
H	-1.2083541	0.2771432	1.5060017
C	-3.0388876	-0.8562207	-0.1567063
H	-3.3295539	-1.8215541	0.2394470
C	-4.0022299	0.0920490	-0.3097686
H	-3.7772111	1.0866020	-0.6810316
C	-6.2393375	0.8550123	-0.3023798
H	-6.3263246	0.9896175	-1.3785816
H	-7.1756450	0.4979247	0.1093848
H	-5.9435787	1.7856127	0.1774754
O	-5.2652142	-0.1761437	-0.0215226
H	1.2352846	-2.2527114	0.3054165
H	0.4226852	1.9415909	0.7697991
C	5.5759862	-0.2220684	-0.6209779
H	6.4841940	0.3393527	-0.8063442
H	5.7219852	-0.9000951	0.2179227
H	5.2912060	-0.7760547	-1.5135726
O	4.5777356	0.7651675	-0.3024845

Cartesian Coordinates of the Optimized Structure for the Ground State of *ortho*-Methoxy Enol Ether (**30**) Calculated at the B3LYP/6-311++G(2d,2p) Level in Nitromethane (PCM model). Total Energy: -617.51918586 hartree/particle.

Symbol	X	Y	Z
C	1.4151959	-0.6881788	0.3467084
C	2.2665200	-1.7795511	0.1979230
C	1.9447734	0.5972955	0.1173859
C	3.6036724	-1.6293172	-0.1686873
C	3.2819256	0.7609694	-0.2457986
C	4.1058358	-0.3546937	-0.3891629
H	4.2397192	-2.4969510	-0.2750551
H	3.6890009	1.7449447	-0.4179399
C	-0.9947071	-0.8209623	-0.4894530
H	-0.6711433	-1.5747623	-1.2137130
H	-0.8991072	0.1481248	-0.9808088
C	-0.0343804	-0.8775970	0.7222862
H	-0.1466529	-1.8451387	1.2145382
H	-0.3374315	-0.1154089	1.4407604
C	-2.4256378	-1.0643786	-0.1084024
H	-2.6738136	-2.0213814	0.3394456
C	-3.3963254	-0.1718781	-0.2853687
H	-3.2111347	0.8044984	-0.7224736
C	-5.5763841	0.6960952	-0.0420280
H	-5.5802750	1.1072770	-1.0532093
H	-6.5697935	0.3328848	0.2034826
H	-5.2882452	1.4739536	0.6673442
O	-4.6970278	-0.4278223	0.0481249
C	1.5528078	2.9666784	0.0757050
H	2.3568467	3.2088067	0.7723821
H	1.9017694	3.1088063	-0.9482575
H	0.7049150	3.6186286	0.2618447
O	1.0738339	1.6384520	0.2792140
H	1.8707987	-2.7712478	0.3784463
H	5.1403234	-0.2149625	-0.6721438

Cartesian Coordinates of the Optimized Structure for the Ground State of the Radical Catiion of *ortho*-Methoxy Enol Ether (**30**$^{\cdot+}$) Calculated at the B3LYP/6-311++G(2d,2p) Level in Nitromethane (PCM model). Total Energy: -617.30565139 hartree/particle.

Symbol	X	Y	Z
C	1.3855675	-0.6920663	0.3498167
C	2.2613833	-1.7703419	0.2092575
C	1.8871244	0.6167731	0.1184206
C	3.5956456	-1.5790942	-0.1126774
C	3.2348886	0.8136862	-0.2022116
C	4.0769528	-0.2809523	-0.3160572
H	4.2626591	-2.4247187	-0.1963563
H	3.6210635	1.8059998	-0.3704997
C	-0.9642585	-0.9245321	-0.6032323
H	-0.6028587	-1.7496005	-1.2155818
H	-0.8210500	0.0131361	-1.1347670
C	-0.0431475	-0.9022626	0.7098325
H	-0.1713731	-1.8530885	1.2213590
H	-0.4087954	-0.1054544	1.3503930
C	-2.3654040	-1.1406178	-0.2396132
H	-2.6861237	-2.1237689	0.0825481
C	-3.3002837	-0.1327589	-0.2397873
H	-3.0545702	0.8830925	-0.5318487
C	-5.5105754	0.6823841	0.0156645
H	-5.8388501	0.7589145	-1.0179969
H	-6.3327897	0.3866479	0.6555017
H	-5.0700930	1.6161544	0.3545702
O	-4.5345264	-0.3884040	0.1087018
C	1.4099932	2.9696091	0.0338659
H	2.1713149	3.2428846	0.7634520
H	1.7900472	3.1147302	-0.9766594
H	0.5225595	3.5745660	0.1833748
O	0.9857916	1.6129761	0.2267307
H	1.8852282	-2.7704575	0.3783098
H	5.1161924	-0.1245731	-0.5689312

Table S5. Cartesian Coordinates of the Optimized Structure for the Ground State of *meta*-Methoxy Enol Ether (**31**) Calculated at the B3LYP/6-311++G(2d,2p) Level in Nitromethane (PCM model). Total Energy: -617.52029369 hartree/particle.

Symbol	X	Y	Z
C	-0.8375077	0.7486319	0.4252496
C	-1.5072508	1.9160108	0.0347592
C	-1.5415911	-0.4507392	0.4430634
C	-2.8459760	1.8644172	-0.3268193
C	-2.8910389	-0.5027168	0.0790191
C	-3.5525931	0.6615170	-0.3104876
H	-3.3587399	2.7696627	-0.6235937
C	1.5539804	0.6395284	-0.4466869
H	1.2927509	1.4254969	-1.1615747
H	1.3490980	-0.3116411	-0.9423936
C	0.6293443	0.7811617	0.7849561
H	0.8598753	1.7208858	1.2912518
H	0.8566977	-0.0221750	1.4872610
C	3.0104188	0.7314507	-0.0971413
H	3.3668437	1.6564140	0.3445062
C	3.8774650	-0.2578683	-0.2960720
H	3.5804390	-1.2091372	-0.7272146
C	5.9500049	-1.3584005	-0.0557812
H	5.8660438	-1.8206267	-1.0411072
H	6.9870643	-1.0981897	0.1334695
H	5.6061517	-2.0594467	0.7068565
O	5.2061392	-0.1383484	0.0000783
H	-0.9793173	2.8604831	0.0213018
H	-4.5935457	0.6481558	-0.5922230
H	-1.0543927	-1.3685943	0.7457144
C	-4.8515753	-1.8526011	-0.2132211
H	-5.1018591	-2.9020371	-0.0932834
H	-5.4801688	-1.2515057	0.4455624
H	-5.0189464	-1.5551172	-1.2495072
O	-3.4736489	-1.7372738	0.1411648

Table S6. Cartesian Coordinates of the Optimized Structure for the Ground State of the Radical Catiion of *meta*-Methoxy Enol Ether (**31**$^{\cdot+}$) Calculated at the B3LYP/6-311++G(2d,2p) Level in Nitromethane (PCM model). Total Energy: -617.30432510 hartree/particle.

Symbol	X	Y	Z
C	-0.8169273	0.7638682	0.4096044
C	-1.5047236	1.9294104	0.0432805
C	-1.4938678	-0.4514042	0.4166655
C	-2.8473883	1.8601762	-0.2939982
C	-2.8475501	-0.5190773	0.0755273
C	-3.5313998	0.6439543	-0.2837233
H	-3.3810522	2.7599936	-0.5676446
C	1.5542578	0.7443055	-0.5129107
H	1.3204490	1.6249699	-1.1143689
H	1.3058206	-0.1496339	-1.0807221
C	0.6400473	0.8173829	0.7783574
H	0.8715600	1.7407285	1.3064195
H	0.8978824	-0.0163169	1.4276734
C	2.9701472	0.7758758	-0.1427376
H	3.3931889	1.6749167	0.2893641
C	3.8110933	-0.3248600	-0.2776252
H	3.4646025	-1.2695052	-0.6839686
C	5.9485283	-1.3546269	-0.0694329
H	5.4037472	-2.2258795	-0.4180512
H	6.7095710	-1.0477327	-0.7798714
H	6.3864292	-1.5214398	0.9089319
O	5.0466043	-0.2207362	0.0817912
H	-0.9903674	2.8808628	0.0330791
H	-4.5760917	0.6177813	-0.5500665
H	-0.9853458	-1.3639072	0.6980535
C	-4.7957990	-1.8904016	-0.1961527
H	-5.0254374	-2.9453370	-0.0860726
H	-5.4156815	-1.3093528	0.4877811
H	-4.9912907	-1.5803720	-1.2234109
O	-3.4099159	-1.7589383	0.1271771

Cartesian Coordinates of the Optimized Structure for the Ground State of 2,4-Dimethoxy Enol Ether (**32**) Calculated at the B3LYP/6-311++G(2d,2p) Level in Nitromethane (PCM model). Total Energy: -732.08133755 hartree/particle.

Symbol	X	Y	Z
C	0.6227016	-0.5517552	0.5085452
C	1.5434770	-1.5869076	0.4355728
C	1.1007434	0.7534736	0.2619896
C	2.8925563	-1.3866599	0.1298109
C	2.4375602	0.9817036	-0.0411547
C	3.3344844	-0.0908098	-0.1096073
H	3.5626991	-2.2300400	0.0885995
H	2.8151685	1.9741457	-0.2286283
C	-1.7372308	-0.8251495	-0.4362014
H	-1.3441351	-1.5769534	-1.1276098
H	-1.6653914	0.1369763	-0.9452100
C	-0.8317951	-0.8096135	0.8178188
H	-0.9178323	-1.7726471	1.3244506
H	-1.2083515	-0.0531668	1.5076712
C	-3.1714459	-1.1301057	-0.1162857
H	-3.3940542	-2.0860127	0.3471931
C	-4.1750021	-0.2928107	-0.3648325
H	-4.0167925	0.6793084	-0.8215276
C	-6.4042139	0.4707074	-0.2511991
H	-6.3788605	0.8532561	-1.2732812
H	-7.3895700	0.0651175	-0.0422511
H	-6.1895402	1.2814555	0.4473684
O	-5.4765980	-0.6047071	-0.0859615
C	0.5949428	3.0976824	0.1265653
H	1.3503224	3.4002190	0.8533444
H	0.9868963	3.2275248	-0.8833211
H	-0.2928114	3.7099081	0.2512764
C	5.5883254	-0.7999627	-0.5084312
H	5.6926099	-1.3254182	0.4420519
H	5.3242577	-1.5117011	-1.2920796
H	6.5274623	-0.3169166	-0.7596759
O	4.6232176	0.2473308	-0.4163353
O	0.1739746	1.7527085	0.3482972
H	1.2025496	-2.5964671	0.6280800

Cartesian Coordinates of the Optimized Structure for the Ground State of the Radical Catiion of 2,4-Dimethoxy Enol Ether (**32**$^{\cdot+}$) Calculated at the B3LYP/6-311++G(2d,2p) Level in Nitromethane (PCM model). Total Energy: -731.87459490 hartree/particle.

Symbol	X	Y	Z
C	0.6016338	-0.5444606	0.5470457
C	1.5206725	-1.5994929	0.4401405
C	1.0777002	0.7914892	0.2801398
C	2.8403091	-1.3862867	0.1253062
C	2.4022720	1.0239260	-0.0350196
C	3.2896699	-0.0557156	-0.1151979
H	3.5254003	-2.2158718	0.0685735
H	2.7822872	2.0132708	-0.2277559
C	-1.6933226	-0.9617723	-0.4522503
H	-1.2720340	-1.8018930	-1.0031006
H	-1.5788936	-0.0639606	-1.0568590
C	-0.8188086	-0.7925577	0.8724464
H	-0.9179045	-1.7079493	1.4518973
H	-1.2413281	0.0336088	1.4360511
C	-3.1161366	-1.2095783	-0.1258070
H	-3.3880435	-2.1623436	0.3129279
C	-4.0775313	-0.2901948	-0.3192602
H	-3.8638424	0.6850045	-0.7451044
C	-6.3081472	0.4800596	-0.3731750
H	-6.3591733	0.5715677	-1.4576477
H	-7.2669529	0.1542503	0.0150197
H	-6.0338233	1.4363033	0.0712345
O	-5.3594852	-0.5353250	-0.0029222
C	0.5108034	3.1133590	0.1231670
H	1.2609722	3.4391320	0.8417548
H	0.8822526	3.2313226	-0.8934212
H	-0.4028280	3.6809956	0.2547027
C	5.5452202	-0.7845584	-0.5455961
H	5.6631593	-1.3094303	0.3995088
H	5.2809872	-1.4761193	-1.3423389
H	6.4596738	-0.2605436	-0.7962966
O	4.5435689	0.2489730	-0.4254067
O	0.1468012	1.7430944	0.3671571
H	1.1770015	-2.6065825	0.6285908

Cartesian Coordinates of the Optimized Structure for the Ground State of 2,4,6-Trimethoxy Enol Ether (**33**) Calculated at the B3LYP/6-311++G(2d,2p) Level in Nitromethane (PCM model). Total Energy: -846.64168365 hartree/particle.

Symbol	X	Y	Z
C	-0.4451176	-0.0660174	-0.4413744
C	-1.3863635	-1.0841333	-0.2543742
C	-0.8956711	1.2567247	-0.2887678
C	-2.7252489	-0.8175097	0.0594624
C	-2.2202405	1.5526941	0.0220506
C	-3.1274885	0.5075092	0.1937604
H	-3.4250174	-1.6219752	0.1952973
H	-2.5698598	2.5652120	0.1370193
C	1.8925382	-0.5553995	0.4690077
H	1.4505822	-1.3339872	1.0972877
H	1.8842481	0.3642797	1.0570929
C	0.9933712	-0.3738594	-0.7770290
H	1.0354306	-1.2850080	-1.3733416
H	1.4034367	0.4298010	-1.3868790
C	3.3045487	-0.9250282	0.1197454
H	3.4655857	-1.8556870	-0.4151843
C	4.3586960	-0.1704194	0.4188192
H	4.2622422	0.7727971	0.9475739
C	6.6344803	0.4500143	0.3770619
H	6.6403142	0.7126541	1.4365973
H	7.5898976	0.0085766	0.1097945
H	6.4697240	1.3483339	-0.2206972
O	5.6374546	-0.5368555	0.1014558
C	-0.3327324	3.5921136	-0.3476431
H	-1.0940469	3.8551473	-1.0834723
H	-0.7018882	3.8125563	0.6550321
H	0.5669576	4.1697916	-0.5362261
C	-5.3885146	-0.1306387	0.6891267
H	-5.5199812	-0.7283468	-0.2140864
H	-5.1265844	-0.7816389	1.5246292
H	-6.3134702	0.3910298	0.9143900
C	-1.8148739	-3.4529394	-0.2488542
H	-2.2357217	-3.4838596	0.7572210
H	-2.6211997	-3.4068423	-0.9822397

H	-1.2236836	-4.3475117	-0.4190924
O	-4.4054251	0.8858730	0.4978675
O	-0.9125664	-2.3586682	-0.4001522
O	0.0528786	2.2241522	-0.4675042

Cartesian Coordinates of the Optimized Structure for the Ground State of the Radical Catiion of 2,4,6-Trimethoxy Enol Ether (**33**$^{\cdot+}$) Calculated at the B3LYP/6-311++G(2d,2p) Level in Nitromethane (PCM model). Total Energy: -846.44026800 hartree/particle.

Symbol	X	Y	Z
C	-0.4325734	-0.0648823	-0.4968521
C	-1.3977511	-1.1070141	-0.2741472
C	-0.8605979	1.2902505	-0.3181510
C	-2.7074298	-0.8261886	0.0620741
C	-2.1616227	1.5786290	0.0158381
C	-3.0821213	0.5193509	0.2035280
H	-3.4222092	-1.6141380	0.2130314
H	-2.5196658	2.5859966	0.1442810
C	1.8320607	-0.7002645	0.4479156
H	1.3692472	-1.5552211	0.9401247
H	1.7721779	0.1536111	1.1211055
C	0.9631964	-0.3899186	-0.8500084
H	0.9996050	-1.2730197	-1.4828322
H	1.4246405	0.4446657	-1.3668586
C	3.2412597	-0.9951208	0.0909007
H	3.4541751	-1.9047413	-0.4586785
C	4.2537034	-0.1697869	0.3921968
H	4.0968604	0.7597262	0.9303008
C	6.5218016	0.4640509	0.5344544
H	6.5568585	0.4463368	1.6236261
H	7.4697979	0.1243218	0.1311527
H	6.3130718	1.4749694	0.1845293
O	5.5267154	-0.4510692	0.0494350
C	-0.2377654	3.5980693	-0.3586274
H	-1.0027839	3.8857096	-1.0789934
H	-0.5788574	3.8024364	0.6556527
H	0.6797927	4.1400310	-0.5570122
C	-5.3500530	-0.0598314	0.7567622
H	-5.5246650	-0.6487275	-0.1410442
H	-5.0864404	-0.7011575	1.5950403
H	-6.2306341	0.5239418	0.9963658
C	-1.7713750	-3.4722429	-0.2173701
H	-2.1505400	-3.4789465	0.8033452
H	-2.5950075	-3.4562505	-0.9293260

H	-1.1482975	-4.3419980	-0.3891281
O	-4.3081126	0.9109902	0.5233781
O	-0.9090611	-2.3396920	-0.4236698
O	0.0977684	2.2100024	-0.5073640

Cartesian Coordinates of the Optimized Structure for the Ground State of the Cycloadduct (**3**) Calculated at the B3LYP/6-311++G(2d,2p) Level in Nitromethane (PCM model). Total Energy: -735.48966883 hartree/particle.

Symbol	X	Y	Z
C	2.8750711	-1.4993386	-0.6552218
C	4.2212934	-0.9088698	-0.1504588
C	3.4168520	0.3434149	0.2996039
C	2.2727436	-0.0659022	-0.6430867
H	2.8881770	-2.0339741	-1.6025167
H	2.4110263	-2.1342217	0.1018008
H	4.8391119	-0.6297787	-1.0066216
H	3.1173348	0.2504737	1.3517897
H	2.4460733	0.4076925	-1.6126885
C	-1.6296518	-0.1542068	-0.7736753
C	-2.3295515	-1.1357725	-0.0758428
C	-2.2925570	1.0538476	-1.0248690
C	-3.6381863	-0.9380990	0.3671208
H	-1.8518177	-2.0855097	0.1303272
C	-3.5919913	1.2714357	-0.5939969
H	-1.7839012	1.8378885	-1.5719429
C	-4.2752262	0.2747156	0.1091137
H	-4.1407898	-1.7298529	0.9006013
H	-4.0948157	2.2069282	-0.7975406
C	0.8346770	0.1568805	-0.2006055
H	0.6713710	-0.3318306	0.7642466
H	0.6668536	1.2257804	-0.0400481
C	-0.1998393	-0.3681115	-1.2128602
H	-0.0273287	-1.4337382	-1.3774102
H	-0.0340619	0.1269765	-2.1728743
O	-5.5519445	0.5789631	0.4935738
C	-6.2904228	-0.4051518	1.2160974
H	-7.2588080	0.0408150	1.4205515
H	-6.4260451	-1.3115708	0.6238565
H	-5.7994411	-0.6549471	2.1580897
O	3.9334185	1.6405452	0.0673624
C	4.9297259	2.0355337	1.0025729
H	4.5492806	1.9834896	2.0276634
H	5.8240303	1.4118971	0.9261079

H	5.1965437	3.0646186	0.7731062
C	5.0345602	-1.7000417	0.8608689
H	4.4353755	-1.9390749	1.7418383
H	5.3805303	-2.6426614	0.4315016
H	5.9145277	-1.1474713	1.1941095

Cartesian Coordinates of the Optimized Structure for the Ground State of the Radical Catiion of the Cycloadduct ($\mathbf{3}^{\bullet+}$) Calculated at the B3LYP/6-311++G(2d,2p) Level in Nitromethane (PCM model). Total Energy: -735.27399896 hartree/particle.

Symbol	X	Y	Z
C	-1.4328896	0.2965676	-0.4297373
C	-1.8796763	1.0178149	0.7089399
C	-2.3782625	-0.4761576	-1.1639397
C	-3.1880959	0.9838285	1.0880005
H	-1.1695206	1.6052215	1.2727269
C	-3.6944237	-0.5290123	-0.8048342
H	-2.0403359	-1.0260716	-2.0306261
C	-4.1231676	0.2059867	0.3360737
H	-3.5533114	1.5302774	1.9445387
H	-4.3964341	-1.1130859	-1.3771557
C	0.7692838	-0.8760925	-0.1654812
H	0.3116748	-1.8180995	-0.4739960
H	0.6651268	-0.8104215	0.9190975
C	-0.0015901	0.3076807	-0.8256920
H	0.0872248	0.2151105	-1.9084270
H	0.4659142	1.2429005	-0.5207270
O	-5.3541014	0.2355519	0.7794183
C	-6.4152346	-0.5108219	0.1258003
H	-7.3041824	-0.2873414	0.7012446
H	-6.5259193	-0.1680053	-0.8990740
H	-6.1909576	-1.5731816	0.1644052
C	2.2428844	-0.8742042	-0.5437780
C	3.1752872	0.2142337	0.0173347
C	3.1733771	-1.9331823	0.1091221
H	2.3553664	-0.9034400	-1.6291347
C	4.2901720	-0.8562667	0.1984132
H	2.8259480	0.5737854	0.9943951
H	2.8196193	-2.2232844	1.0994375
H	3.3830194	-2.8305363	-0.4684510
H	4.8930108	-0.8804249	-0.7114502
C	5.1773748	-0.8305042	1.4317933
H	5.8679852	0.0139343	1.4155930
H	4.5783504	-0.7569127	2.3415598
H	5.7729961	-1.7429415	1.5010118

C	4.2201572	2.3232912	-0.2969079
H	5.2387832	1.9604541	-0.1392665
H	4.2438375	3.1439458	-1.0099071
H	3.8219231	2.6862132	0.6557902
O	3.3839395	1.3123149	-0.8484471

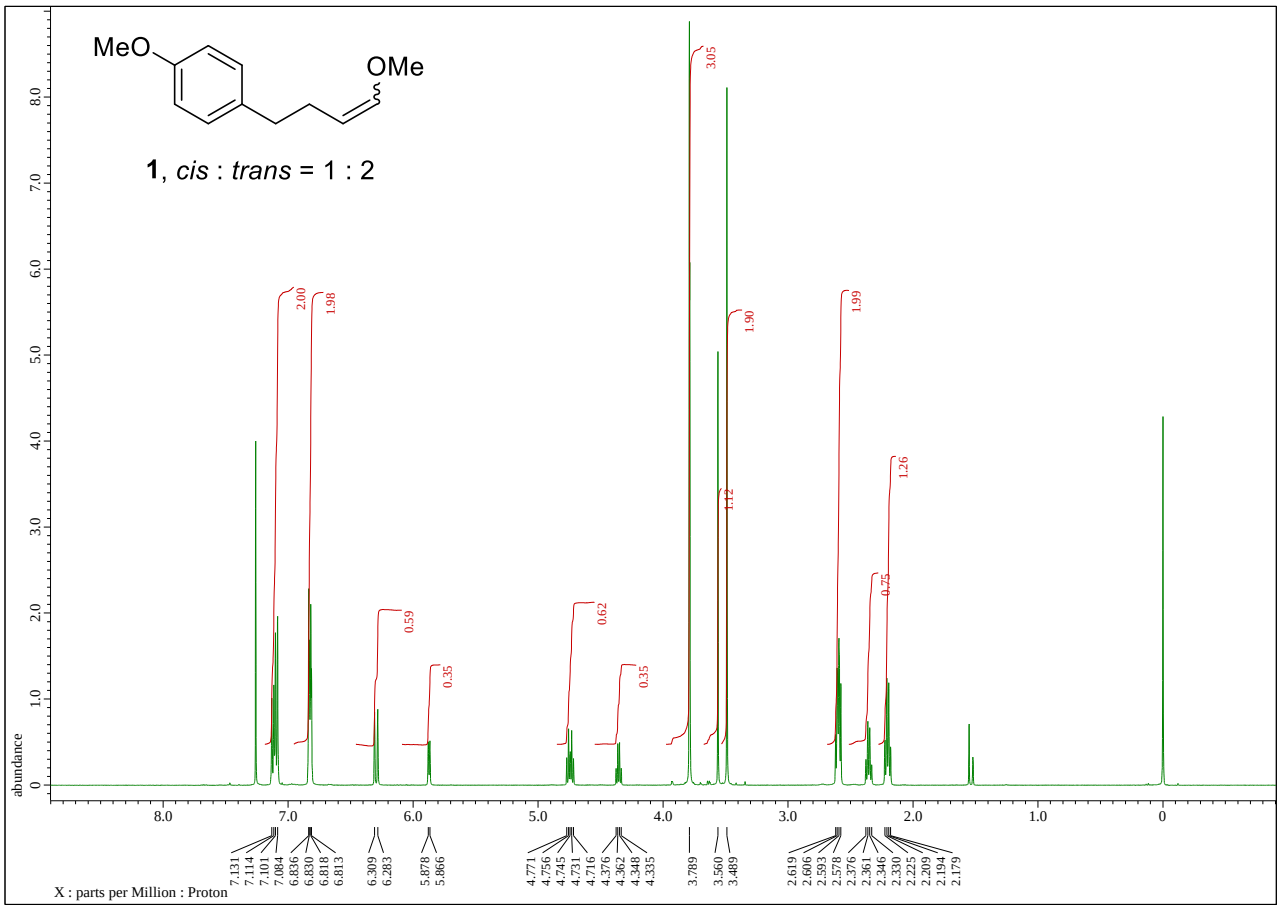
MeO
OMe
1, cis : trans = 1 : 2
abundance
X : parts per Million : Proton

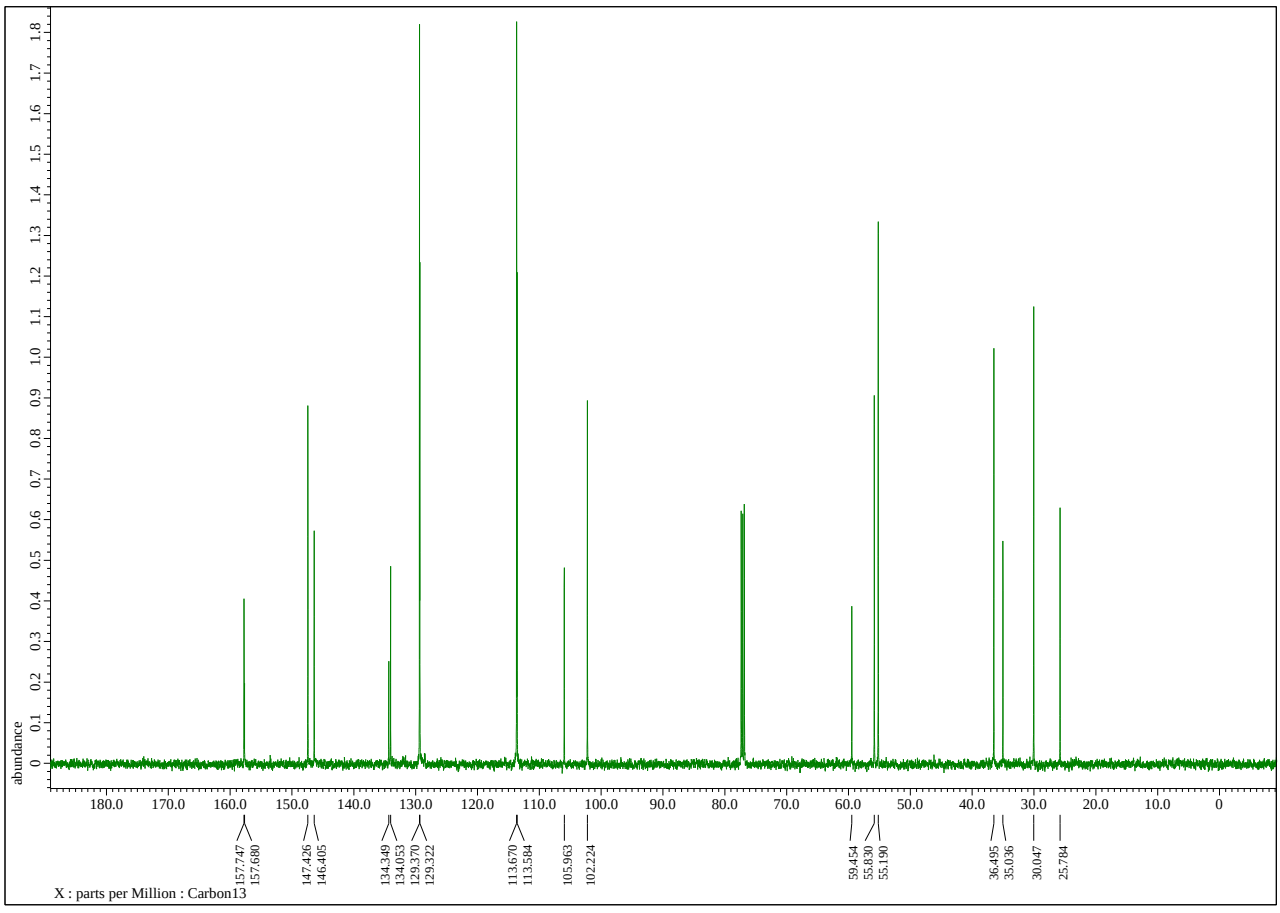
abundance
X : parts per Million : Carbon13

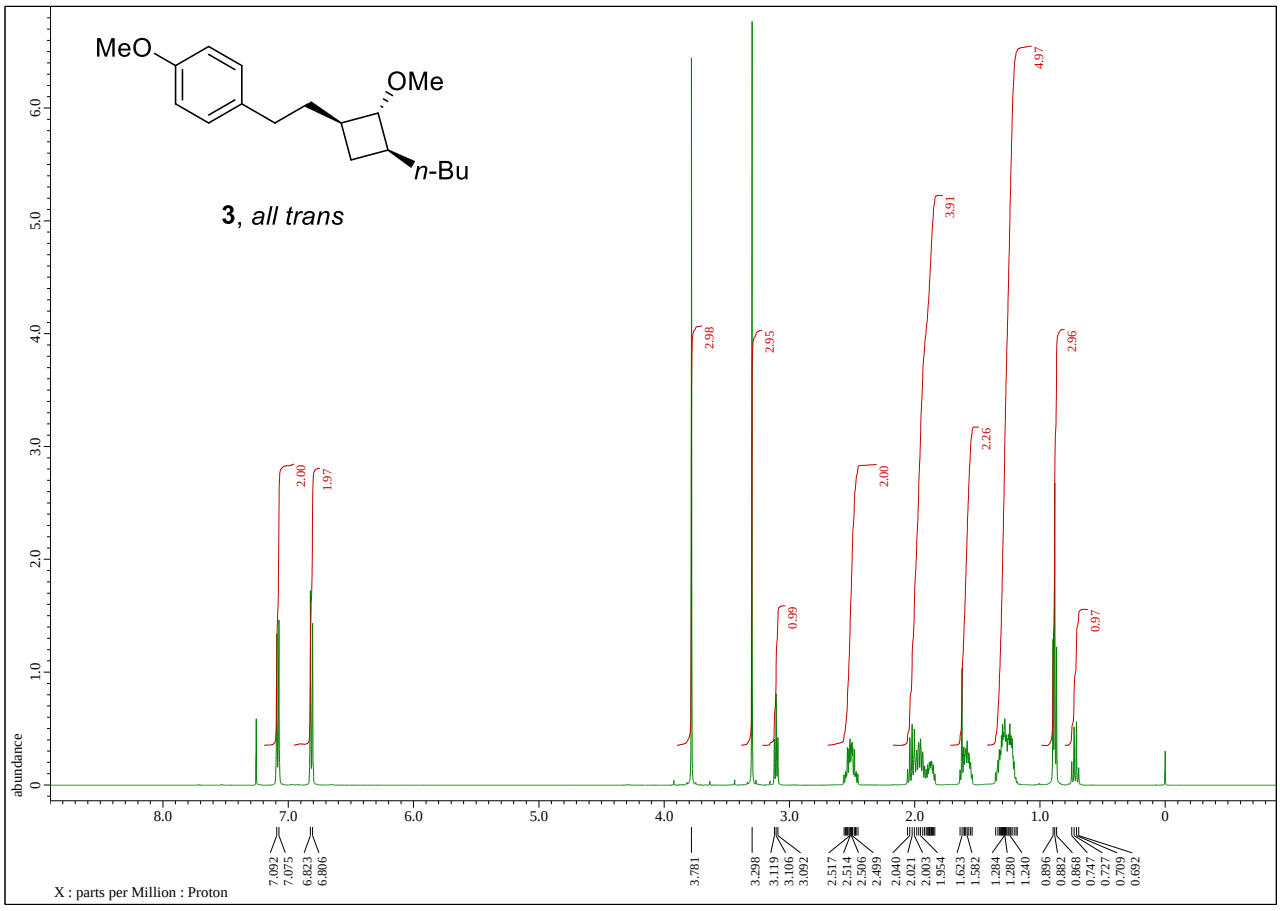
MeO
OMe
n-Bu
3, all trans
abundance
X : parts per Million : Proton

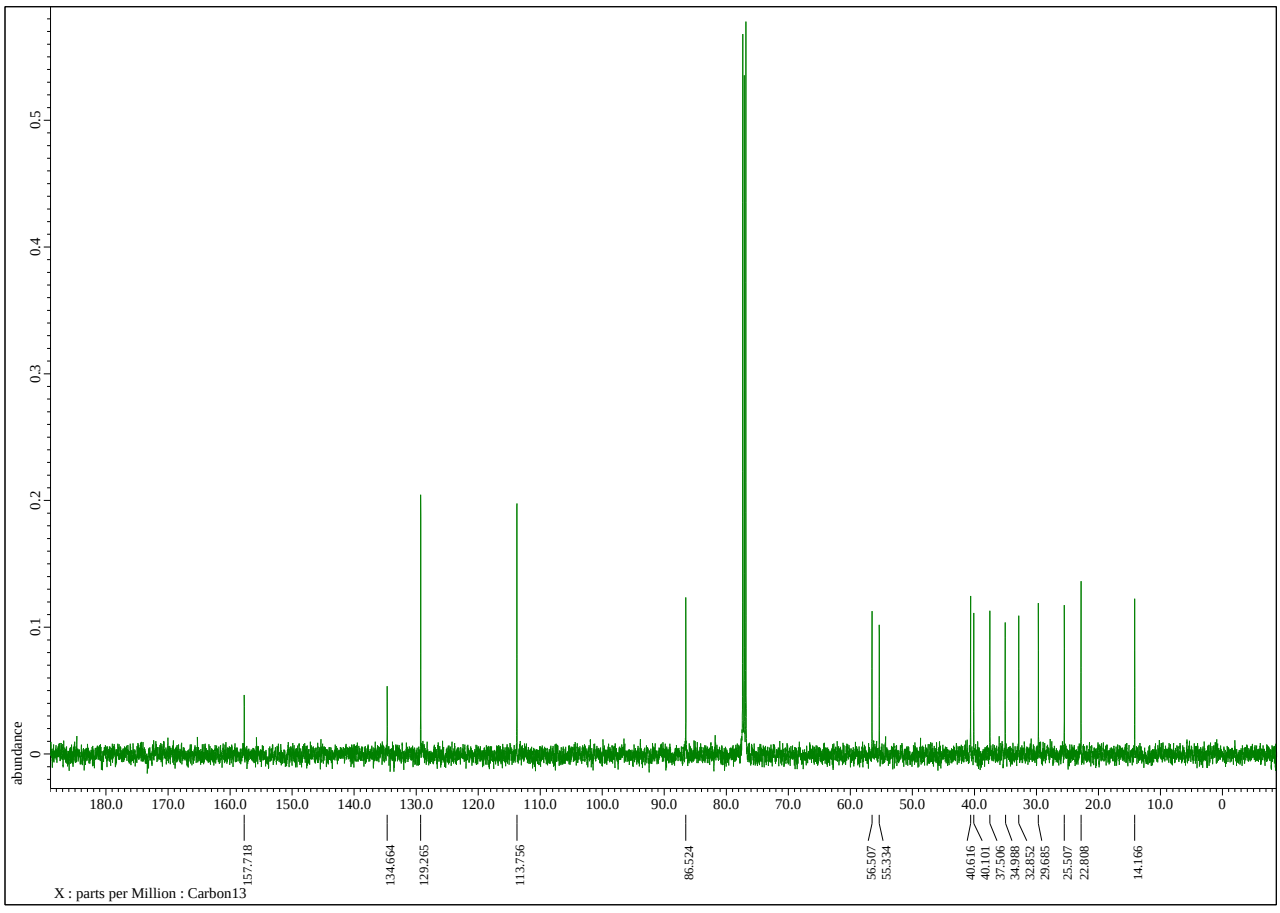
abundance
X : parts per Million : Carbon13

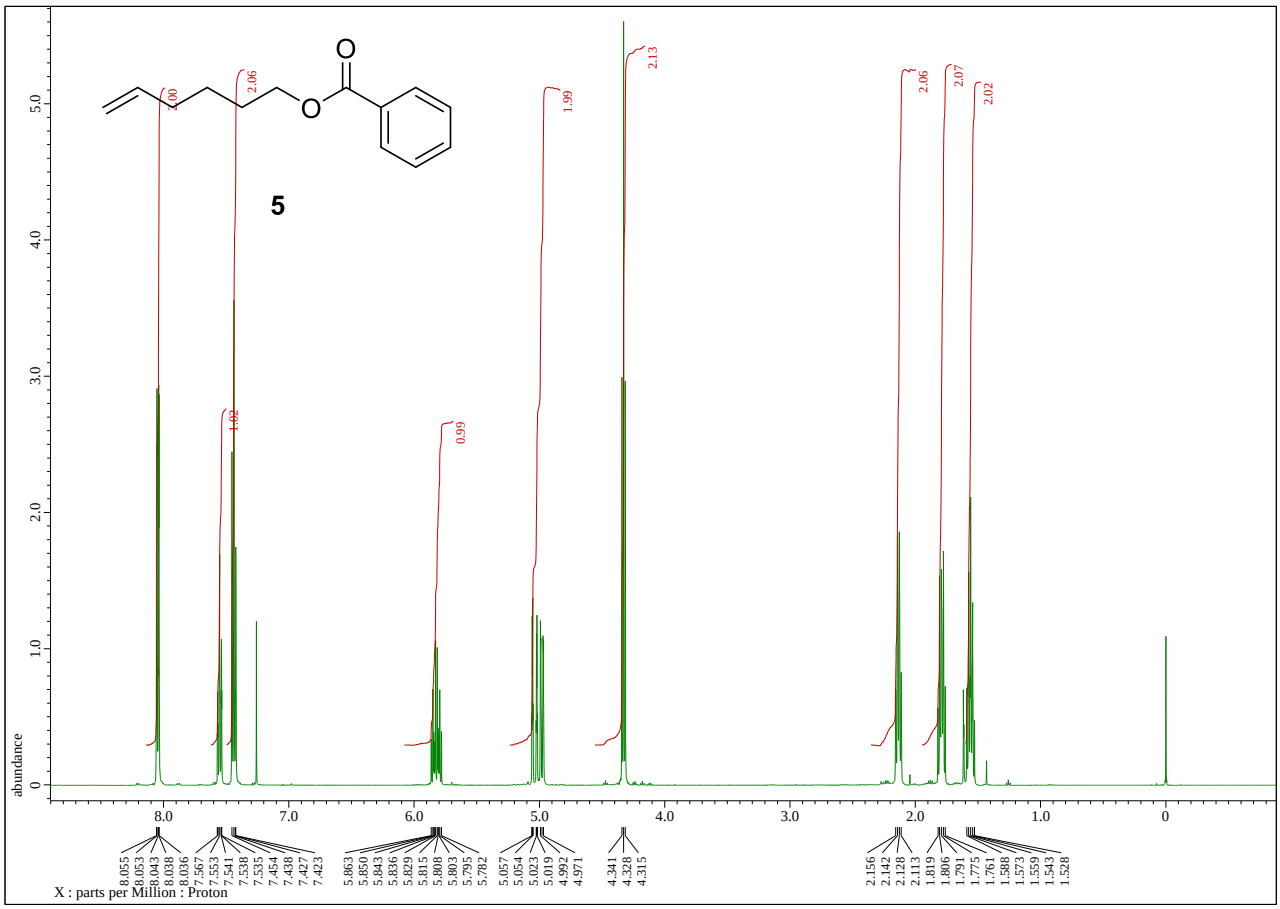
5
4.00
2.06
1.03
0.99
1.99
2.13
2.06
2.07
2.02
abundance
X : parts per Million : Proton

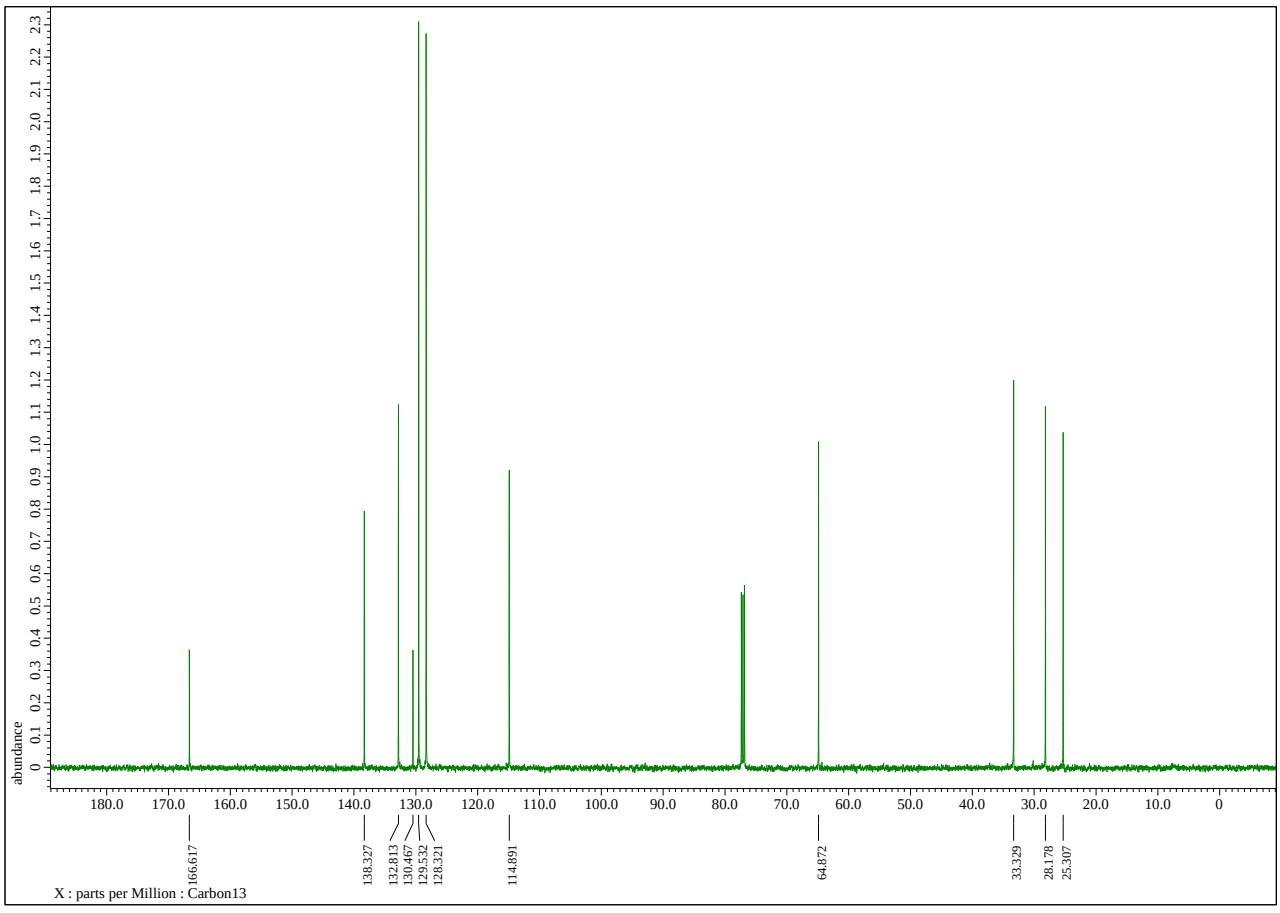
abundance
166.617
138.327
132.813
130.467
129.532
128.321
114.891
64.872
33.329
28.178
25.307
X : parts per Million : Carbon13

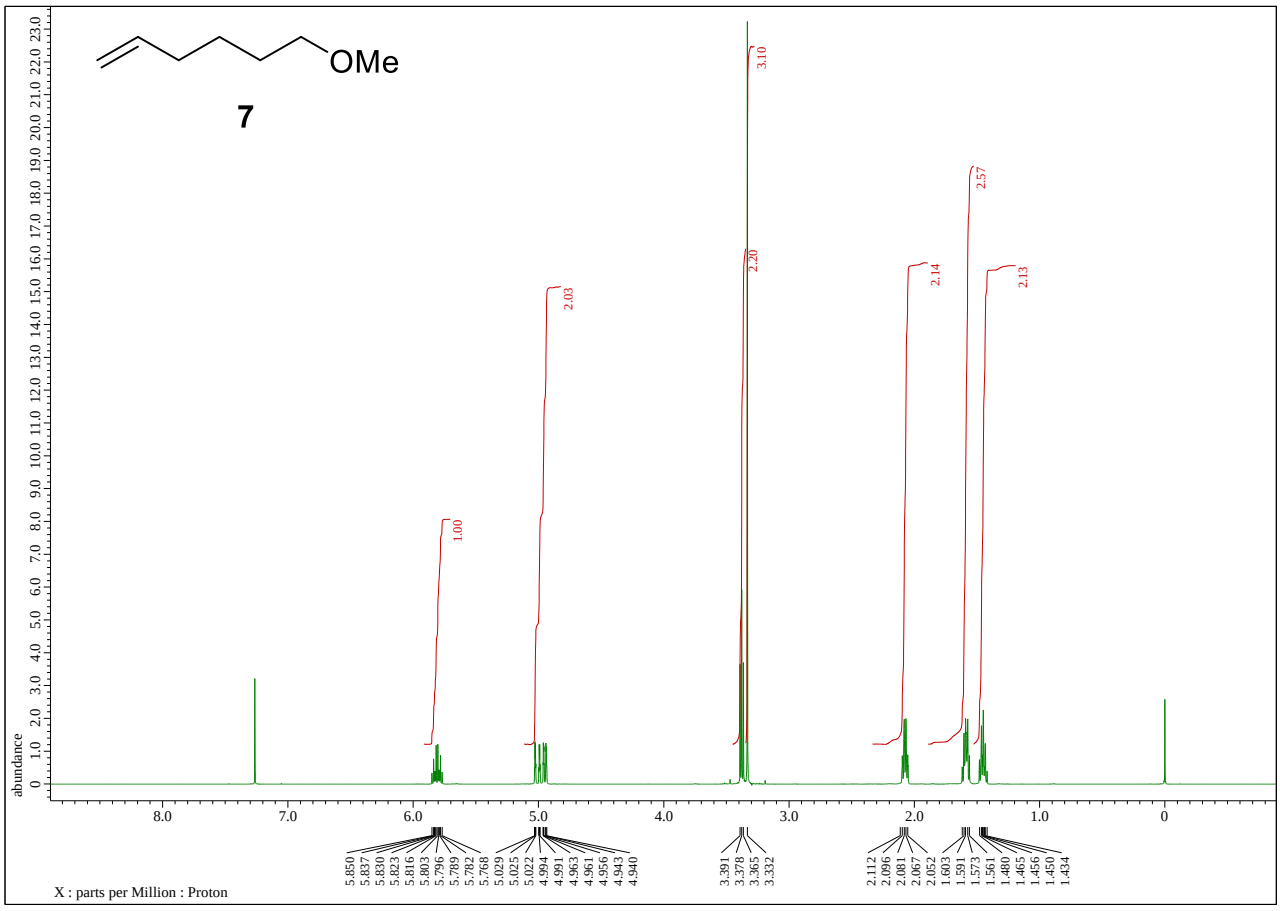
OMe
7
abundance
X : parts per Million : Proton
1.00
2.03
3.10
2.20
2.14
2.57
2.13
5.850
5.837
5.830
5.823
5.816
5.903
5.796
5.789
5.782
5.768
5.029
5.025
5.022
4.994
4.991
4.963
4.961
4.956
4.943
4.940
3.391
3.378
3.365
3.332
2.112
2.096
2.081
2.067
2.052
1.603
1.591
1.573
1.561
1.480
1.465
1.456
1.450
1.434

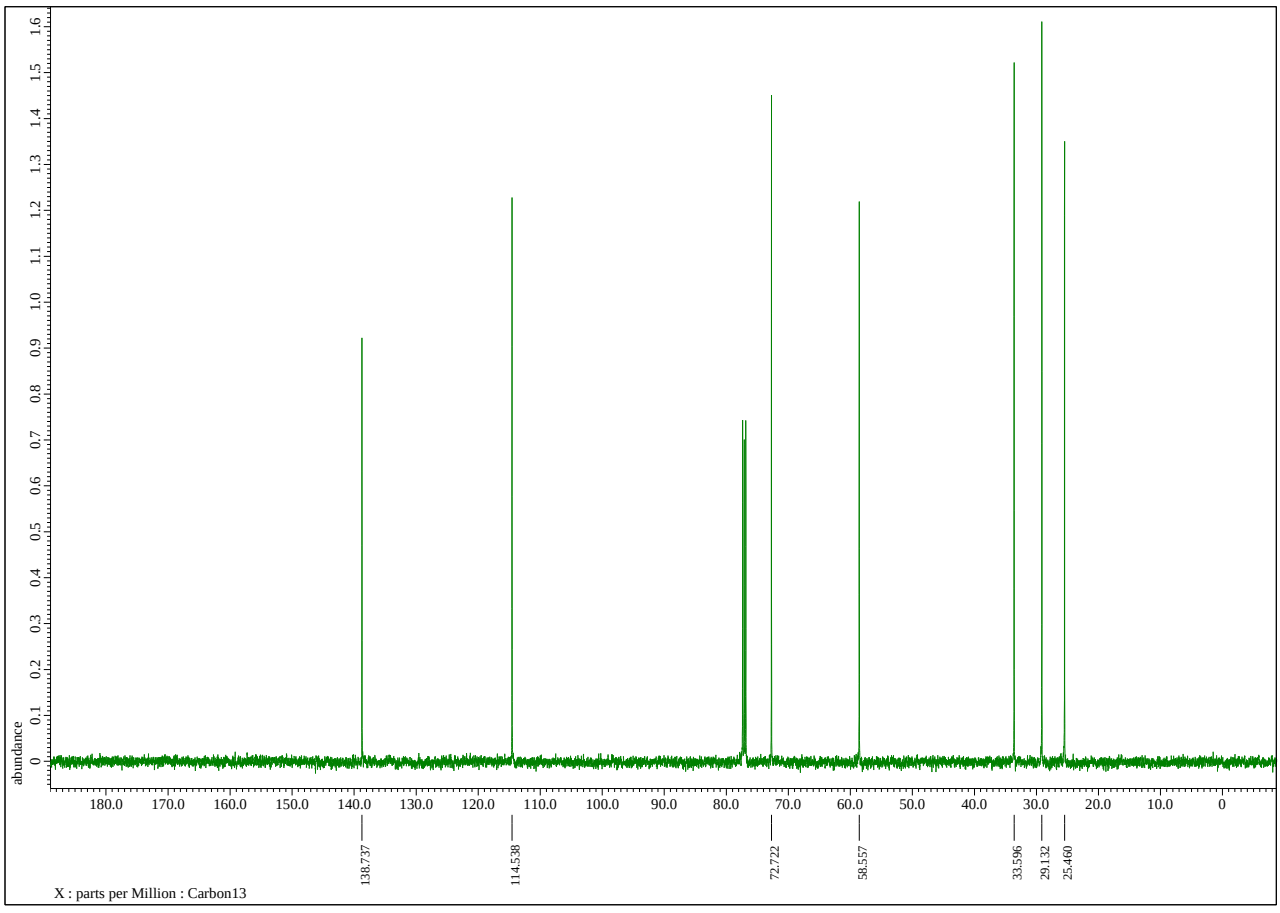
abundance
X : parts per Million : Carbon13
138.737
114.538
72.722
58.557
33.596
29.132
25.460

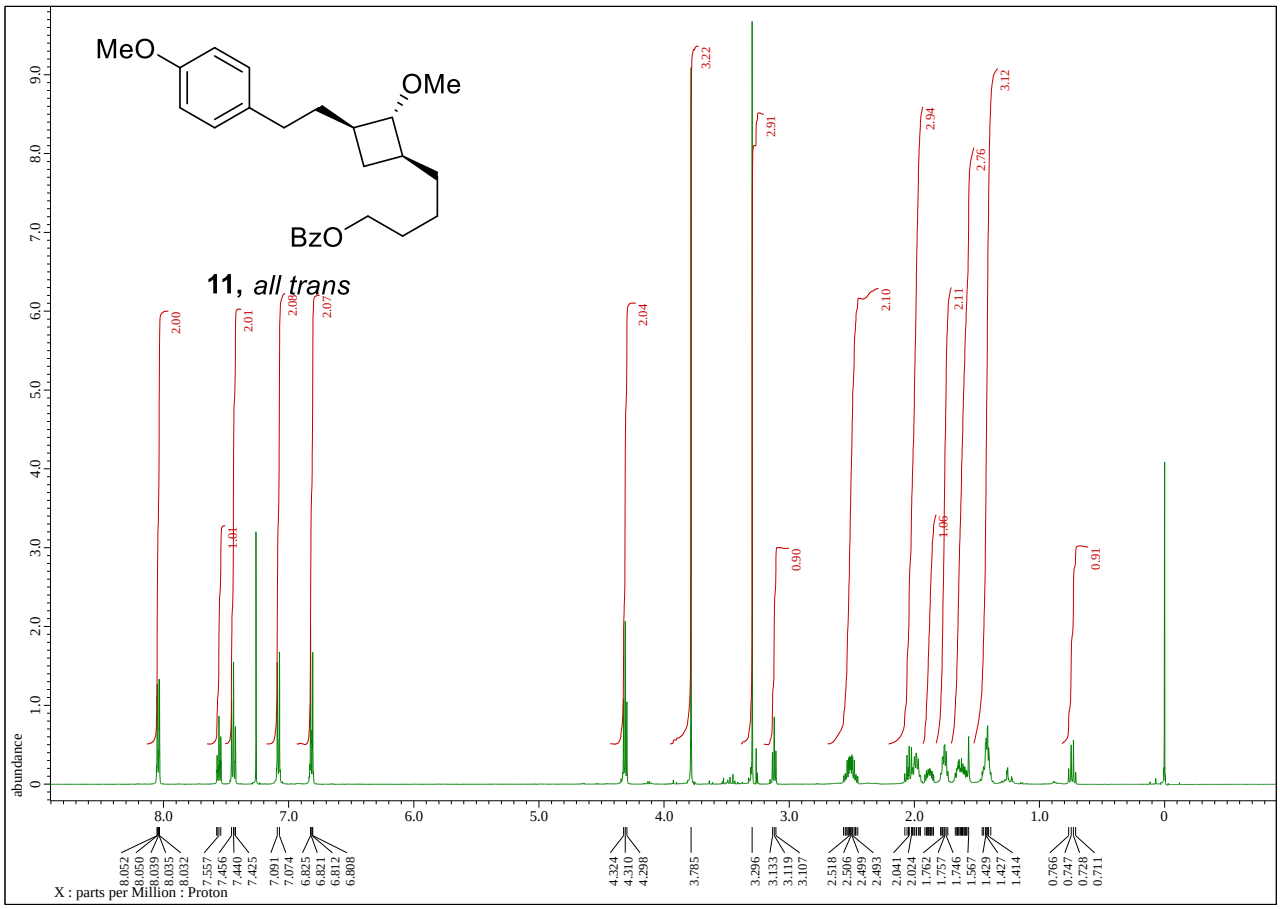
MeO
OMe
BzO
11, all trans
abundance
X : parts per Million : Proton

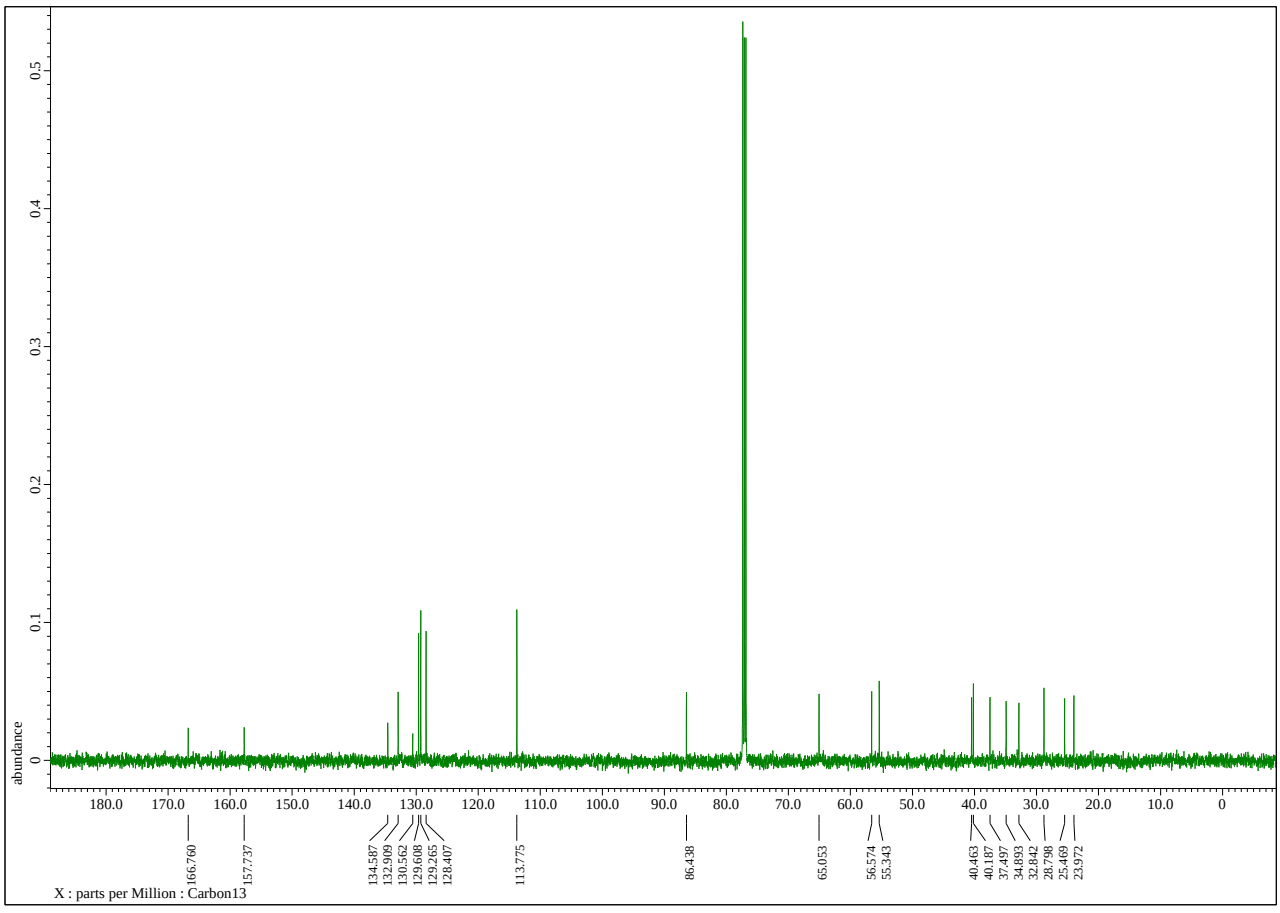
abundance
X : parts per Million : Carbon13

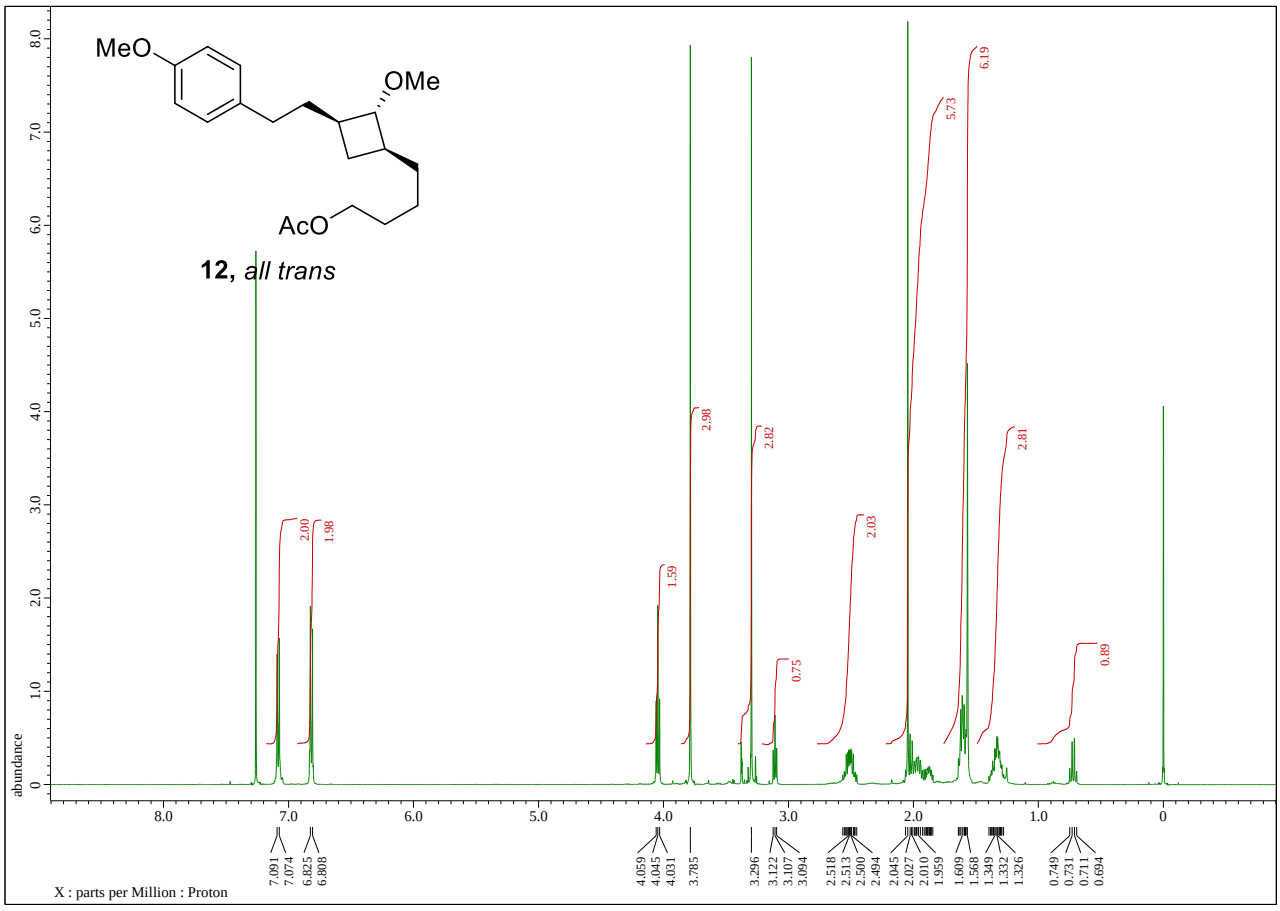
MeO
OMe
AcO
12, all trans
abundance
X : parts per Million : Proton

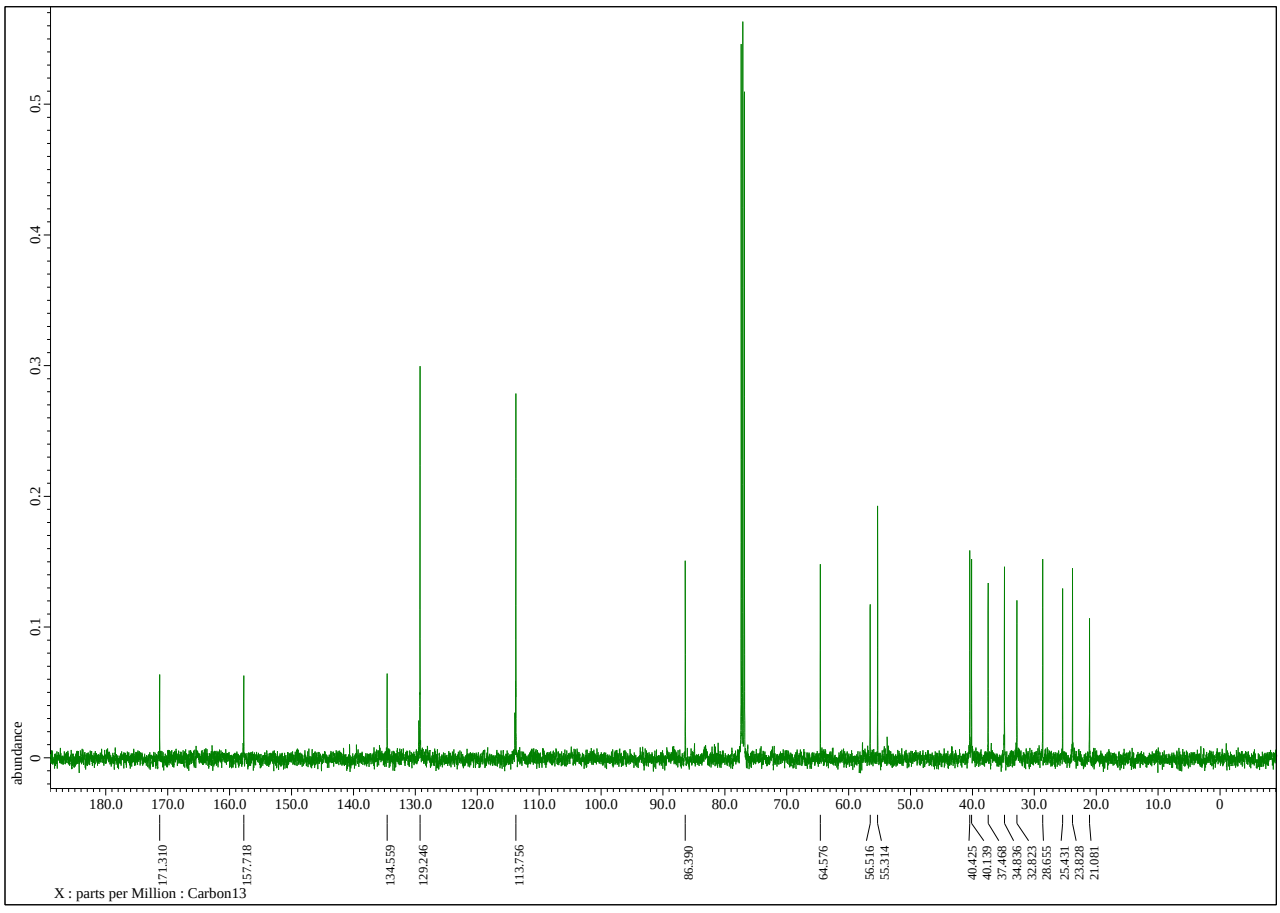
abundance
X : parts per Million : Carbon13

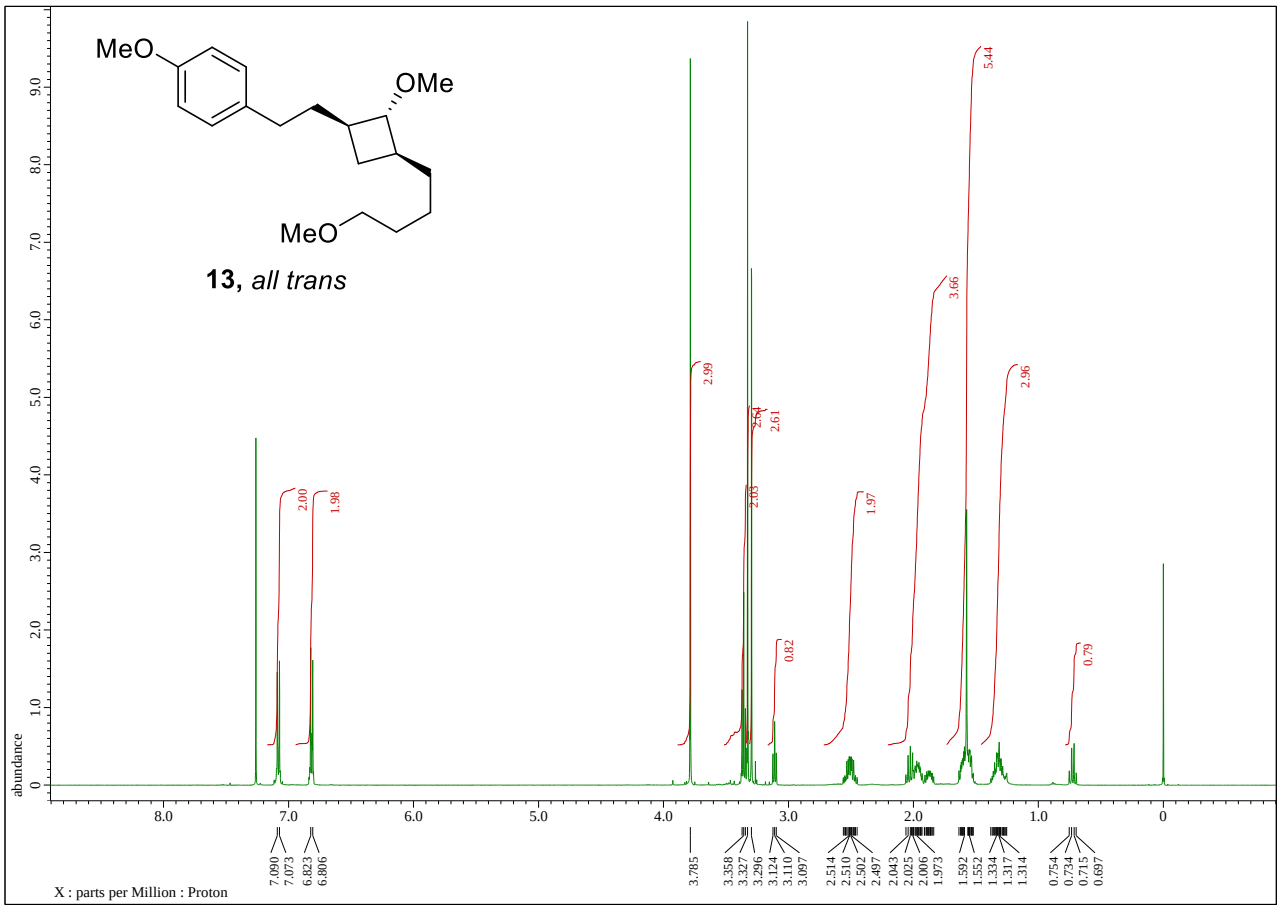
MeO
OMe
MeO
13, all trans
abundance
X : parts per Million : Proton

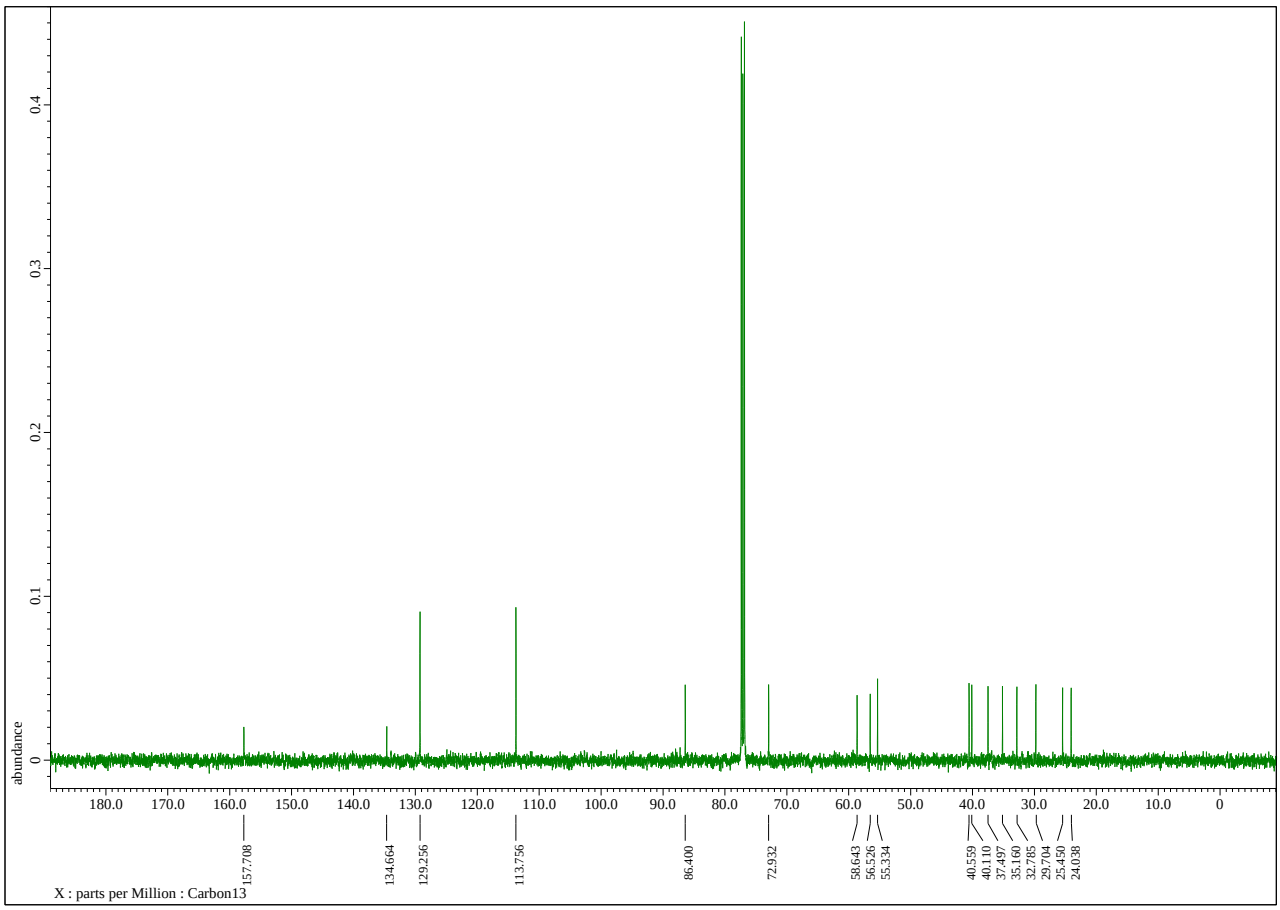
abundance
X : parts per Million : Carbon13

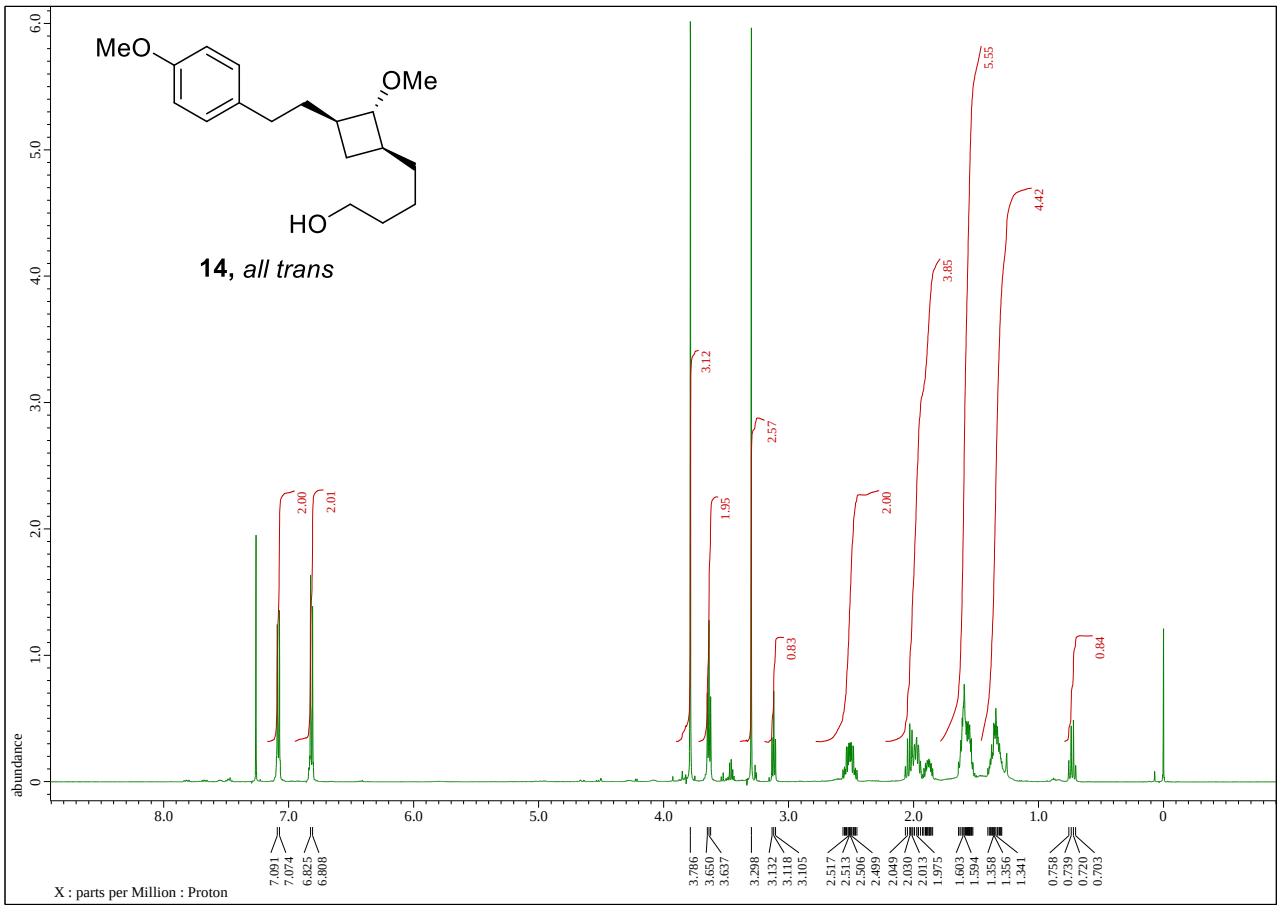
MeO
OMe
HO
14, all trans
abundance
X : parts per Million : Proton

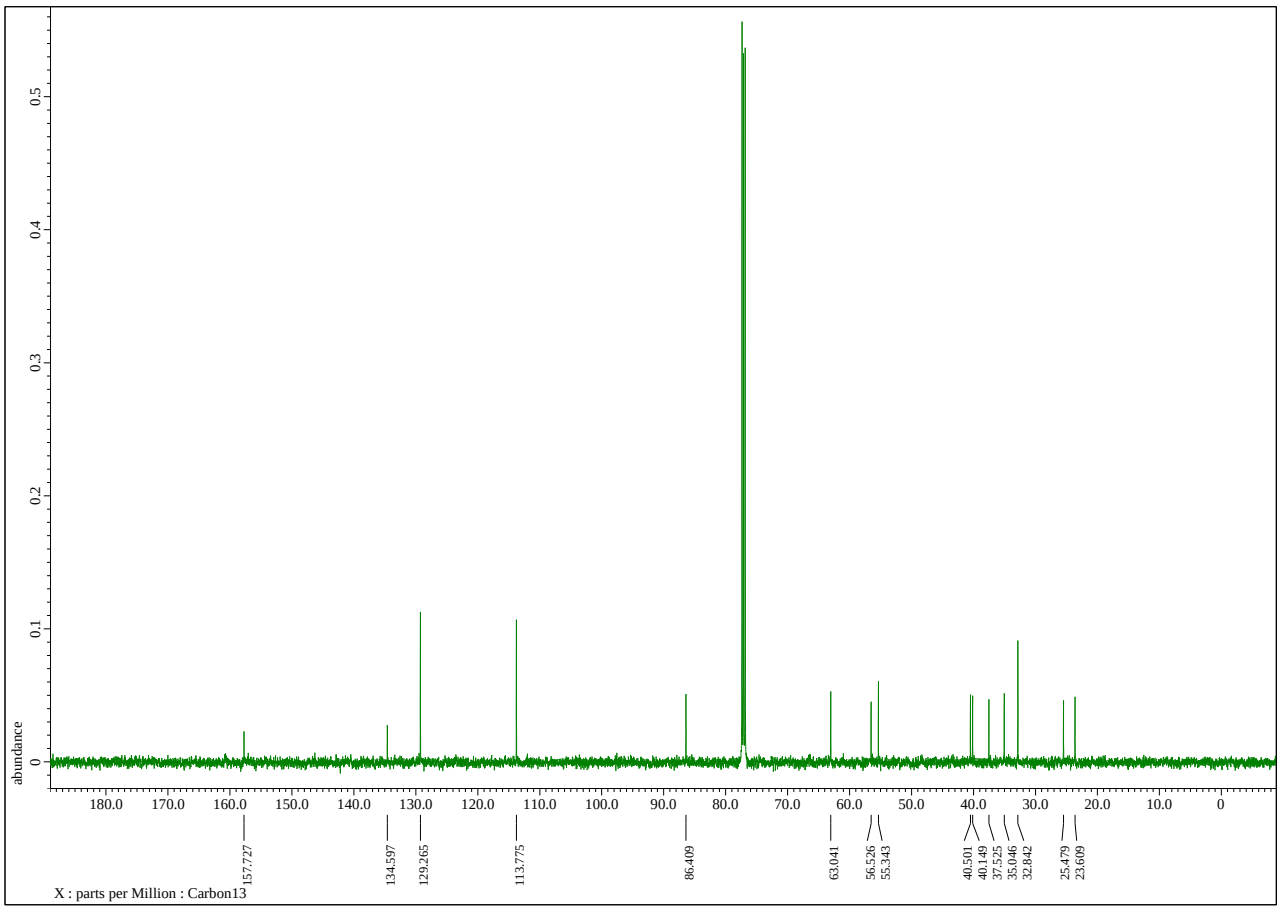
abundance
X : parts per Million : Carbon13

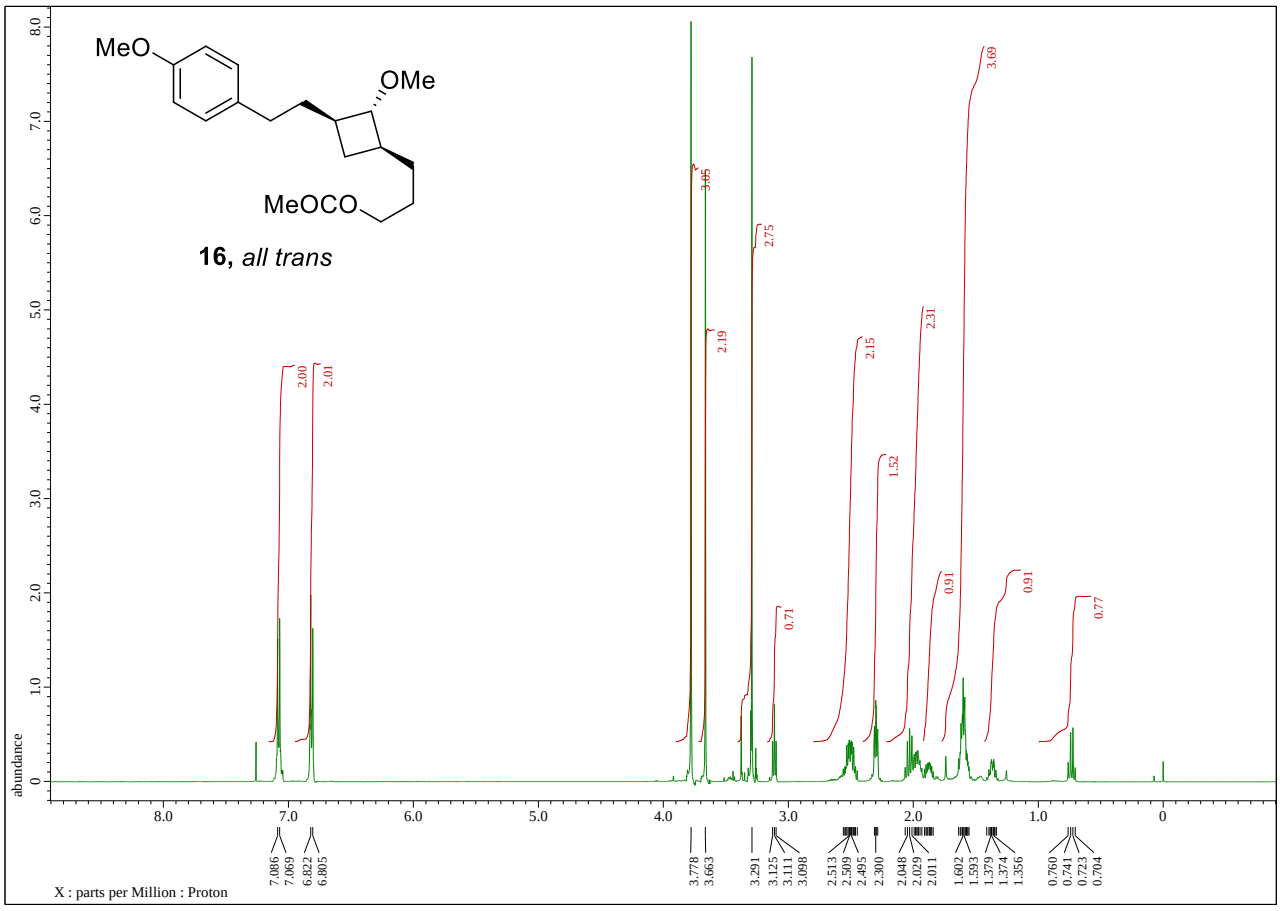
MeO
OMe
MeOCO
16, all trans
abundance
X : parts per Million : Proton

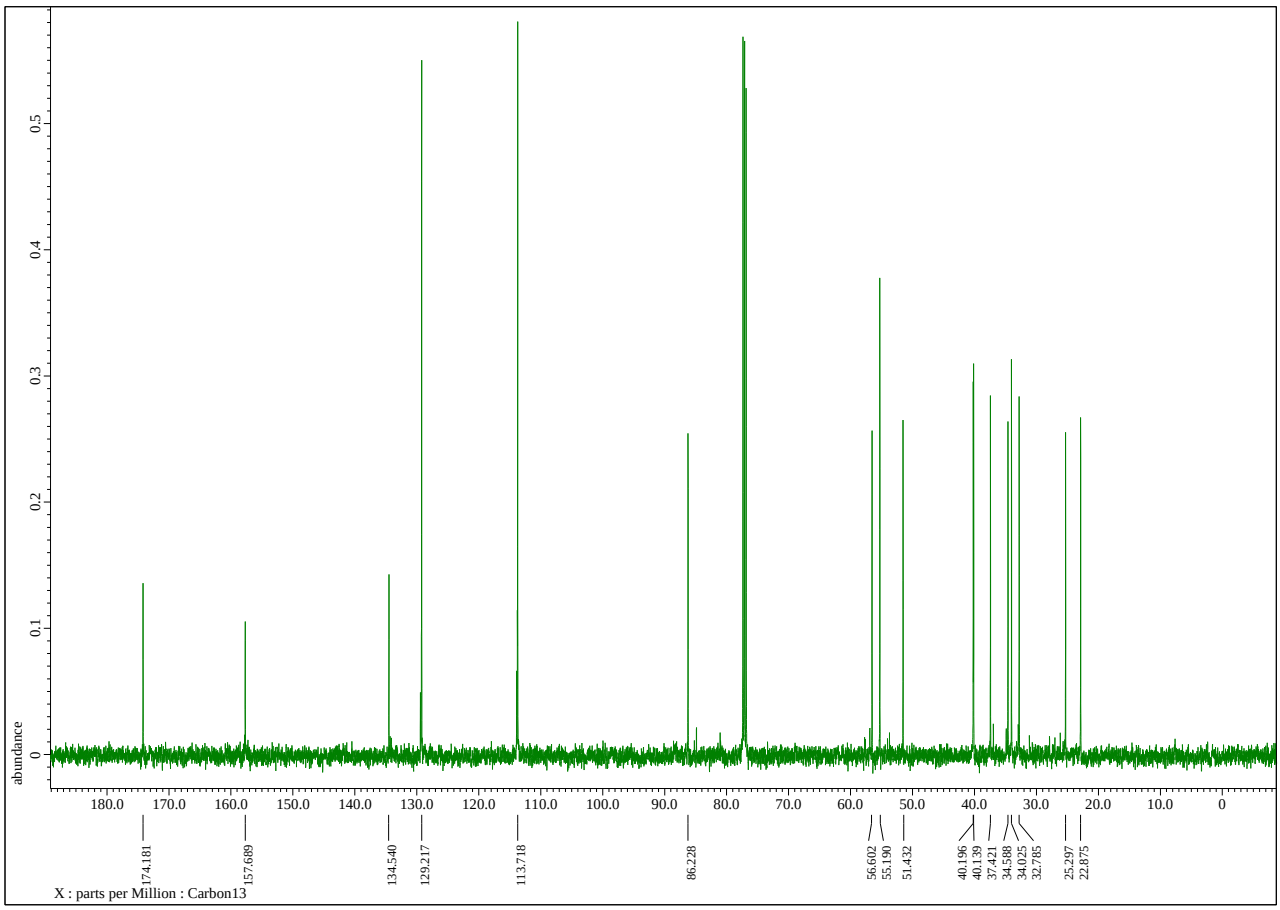
abundance
X : parts per Million : Carbon13

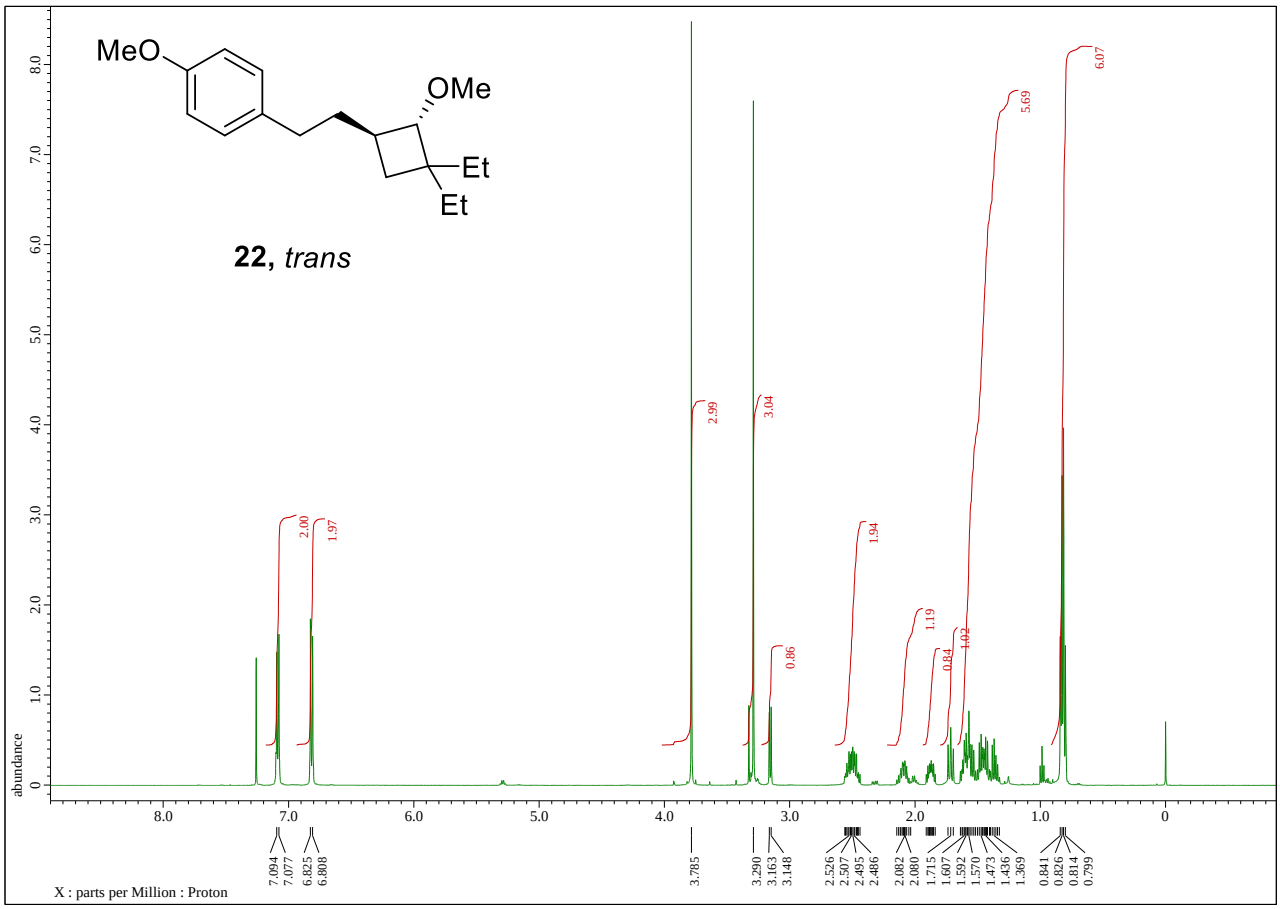
MeO
OMe
Et
Et
22, trans
abundance
X : parts per Million : Proton

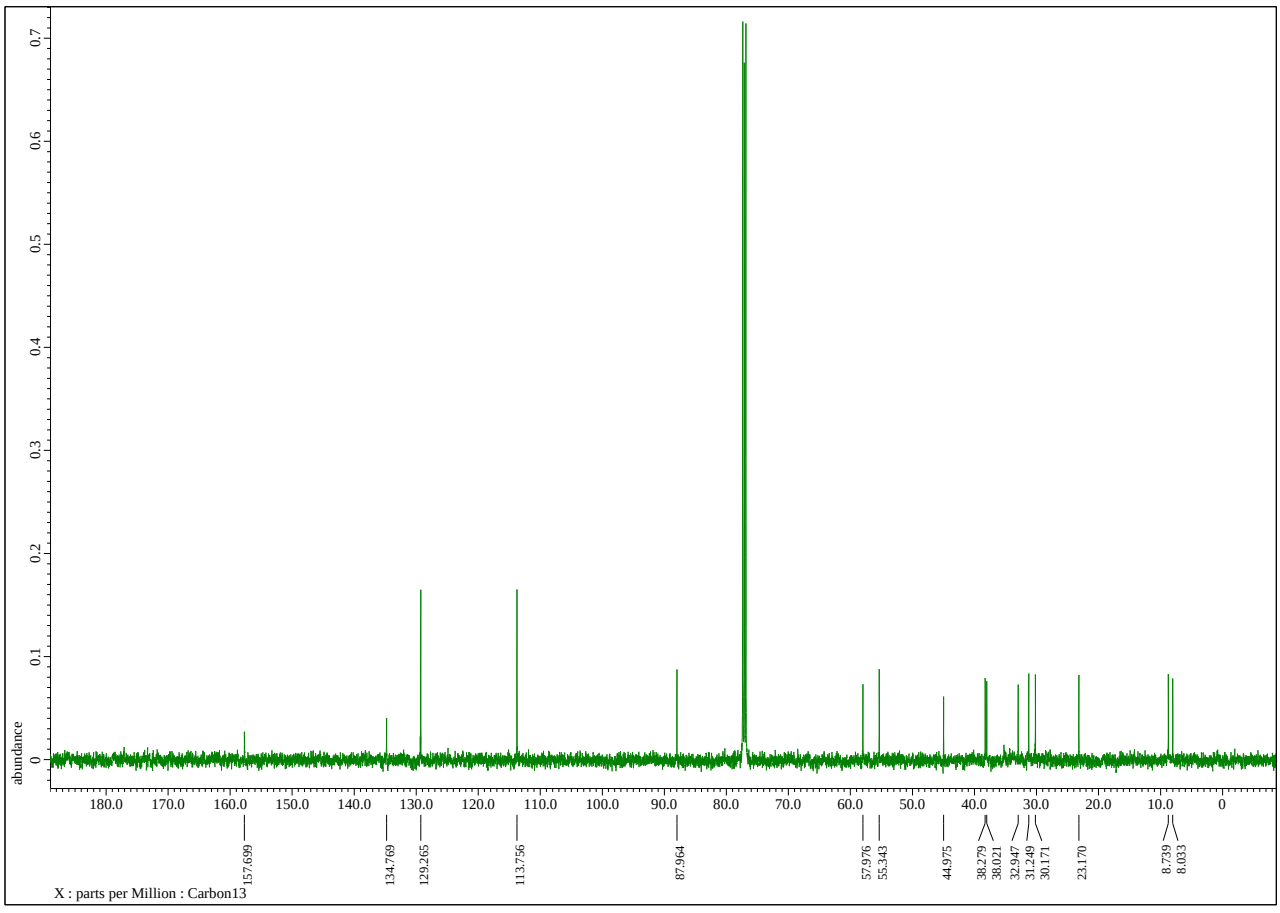
abundance
X : parts per Million : Carbon13

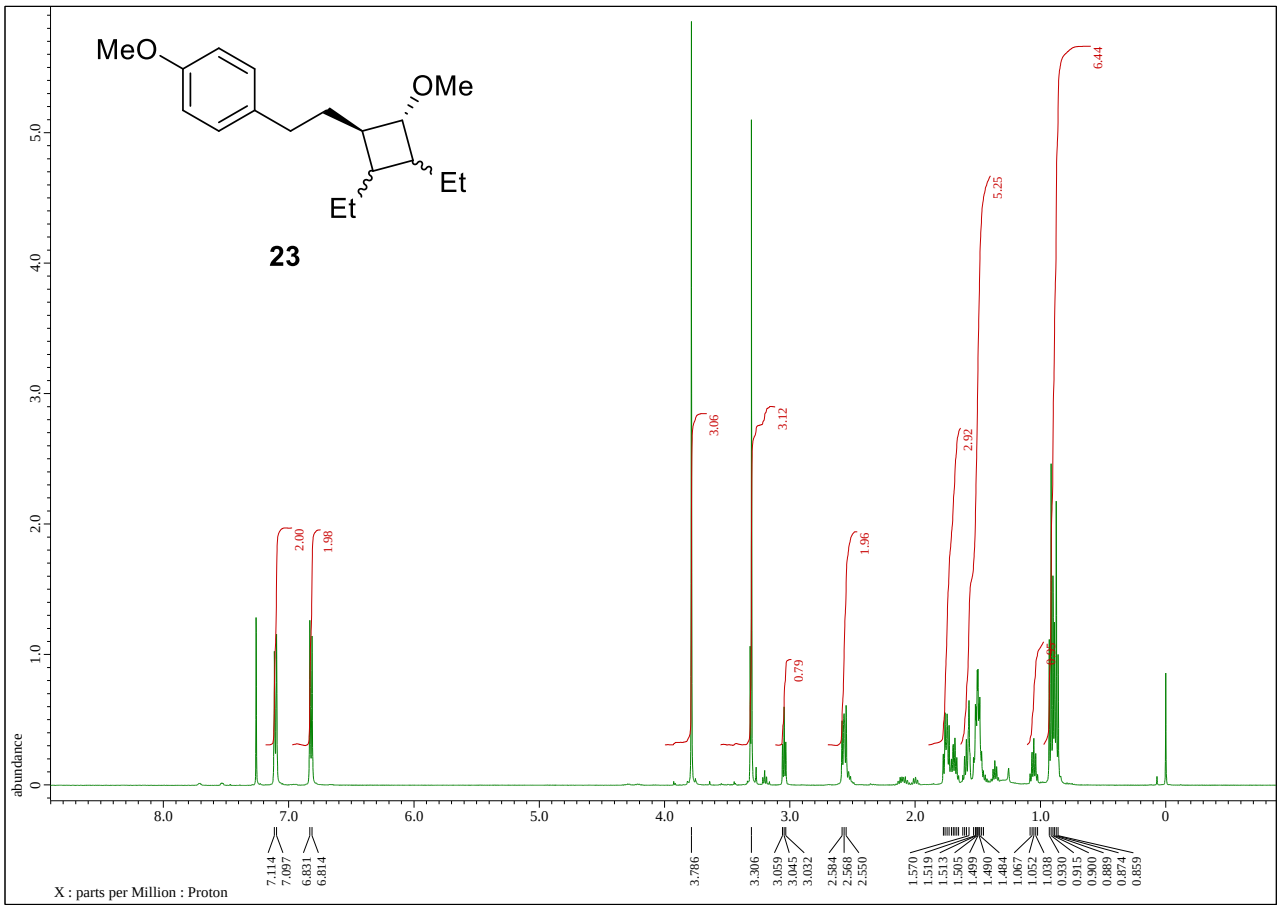
MeO
OMe
Et
Et
23
abundance
X : parts per Million : Proton

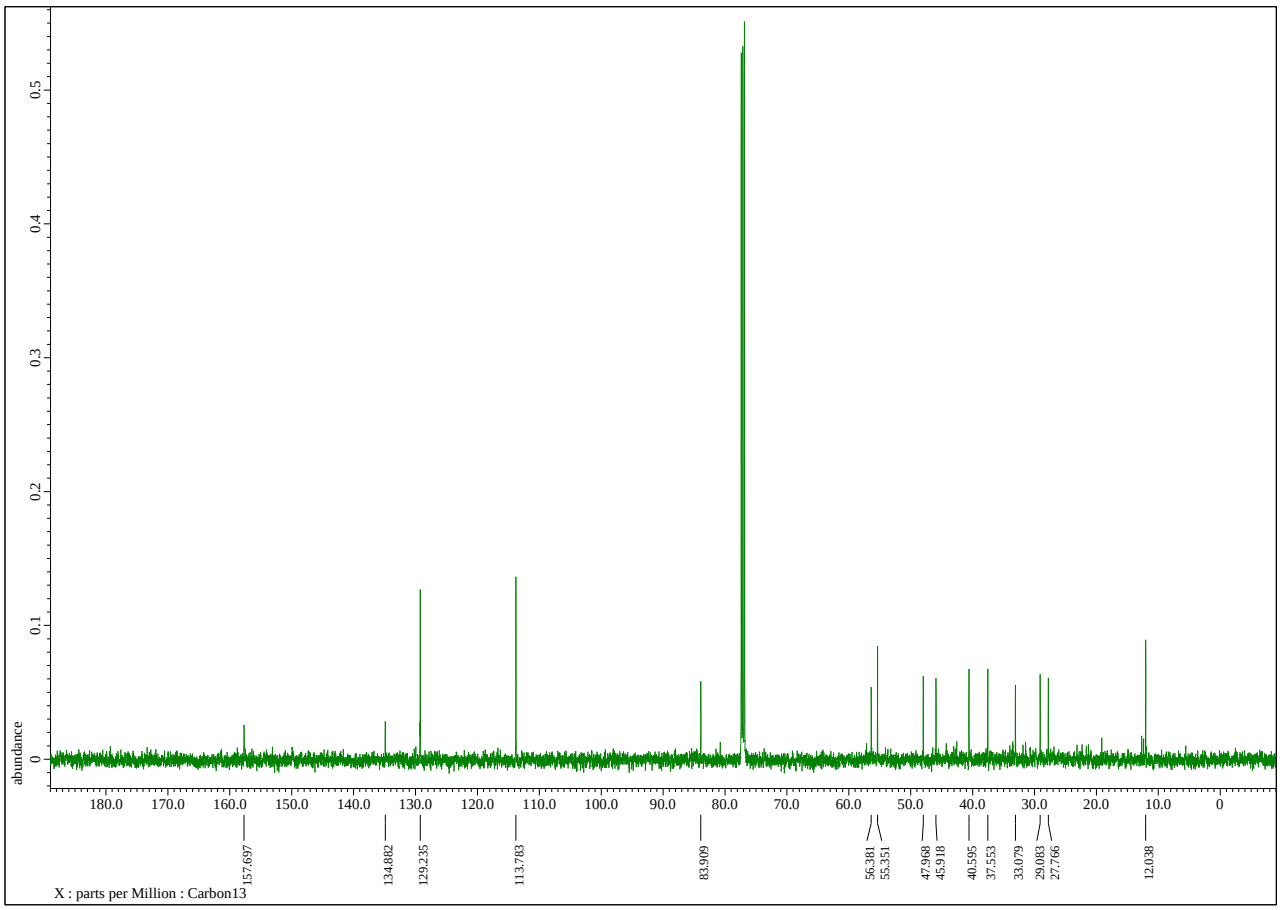
abundance
X : parts per Million : Carbon13

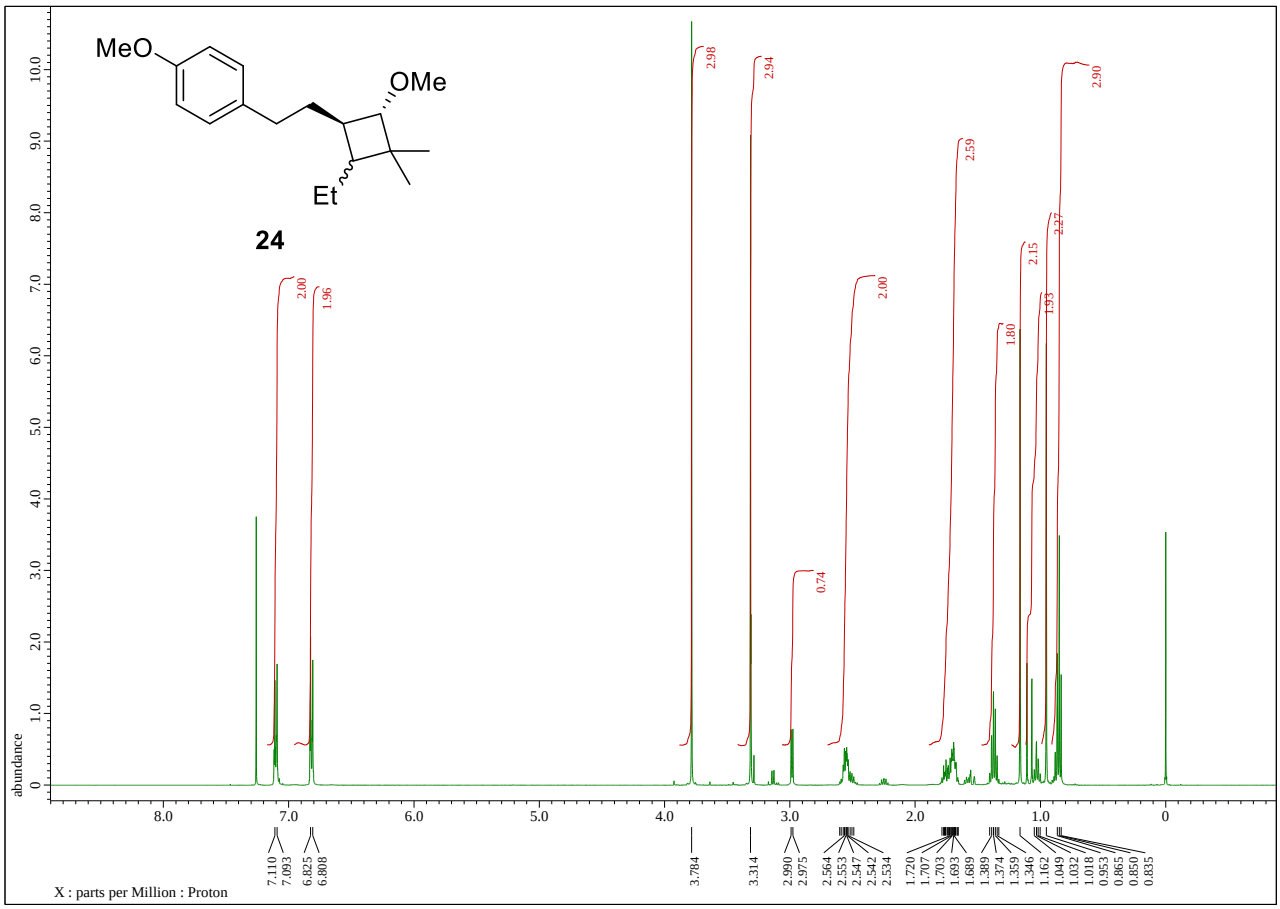
MeO
OMe
Et
24
abundance
X : parts per Million : Proton

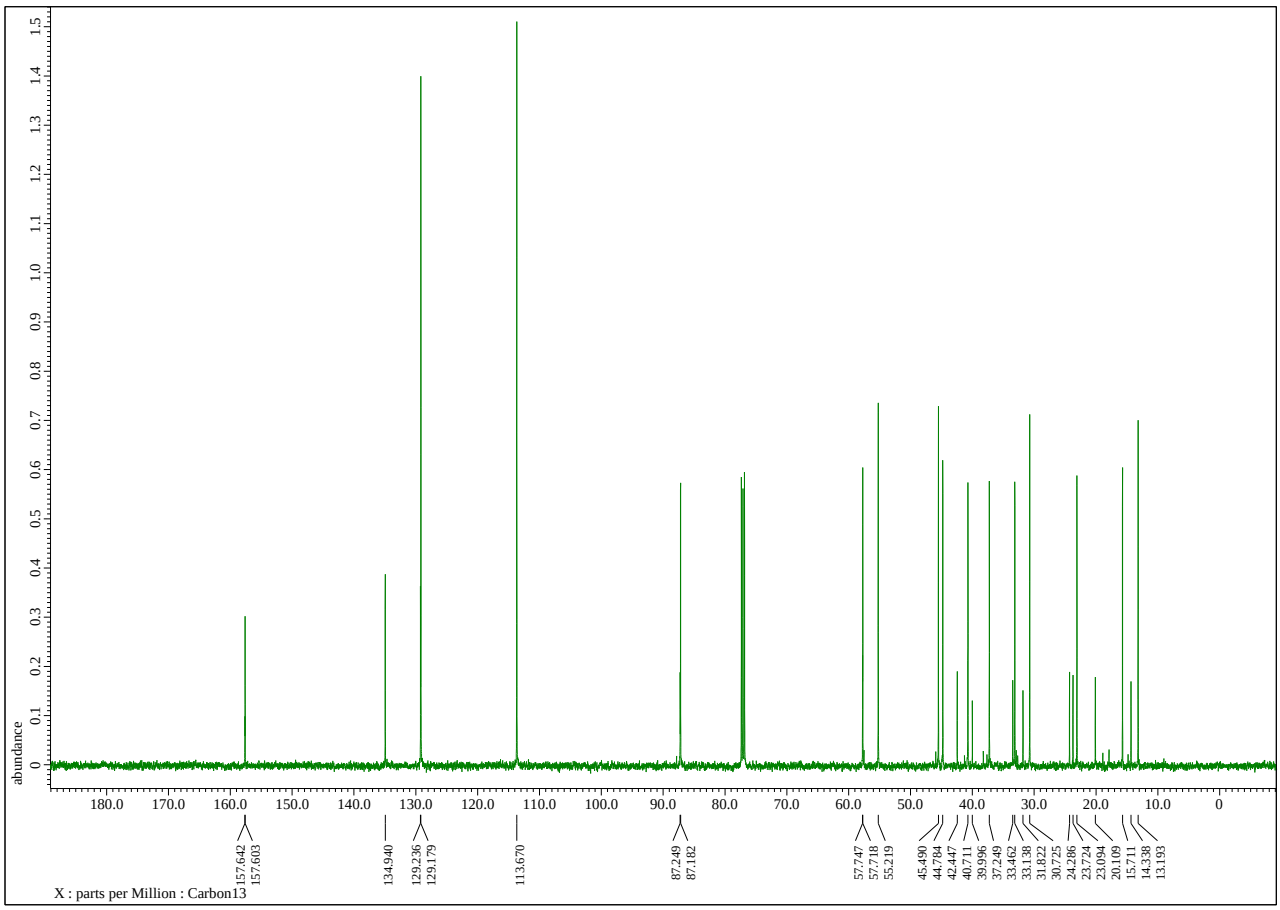
abundance
X : parts per Million : Carbon13

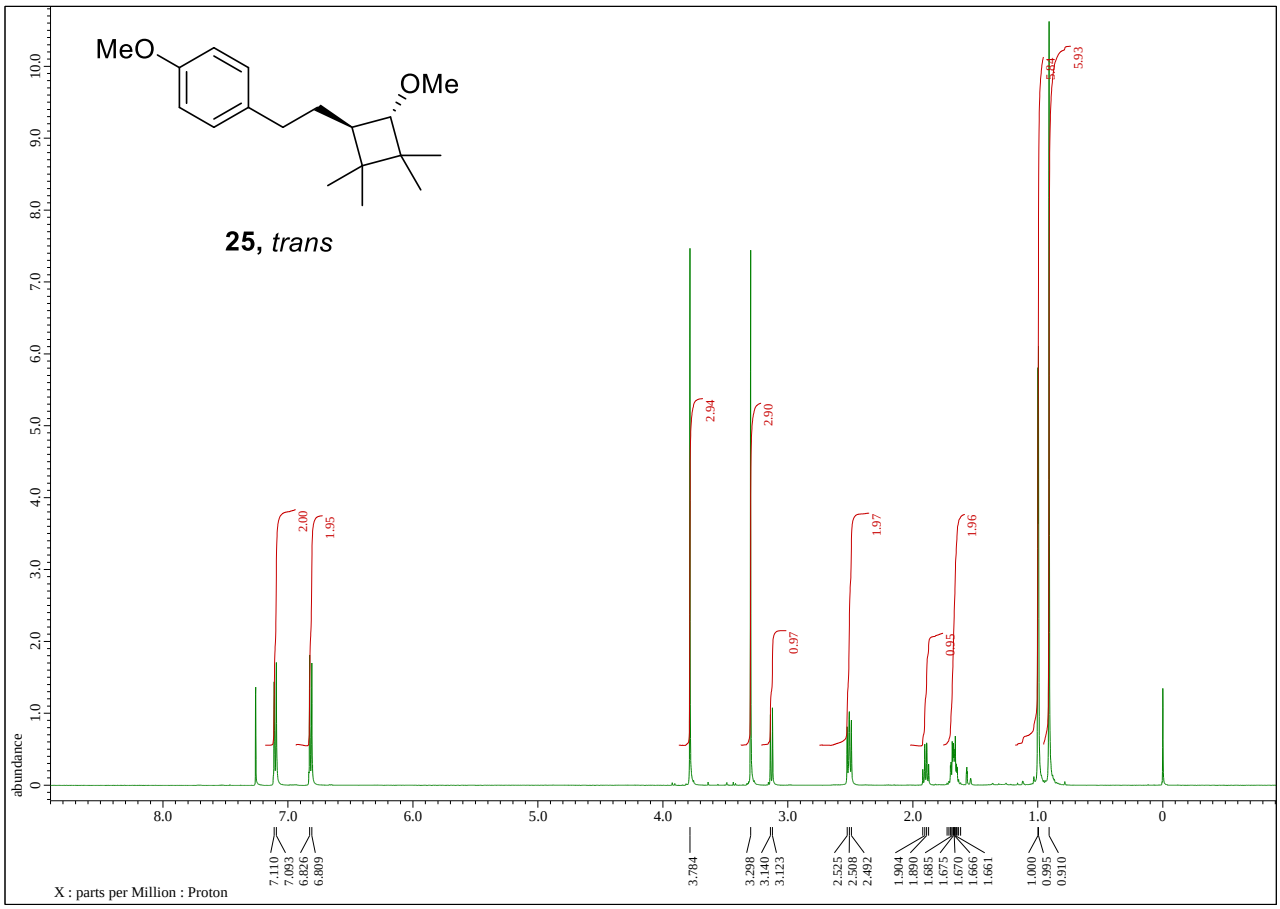
MeO
OMe
25, trans
abundance
X : parts per Million : Proton

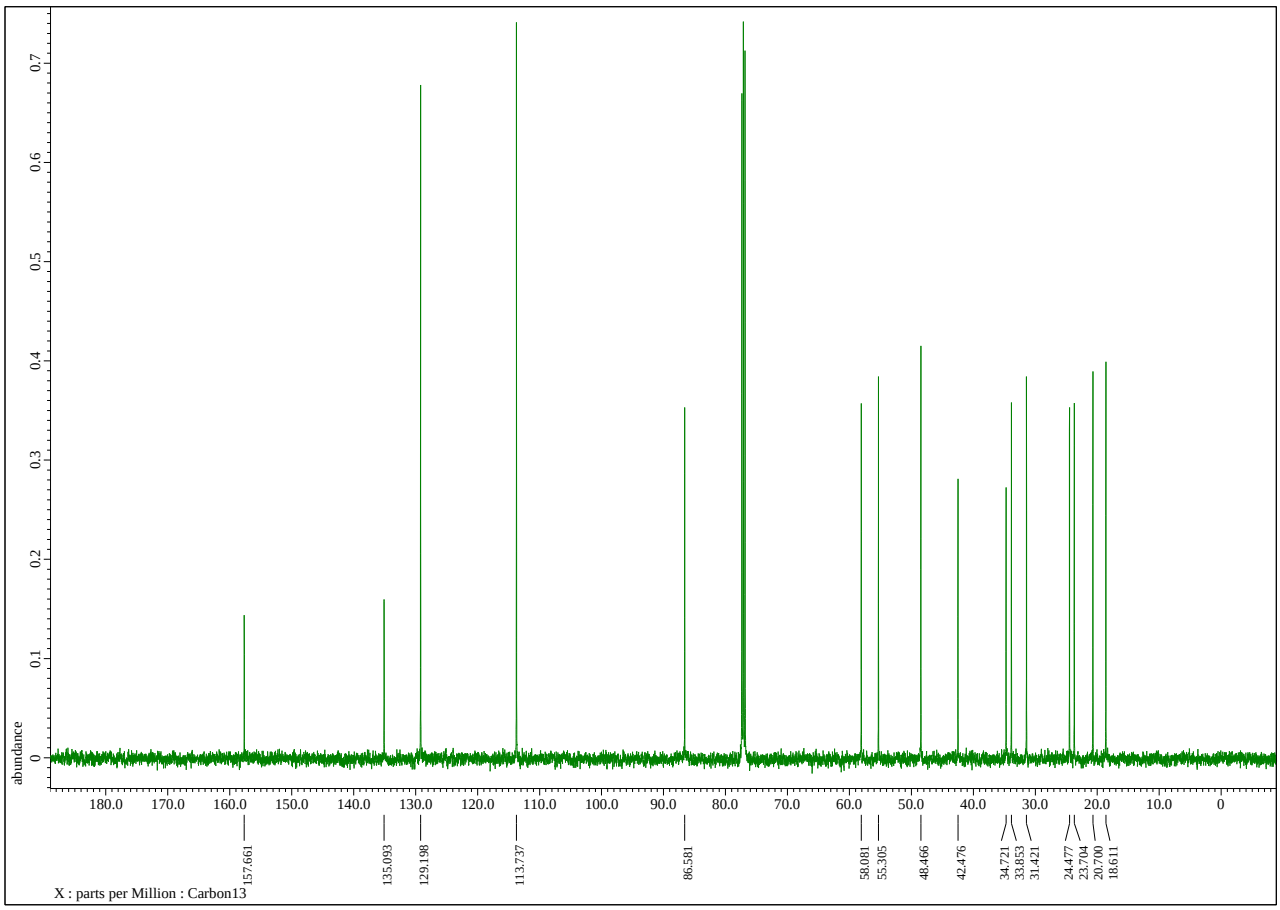
abundance
X : parts per Million : Carbon13

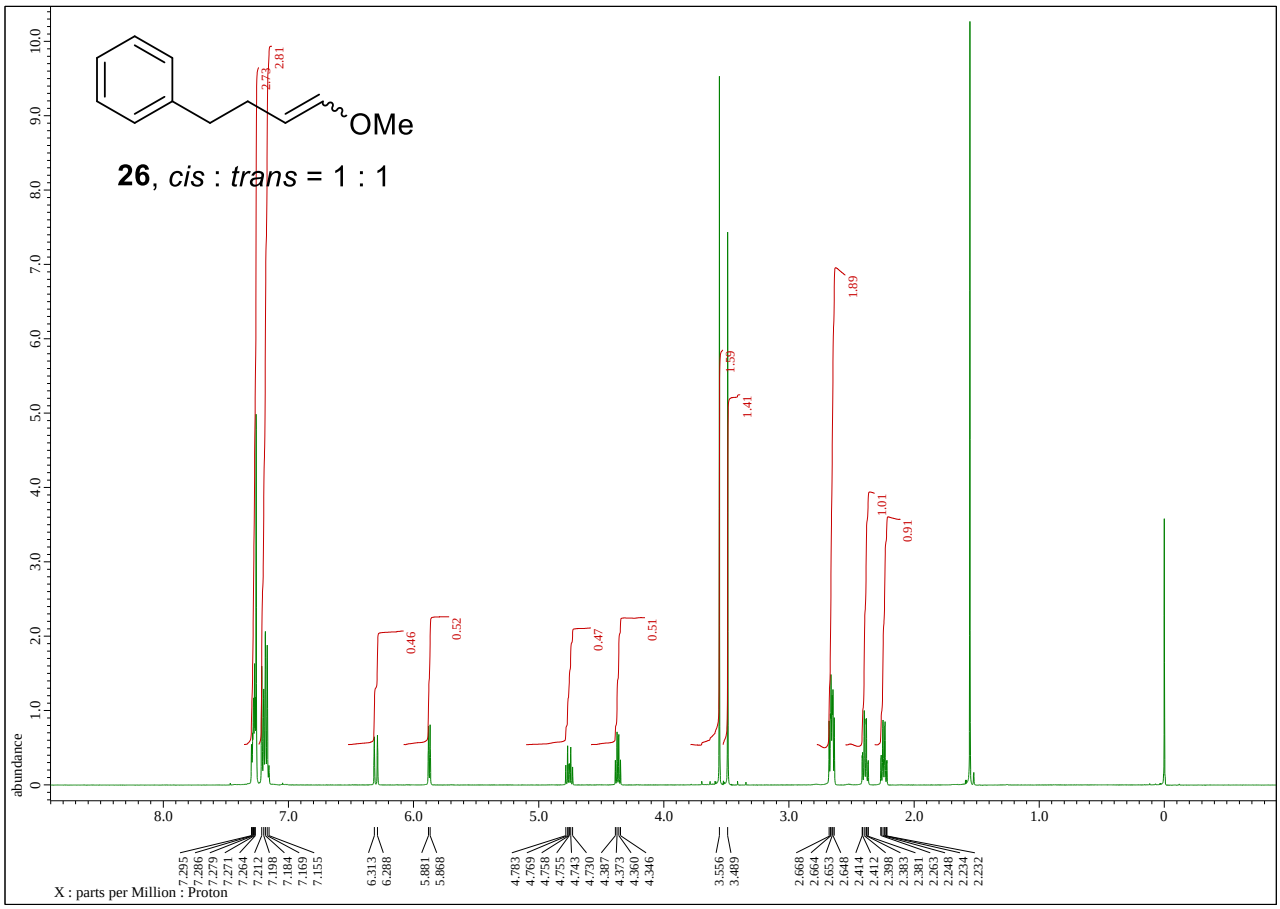
OMe
26, cis : trans = 1 : 1
abundance
X : parts per Million : Proton

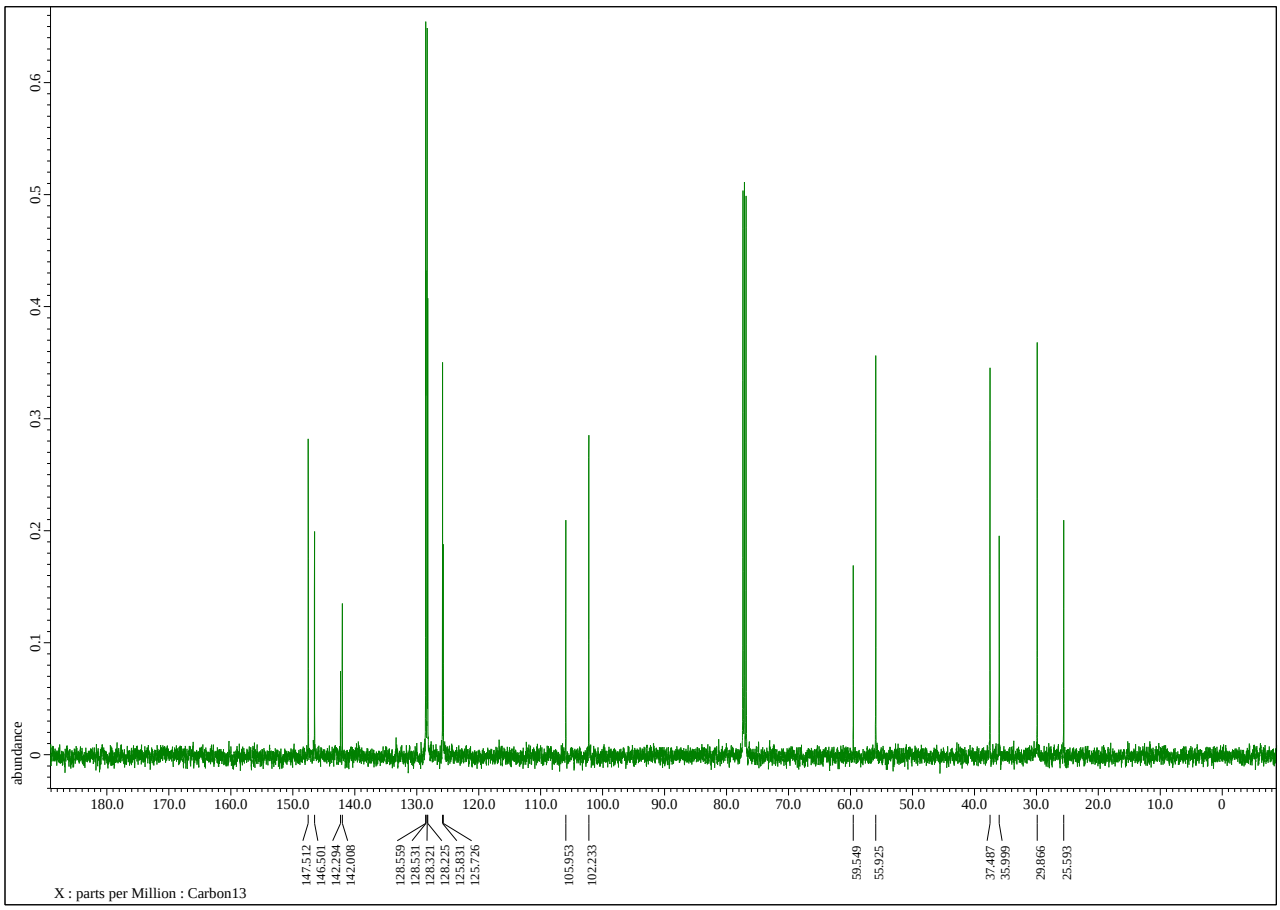
abundance
X : parts per Million : Carbon13

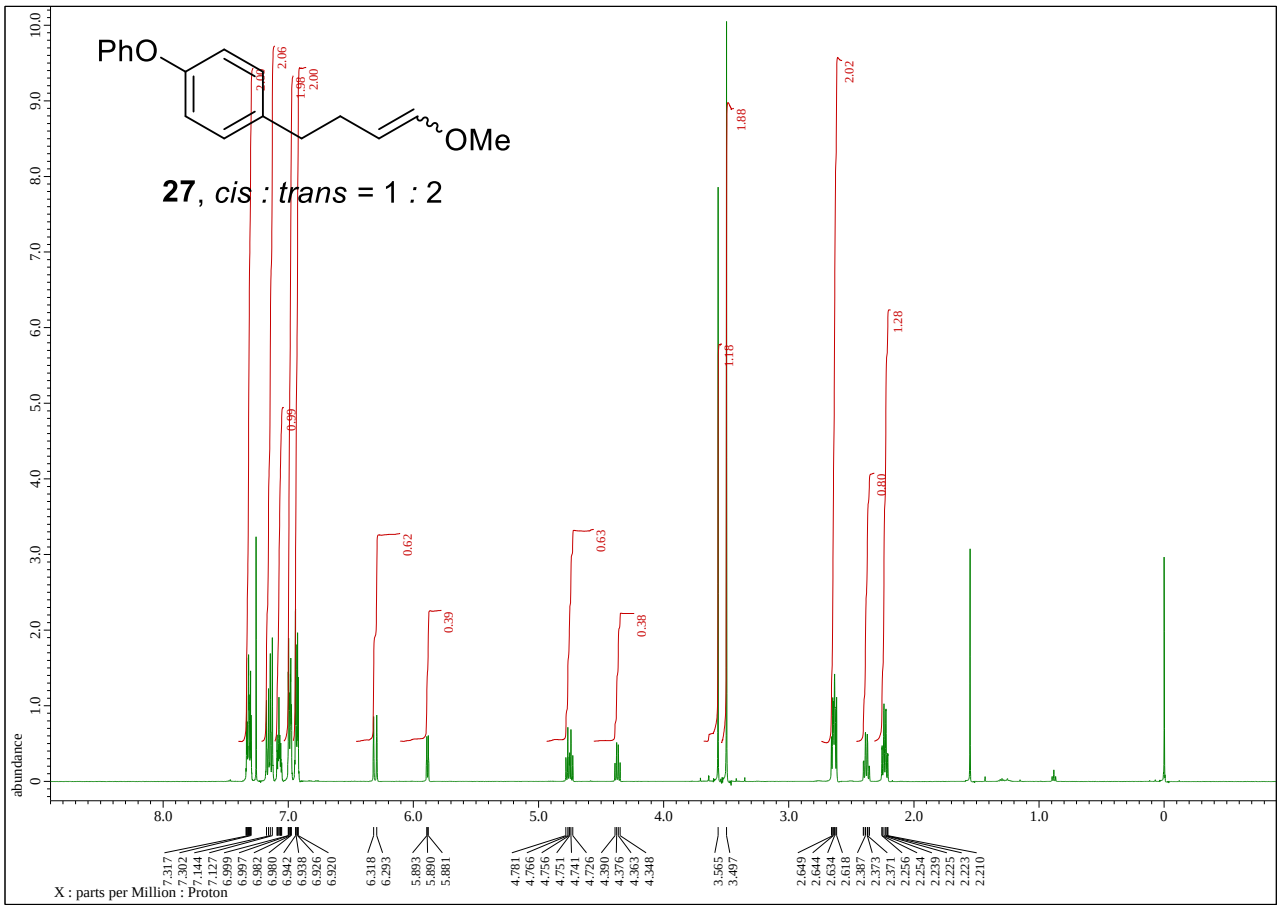
PhO
OMe
27, cis : trans = 1 : 2
abundance
X : parts per Million : Proton

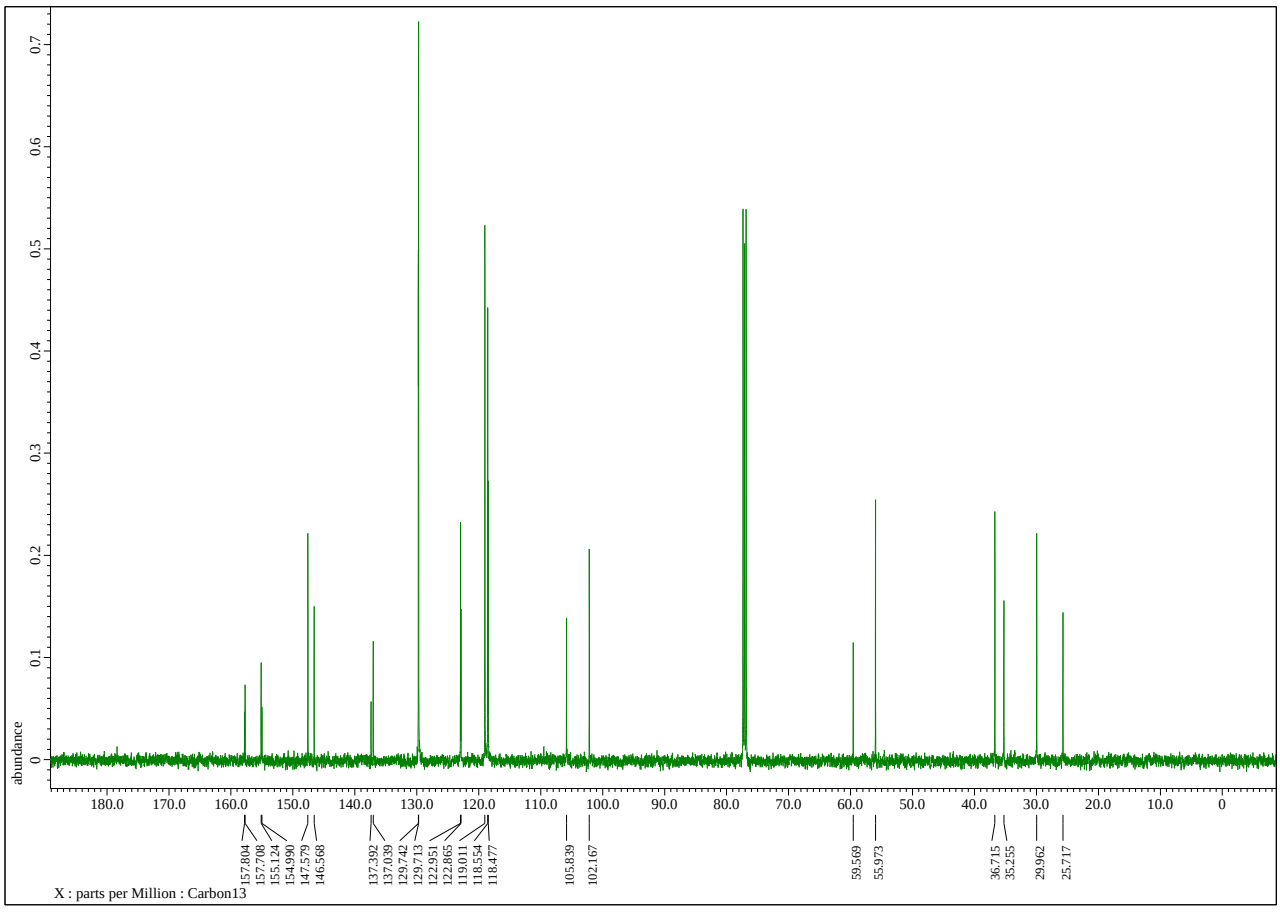
abundance
X : parts per Million : Carbon13

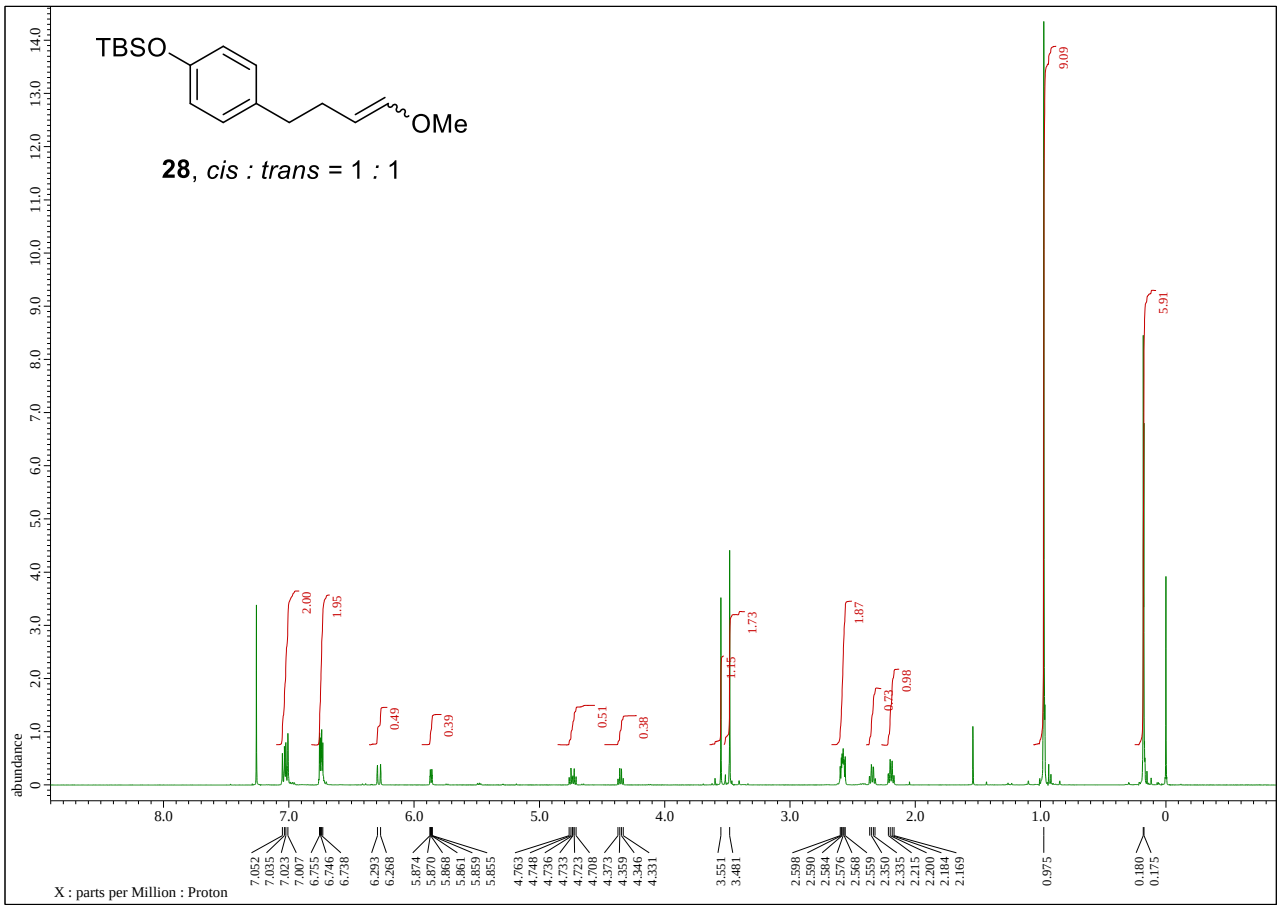
TBSO
OMe
28, cis : trans = 1 : 1
abundance
X : parts per Million : Proton

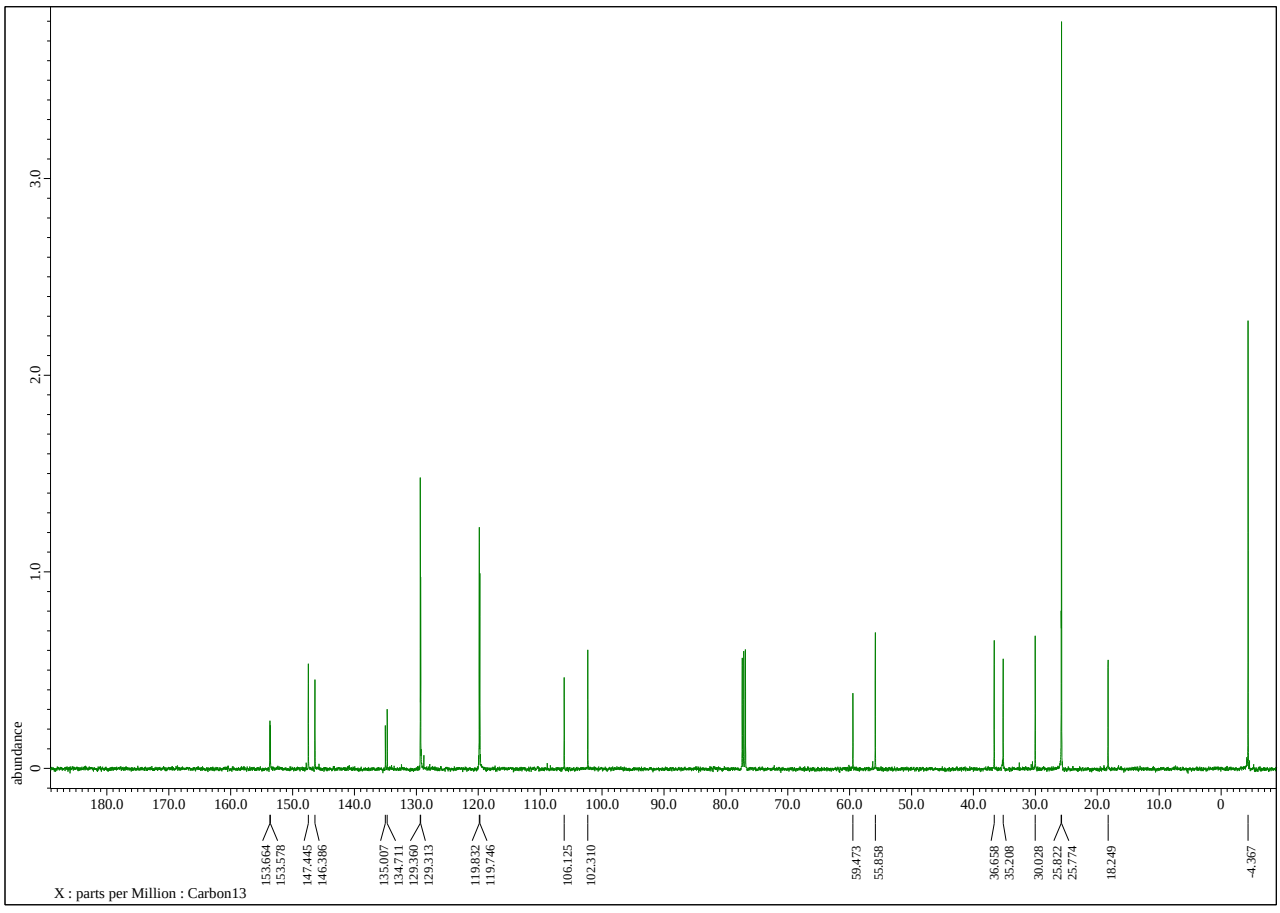
abundance
X : parts per Million : Carbon13

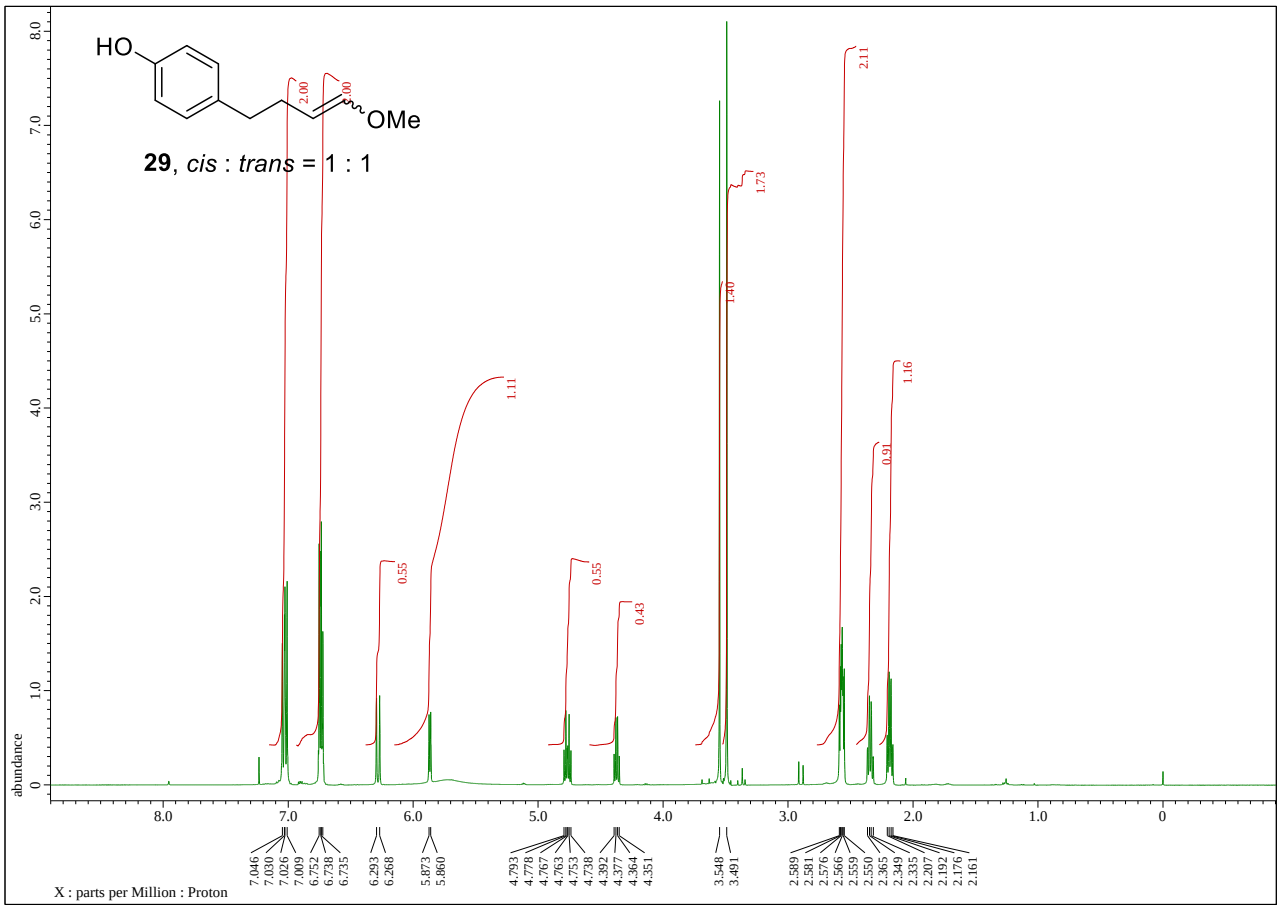
HO
OMe
29, cis : trans = 1 : 1
2.00
3.00
abundance
X : parts per Million : Proton
7.046
7.030
7.026
7.009
6.752
6.738
6.735
6.293
6.268
5.873
5.860
4.793
4.778
4.767
4.763
4.753
4.738
4.393
4.377
4.364
4.351
3.548
3.491
2.589
2.581
2.576
2.566
2.559
2.550
2.365
2.349
2.335
2.207
2.192
2.176
2.161

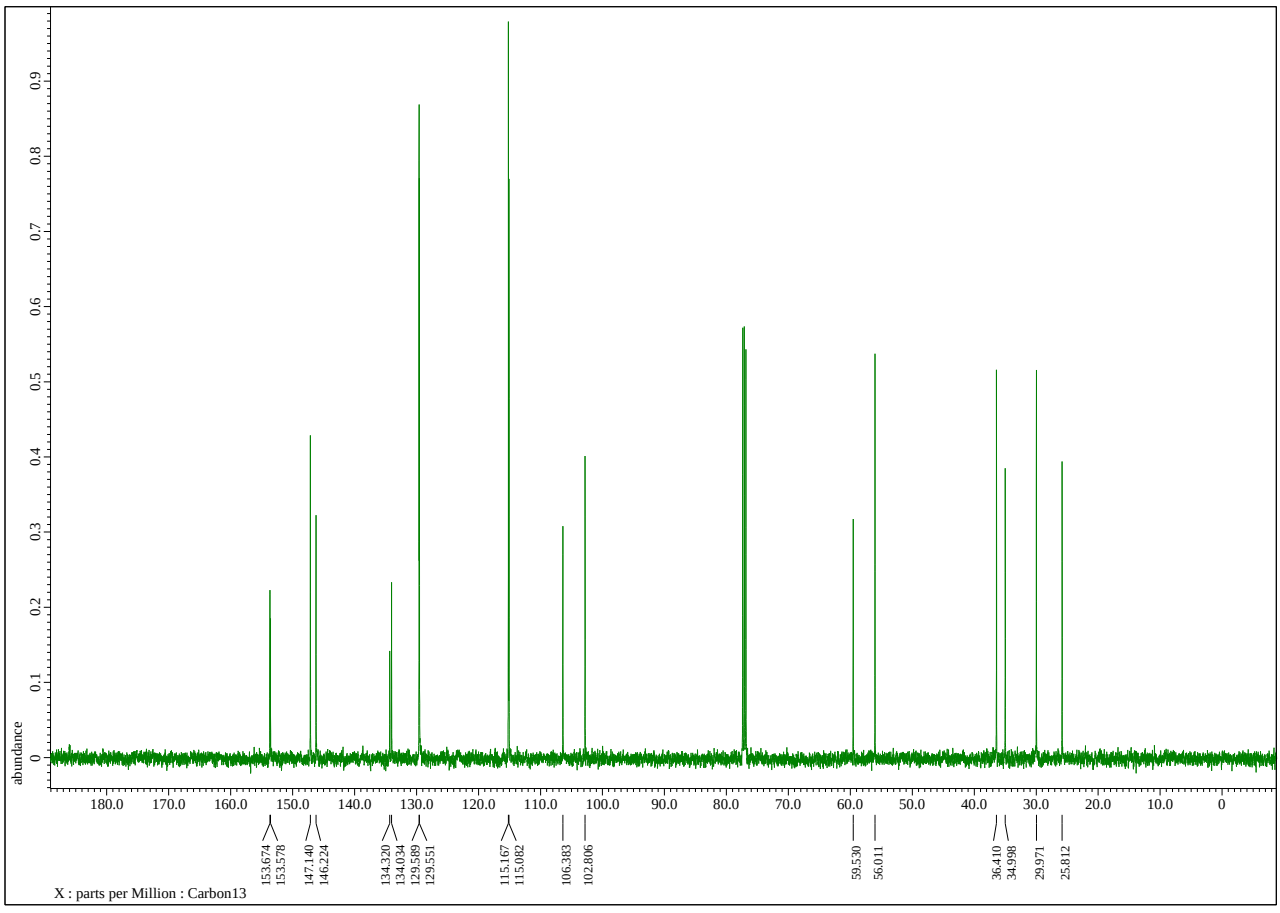
abundance
X : parts per Million : Carbon13
153.674
153.578
147.140
146.224
134.320
134.034
129.589
129.551
115.167
115.082
106.383
102.806
59.530
56.011
36.410
34.998
29.971
25.812

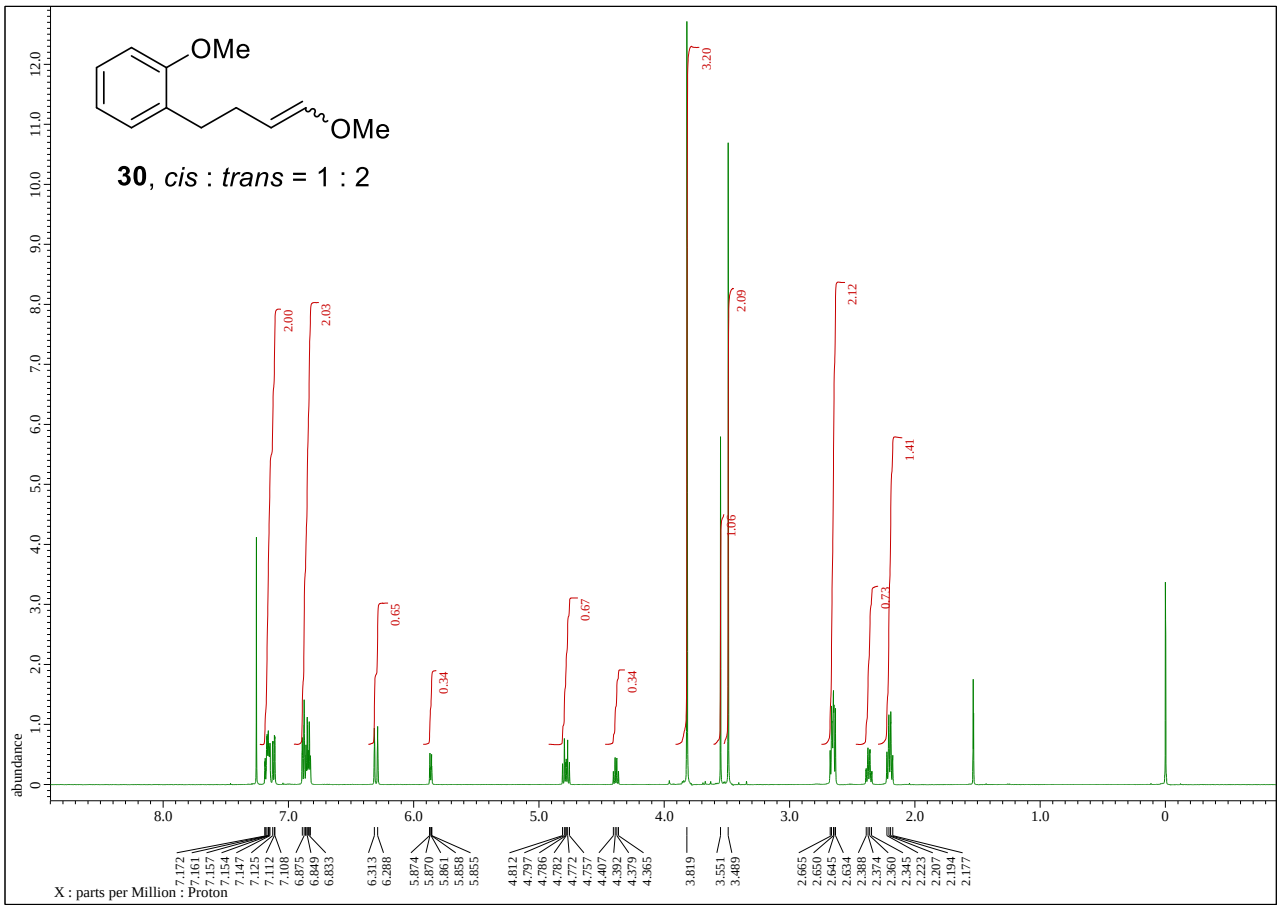
OMe
OMe
30, *cis* : *trans* = 1 : 2
abundance
X : parts per Million : Proton

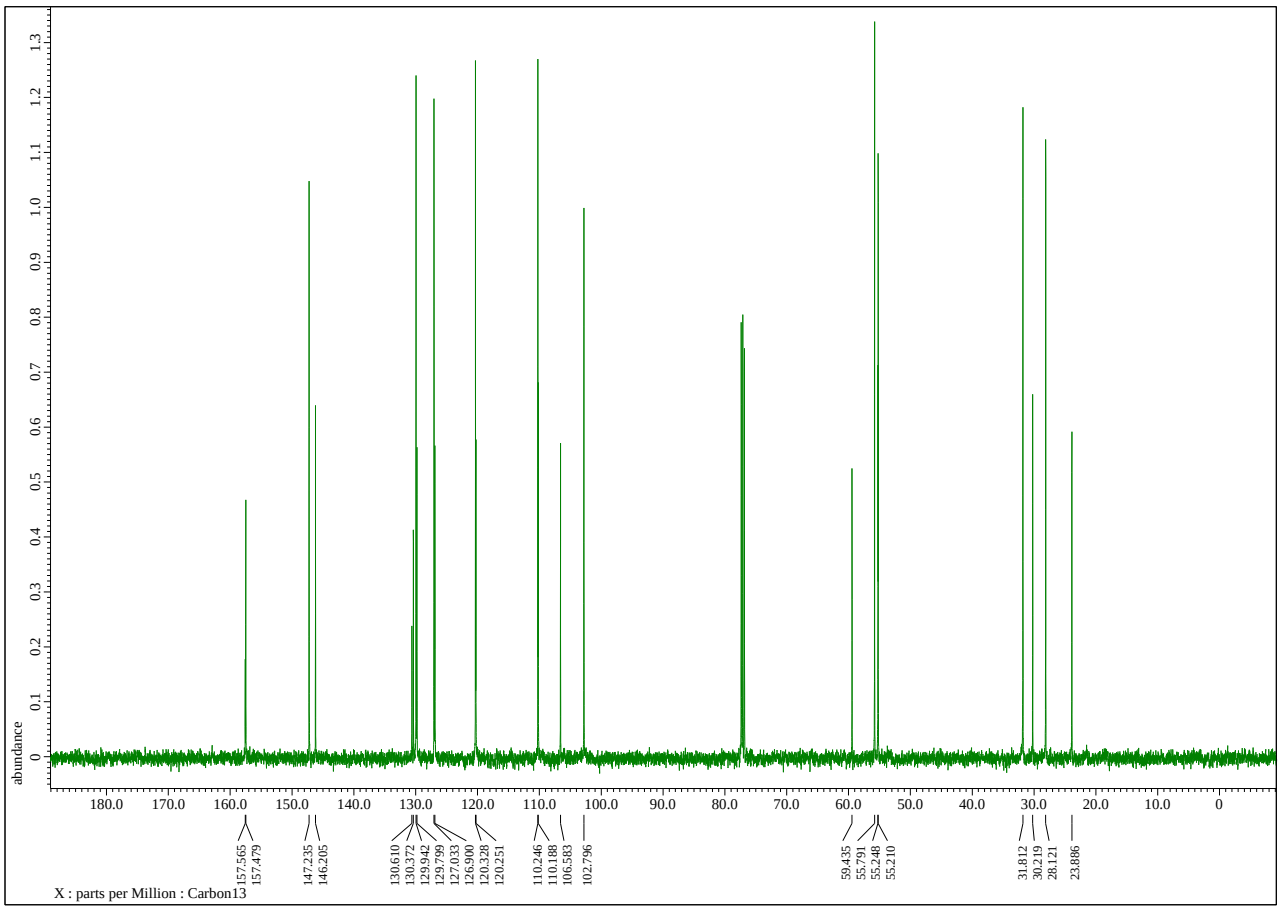
abundance
X : parts per Million : Carbon13

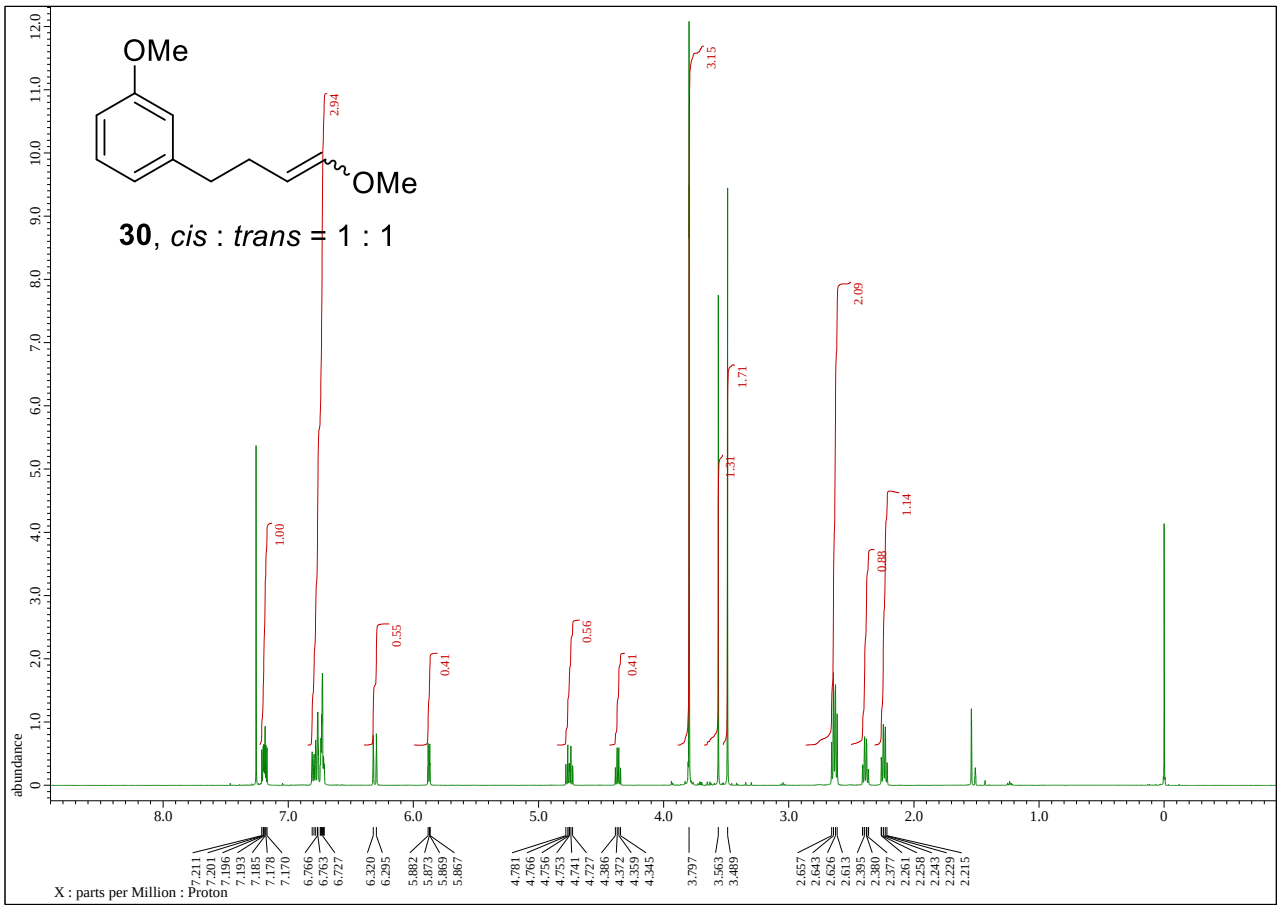
OMe
OMe
30, *cis* : *trans* = 1 : 1
abundance
X : parts per Million : Proton

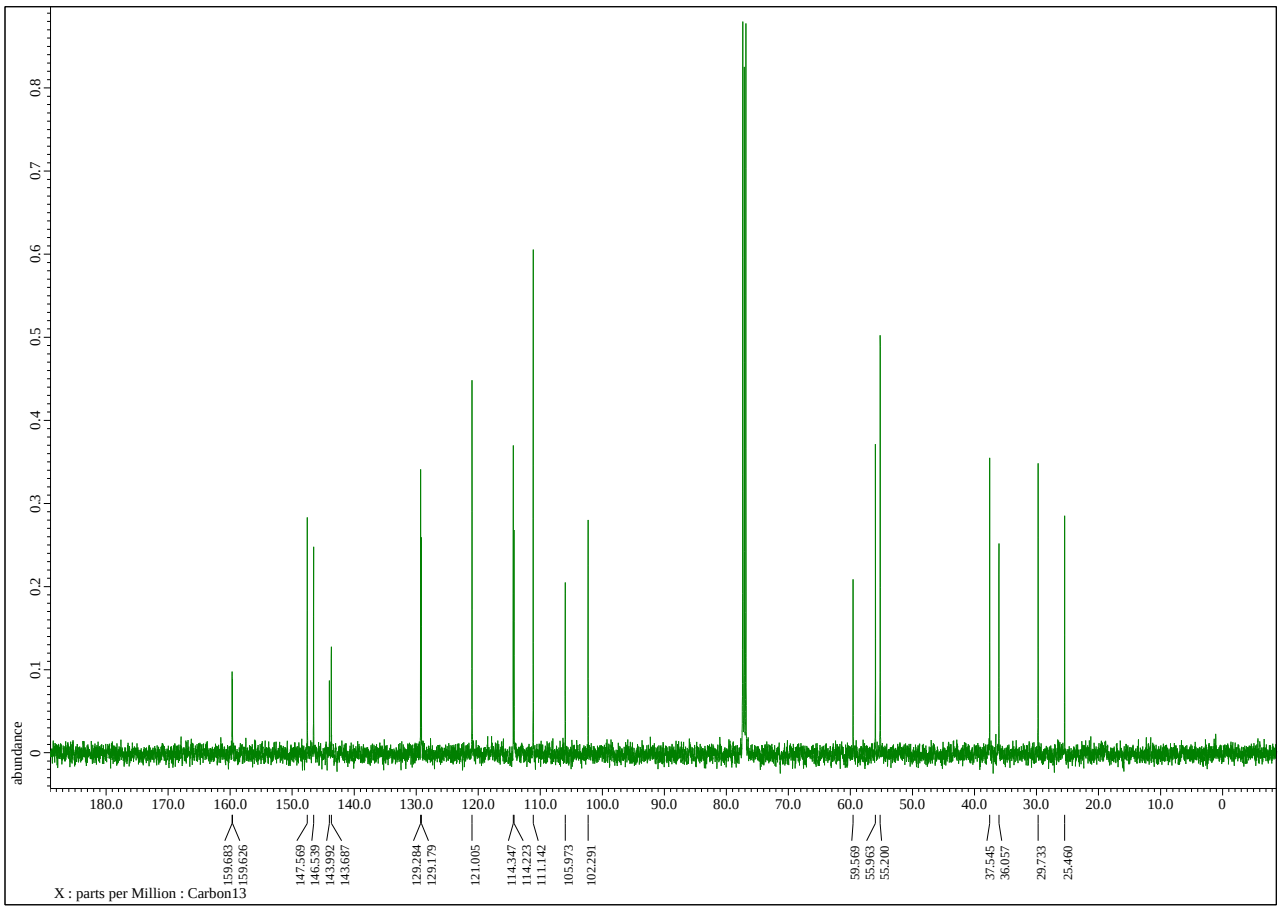
abundance
X : parts per Million : Carbon13

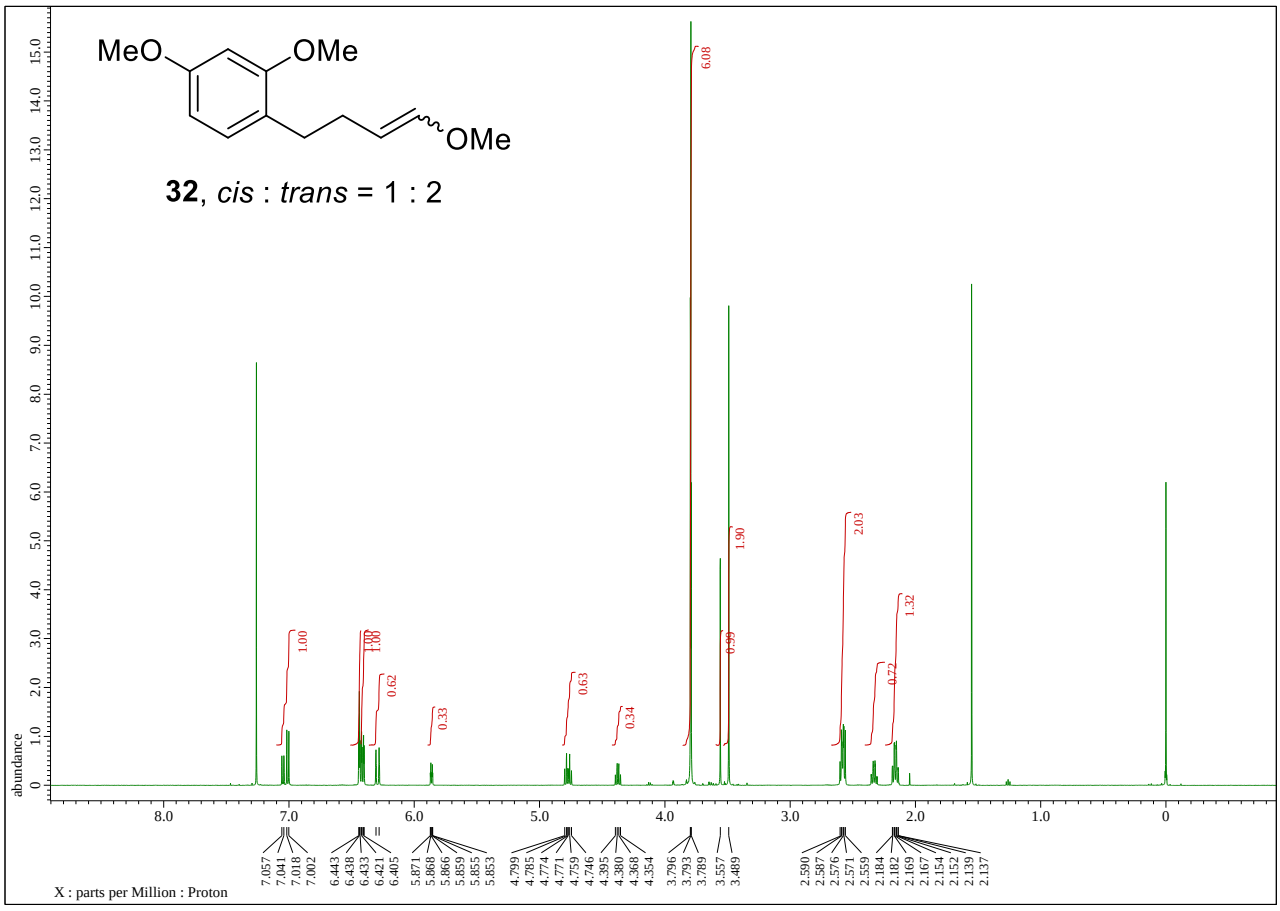
MeO
OMe
OMe
32, cis : trans = 1 : 2
abundance
X : parts per Million : Proton

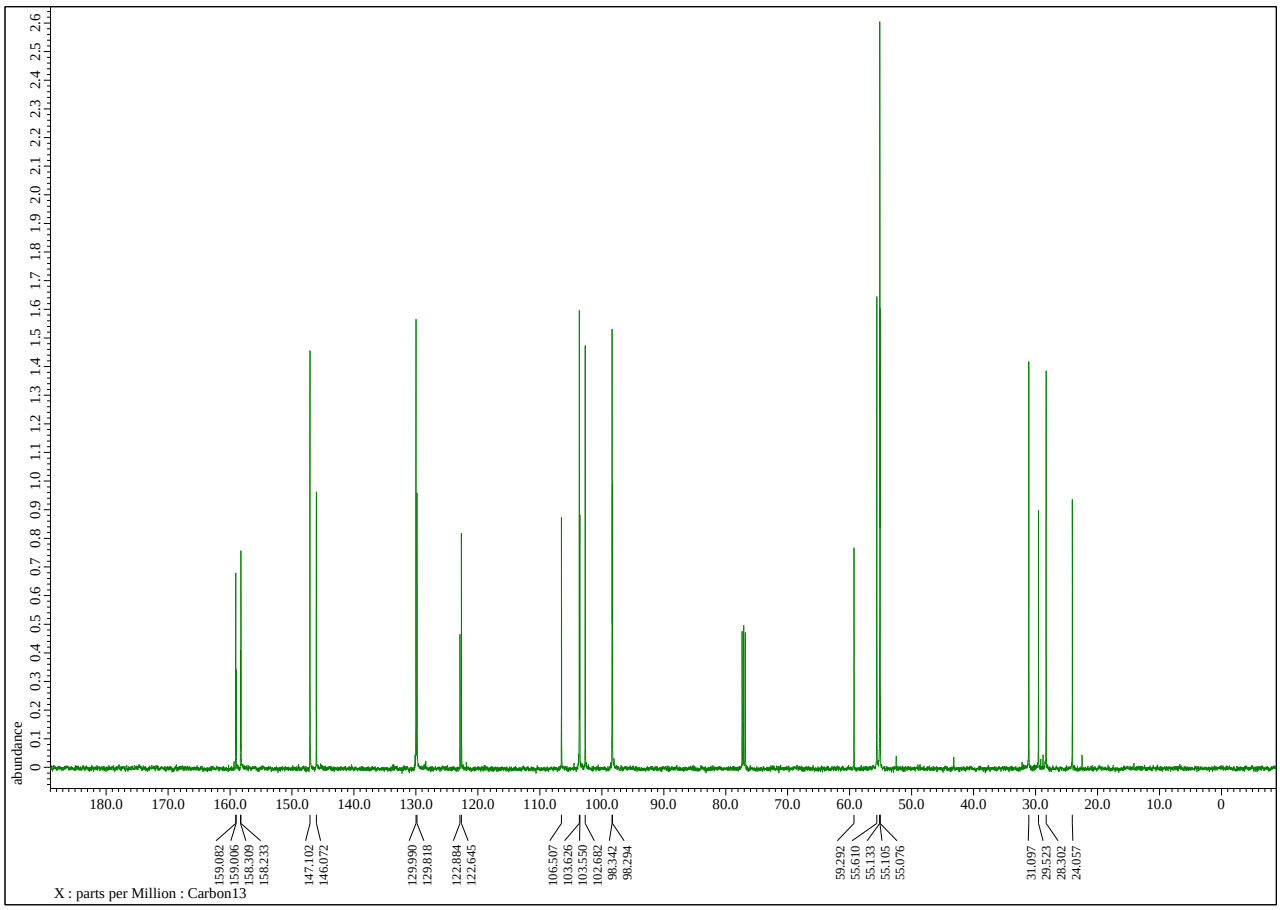
abundance
X : parts per Million : Carbon13

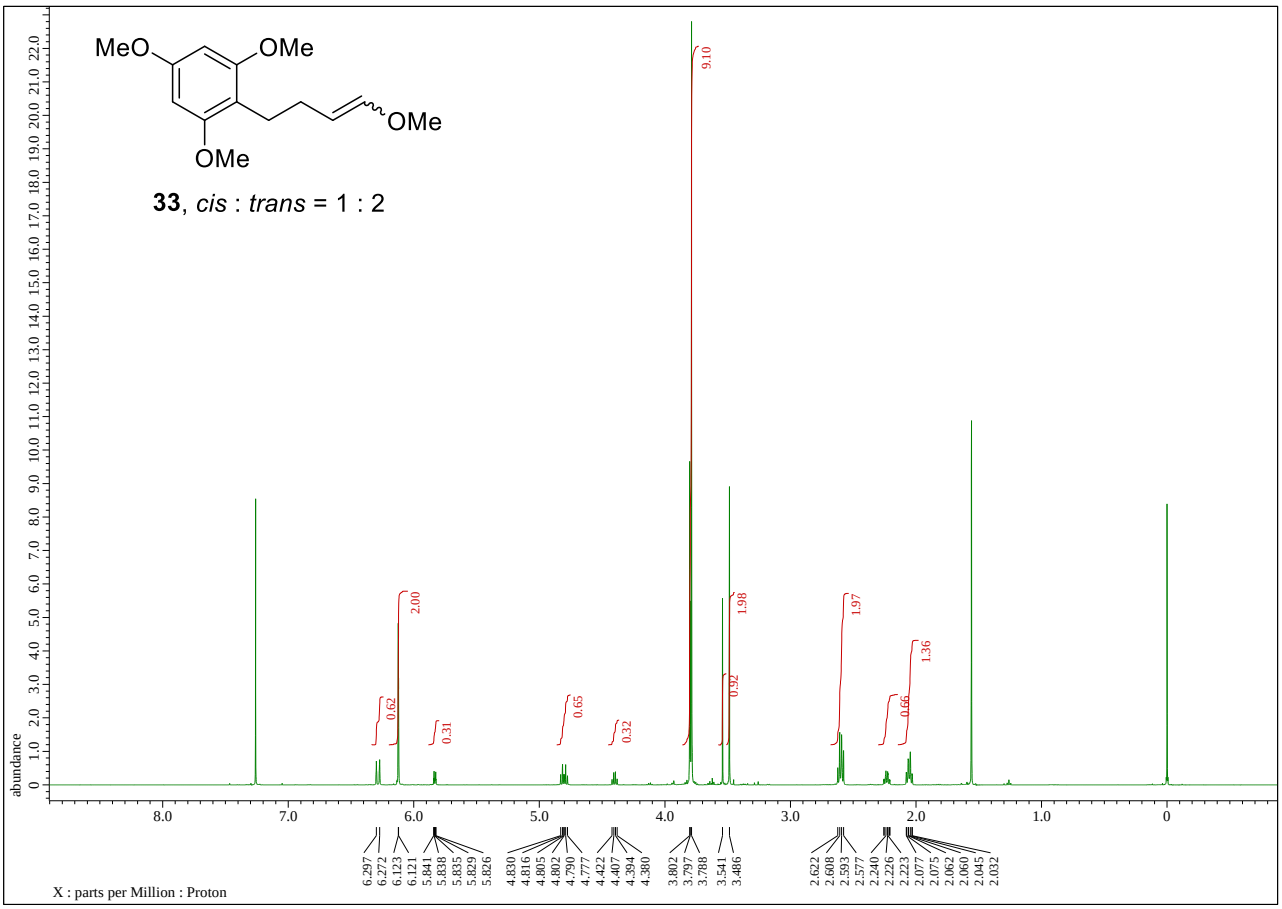
MeO
OMe
OMe
OMe
33, cis : trans = 1 : 2
abundance
X : parts per Million : Proton

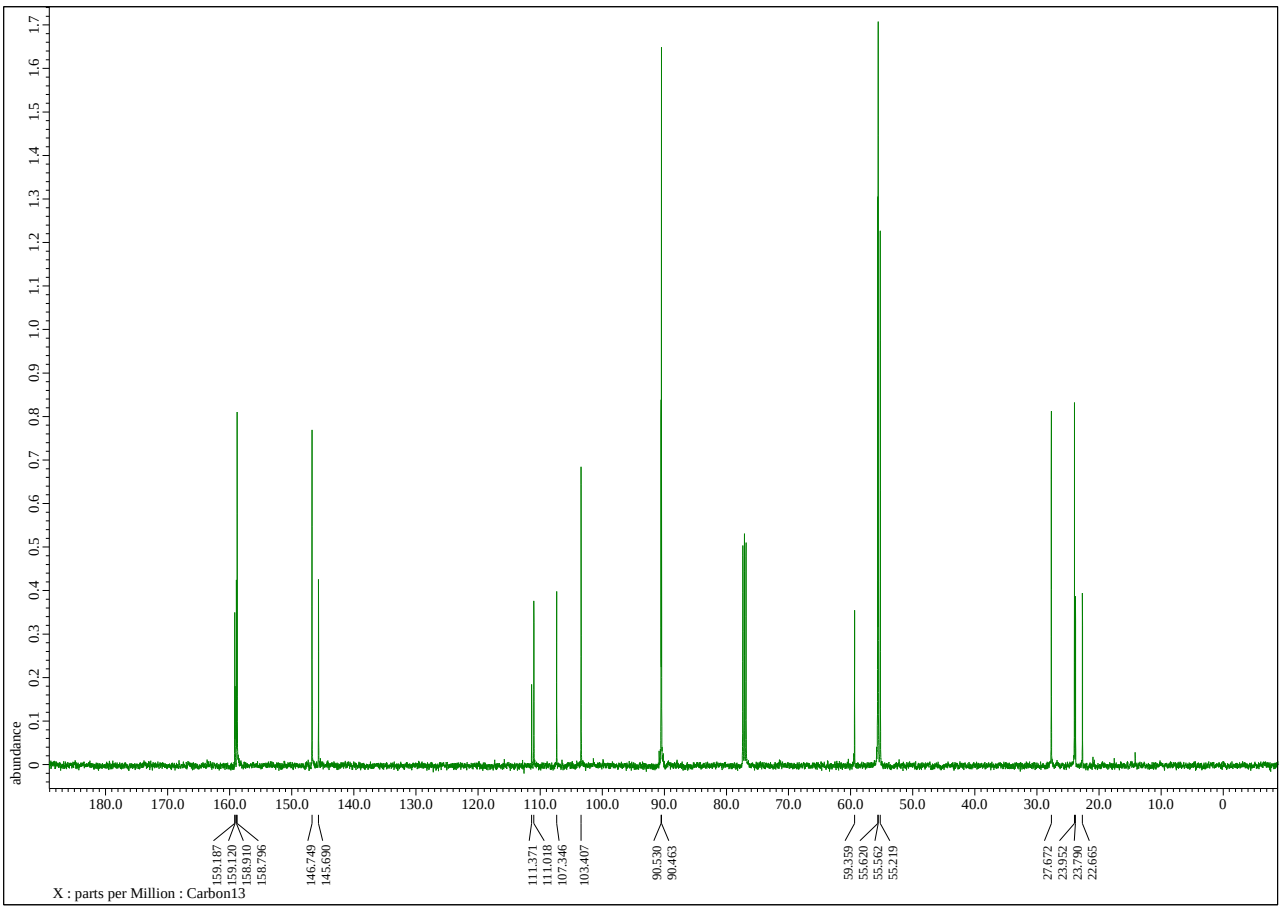
abundance
X : parts per Million : Carbon13

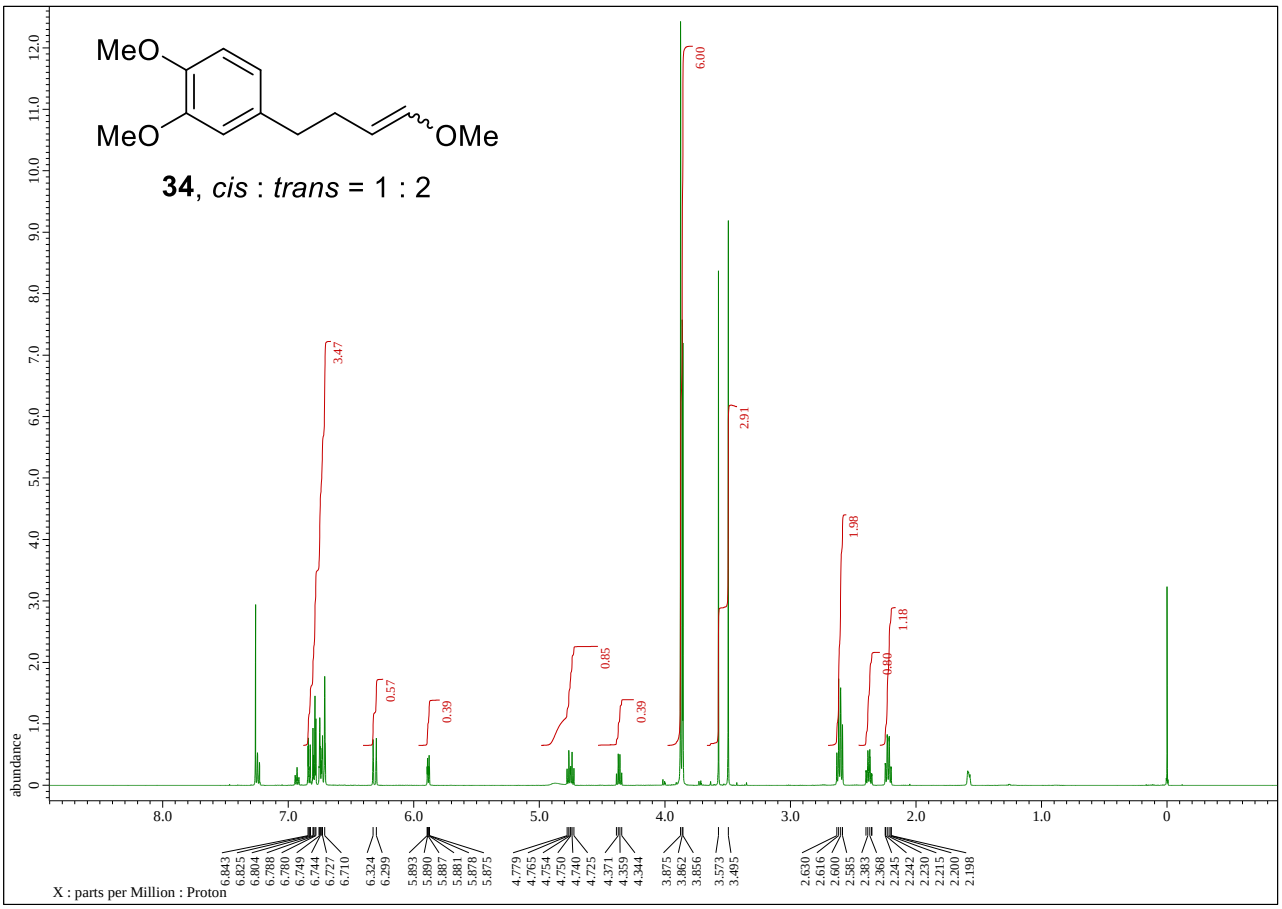
MeO
MeO
OMe
34, cis : trans = 1 : 2
abundance
X : parts per Million : Proton

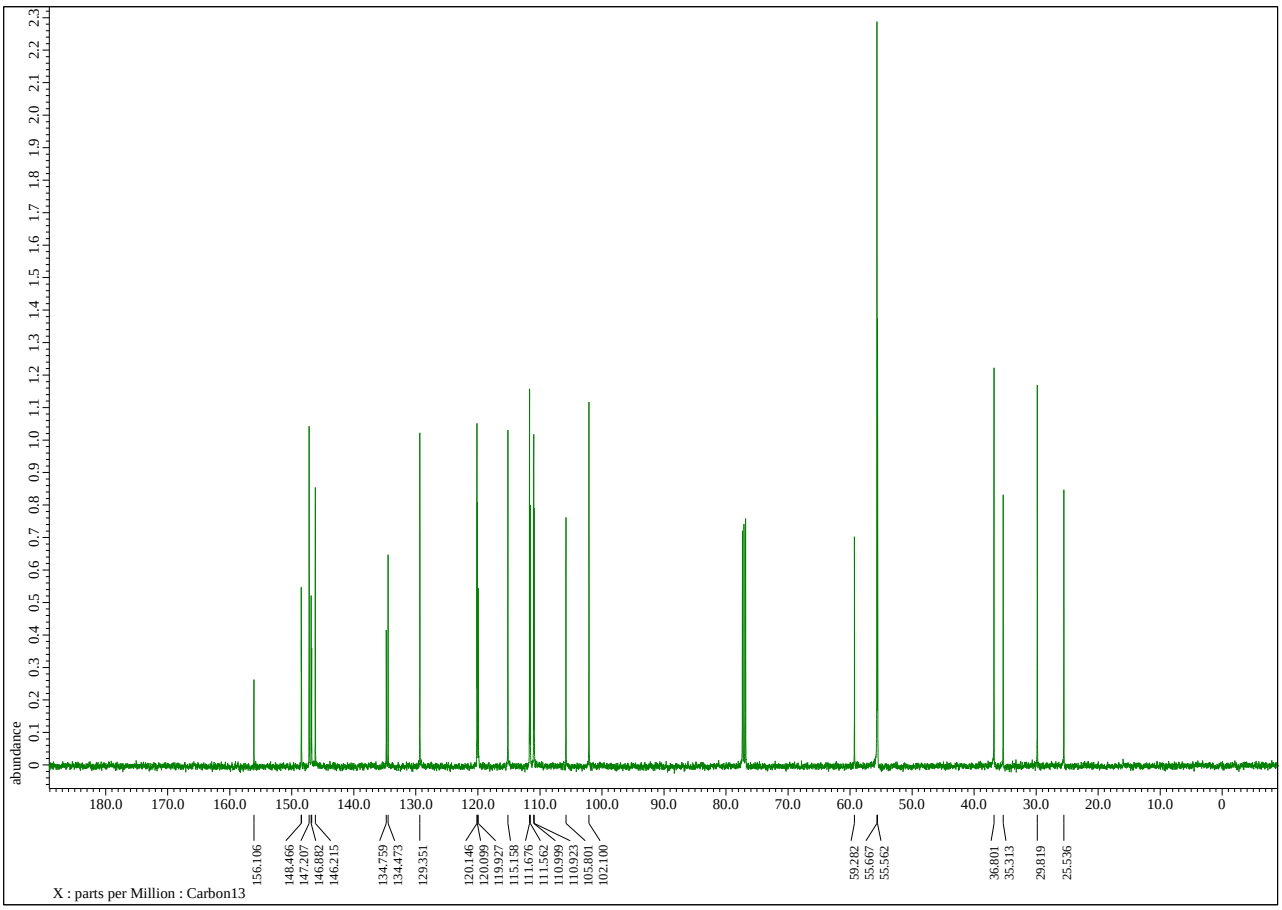
abundance
X : parts per Million : Carbon13

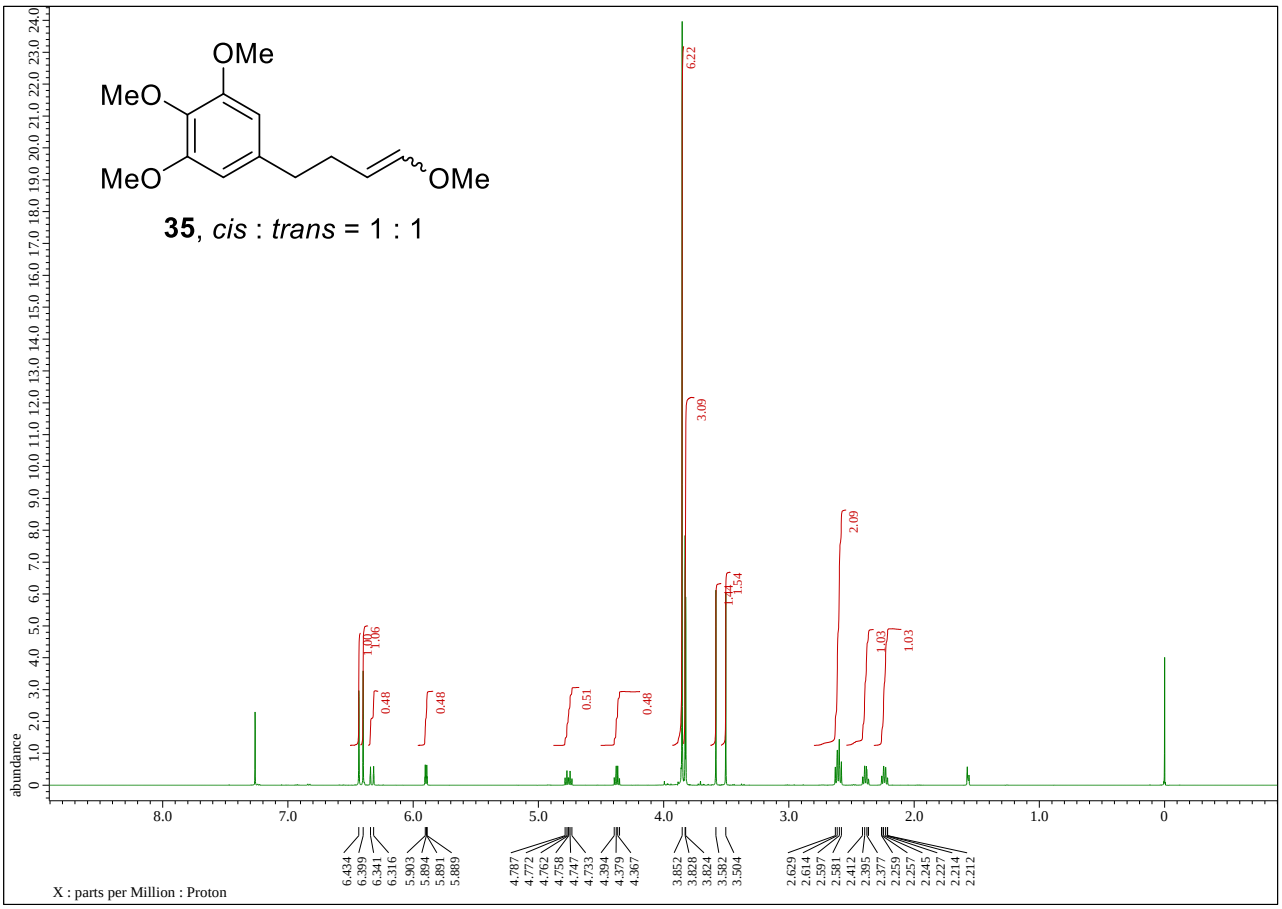
OMe
MeO
MeO
OMe
35, cis : trans = 1 : 1
abundance
X : parts per Million : Proton

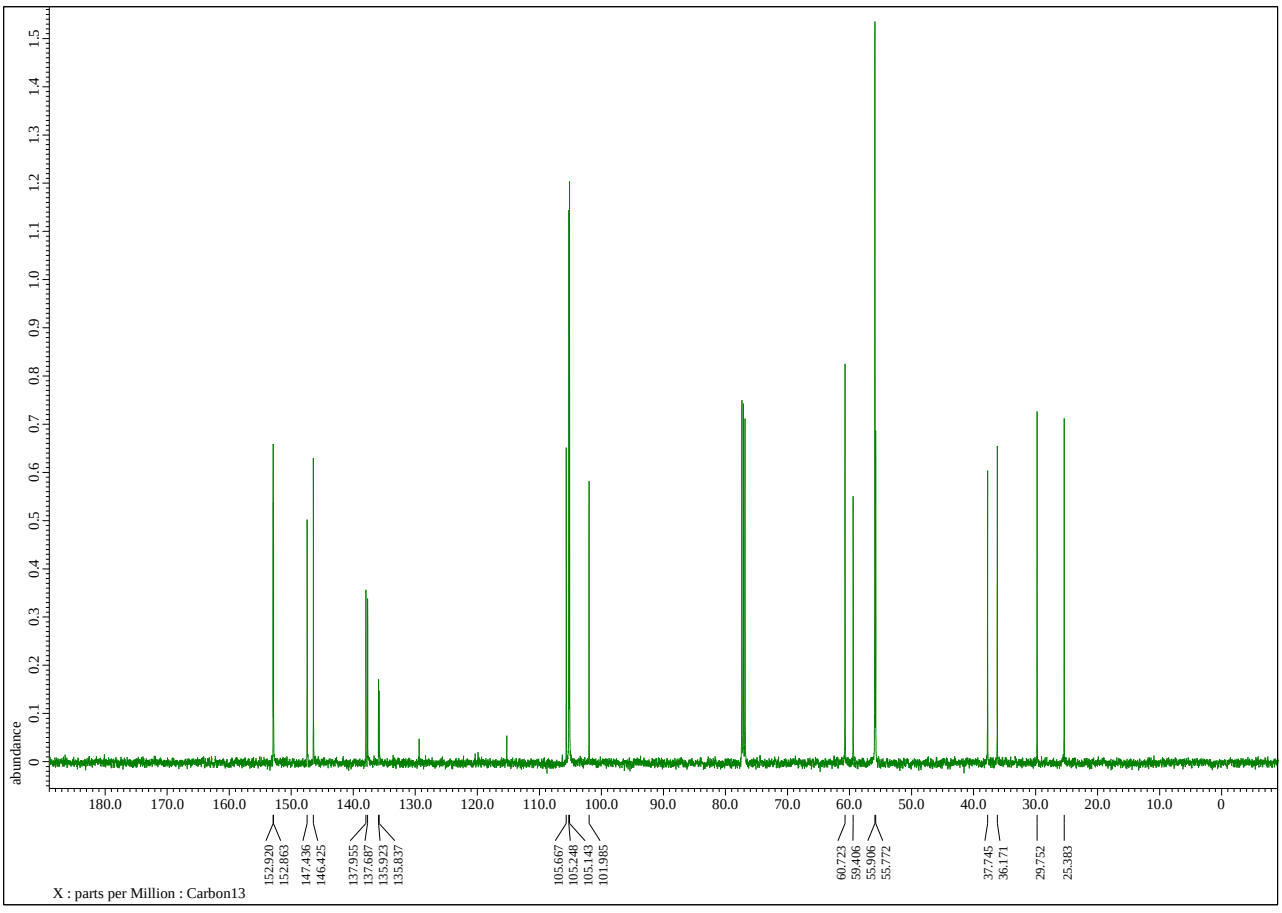
abundance
X : parts per Million : Carbon13

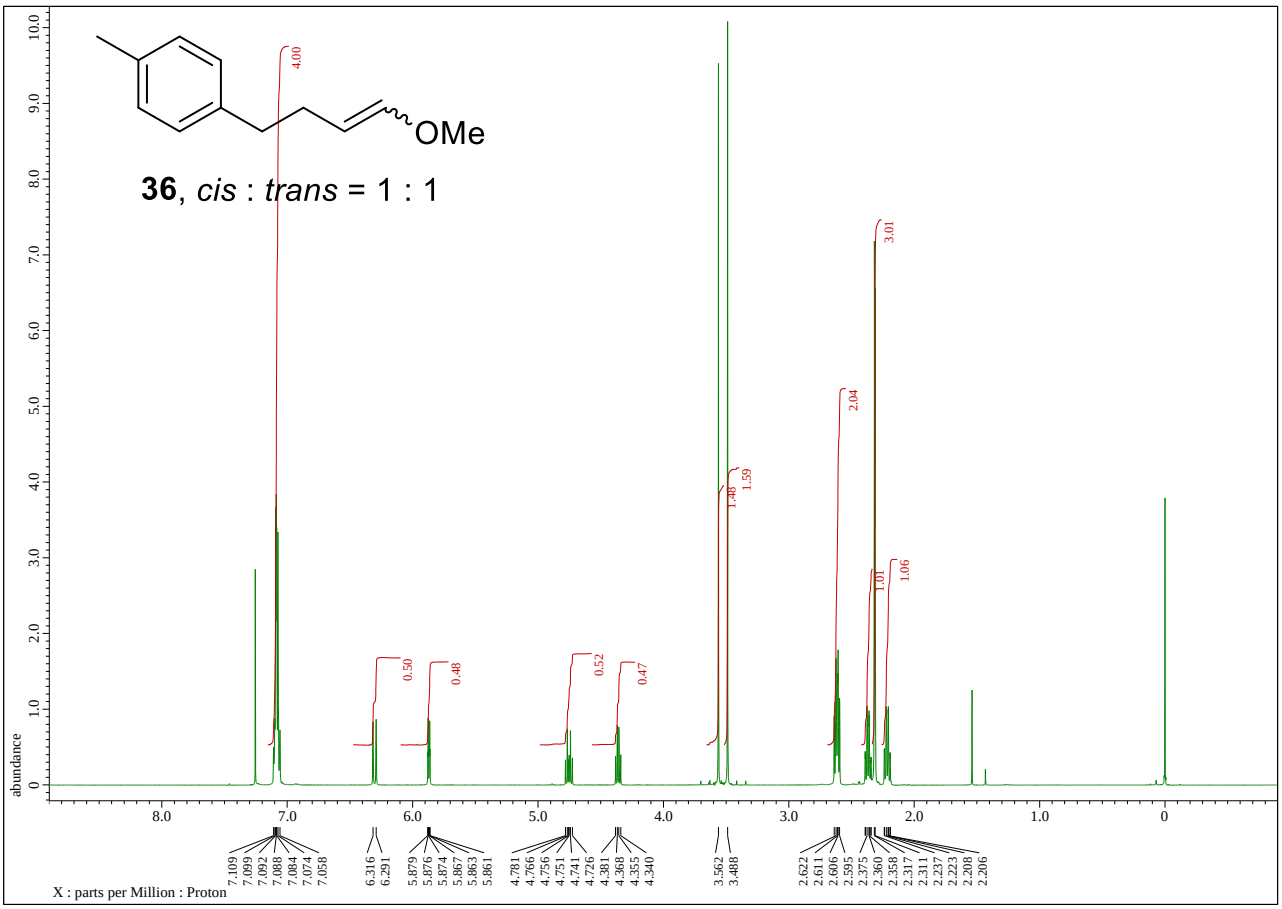
OMe
36, cis : trans = 1 : 1
4.00
3.01
2.04
1.59
1.48
1.06
1.01
0.50
0.48
0.52
0.47
abundance
X : parts per Million : Proton

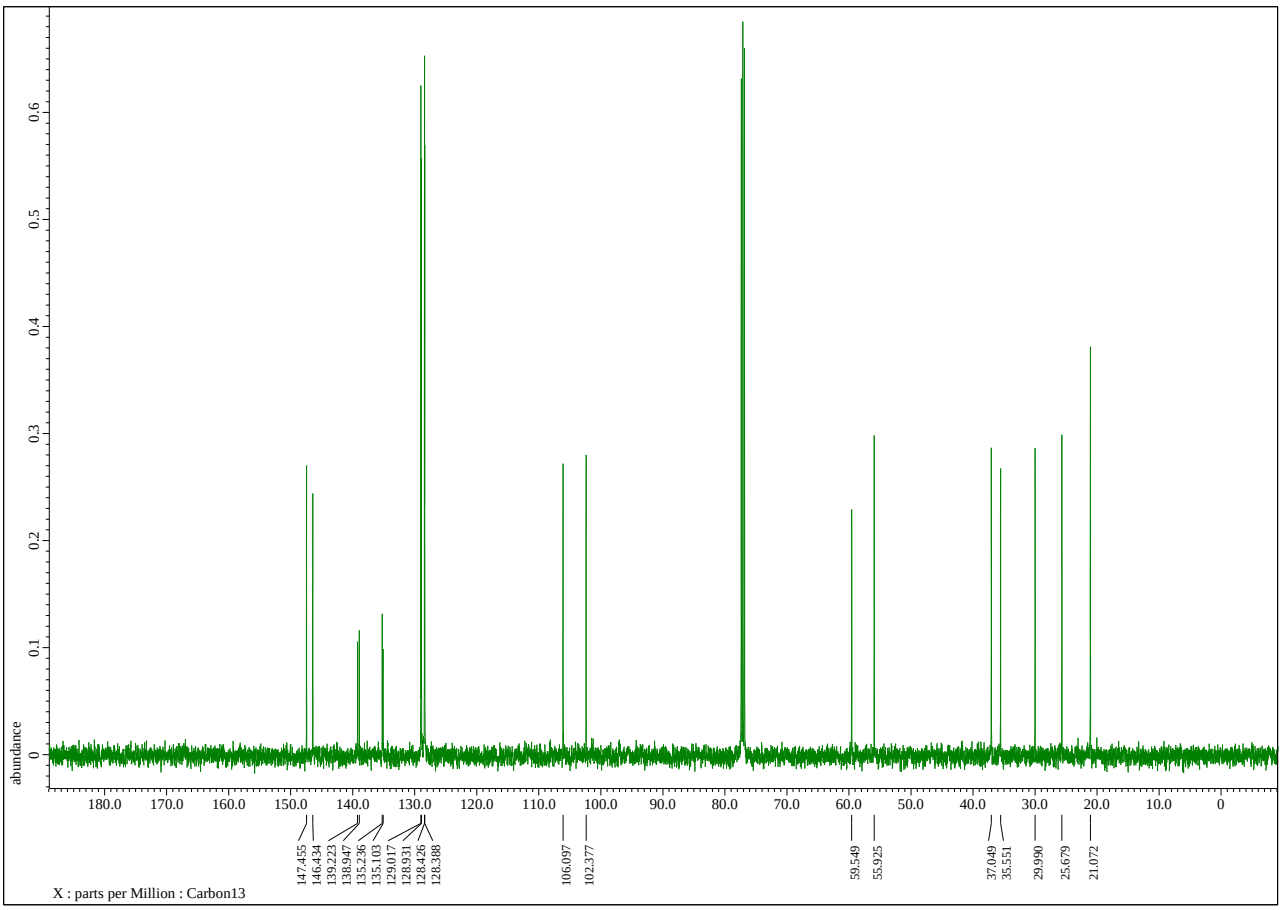
abundance
X : parts per Million : Carbon13

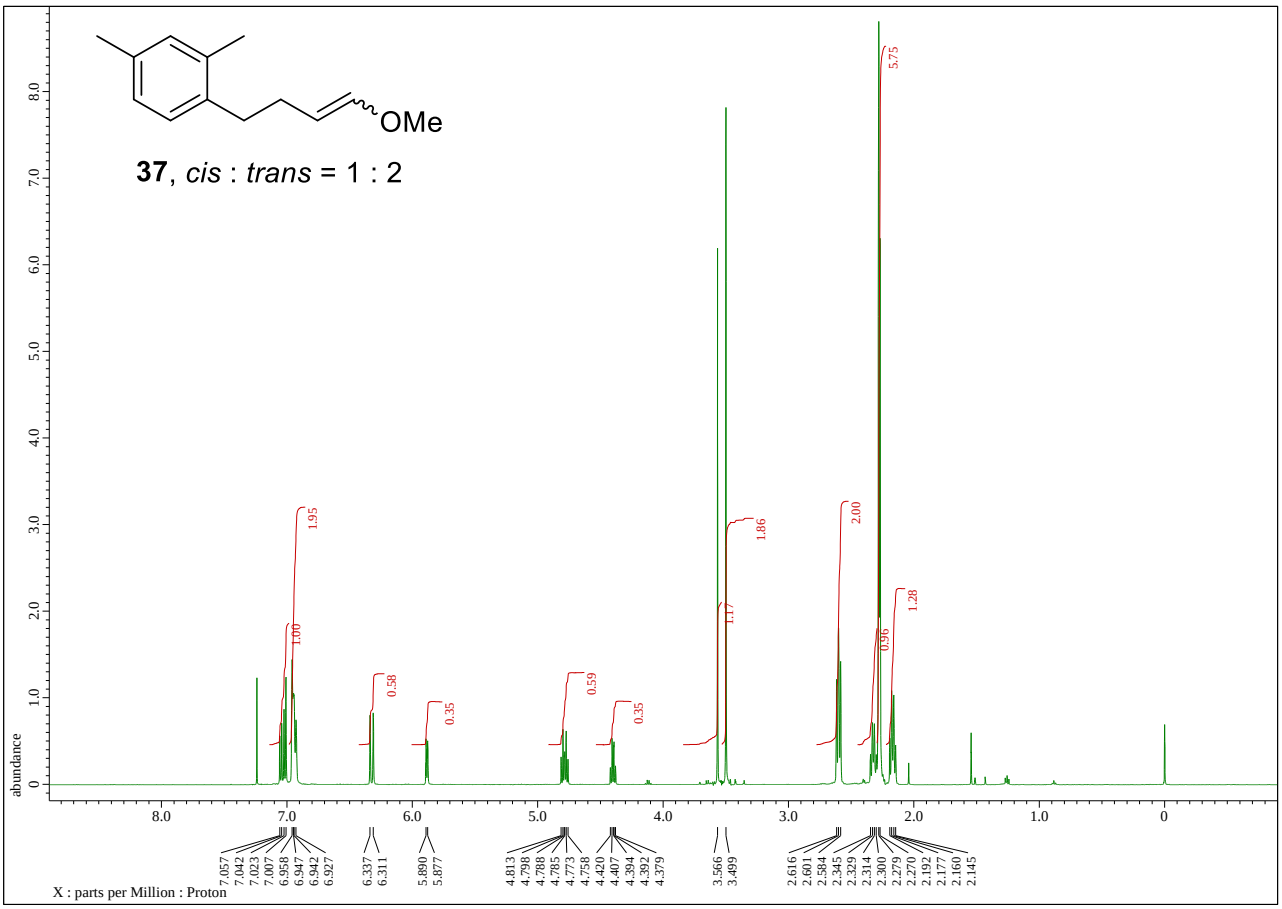
OMe
37, cis : trans = 1 : 2
abundance
X : parts per Million : Proton

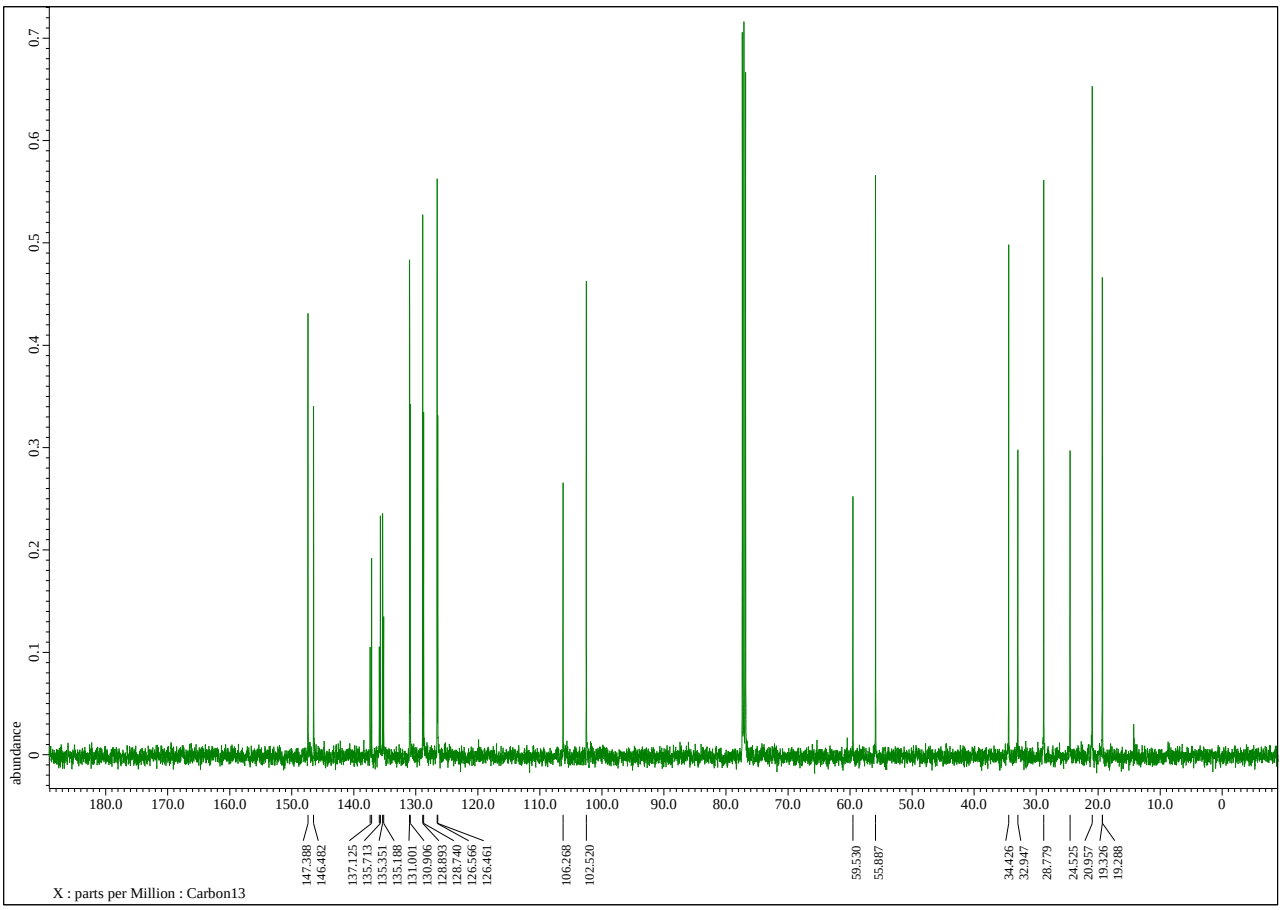
abundance
X : parts per Million : Carbon13

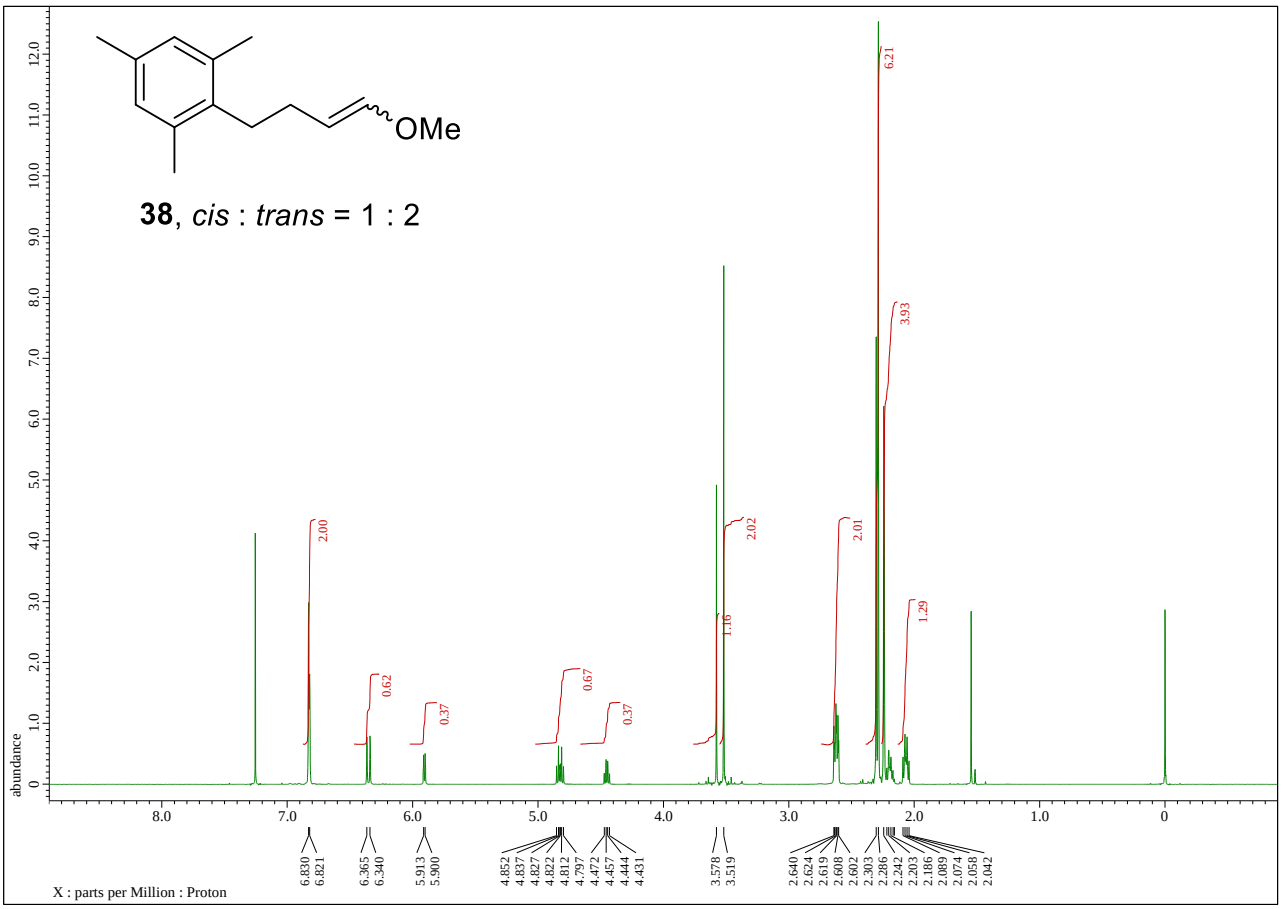
OMe
38, cis : trans = 1 : 2
abundance
X : parts per Million : Proton

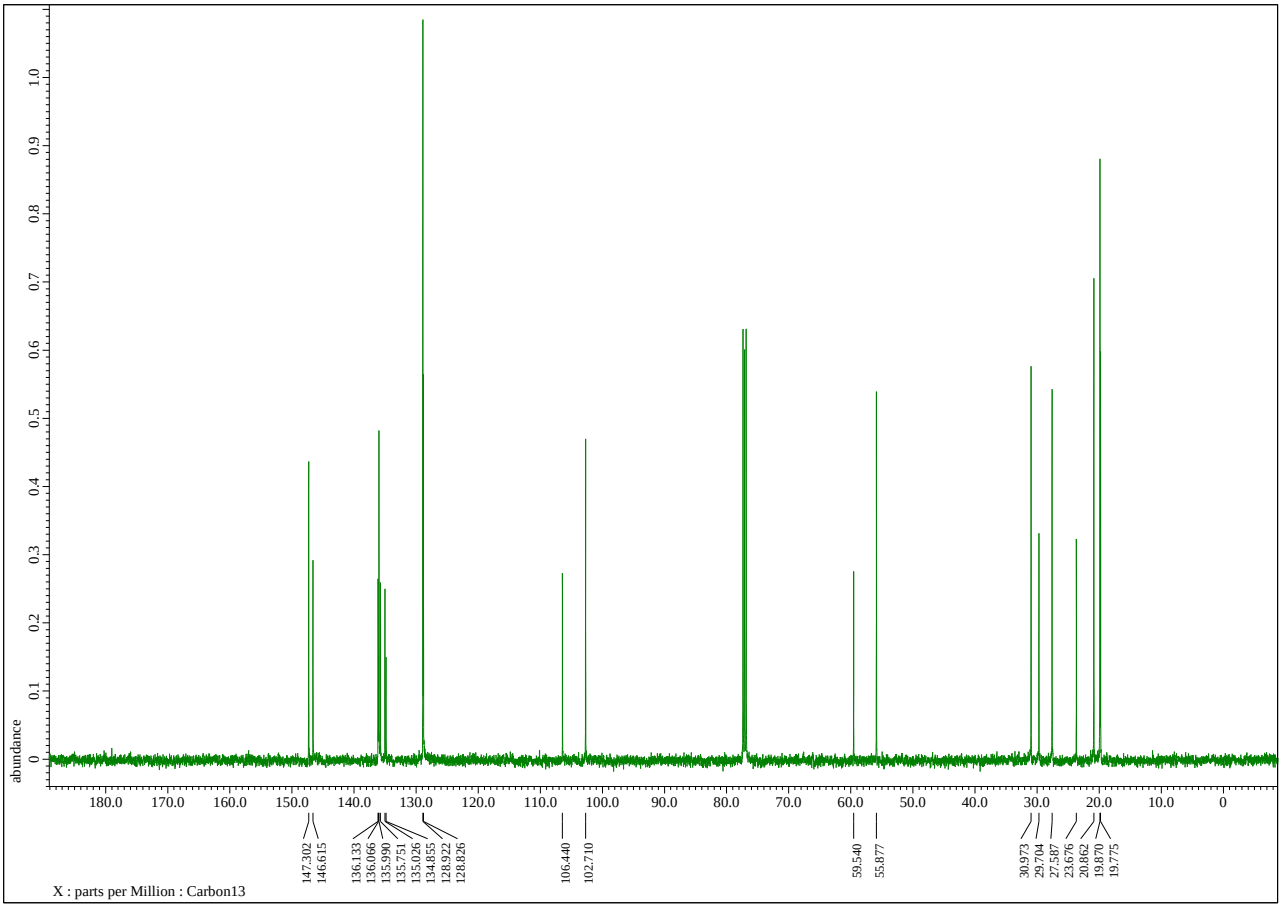
abundance
X : parts per Million : Carbon13

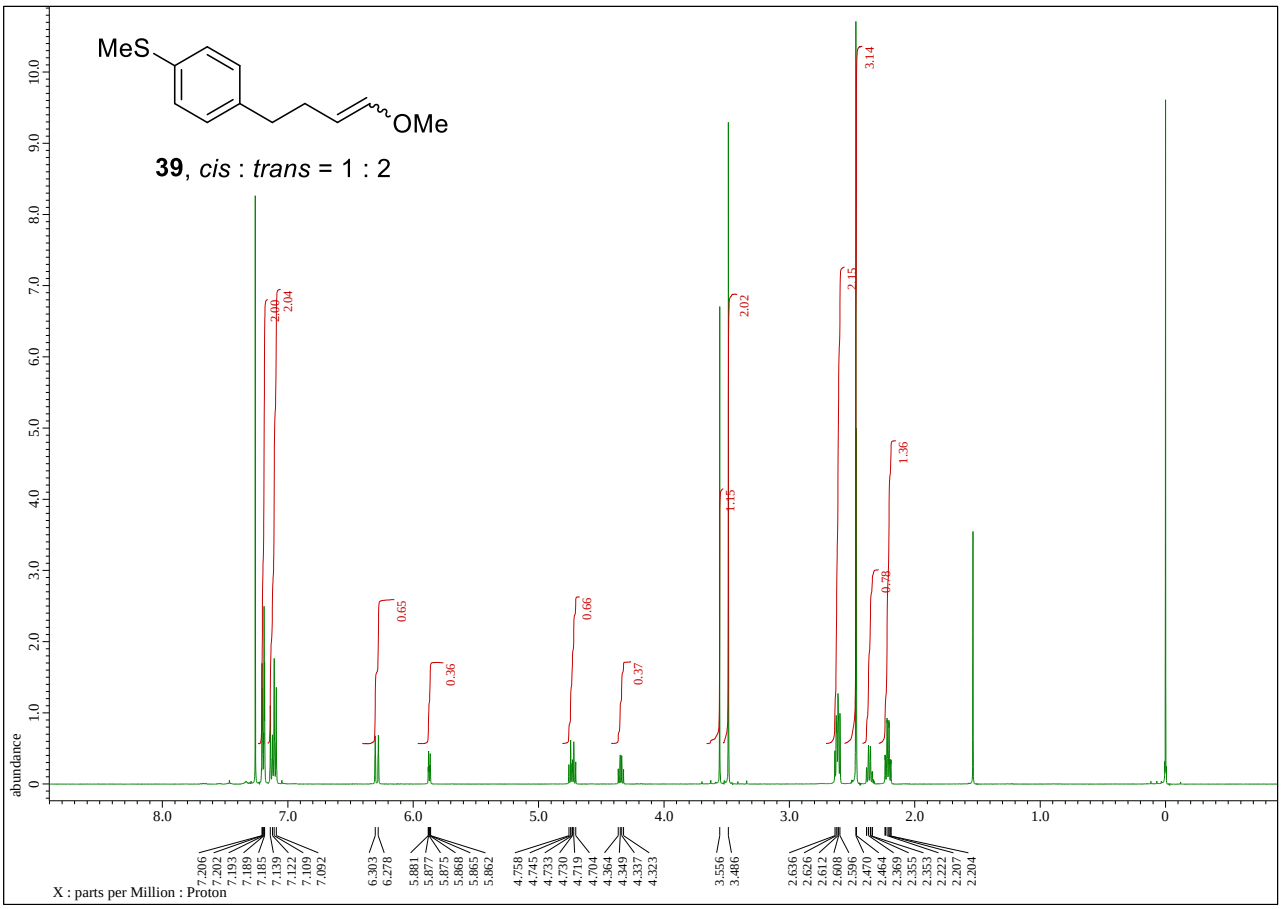
MeS
OMe
39, cis : trans = 1 : 2
abundance
X : parts per Million : Proton

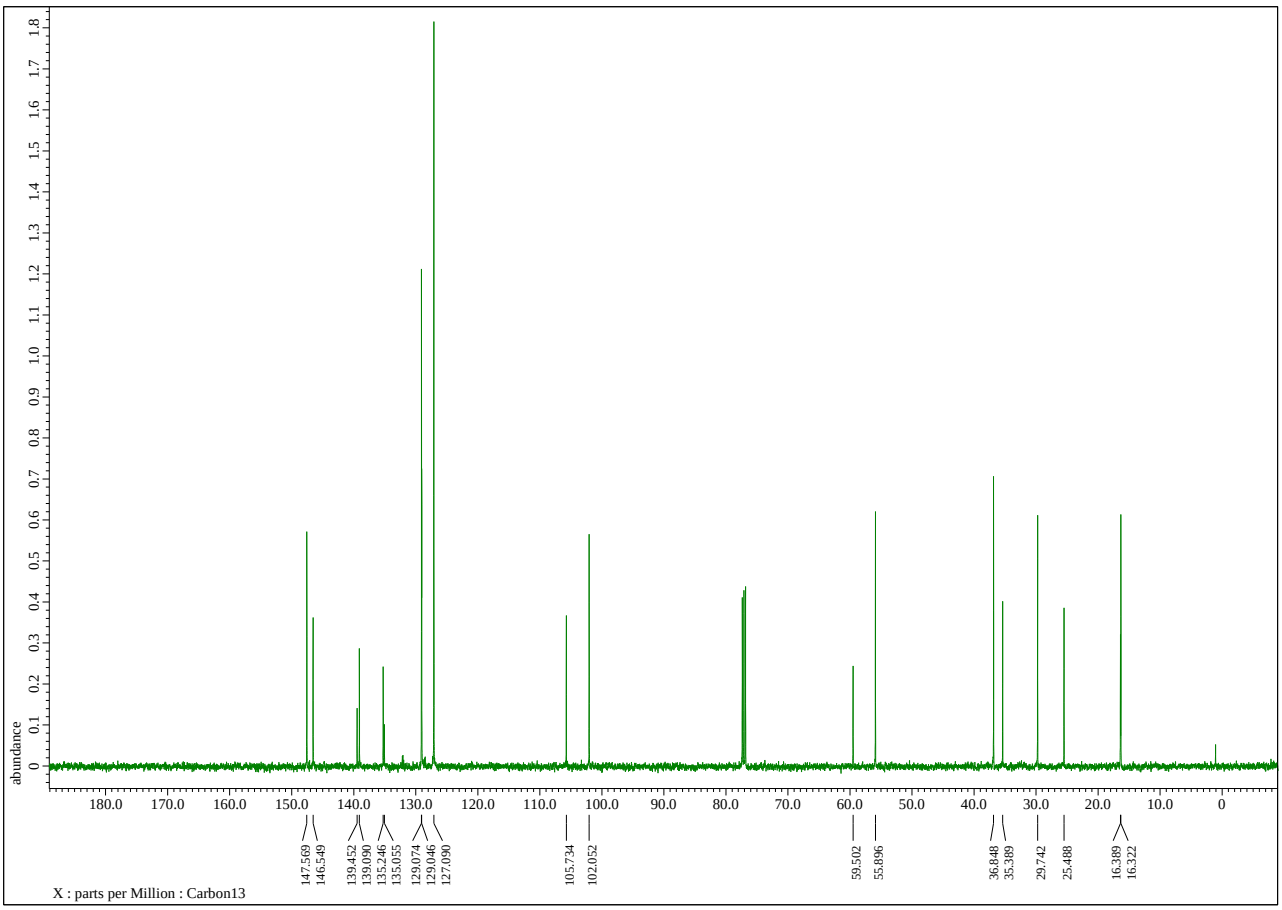
abundance
X : parts per Million : Carbon13

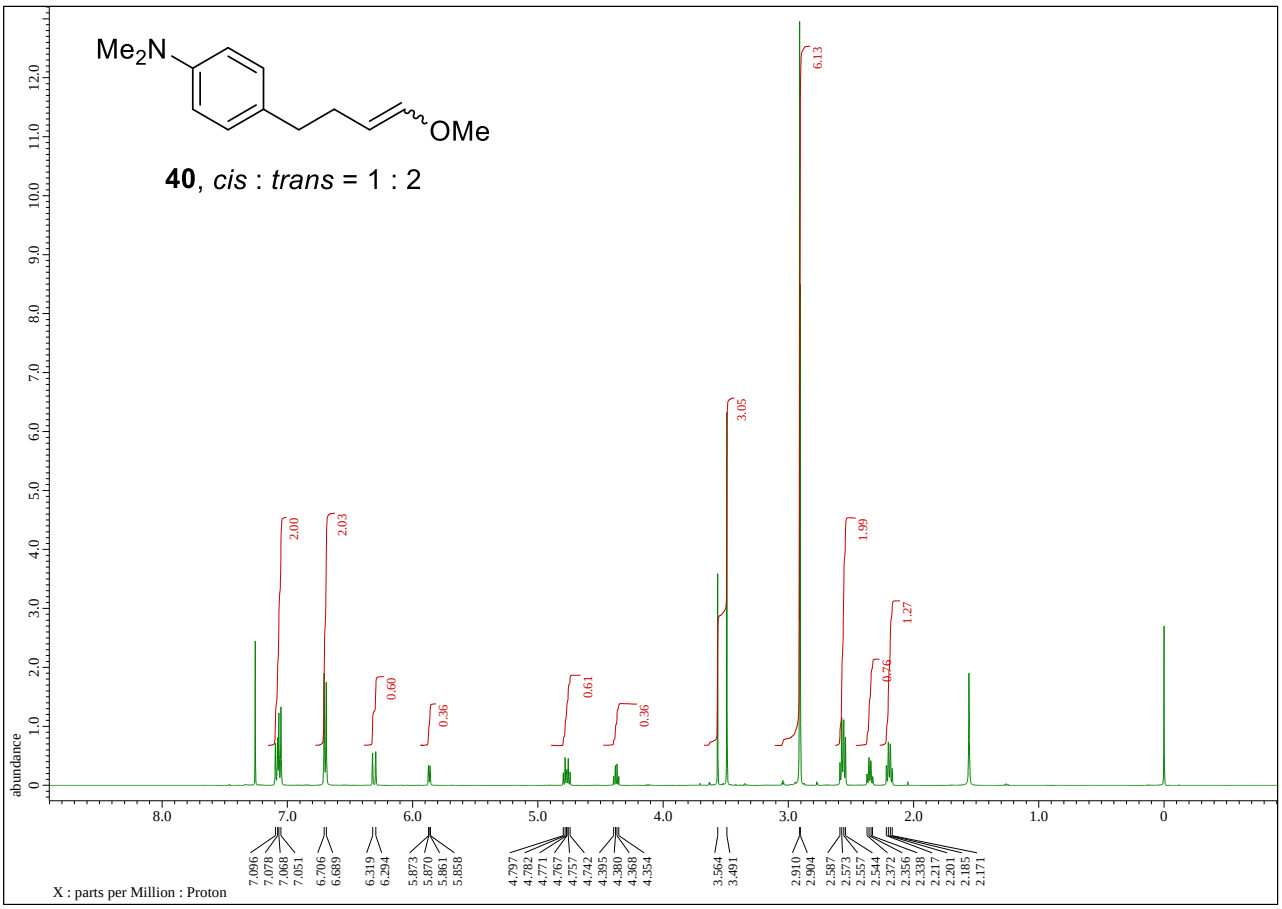
Me2N
OMe
40, cis : trans = 1 : 2
abundance
X : parts per Million : Proton

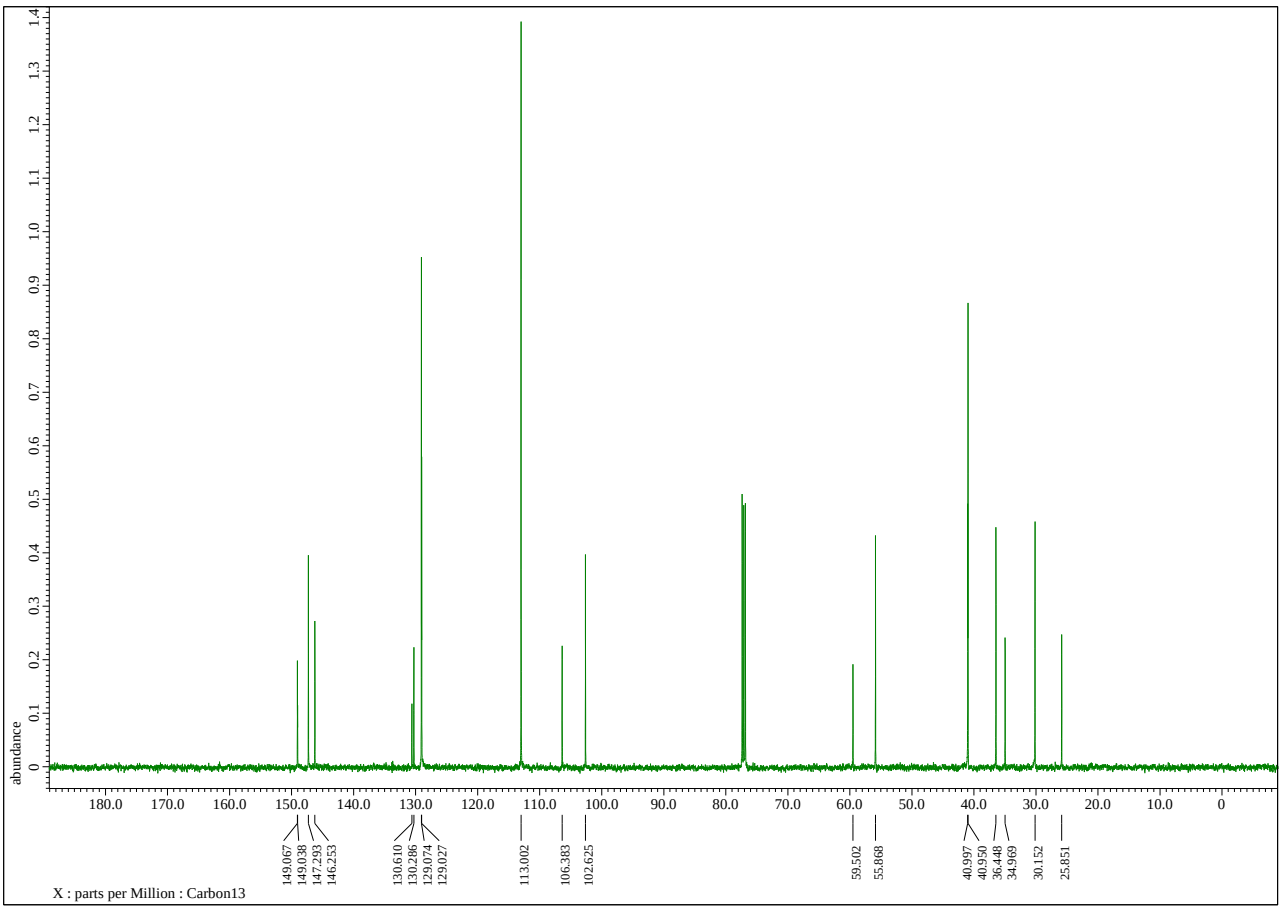
abundance
X : parts per Million : Carbon13

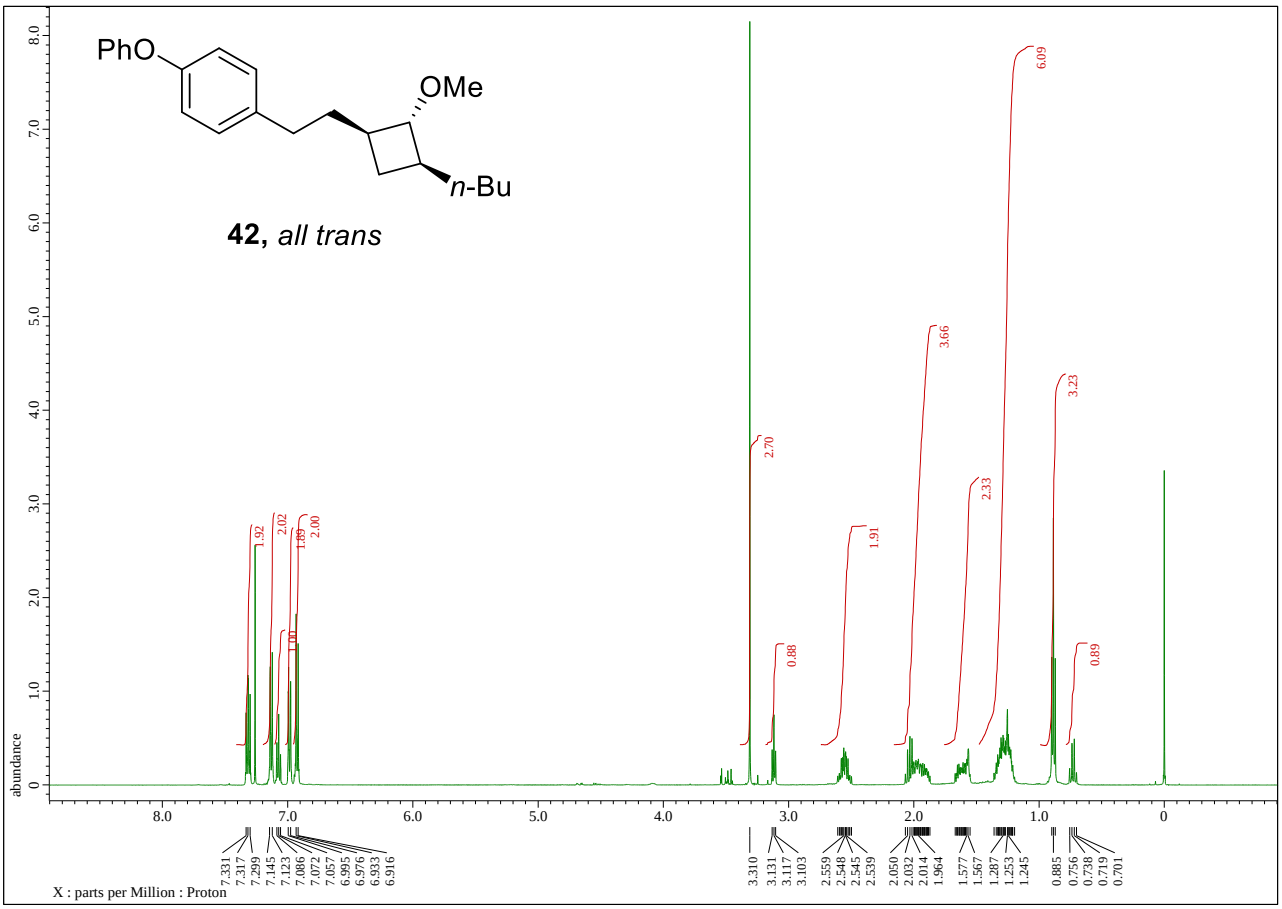
PhO
OMe
n-Bu
42, all trans
abundance
X : parts per Million : Proton

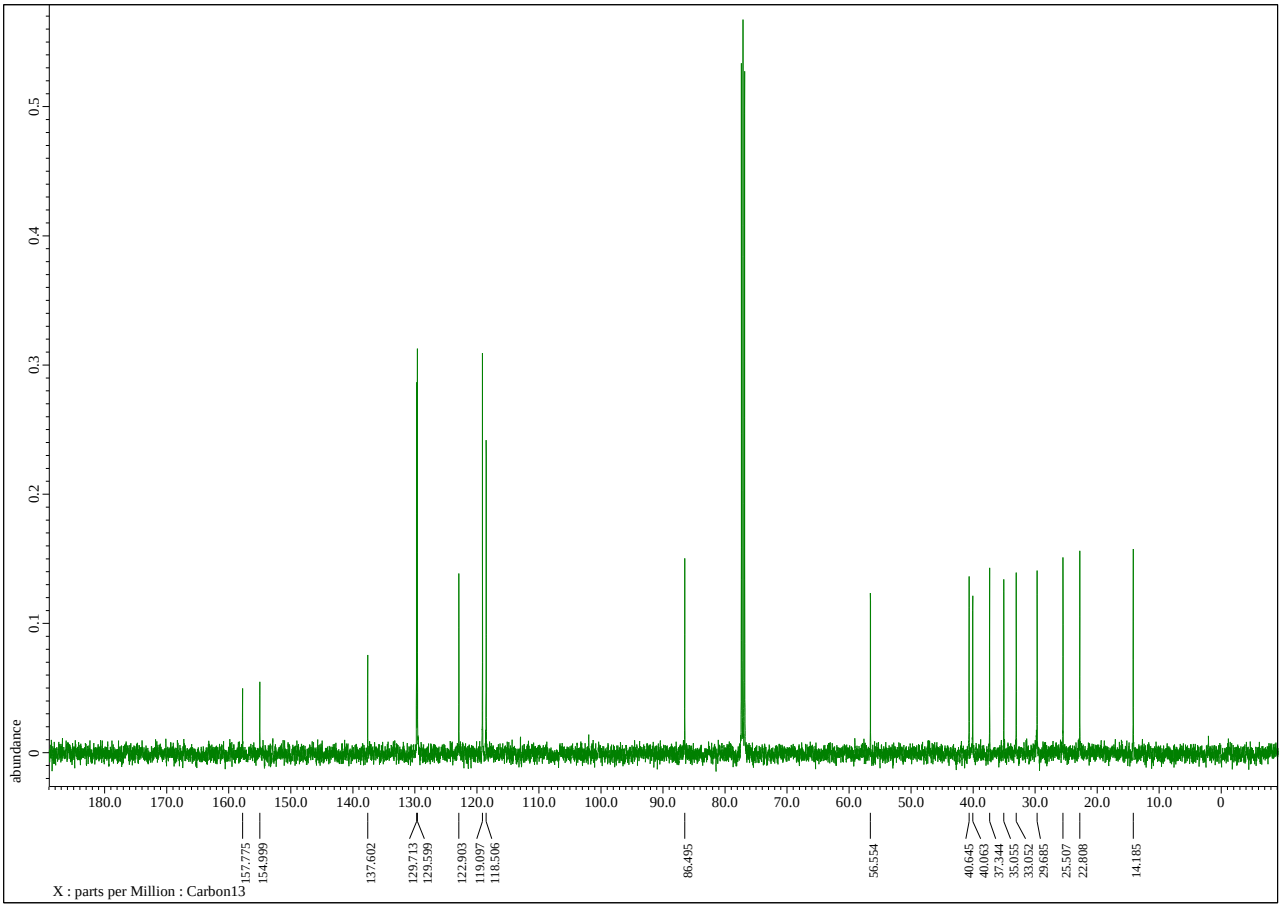
abundance
X : parts per Million : Carbon13

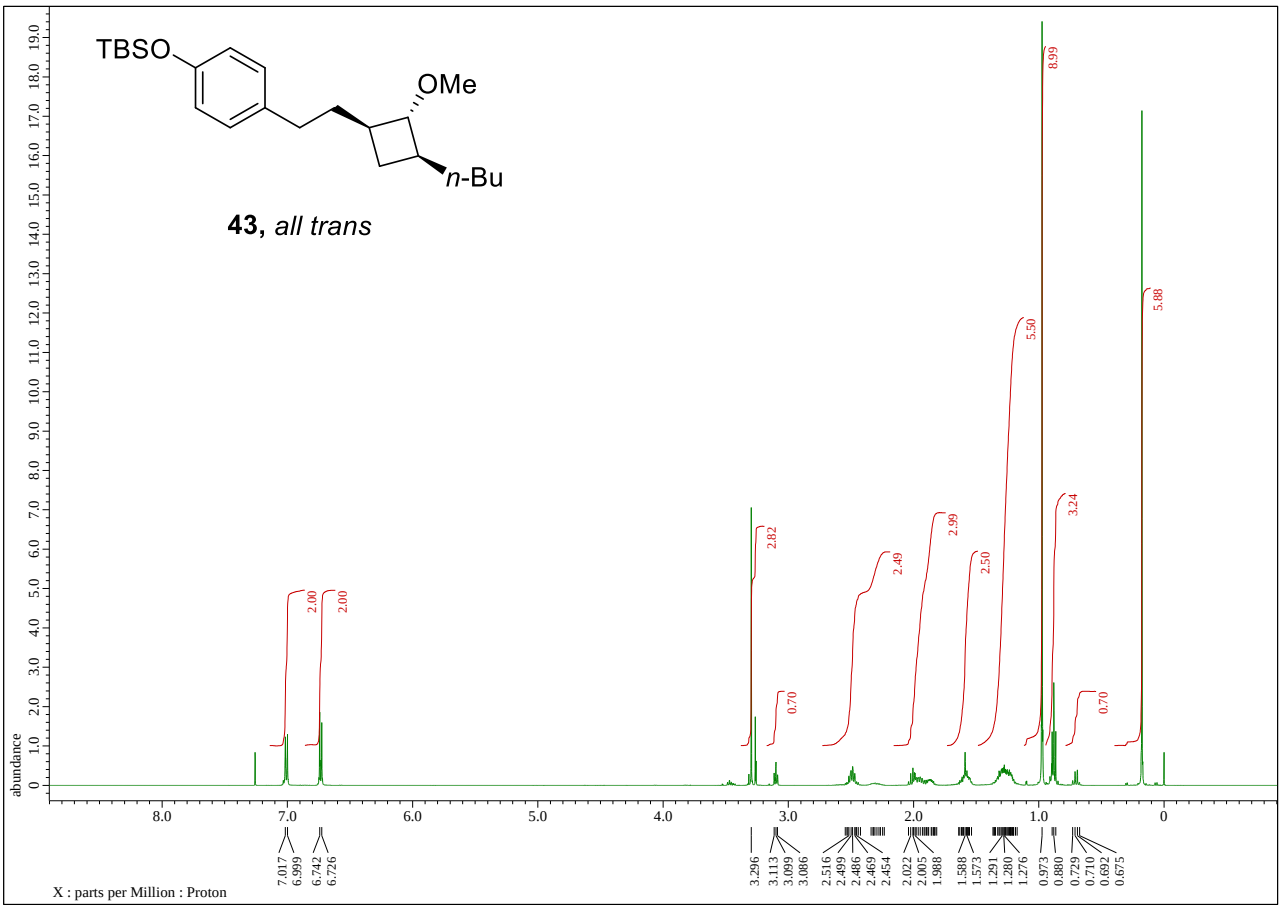
TBSO
OMe
n-Bu
43, all trans
abundance
X : parts per Million : Proton

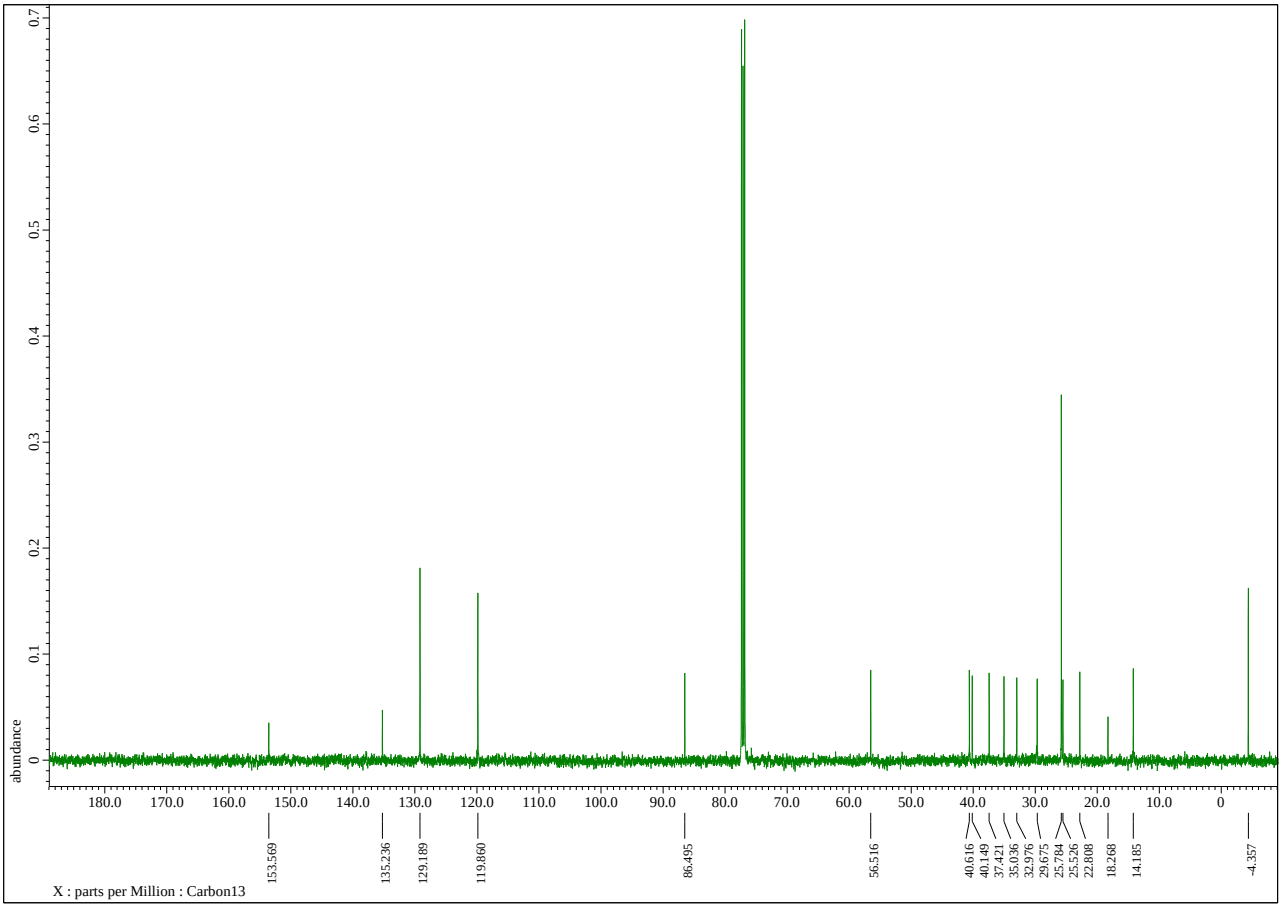
abundance
X : parts per Million : Carbon13

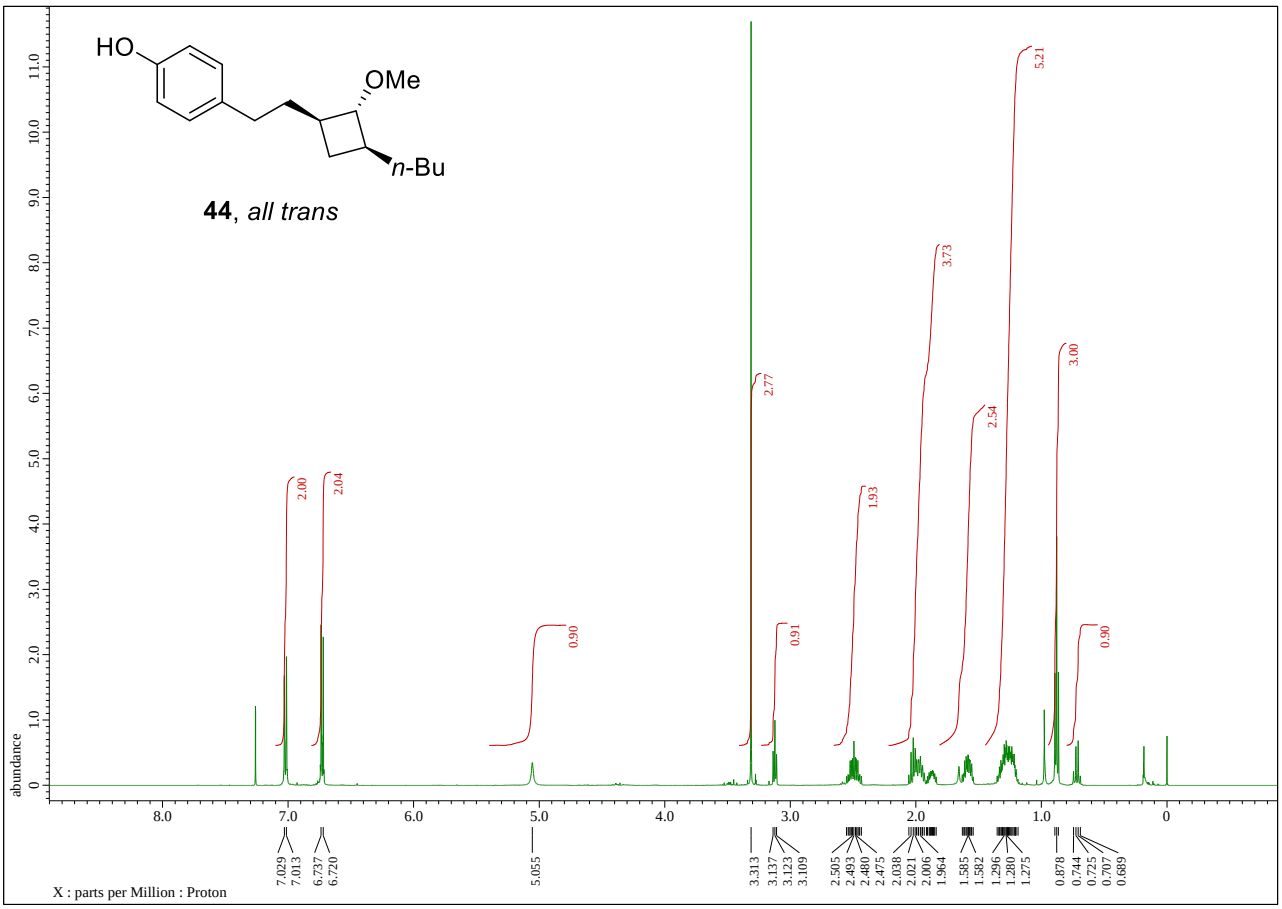
HO
OMe
n-Bu
44, all trans
abundance
X : parts per Million : Proton

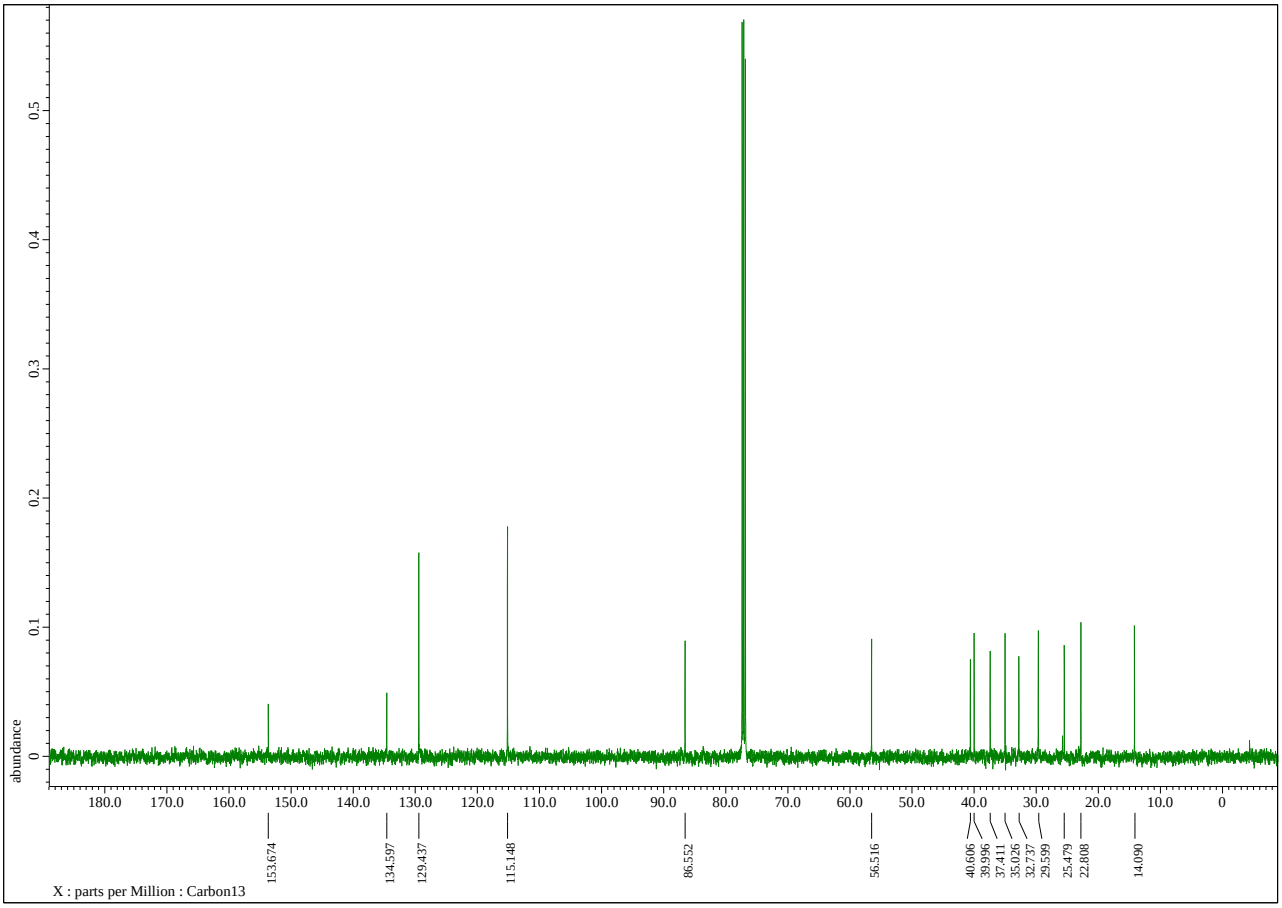
abundance
X : parts per Million : Carbon13

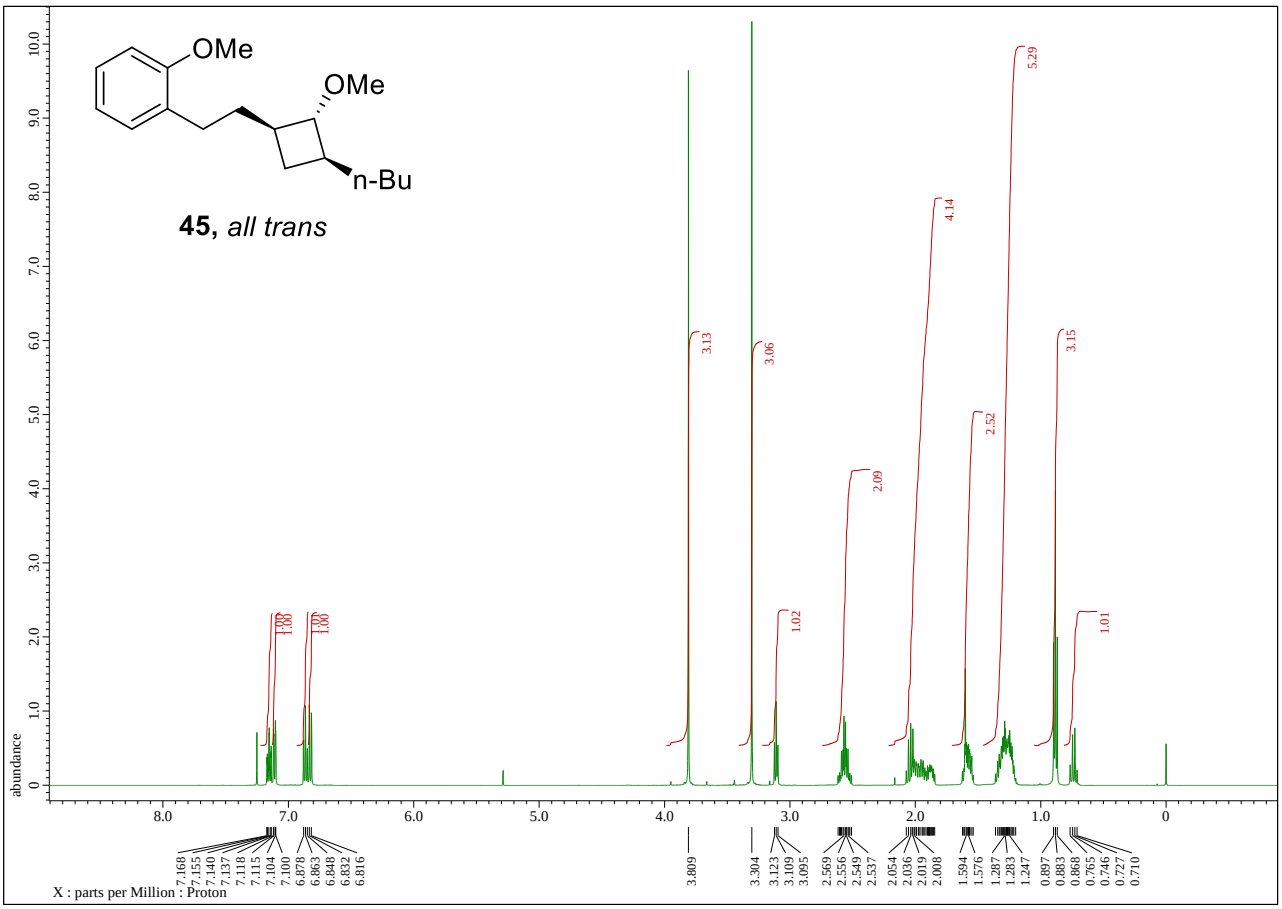
OMe
OMe
n-Bu
45, all trans
abundance
X : parts per Million : Proton

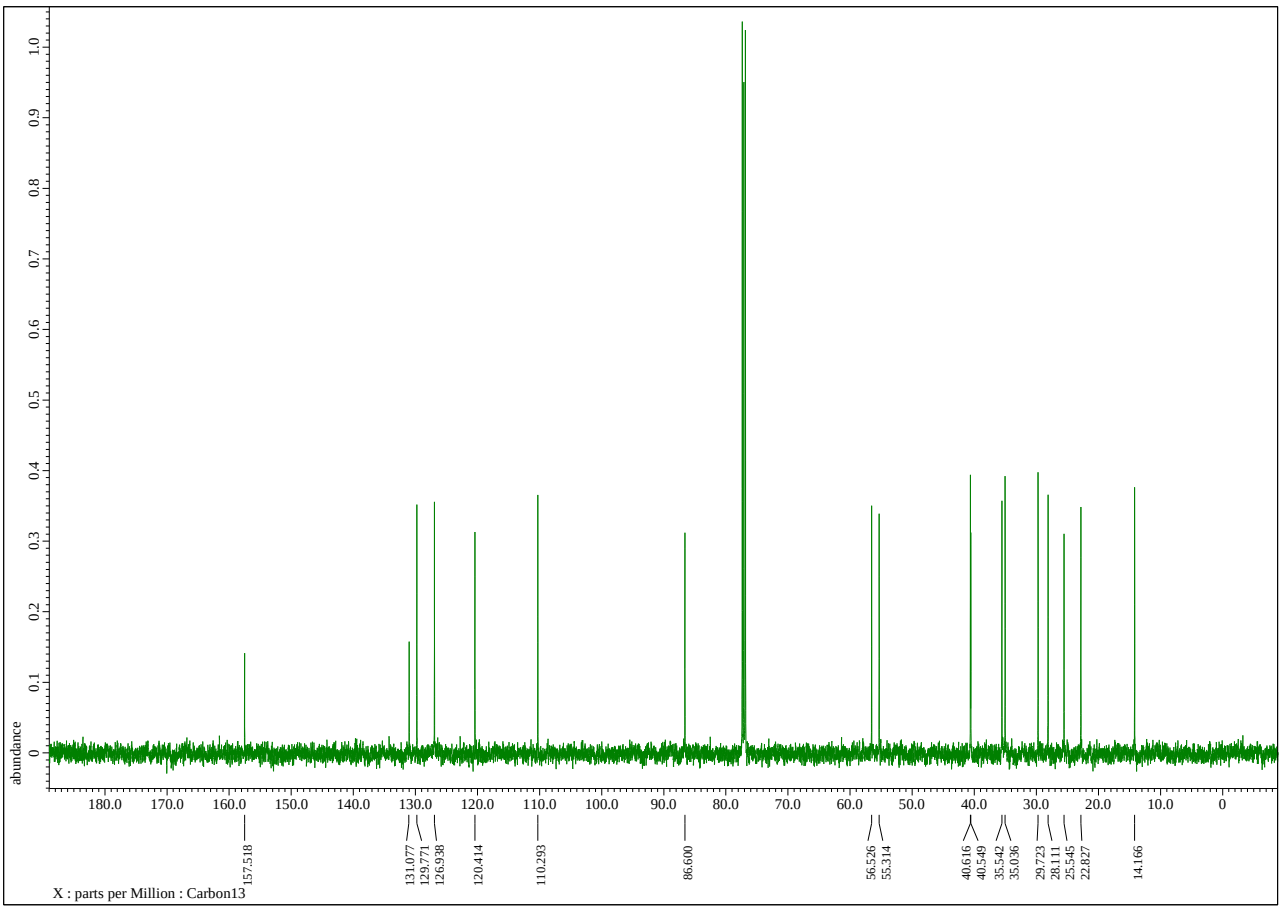
abundance
X : parts per Million : Carbon13

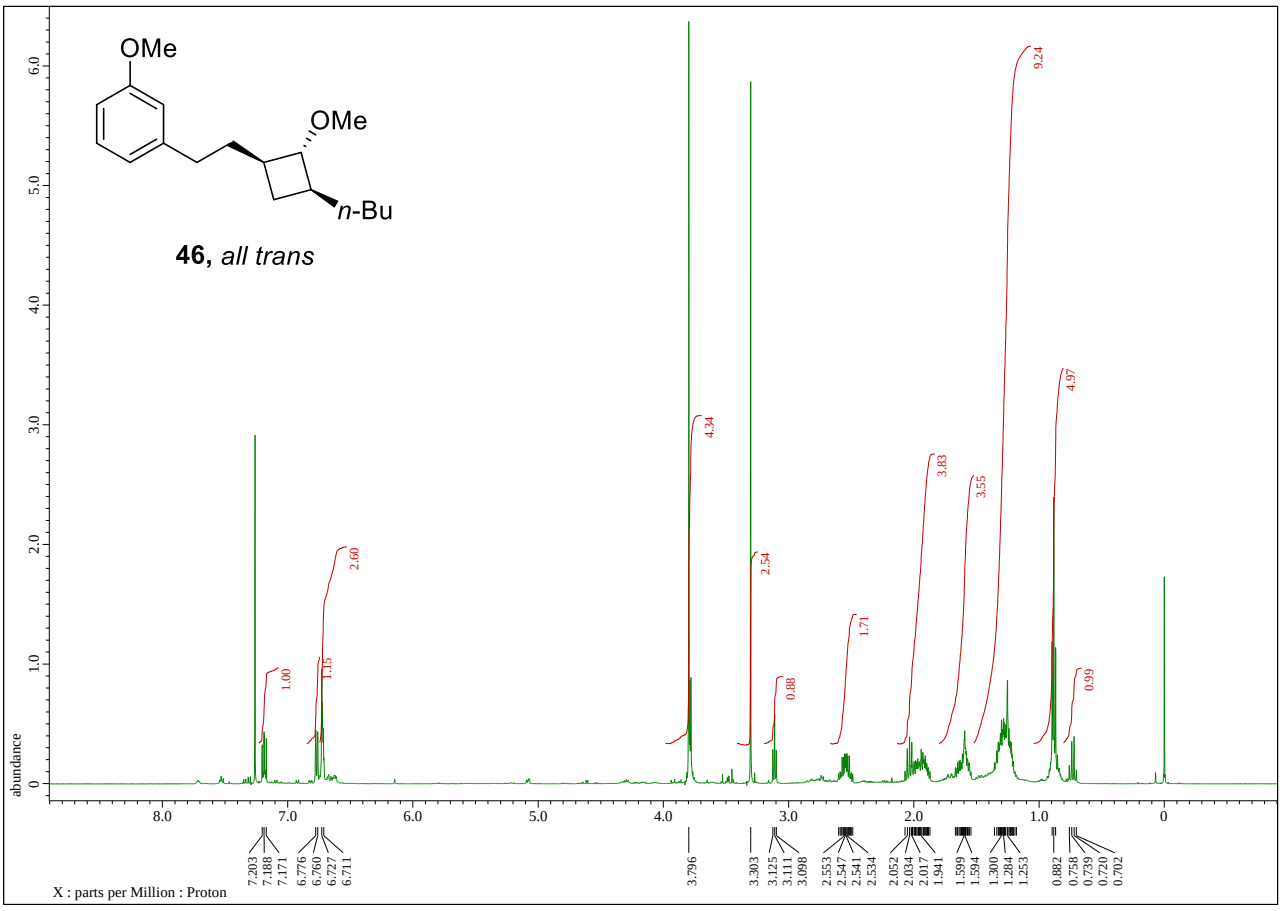
OMe
OMe
n-Bu
46, all trans
abundance
X : parts per Million : Proton
9.24
4.97
4.34
3.83
3.55
2.60
2.54
1.71
1.00
1.15
0.88
0.99

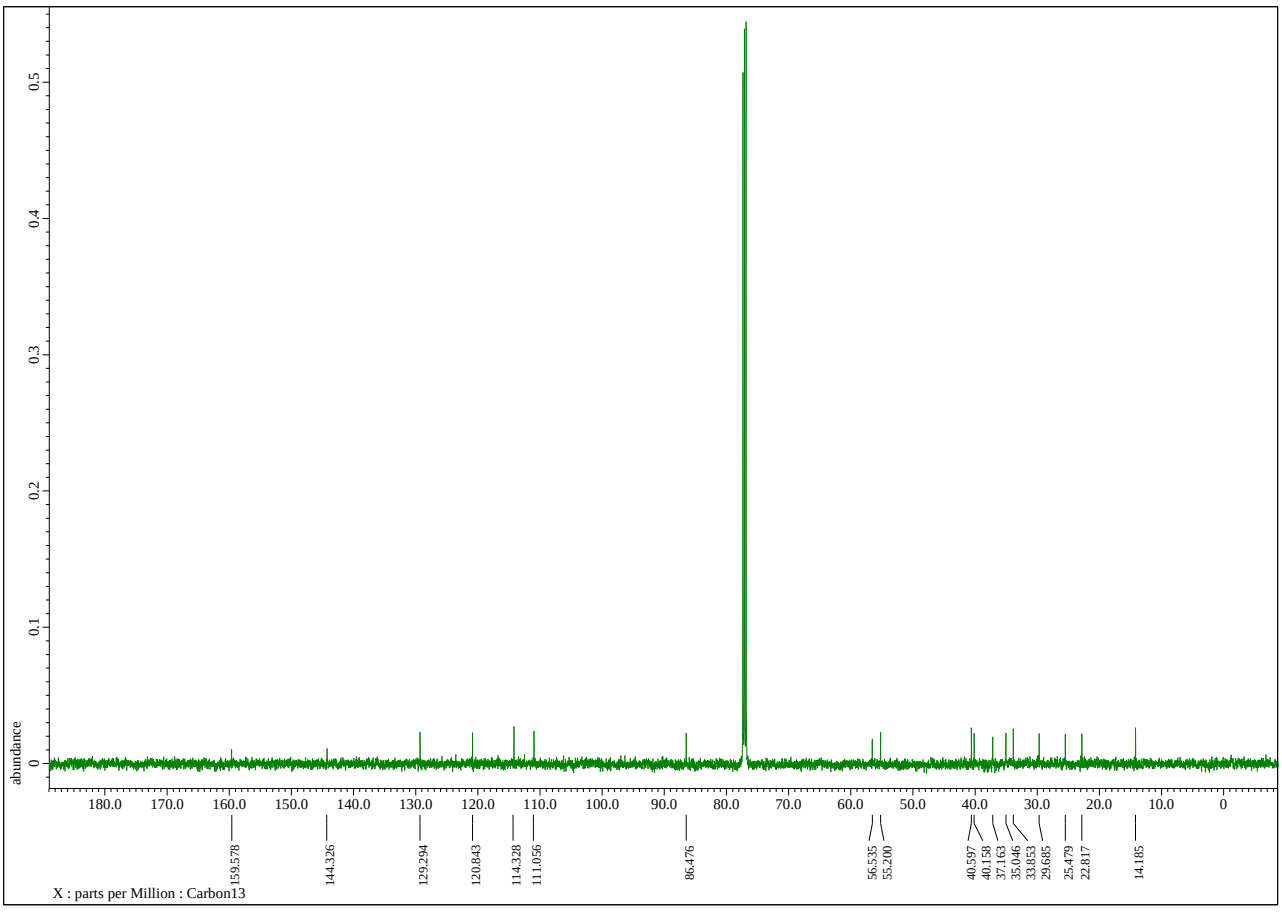
abundance
X : parts per Million : Carbon13

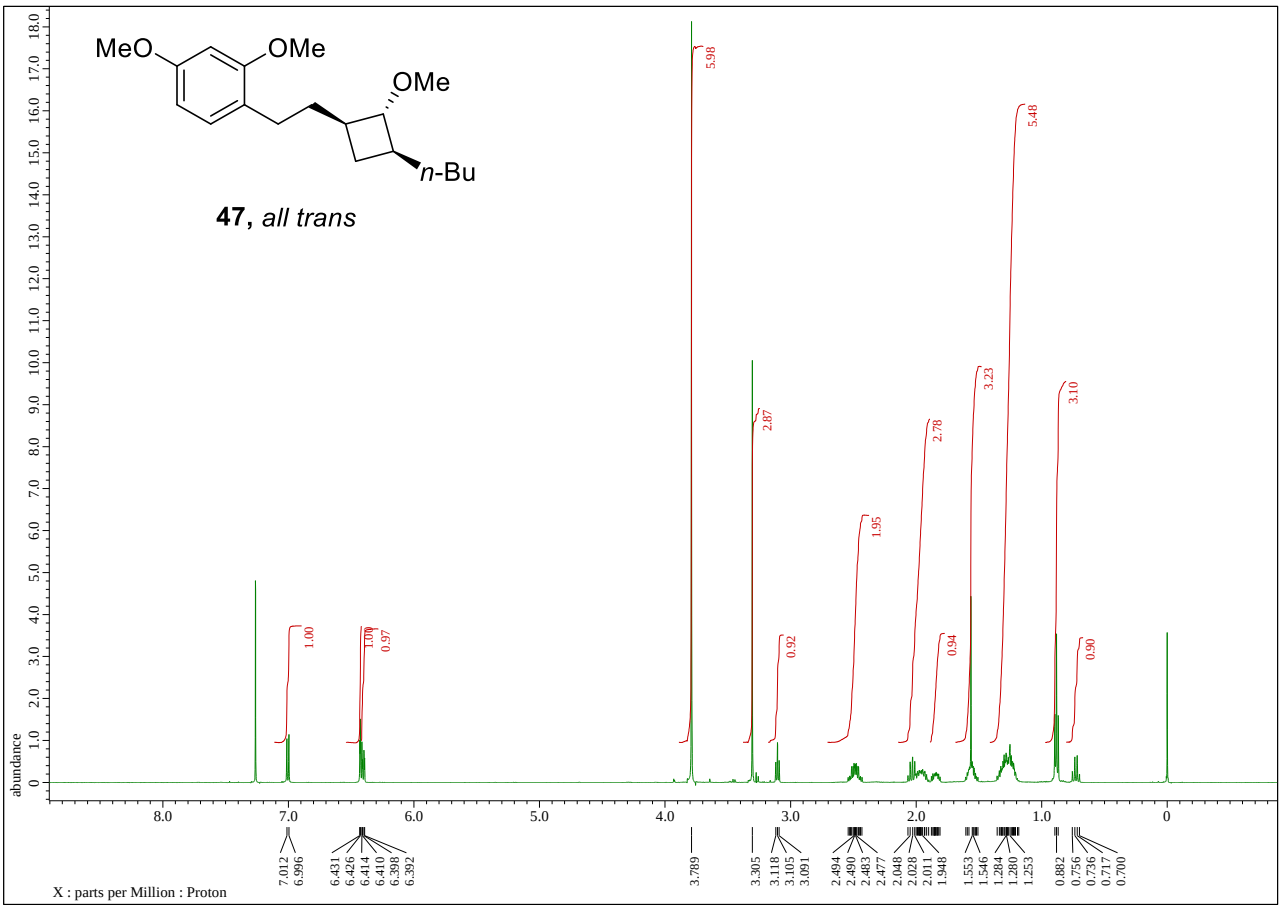
MeO
OMe
OMe
n-Bu
47, all trans
abundance
X : parts per Million : Proton

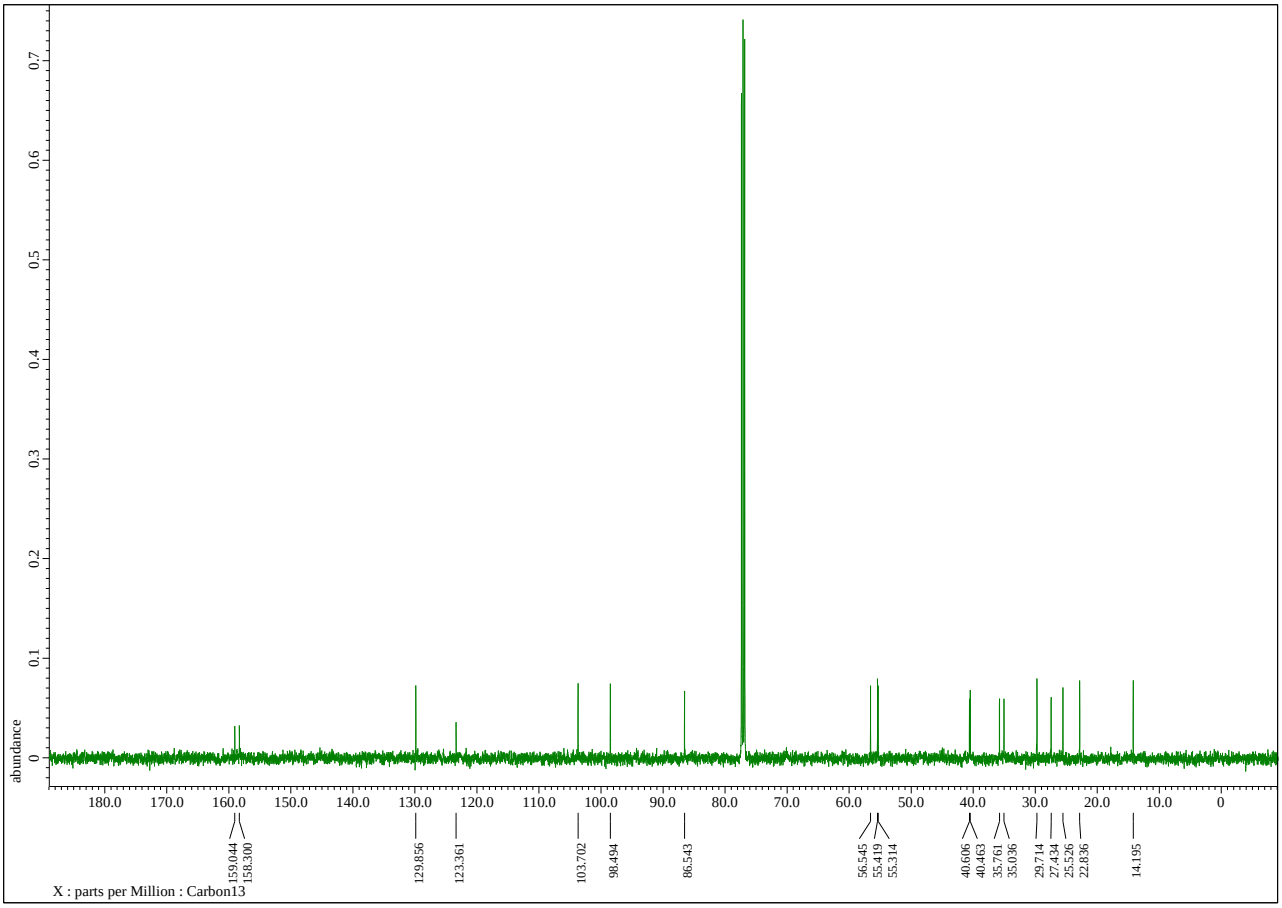
abundance
X : parts per Million : Carbon13

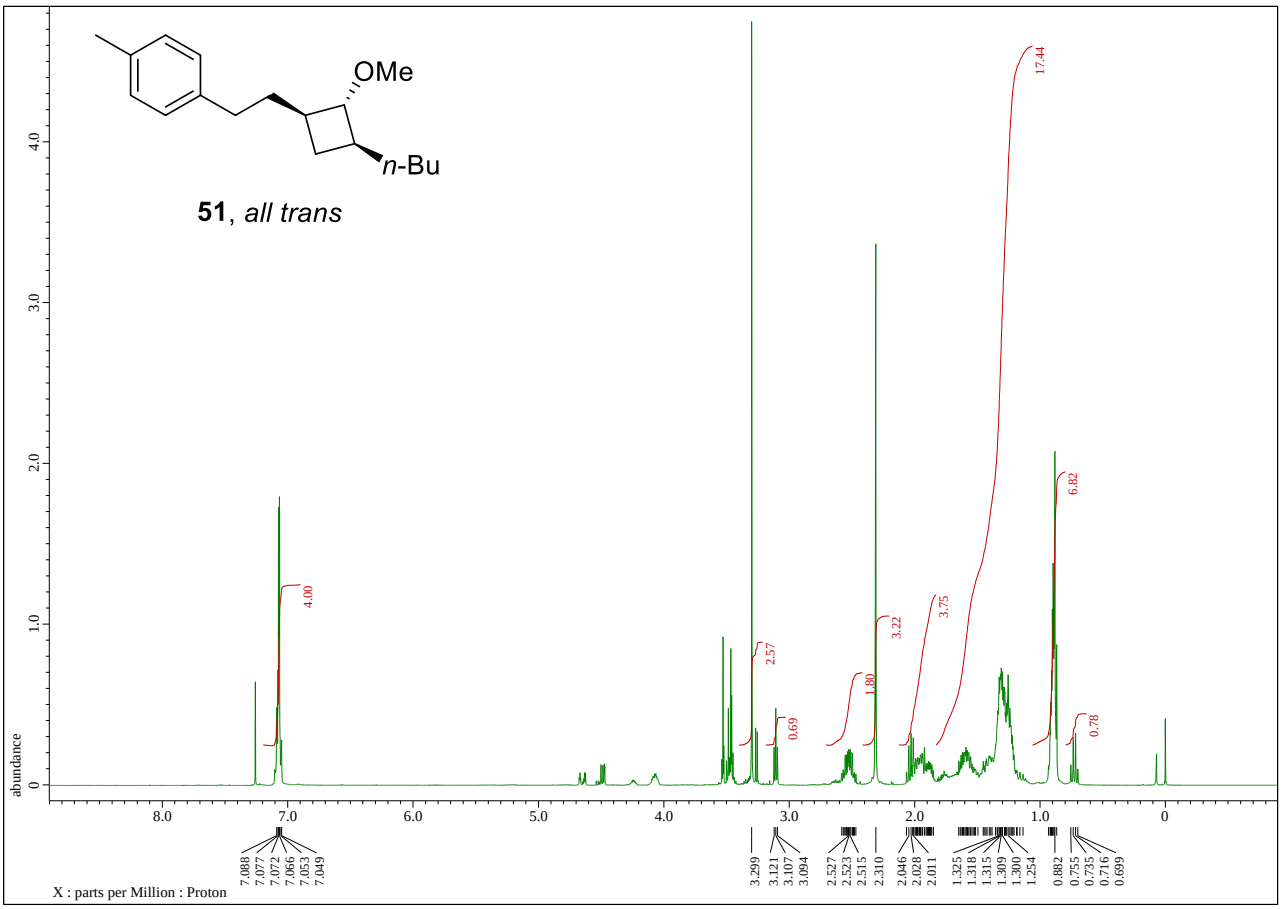
OMe
n-Bu
51, all trans
abundance
X : parts per Million : Proton

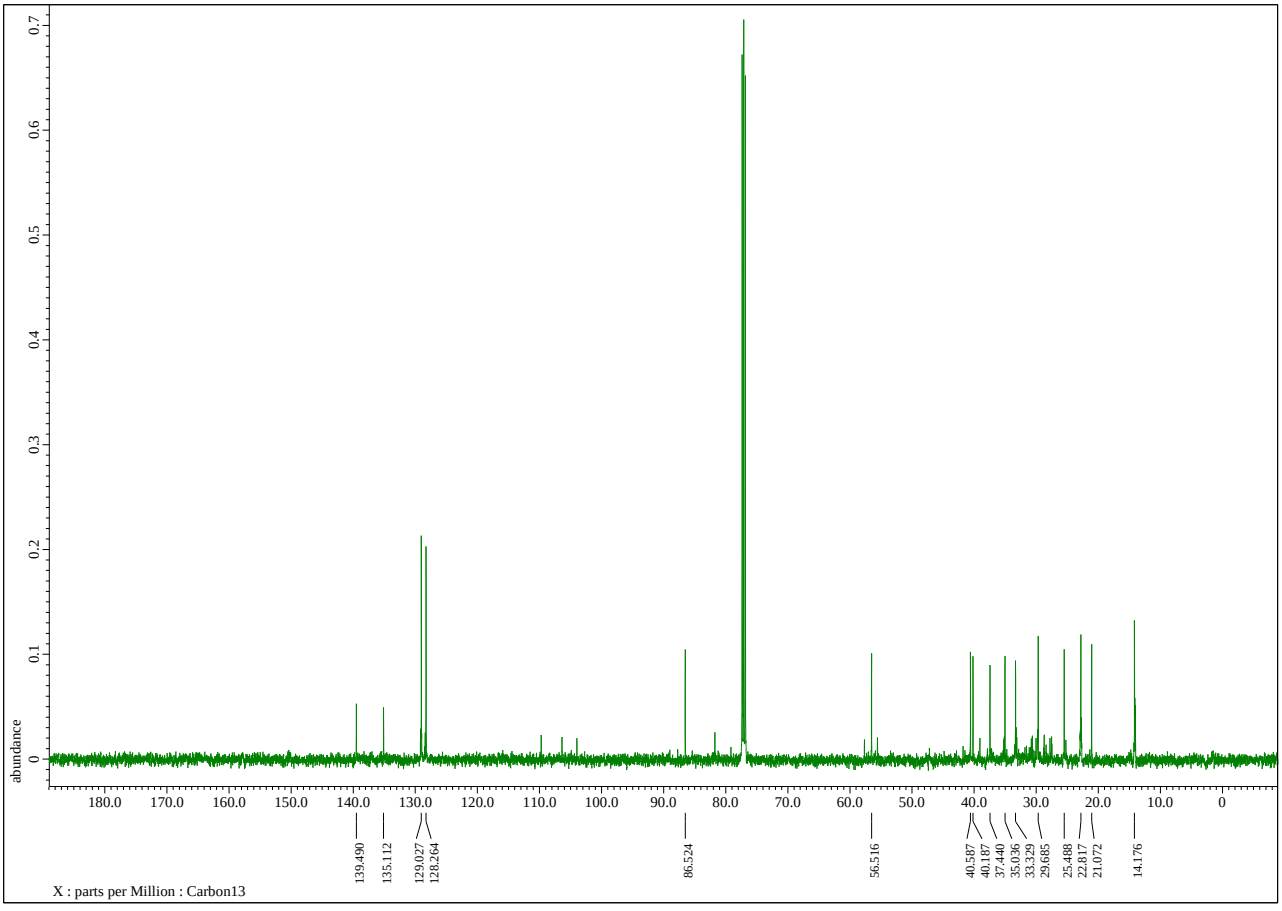
abundance
X : parts per Million : Carbon13

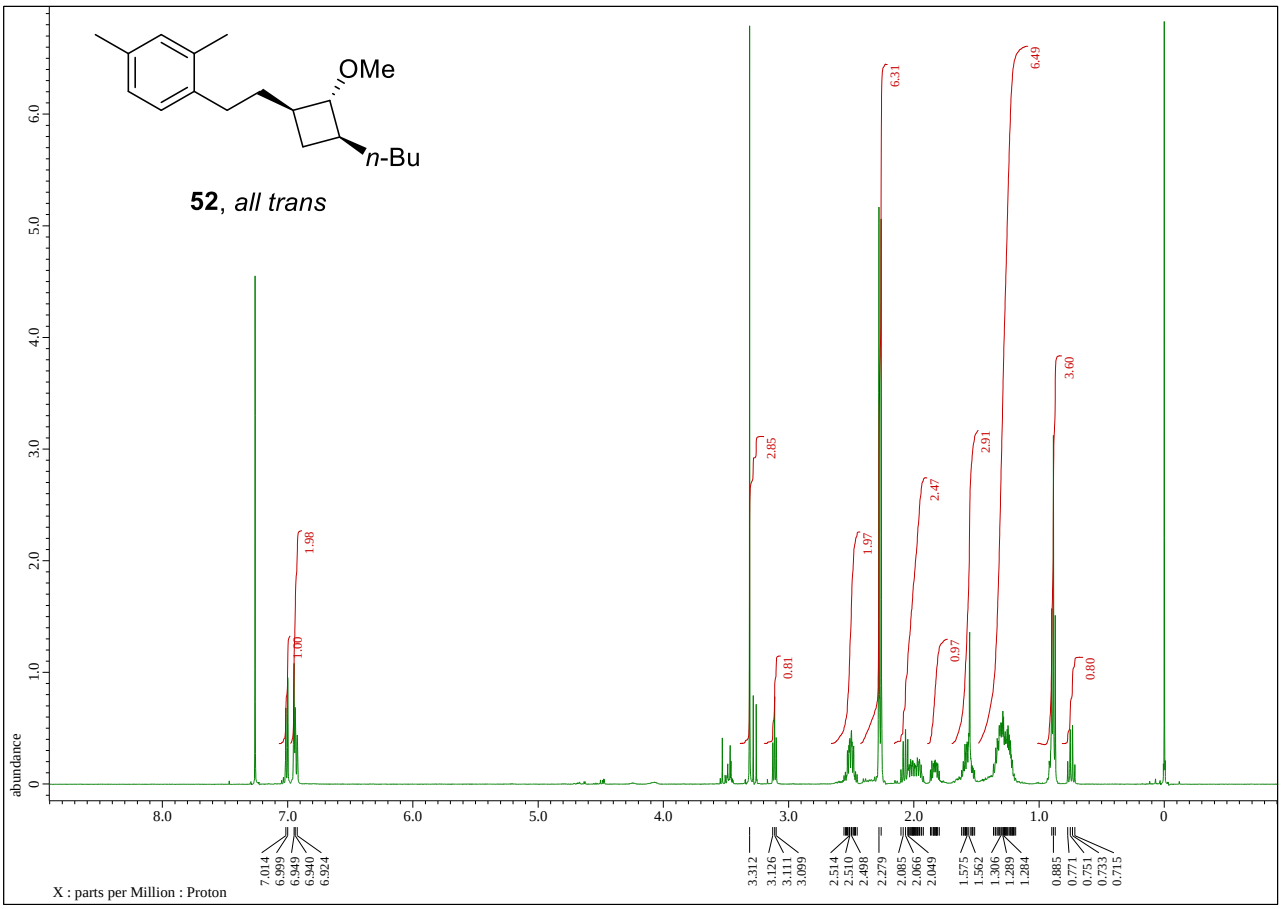
OMe
n-Bu
52, all trans
abundance
X : parts per Million : Proton

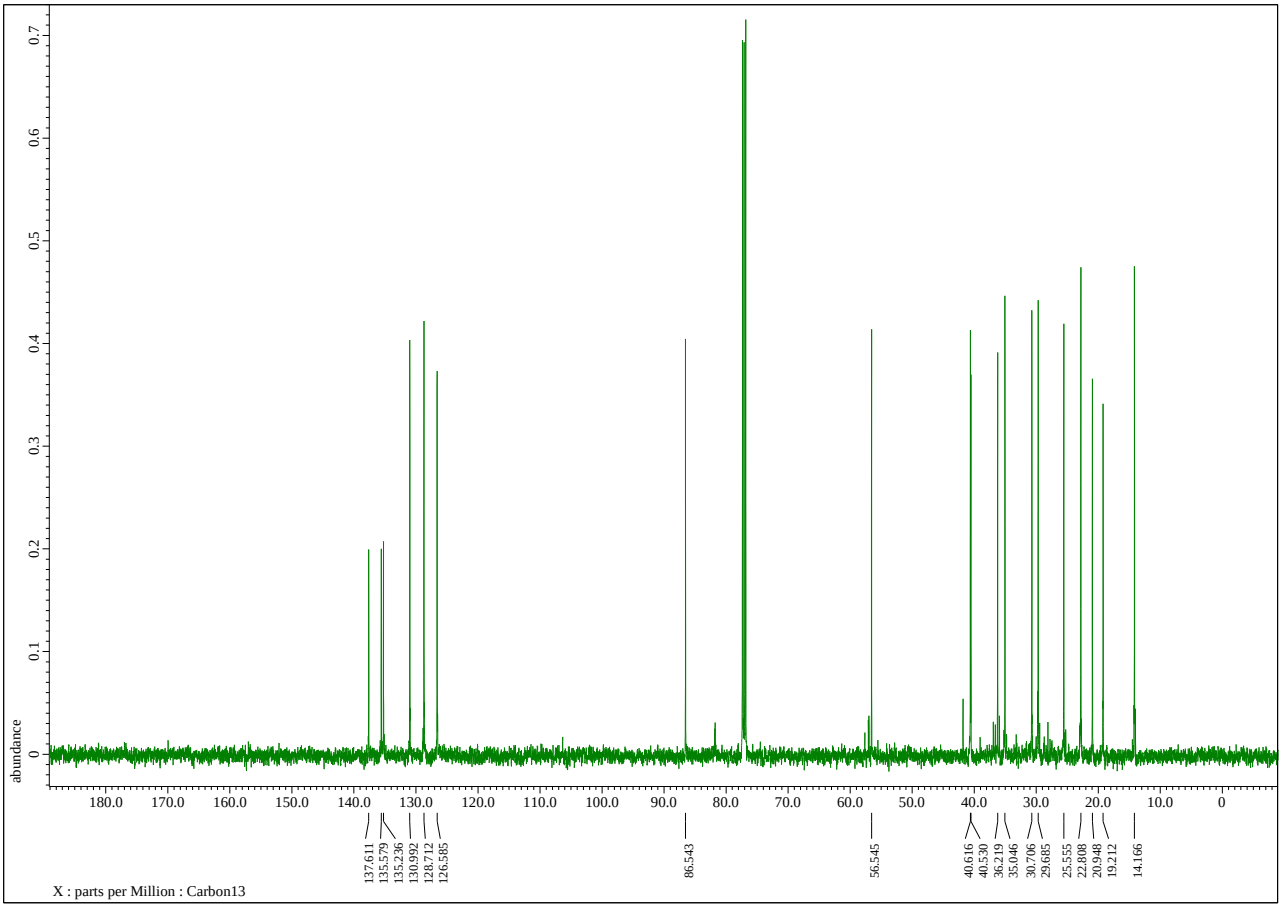
abundance
X : parts per Million : Carbon13

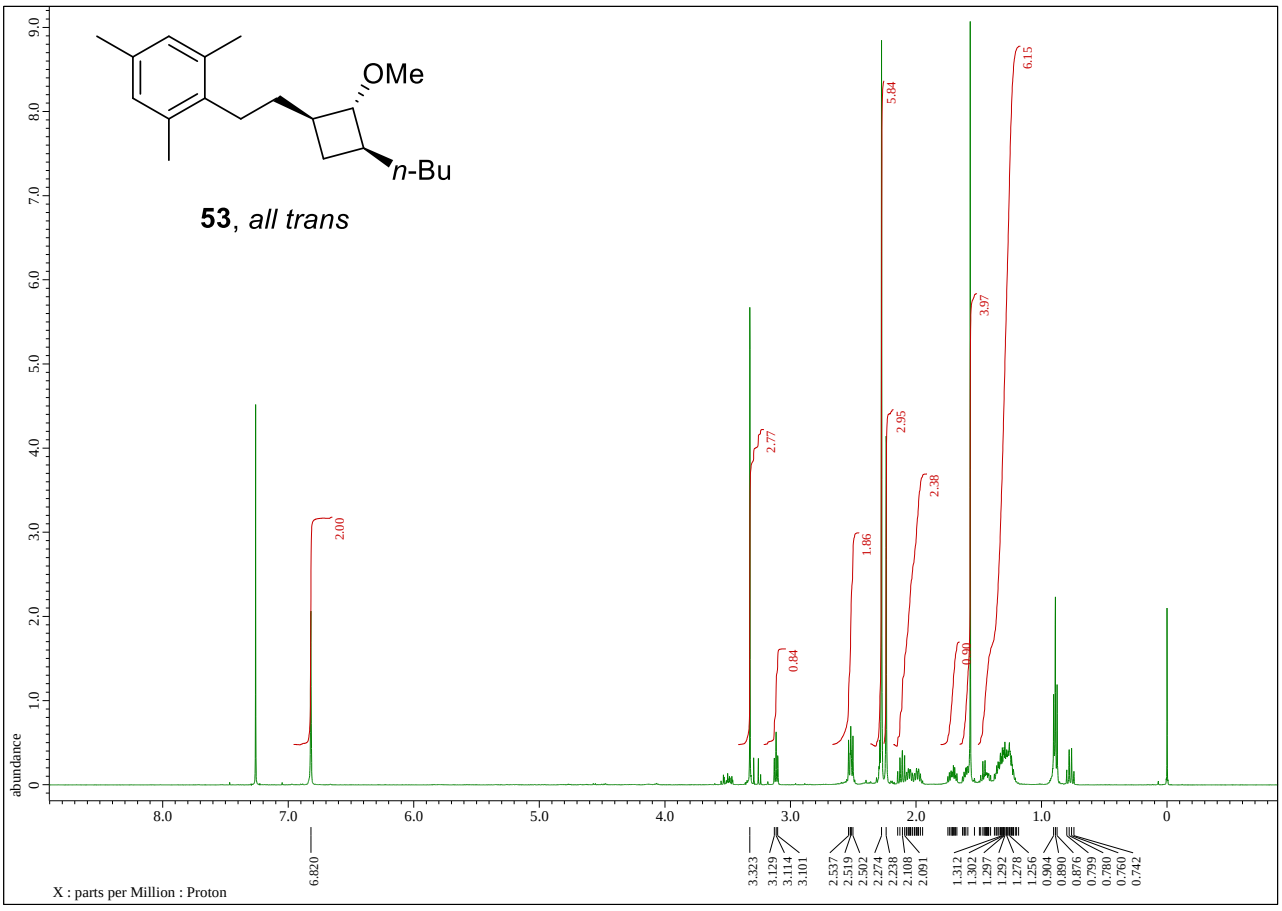
OMe
n-Bu
53, all trans
abundance
X : parts per Million : Proton

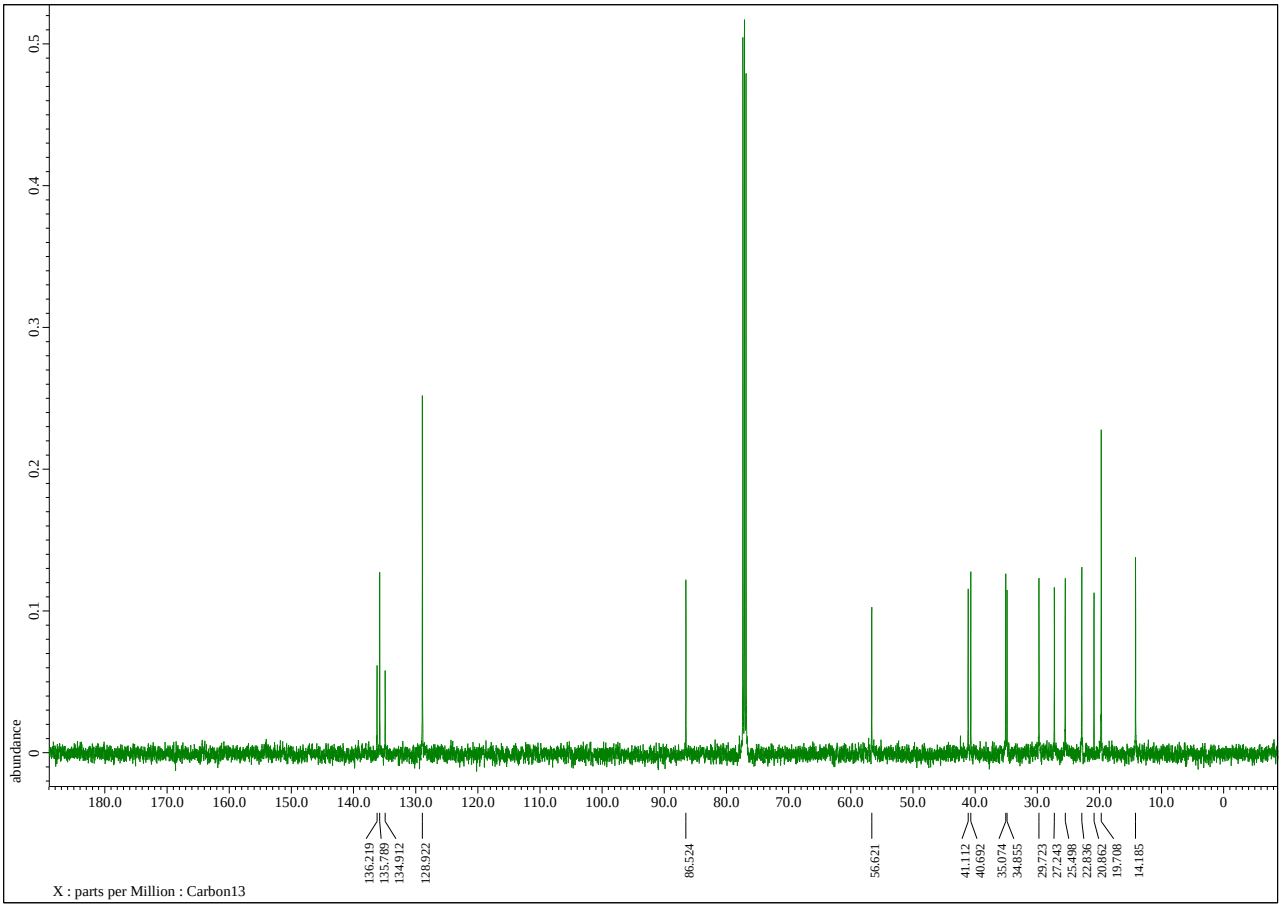
abundance
X : parts per Million : Carbon13

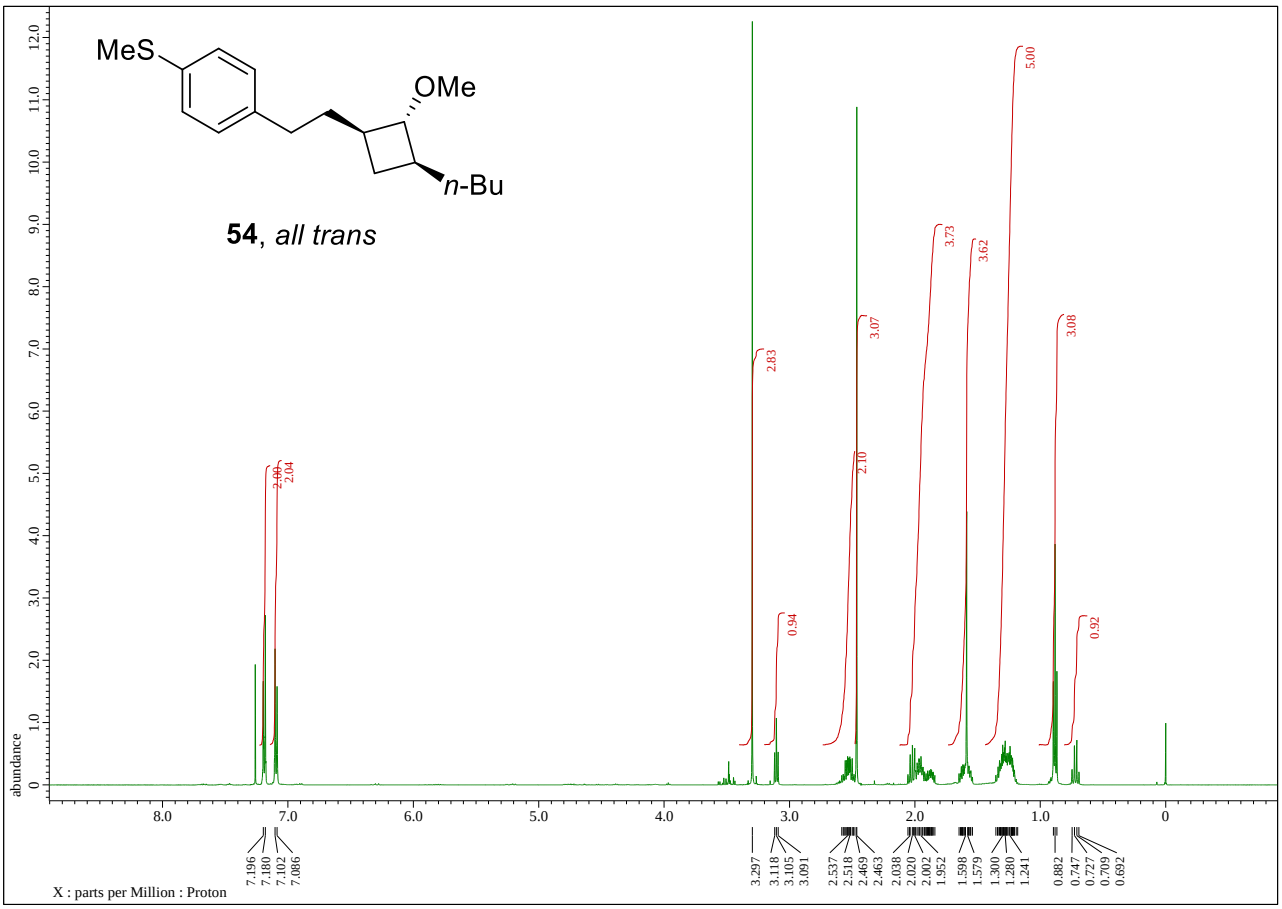
MeS
OMe
n-Bu
54, all trans
abundance
X : parts per Million : Proton

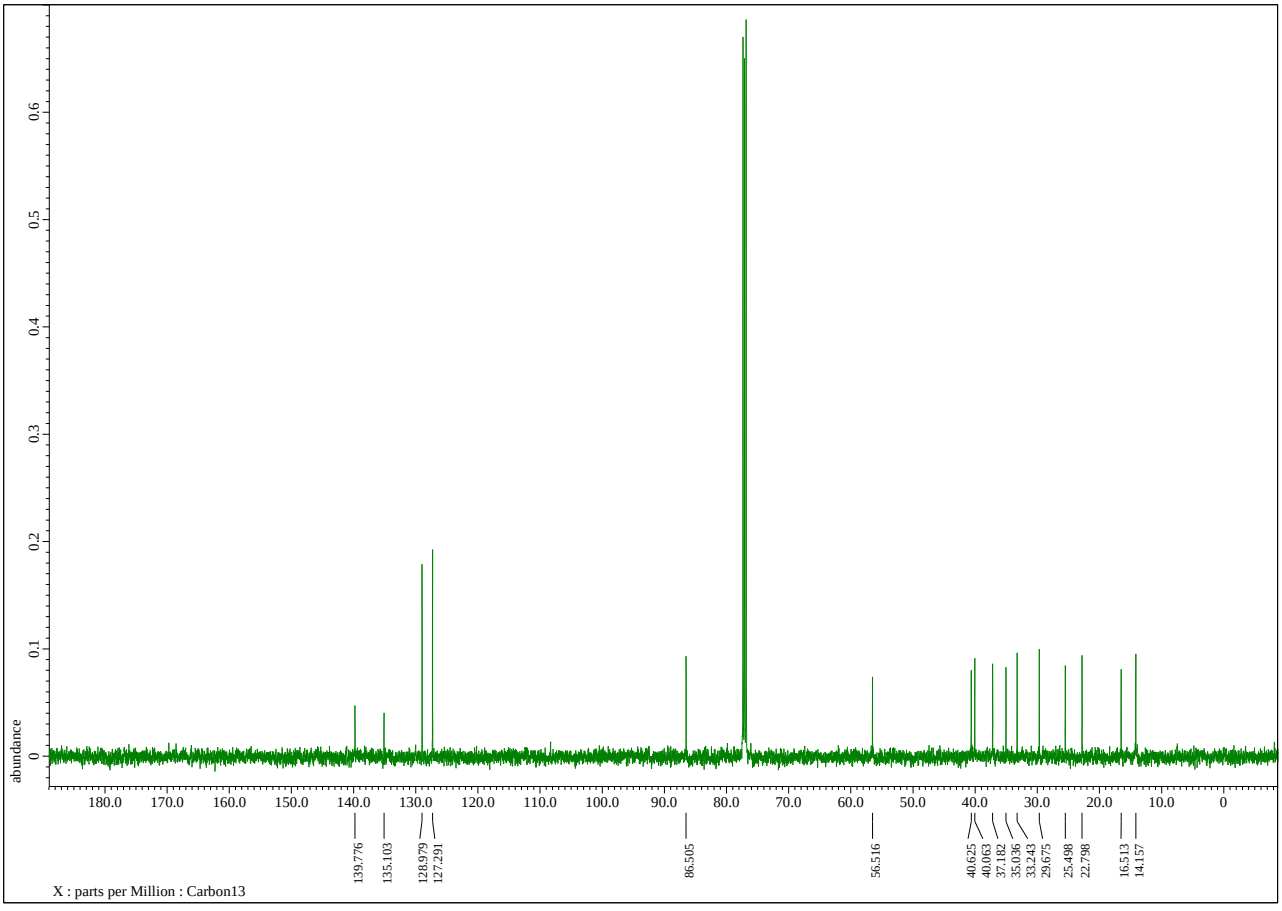
abundance
X : parts per Million : Carbon13

8.4. NMR and DFT Information in Chanter 5

*1-(2-(3-Butyl-2-methoxycyclobutyl)ethyl)-4-methoxybenzene (**3**, all trans).* Colorless oil.

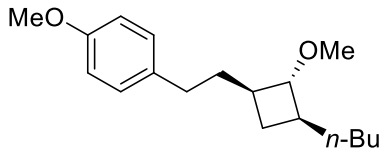

3, *all trans*

Product yield (1.0 mmol); 71% (determined by NMR), isolated in 65% (180 mg, 0.65 mmol).
^{1}H NMR ($CDCl_3$, 500 MHz) δ 7.08 (2H, d, J = 8.6 Hz), 6.81 (2H, d, J = 8.6 Hz), 3.78 (3H, s), 3.30 (3H, s), 3.11 (1H, t, J = 6.8 Hz), 2.59−2.43 (2H, m), 2.07−1.82 (4H, m), 1.65−1.53 (2H, m), 1.36−1.17 (5H, m), 0.88 (3H, t, J = 7.1 Hz), 0.72 (1H, q, J = 9.1 Hz); ^{13}C NMR (125 MHz, $CDCl_3$) δ 157.8, 134.8, 129.4, 113.9, 86.6, 56.6, 55.4, 40.7, 40.2, 37.6, 35.1, 33.0, 29.8, 25.6, 22.9, 14.3; HRMS $[M + H]^+$ calcd for $C_{18}H_{29}O_2$ 277.2168, found 277.2177.

*4-Phenyl-1-butene (**5**).* Colorless oil.

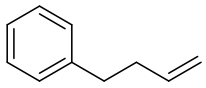

5

Product yield; 68% (determined by NMR), isolated (pentane) in 43% (23 mg, 0.17 mmol).
^{1}H NMR ($CDCl_3$, 500 MHz) δ 7.28 (2H, t, J = 7.5 Hz), 7.21-7.16 (3H, m), 5.86 (1H, ddt, J = 17.2, 10.3, 6.9 Hz), 5.05 (1H, dq, J = 17.2, 1.7 Hz), 4.98 (1H, dq, J = 10.3, 1.7 Hz), 2.38 (2H, q, J = 6.9 Hz); ^{13}C NMR (125 MHz, $CDCl_3$) δ 142.0, 138.2, 128.6, 128.4, 126.0, 115.1, 35.7, 35.5; HRMS $[M + H]^+$ calcd for $C_{10}H_{13}$ 133.1017, found 132.0995.

*1-Methoxy-4-(3-methoxyallyl)benzene (**6**, cis : trans = 1 : 1).* Colorless oil.

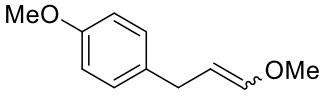

6, *cis* : *trans* = 1 : 1

Product yield; isolated in 61% (1.09 g, 6.09 mmol) over 3 steps from 2-(4-methoxyphenyl)acetic acid.
cis: ^{1}H NMR ($CDCl_3$, 500 MHz) δ 7.13 (2H, d, J = 8.6 Hz), 6.82 (2H, d, J = 8.6 Hz), 5.98 (1H, dt, J = 6.3, 1.7 Hz), 4.54 (1H, dt, J = 7.5, 6.3 Hz), 3.78 (3H, s), 3.63 (3H, s), 3.35 (2H, d, J = 7.5 Hz); ^{13}C NMR (125 MHz, $CDCl_3$) δ 157.9, 146.6, 134.0, 129.3, 113.9, 106.1, 59.8, 55.4, 29.3.
trans: ^{1}H NMR ($CDCl_3$, 500 MHz) δ 7.12 (2H, d, J = 8.6 Hz), 6.83 (2H, d, J = 8.6 Hz), 6.38 (1H, dt, J = 12.6, 1.3 Hz), 4.87 (1H, dt, J = 12.6, 7.5 Hz), 3.79 (3H, s), 3.53 (3H, s), 3.21 (2H, d, J = 6.9 Hz); ^{13}C NMR (125 MHz, $CDCl_3$) δ 158.1, 148.0, 133.9, 129.3, 113.9, 102.5, 56.1, 55.4, 33.3; HRMS $[M + H]^+$ calcd for $C_{11}H_{15}O_2$ 179.1072, found 179.1092.

(3-Methoxyallyl)benzene (7, cis : trans = 2 : 1). Colorless oil.

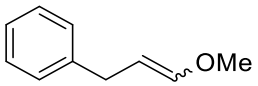

7, *cis* : *trans* = 2 : 1

Product yield; isolated in 58% (860 mg, 5.82 mmol) over 4 steps from ethyl 2-phenylacetate.

cis: ^{1}H NMR ($CDCl_3$, 500 MHz) δ 7.27 (2H, t, *J* = 7.5 Hz), 7.24-7.15 (3H, m), 6.00 (1H, dt, *J* = 6.3, 1.3 Hz), 4.56 (1H, dt, *J* = 7.5, 6.9 Hz), 3.64 (3H, s), 3.42 (2H, d, *J* = 7.5 Hz); ^{13}C NMR (125 MHz, $CDCl_3$) δ 146.8, 141.8, 128.5, 128.4, 125.9, 105.6, 59.8, 30.3.

trans: ^{1}H NMR ($CDCl_3$, 500 MHz) δ 7.29 (2H, t, *J* = 8.0 Hz), 7.24-7.15 (3H, m), 6.41 (1H, d, *J* = 12.6 Hz), 4.89 (1H, dt, *J* = 12.6, 7.5 Hz), 3.53 (3H, s), 3.27 (2H, d, *J* = 7.5 Hz); ^{13}C NMR (125 MHz, $CDCl_3$) δ 148.2, 141.8, 128.5, 128.4, 126.1, 102.0, 56.1, 34.2; HRMS $[M + H]^+$ calcd for $C_{10}H_{13}O$ 149.0966, found 149.0953.

*1-Methoxy-4-(4-methoxybut-3-en-1-yl)benzene (**8**, cis : trans = 1 : 1).* Colorless oil.

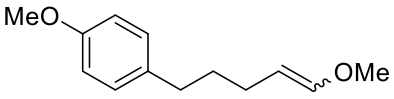

8, *cis* : *trans* = 1 : 1

Product yield; isolated in 62% (1.28 g, 6.21 mmol) over 3 steps from 4-(4-methoxyphenyl)butanoic acid.

cis: ^{1}H NMR ($CDCl_3$, 500 MHz) δ 7.10 (2H, d, *J* = 8.6 Hz), 6.81 (2H, d, *J* = 8.6 Hz), 5.89 (1H, dt, *J* = 5.7, 1.7 Hz), 4.35 (1H, dt, *J* = 6.9, 6.3 Hz), 3.78 (3H, s), 3.58 (3H, s), 2.55 (2H, t, *J* = 6.3 Hz), 2.10 (2H, dq, *J* = 7.5, 1.2 Hz), 1.63 (2H, quin, *J* = 7.5 Hz); ^{13}C NMR (125 MHz, $CDCl_3$) δ 157.7, 146.4, 135.0, 129.4, 113.8, 106.7, 59.6, 55.3, 34.8, 32.0, 23.7.

trans: ^{1}H NMR ($CDCl_3$, 500 MHz) δ 7.09 (2H, d, *J* = 8.6 Hz), 6.82 (2H, d, *J* = 8.6 Hz), 6.28 (1H, dt, *J* = 12.6, 1.1 Hz), 4.74 (1H, dt, *J* = 12.6, 7.5 Hz), 3.79 (3H, s), 3.50 (3H, s), 2.56 (2H, t, *J* = 6.3 Hz), 1.95 (2H, q, *J* = 6.3 Hz), 1.63 (2H, quin, *J* = 7.5 Hz); ^{13}C NMR (125 MHz, $CDCl_3$) δ 157.8, 147.4,134.7, 129.4, 113.8, 102.8, 56.0, 55.3, 34.4, 32.8, 27.4; HRMS $[M + H]^+$ calcd for $C_{13}H_{19}O_2$ 207.1385, found 207.1400.

*1-Methoxy-4-(6-methoxyhex-5-en-1-yl)benzene (**9**, cis : trans = 1 : 1).* Colorless oil.

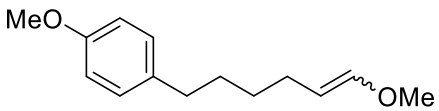

9, *cis* : *trans* = 1 : 1

Product yield; isolated in 29% (639 mg, 2.90 mmol) over 5 steps from 4-(4-methoxyphenyl)butanoic acid.

cis: ^{1}H NMR ($CDCl_3$, 500 MHz) δ 7.09 (2H, d, *J* = 8.6 Hz), 6.82 (2H, d, *J* = 8.6 Hz), 5.86 (1H, dt, *J* = 6.3, 1.7 Hz), 4.32 (1H, q, *J* = 6.9 Hz), 3.78 (3H, s), 3.57 (3H, s), 2.55 (2H, t, *J* = 7.5 Hz), 2.08 (2H, dq, *J* = 7.5, 1.2 Hz), 1.63-1.55 (2H, m), 1.37 (2H, quin, *J* = 8.0 Hz); ^{13}C NMR (125 MHz, $CDCl_3$) δ 157.8, 146.3, 135.0, 129.4, 113.8, 107.0, 59.6, 55.4, 35.0, 31.2, 30.5, 27.7.

trans: ^{1}H NMR ($CDCl_3$, 500 MHz) δ 7.09 (2H, d, *J* = 8.6 Hz), 6.81 (2H, d, *J* = 8.6 Hz), 6.27 (1H, dt, *J* = 12.6,

1.2 Hz), 4.71 (1H, dt, *J* = 12.0, 7.5 Hz), 3.78 (3H, s), 3.49 (3H, s), 2.54 (2H, t, *J* = 7.5 Hz), 1.94 (2H, dq, *J* = 6.9, 1.2 Hz), 1.63-1.55 (2H, m), 1.37 (2H, quin, *J* = 8.0 Hz); ^{13}C NMR (125 MHz, $CDCl_3$) δ 157.8, 147.2, 135.2, 129.4, 113.8, 103.1, 59.6, 55.4, 35.0, 31.2, 30.5, 27.7; HRMS $[M + H]^+$ calcd for $C_{14}H_{21}O_2$ 221.1542, found 221.1530.

*1-((3-Butyl-2-methoxycyclobutyl)methyl)-4-methoxybenzene (**10**, all trans).* Colorless oil.

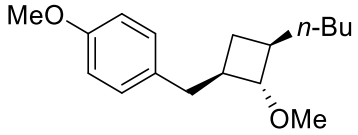

10, *all trans*

Product yield; 87% (determined by NMR), isolated in 65% (68 mg, 0.26 mmol).

^{1}H NMR ($CDCl_3$, 500 MHz) δ 7.07 (2H, d, *J* = 8.6 Hz), 6.81 (2H, d, *J* = 8.6 Hz), 3.78 (3H, s), 3.30 (3H, s), 3.11 (1H, t, *J* = 6.8 Hz), 2.59-2.43 (2H, m), 2.07-1.82 (4H, m), 1.65-1.53 (2H, m), 1.36-1.17 (5H, m), 0.88 (3H, t, *J* = 7.1 Hz), 0.72 (1H, q, *J* = 9.1 Hz); ^{13}C NMR (125 MHz, $CDCl_3$) δ 157.8, 134.8, 129.4, 113.9, 86.6, 56.6, 55.4, 40.7, 40.2, 37.6, 35.1, 33.0, 29.8, 25.6, 22.9, 14.3; HRMS $[M + H]^+$ calcd for $C_{17}H_{27}O_2$ 263.2011, found 263.2020.

*Allylbenzene (**13**).* Colorless oil.

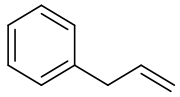

13

Product yield; 68% (determined by NMR), isolated (pentane) in 28% (13 mg, 0.11 mmol).

^{1}H NMR ($CDCl_3$, 500 MHz) δ 7.37-7.15 (5H, m), 5.97 (1H, ddt, *J* = 17.2, 10.3, 6.9 Hz), 5.12-5.04 (2H, m), 3.40 (2H, d, *J* = 6.9 Hz); ^{13}C NMR (125 MHz, $CDCl_3$) δ 140.2, 137.6, 128.7, 128.5, 126.2, 115.9, 40.4; HRMS $[M + H]^+$ calcd for C_9H_{11} 119.0861, found 119.0834.

*1-(3-(3-Butyl-2-methoxycyclobutyl)propyl)-4-methoxybenzene (**16**, all trans).* Colorless oil.

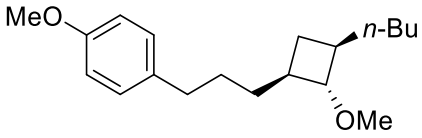

16, *all trans*

Product yield; 63% (determined by NMR), isolated in 38% (44 mg, 0.15 mmol).

^{1}H NMR ($CDCl_3$, 500 MHz) δ 7.08 (2H, d, *J* = 8.6 Hz), 6.82 (2H, d, *J* = 8.6 Hz), 3.78 (3H, s), 3.29 (3H, s), 3.06 (1H, t, *J* = 6.8 Hz), 2.58-2.48 (2H, m), 2.04-1.89 (3H, m), 1.63-1.50 (4H, m), 1.39-1.18 (6H, m), 0.88 (3H, t, *J* = 6.9 Hz), 0.68 (1H, q, *J* = 9.7 Hz); ^{13}C NMR (125 MHz, $CDCl_3$) δ 157.8, 135.0, 129.4, 113.8, 86.6, 56.6, 55.4, 40.7, 40.5, 35.2, 35.1, 34.9, 29.8, 29.7, 25.6, 22.9, 14.3; HRMS $[M + H]^+$ calcd for $C_{19}H_{31}O_2$ 291.2324, found 291.2317.

*1-Methoxy-4-(pent-4-en-1-yl)benzene (**17**).* Colorless oil.

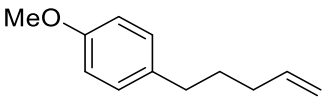

17

Product yield; 21% (determined by NMR), isolated in 16% (11 mg, 0.062 mmol).
^{1}H NMR ($CDCl_3$, 500 MHz) δ 7.09 (2H, d, *J* = 8.0 Hz), 6.83 (2H, d, *J* = 8.6 Hz), 5.83 (1H, ddt, *J* = 17.2, 10.3, 6.3 Hz), 5.02 (1H, dq, *J* = 17.2, 1.7 Hz), 4.97 (1H, d, *J* = 10.3 Hz), 3.79 (3H, s), 2.56 (2H, t, *J* = 7.5 Hz), 2.08 (2H, q, *J* = 6.9 Hz), 1.68 (2H, quin, *J* = 7.5 Hz); ^{13}C NMR (125 MHz, $CDCl_3$) δ 157.8, 138.8, 134.6, 129.4, 114.8, 113.8, 5.3, 34.5, 33.4, 31.0; HRMS $[M + H]^+$ calcd for $C_{12}H_{17}O$ 177.1279, found 177.1268.

*1-(Hex-5-en-1-yl)-4-methoxybenzene (**19**).* Colorless oil.

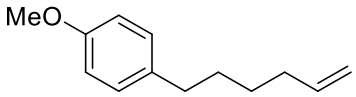

19

Product yield; 67% (determined by NMR), isolated in 63% (48 mg, 0.25 mmol).
^{1}H NMR ($CDCl_3$, 500 MHz) δ 7.09 (2H, d, *J* = 8.6 Hz), 6.82 (2H, d, *J* = 8.6 Hz), 5.80 (1H, ddt, *J* = 16.6, 9.7, 6.9 Hz), 4.99 (1H, dq, *J* = 17.2, 1.7 Hz), 4.93 (1H, d, *J* = 9.7 Hz), 3.79 (3H, s), 2.55 (2H, t, *J* = 7.5 Hz), 2.07 (2H, ddt, *J* = 7.5, 6.9, 1.6 Hz), 1.60 (2H, quin, *J* = 7.5 Hz), 1.42 (2H, quin, *J* = 8.0 Hz); ^{13}C NMR (125 MHz, $CDCl_3$) δ 157.7, 139.0, 134.9, 129.3, 114.4, 113.8, 55.3, 35.0, 33.7, 31.2, 28.6; HRMS $[M + H]^+$ calcd for $C_{13}H_{19}O$ 191.1436, found 191.1445.

*6-Methoxy-2-(2-methoxyvinyl)-1,2,3,4-tetrahydronaphthalene (**20**, cis : trans = 1 : 2).* Colorless oil.

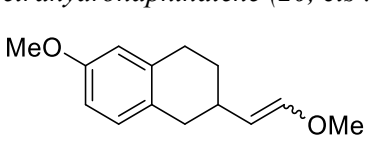

20, *cis* : *trans* = 1 : 2

cis: ^{1}H NMR ($CDCl_3$, 500 MHz) δ 6.95 (1H, d, *J* = 8.0 Hz), 6.67 (1H, dt, *J* = 8.6, 2.9 Hz), 6.63-6.60 (1H, m), 5.88 (1H, d, *J* = 6.3 Hz), 4.34 (1H, dd, *J* = 8.6, 6.3 Hz), 3.76 (3H, s), 3.59 (3H, s), 2.91-2.85 (1H, m), 2.85-2.74 (3H, m), 2.54-2.41 (1H, m), 1.93-1.86 (1H, m), 1.59-1.49 (1H, m); ^{13}C NMR (125 MHz, $CDCl_3$) δ 157.5, 145.7, 137.6, 130.0, 128.7, 113.5, 111.9, 111.7, 59.7, 55.3, 35.6, 30.3, 29.8, 29.2.
trans: ^{1}H NMR ($CDCl_3$, 500 MHz) δ 6.97 (1H, d, *J* = 8.0 Hz), 6.67 (1H, dt, *J* = 8.6, 2.9 Hz), 6.63-6.60 (1H, m), 6.40 (1H, d, *J* = 12.6 Hz), 4.80 (1H, dd, *J* = 12.6, 8.0 Hz), 3.77 (3H, s), 3.52 (3H, s), 2.85-2.74 (3H, m), 2.54-2.41 (1H, m), 2.54-2.41 (1H, m), 2.38-2.30 (1H, m), 1.93-1.86 (1H, m), 1.59-1.49 (1H, m); ^{13}C NMR (125 MHz, $CDCl_3$) δ 157.6, 146.7, 137.5, 129.9, 128.5, 113.5, 112.0, 108.1, 55.9, 55.3, 36.5, 34.0, 30.9, 29.4; HRMS $[M + H]^+$ calcd for $C_{14}H_{19}O_2$ 219.1385, found 219.1412.

*4-Methoxy-1-(4-methoxybut-3-en-1-yl)-2-methylbenzene (**21**, cis : trans = 1 : 1).* Colorless oil.

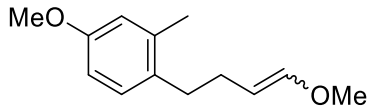

21, *cis* : *trans* = 1 : 1

cis: ^{1}H NMR ($CDCl_3$, 500 MHz) δ 7.06 (2H, d, *J* = 8.6 Hz), 6.71-6.65 (2H, m), 5.88 (1H, dt, *J* = 6.3, 1.6 Hz), 4.39 (1H, dt, *J* = 7.3, 6.3 Hz), 3.76 (3H, s), 3.56 (3H, s), 2.58 (2H, t, *J* = 7.5 Hz), 2.31 (2H, dt, *J* = 8.0, 7.5 Hz), 2.29 (3H, s); ^{13}C NMR (125 MHz, $CDCl_3$) δ 157.7, 146.5, 137.4, 132.8, 129.7, 115.8, 110.9, 106.3 59.6, 55.3, 32.6, 24.8, 19.7.

trans: ^{1}H NMR ($CDCl_3$, 500 MHz) δ 7.03 (2H, d, *J* = 8.6 Hz), 6.71-6.65 (2H, m), 6.31 (1H, dt, *J* = 12.6, 1.5 Hz), 4.78 (1H, dt, *J* = 12.6, 7.5 Hz), 3.77 (3H, s), 3.50 (3H, s), 2.58 (2H, t, *J* = 7.5 Hz), 2.28 (3H, s), 2.15 (2H, dt, *J* = 8.6, 8.0 Hz); ^{13}C NMR (125 MHz, $CDCl_3$) δ 157.8, 147.5, 137.2, 132.5, 129.9, 115.9, 111.1, 102.6, 56.0, 55.3, 34.1, 29.0, 19.8; HRMS $[M + H]^+$ calcd for $C_{13}H_{19}O_2$ 207.1385, found 207.1411.

*2-(2-Methoxyvinyl)-1,2,3,4-tetrahydronaphthalene (**22**, cis : trans = 3 : 1).* Colorless oil.

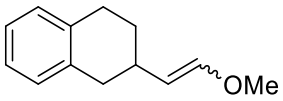

22, *cis* : *trans* = 3 : 1

cis: ^{1}H NMR ($CDCl_3$, 500 MHz) δ 7.12-7.02 (4H, m), 5.89 (1H, d, *J* = 6.3 Hz), 4.35 (1H, dd, *J* = 7.5, 6.3 Hz), 3.60 (3H, s), 2.94-2.90 (1H, m), 2.90-2.78 (3H, m), 2.63-2.49 (1H, m), 1.96-1.88 (1H, m), 1.61-1.51 (1H, m); ^{13}C NMR (125 MHz, $CDCl_3$) δ 145.8, 136.7, 136.6, 129.3, 129.0, 125.6, 125.5, 111.7, 59.8, 36.4, 30.2, 29.9, 28.9.

trans: ^{1}H NMR ($CDCl_3$, 500 MHz) δ 7.12-7.02 (4H, m), 6.41 (1H, d, *J* = 13.2 Hz), 4.80 (1H, dd, *J* = 12.6, 8.0 Hz), 3.53 (3H, s), 2.90-2.78 (3H, m), 2.63-2.49 (1H, m), 2.41-2.33 (1H, m), 1.96-1.88 (1H, m), 1.61-1.51 (1H, m); ^{13}C NMR (125 MHz, $CDCl_3$) δ 146.7, 136.7, 136.5, 129.3, 129.2, 125.7, 125.6, 108.1, 56.0, 37.4, 33.8, 30.9, 29.1; HRMS $[M + H]^+$ calcd for $C_{13}H_{17}O$ 189.1279, found 189.1303.

*1-(4-Methoxybut-3-en-1-yl)-2-methylbenzene (**23**, cis : trans = 1 : 1).* Colorless oil.

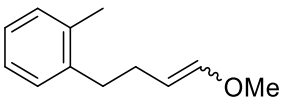

23, *cis* : *trans* = 1 : 1

cis: ^{1}H NMR ($CDCl_3$, 500 MHz) δ 7.18-7.06 (4H, m), 5.89 (1H, dt, *J* = 6.3, 1.2 Hz), 4.41 (1H, dt, *J* = 13.8, 7.5 Hz), 3.56 (3H, s), 2.64 (2H, t, *J* = 6.9 Hz), 2.35 (2H, q, *J* = 8.0 Hz), 2.32 (3H, s); ^{13}C NMR (125 MHz, $CDCl_3$) δ 146.7, 140.6, 136.2, 130.3, 128.9, 126.1, 125.9, 106.3, 59.6, 33.5, 24.5, 19.5.

trans: ^{1}H NMR ($CDCl_3$, 500 MHz) δ 7.18-7.06 (4H, m), 6.32 (1H, dt, *J* = 12.6, 1.1 Hz), 4.79 (1H, dt, *J* = 12.6, 7.5 Hz), 3.50 (3H, s), 2.64 (2H, t, *J* = 6.9 Hz), 2.31 (3H, s), 2.20 (2H, q, *J* = 8.0 Hz); ^{13}C NMR (125 MHz,

$CDCl_3$) δ 147.6, 140.3, 136.0, 130.2, 129.0, 126.0, 125.9, 102.5, 56.0, 35.0, 28.7, 19.5; HRMS $[M + H]^+$ calcd for $C_{12}H_{17}O$ 177.1279, found 177.1293.

*2-(3-Butyl-2-methoxycyclobutyl)-6-methoxy-1,2,3,4-tetrahydronaphthalene (**24**, all trans).* Colorless oil.

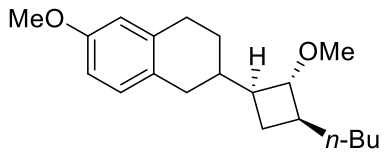

24, *all trans*

Product yield; 87% (determined by NMR), isolated in 73% (87 mg, 0.29 mmol).
Minor Diastereomer: ^{1}H NMR ($CDCl_3$, 500 MHz) δ 6.99 (1H, d, J = 8.6 Hz), 6.67 (1H, dd, J = 8.6, 2.3 Hz), 6.62-6.59 (1H, m), 3.76 (3H, s), 3.34 (3H, s), 3.25 (1H, t, J = 6.9 Hz), 2.84-2.68 (3H, m), 2.39 (1H, dd, J = 16.0, 10.9 Hz), 2.08-1.82 (4H, m), 1.69-1.58 (2H, m), 1.43-1.20 (6H, m), 0.89 (3H, t, J = 6.9 Hz), 0.82 (1H, q, J = 9.7 Hz); ^{13}C NMR (125 MHz, $CDCl_3$) δ 157.6, 138.0, 130.2, 128.9, 113.6, 112.0, 85.2, 56.5, 55.4, 45.4, 40.4, 39.8, 35.3, 33.4, 29.8, 29.6, 26.9, 23.6, 22.9, 14.3.
Major Diastereomer: ^{1}H NMR ($CDCl_3$, 500 MHz) δ 6.96 (1H, d, J = 8.6 Hz), 6.67 (1H, dd, J = 8.6, 2.3 Hz), 6.62-6.59 (1H, m), 3.76 (3H, s), 3.33 (3H, s), 3.25 (1H, t, J = 6.9 Hz), 2.84-2.68 (3H, m), 2.29 (1H, dd, J = 16.0, 10.9 Hz), 2.08-1.82 (4H, m), 1.69-1.58 (2H, m), 1.43-1.20 (6H, m), 0.89 (3H, t, J = 6.9 Hz), 0.82 (1H, q, J = 9.7 Hz); ^{13}C NMR (125 MHz, $CDCl_3$) δ 157.6, 138.1, 130.1, 128.7, 113.6, 112.1, 85.2, 56.5, 55.4, 45.4, 40.6, 39.7, 35.3, 32.9, 29.8, 29.6, 27.2, 23.6, 22.9, 14.3; HRMS $[M + H]^+$ calcd for $C_{20}H_{31}O_2$ 303.2324, found 303.2323.

*2-Vinyl-1,2,3,4-tetrahydronaphthalene (**27**).* Colorless oil.

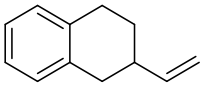

27

Product yield; 58% (determined by NMR), isolated in 55% (34 mg, 0.22 mmol).
^{1}H NMR ($CDCl_3$, 500 MHz) δ 7.13-7.06 (4H, m), 5.92 (1H, ddd, J = 17.2, 10.3, 6.9 Hz), 5.09 (1H, dt, J = 17.2, 1.9 Hz), 5.01 (1H, dq, J = 10.3, 1.7 Hz), 2.91-2.83 (3H, m), 2.67-2.59 (1H, m), 2.49-2.40 (1H, m), 2.02-1.95 (1H, m), 1.62-1.52 (1H, m); ^{13}C NMR (125 MHz, $CDCl_3$) δ 143.4, 136.6, 136.3, 129.3, 129.0, 125.8, 125.7, 113.1, 38.4, 35.4, 29.2, 29.0; HRMS $[M + H]^+$ calcd for $C_{12}H_{15}$ 159.1174, found 159.1150.

*1-(2-(3-Butyl-2-methoxycyclobutyl)ethyl)-4-methoxy-2-methylbenzene (**28**, all trans).* Colorless oil.

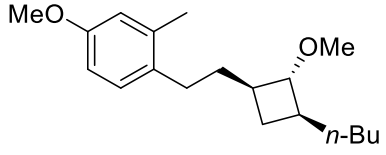

28, *all trans*

Product yield; 86% (determined by NMR), isolated in 65% (76 mg, 0.26 mmol).
^{1}H NMR ($CDCl_3$, 500 MHz) δ 7.02 (2H, d, *J* = 8.6 Hz), 6.69 (1H, d, *J* = 2.3 Hz), 6.67 (1H, dd, *J* = 8.0, 2.3 Hz), 3.77 (3H, s), 3.31 (3H, s), 3.11 (1H, t, *J* = 6.9 Hz), 2.54-2.43 (2H, m), 2.27 (3H, s), 2.10-1.92 (3H, m), 1.86-1.78 (1H, m), 1.62-1.50 (2H, m), 1.37-1.20 (5H, m), 0.89 (3H, t, *J* = 6.9 Hz), 0.74 (1H, q, *J* = 9.7 Hz); ^{13}C NMR (125 MHz, $CDCl_3$) δ 157.8, 137.2, 133.0, 129.7, 115.9, 111.1, 86.7, 56.6, 55.4, 40.8, 40.6, 36.4, 35.1, 30.4, 29.8, 25.7, 22.9, 19.7, 14.3; HRMS $[M + H]^+$ calcd for $C_{19}H_{31}O_2$ 291.2324, found 291.2300.

*1-(But-3-en-1-yl)-2-methylbenzene (**31**).* Colorless oil.

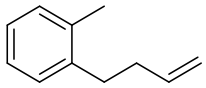

31

Product yield; 74% (determined by NMR), isolated (pentane) in 70% (41 mg, 0.28 mmol).
^{1}H NMR ($CDCl_3$, 500 MHz) δ 7.17 (4H, m), 5.90 (1H, ddt, *J* = 16.6, 10.3, 6.9 Hz), 5.06 (1H, dq, *J* = 17.2, 1.7 Hz), 4.99 (1H, dq, *J* = 10.3, 1.7 Hz), 2.69 (2H, t, *J* = 8.0 Hz), 2.36-2.29 (2H, m), 2.31 (3H, s); ^{13}C NMR (125 MHz, $CDCl_3$) δ 140.2, 138.5, 136.1, 130.3, 128.9, 126.1, 126.0, 115.0, 3.5, 32.9, 19.5; HRMS $[M + H]^+$ calcd for $C_{11}H_{15}$ 147.1174, found 147.1177.

Cartesian Coordinates.

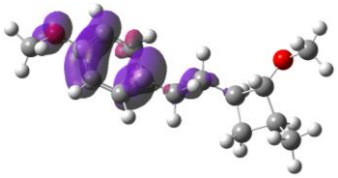

$3^{\bullet+}$ Total Energy = -734.933282 hartree/particle

Atom	X	Y	Z
C	2.84753777	-1.48890620	-0.68564397
C	4.18100004	-0.89685143	-0.14872264
C	3.36431617	0.34582904	0.31023433
C	2.23965491	-0.06065815	-0.65991034
H	2.87959916	-2.00460857	-1.64246446
H	2.37592343	-2.13995266	0.05238784
H	4.81109573	-0.59983875	-0.98923331
H	3.05001007	0.23450986	1.35588785
H	2.41771668	0.43393463	-1.61677712
C	-1.61169252	-0.16023559	-0.82478463
C	-2.27419178	-1.14954112	-0.04336124
C	-2.29801351	1.04735598	-1.12056994
C	-3.54646569	-0.96584077	0.41690071
H	-1.75418405	-2.06970523	0.18113450
C	-3.56785856	1.25667518	-0.67275747
C	-4.21674681	0.25182622	0.11054456
H	-4.03451813	-1.73010180	0.99931030
H	-4.11202872	2.16379573	-0.88892230
C	0.80055633	0.15333333	-0.21673488
H	0.62352662	-0.35959202	0.73029030
H	0.61981033	1.21650242	-0.04686625
C	-0.21341902	-0.37151070	-1.27854526
H	-0.02959654	-1.43340739	-1.44196747
H	-0.04012468	0.15820835	-2.21518132
O	-5.43005598	0.54826224	0.50158909
C	-6.21034614	-0.36693725	1.31651094
H	-7.14741702	0.14699226	1.48716442
H	-6.37531593	-1.29209689	0.77123486
H	-5.69614572	-0.54809648	2.25645680
O	3.87091044	1.64672906	0.09955996

C	4.83735880	2.05022443	1.06400055
H	4.43063232	1.98531024	2.07782839
H	5.74205349	1.44019739	1.00542615
H	5.09348959	3.08445644	0.84712379
C	4.97961191	-1.69801352	0.86598968
H	4.36552746	-1.95399002	1.73158709
H	5.33921858	-2.63127085	0.42793329
H	5.84930935	-1.14449130	1.22316596
H	-1.80322911	1.80281742	-1.71361405

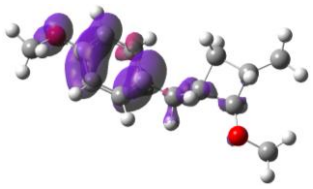

$10^{\bullet+}$ Total Energy = -695.635563 hartree/particle

Atom	X	Y	Z
C	-1.69979626	1.36627601	-0.54015261
C	-3.17566152	0.96361373	-0.81177787
C	-2.94454485	-0.26346638	0.12407088
C	-1.43200536	-0.09217754	-0.09200102
H	-1.11894295	1.74514314	-1.37714210
H	-1.62819014	2.06782396	0.29149700
H	-3.27115083	0.59695044	-1.83503539
H	-3.23320548	-0.01695073	1.15279394
H	-1.13549460	-0.69711126	-0.94914124
C	-0.50511041	-0.39170821	1.11345754
H	-0.78776976	0.24592244	1.94946526
H	-0.66841140	-1.43277891	1.40096587
O	-3.44015120	-1.53212322	-0.22703803
C	-4.79965822	-1.74816698	0.14328015
H	-4.94224305	-1.59020402	1.21609262
H	-5.47316900	-1.08713703	-0.40688393
H	-5.03605447	-2.78031258	-0.10224772
C	-4.27791223	1.95770991	-0.48702343
H	-4.21212387	2.28919595	0.55080121
H	-4.20100276	2.84135700	-1.12344271
H	-5.26705937	1.52427990	-0.64070889
C	0.92462343	-0.19028999	0.76438094
C	1.60752675	1.00362629	1.11168123
C	1.62893026	-1.19313494	0.03615148
C	2.91438566	1.18596561	0.76702674
H	1.08496585	1.77068783	1.66416024
C	2.93842523	-1.03754974	-0.31711670
H	1.11133861	-2.10353051	-0.23048492
C	3.60613373	0.16526834	0.04449269
H	3.45698579	2.08271908	1.02614619
H	3.45635421	-1.81364230	-0.85656555

O	4.85681822	0.43338192	-0.23657765
C	5.68834792	-0.51033860	-0.96235233
H	6.64786407	-0.01827572	-1.05522163
H	5.78327163	-1.42836929	-0.38888042
H	5.25859629	-0.69960195	-1.94194859

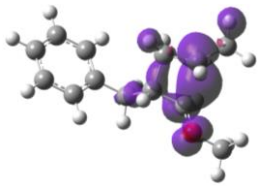

$12^{\bullet+}$ Total Energy = -581.092016 hartree/particle

Atom	X	Y	Z
C	-0.80412204	1.31714850	-0.43548217
C	-2.26721584	1.37435139	-0.75571036
C	-2.11639405	-0.44823274	0.27598312
C	-0.69569847	-0.20237059	-0.14488985
H	-0.16923584	1.63287661	-1.26303233
H	-0.56705916	1.91185195	0.44451286
H	-2.56161782	0.93909286	-1.70501698
H	-2.48235393	-0.04811402	1.21965114
H	-0.52751420	-0.74135108	-1.07614562
C	0.34658909	-0.63558815	0.91345253
H	0.14672473	-0.11399181	1.84919489
H	0.20900307	-1.70191512	1.09931742
O	-2.75785393	-1.45451459	-0.23074611
C	-4.09341990	-1.76369713	0.26369008
H	-4.17561643	-1.48007282	1.30891316
H	-4.80957782	-1.22419028	-0.34923037
H	-4.21210782	-2.83312859	0.13832698
C	-3.20493768	2.33994977	-0.14430494
H	-2.96761715	2.55518381	0.89633399
H	-3.10562546	3.28486669	-0.69849588
H	-4.24234980	2.02531903	-0.23985744
C	1.76239290	-0.36768846	0.46091641
C	2.47322204	0.73665936	0.93714554
C	2.38667431	-1.22101728	-0.45475655
C	3.77488431	0.98442154	0.50917609
H	2.01134867	1.40261504	1.65439840
C	3.68632260	-0.97621486	-0.88395423
H	1.85548667	-2.08798670	-0.82670288
C	4.38459041	0.12968815	-0.40393934
H	4.31164980	1.84155500	0.89224813
H	4.15566479	-1.65028933	-1.58742782

H	5.39630304	0.31933854	-0.73497669

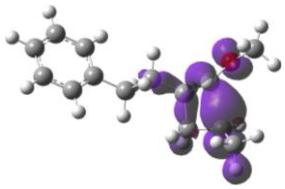

$15^{\bullet+}$ Total Energy = -620.390487 hartree/particle

Atom	X	Y	Z
C	-1.93054285	-1.47946312	0.64077115
C	-3.38296908	-1.20590594	0.39291478
C	-2.47701685	0.58438477	-0.25538639
C	-1.40068529	-0.01909848	0.60015856
H	-1.74873748	-1.96582341	1.59907066
H	-1.49701500	-2.08343770	-0.15426879
H	-3.92479648	-0.74995468	1.21475950
H	-2.53474301	0.33738160	-1.31366408
H	-1.47655735	0.42585761	1.59185282
C	2.48847335	-0.19247505	0.39731081
C	3.08047575	-1.12373727	-0.46010780
C	3.20418754	0.96435676	0.71811924
C	4.35155860	-0.90617630	-0.98432571
H	2.54491012	-2.02963178	-0.71489940
C	4.47544227	1.18634659	0.19642200
C	5.05340383	0.25126724	-0.65821531
H	4.79446894	-1.64149599	-1.64247544
H	5.01516962	2.08576697	0.46057849
C	0.01197557	0.18462417	0.03063255
H	0.07454652	-0.26323889	-0.96290629
H	0.18763361	1.25552254	-0.08846222
C	1.09684809	-0.41683512	0.94256142
H	0.92036076	-1.48701747	1.05938333
H	1.01359367	0.03111410	1.93429203
O	-3.05055582	1.67936285	0.13291929
C	-4.02060032	2.31725080	-0.74863226
H	-3.71650799	2.19082175	-1.78361770
H	-4.99049904	1.86426920	-0.56463576
H	-4.02647548	3.36326070	-0.46794993
C	-4.18774432	-1.90081447	-0.63409539
H	-3.61849308	-2.12408028	-1.53498545

H	-4.50015347	-2.86440334	-0.20521680
H	-5.09693835	-1.35709950	-0.88376930
H	2.76562165	1.69444325	1.38675597
H	6.04222065	0.42049511	-1.06196185

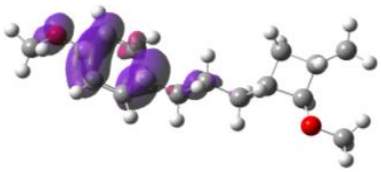

$16^{\bullet+}$ Total Energy = -774.231095 hartree/particle

Atom	X	Y	Z
C	-2.95764845	1.44188166	-0.57188858
C	-4.45972736	1.07429458	-0.72773539
C	-4.13333278	-0.26088430	0.00037338
C	-2.64407059	-0.06108086	-0.33219928
H	-2.47295784	1.93038336	-1.41425921
H	-2.78474124	2.03510524	0.32781514
H	-4.67198820	0.84972485	-1.77497455
H	-4.31721972	-0.16585953	1.07846586
H	-2.44269194	-0.54799840	-1.28917770
C	-1.60115224	-0.47328659	0.69702039
H	-1.80428152	0.03606361	1.64310405
H	-1.68984332	-1.54577761	0.89158725
O	-4.67822175	-1.47776683	-0.46983304
C	-6.02968344	-1.69037827	-0.07838672
H	-6.13384399	-1.65271325	1.01047785
H	-6.69856142	-0.94942213	-0.52328222
H	-6.31405234	-2.67927602	-0.43025432
C	-5.50698443	2.01719251	-0.15862648
H	-5.32833197	2.20375821	0.90219854
H	-5.48366253	2.98066534	-0.67205593
H	-6.51499020	1.61265743	-0.26287969
C	-0.17266010	-0.15800672	0.24527296
H	-0.06836532	0.90967243	0.04583278
H	0.04446691	-0.67953483	-0.68874803
C	0.87523973	-0.57591930	1.31879836
H	0.76269518	-1.64176622	1.51861453
H	0.66922743	-0.02873103	2.23871640
C	2.25707763	-0.28915193	0.85472020
C	2.86347806	0.97024543	1.10573553
C	2.98220660	-1.26081275	0.10690366
C	4.11677084	1.24547411	0.64714307
H	2.32106760	1.71277618	1.67288760

C	4.23924137	-1.01124175	-0.36374853
H	2.52254638	-2.22004042	-0.08359112
C	4.82911452	0.25735464	-0.10191190
H	4.60131654	2.19296935	0.82914047
H	4.77579266	-1.76118319	-0.92161792
C	6.85749261	-0.27598517	-1.28879972
H	7.07069362	-1.17408185	-0.71579151
H	6.35988158	-0.51339781	-2.22514209
H	7.76489633	0.28525788	-1.47031641
O	6.02081866	0.61683891	-0.50551390

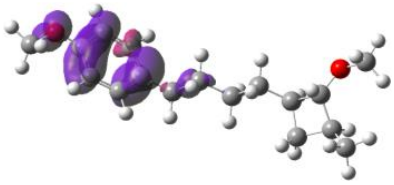

$18^{\bullet+}$ Total Energy = -813.528837 hartree/particle

Atom	X	Y	Z
C	4.00042589	-1.46791866	-0.47764204
C	5.38653369	-0.89679294	-0.06726618
C	4.64008453	0.39256897	0.37827347
C	3.43700394	-0.01929323	-0.48710839
H	3.94857263	-2.03628007	-1.40372301
H	3.56184125	-2.06222451	0.32608707
H	5.96421464	-0.66529554	-0.96453476
H	4.39574479	0.34534865	1.44763727
H	3.57001757	0.41460672	-1.48110239
C	2.02994885	0.25897838	0.02239722
H	1.91315245	-0.18643708	1.01495831
H	1.90150743	1.33835171	0.14859579
C	0.93534216	-0.27518676	-0.90703629
H	1.05931054	-1.35322644	-1.03811650
H	1.04875625	0.17402552	-1.89744313
O	5.17523751	1.66547148	0.06997065
C	6.23519853	2.06526063	0.93043350
H	5.91604411	2.05683973	1.97744808
H	7.10809164	1.41650785	0.82223116
H	6.51202681	3.07893220	0.65007846
C	6.23194033	-1.67339400	0.92886235
H	5.67446861	-1.86355485	1.84823387
H	6.52958099	-2.64012594	0.51733959
H	7.14260199	-1.13418570	1.19460764
C	-0.47227044	0.01023605	-0.37967111
H	-0.61421785	1.08557017	-0.25709794
H	-0.60006218	-0.44217512	0.60550208
C	-1.56800971	-0.54030653	-1.33951818
H	-1.43844674	-0.07848514	-2.31825720
H	-1.42731385	-1.61647785	-1.44492354
C	-2.93065681	-0.25562902	-0.82028471
C	-3.56378478	-1.16014130	0.08028314

C	-3.61046945	0.93900869	-1.17691302
C	-4.80340488	-0.90968192	0.59469420
H	-3.04773909	-2.06955794	0.35310333
C	-4.84858060	1.21339648	-0.67851267
H	-3.13729787	1.63145338	-1.85794655
C	-5.46993292	0.29132529	0.22083308
H	-5.26952456	-1.61018659	1.26823978
H	-5.38853202	2.11103885	-0.94001430
C	-7.40962414	-0.18599202	1.56978326
H	-6.85871771	-0.28846607	2.50061042
H	-8.33491056	0.35169194	1.73126323
H	-7.60312351	-1.15403263	1.11631594
O	-6.65580136	0.64424304	0.64643703

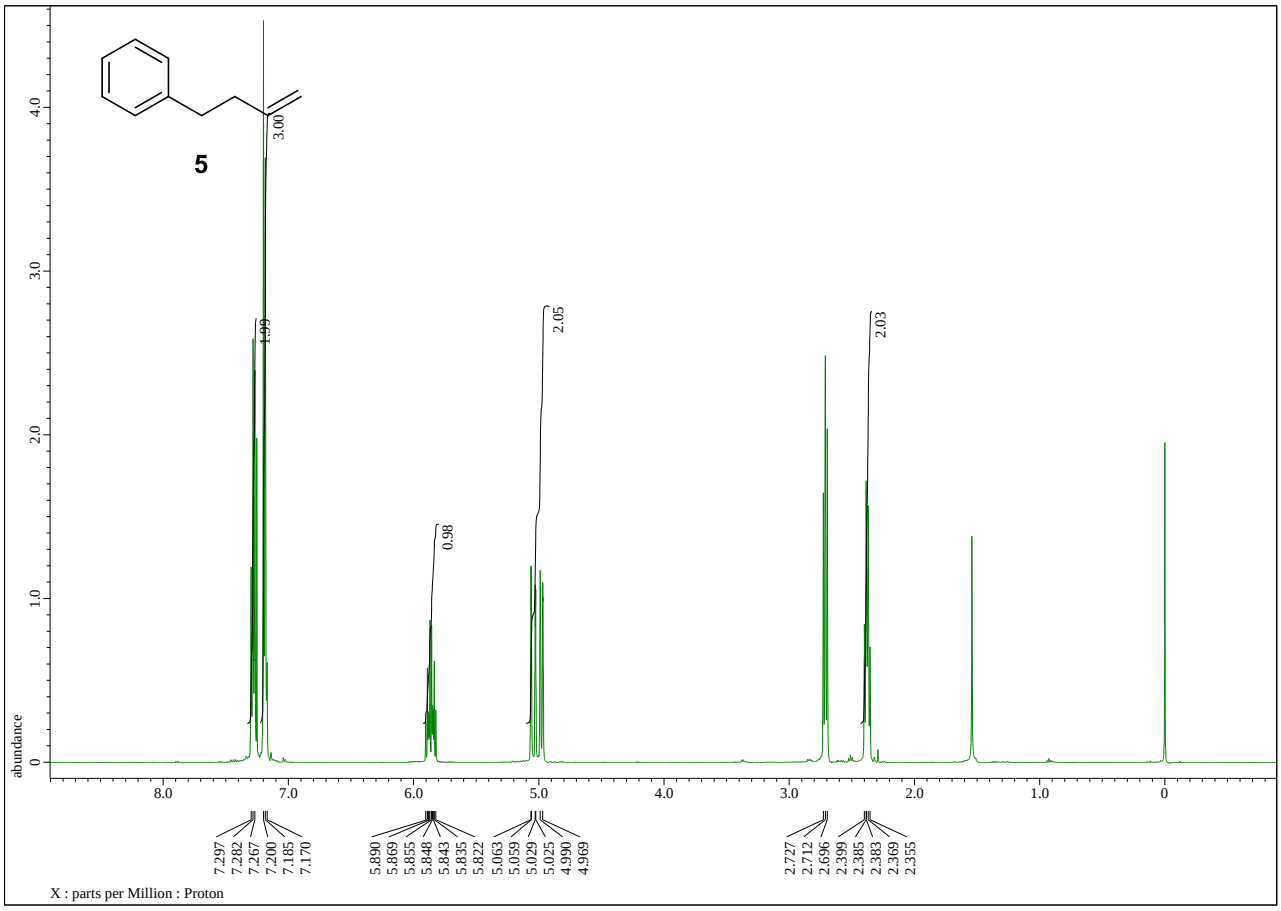
5
3.00
1.99
0.98
2.05
2.03
abundance
X : parts per Million : Proton

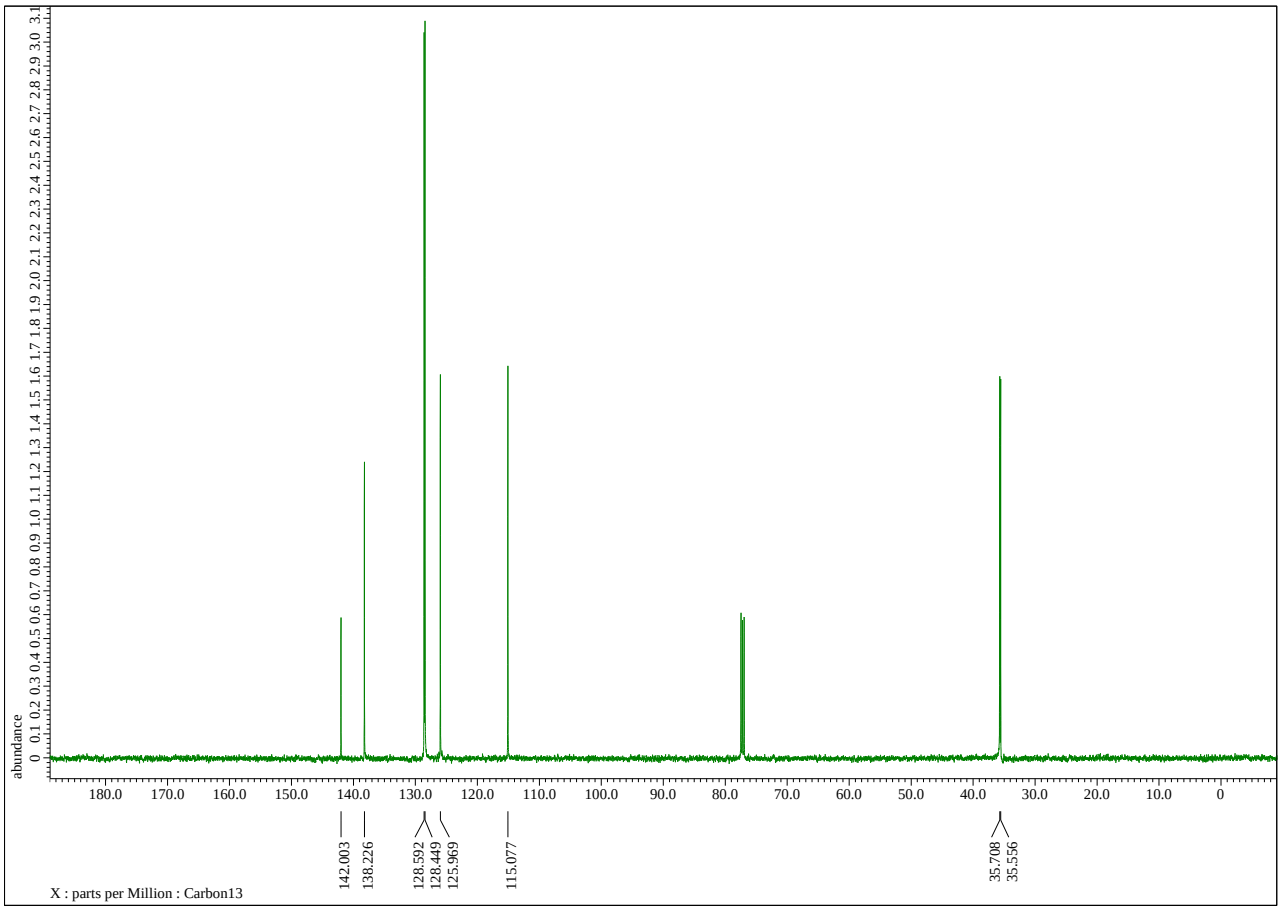
abundance
142.003
138.226
128.592
128.449
125.969
115.077
35.708
35.556
X : parts per Million : Carbon13

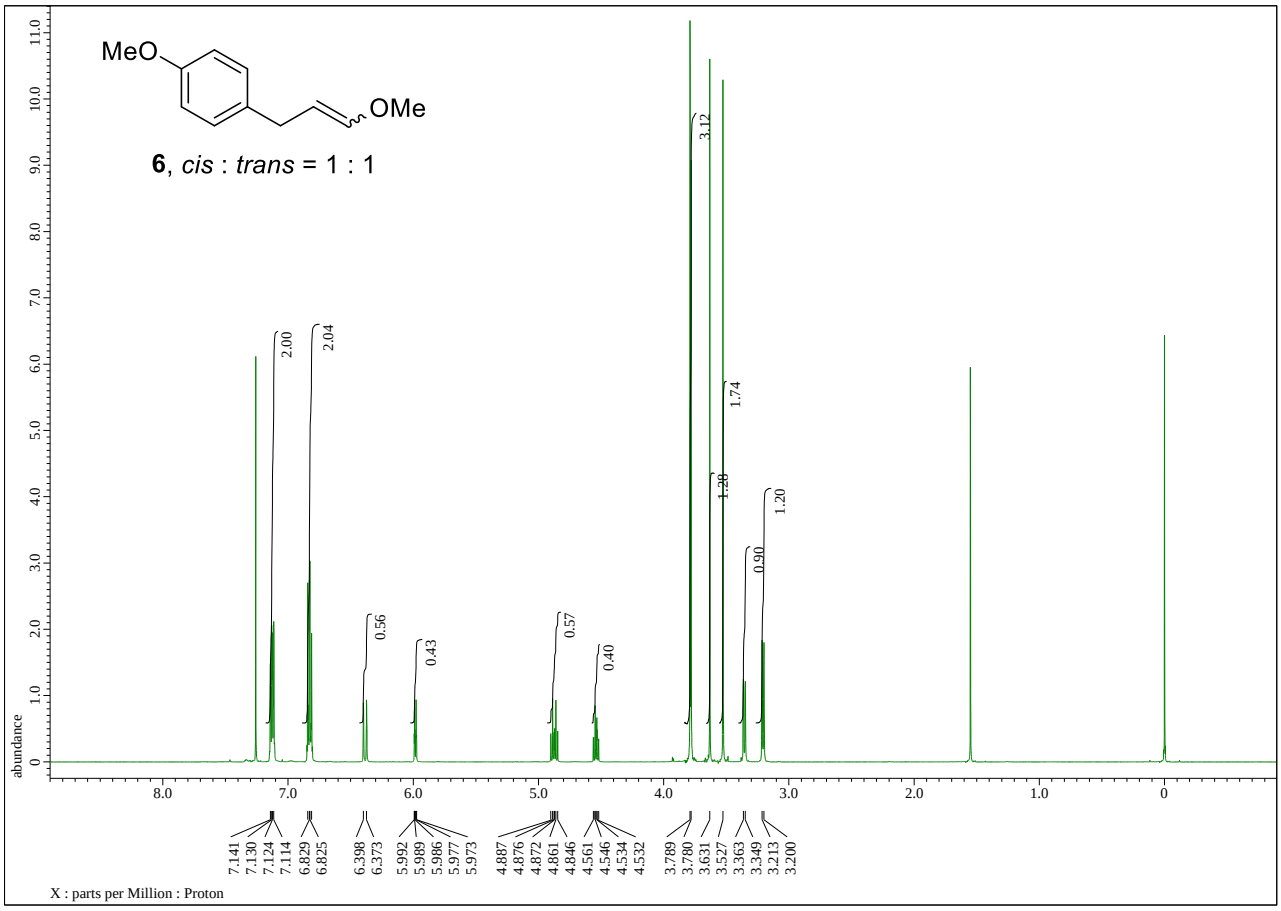
MeO
OMe
6, cis : trans = 1 : 1
abundance
X : parts per Million : Proton

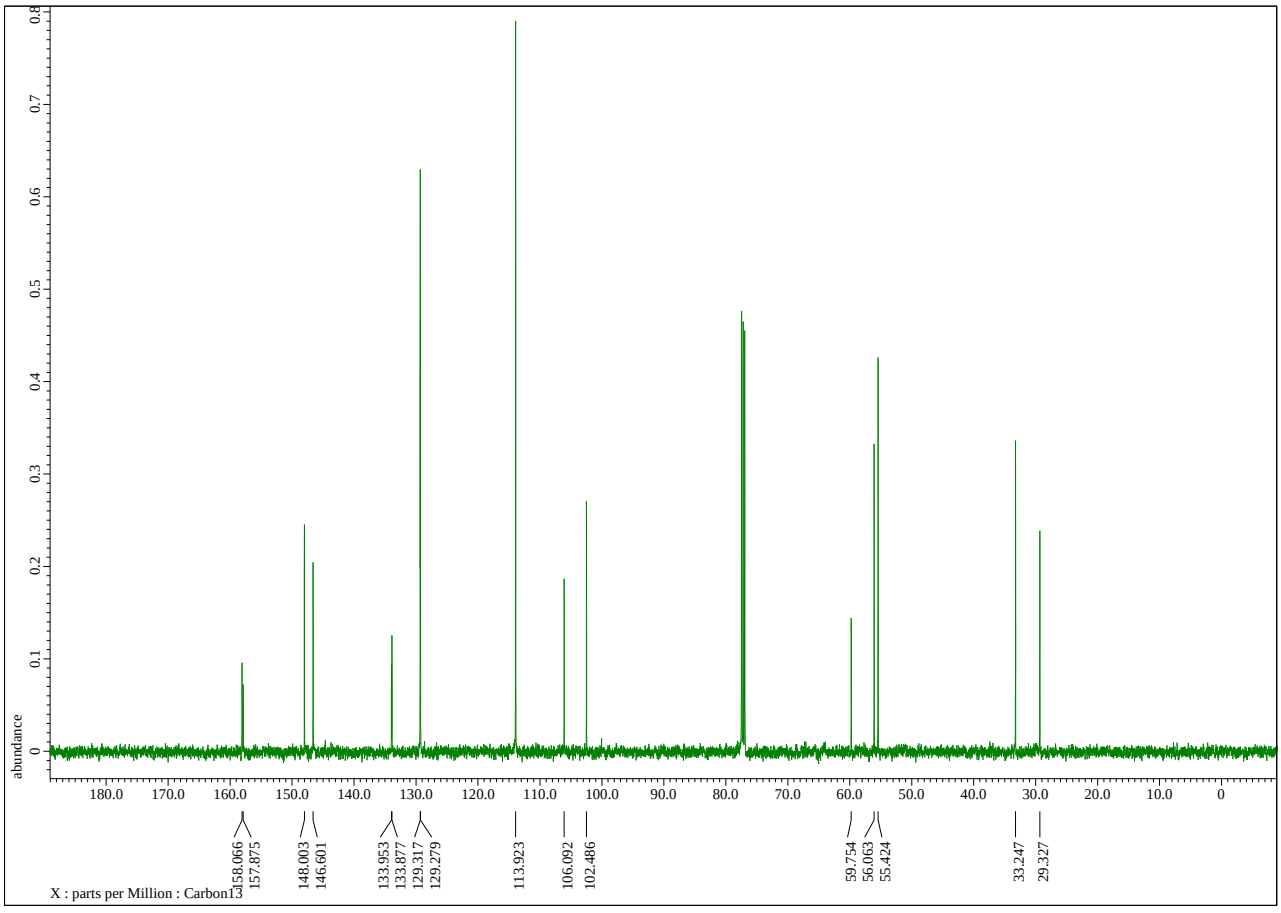
abundance
X : parts per Million : Carbon13

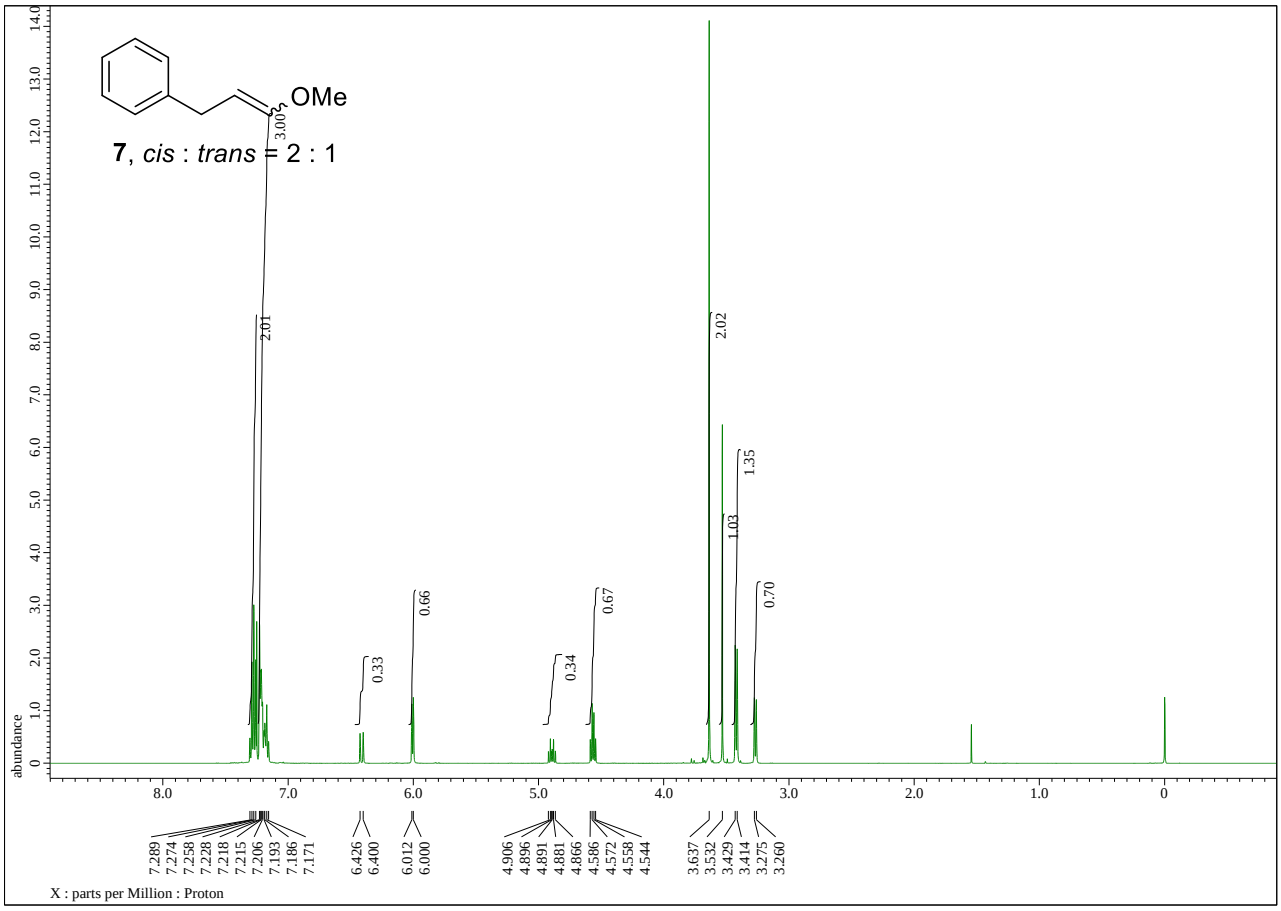
OMe
3.00
7, cis : trans = 2 : 1
2.01
2.02
1.35
1.03
0.70
0.67
0.66
0.33
0.34
abundance
X : parts per Million : Proton

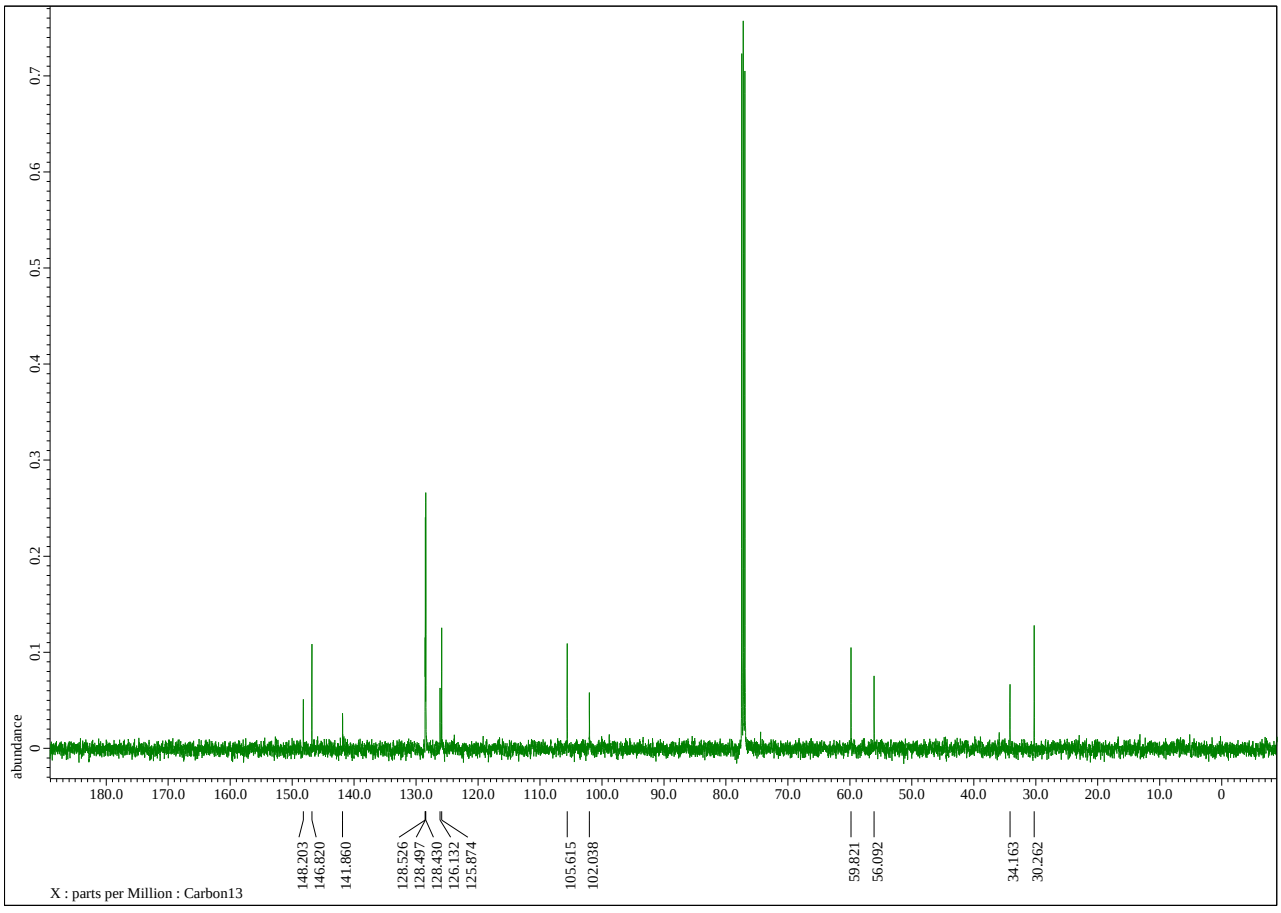
abundance
X : parts per Million : Carbon13

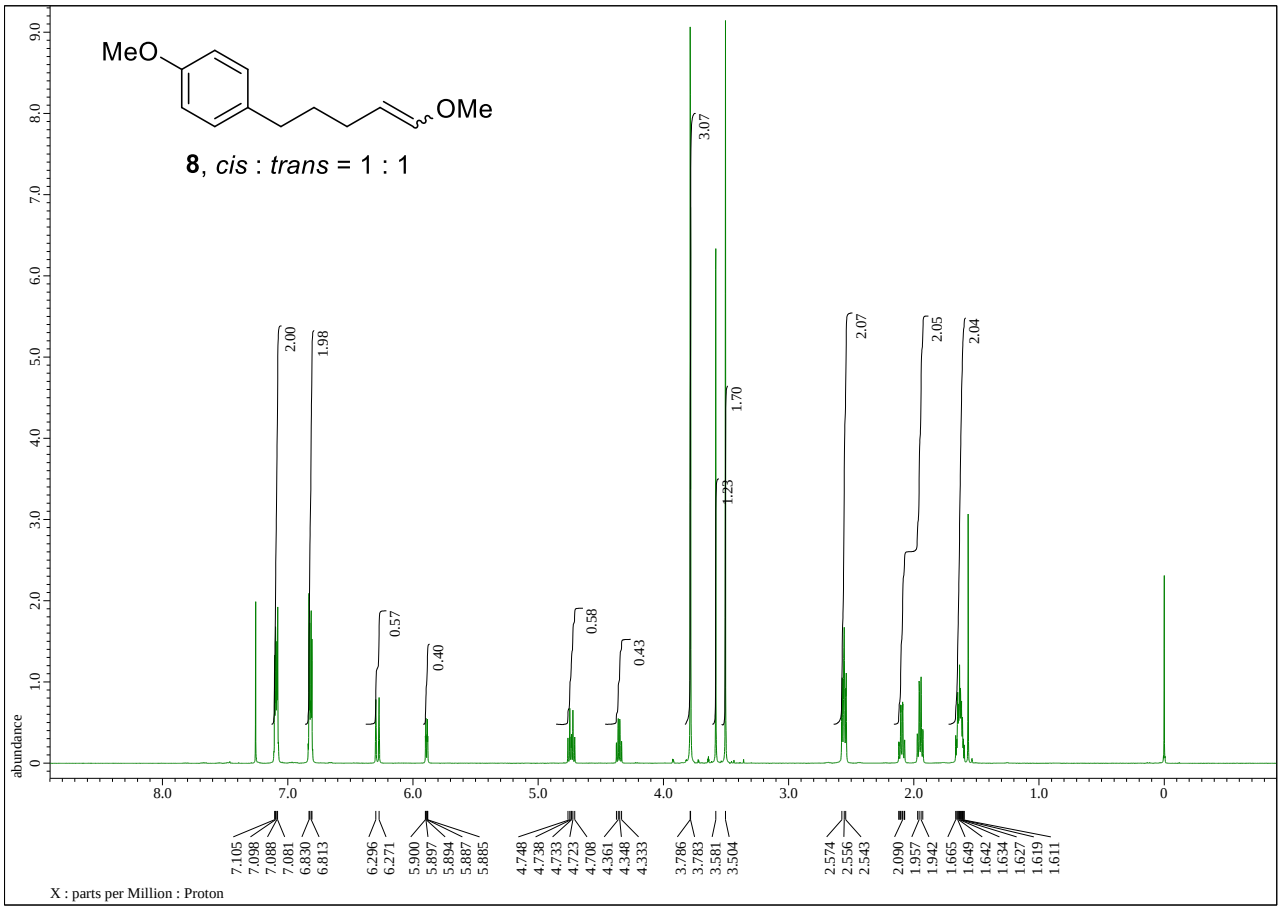
MeO
OMe
8, cis : trans = 1 : 1
abundance
X : parts per Million : Proton

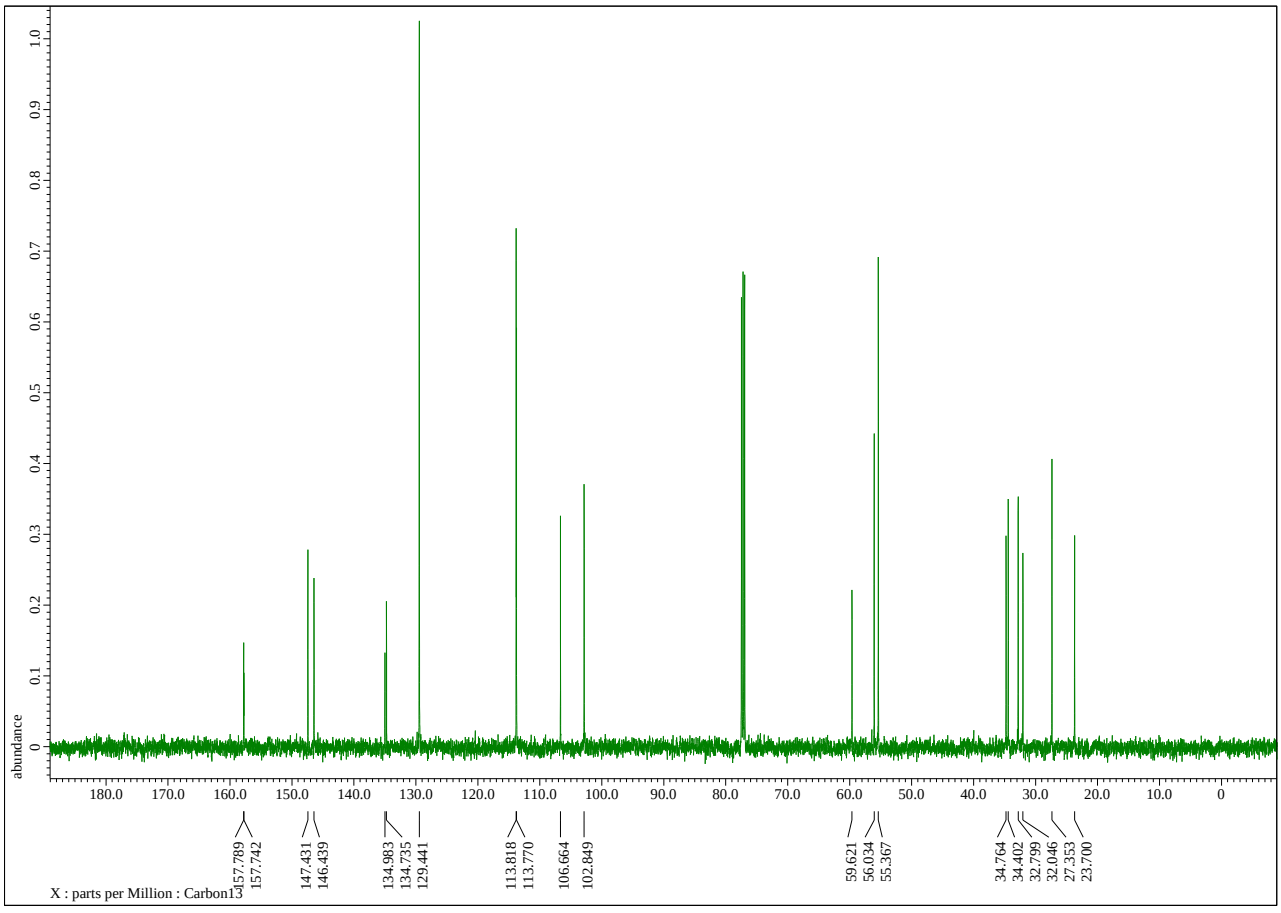
abundance
X : parts per Million : Carbon13

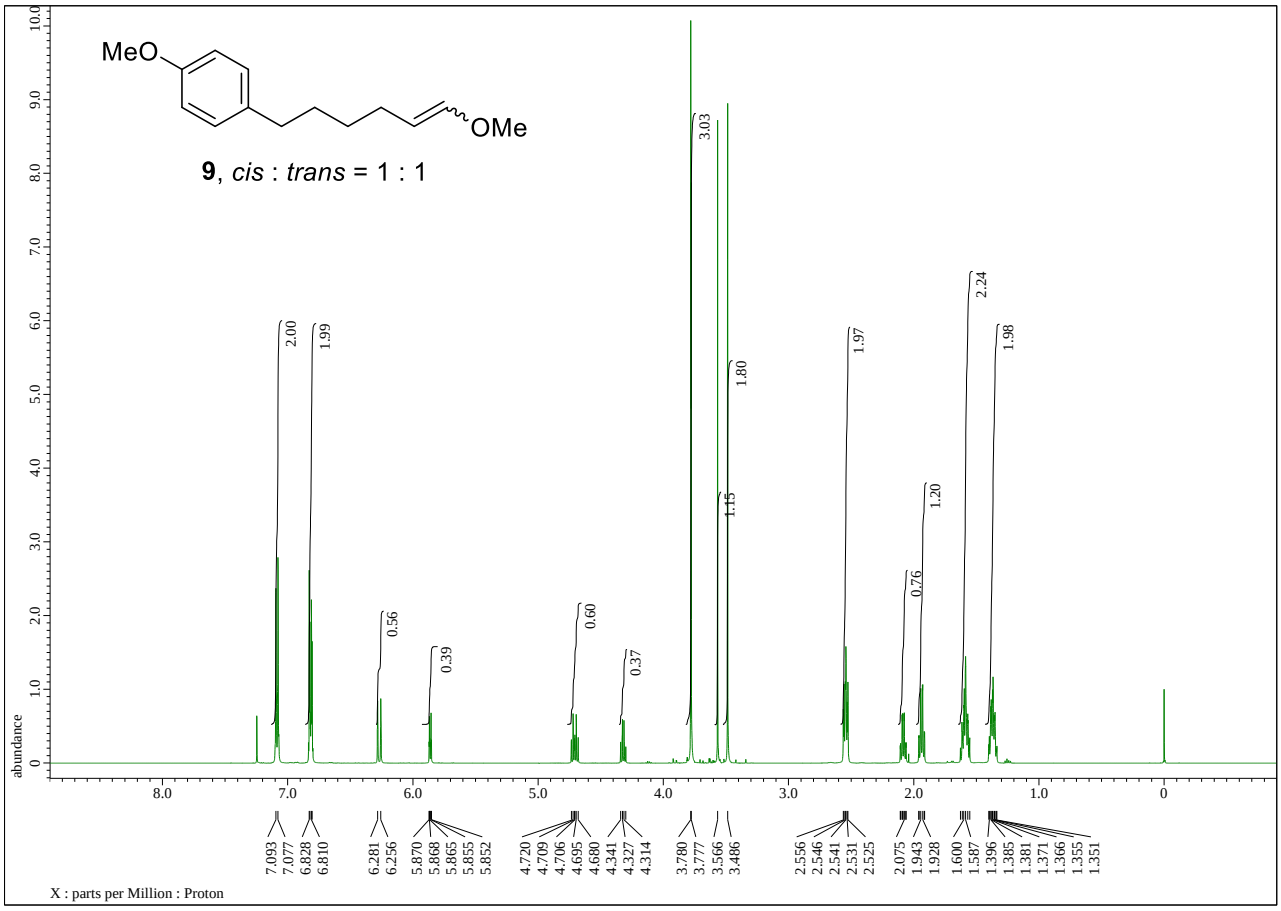
MeO
OMe
9, cis : trans = 1 : 1
abundance
X : parts per Million : Proton

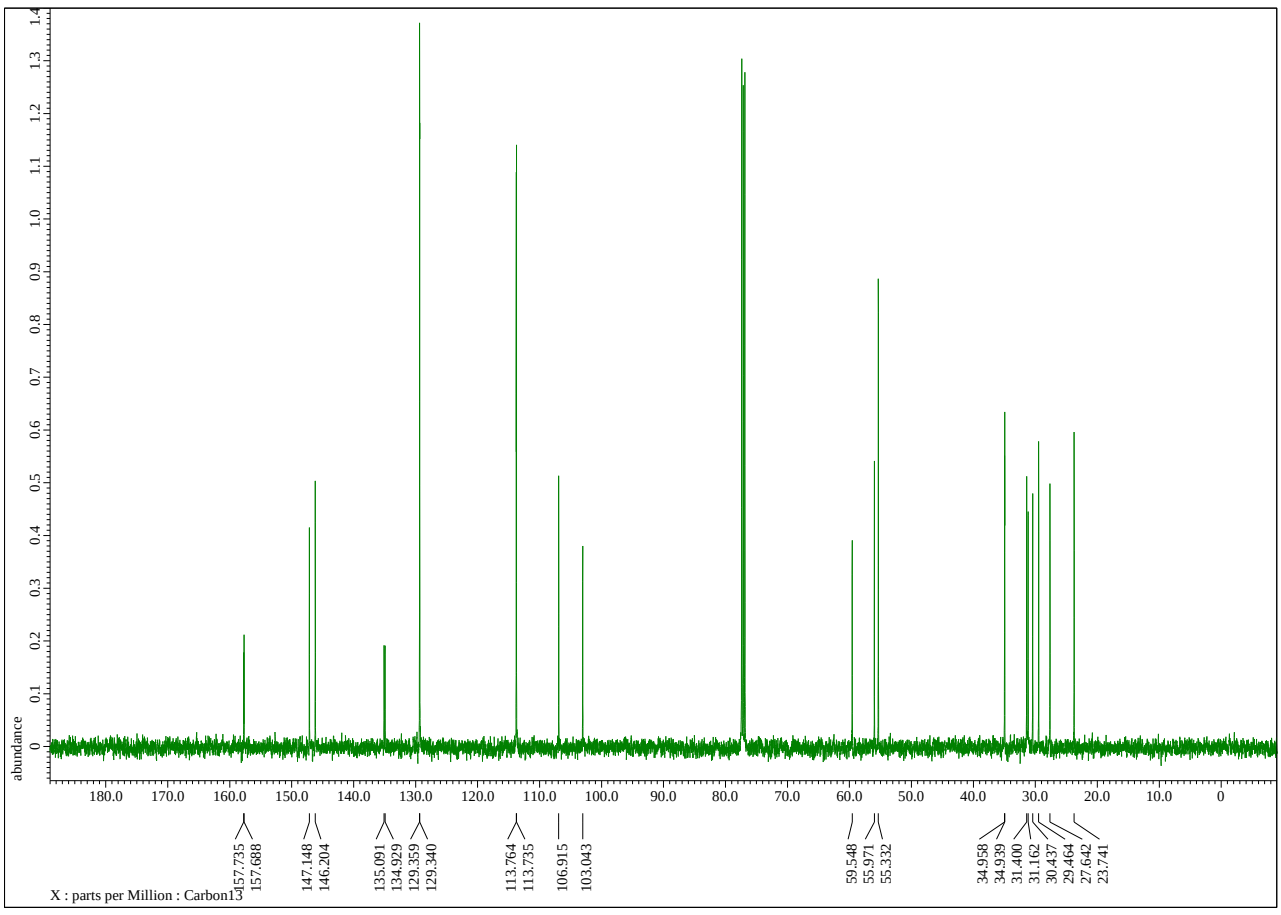
abundance
X : parts per Million : Carbon13

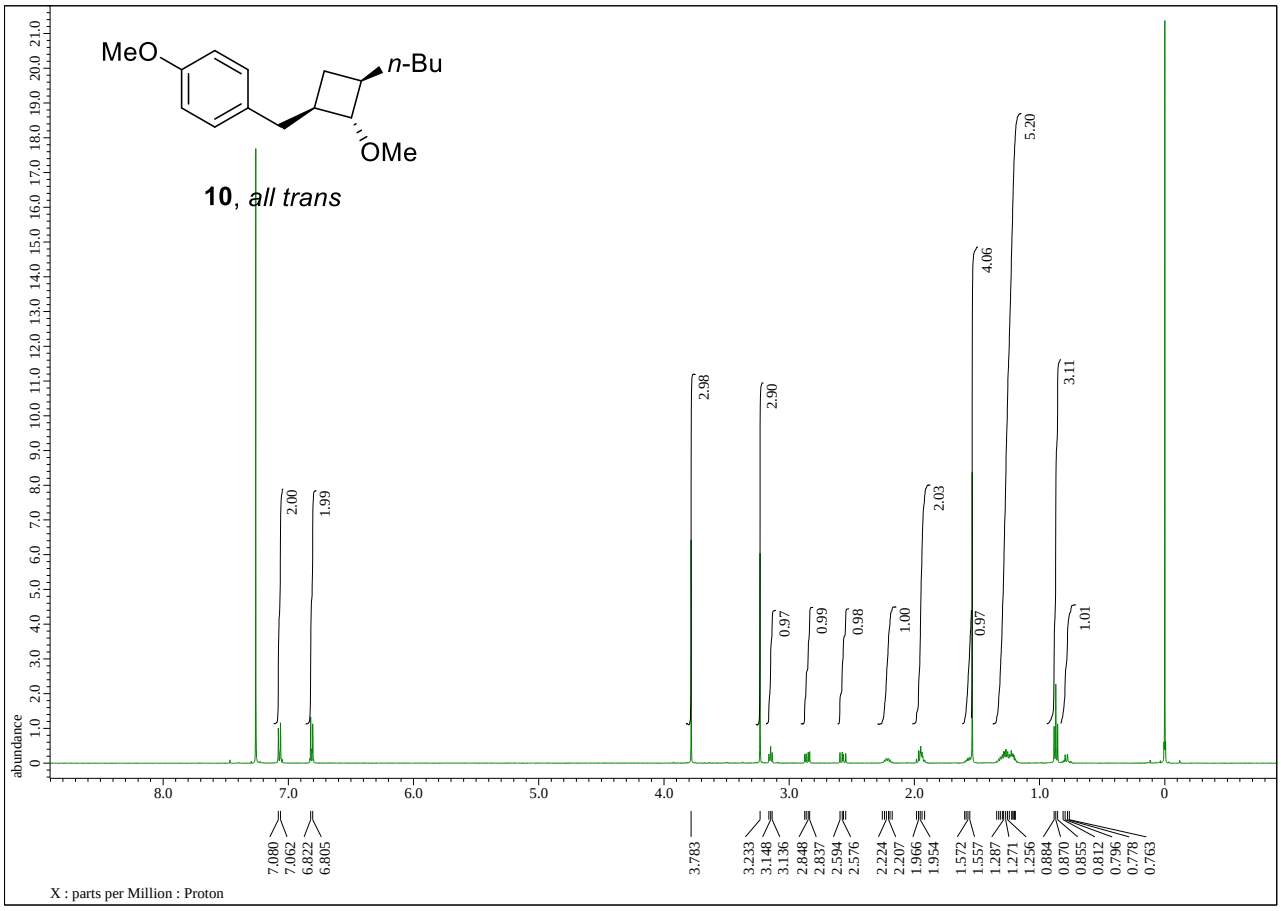
MeO
n-Bu
OMe
10, all trans
abundance
X : parts per Million : Proton

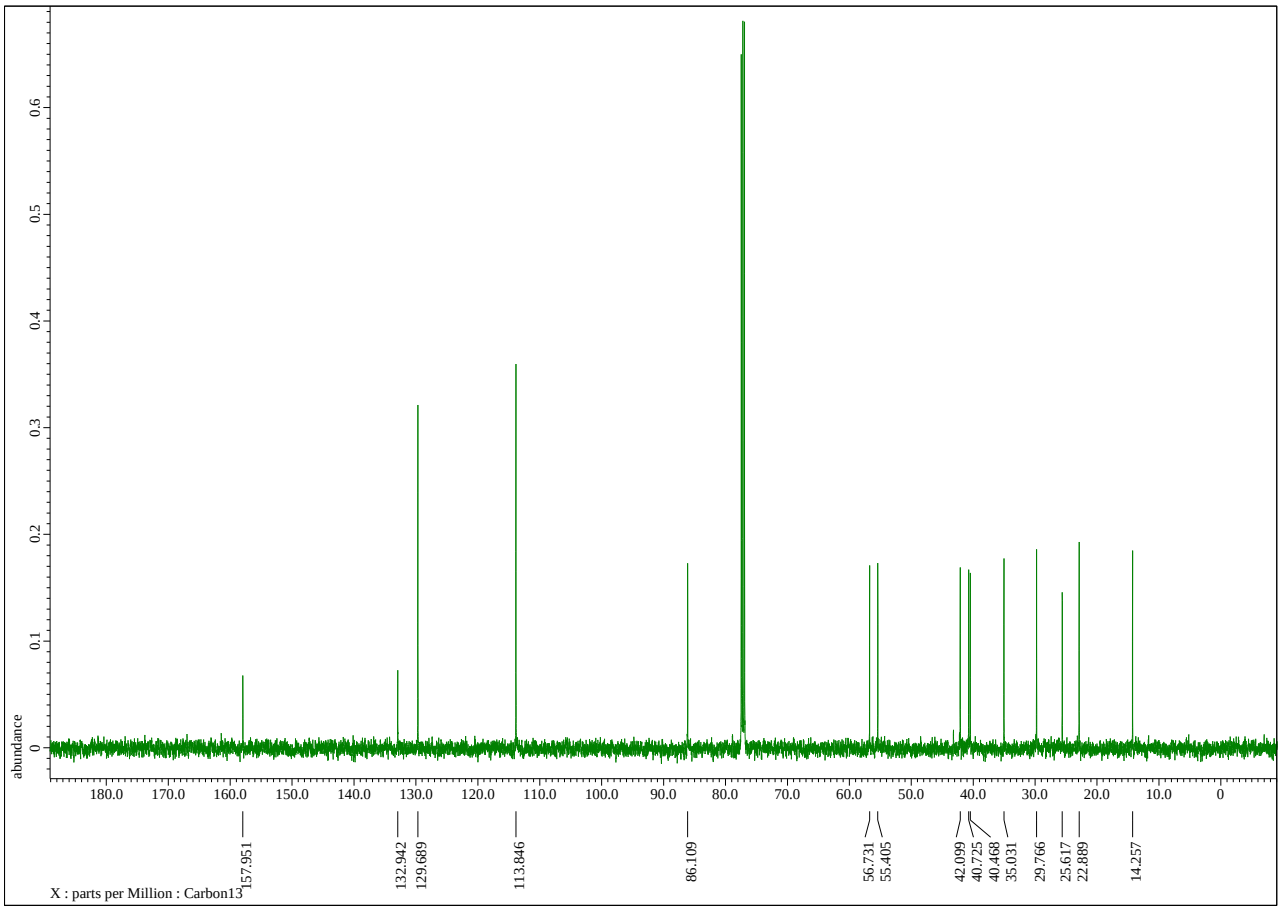
abundance
X : parts per Million : Carbon13

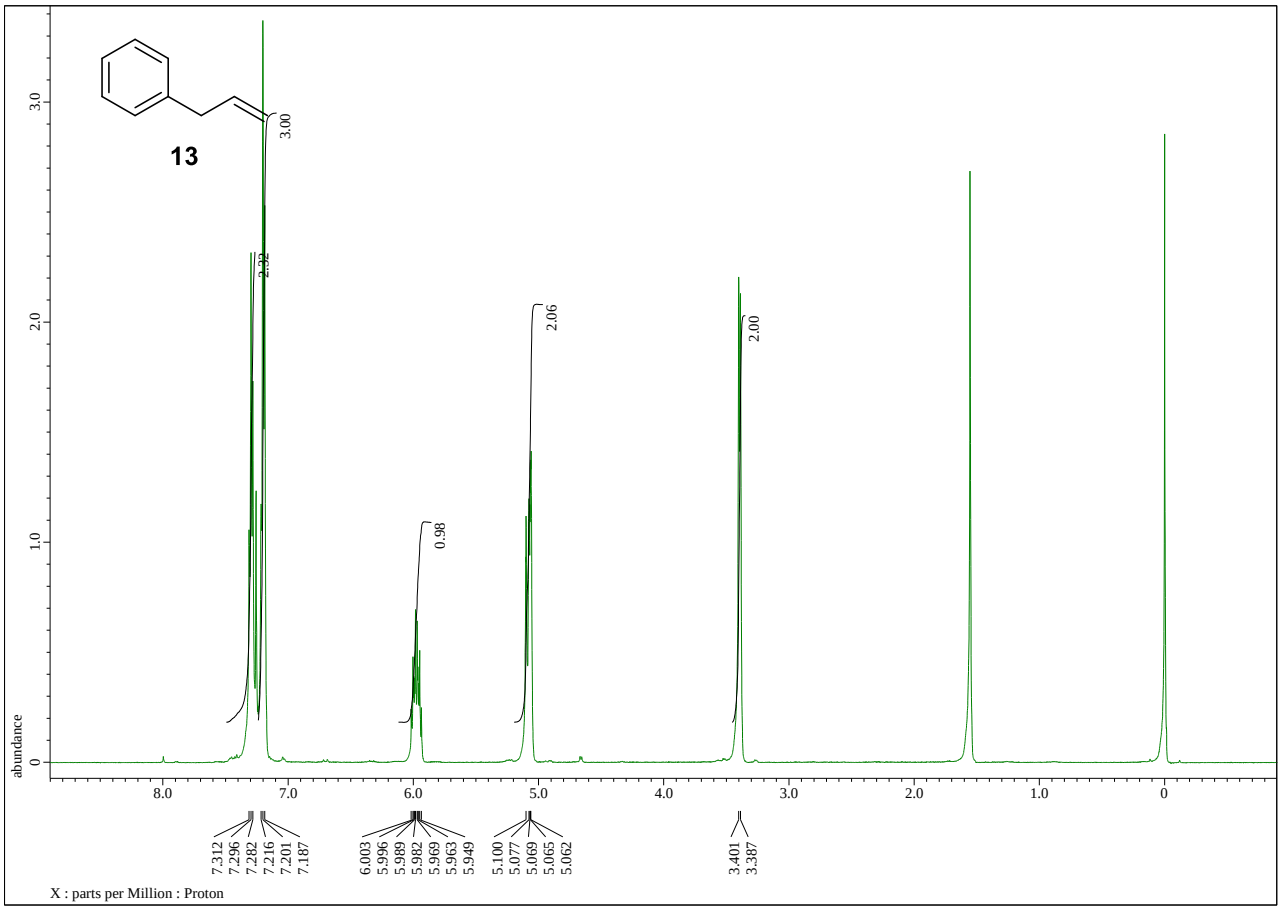
13
3.00
2.32
0.98
2.06
2.00
abundance
X : parts per Million : Proton

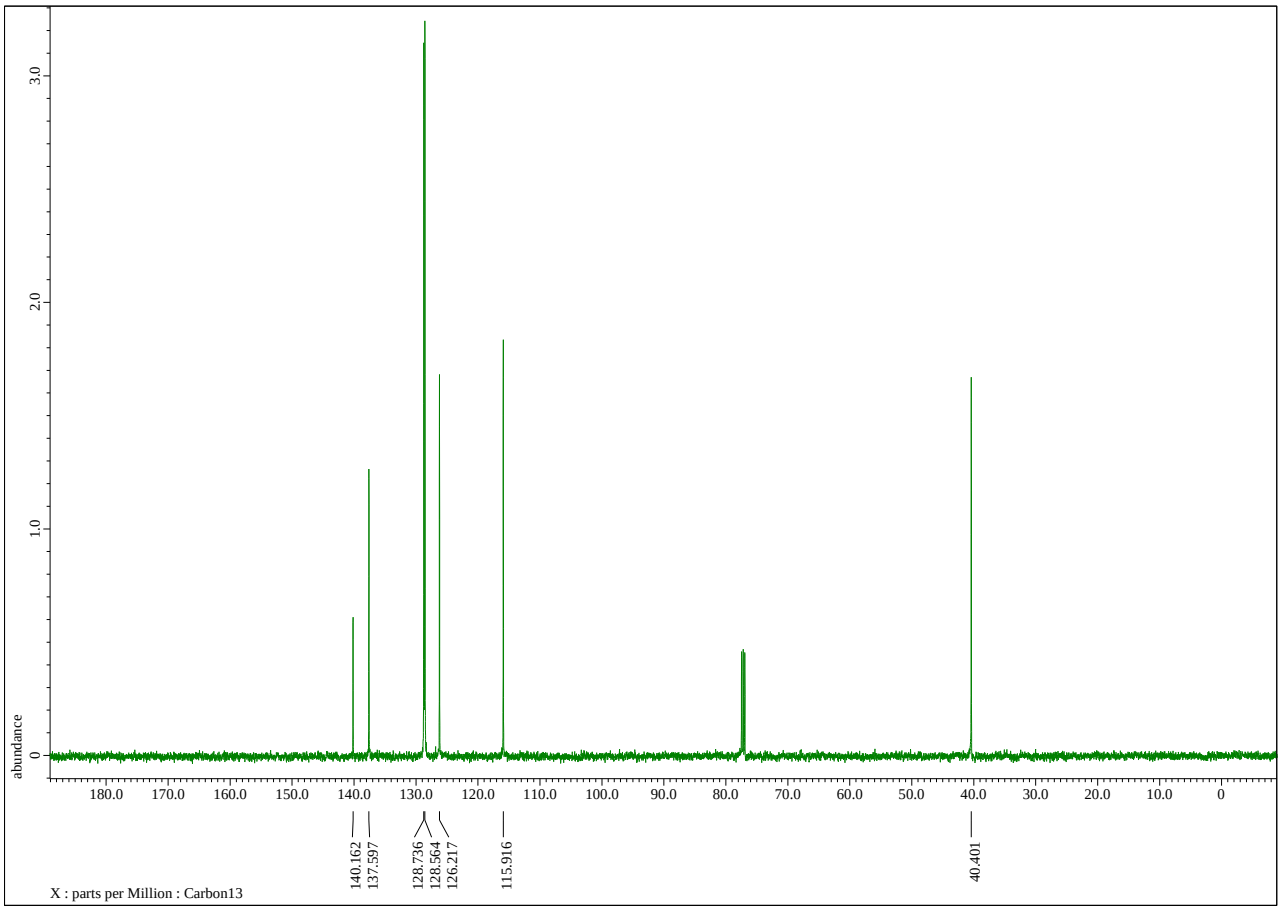
abundance
X : parts per Million : Carbon13

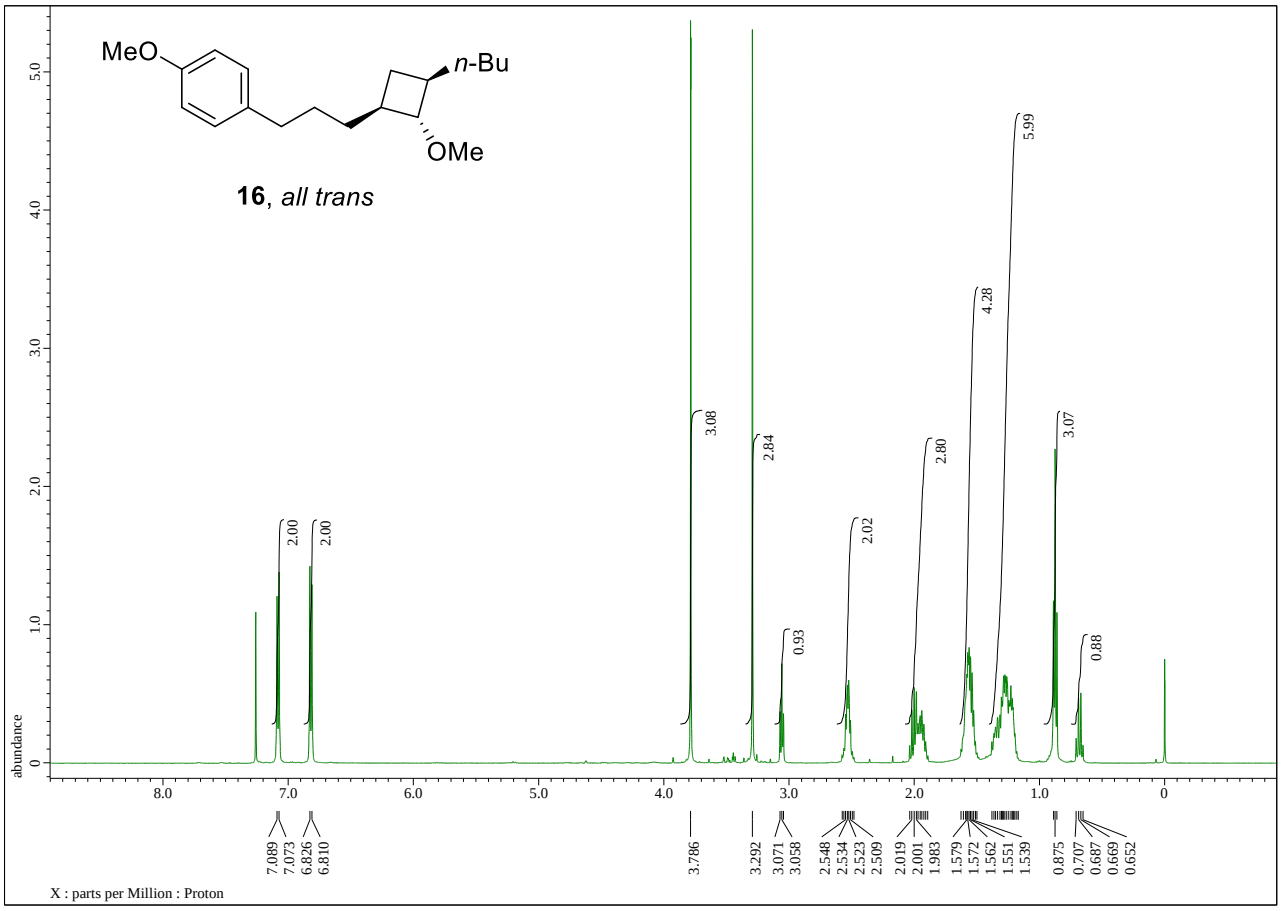
MeO
n-Bu
OMe
16, all trans
abundance
X : parts per Million : Proton

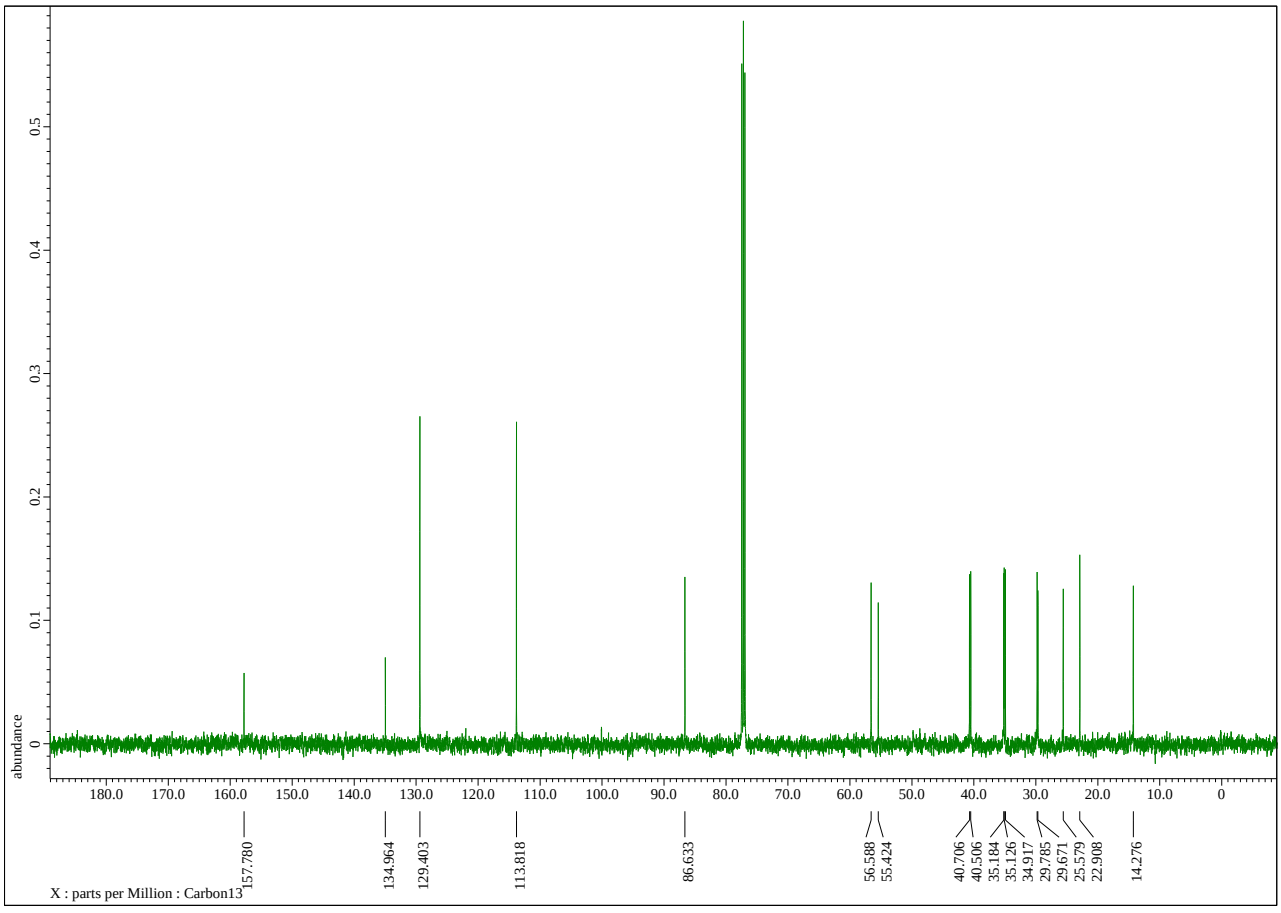
abundance
X : parts per Million : Carbon13

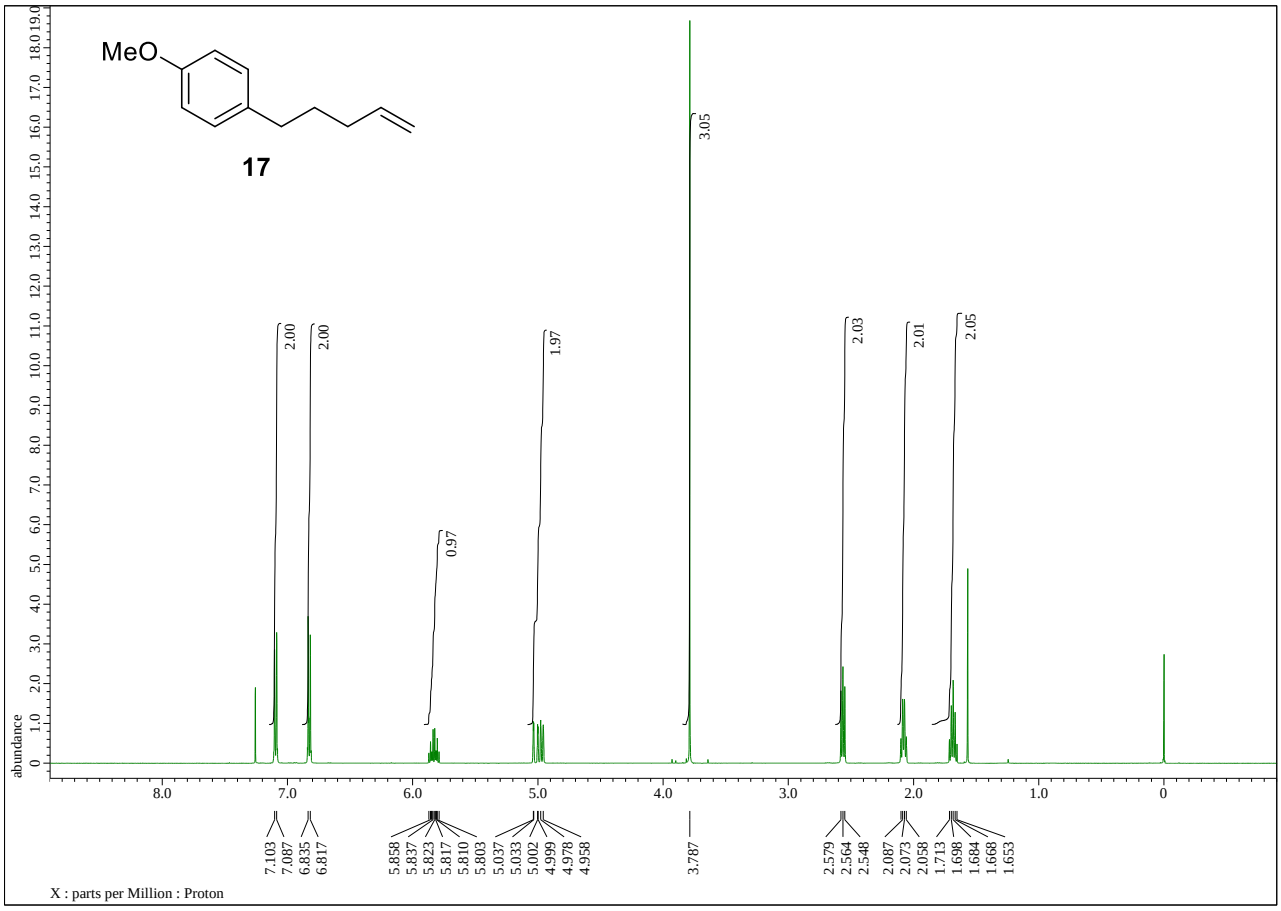
MeO
17
abundance
X : parts per Million : Proton
7.103
7.087
6.835
6.817
5.858
5.837
5.823
5.817
5.810
5.803
5.037
5.033
5.002
4.999
4.978
4.958
3.787
2.579
2.564
2.548
2.087
2.073
2.058
1.713
1.698
1.684
1.668
1.653
2.00
2.00
0.97
1.97
3.05
2.03
2.01
2.05

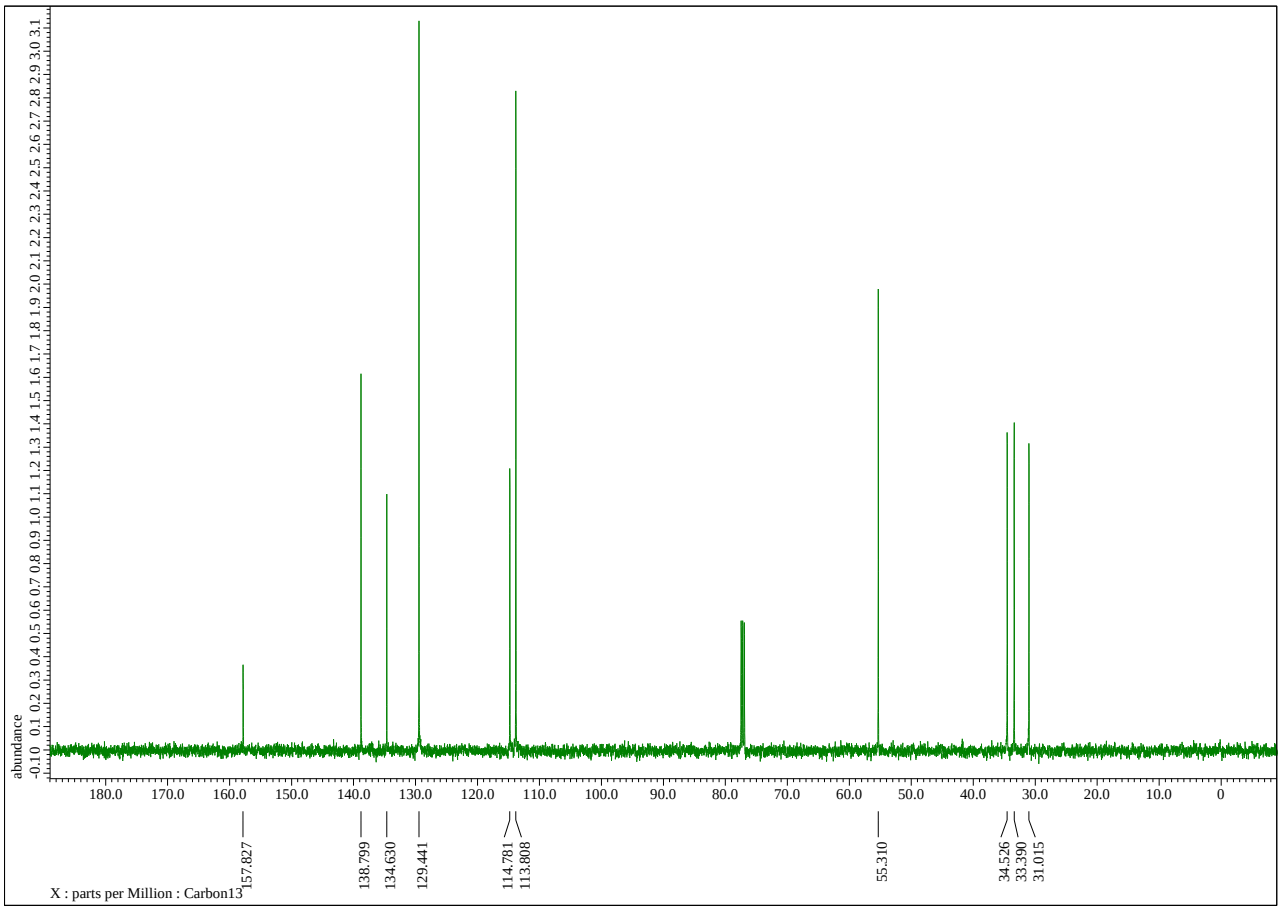
abundance
X : parts per Million : Carbon13
157.827
138.799
134.630
129.441
114.781
113.808
55.310
34.526
33.390
31.015

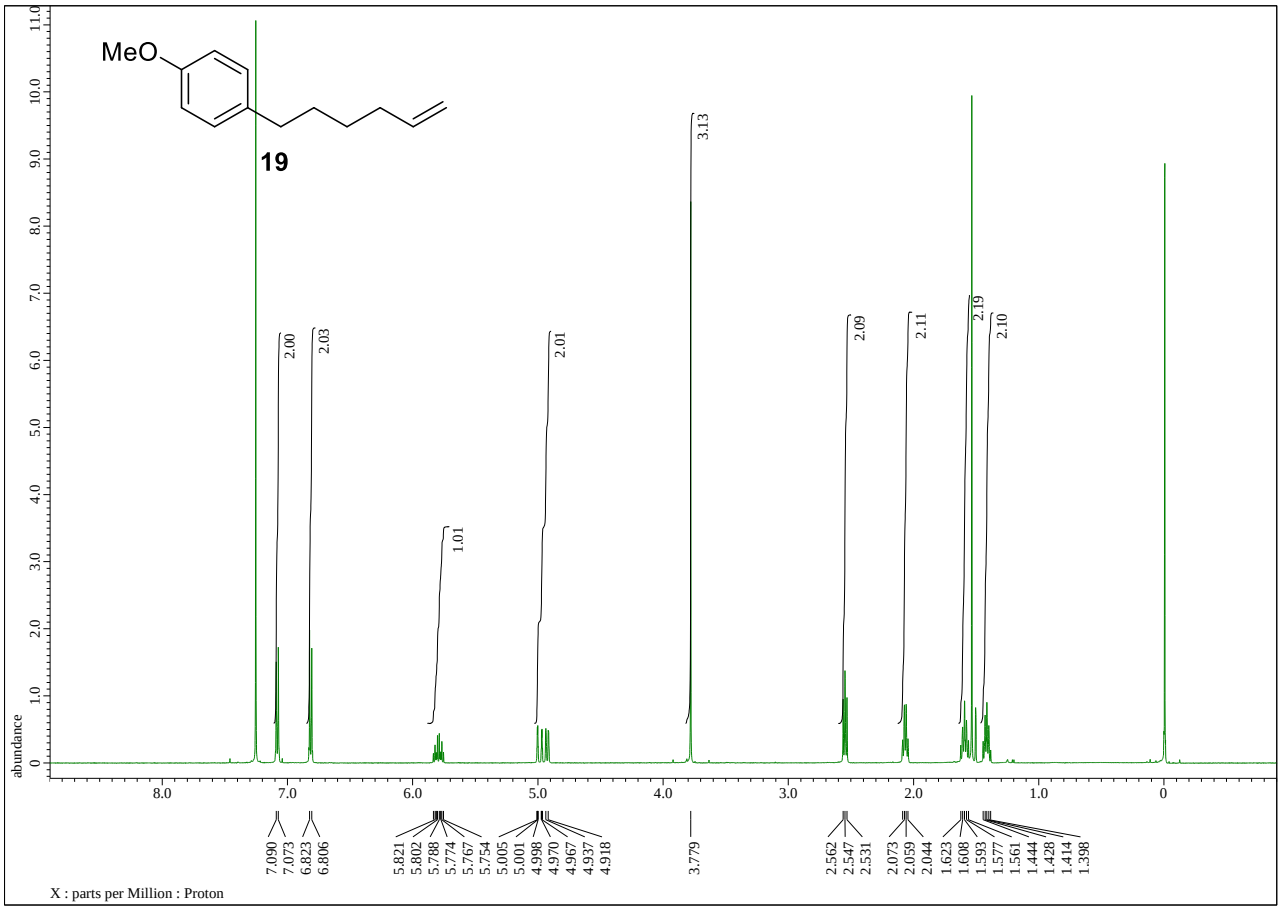
MeO
19
abundance
X : parts per Million : Proton
2.00
2.03
1.01
2.01
3.13
2.09
2.11
2.19
2.10
7.090
7.073
6.823
6.806
5.821
5.802
5.788
5.774
5.767
5.754
5.005
5.001
4.998
4.970
4.967
4.937
4.918
3.779
2.562
2.547
2.531
2.073
2.059
2.044
1.623
1.608
1.593
1.577
1.561
1.444
1.428
1.414
1.398

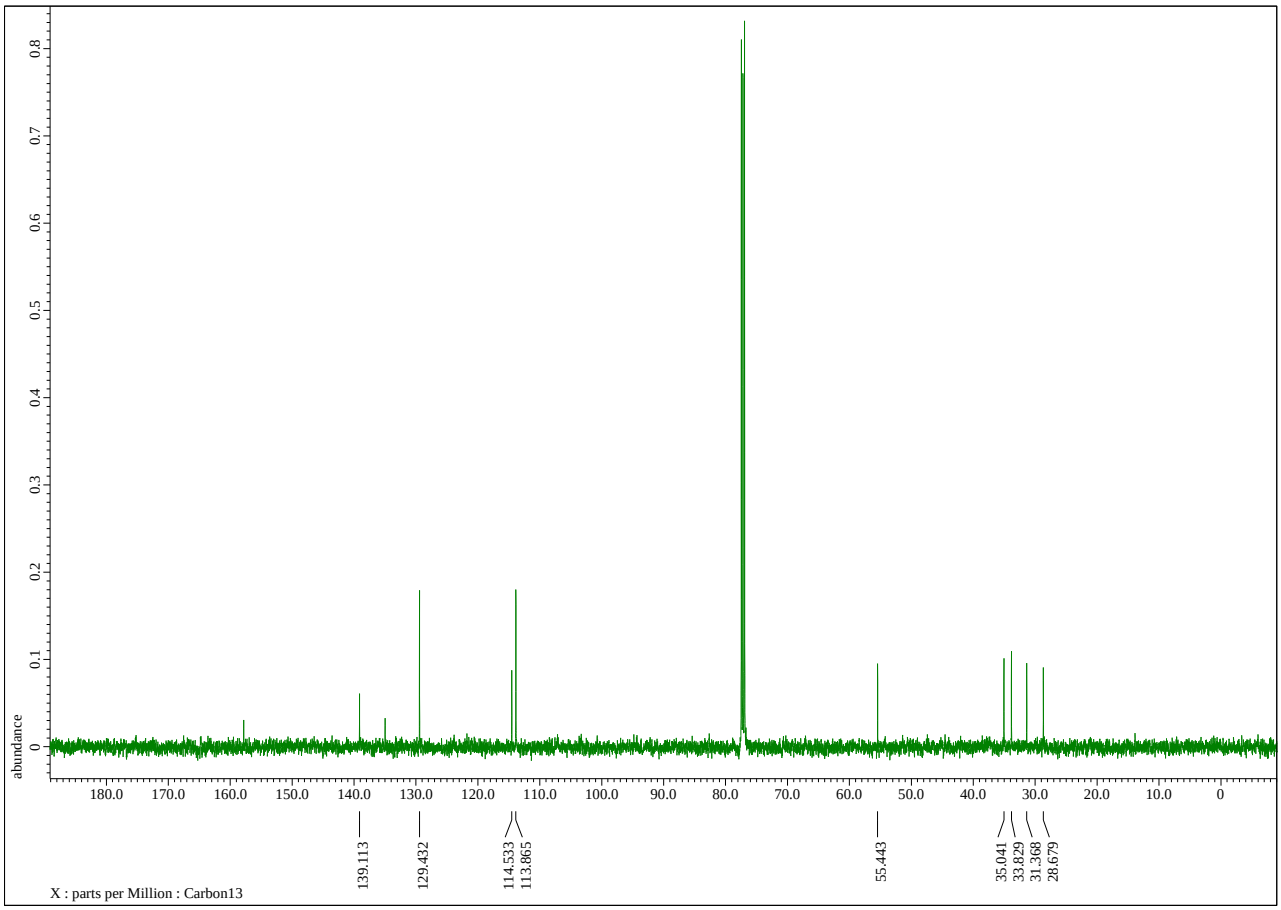
abundance
X : parts per Million : Carbon13
139.113
129.432
114.533
113.865
55.443
35.041
33.829
31.368
28.679

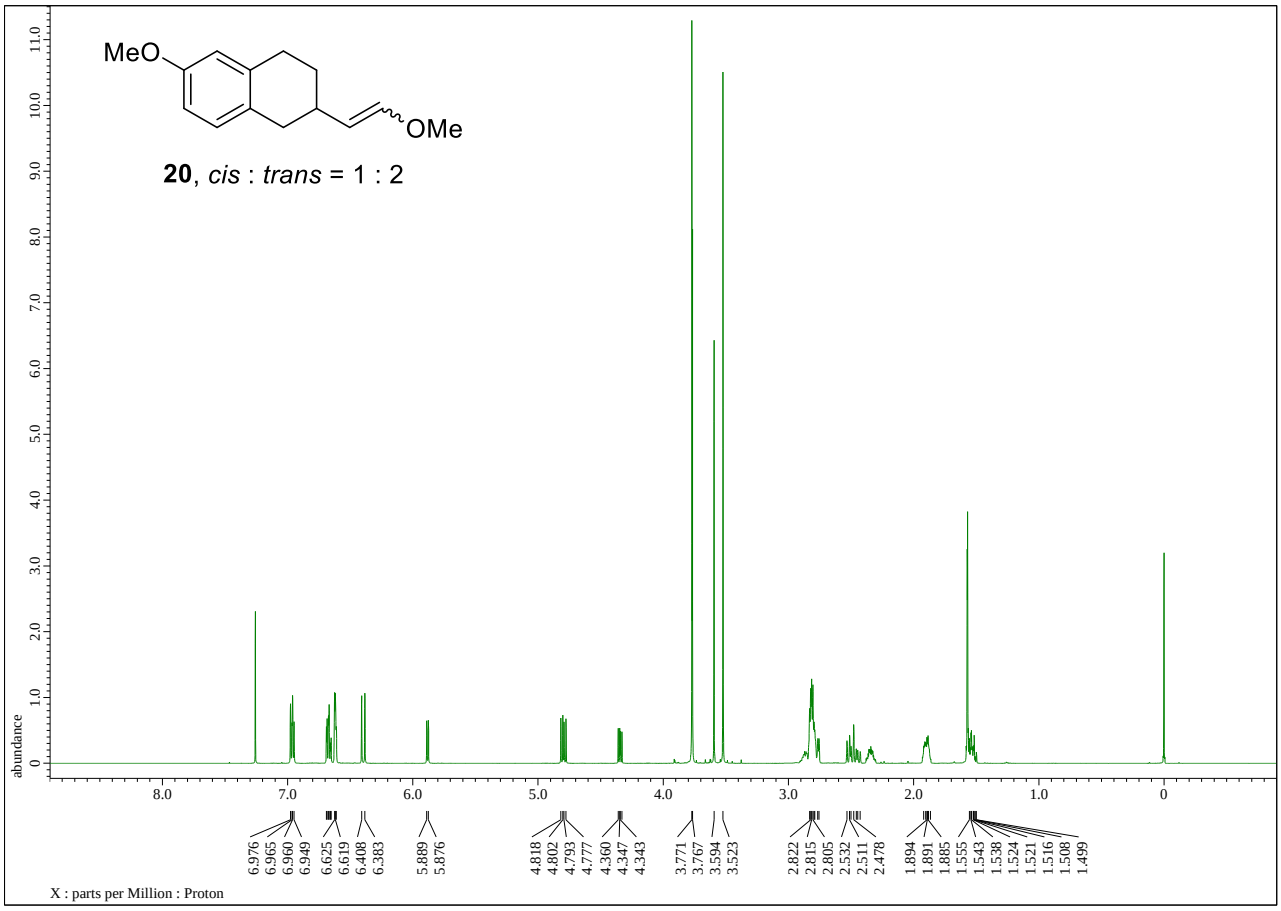
MeO
OMe
20, cis : trans = 1 : 2
abundance
X : parts per Million : Proton

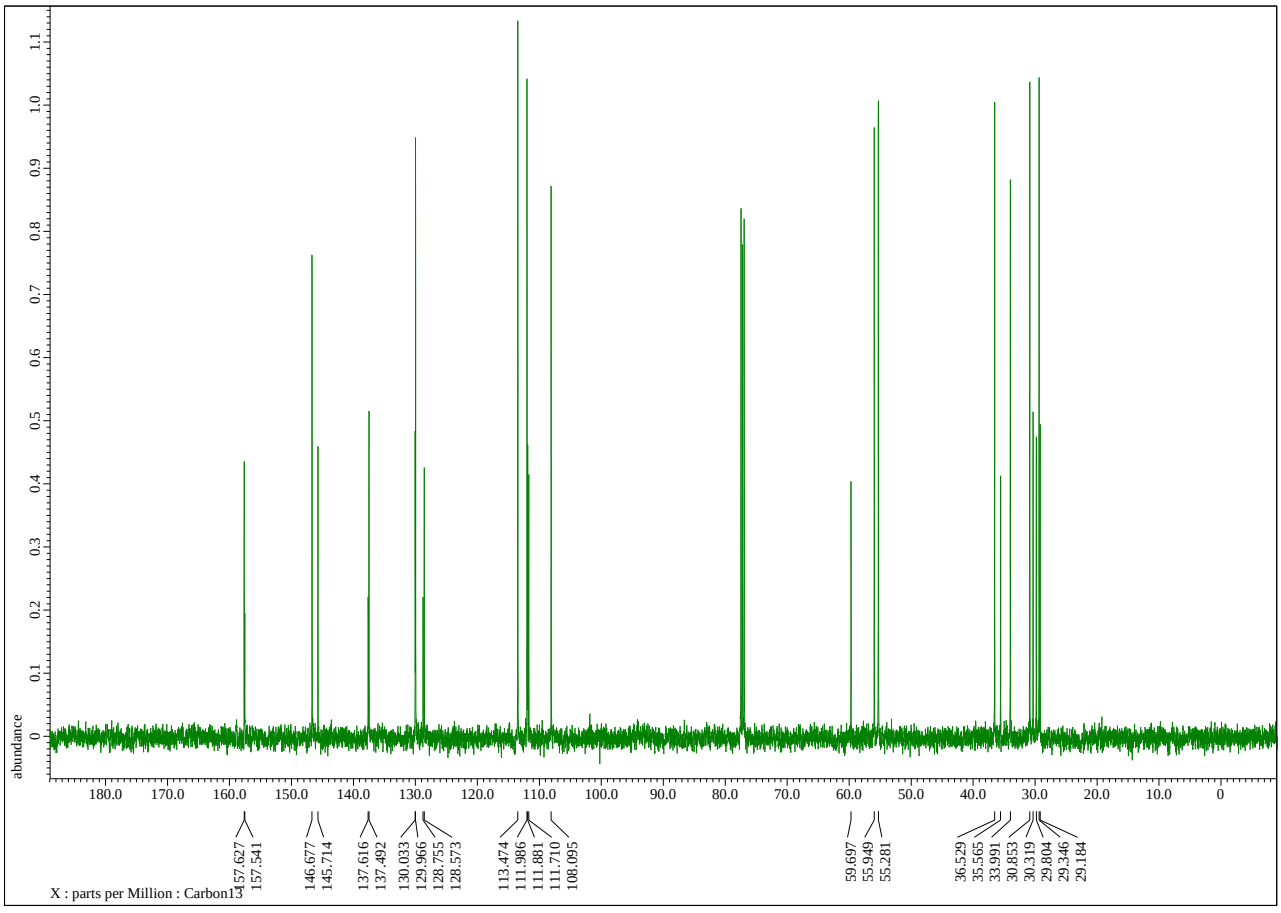
abundance
X : parts per Million : Carbon13

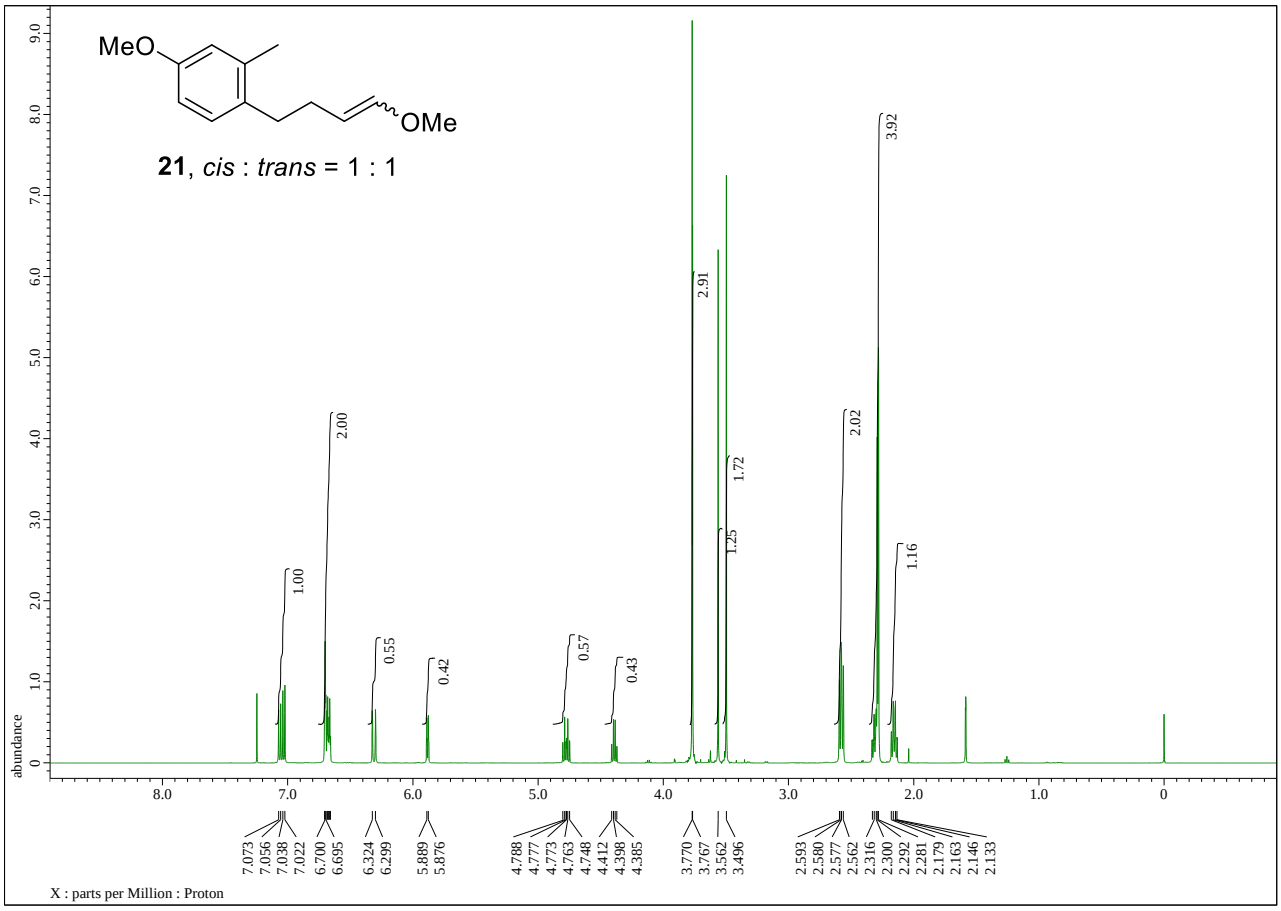
MeO
OMe
21, cis : trans = 1 : 1
abundance
X : parts per Million : Proton

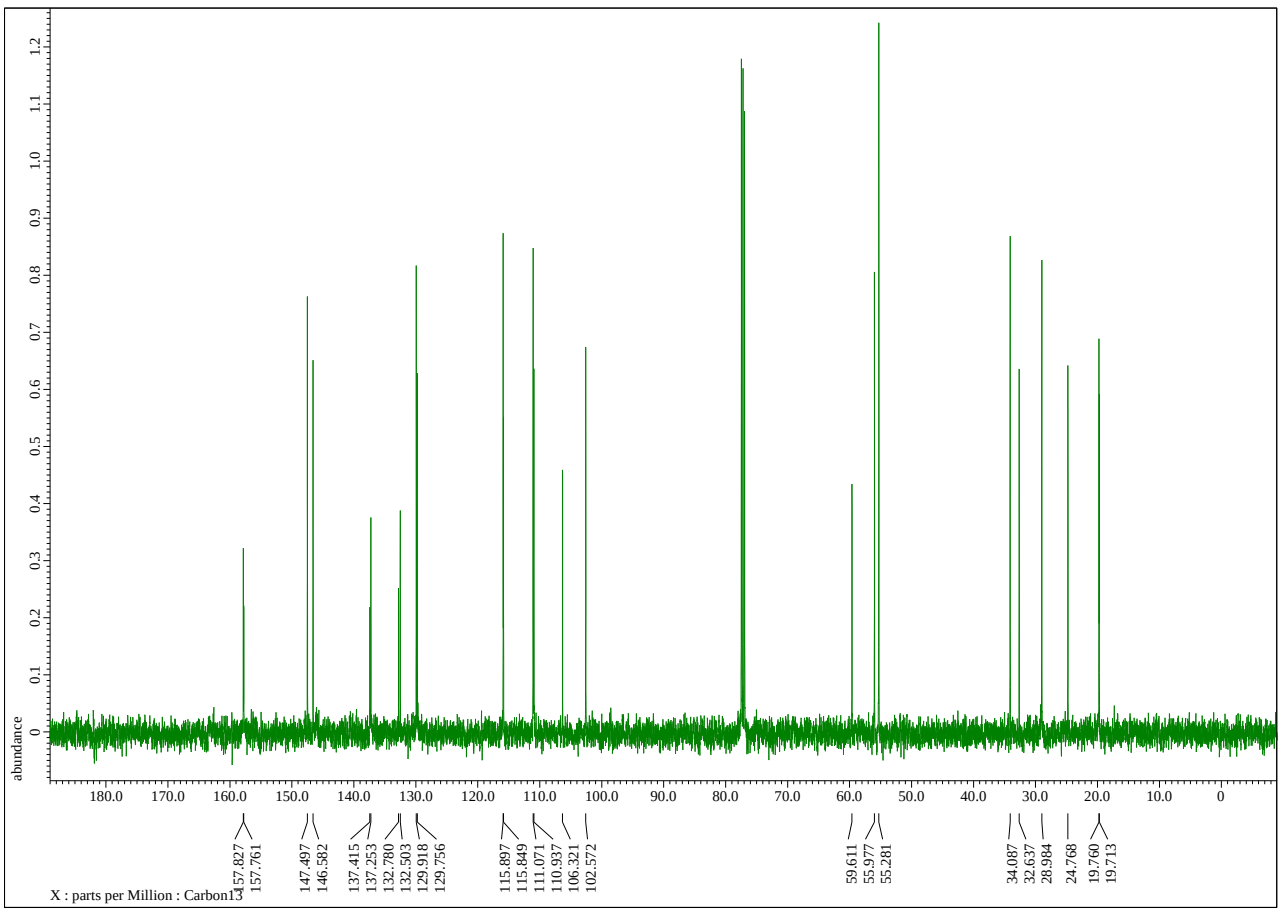
abundance
X : parts per Million : Carbon13

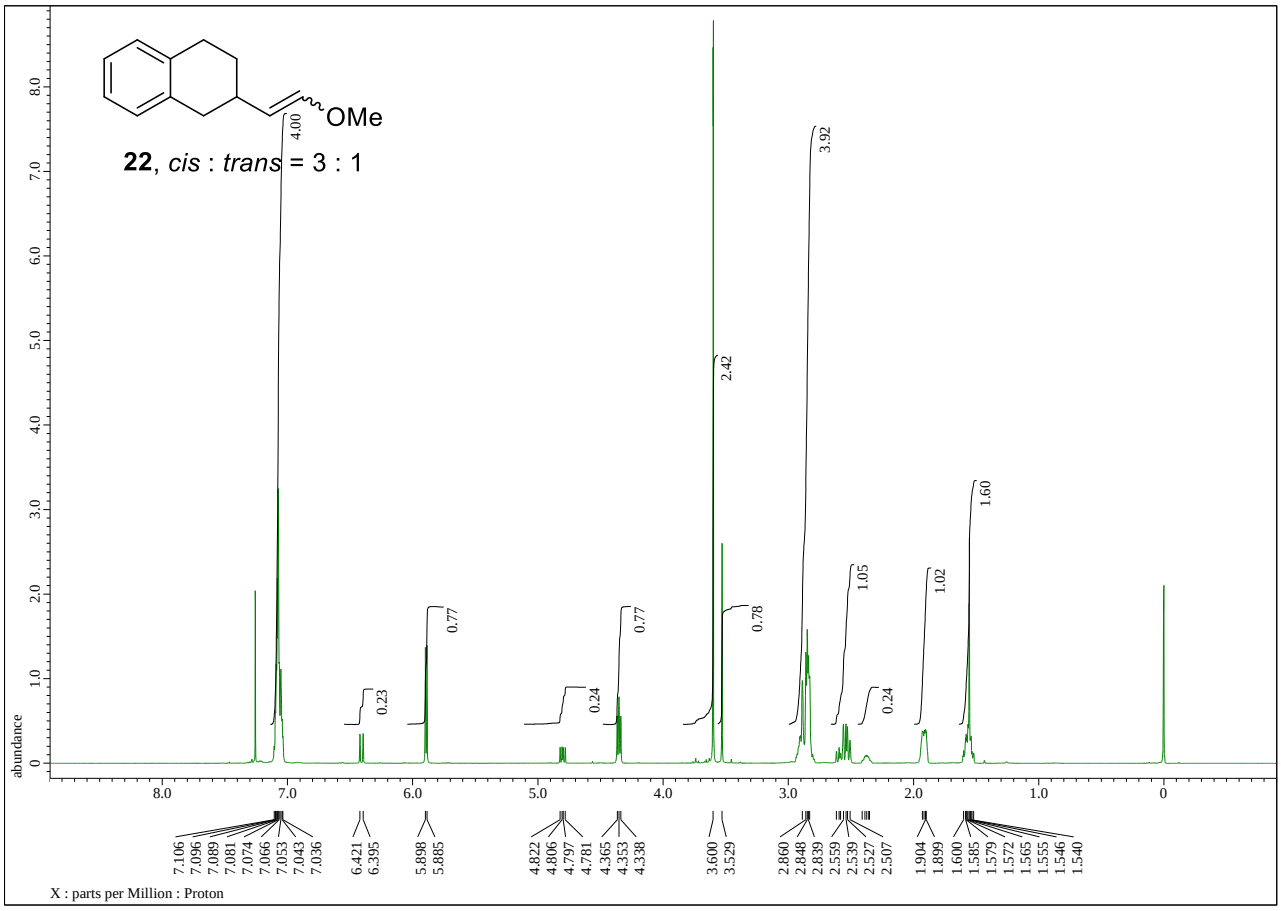
OMe
22, cis : trans = 3 : 1
abundance
X : parts per Million : Proton

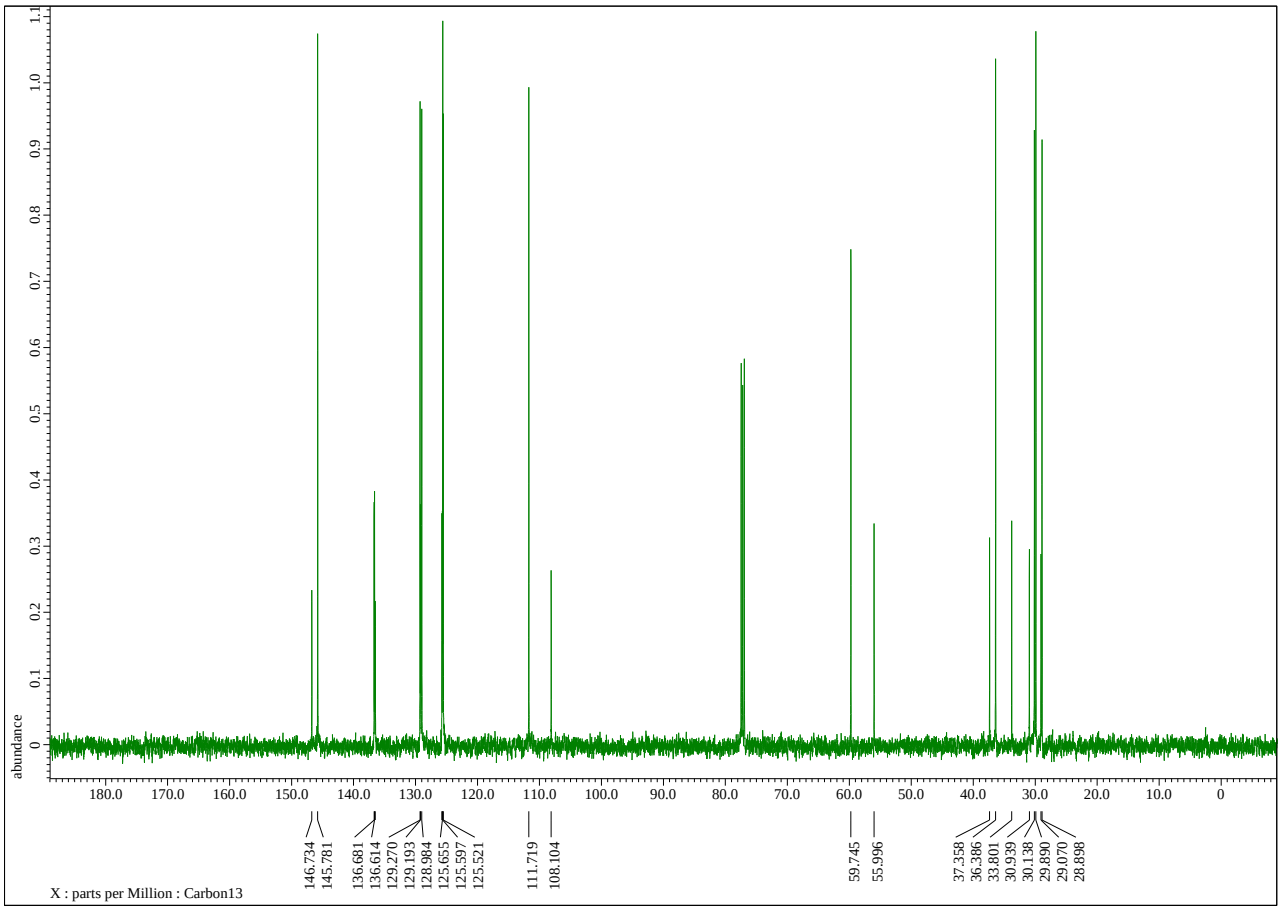
abundance
X : parts per Million : Carbon13

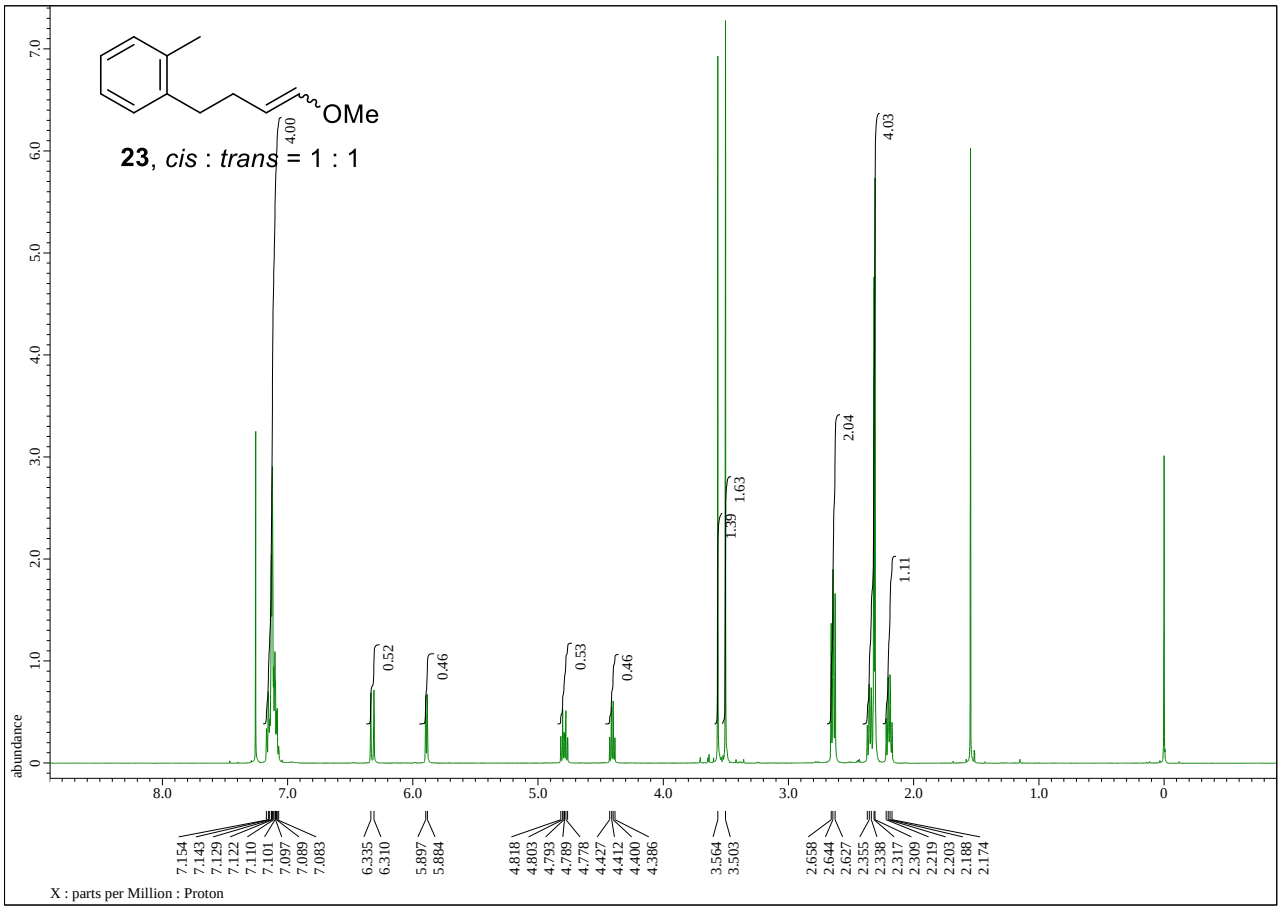
OMe
23, cis : trans = 1 : 1
abundance
X : parts per Million : Proton

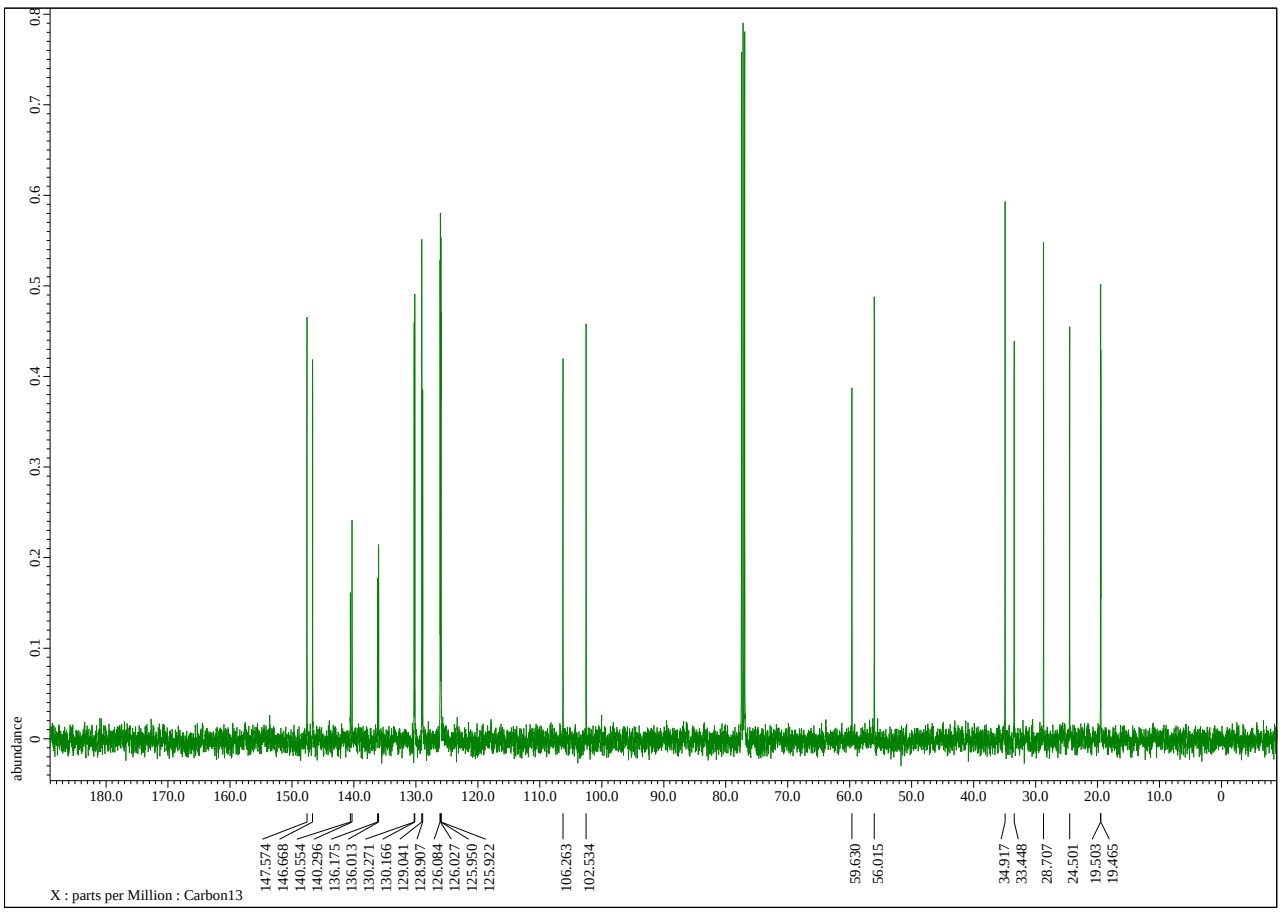
abundance
X : parts per Million : Carbon13

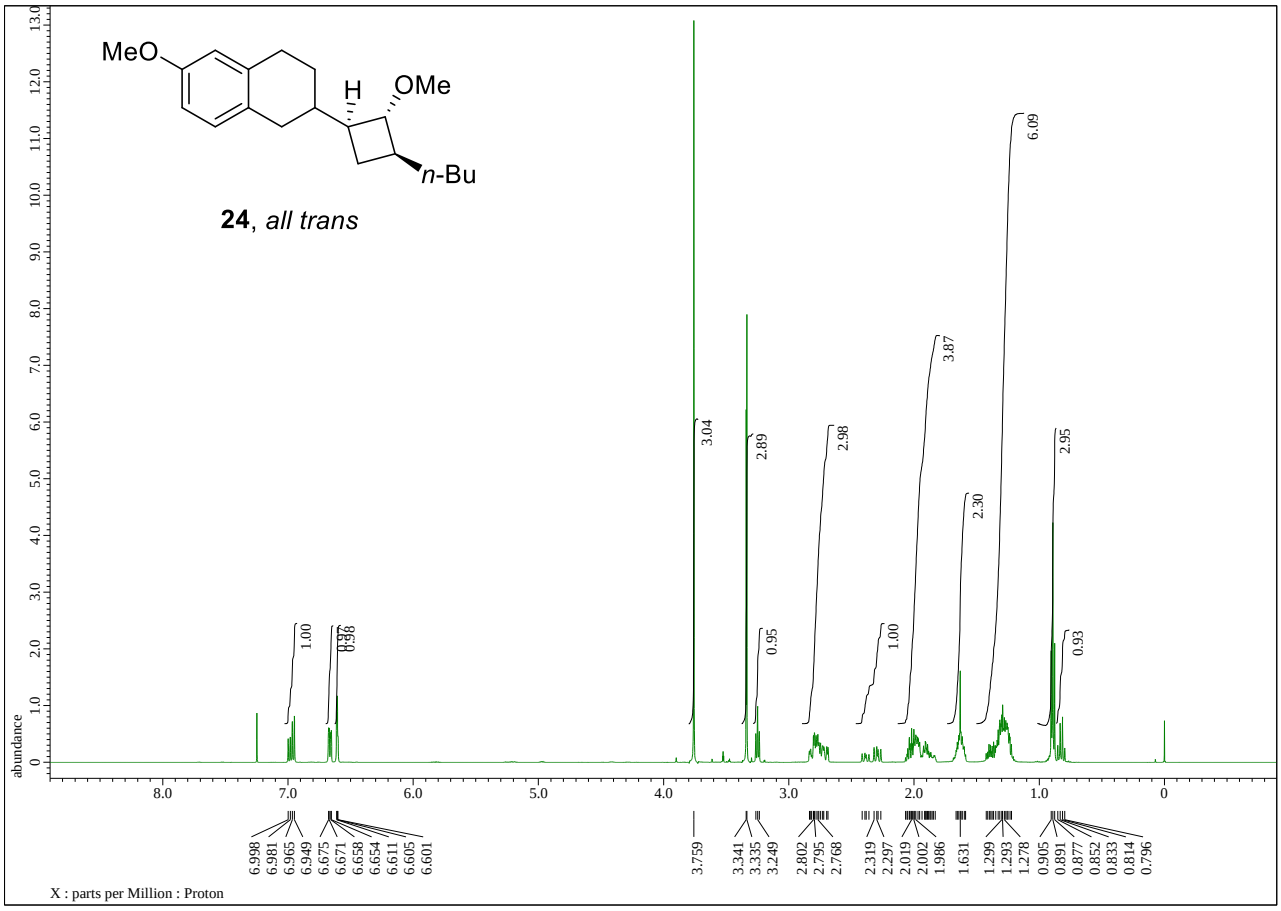
MeO
H
OMe
n-Bu
24, all trans
abundance
X : parts per Million : Proton

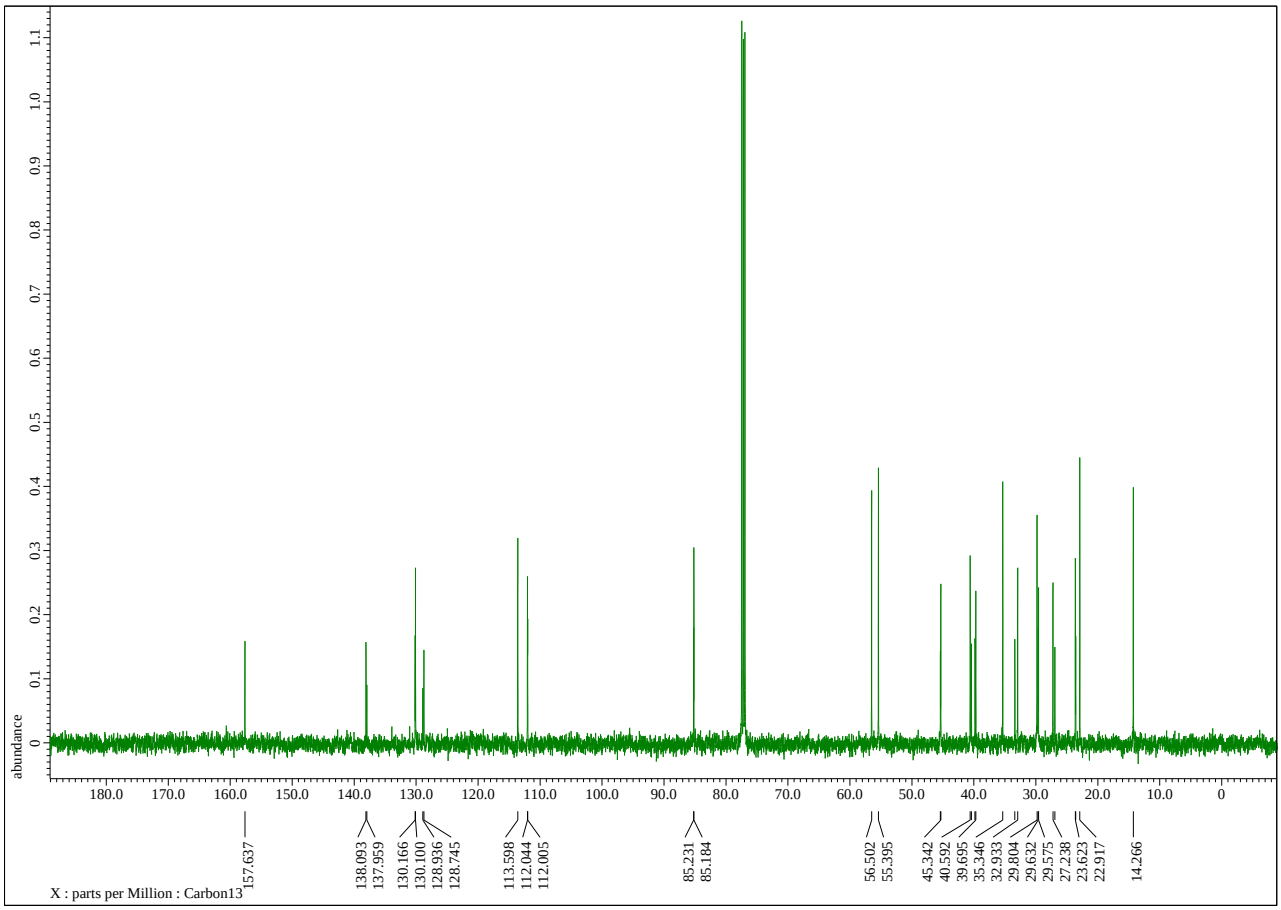
abundance
X : parts per Million : Carbon13

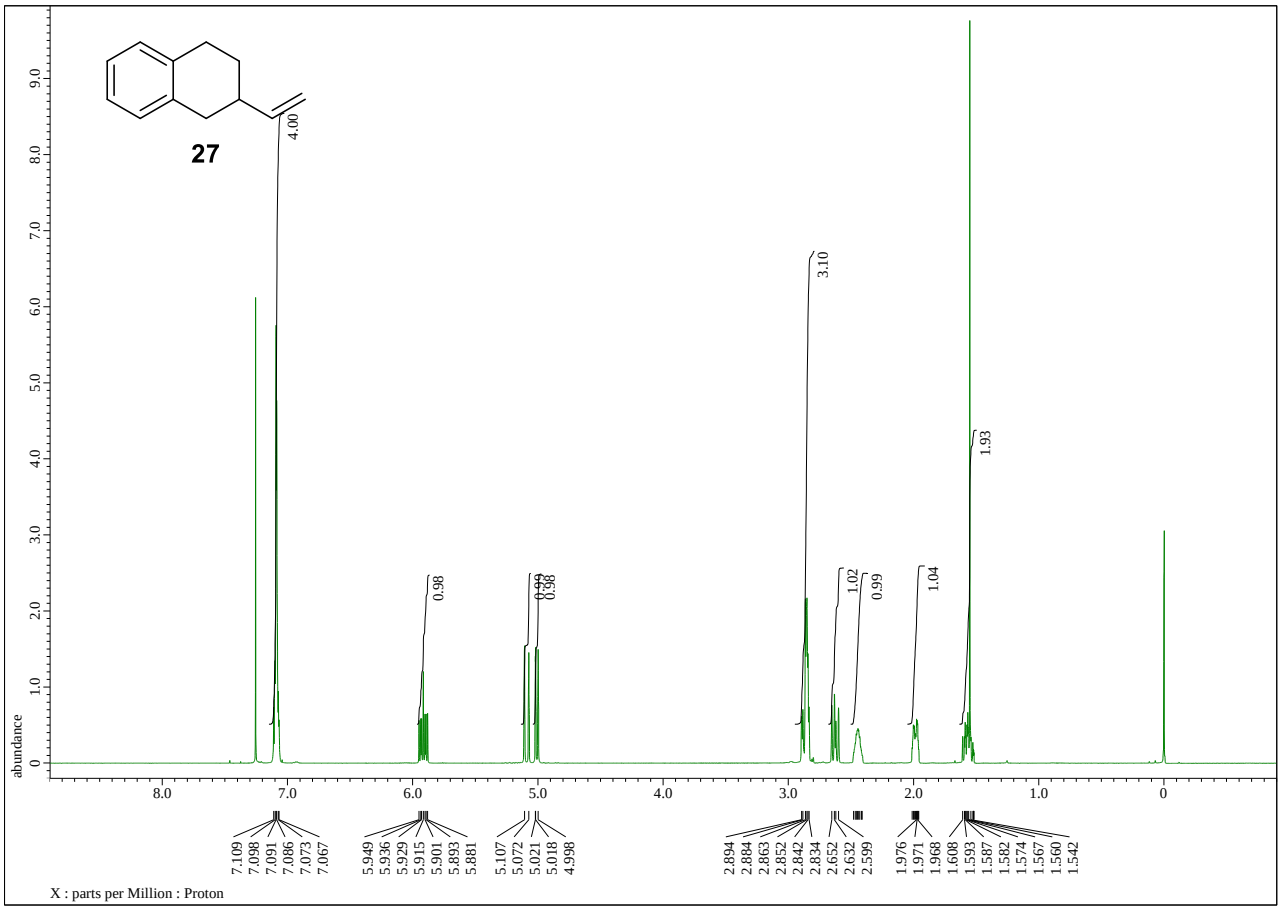
27
4.00
3.10
1.93
0.98
0.99
1.02
0.99
1.04
abundance
X : parts per Million : Proton

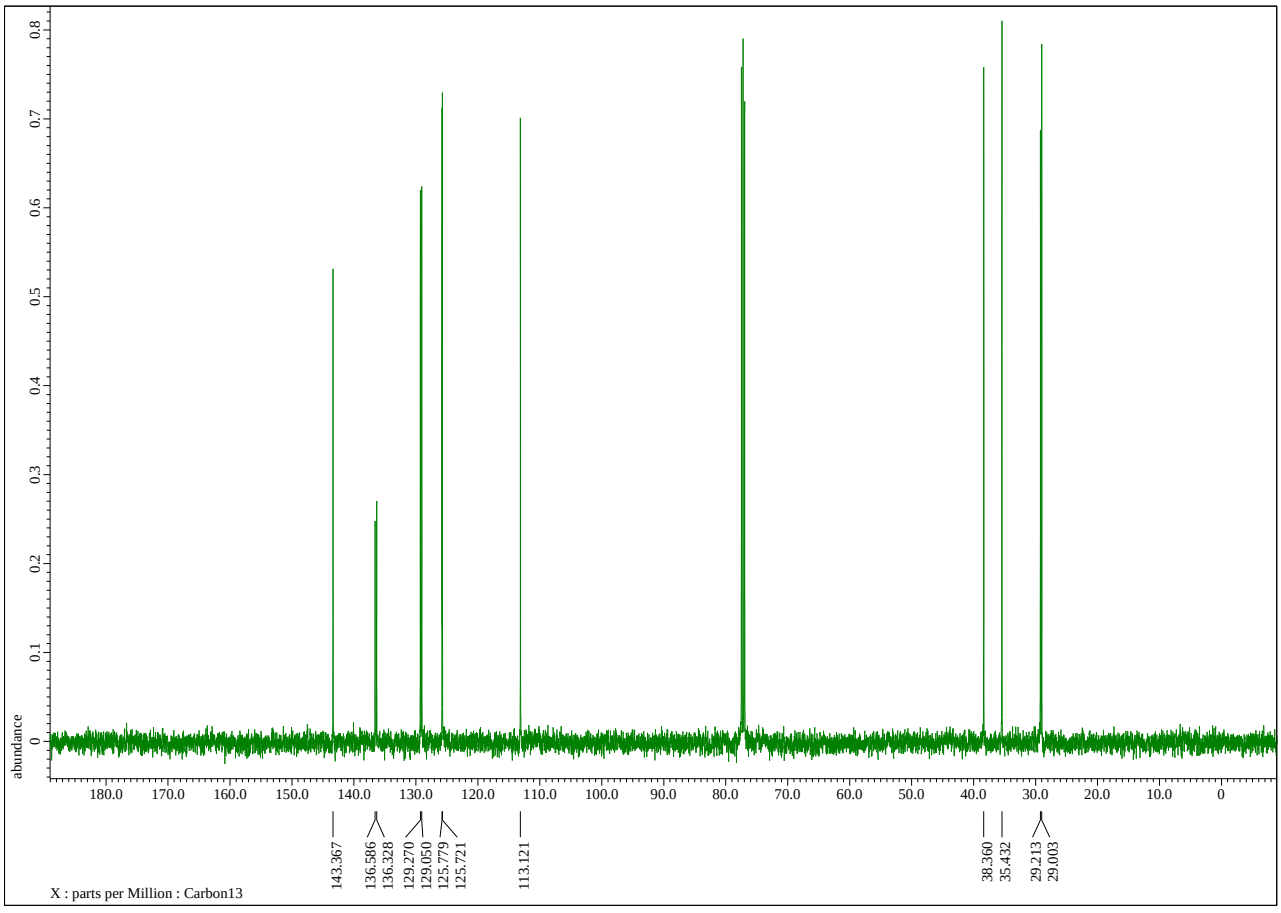
abundance
X : parts per Million : Carbon13

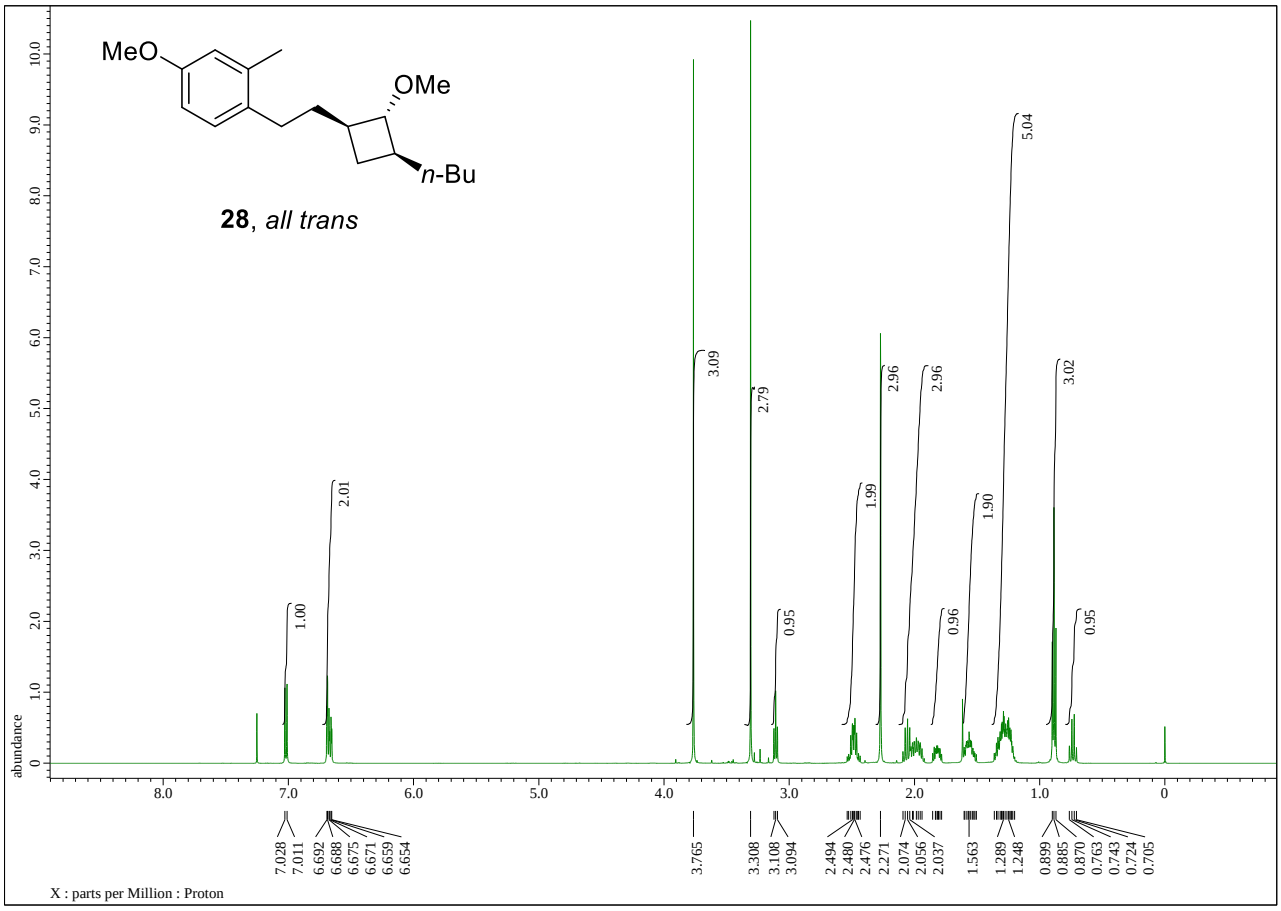
MeO
OMe
n-Bu
28, all trans
abundance
X : parts per Million : Proton

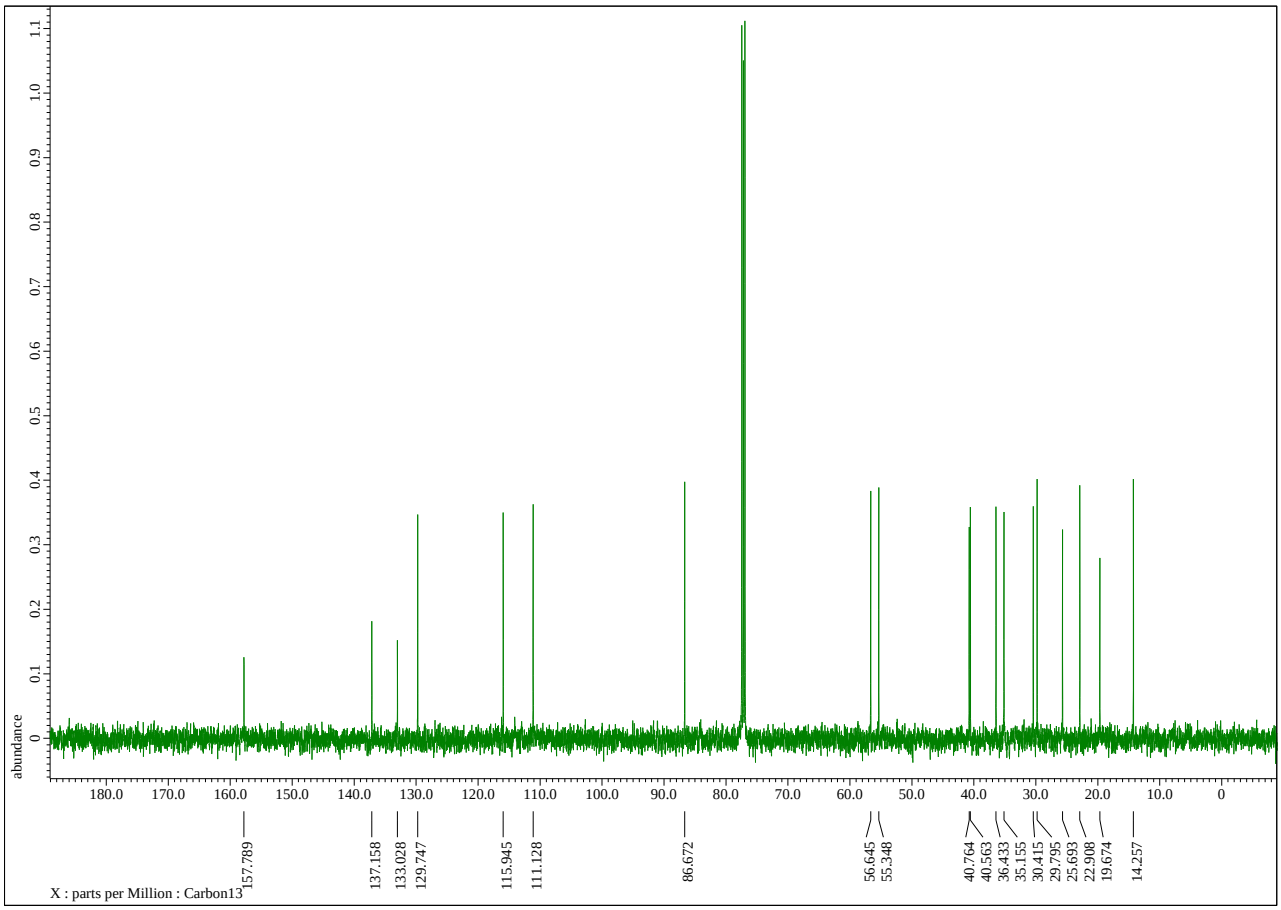
abundance
X : parts per Million : Carbon13

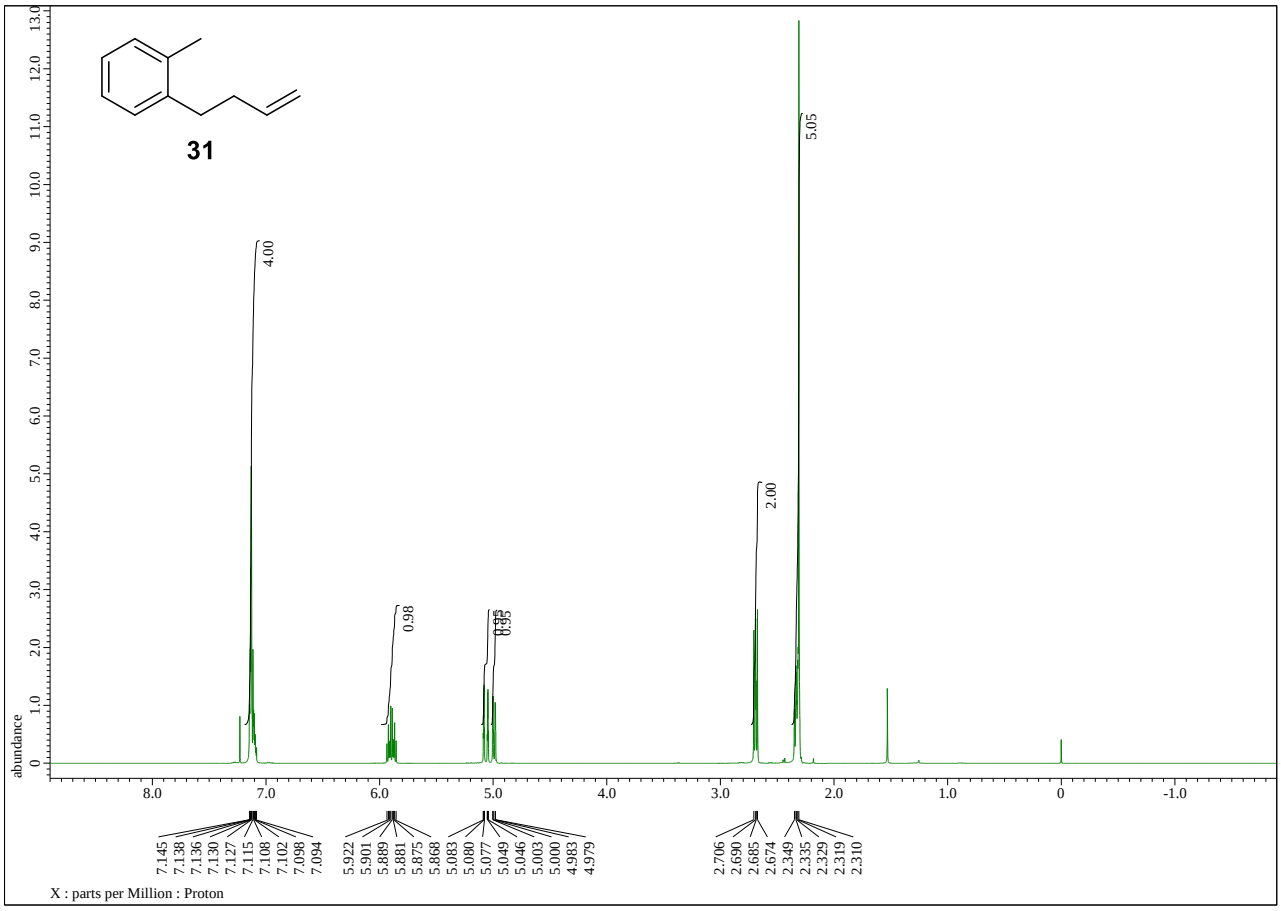
31
4.00
0.98
0.95
2.00
5.05
abundance
X : parts per Million : Proton

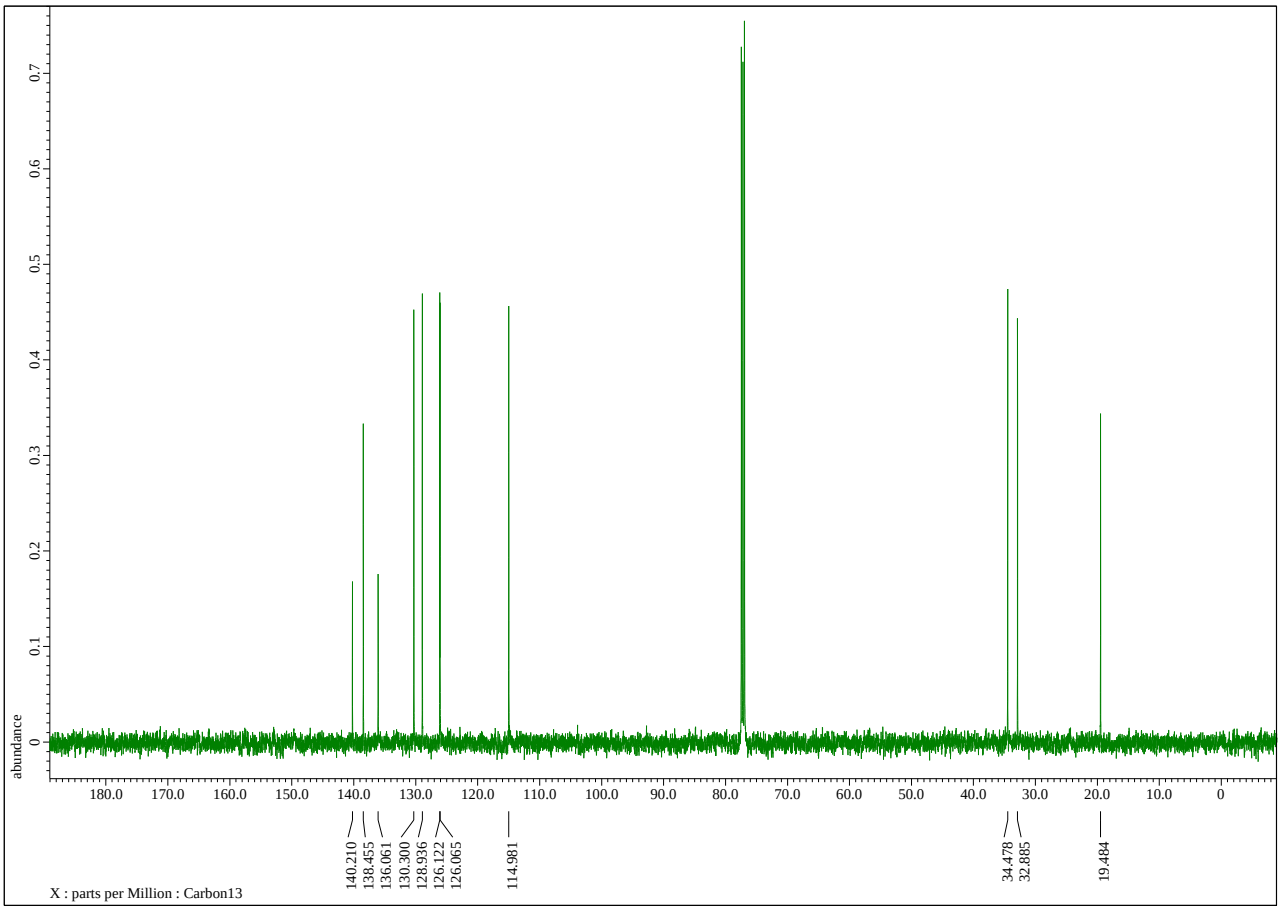
abundance
X : parts per Million : Carbon13